Terrestrial response to abrupt climate changes during the Late Quaternary in Southern Spain

Claire Elizabeth Gallant

Thesis submitted for the degree of Doctor of Philosophy,
Royal Holloway, University of London

September 2012

Institution of study:
Centre for Quaternary Research
Department of Geography
Royal Holloway
University of London

Declaration of Authorship

I Claire Elizabeth Gallant hereby declare that this thesis and the work presented in it is entirely my own. Where I have consulted the work of others, this is always clearly stated.

Signed:

Abstract

The Mediterranean region is located on a climatic boundary between arid North Africa and temperate Europe and lies proximal to the North Atlantic. As such, the region is thought to have been highly sensitive to past climate changes, and is predicted to be acutely sensitive to future changes. The impact of both glacial/interglacial and stadial/interstadial climate shifts have been identified within long pollen records of the eastern Mediterranean and western Mediterranean marine sequences. However, our understanding of the impact of these changes within terrestrial settings is relatively poor with little understanding of either the scale or rapidity of response.

This thesis presents sedimentological, geochemical, micromorphological and isotopic data from three previously unidentified loess-palaeosol sequences within southern Spain; covering MIS 5, MIS 2 and MIS 1. Bulk sedimentological data from each site is presented within a chronological framework provided by OSL dating. Additionally, results from micromorphological analysis of sediments and oxygen and carbon isotopic composition of secondary carbonates are presented for each site.

The thesis provides discussion of:

1. The description and recognition of loess within southern Spain, using bulk sedimentological properties, mineralogy (XRD) and isotopic composition (Sr/Nd).
2. Geomorphic response of the landscape to both Milankovitch and sub-Milankovitch timescales.
3. The use of oxygen and carbon isotopic composition of secondary carbonates to identify shifting temperatures and/or aridity through loess deposition and alteration.

Shifts in depositional environments and geomorphic processes recorded at each site identifies that the landsystem of southern Spain is highly responsive and capable of large scale changes on Milankovitch and sub-Milankovitch timescales. Contrary to current understanding loess in southern Spain is not exclusively a glacial phenomenon, nor is its provenance as straightforward as previously suggested. As such, existing literature regarding atmospheric processes and loess transport in the region during the last glacial appear over simplified.

Acknowledgements

First and foremost, I wish to thank my supervisors Dr I. Candy and Dr S. Armitage for their endless encouragement, support and patience over the last four years. Thank you to all of the staff of the CQR for their discussions and useful insights, and for making the department such a great place to be.

I would like to thank Dr C. Manning and Prof M. Thirlwall (RHUL) for their assistance with sample preparation and analysis of strontium and neodymium isotopes and am particularly grateful to Dr C. Manning for guidance in data analysis. Thanks also to Dr D. Alderton (RHUL) for providing XRD analysis data and guidance of data analysis. A huge thanks is due to the RHUL geography laboratory and support staff Dr Adrian Palmer, Iñaki Valcarcel, Robyn Christie, Jenny Kynaston and Elaine Turton for all of their assistance over the last four years. In particular I'd like to thank Adrian for his assistance with all things sedimentological and micromorphological and Iñaki for all of his help during sample preparation.

Thanks to all of the CQR PhD students for making my time at RHUL so enjoyable; and a special thanks to Gareth Tye, Jenni Sherriff, Mark Hardiman, Chris Satow, Ruth Sowa and Caroline Juby for all of their support and making the past four years so enjoyable! I'd also like to thank Clare Daly and Mark Hardiman for being the best field assistants I could ever have hoped for, and for never moaning (even when I was being a slave driver!). This thesis is dedicated to my family and to Gareth Tye for their endless support and for always believing in me. Thank you.

List of contents

Chapter 3 Loess as a palaeoenvironmental archive

Chapter 4 Composition of secondary carbonates

Chapter 5 Methodology

Chapter 9 – Maro

List of Figures

Chapter 8: Chimeneas

Chapter 9: Maro

List of Tables

Chapter 1 – Introduction

This introduction chapter provides the rationale and scientific context of the research undertaken. Brief summaries of the current understanding of Mediterranean Quaternary climates and the use of loess-palaeosol sequences within Quaternary research are presented, with full reviews presented in chapters 2, 3 and 4. The rationale and academic context provides the basis for the aims and objectives stated. The chapter concludes with an introduction to the three study sites including an introduction to the modern climate of the region.

1.1 Rationale

The IPCC has highlighted the Mediterranean as a region especially vulnerable to future climate changes; with the region predicted to warm at a rate greater than the global mean (Harding *et al.* 2009) and for summer droughts to increase (Giorgi *et al.* 2001 (IPCC report)). The climatic sensitivity of the region is due to its geographic position on a climatic boundary between arid North Africa and temperate Europe and additionally, due to the regions proximity to the North Atlantic (Giorgi and Lionello 2008). Positioned as it is at the transition between temperate and arid climates and close to the North Atlantic, considered to be a communicator of climate change, the region is thought to have been particularly sensitive to past climate changes. Understanding communication of climatic changes to the region, and within the region itself and the impact of such changes upon land-systems could help further understanding of how the region will respond to future climate shifts (Fletcher and Zielhofer 2011).

At present, there is a lack of understanding of western Mediterranean terrestrial response to Quaternary climate changes. This is due to the paucity of long terrestrial sequences in the western Mediterranean. Currently, understanding of Mediterranean Quaternary climates is based upon the marine sequences in the western Mediterranean and the long terrestrial records of the central and eastern Mediterranean. This thesis seeks to examine the potential for using loess sequences in southern Spain as a record of western Mediterranean response to late Quaternary climate changes.

1.2 Scientific context

1.2.1 Mediterranean Quaternary climates

Quaternary climates are characterised by orbitally driven (Milankovitch) variations between glacial and interglacial periods (Berger *et al.* 2007). The chronology of these variations is derived from isotopic shifts recorded within continuous marine sequences and ice core records (e.g.

Shackleton 1967, Imbrie *et al.* 1984, Jouzel *et al.* 2007 and Rasmussen *et al*., 2008) with the different climatic periods assigned a Marine Isotope Stage (MIS) or Oxygen Isotope Stage (OIS) number. Superimposed upon these large scale climate changes paced according to Milankovitch forcing (chapter 2) are rapid, quasi-periodic relatively low amplitude events; such as the Dansgaard-Oeschger cycles of the last glacial (Bond *et al.* 1997). This thesis focusses on the late Quaternary, a period covering the previous Interglacial (MIS 5e), the last Glacial (MIS 4-2) and the current Interglacial (MIS 1) (figure 1.1).

Through correlation of Mediterranean marine sequences with those located within the North Atlantic it is suggested that the Mediterranean region shows a clear climatic response to both glacial/interglacial changes and rapid climate events recorded within the North Atlantic and Greenland (e.g. Shackleton *et al.* 2000, Martrat *et al.* 2004). Through the analysis of terrestrial pollen contained within western Mediterranean and North Atlantic Iberian peninsula marine cores it has been possible to assess the timing and style of vegetation response to the climatic and oceanographic changes recorded by the marine sequences (e.g.MD95-2042 Shackleton *et al.* 2000, MD95-243 Sánchez Goñi *et al.* 2002). The pattern of response is also recorded within the long, terrestrial sequences from the central and eastern Mediterranean (e.g. Monticchio, Allen *et al.* 1999 and Ioannina and Tenaghi Phillipon, Tzedakis *et al.* 2001). These records indicate that in the Mediterranean Interglacial episodes are associated with forested conditions and glacial stages associated with large declines in forest cover and the dominance of steppic taxa (Tzedakis 2009) (figure 1.1). From these records it is also evident that Mediterranean vegetation responded to sub-Milankovitch climate variations with steppic taxa associated with stadial (cold) conditions and increases in forest cover associated with interstadial (warm) conditions (for discussion see Allen *et al.* 1999 and Fletcher and Sánchez Goñi 2008).

It is suggested that available moisture is the key control on Mediterranean vegetation (Tzedakis 2003) and therefore the pattern of warm interglacial forests suggests humid conditions and cold, glacial steppe associated with aridity (Tzedakis 2009). Prentice *et al.* (1992) has suggested that glacial steppic conditions are related to a change in effective precipitation. Through construction of a water balance model Prentice *et al.* (1992) was able to reconstruct effective precipitation levels based upon the vegetation record at Tenaghi Phillipon, where effective precipitation describes the precipitation contribution to soil moisture i.e. precipitation not lost via evapotranspiration or as surface run-off. Prentice *et al.* (1992) suggest that steppic taxa indicative of arid conditions are reflecting increased seasonality of the rainfall season, with a shorter wet winter period and longer summer droughts.

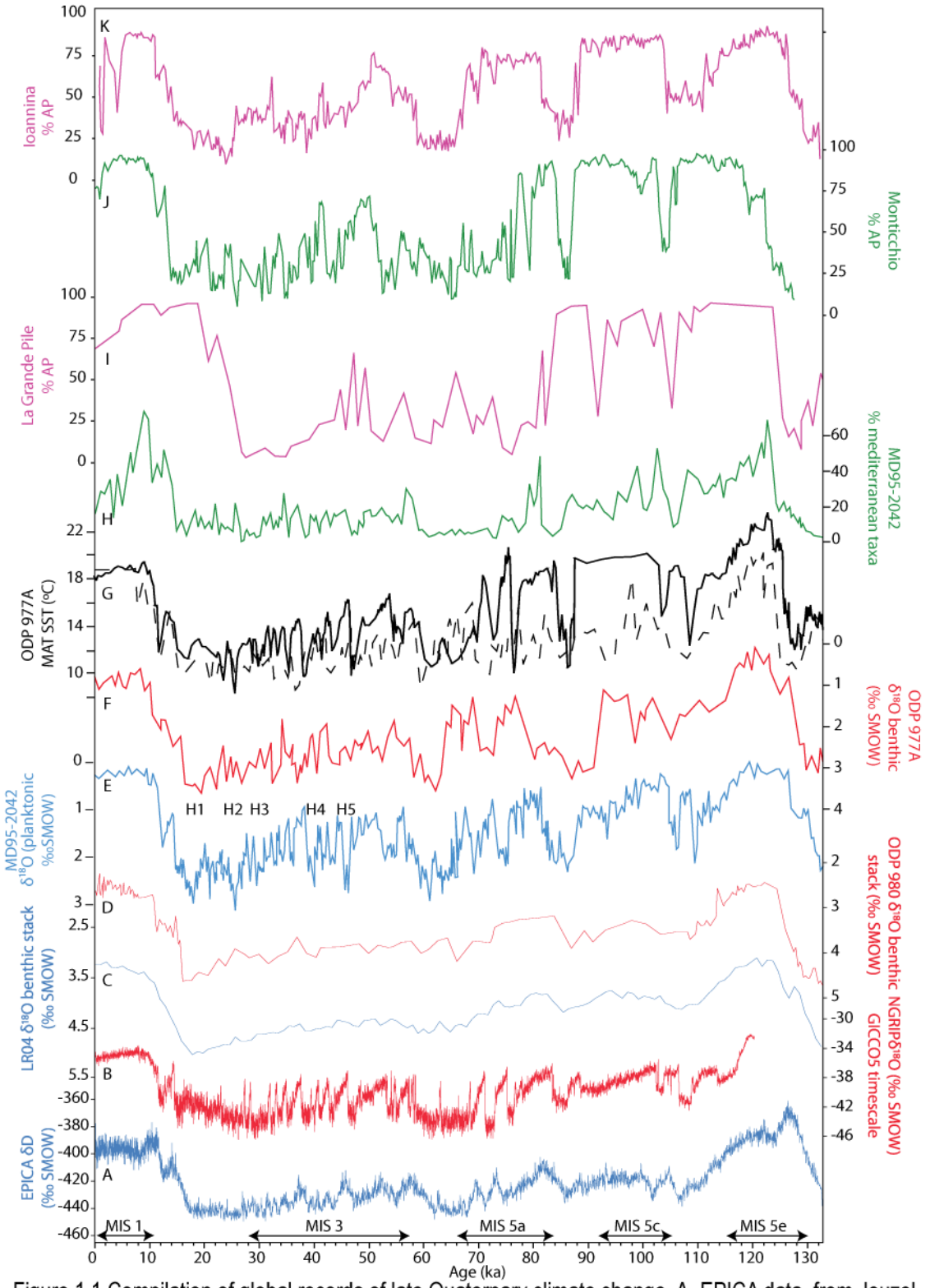

Figure 1.1 Compilation of global records of late Quaternary climate change. A. EPICA data from Jouzel *et al.* 2007. B. NGRIP data from Wolff *et al.* (2010). C. LR04 data from Lisiecki and Raymo (2005) (insolation tuned). D. ODP 980 data from McManus 1999. E. MD95-2042 data from Shackleton *et al.* 2000 (GISP2 correlated). F-G. ODP 977A: benthic $\delta^{18}O$ record from Martrat *et al.* (2004), dashed line is MAT estimate based on the modern analogue reconstruction of planktonic foraminifera assemblage (Pérez-Folgado *et al.* 2004), solid line is alkenone derived MAT estimate (Martrat *et al.* 2004). MD95-2042 record of % Mediterranean taxa from Sánchez Goñi *et al.* (2000, 2008). La Grande Pile %arboreal pollen (AP) from Woillard and Mook (1987) plotted to age model shown in Heusser (2000). Monticchio %AP from Brauer *et al.* 2007. Ionnanina %AP from Tzedakis *et al.* (2001). Site locations in figure 1.8.

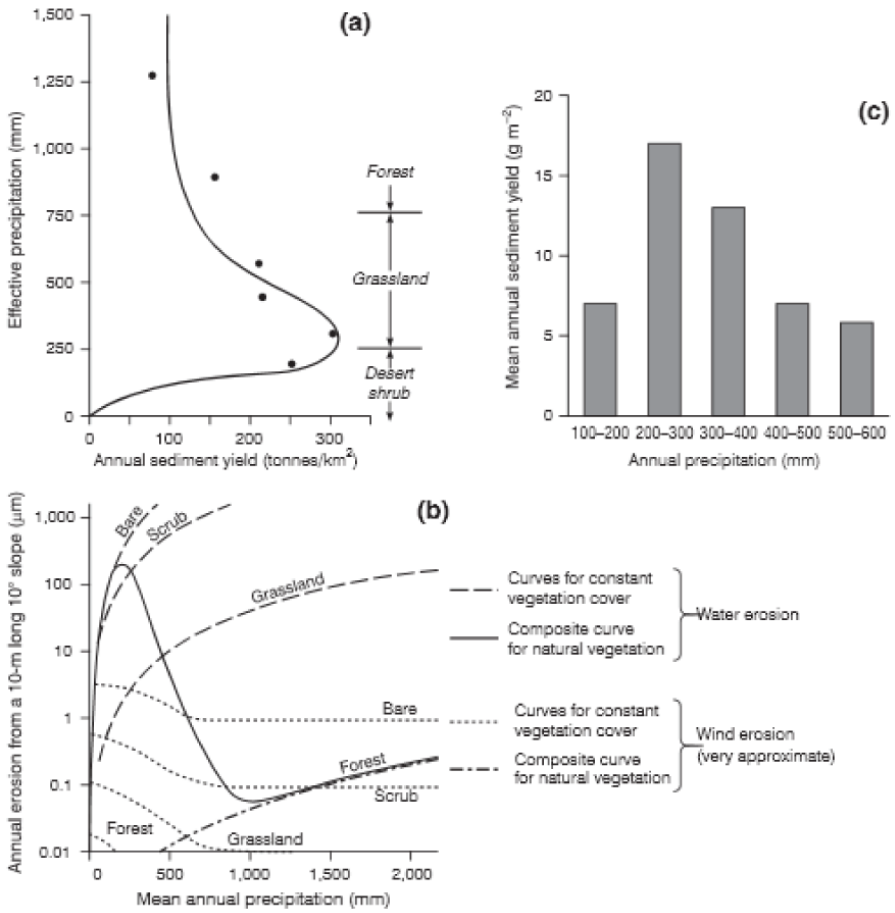

Figure 1.2 Taken from Thornes (2009) (and references therein). Showing the relationship between vegetation,precipitation and sediment availability.
a) Relationship between sediment yield and annual effective precipitation.
b) Wind and water erosion rates as a function of ranfall and vegetation cover.
c) Erosion rates, vegetation cover and rainfall.

Terrestrial evidence of western Mediterranean response to Quaternary climate change is based primarily on the interpretation of pollen from marine cores located off the Iberian coast. There have, however, been attempts to reconstruct geomorphic response from terrestrial sediment sequences. Through the analysis of western Mediterranean fluvial sequences Macklin *et al.* (2002) have suggested glacial and stadial events are associated with alluviation events suggesting increased sediment availability during these events. This view is supported by Rose *et al.* (1999) who highlight landscape instability during glacial and stadial events, countered by soil development associated with stable land systems during interglacial periods expressed in sediment sequences on Mallorca. As such, it is suggested that there is a geomorphic response associated with both Milankovitch and sub-Milankovitch climate changes within the western Mediterranean, in response to both changing precipitation regimes and vegetation dynamics (figure 1.2). However, the regional assessment of terrestrial response undertaken by Macklin *et al.* (2002) is based upon fragmentary fluvial sequences, where sub-stage and sub-Milankovitch correlations are based upon age estimates with large uncertainties, often larger than the duration of the correlated event. In addition to difficulties associated with constraining the timing of fluvial

change, Candy *et al.* (2004a) highlight the issues of identifying climate change as the primary driver of response within a tectonically active area such as southern Spain.

As a semi-arid region southern Spain is particularly sensitive to climate changes as shifts in the precipitation regime can easily affect vegetation composition and therefore sediment mobilisation (Fletcher *et al.* 2012). However, despite clear indications that Quaternary climate changes drove significant changes in sediment availability and landscape stability (Macklin *et al.* 2002, Rose *et al.* 1999), the region may have additionally been affected by sediment mobilisation from the nearby semi-arid region of North Africa.

It is suggested that marine cores from within the Alboran sea record an increase in the input of North African dust during stadial events of the last glacial (e.g. Moreno *et al.* 2002, 2004 (MD95-2043), Bout-Roumazeilles *et al.* 2007 (ODP976)). Peaks in North African dust contribution are identified on the basis of increased input of silt sized material and peaks in silica vs. potassium, where silica is regarded as a proxy for North African derived sediments (Moreno *et al.* 2002) or increased occurrence of palygorskite clay, a clay destroyed by fluvial transport (Bout-Roumazeilles *et al.* 2007). It has been suggested that stadial conditions were associated with a long lived positive NAO type atmospheric system (Moreno *et al.* 2002, 2004, Bout-Roumazeilles *et al.* 2007) (figure 1.3). This assertion is based on the modern day relationship between atmospheric pressure systems and short lived dust events (e.g. Moulin *et al.* 1997), where positive North Atlantic Oscillation (NAO) phases are shown to correlate with increased transport of North African dust to the Mediterranean.

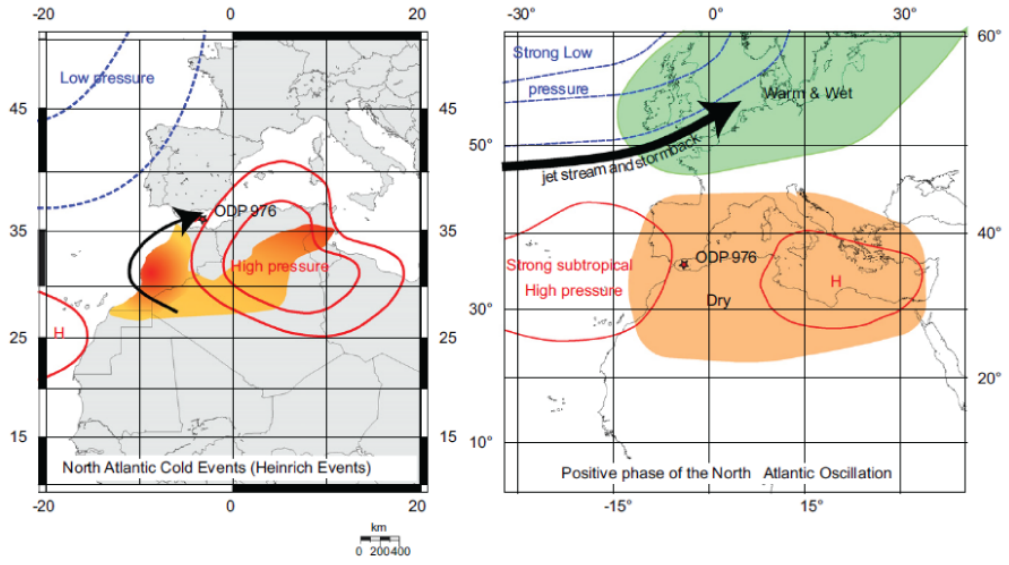

Figure 1.3 Taken from Bout-Roumazeilles *et al.* (2007). Comparison of: a) proposed atmospheric conditions resulting in enhanced aeolian transport of clays and silt from North Africa during stadial events and b) atmospheric conditions during the positive phase of the NAO cycle

It has been suggested (Rose *et al.* 1999) that the western Mediterranean may have experienced periods of far travelled loess accumulation during the late Quaternary. As one of the major contributors to global dust flux (McGee *et al.* 2010), North Africa is an obvious potential source. Despite the large apparent dust inputs to the Alboran sea during the last glacial, to date, no far travelled loess has been identified within southern Spain (e.g. Günster *et al.* 2001) and no other Mediterranean loess deposits have been identified as North African in origin.

1.2.2 Loess-palaeosol sequences as records of Quaternary climate

The thick loess-palaeosol sequences of Northern Europe, Eastern Europe and China are frequently used as multi-proxy records of terrestrial response to Quaternary climate changes (e.g. Kukla 1987, Markovíc *et al.* 2011). Although these regions have accumulated some of the most extensive, thick deposits of loess, the occurrence of loess is not restricted to these locations (for example; Coude-Gaussen 1991).

Loess-palaeosol sequences are frequently described in terms of glacial loess accumulation and interglacial pedogenic alteration (Muhs and Bettis 2003) and on this basis are correlated to Milankovitch timescales (figure 1.4a). This Milankovitch driven accumulation and alteration provides the basis for regional correlation of loess deposits and correlation with global records of Quaternary climate (figure 1.4a, b). However, it has recently been demonstrated that loess accumulation and alteration is a highly dynamic system capable of responding to and recording sub-Milankovitch climate events (figure 1.4c, Moine *et al.* 2008).

In addition to the ability of loess to record climate change on different timescales, it is also a readily dateable deposit (Roberts 2008) via OSL methods and contains a variety of sediment proxies (chapters 3, 4, 5) enabling multi-proxy analysis to be undertaken. Therefore, loess offers the potential to produce multiple lines of evidence for palaeoclimate change within an independently dated timescale. Furthermore these deposits are capable of recording both Milankovitch and sub-Milankovitch events. Loess is frequently reported within the Mediterranean region (e.g. Coude-Gaussen 1991, Günster *et al.* 2001, Garcia *et al.* 2011), to date however, very little work has been undertaken on the reported sequences. This thesis will examine the potential for using loess-palaeosol sequences within southern Spain as records of terrestrial response to Milankovitch and sub-Milankovitch climate events.

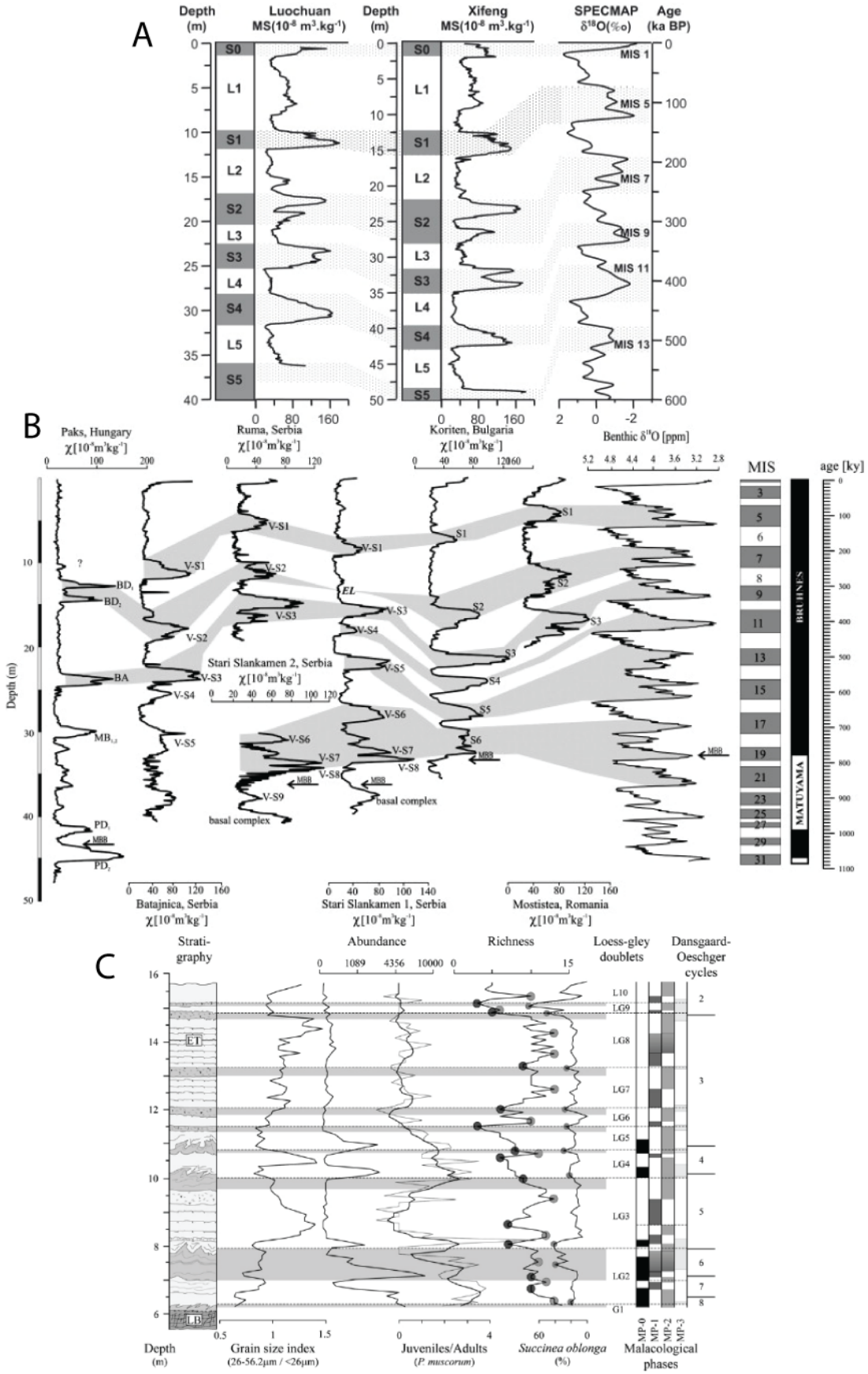

Figure 1.4 Milankovitch and sub-Milankovitch climate changes recorded in loess-palaeosol sequences. A. Chinese loess plateau stratigraphy (Wu *et al.* 2007), where soil horizons marked by magnetic susceptibility peaks relate to interglacial climates and loess accumulation to glacial climates. B. East European loess correlation (Markovic *et al.* 2011), interglacial soils marked by magnetic susceptibility peaks are used to produce a regional correlation from multiple sites. C. Record of sub-Milankovitch change recorded through multiple palaeosols within last glacial loess in Belgium (Moine *et al.* 2008)

1.3 Aims and objectives

1.3.1 Aims

This thesis aims to examine the potential of using loess-palaeosol sequences within southern Spain to reconstruct landscape response to late Quaternary climate change. The work undertaken will also address a series of subsidiary aims listed below;

1. Provide the first quantitative characterisation of loess deposits in southern Spain.

2. Identify the timing of loess accumulation in the western Mediterranean.

3. Attempt to provenance each deposit to at least a local or non-local level.

4. Derive palaeoclimatic and geomorphic information from each deposit through the multi-proxy analysis of the sediments in order to reconstruct accumulation and alteration models.

5. Examine the potential of combining micromorphological and stable isotopic geochemistry analyses on loess-palaeosol sequences.

1.3.2 Objectives

For each study site, sediments will be analysed in terms of particle size, carbonate content, and magnetic susceptibility in order to produce a quantitative assessment of the sedimentary characteristics of each loess deposit. In addition, semi-quantitative bulk mineralogy (XRD) will be undertaken alongside geochemical analysis of Sr/Nd isotope content to enable comparison with local sediments and data relating to potential remote dust sources. This study will provide the first quantitative assessment of the properties and composition of loess in southern Spain, enabling it to be compared with loess elsewhere in the Mediterranean and beyond.

Through independent dating (OSL and where possible U-series) of each loess sequence, site chronologies will be produced. This will not only constrain the timing of loess accumulation in the region but enable the correlation of the sequences to MIS or sub-stage level and aid comparisons with global and regional climate records. It may therefore be possible to identify different periods of loess accumulation and identify the climatic context of accumulation episodes.

The geomorphic response of the landscape to both Milankovitch and sub-Milankovitch climate forcing will be established by combining results from multiple lines of evidence (sediment descriptions (e.g. texture, colour and structure), particle size analysis (PSA), magnetic susceptibility, calcium carbonate content and thin section micromorphology). This will make it possible to discriminate between periods of accumulation and alteration of the sediment profiles.

Given current understanding of landscape response to climate change in the region, it is hypothesised that loess accumulation occurs during cold, arid climates, which are characterised by landscape instability, low vegetation cover and high sediment availability (Prentice *et al.* 1992, Allen *et al.* 1999, Macklin *et al.* 2002, Fletcher and Sánchez Goñi 2008, Tzedakis 2009). Conversely, during warm/wet periods, correlated with high vegetation levels, and landscape stability (Rose *et al.* 1999, Tzedakis 2009), it is proposed that loess accumulation ceases, and post-depositional pedogenic alteration of the loess occurs.

Pedo-sedimentary reconstructions based upon micromorphological investigation of loess-palaeosol sequences have been used extensively in the analysis of thick loess sequences (e.g. Kemp 1999). However, the technique is also used in order to support analysis of the isotopic composition of pedogenic carbonates found within loess sequences. It has been demonstrated that the oxygen and carbon isotopic composition of soil carbonates can be used to reconstruct vegetation (e.g. Wang and Greenberg 2006), temperature (e.g. Cerling 1984, Cerling and Quade 1993, Gallant *et al.* in prep) and aridity (Candy *et al.* 2012), accompanying micromorphological analysis is generally presented as a means of demonstrating the authigenic, unaltered nature of the carbonates analysed (e.g. Łącka *et al.* 2009). Therefore, through the production of a pedo-sedimentary model of evolution for each deposit, together with a record of the isotopic composition of pedogenic carbonates, it will be possible to assess the value of using the two techniques together and their potential to further the understanding of loess-palaeosol sequences.

1.4 Introduction to study sites

Günster *et al.* (2001) have produced the most recent review of loess deposits within southern Spain (figure 1.5). Attempts were made to locate each deposit listed by Günster *et al.* (2001). However, a lack of detail contained within the review meant that it was not possible to identify each loess accumulation mentioned in the text. Sites from Günster *et al.* (2001) that were located appeared to lack both the silt dominant grain size and cohesive nature that typifies loess accumulations (e.g. Pesci 1990, chapter 3). Through this investigative fieldwork however, three deposits were identified which appeared to fulfil the necessary criteria, these were; La Malaha, Chimeneas and Maro (figure 1.5). La Malaha and Chimeneas are located within the Granada basin and Maro is located on the coast.

Table 1.1 Study site coordinates and elevations (m a.s.l.)

Site	GPS coordinates	Elevation
La Malaha	+37° 5' 23.78", -3° 42' 42.19"	~690 m
Chimeneas	+37° 7' 48.04", -3° 49' 43.18"	~730 m
Maro	+36° 45' 7.41", -3° 48' 48.73"	~ 30 m

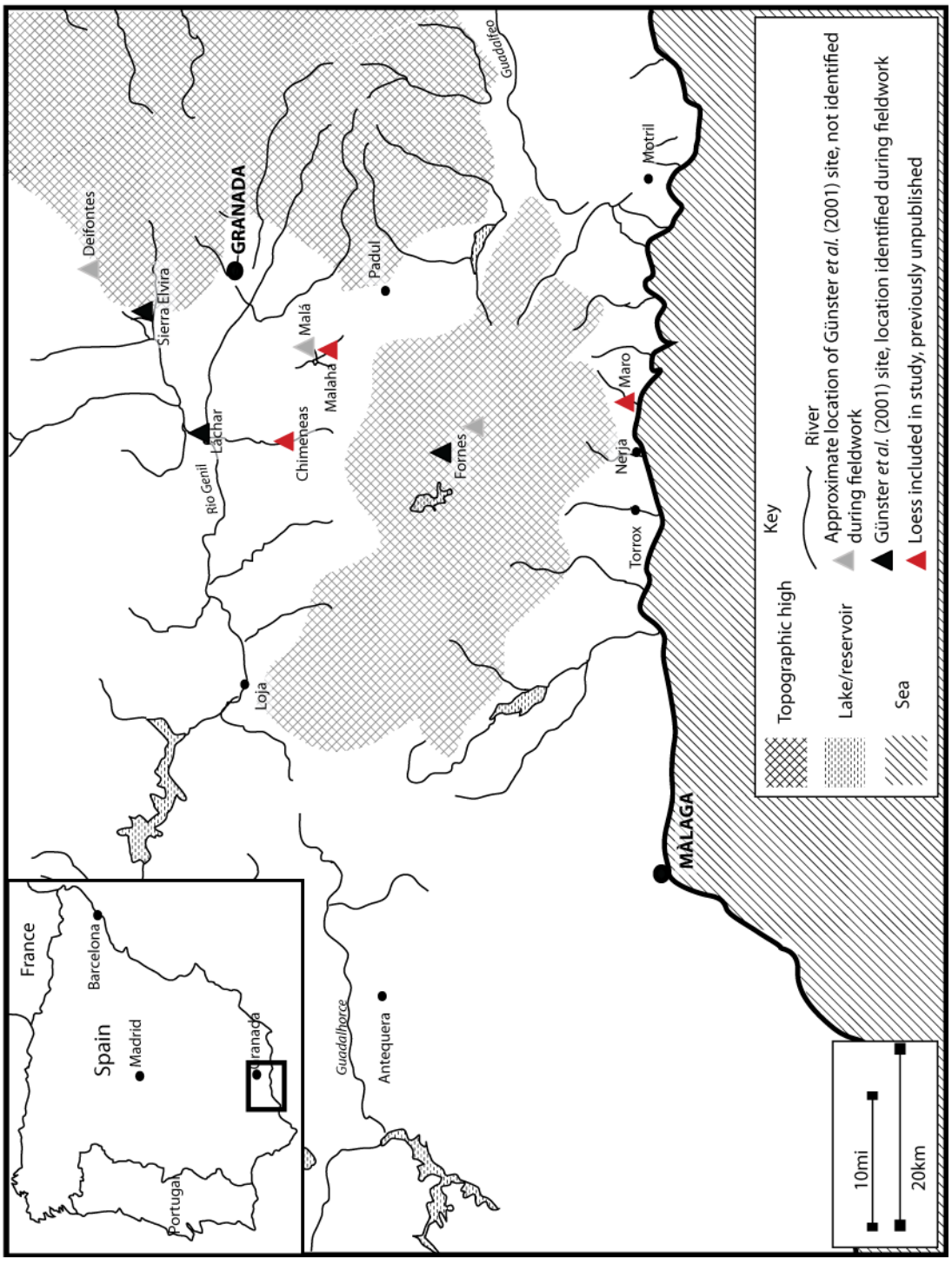

Figure1.5 Map showing the location of the study sections, with key towns and loess sites (chapter 3) for reference.

1.4.1 Local climate

As shown in figure 1.6 southern Spain contains a variety of climatic zones related to the varied topography of the region. The modern climate of all three study sites is characterised as temperate, with minimum winter temperatures from 0-18 ˚C accompanied by warm or dry summers (figure 1.2). Meteorological data (1971-2000) from the closest weather station to each site is listed in table 1.2, with Granada being the closest available data to La Malaha and Chimeneas and Malaga being closest to Maro.

This data indicates that the modern climate of each site is subject to highly seasonal rainfall regimes, with precipitation concentrated in winter, a characteristic that is typical of Mediterranean climates (Harding *et al.* 2009). The data from the Granada basin indicates that the area receives a much lower rainfall total than the coast and is subject to larger seasonal temperature variations.

Table 1.2 Local weather data from closest monitoring stations; Malaga data for Maro and Granada data for Chimeneas and La Malaha. Data presented is from 1971-2000, taken from Agencia Estatal de Meteorologia.

Location:	*Granada base area (37° 8' 10'' N, 3° 38' 0''W)*			
	Temperature (˚C)			
Period	Average	Average maximum	Average minimum	Precipitation (mm)
Mean annual	15.2	21.7	8.7	361(total) 30.08 (mean)
Coldest month (January)	6.8	12.2	1.3	44
Warmest month (July)	25.3	33.5	17.1	3
Location:	*Malaga airport (36° 40' 37'' N, 4° 29' 26''W)*			
	Temperature (˚C)			
Period	Average	Average maximum	Average minimum	Precipitation (mm)
Mean annual	18	22.9	13.1	524(total) 43.83 (mean)
Coldest month (January)	11.9	16.6	7.3	81
Warmest month (July)	24.8	29.9	19.7	2

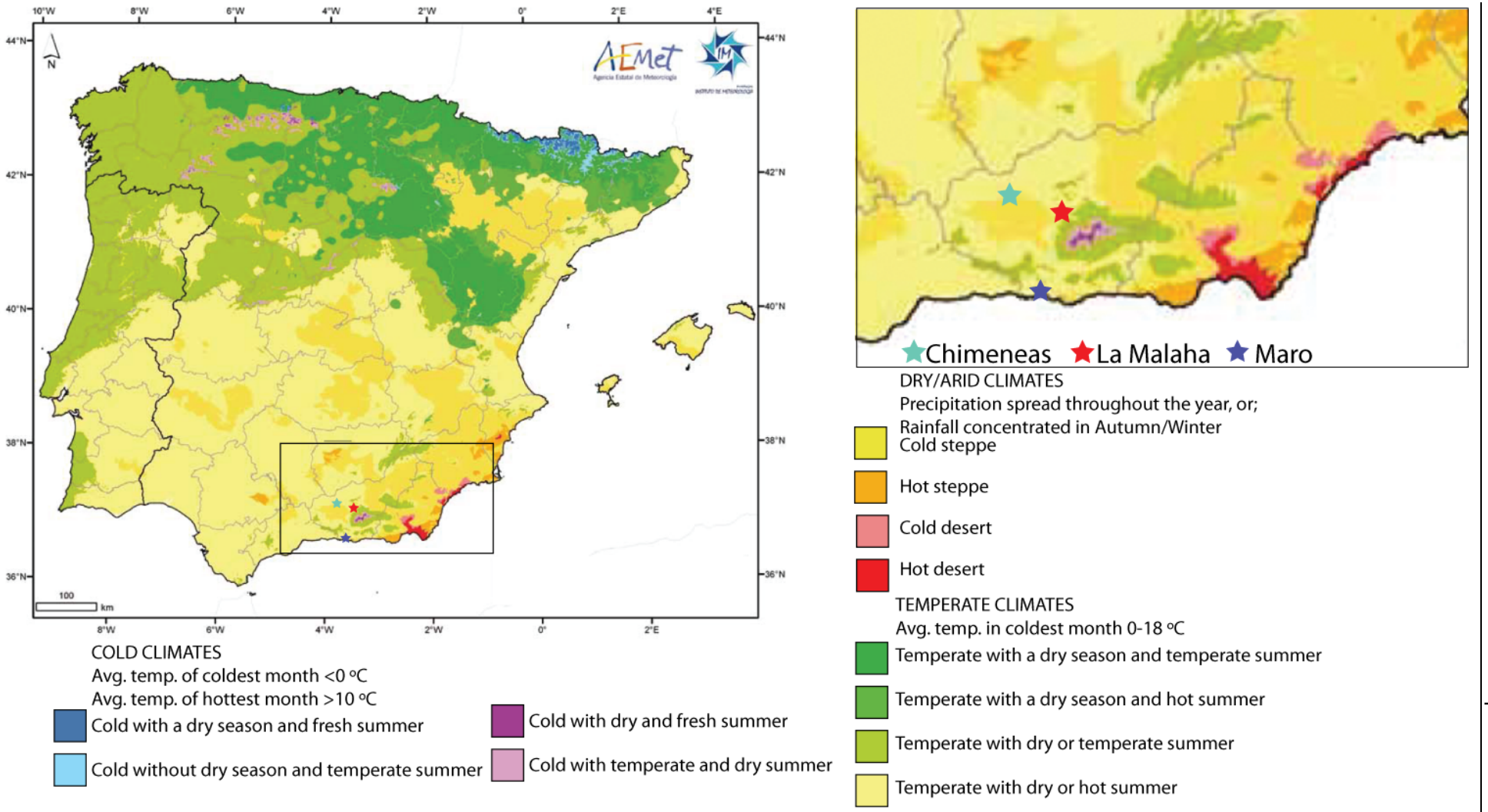

Figure 1.6 Climatic map of Spain. Site locations marked with stars. The map was compiled by Agencia Estatal de Meteorologia compiled from weather station data from 1971-2001 using the Köppen-Geiger climatic zonation scheme.

1.4.2 Vegetation

Mediterranean biomes are defined by their climate, typified by long, dry, warm summers and short, wet winters (Medaíl 2008, Allen 2009). The regions climate is divided, on the basis of mean annual precipitation (figure 1.7b), from per humid through to per arid reflected by deciduous forest through to Saharan type vegetation communities (Medaíl 2008). The relationship between precipitation and vegetation is subdivided into eight main bioclimatic zones of the Mediterranean (figure 1.7a). These zones are divided on the basis of the relationship between temperature and precipitation (given as a factor of latitude and altitude) (Allen 2009).

The Mediterranean region, as a tectonically active zone, is composed of basin and range topography composed of a wide range of lithologies and therefore varying soils. This complex landscape results in a heterogeneous vegetation cover related to the varied climatic and lithogenic conditions (Allen 2009, Tzedakis 2009).

The climate of each site (table 1.2, figure 1.6, 1.7) indicates that each location would be suitable to support the development of Mediterranean forest vegetation (Sánchez Goñi *et al.* 2008). However, at all sites the surrounding land has been extensively cleared for agricultural purposes.

1.4.3 Modern climatic controls

The modern climate of the Mediterranean is controlled by the shifting dominance of regional climate systems, with systems of North African origin dominating in summer and temperate, westerlies dominated systems of northern Europe emplaced during winter (Rohling *et al.* 2009). The region experiences a shift from hot, dry conditions during the summer when sub-tropical high pressure systems dominate, to a mild and wet winter when the sub-tropical high moves southward and the region becomes affected by westerlies (Harding *et al.* 2009, Nicholson 2011) (figure 1.7a).

A

Vegetation zonation	Vegetation communities	Bioindicator taxa
Cryo-Mediterranean	Alpine on rock, scree, and gravel	*Saxifraga, Androsace, Aubretia*
Alti-Mediterranean	Sub-alpine grasslands, herbaceous perennials, and dwarf junipers	*Juniperus , Bromus, Festuca, Poa, Phleum*
Oro-Mediterranean	Coniferous woodland	*Pinus uncinata, Pinus mugo*
Montane Mediterranean	Deciduous woodland	*Fagus sylvatica*; conifers (*Pinus, Cedrus, Abies*), *Juniperus*
Supra-Mediterranean	Deciduous oak forests and semi-deciduous in North Africa and Spain	*Quercus humilis, Quercus cerris, Quercus frainetto, Quercus macedonia, Ostrya carpinus, Carpinus orientalis, Corylus* sp ,*Tilia* sp., *Fraxinus ornus, Acer* sp.s
Meso-Mediterranean	Evergreen oak woodands and shrublands	*Quercus ilex, Quercus calliprinos, Pinus halepensis, Pinus brutia*. Where heavy anthropogenic activity: *Quercus coccifera, Calycotome villosa, Genista acanthoclada*
Thermo-Mediterranean	Dense coastal woodand; sclerophyllous, evergreen; significant human impact	*Olea europea, Ceratonia siliqua, Phillyrea media, Pistacia lentiscus, Laurus nobilis, Quercus suber, Pinus pinaster, Chamaerops humilis*
Infra-Mediterranean (Western Morocco)		*Argania spinosa* and *Acacia gummifera*

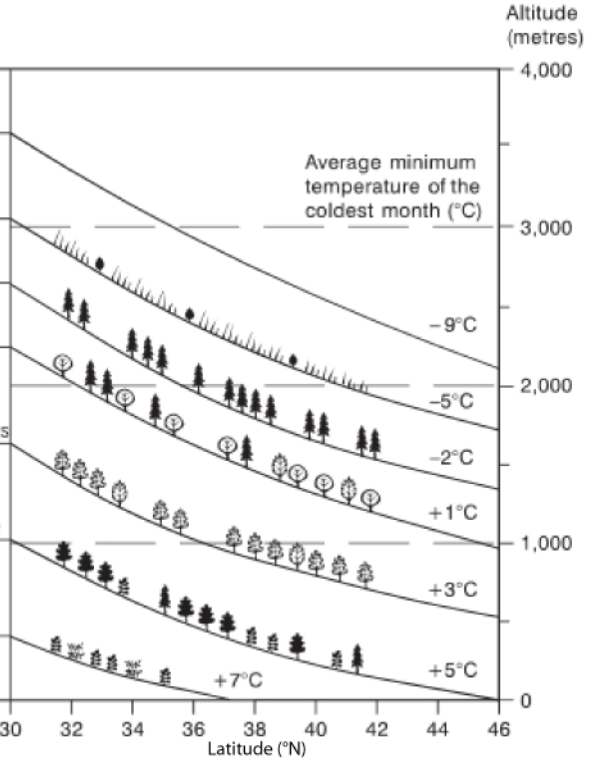

B

Bioclimate	*Mean annual rainfall (for m = 0 °C)*	*Number of months without rainfall*	*Main vegetation type*
Per-Arid	< 100 mm	11–12	Saharan
Arid	100–400 mm	7–10	Steppe and pre-steppe (*Juniperus turbinata, Pinus halepensis, Pistacia atlantica*)
Semi-Arid	400–600 mm	5–7	Pre-forest (*Pinus halepensis, P. brutia, Juniperus* spp., *Quercus*)
Sub-Humid	600–800 mm	3–5	Forest (Mostly sclerophyllous *Quercus*, *Pinus halepensis, P. brutia, P. pinaster, P. pinea, P. nigra, Cedrus*)
Humid	800–1000 mm	1–3	Forest (Mostly deciduous *Quercus*, *Pinus brutia, P. pinaster, P. nigra, Cedrus, Abies, Fagus*)
Per-Humid	>1000 mm	<1	Forest (Deciduous *Quercus*, *Cedrus, Abies, Fagus*)

m: mean minimum temperatures of the coldest month.

Figure 1.7 Controls on Mediterranean vegetation types: A. Bioclimatic zones according to temperate, altitude and latitudinal controls, taken from Allen (2009), B. Vegetation according to precipitation levels, taken from Médail (2008).

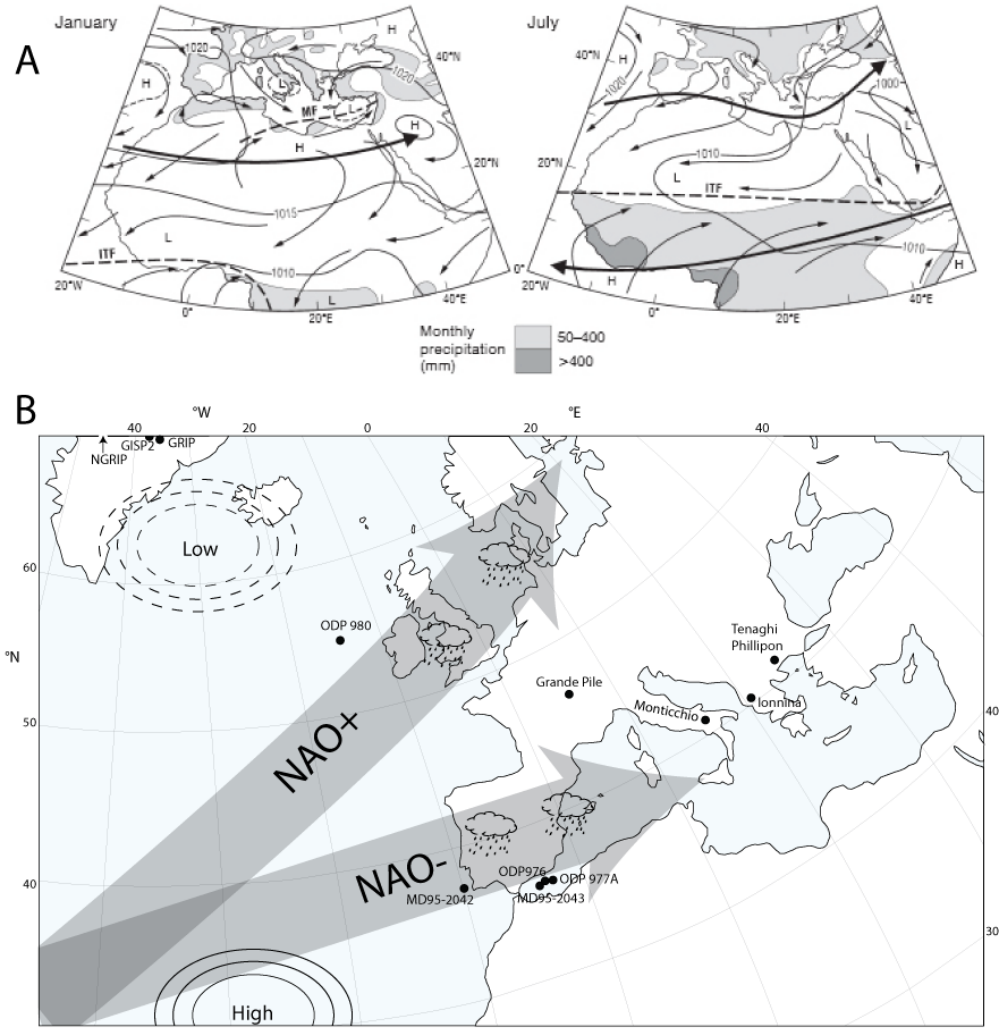

Figure 1.8 A. From Harding *et al.* (2009), location of the Mediterranean region in relation to large-scale atmospheric circulation. B. Adapted from Mayers and Pagani (2006), positive and negative phases of the North Atlantic oscillation. Also showing location of sites mentioned in text.

These climatic controls are then influenced by a number of factors which modify Mediterranean climate on a seasonal to decadal scale (Harding *et al.* 2009). The NAO (figure 1.8) is a storm track system controlled by the strength of opposing pressure systems which are centred over Iceland and the Azores (Meyers and Pagani 2006). In a positive NAO cycle the gradient between the arctic (Icelandic) and sub-tropic (Azores) pressure systems is most pronounced, resulting in the westerlies system being displaced and positioned over Northern Europe (figure 1.7b) (Meyers and Pagani 2006, Harding 2009). This results in increased levels of precipitation over Northern Europe and drier conditions within the Mediterranean. Conversely, during negative NAO cycles, when the pressure gradient between the arctic and sub-arctic is reduced, westerlies are positioned over southern Europe, resulting in increased precipitation over the Mediterranean (Harding 2009, Moreno *et al.* 2004). The NAO cycle is suggested to influence European climates in ~25 year cycles (Meyers and Pagani 2006); although some authors have suggested that sustained NAO type systems may have occurred during previous climate periods (e.g. Moreno *et al.* 2004, Bout-Roumazeilles *et al.* 2007).

1.5 Thesis structure

This thesis is divided into thirteen chapters. Chapter 2 provides a review of late Quaternary climate in order to place both the geomorphic and vegetational changes of the western Mediterranean within a climatic context. Chapter 3 provides a review of loess in the Mediterranean and the use of loess-palaeosol sequences as palaeoenvironmental records. Chapter 4 outlines the background and potential of using the stable isotopic composition of soil carbonates from loess-palaeosol sequences as palaeoclimatic indicators. Chapter 5 provides a brief explanation of the methods used in this study and an explanation of the OSL dating procedure. Chapter 6 presents a comparison of the sedimentological, morphological and geochemical characteristics of loess sediments from each study site with those of local fluvial and slope system sediments, providing an outline of the origin and nature of the loess sediments at each location. Chapters 7, 8 and 9 provide the sedimentological, micromorphological, geochronological and stable isotope composition results from La Malaha, Chimeneas and Maro (respectively). For each site results obtained from each analysis are presented, a palaeoenvironmental significance is suggested and a pedo-sedimentary model of deposition and alteration is discussed. In Chapter 10 the stable isotopic composition of soil carbonates from Chimeneas and Maro are discussed in terms of the current understanding of the controls on the isotopic composition of Mediterranean soil carbonates. Chapter 11 summarises the results presented in this thesis. Evidence of the timing and nature of loess deposition in southern Spain gained within this study is discussed within the context of regional palaeoenvironmental studies and a geomorphic model of loess deposition is proposed. Chapter 12 discussed the significance of the findings of this thesis in relation to current understanding of late Quaternary dust flux within the western Mediterranean. The main conclusions of this study are presented in Chapter 13.

Chapter 2 - Late Quaternary Mediterranean climate

This chapter aims to introduce Quaternary climate cycles, with a focus on the period from the last interglacial through to the present interglacial. It will introduce the main climate records associated with key localities for each period (figure 2.1), with an ultimate focus on placing Mediterranean climate changes within a global context. This will provide both a climatic and geomorphic context to the sediments studied in this thesis, on both a global and a regional scale.

The Mediterranean is located on the boundary between arid North Africa and temperate Europe, making the Mediterranean sensitive to changes within either region (e.g. Giorgi and Lionello 2008). Additionally, the Mediterranean Sea is fed by North Atlantic waters, allowing for the communication of high-latitude climate signals into the Mediterranean Basin. Such changes in Mediterranean Sea waters impact upon the regional climate, which is further modified by North Atlantic control on the atmospheric systems that affect the Mediterranean region.

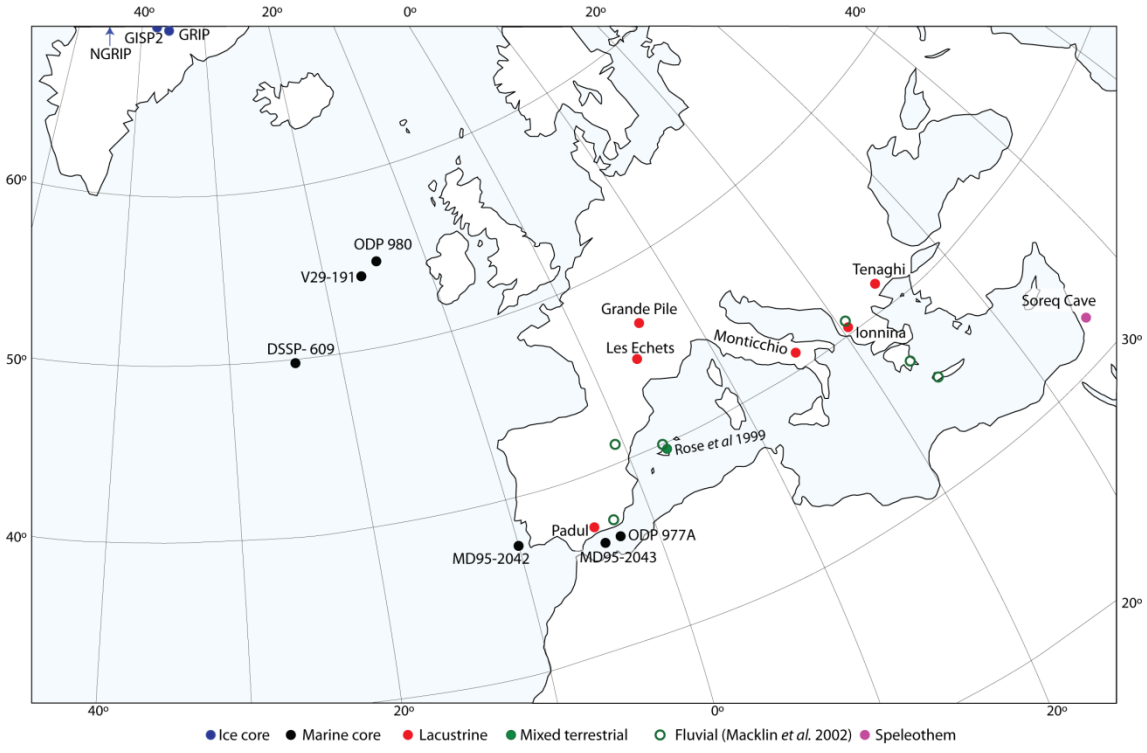

Figure 2.1 Map showing location of key sequences discussed in chapter. N.B. location of Antarctic ice cores are omitted for clarity.

This chapter will discuss the evidence for the impact of Milankovitch and sub-Milankovitch scale climate changes within Mediterranean records (figure 2.1). Such climatic events can be clearly linked with changes in vegetation composition throughout the region, which can be tied in to the landsystem response of the region.

2.1 Quaternary climate characteristics

Milankovitch theory explains the variability of the Earth's rotation around the sun which controls the distribution of solar radiation (insolation). Milankovitch described three components of the Earth's orbit (eccentricity, obliquity and precession); each component works on a different timescale (100 ka, 41 ka and 21 ka respectively) (figure 2.2).The total amount of radiation received by the Earth does not change with orbital parameters; however, the seasonal and hemispheric distribution of radiation is affected. It is thought that the total radiation received within the northern Hemisphere summer is key to driving glacial-interglacial cycles (For a review of current understanding of Milankovitch theory see Berger *et al.* 2007).

Maslin *et al.* (2001) argue that it is the strong feedback processes related to the survial and subsequent growth of Northern Hemisphere glaciers during periods of reduced Northern Hemisphere summer insolation (such as increased albedo and reduced North Atlantic deep water (NADW) formation) that result in orbital parameters being translated into glacial-interglacial cycles. Seidov and Maslin (2001) and Maslin *et al.* (2001) highlight the importance of the oceans, arguing that they are the key to long-term climate cycles, through communication of high-latitude events by oceanic heat transfer processes.

Additionally, feedback processes involving greenhouse gases are thought to be responsible for the amplification of changes in orbital parameters (Petit *et al.* 1999). The Antarctic temperature and atmospheric gas record shows strong correlation (Petit *et al.* 1999), indicating a close relationship between the two systems. It is thought that through the high greenhouse gas levels witnessed during interglacials, and the low greenhouse gas levels seen in glacial periods (Petit *et al.* 1999), that gases are likely to contribute to the amplification of orbitally induced climate changes. Many hypotheses exist surrounding the sources and sinks of atmospheric gases; however, it is thought likely that oceanic processes and terrestrial storage (vegetation) are key (e.g. Köhler *et al.* 2005).

Not all of the Earth's climate cycles appear to correlate with Milankovitch timescales. Evidence from Greenland ice cores and the North Atlantic marine cores were key in the identification of rapid climate cycles (e.g. Bond *et al.* 1992, 1993, Dansgaard *et al.* 1993). Such cycles are termed sub-Milankovitch cycles as they occur on timescales too short to be explained by orbital parameters; they include Dansgaard-Oeschger (D-O) cycles and Heinrich events (HEs) occurring on ~1500 year and 7200 ± 2400 year cycles respectively (Maslin *et al.* 2001 and references therein).

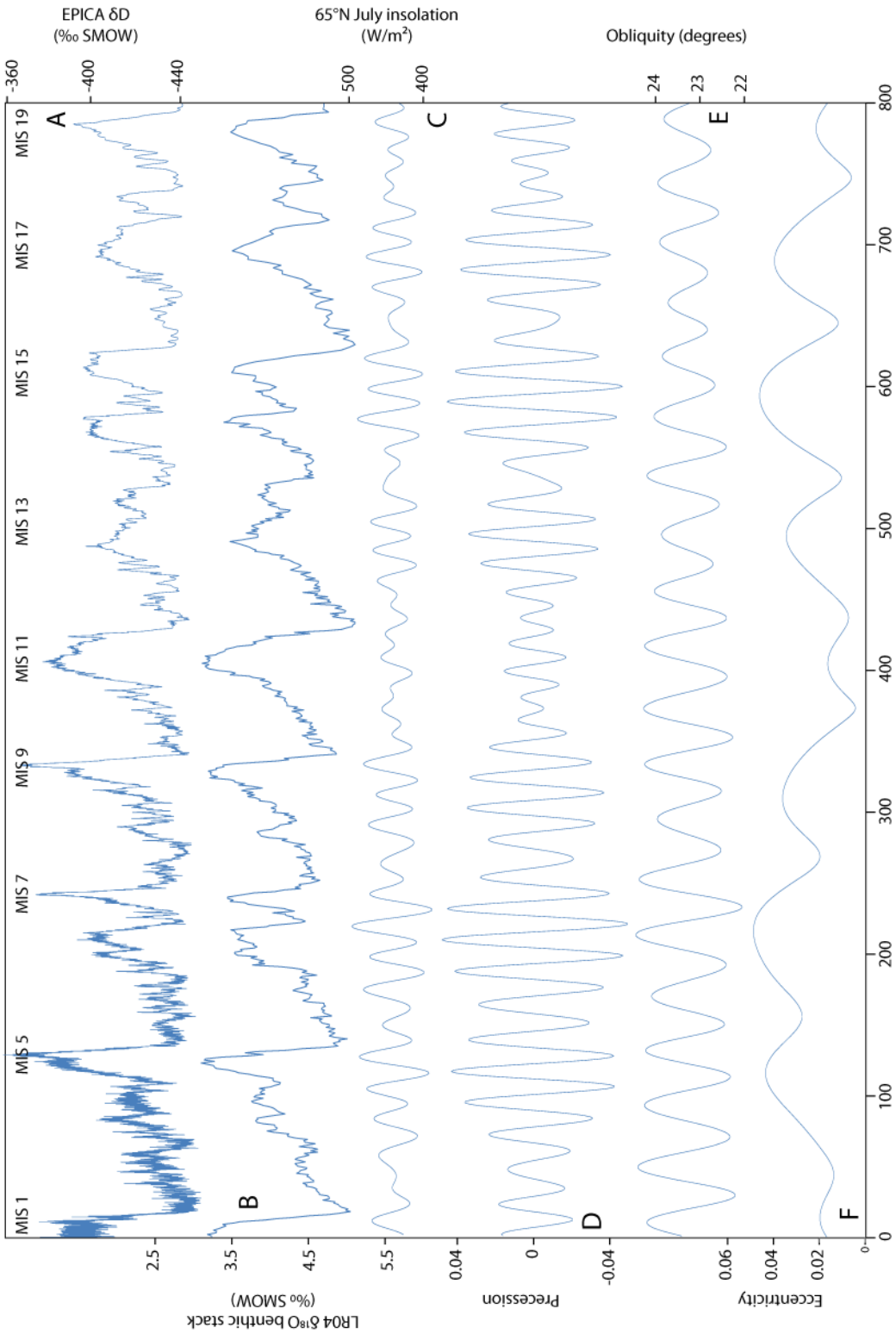

Figure 2.2 Comparison of ice and marine core records with Milankovitch forcing cycles. A. EPICA deuterium record (Jouzel et al. 2007) (insolation tuned, with tie points and flow models), B. LR04 marine benthic stack (Lisiecki and Raymo 2005) (insolation tuned), C-F Insolation and orbital parameters modelled over the last 800ky (Berger and Loutre 1991).

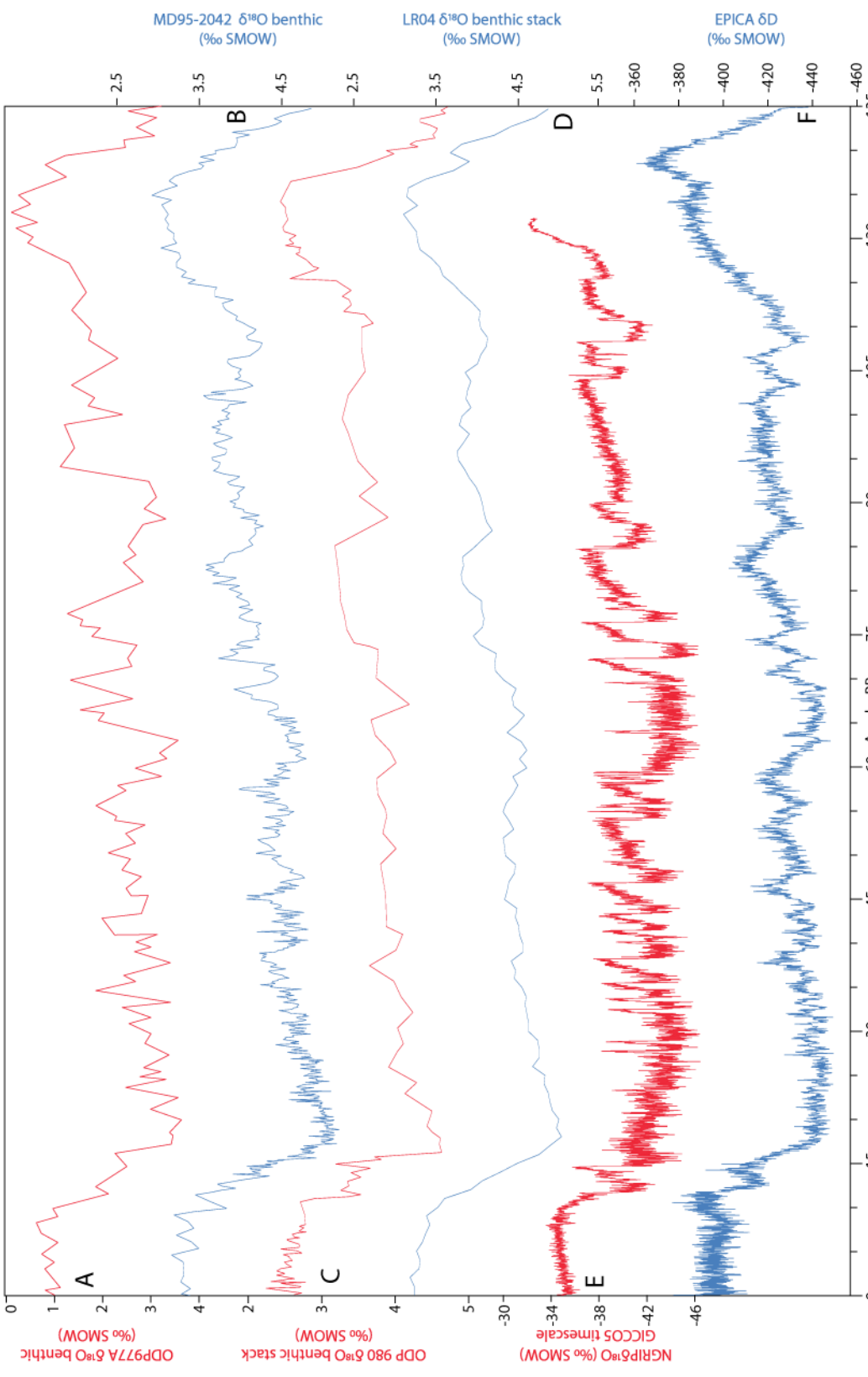

Figure 2.3 Compilation of climate records for MIS5-1. A. ODP977A (14C and GISP2 correlated) Perez-Fogaldo et al (2004), B. MD95-2042 data from Shackleton et al (2000) (GISP2 correlated), C. ODP980 Oppo et al. (2002) , D. LR04 data from Lisiecki and Raymo (2004) (insolation tuned), E. NGRIP Andersen et al. (2006) , F. EPICA data from Jouzel et al 2007 (insolation tuned, with age tie points and flow model).

This work will focus on the last climatic cycle; covering the last interglacial through to the current interglacial and the glacial stage between (see figure 2.3). Although the Eemian (last interglacial) is not thought of as a strong analogue for the Holocene (current stage) due to differences in orbital parameters (Loutre and Berger 2003), sediments of Eemian age are more widely preserved than those of older interglacials and as such provide an opportunity to understand Earth's climate and land-systems during an interglacial period.

The last glacial allows us to understand both the transition into and out of a glacial stage and additionally allows the study of Earth systems under a less stable climate regime. Although the rapid climate transitions that occur during this interval are not an analogue for future climate changes, they do allow an assessment of how land-systems respond to rapid climate changes such as those that might be invoked by human induced modification of climate. Through comparison of global climate records (e.g. ice cores, benthic stacks) with those reflecting regional or local signals (e.g. marine, lacustrine, terrestrial sediments) it is possible to identify the general structure of this climatic cycle; importantly, it also highlights regional and local scale responses.

2.2 Stage 5

Stage 5 contains MIS 5e, which is the last interglacial period prior to the Holocene (MIS 1). As the most recent interglacial in the geological past, terrestrial deposits of this age are, generally, the most widespread and best preserved of any interglacial sediments. Despite significant differences in orbital parameters between MIS 5e and MIS 1 (Loutre and Berger 2003) (figure 2.4), and therefore significant differences in the forcing mechanisms responsible for the duration, climate and stability of the two periods, terrestrial sediments from MIS 5e enable us to assess terrestrial systems operating during an interglacial, prior to human interference. Additionally, many chronological techniques are applicable to sediments of MIS 5e age, and, as such, interpretations of terrestrial systems and their response to climate forcing can be explored within chronological constraints.

2.2.1 Greenland

As shown in figures 2.2 and 2.3, over glacial/interglacial timescales Antarctic and Arctic climate follows the same trends. However, over sub-Milankovitch timescales the two hemispheres are thought to be out of phase (e.g. Blunier and Brook 2001), it is hypothesised that this is due to oceanic heat transfer (e.g. Seidov and Maslin 2001). Therefore, northern hemisphere climate signals are more appropriate when discussing Mediterranean climate systems.

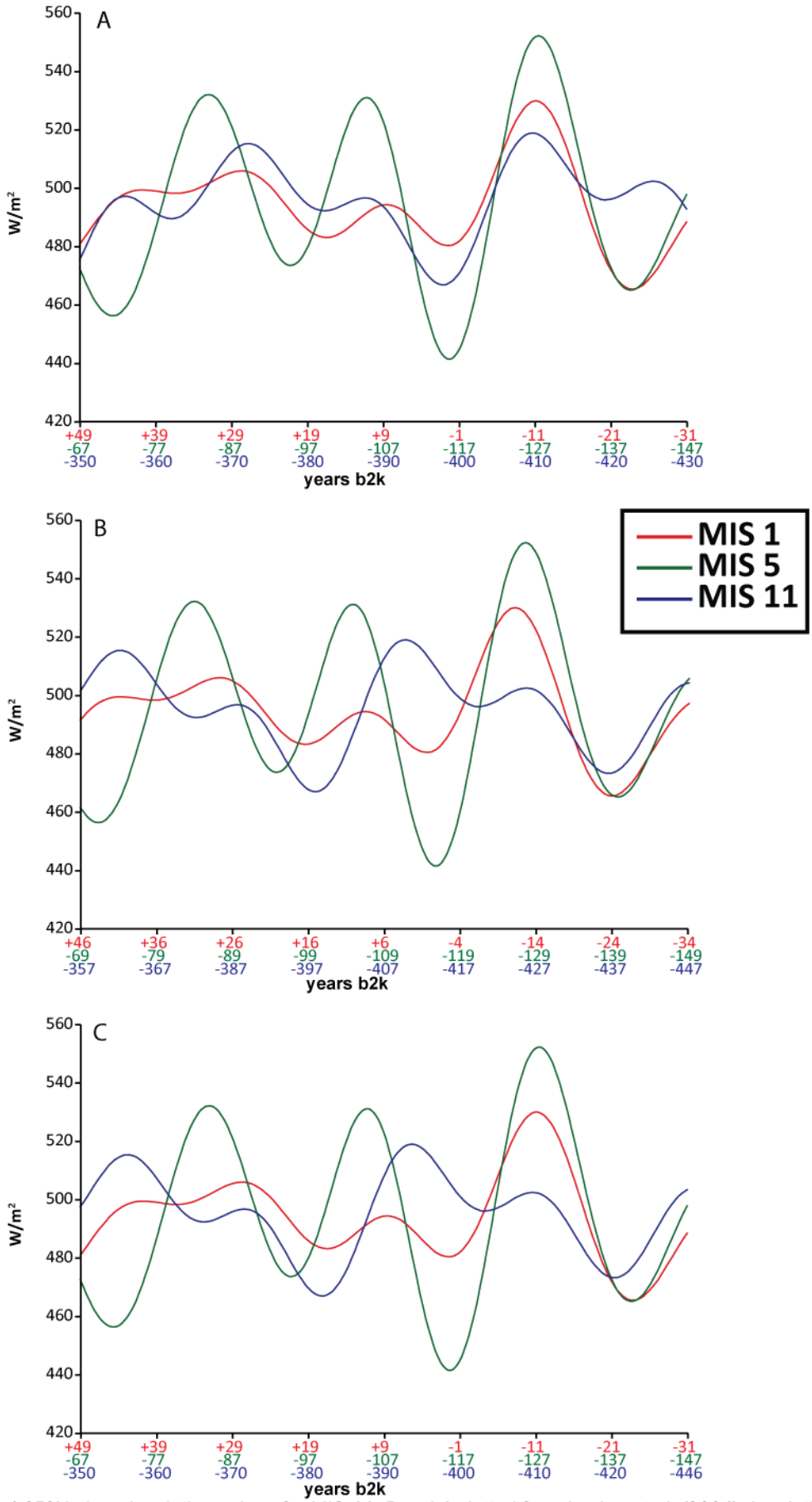

Figure 2.4 65°N, June insolation values for MIS 11, 5 and 1 plotted from Laskar et al. (2004). Insolation parameters can be aligned in a number of ways; A) insolation peaks aligned, B) preceding minima aligned, C) first insolation peak aligned. This plot demonstrates that MIS 5 is not a strong climatic analogue for the Holocene.

Currently, however, there is no reliable, complete record of MIS 5 climate from Greenland (Dye 3, Renland, Camp Century, GISP 2, GRIP and NGRIP) (Grootes *et al.* 1993, Johnsen *et al.* 2001, Suwa *et al.* 2006, Chappellaz *et al.* 1997 and Svensson et al. 2011), due to basal disturbance of the cores and/or basal melting (NGRIP). Svensson *et al.* (2011) report that the NGRIP record can be annually resolved to the base, at ~123 ka, as the dust input appears undisturbed. However, Svensson *et al.* (2011) highlight that other proxies contained within the core have been affected by significant diffusion and post-depositional alteration. The NEEM ice core record potentially will resolve the absence of a complete MIS 5 Greenland record (Buchardt and Dahl-Jensen 2008).

The Greenland $\delta^{18}O$ record (MIS 1-5) can be seen in figure 2.3, which demonstrates that on glacial/interglacial timescales, the climate of both Polar Regions follows a similar structure.

2.2.2 North Atlantic

As demonstrated by figure 2.3 variations in $\delta^{18}O$ within the North Atlantic broadly follow the same pattern exhibited by other regional and global climate records (figure 2.2 shows ODP 980 $\delta^{18}O$ benthic record). However, $\delta^{18}O$ of benthic foraminifera is controlled by global ice volume (see Shackleton 1967) and should, therefore, follow climatic changes seen within both Polar Regions and mid-latitudes. This close association of proxies within the marine cores and ice cores is often used as a means of correlation between records and a tool for extending marine core chronologies where direct dating techniques are no longer applicable.

Marine cores often contain a wealth of proxy records, which, through comparison with $\delta^{18}O$ data, allow marine system (and sometimes terrestrial) response to be assessed relative to the timing and scale of apparent ice volume changes. $\delta^{18}O$ benthic records are used as a chronostratigraphic anchor for the records, $\delta^{13}C$ of benthic foraminifera provides a proxy for changes in circulation strength and shifts in *pachyderma* assemblages are used to indicate changing sea surface temperatures (McManus *et al.* 2002).The compilation of multiple marine records within the North Atlantic gives a comprehensive review of the region's behaviour during stage 5 (McManus *et al* 1994, 2002, Oppo and Lehman 1995 and Oppo *et al.* (2006) (see figures 2.5 and 2.6).

The $\delta^{18}O$ record from these marine cores indicates that the North Atlantic records shifts within global ice volume in agreement with temperature changes seen within Antarctic and Arctic ice cores. With low ice volumes and relative stability through the last interglacial (MIS 5e), increases in ice volume at the times of stadials (MIS 5d, 5b) and a reduction in ice volume during interstadial events MIS 5c and 5a (McManus *et al.* 1994, 2002, Oppo *et al.* 2006).

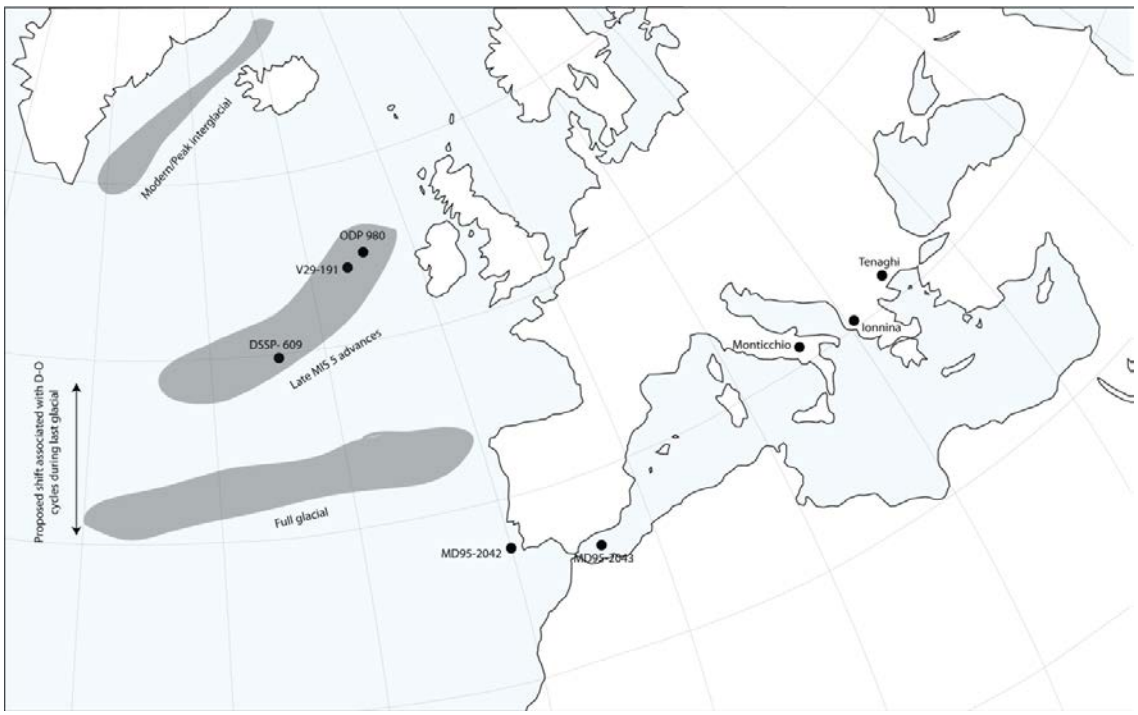

Figure 2.5 Location of marine cores discussed by McManus et al. (1994, 2002), Oppo and Lehman (1995) and Oppo et al. (2006) and including the location of some key Mediterranean sequences. The grey shading represents the position of the polar water boundaries during different climate periods, suggested by McManus et al. (1994) and Oppo and Lehman (1995).

This general climatic pattern is corroborated by the Sea Surface Temperature (SST) estimates for core ODP-980 (Oppo *et al.* 2006) gained from planktonic foraminiferal assemblages using the modern analogue technique. The SST record from ODP 980 indicates a warming of ~10 ˚C associated with the transition from MIS 6 to MIS 5e, minimal temperature fluctuations during the interglacial and then a reduction in SST of ~4 ˚C into the following stadial (5d), followed by fluctuations of 1-2 ˚C during the stadial/interstadial events of stage 5.

North Atlantic cores contain bands of coarse grained clastic material inferred to be ice rafted debris (IRD) resulting from significant iceberg discharge into the ocean. The transition from MIS 6 into MIS 5e was marked by a pronounced IRD event, termed Heinrich Event 11 (H11) (Oppo *et al.* 2006, McManus *et al.* 2004), IRD input is negligible through stage 5, except within the stadials of 5d and 5b (McManus *et al* 1994, Oppo *et al.* 2006). IRD input events are associated with an increase in *N. pachyderma* (a polar foraminifera) which indicates a southward migration of polar waters. These events are referred to as Cold events (C) within the North Atlantic records, the first major cold event within stage 5 is C24 which occurs within 5d (Oppo *et al.* 2006). Oppo *et al.* (2006) highlight the existence of cold events (C25-27) during 5e, however, such events are not associated with marked increases in *N. pachyderma* or IRD and as such appear to be recorded by only minor changes in SST.

Within the North Atlantic records, SSTs remain high after the insolation maxima (~125 ka). McManus *et al.* (2002) argue that the absence of polar foraminifera, relatively high SSTs and absence of IRD post peak interglacial conditions (prior to C24) indicate regional warmth during a period of reduced insolation and ice growth. McManus *et al.* (2002) argue that elevated $\delta^{13}C$ values during this period of prolonged warmth are indicative of a reinvigoration of the Thermohaline Circulation (THC). With enhanced NADW formation due to increased salinity of waters resulting from glacial growth, leading to enhanced THC. Such a reinvigoration would result in enhanced oceanic 'heat piracy' from the southern oceans, resulting in prolonged warmth in the North Atlantic. McManus *et al.* (2002) state that such a response is unlikely to cause prolonged interglacial warmth on a global scale, but regionally, may result in prolonged warmth, beyond that suggested by the timing of the insolation maximum.

Oppo *et al.* (2006) identify that each cooling event was coincident with a low $\delta^{13}C$ (benthic foraminifera) excursion. Oppo *et al.* (2006) suggest that this is consistent with a reduced meridional overturning circulation (MOC) supplying less heat to the region and affecting surface climate. However, within their record, the phasing of IRD/*N. pachyderma* shifts and those of $\delta^{13}C$ do not follow a consistent pattern. At times $\delta^{13}C$ leads (consistent with an MOC invoked surface climate change), but during other cold events $\delta^{13}C$ lags. This shift in phasing may indicate that at times surface climate is driven by changes in MOC and at times MOC is driven by terrestrial processes, e.g. increased iceberg discharge reducing NADW and impacting MOC. However, this work indicates that the North Atlantic cold events are associated with significant shifts in oceanic circulation; such changes impact upon Seas fed by the North Atlantic and, additionally, alters atmospheric circulation impacting weather systems.

Marine core MD95-2042 is located off the south-western coast of Portugal. The core's location offers the opportunity to assess communication of climate events through the North Atlantic region, and, importantly, to an area which influences both the Mediterranean Sea and the western Mediterranean land masses. By analysing terrestrial pollen from the same archive as benthic $\delta^{18}O$ and SST records are constructed it is possible to assess the phase relationship between ocean and land systems without chronological uncertainties, assuming no lag in either proxy (Tzedakis 2003).

Shackleton *et al.* (2000) were able to demonstrate the synchronous nature of oceanic changes witnessed within core MD95-2043 with those seen in higher latitude North Atlantic cores and Greenland ice cores. Shackleton *et al.* (2000) state that the timing, amplitude and structure of climatic events witnessed in MD95-2042 is the same as those seen in high-latitude climate records. This close correlation, in terms of both timing and structure of climatic changes, was

used by Shackleton *et al.* (2000) as evidence to support the rapid communication of high latitude climate signals to the western Mediterranean.

Shackleton *et al.* (2000, 2003) were able to demonstrate that the vegetation response lagged that of the oceans. The proposed timing of MIS 5e based upon the benthic record was 132-115 ka, but interglacial forest conditions were not reached until 126 ka and remained until 110 ka. The timing of terrestrial response is closely linked to peak SST estimates from both MD95-2042 (Shackleton *et al.* 2003) and ODP 977A (Pérez-Folgado *et al.* 2004, Martrat *et al.* 2004). However, forested conditions prevailed after SSTs were declining (Tzedakis 2003). Tzedakis (2003) suggests that the decline in tree populations at 110 ka was linked to the timing of a significant North Atlantic cold event (C24), which marked the onset of significant ice rafting resulting in disruption of the THC and a shift in the Mediterranean precipitation regime.

2.2.3 Mediterranean Sea

The impact of North Atlantic and Greenland climate changes on the Mediterranean region is discussed with reference to specific regional records shown in figure 2.6.

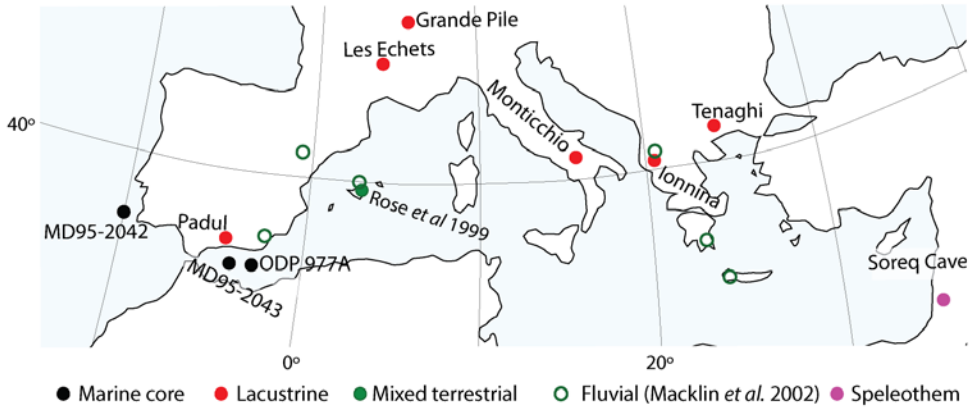

Figure 2.6 Map showing location of Mediterranean sites discussed in chapter.

ODP 977A is located within the Alboran Sea and covers the last 150 ka. The age model for the core is constructed from ^{14}C dating, together with correlation of $\delta^{18}O$ benthic variations with $\delta^{18}O$ variations in Greenland cores and SPECMAP (Pérez-Folgado *et al.* 2004). The timing of events during stage 5 within ODP 977A are; 5e 130-~117 ka, 5d ~117-104 ka, 5c ~104-93 ka, 5b ~93-80 ka, 5a ~80-72 ka. The timing of stage 5 events within the western Mediterranean Sea appears closely related to the timing of events within the North Atlantic and within the Antarctic (Oppo *et al* 2006, McManus *et al.* 2002, Shackleton *et al.* 2000, Jouzel *et al.* 2007) (figure 2.3). However, this may be a product of the tuning used to construct the chronology of the marine cores. As the marine records are insolation tuned, it is impossible to assess leads and lags between the different marine basins. ODP-977A does however show that the Mediterranean Sea experienced

the same number of stage 5 sub-stages as recorded in high-latitude climate records and, additionally, that these sub-stages appear to be of similar amplitude.

Two SST reconstructions exist for ODP 977A: one is constructed from alkenones (Martrat *et al.* 2004) and one constructed using modern analogue temperature relationships of planktonic foraminifera (Pérez-Folgado *et al.* 2004). Alkenone (UK_{37}) SST reconstructions are based upon the relationship between temperature and production rate of alkenones by Coccolithophores (Müller *et al.* 1997). It has become a widely used technique for generating SST estimates from Quaternary marine sediments. Despite uncertainties over species dependence and preservation, it is generally considered to produce reliable SST estimates in most instances (Pelejero and Grimalt 1997). Both estimates show peak 5e SSTs to be ~20˚C, slightly higher than peak Holocene values, however, there is substantial variation between estimates for the SSTs of the sub-stages of 5 (figure 2.7). The alkenone record of Martrat *et al.* (2004) perhaps appears more consistent with the $\delta^{18}O$ record from ODP 977A, but alkenone SST estimates suggest sustained warmth through the interstadials 5c and 5a.

Pérez-Folgado (2004) identified the occurrence of organic rich layers within ODP 977A, they suggest that these are equivalent to sapropel formation which can be seen in the eastern Mediterranean (e.g. Rossignol-Strick *et al.* 1982, Bethoux and Pierre 1999). Organic rich layers are present during 5e, 5c and 5a, they are thought to occur during times of reduced salinity and increased sea surface productivity, and as such organic rich layers indicate warm, wet conditions (Pérez-Folgado 2004, Bardaji *et al.* 2009).

2.2.4 Mediterranean vegetational response

Key Mediterranean vegetation records can be seen in figures 2.7 and 2.8, showing Western Mediterranean records (MD95-2042) through to eastern Mediterranean records (Ioannina, Tenaghi Phillipon). Records are typically discussed in terms of % arboreal pollen, which gives an assessment of the shift in dominance of forest vs. steppic conditions. An alternative is to express this in % Mediterranean taxa, allowing assessment of variation away from typical (modern) vegetation. Within the Mediterranean, it is effective precipitation that is the key climatic control of vegetation communities (Tzedakis 2003). Such shifts in vegetation and inferred effective precipitation allow for inferences regarding landscape stability and sediment availability to be made. As discussed in chapter 1 there is a direct relationship between vegetation cover, soil cover, precipitation regime and landscape stability (Thornes *et al.* 2009). Periods of high vegetation cover, high soil cover and a moderate to high effective moisture regime are associated with low rates of sediment erosion and landscape stability.

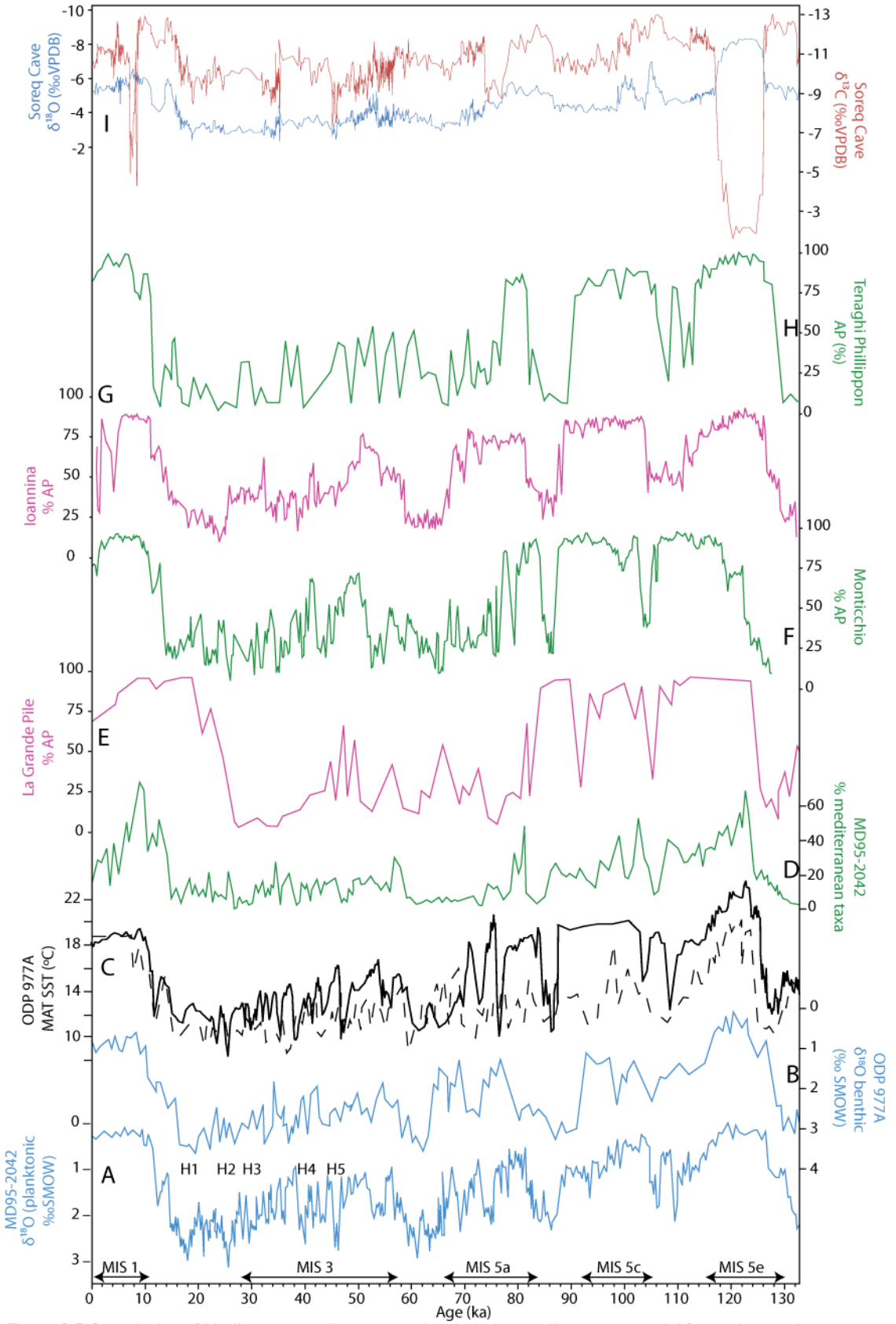

Figure 2.7 Compilation of Mediterranean climate records, plotted according to age model for each record. A. MD95-2042 benthic $\delta^{18}O$ record from Shackleton et al. (2000). B. ODP 977A: benthic $\delta^{18}O$ record from Martrat et al. (2004), C. ODP977A SST estimates: dashed line based on the modern analogue reconstruction of planktonic foraminifera assemblage (Pérez-Folgado et al. 2004), solid line is alkenone derived (Martrat et al. 2004). D. MD95-2042 record of % Mediterranean taxa from Sánchez Goñi et al. (2000, 2008). E. La Grande Pile %arboreal pollen (AP) from Woillard and Mook (1987) plotted to age model shown in Heusser (2000). F. Monticchio %AP from Brauer et al 2007. G-H. onnanina and Tenaghi Phillipon %AP from Tzedakis et al. (2001). I. Soreq cave data from Bar-Matthews et al. 2000.

Tzedakis (2009) outlines typical Mediterranean vegetation succession, following the scheme of van der Hammen *et al.* (1971); where glacial steppe is succeeded by sclerophyllous (e.g. pine) woodland, then a shift to deciduous mixed oak forest. However, Tzedakis (2009) highlights regional variation within this proposed typical sequence, arguing for regional variability due to the heterogenetic nature of Mediterranean landscapes resulting in diverse biomes.

As the chronology of each record is age modelled, and some tuned, it is difficult to assess the existence of leads/lags within records, or to investigate the existence of a west-east gradient associated with stronger North Atlantic influence. Instead, it is perhaps more valid to focus on large scale features within the records. As such the following discussion of Mediterranean vegetational response will focus on the structure of response.

There is a shared structure of vegetation response across the Mediterranean during the climatic evolution of stage 5, where the timing of response is tied to key climate events. The 5e pollen records of the Mediterranean show that peak forest conditions were reached ~126 ka (figures 2.8, 2.9), as discussed previously for MD95-2042. This pattern of expansion is linked closely with peak insolation (Tzedakis 2005) (figure 2.7). It is argued that this relationship between insolation and vegetation dominates the nature of interglacial successions in the Mediterranean, with Mediterranean and sclerophyll, drought resistant, type forests dominating the periods of peak insolation, followed by a transition to more deciduous forests following the insolation maxima (Tzedakis 2003, 2009). Tree populations within the Mediterranean remained high until ~110 ka, where ice growth within the North Atlantic was sufficient to produce major ice rafting events, in this case C24 (figure 2.8). Such events interrupt the THC, resulting in a major shift in atmospheric systems. In this instance, Tzedakis (2003) suggests that C24 was sufficient to invoke atmospheric changes resulting in reduced moisture availability within the Mediterranean, leading to a reduction in tree cover.

Figure 2.8 highlights some differences in the style and timing of changes within vegetation communities across the Mediterranean region. In particular, the timing of arboreal reductions within the record from Grande Pile appears different from the records closer to the Mediterranean Sea. It has been suggested that a North-South gradient of response exists throughout stage 5, affecting vegetation composition and also the timing of vegetation changes (Sánchez Goñi *et al.* 2000, 2005). It could be that as the most northern and least typically Mediterranean location, the timing of changes at Grande Pile are linked to Northern European changes. However, Tzedakis (2003) suggests that lags between Mediterranean and Northern European response are unlikely to be of significant scale, particularly when considering the errors associated with the age models of such records.

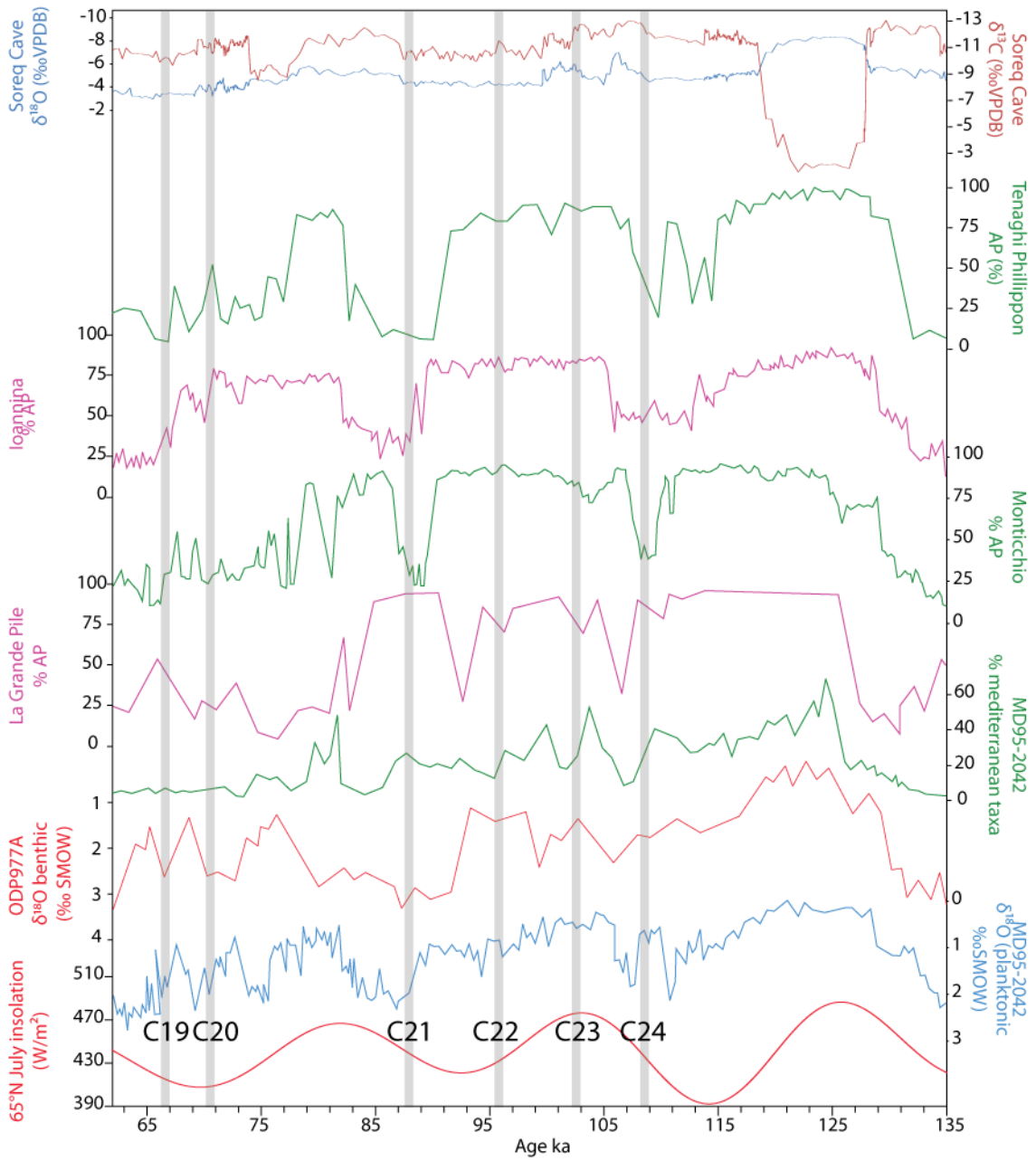

Figure 2.8 Mediterranean records of vegetation and climate response during the evolution of stage 5. A. Insolation curve from Berger and Loutre 1991, B. MD95-2042 benthic $\delta^{18}O$ record from Shackleton et al. (2000). C. ODP 977A benthic $\delta^{18}O$ record from Martrat et al. (2004), D. MD95-2042 record of % Mediterranean taxa from Sánchez Goñi et al. (2000, 2008). E. La Grande Pile %arboreal pollen (AP) from Woillard and Mook (1987) plotted to age model shown in Heusser (2000). F. Monticchio %AP from Brauer et al 2007. G-H. onnanina and Tenaghi Phillipon %AP from Tzedakis et al. (2001). I. Soreq cave data from Bar-Matthews et al. 2000. Cold Events assigned using the chronology of Oppo et al. (2006).

Overall, the vegetation records suggest that vegetation associated with the warm stages of 5 (5e, 5c, 5a) prevailed for longer than warmth recorded by the ocean records. As Mediterranean vegetation is related to moisture availability as opposed to temperature (Tzedakis 2003), it appears that only once large scale changes in atmospheric conditions occurred in response to sustained ice growth, tree populations decline substantially.

2.2.5 Summary

Shackleton *et al.* (2000) were able to demonstrate the near synchronous nature of changes observed within the North Atlantic and Greenland ice core records. Communication of the North Atlantic signal to the Mediterranean Sea has resulted in the Mediterranean structure of climate throughout stage 5 being closely linked to the North Atlantic and Greenland. Despite some criticism of the alignment of such records (e.g. Blaauw *et al.* 2008), analysis of terrestrial pollen within marine records has demonstrated synchroneity between terrestrial and marine changes in Iberia (e.g. Shackleton *et al.* 2000, Sánchez Goñi *et al.* 2008).

Vegetation records from across the Mediterranean basin indicate the dominance of Mediterranean forest conditions prevailing during the last interglacial, and returning to near interglacial levels during interstadials 5c and 5a. The dominance of a North Atlantic/Greenland signal within Mediterranean vegetation records can be seen through tree decline which appear to be related to North Atlantic cold events. The rapid response of vegetation within the Mediterranean to both Milankovitch (interglacial, stadial, interstadial) events during stage 5 and sub-Milankovitch events (North Atlantic cold events) demonstrates the importance of placing Mediterranean Quaternary climate shifts within a North Atlantic framework. Additionally, through changes in vegetation thought to primarily reflect shifts in moisture availability, it demonstrates the importance of high latitude changes in controlling the moisture regime of the Mediterranean.

The last interglacial of the Mediterranean was a period characterised by warm, stable, forested conditions. During the transition to full glacial conditions (MIS 4), the region underwent transition from stadial to interstadial climates, apparently in phase with changes in insolation. Within the vegetational records of the Mediterranean, it appears that there is something of a west-east gradient of response. Where, during interstadials (5c, 5a), vegetation communities in the east recover to close to interglacial maximum values and remain relatively stable, in the west there is some recovery of vegetation but the recovery is a less consistent feature. Differences in the amplitude of vegetation recovery associated with interstadial climates through the Mediterranean could reflect regional differences in the amplitude of climatic changes, or it could relate to local ecological thresholds (Tzedakis *et al.* 2004).

2.3 Last glacial

2.3.1 Greenland and North Atlantic

During the last glaciation there is particularly strong evidence to support the existence of sub-Milankovitch events. Dansgaard-Oeschger cycles (D-O) are the dominant climate signal (Alley *et al.* 1999) throughout the last glacial, occurring as quasi-periodic warming/cooling events. The

term describes the series of interstadials and stadials beginning during the stepwise cooling transition of MIS 5a – MIS 4 (Bond *et al.* 1993).

These events were first identified by Dansgaard *et al.* (1993) within the $\delta^{18}O$ record of the Greenland ice cores. Dansgaard-Oeschger events are characterised by asymmetrical warming and cooling (see figure 2.9); rapid warming into peak interstadial conditions (of 3-5˚C/century) followed by slower cooling which occurs in two steps before peak stadial conditions are achieved (gradual cooling of ~5-10 ˚C over ~600-200 years followed by a rapid decline of ~5-10˚C maintained for a further 300-700 years) (Labeyrie *et al.* 2007). Each successive D-O event fails to reach the peak interstadial warmth achieved by the previous event, resulting in a stepwise cooling. This cooling trend is then punctuated by a dramatic cooling event associated with iceberg discharge, referred to as an HE (Maslin *et al.* 2001).

HEs were first recognised by their namesake in 1988 who identified IRD deposits within North Atlantic cores, occurring roughly every 11 ka during the last glacial. The deposits were interpreted as representing periodic glacial surge events, containing sediments predominantly derived from the Laurentide ice sheet. The North Atlantic marine cores revealed that each HE was preceded by oceanic cooling (Bond *et al.* 1992), indicating that the cause of the events was not solely ice dynamics, but possibly prompted by climatic cooling (Alley *et al.* 1999). It may be that HEs occur in response to D-O stadials, but only when ice has had enough time to build up and lead to instabilities, these instabilities then resulting in iceberg discharge, with further cooling following (Alley *et al* 1999).

Bond *et al.* (1993) correlated North Atlantic deep ocean cores with Greenland ice cores and identified a common pattern of climate change within both records. Bond *et al.* (1993) correlated D-O events within both records and noticed that the events could be grouped into 3 or 4 D-O events terminated by a deep stadial associated with a HE. This millennial scale climate cycle is referred to as a Bond cycle (see figure 2.9).

It is important to remember that the evidence from Greenland and the North Atlantic should be considered as evidence of local/regional phenomena. Studies from the mid 1990s onwards sought to investigate whether the effects of D-O or HEs were present in other areas and to identify any leads/lags that may be present in order to try to help understand the forcing factors involved with these processes.

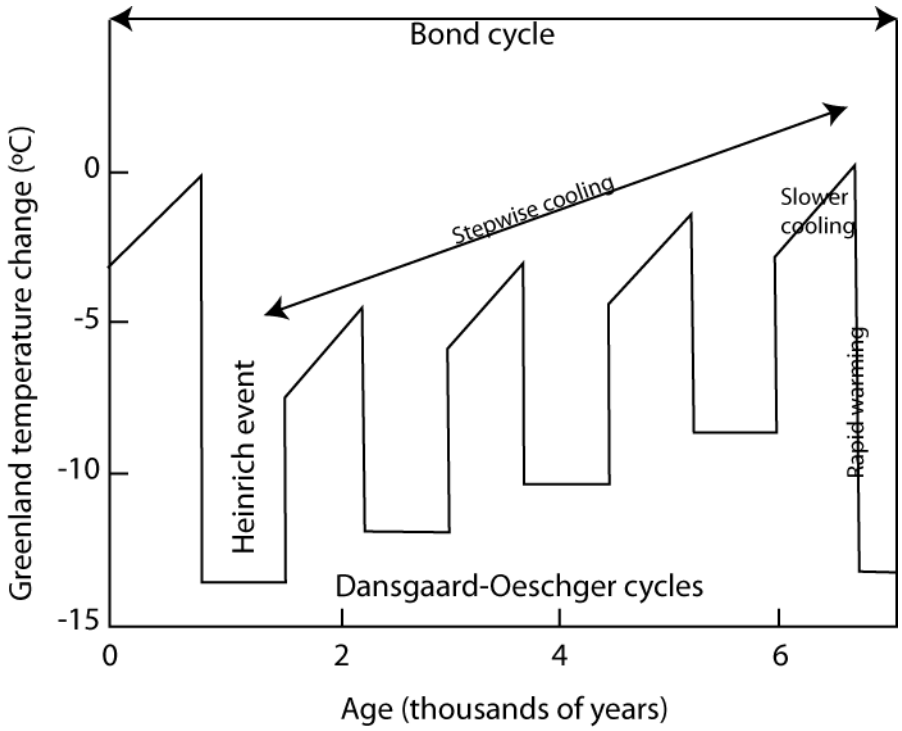

Figure 2.9 Schematic showing the general structure of a Bond cycle. Adapted from Alley et al. 1999.

2.3.2 Mid-latitudes – terrestrial evidence

Evidence of rapid climate events from within the North Atlantic marine records and Greenland ice cores do not demonstrate how climate within other regions may be changing, and more importantly what this might mean in terms of a terrestrial system response to such changes. In fact, the presence of D-O and HE signatures within terrestrial sequences is much less clear.

Speleothems from Europe offer a high resolution record of terrestrial climate; the records can be placed within tight chronological frameworks through Uranium Thorium (U/Th) dating. U/Th dating has minimal errors, meaning that shifts seen within those records can be constrained on sub-Milankovitch timescales through the last glacial. Genty *et al.* (2005) reported a speleothem record located in South-western France (Villars cave) covering 83 to 32 ka. Genty *et al.* (2005) suggest that the carbon isotopic shifts seen within the record are synchronous with those occurring in the $\delta^{18}O$ records of Greenland. Such carbon isotopic shifts within the Speleothem record are, in this instance, thought to reflect changes in the proportional input of atmospheric CO_2.

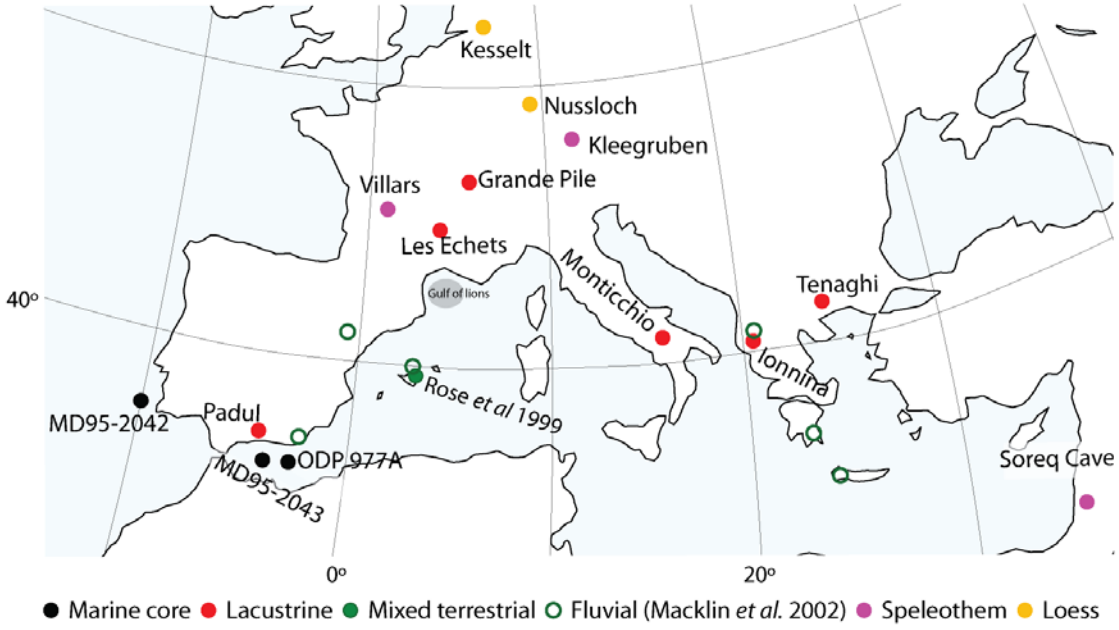

Figure 2.10 Map showing locations of Mediterranean sites discussed

During periods of reduced vegetation cover there is a greater atmospheric component to the $\delta^{13}C$ record of the speleothem, and so $\delta^{13}C$ increases. The record of Genty *et al.* (2005) indicates that vegetation was responding rapidly with the sub-Milankovitch oscillations of the last glacial. Such changes in vegetation structure require rapid changes in moisture and/or temperature, and so the record of Villars Cave reported by Genty *et al.* (2005) demonstrates rapid climatic and ecological response to last glacial sub-Milankovitch events. However, this site is located within 200km of the Atlantic Ocean and so the record could reflect the maritime type climate of the area, with terrestrial fluctuations potentially tied to the oceanographic changes witnessed within North Atlantic marine cores, and may not necessarily be representative of mid-latitude climate shifts.

A further insight into mid-latitude continental climates comes from a speleothem within Austria, removed from maritime climatic influence. Spötl and Mangini (2002) reported the findings of a speleothem covering the period 57 to 46 ka located within Austria (Kleegruben cave). The $\delta^{18}O$ record of the speleothem reflects the $\delta^{18}O$ of precipitation, where the isotopic composition of precipitation is closely related to mean annual temperature (chapter 4). Spötl and Mangini (2002) demonstrate through the $\delta^{18}O$ record of the speleothem that the region is warming and cooling rapidly in response to the sub-Milankovitch oscillations witnessed within Greenland records. This demonstrates that areas away from direct modification by North Atlantic processes are still dominated by climatic oscillations witnessed within the high latitudes; therefore the sub-Milankovitch oscillations of the last glacial appear to be more than just localised occurrences.

Terrestrial response studies are not limited to the analysis of speleothem data. During the last glacial period much of continental Europe that remained ice free was subject to loessic deposition (Moine *et al.*2008). Moine *et al.* (2008) and Vandenberghe *et al.* (1998) present last glacial European loess sequences, which they argue demonstrate terrestrial response to sub-Milankovitch events. Moine *et al*. (2008) undertook a multiproxy study of a loess section within the Rhine valley region of Germany (Nussloch) focussing on molluscan assemblages. The section studied is believed to date from 34 to 20 ka and contains alternating loessic and palaeosol sediments. Moine *et al.* (2008) argue that sediment properties (grain size, pedogenic alteration) and molluscan assemblages appear to vary on D-O type timescales, demonstrating sub-Milankovitch variations within Europe during the last glacial.

Vandenberghe *et al.* (1998) argue that the loess section at Kesselt demonstrates changes in wind strength through the last glacial, with deposition of coarser silts during stadials in response to stronger winds and reduced vegetation. Warmer and more humid climates are indicated by multiple soil horizons which they correlate to interstadial events, indicating increased moisture, vegetation cover and land surface stability.

Both Moine *et al.* (2008) and Vandenberghe *et al.* (1998) have demonstrated variability through European last glacial loess sequences. The occurrence of multiple soil horizons through the last glacial, is perhaps the best evidence of sub-Milankovitch oscillations, and clearly demonstrates rapid landsystem response to a changing climate. However, the dating of both sequences is problematic and in the case of Vandenberghe *et al.* (1998), outdated (chapter 5). Such issues are often 'overcome' by tuning to Greenland records, as carried out by Moine *et al.* (2008). By correlating their record with D-O occurrences in Greenland (dust variations are thought to be synchronous with $\delta^{18}O$ changes in the ice cores) they have assumed synchrony of events and assumed the cause of grain size variations within the loess record to be the same factor controlling Greenland air temperatures. This methodology introduces a certain circularity to their argument. They have correlated their record with the dust record of Greenland which also follows the D-O cycles and therefore presents the same overall trend as the Greenland $\delta^{18}O$ record; they then use this correlation to state that the Nussloch molluscan abundance peaks occur at the same time as peaks within the $\delta^{18}O$ Greenland record.

The methodology employed by Moine *et al.* means that they are unable to make any inferences about synchroneity between the two regions (although it is unlikely they would have been able to if they had relied on a radiometrically dated chronology due to associated uncertainties), and so although the proxies indicate that this site has been subject to frequent climatic shifts during the last glacial, it is not at present clear whether these are synchronous with those experienced within

and around Greenland. However, such studies do illustrate the potential for Northern European loess sections for recording rapid and short lived climatic shifts.

Combining the speleothem records with that of the European loess sequences indicates that the terrestrial environment of Northern Europe is responding to sub-Milankovitch oscillations present through the last glacial. The speleothem records indicate that both vegetation and mean annual temperature are responding in a near synchronous manner to D-O cycles and HEs. The loess sequences indicate that there is an associated geomorphic response across Europe, with episodes of soil formation associated with interstadials, and increased sediment mobilisation during stadials. However, the chronological uncertainties associated with the loess studies means that it is not possible to discuss synchroneity, or whether such changes occur in association with all D-O cycles or only the most pronounced.

2.3.3 Mediterranean Sea

As discussed previously for MIS 5, the Mediterranean Sea receives North Atlantic waters, and often there appears to be a close relationship between Mediterranean climate changes and those occurring within the North Atlantic region. This section will discuss this relationship through the fluctuating climate of the last glacial.

Marine cores located off the coast of Portugal are key for identifying the potential for the high latitude signals of D-O cycles and HEs being transmitted to the mid-latitudes, and into an area with a direct impact upon both the Mediterranean Sea and the terrestrial climate of the Western Mediterranean. Figure 2.11 shows the close relationship between the records of Greenland and MD95-2042, indicating the rapid transmission of events from the high to the mid-latitudes. It is difficult to discuss synchroneity, due to differences in the composition of the age models of the two records.

Shackleton *et al.* 2000 highlight that the benthic $\delta^{18}O$ record is responding rapidly to changes in ice volume in Greenland, with ice sheet growth stadials and ice reduction during interstadials. This close relationship was used to construct the age model for the marine core, by assuming near synchroneity of changes. The occurrence of HEs within the core is marked by the input of IRD and arrival of *N. pachyderma*, such events are marked also by decreases in SSTs and additionally with reduced deep water ventilation ($\delta^{13}C$ benthic); such a response was discussed previously for the high latitude North Atlantic.

This pattern of response was highlighted by Abreu *et al.* (2003) from a marine core (MD95-2040) located slightly north of MD95-2042. In addition to the response to HEs both marine records also

record millennial scale variability in association with D-O events; however, such response is on a muted scale compared to the stadials associated with HEs. The mid-latitude North Atlantic appears to warm and cool in response to each D-O event, following the pattern and style of warming and cooling witnessed within the Greenland cores. The response of the Mediterranean Sea to last glacial climate events is often discussed alongside apparent impacts upon local vegetation; this will be discussed in section 2.3.4.

The Alboran Sea, located at the western edge of the Mediterranean basin, receives inflow in the form of North Atlantic surface waters (Fletcher and Sánchez Goñi 2008). As noted, the temperature of the surface waters of the North Atlantic has been shown to vary in accordance to D-O and HE timescales. As such, the characteristics of North Atlantic waters feeding in to the Alboran Sea would also vary, therefore an Alboran Sea change should be expected. Change in the Alboran Sea could therefore be simply down to changing North Atlantic inflow conditions, or, additionally, through climatic forcing directly affecting the region.

Changes in SST, inferred from shifts in alkenone chemistry, of the Alboran Sea during HEs appear to be similar to those reported for the North Atlantic (Cacho *et al.* 1999). However the response to D-O stadials not associated with HEs appears muted, with shifts of only 1-3°C recorded.

It is not just the surface water temperature that is changing within the Alboran Sea, Cacho *et al.* (2000, 2006) inferred changes of deep water formation ($\delta^{13}C$ benthic), temperature and circulation associated with the sub-Milankovitch cycles evident within the last glacial. Records suggest that Mediterranean THC was increased during stadials and relatively reduced during interstadials, opposite to the situation presented within the North Atlantic. Cacho *et al.* (2006) have suggested that the mechanisms responsible for increased Mediterranean THC during stadials are increased regional evaporation (aridity) and increased westerly wind strength over the Gulf of Lions (figure 2.10).

The mechanisms suggested by Cacho *et al.* (2006) have previously been identified as responsible for increases in THC witnessed within the Mediterranean Sea over the last century. It is suggested that over the last century it is possible to demonstrate a correlation between westerly wind strength and deep water formation within the Gulf of Lions, ultimately driving Mediterranean THC (e.g. Millot 1990, Cacho *et al.* 2000). However, the Mediterranean Sea and climatic conditions during stadials are significantly different from present day conditions. The mechanism of increased deep water formation suggested by Cacho *et al.* (2006) appears to contradict the theory of Moreno *et al.* (2002), which states that there is a reduction in westerly

winds during stadial episodes (figure 2.12). It is possible that the modern relationship between westerly wind strength and deep water formation may not have existed during a period where Mediterranean Sea conditions were significantly different to the present day, such as the last glacial.

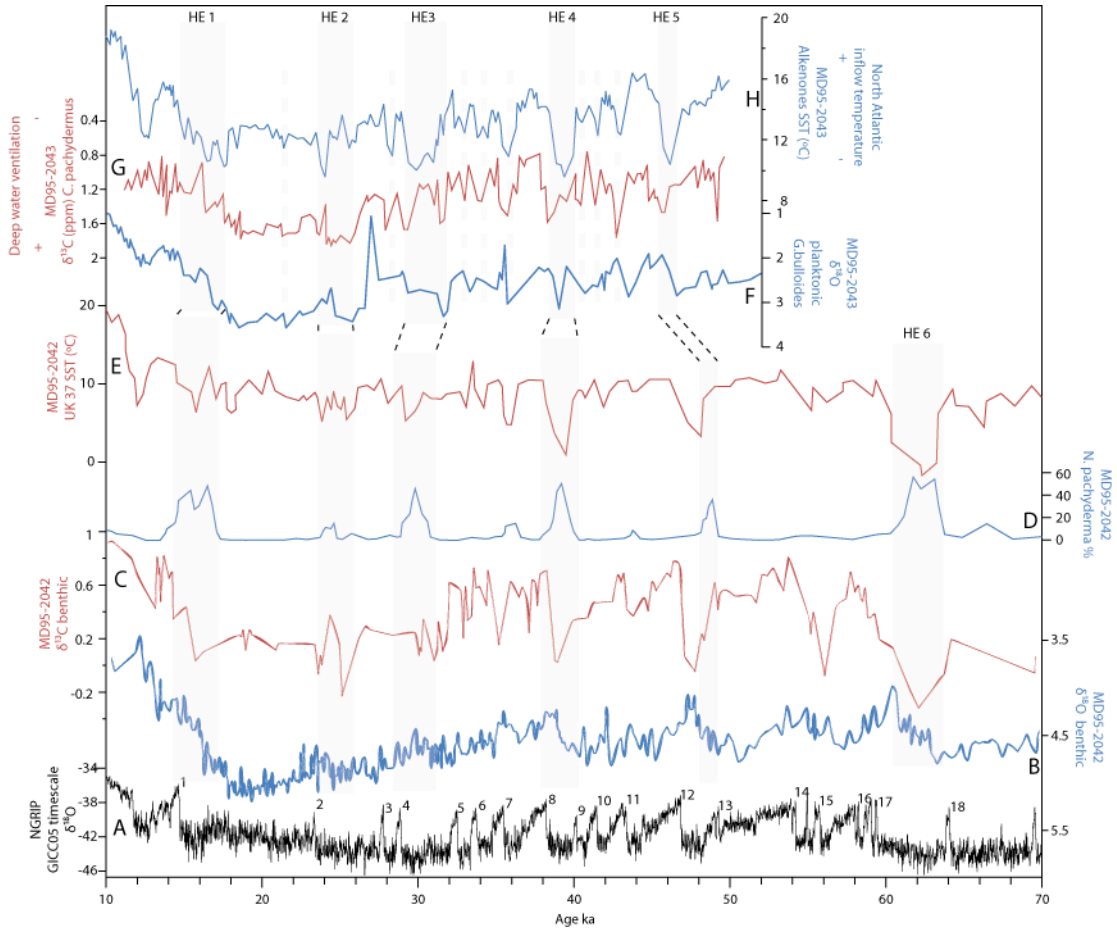

Figure 2.11 Comparison of Greenland, North Atlantic and Mediterranean Sea records through the last glacial. Each record is plotted according to their own timescale. This highlights problems with discussions of synchroneity and leads/lags. However, it is possible to identify sensitivity within Mediterranean records to events witnessed within Greenland and the North Atlantic. A. NGRIP oxygen isotope record (Andersen et al. 2007, Wolff et al. 2010), B-E MD95-2042 (B,C) isotope record from Martrat et al. (2004), (D, E) N. pachyderma and SST from Sánchez Goñi et al. (2008). F-H MD95-2043 data from Cacho et al. (2006).

The deep water temperature (DWT) record of the western Mediterranean also indicates that the cooling maxima in this region were not synchronous with those of the North Atlantic. These observed differences imply that the two regions were at times decoupled exhibiting different responses (amplitudes) to the sub-Milankovitch cycles; however, no mechanism has so far been suggested.

Frigola *et al.* (2008) presented work based on a marine core from within the Balearic Sea and report a similar pattern of variability as reported by Cacho *et al.* (2000, 2006). Frigola *et al.* (2008) state that during stadials associated with HEs Western Mediterranean Deep Water (WMDW) formation is reduced relative to that during D-O stadials. They argue that this is due to freshening

of surface waters caused by the inflow of North Atlantic waters associated with HE iceberg discharges.

As the Mediterranean has increased THC during stadials, it follows that the Mediterranean outflow water (MOW) would have increased salinity during these times, and as such would be a source of salinity for the North Atlantic and a possible trigger for increasing/reinstating North Atlantic overturning (see Cacho *et al.* 2006 and references therein).

It is important to note however, that the age model constructed for the Cacho *et al.* (1999, 2000, 2006) core (MD952043) is not purely based upon radiometric dating. The core has two age models assigned to it, one constructed using ^{14}C dates along with ^{18}O correlation with North Atlantic records and the other consists of correlating Alboran SSTs with the ^{18}O GISP2 record from Greenland. The two age models appear to be in good agreement with each other, however they assume continuous rates of sedimentation between dated/correlated points and also assume synchrony of events thus removing the potential to recognise any important leads/lags.

It has been suggested by Moreno *et al.* (2002) that the same core provides evidence for increased aeolian transport (through analysis of % silt) during times of D-O stadials, which correlates well with the Greenland dust record. Moreno *et al.* suggest that this is indicative of high latitude northwesterlies and low latitude Saharan winds displaying a similar variation during the last glacial. They suggest that this pattern of wind variability is linked to atmospheric pressure gradients. During cold stadials North Atlantic SSTs are reduced, driven by THC overturn slowdown and decreased northward marine heat transport, which Moreno *et al.* (2002, 2004, 2005) argue would result in displacement of northwesterly winds. Displacement of northwesterlies in combination with reduced Mediterranean SST would result in increased aridity for the region and increased Saharan dust transport (see figure 2.12).

Regardless of the mechanism(s) of forcing, it appears that the Mediterranean Sea is responding to the same climatic events that are witnessed within the Greenland and North Atlantic records. Despite major uncertainties existing around the communication mechanism of these events, and therefore uncertainty as to whether or not these mechanisms would impact upon terrestrial climates independently, the fact that there are significant changes within the Mediterranean sea should impact upon terrestrial climates within the surrounding land masses.

It has been illustrated that the increased aridity of the Western Mediterranean as indicated by marine proxies correlated to stadial events during the last glacial can also be identified within terrestrial pollen records (Sánchez Goñi *et al.* 2000, Fletcher and Sánchez Goñi 2008). However, as these studies are based upon sediment from the same marine core as discussed above for

Cacho *et al.* (1999, 2000, 2006) and Moreno *et al.* (2002, 2004, 2005) this work will be considered further when discussing terrestrial response to climate events.

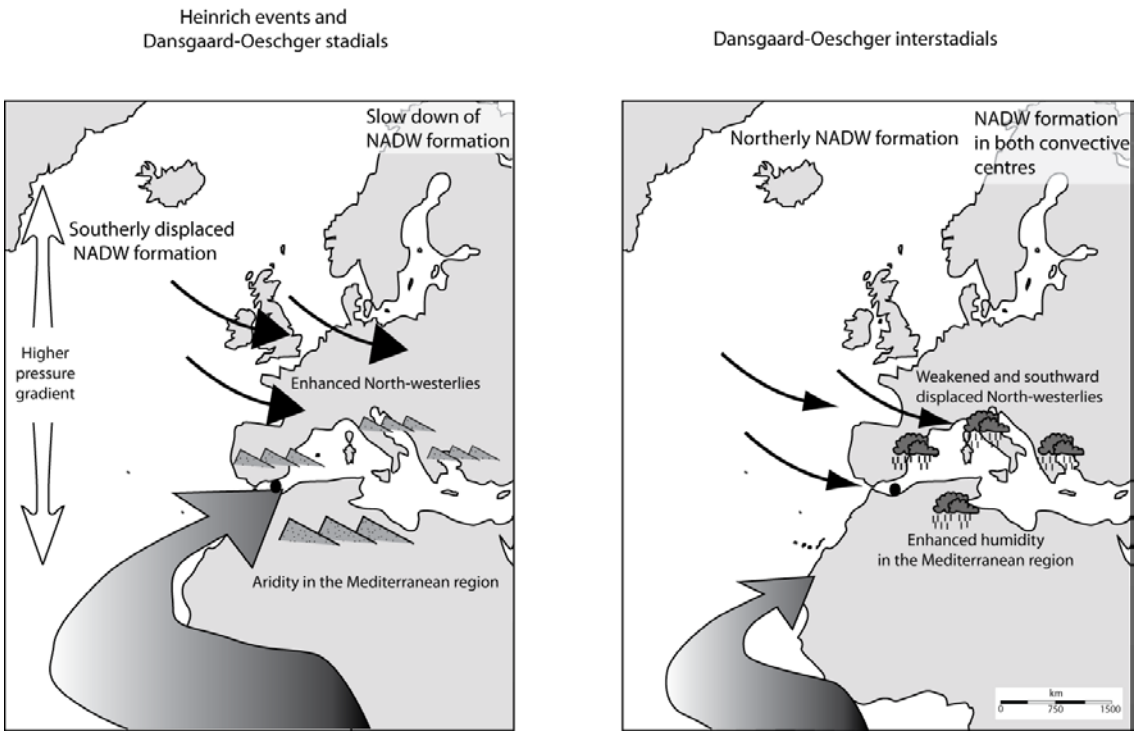

Figure 2.12 Showing the different processes affecting the Mediterranean region during the different phases associated with the last glacial period. Black dot shows location of marine core MD95-2043. Schematic adapted from Moreno et al. (2005).

2.3.4 Mediterranean Vegetation response

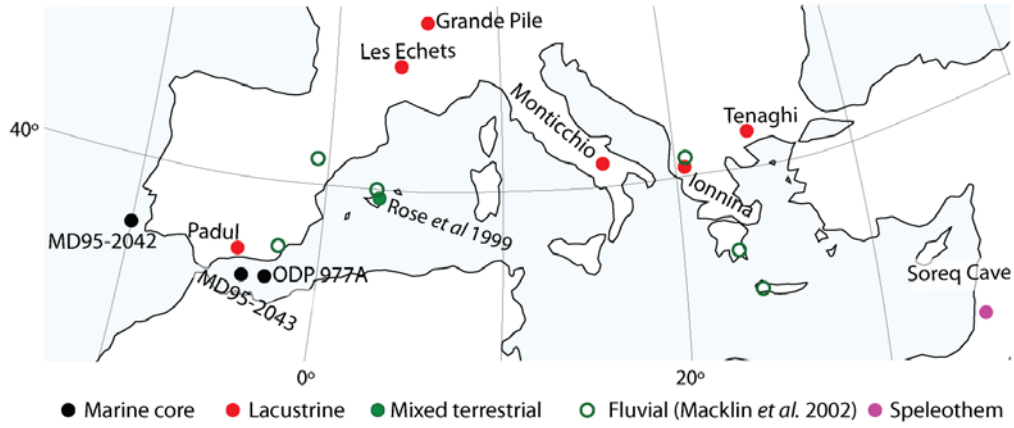

Figure 2.13 Map showing location of Mediterranean sites discussed

The long terrestrial sequences used for palynological reconstructions of Mediterranean response to climate events through the last glacial are located within the central and eastern Mediterranean. Lago Grande di Monticchio (Italy, figure 2.13) is a varved lacustrine sequence containing a number of tephra horizons; as such the chronology of the site is well constrained making it a key record of rapid climate changes in the eastern Mediterranean. This enables the

rapid, sub-Milankovitch events of the last glacial and the timings of such events to be constrained with minimal age uncertainties. Allen *et al.* (1999) argue that the expression of North Atlantic type events during the last glacial within the Mediterranean marine cores is recorded within the vegetational successions of Monticchio. Allen *et al.* (1999) state that rapid vegetation changes which occurred near synchronously with those of the North Atlantic support a close coupling of the regions during this period. The pollen assemblage at Monticchio was converted to represent biomes, and this sequence of biome shifts has been used to demonstrate the close coupling of the record with those of the high latitudes. Within the Monticchio sequence, there are shifts towards steppic biomes during stadials and wooded biomes during interstadials, with evidence for the amplitude of vegetation response being similar to those discussed for the Alboran Sea records.

Tzedakis *et al.* (2004) and Tzedakis (2009) highlight that within the Mediterranean vegetation records it can be difficult to assess the amplitude of climatic changes due to the diverse ecology of the region with the Mediterranean consisting of a mosaic of niches. Therefore, Tzedakis *et al.* (2004) argue that it is likely that variations in regional vegetation response reflect the ecological position of the site. This means that a site located on the edge of the ecological niche will be 'pushed' into a large change in vegetation structure by relatively minor climatic changes; therefore the amplitude of climate change may not necessarily be reflected in the amplitude of vegetational change. Tzedakis *et al.* (2004) argue that this is the case for the discrepancy in amplitude changes seen at Tenaghi and Ioannina (Greece, figure 2.13), where vegetational response is not always a reflection of the strength (amplitude) of the climatic fluctuation. Tzedakis *et al.* (2004) state that at Ioannina it is possible to pick out an amplitude-driven response to D-O stadials vs. HEs, but at Tenaghi the vegetation response appears to be of the same magnitude during both HE and D-O stadial events.

Tenaghi Phillipon shows drastic tree population reductions in association with both HE and D-O stadial events, which, if interpreted in isolation, would suggest that both events were regionally expressed by the same level of reduction in moisture availability. However, when compared with other regional records, such as Ioannina (Tzedakis *et al.* 2004, Tzedakis 2009), where HE and D-O stadials are represented by different levels of tree population contraction, it becomes clear that the amplitude of response seen in records is related to the ecological position of the vegetation community, rather than driven simply by the climatic conditions.

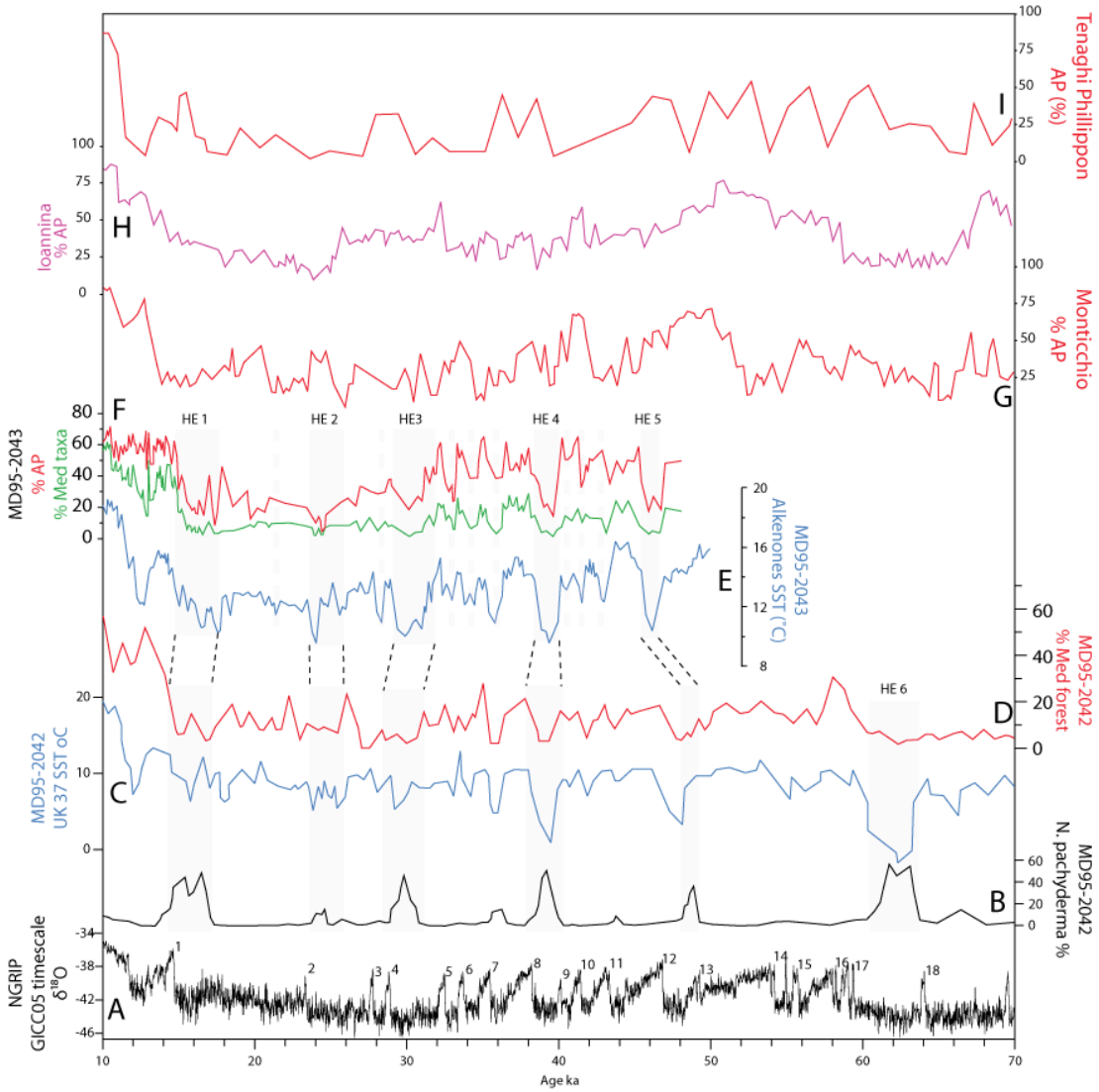

Figure 2.14 Comparison of NGRIP , N.Atlantic and Alboran sea proxies and Mediterranean pollen records. A. NGRIP oxygen isotope data (Andersen et al 2008, Wolff et al 2010), B-D MD95-2042 (C) SST record (Martrat et al. 2004), (B) N. pachyderma and (C) %Med forest from Sánchez Goñi et al. (2008), E. MD95-2043 SSR data from Cacho et al. (2006), F. MD95-2043 pollen records from Fletcher and Sánchez Goñi (2008), G. Monticchio pollen record (Brauer et al 2007), H-I Ioannina and Tenaghi pollen records from Tzedakis et al. (2001)

The events witnessed within the eastern Mediterranean appear to correlate well with the event stratigraphy of the last glacial witnessed within Mediterranean and North Atlantic marine cores (figure 2.14). It might, therefore, be reasonable to assume that rapid and large scale changes occurring within the western Mediterranean Sea would impact upon the vegetation of the surrounding region. Unfortunately, however, there is a lack of long, continuous terrestrial records of the last glacial within the western Mediterranean. The use of terrestrial pollen records from within marine cores is employed within the western Mediterranean to attempt to understand the regional response to last glacial events. Such a strategy prevents chronological uncertainties from masking leads/lags, enabling direct comparison of vegetational response relative to the timing of marine changes (figure 2.14).

Pollen from marine records from the Portuguese coast and within the Alboran Sea have been used to highlight the rapidity of vegetational response to D-O events (Roucoux *et al.* 2001, Sánchez Goñi *et al.* 2000, 2001, 2008, Combourieu Nebout *et al.* 2002). Such records show repeated expansion and contraction of Iberian tree populations on sub-Milankovitch timescales, with a close correlation between arboreal pollen and the timing of D-O events. The records are characterised by steppic vegetation during stadial events and arboreal pollen dominating interstadial events (Sánchez Goñi *et al.* 2000). Sánchez Goñi *et al.* (2000, 2009) state that within the Portuguese margin records, the scale of changes seen in pollen shifts do not correspond to the scale of change witnessed within the oceanic proxies (e.g. SSTs reconstructions). However, within Alboran records there is an apparently proportional response of vegetation to the magnitude of events; with HE stadials showing the most pronounced arboreal contractions and non HE D-O stadials showing a relatively muted contraction (Fletcher and Sánchez Goñi 2008).

Whilst this pattern of response is easily recognised through terrestrial proxies within marine cores and the long records of the eastern Mediterranean, it can be difficult to distinguish the same pattern of events within the terrestrial records of Iberia (González-Sampériz *et al*. 2010). It has, however, been suggested that there is evidence of Heinrich impacts within northern Iberian lake records (Moreno *et al*. 2012); through evidence of increased aridity and low lake levels during HEs. There remains a lack of viable sources of information from terrestrial records of southern Iberia. The one known long terrestrial sequence located within southern Spain, Padul, has been studied on a number of occasions (Florschütz *et al.* 1971, Pons and Reille 1988, Ortiz *et al.* 2004). Fletcher and Sánchez Goñi (2008) highlight similarities between the pollen assemblage of Padul and MD95-2043 during the last 28 ka with Padul recording shifts towards steppic conditions during HEs. Padul, however, is a difficult record to interpret as (1) the chronology is based primarily upon ^{14}C dates from the 1980s (Pons and Reille, 1988), (2) the resolution of the sequence at Padul is particularly poor (~30 ky/8 m) and (3) there are a number of possible hiatuses in the sequence. Recently, Ortiz *et al.* (2004) have re-cored Padul and have constructed an n-alkane record from the Holocene through to 1 Ma dated using U/Th ages from peat. However, fluctuations recorded within the N-alkane record appear minimal, and do not appear to correspond well with the scale of fluctuations recorded within the pollen zones reported by Florschütz *et al.*(1971) and Pons and Reille (1988). The relatively weak chronological controls on the records derived from the site limit the usefulness in recognising ecological response to climate forcing in this region. Despite the palynological difficulties introduced from working within a topographically diverse, and therefore ecologically diverse region, such as the landscape around Granada, the formation of a reliable age model for this site would prove invaluable due to the lack of other long terrestrial sequences within the western Mediterranean.

Due to the lack of long terrestrial records within southern Iberia, work has tended to focus on fragmentary records. The work of Carrión *et al.* (1999, 2001) and Finlayson *et al.* (2008) within the region has tended to focus on pollen records within cave sites, which are recognised as less than ideal due to problems associated with pollen preservation, transportation and reworking as well as with site stratigraphy (Carrión *et al.*1999). Finlayson *et al.*(2008) present evidence based upon bioclimatic reconstructions from bird species assemblage data and pollen collected at Gorham's cave, Gibraltar, which indicates relatively mild conditions present in the region during the last glacial including the LGM. Finlayson *et al.* (2008) conclude that during stadials in the Gorham's cave record, vegetation shifts from Thermo to Meso-Mediterranean occur, indicating a slight reduction in annual temperatures. This, Finlayson *et al.* (2008) argue, indicates that the work of Sánchez Goñi and others suggesting increasing aridity associated with stadials, is perhaps oversimplified. Finlayson *et al.* (2008) argue that aridification within pollen sequences probably represents both aridity in the region and increased North African winds, but also argue that the topographic variations of the region are too great to characterise the response of the region to stadial/interstadial transitions as one of aridity/humidity.

The work of Carrión *et al.* (1999, 2001) has focussed not just on cave records but also upon palynological records within coprolites. Carrión *et al.*(2001) argue that these fragmentary records support the idea of Southern Spain being a mosaic of environments during the last glacial, with evidence for aridification during stadials (increased steppe vegetation) and humidification during interstadials (increased tree pollen). However, Carrión and Finlayson are strongly opposed to the view of d'Errico and Sánchez Goñi (2003) that, during times of stadials, trees were absent (or very close to absent) from the region. Carrión *et al.* (1999, 2001) and Finlayson *et al.* (2008) argue for the persistence of trees in the region throughout the last glacial, with populations exhibiting slight expansion and contraction with climate, not disappearing.

The focus on cave sites and coprolites is a result of the lack of long and suitable terrestrial records; however, the environments are far from ideal for the preservation, collection and interpretation of pollen records. The dating (or archaeological affiliation used to date the site) and stratigraphy of the sites studied by Carrión *et al.* (1999, 2001) and Finlayson *et al.* (2008) are often far from simple.

2.3.5 Summary

Through the last glacial period the northern high-latitudes were subject to rapid, climatic oscillations referred to as Dansgaard-Oeschger cycles, punctuated by extreme cold events known as HEs. These sub-Milankovitch cycles are clear within Greenland ice core records and

through North Atlantic marine records. In addition, there is a growing body of evidence supporting their communication to terrestrial systems, including those of the Mediterranean.

Due to the link between the Mediterranean Sea and the North Atlantic, there is a clear relationship between the two systems, with the Mediterranean exhibiting similar phasing of temperature oscillations through the last glacial. The marine record of the Mediterranean has been used to infer terrestrial conditions of the surrounding land masses. Within the Mediterranean Sea there is evidence supporting aridity through the stadial events (increased THC, increased dust supply) and relative humidity through interstadials. Such cooling and aridity of the Mediterranean in response to stadials is thought to be related to the position of westerlies during these periods, where changes in North Atlantic circulation and pressure gradients result in the displacement of the main westerly system over Northern Europe. Such displacement is thought to be similar to a positive NAO type system, which in studies of modern meteorological systems results in a reduction of precipitation over the Mediterranean, with a particular impact on winter rainfall. Such a decline in rainfall during the peak growing season of Mediterranean vegetation is likely to be the mechanism primarily responsible for driving rapid regional vegetational responses to last glacial D-O events. Additionally, an enhanced pressure gradient over the North Atlantic during stadials is thought to enable intensification of Saharan winds, resulting in increased dust transportation to the region during such events (Moreno *et al.* 2005). A link between positive NAO states and modern dust exportation from North Africa has been established (Moulin *et al.* 1997). Therefore, if a sustained NAO shift occurs during glacial periods, it follows that mobilisation of North African dust would be enhanced.

Vegetation records demonstrate the argued near synchronous response of the terrestrial system to the rapid changes witnessed within the Mediterranean Sea records. Regionally, there are forest declines associated with stadials, in particular HEs, again supporting regional aridity through last glacial cold events. The strength of the vegetational record has added weight to the dismissal of the idea of Mediterranean pluvial periods during the last glacial (section 2.4). Throughout the last glacial, reduced forest conditions relative to interglacial levels persisted, with sharp transitions to steppic dominated conditions during stadial events. Such transitions would invoke drastic changes within the landscape, in terms of stability, sediment supply and alter dominant processes.

2.4 Mediterranean geomorphic response during the last climate cycle (MIS 5-2)

2.4.1 Background

Within the Mediterranean river system geomorphology often represents one of the best available terrestrial records by which terrestrial response to climate changes can be unpicked. As highlighted by Macklin and Woodward (2009), the climatic changes observed during the last 130 ka had a major impact on river behaviour; with direct changes in climatic conditions (e.g. weather systems) altering river hydrology and catchments (vegetation and surface sediment changes), affecting sediment supply and flow regime.

As previously discussed, the vegetation shifts seen within the Mediterranean region to changes in climate over the past 130 ka predominantly involve shifts between forested and steppic conditions (excluding the Holocene, section 2.5) (e.g. Tzedakis 2009). Such dramatic changes in vegetation cover, occurring even in response to the rapid sub-Milankovitch oscillations of the last glacial (e.g. Allen *et al.* 1999, Sánchez Goñi *et al.* 2008, Tzedakis 2009), result in a large change in sediment availability (e.g. Thornes *et al.* 2009); where reduced soil formation and increased bare ground during steppic periods results in increased potential for sediment removal and transport. As such the response of Mediterranean river systems to a climatic shift is often considered in terms of the timing of alluviation events, linked to periods of reduced vegetation cover and increased sediment supply (Fuller *et al.* 1998); therefore, the timing of alluviation or incision events (if tectonics can be excluded or accounted for) allow catchment response to climate change to be inferred (e.g. Macklin *et al.* 2002).

The classical theory proposed by Vita-Finzi (1969) identified an ‘Older’ and a ‘Younger’ alluvial fill within the Mediterranean valley systems (figure 2.15). Vita-Finzi (1969) proposed a last glacial age for the ‘Older’ fill sediments based primarily upon archaeological associations, and despite differences in the composition of the ‘younger’ fills he assigned their occurrence to a cold climate event within the Holocene. However, the lack of human influence ascribed to the formation of younger fill sediments by Vita-Finzi was criticised widely (see Macklin and Woodward 2009). In addition many authors simplified the discussion of Vita Finzi (1969). Macklin and Woodward (2009) state that Vita Finzi (1969) acknowledges the presence of multiple alluvial terraces associated with both the younger and older fill sediments; however, high-resolution studies, particularly those able to produce strong chronological controls, were not possible at the time. It is this lack of chronological constraint that limited geomorphological understanding of alluviation events. As dating techniques have developed, so our ability to constrain alluviation events has

improved and enabled a more detailed understanding of their timing and environmental significance (e.g. Bailey *et al.* 1990, Rose *et al.* 1999, Macklin *et al.* 2002, Candy *et al.* 2004a).

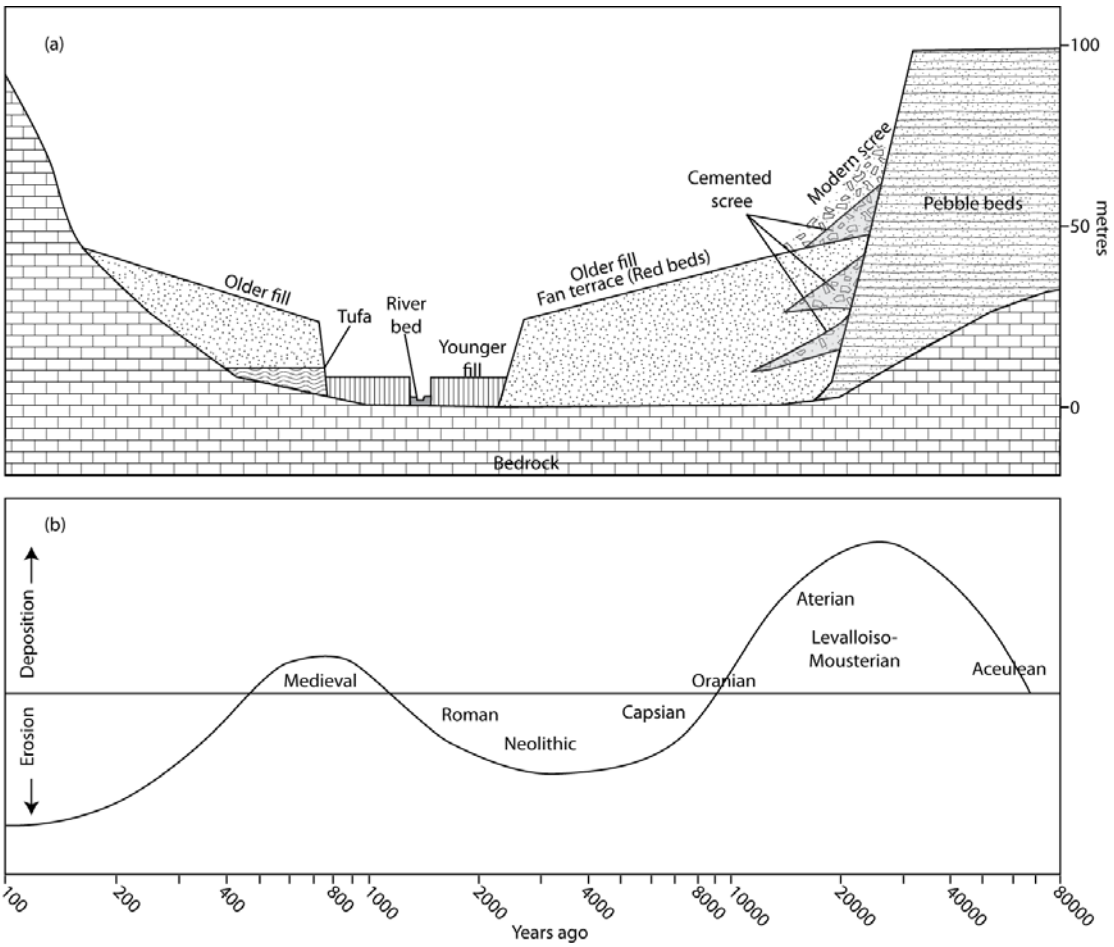

Figure 2.15 Taken from Macklin and Woodward (2009). a) From Higgs and Vita-Finzi (1966) the Quaternary sequence from the Louros valley, Greece, demonstrating a typical older to younger fill succession sequence. b) The model of alluviation events put forward by Vita-Finzi (1969)

2.4.2 Stage 5

As discussed in sections 2.2.4 and 2.2.5 evidence of terrestrial climate derived from vegetation records and marine proxies during stage 5 indicates warm, wet conditions through the interglacial and interstadials and colder, drier conditions through the stadial events. This view is supported by the oxygen and carbon isotopic composition of the speleothem record of Soreq Cave (figures 2.8, 2.9). Here a strong decoupling of $\delta^{18}O$ and $\delta^{13}C$ occurs during periods of enhanced temperature and water availability. At Soreq, the $\delta^{18}O$ signal is thought to be responding to both precipitation levels and temperature (Bar-Matthews *et al.* 1997). Therefore, $\delta^{18}O$ at Soreq is driven by a combination of the 'amount effect' and the temperature dependence of calcite precipitation (chapter 4), resulting in depleted $\delta^{18}O$ values during enhanced temperatures and precipitation (Bar-Matthews *et al.* 1997). During these warm, moist periods the $\delta^{13}C$ signal becomes less

negative due to the increased incorporation of isotopically light bedrock as a result of enhanced weathering (Bar-Matthews *et al.* 2000).

Soreq provides evidence for enhanced weathering during 5e and during 5c and 5a (Bar-Matthews *et al.* 2000). Traditionally, the development of red 'terra rossa' soils, characterised by their strong red colouration, clay illuviation and carbonate redistribution (Yaalon 1997, Federoff 1997), is assigned to the stability and warmth of stage 5e (e.g. Yaalon 1997). However, the Soreq cave record suggests that the conditions for terra rosa soil formation may be present during the interstadials of stage 5. Soreq provides a record of the eastern Mediterranean and so consideration of records surrounding southern Iberia will provide better constraint of conditions for comparison.

Along with soil development, tufa formation also provides evidence for pronounced landscape stability during MIS 5e and earlier interglacials (e.g. Martín-Algarra *et al.* 2003, Pedley 2009, Domínguez-Villar *et al.* 2011). It is thought that tufa formation is restricted to interglacial or interstadial periods where vegetation (particularly forests) levels are high. This is suggested because an increase in vegetation cover will: (1) limit sediment supply to waters and (2) fix sufficient soil CO_2 to drive supersaturation of soil fed waters (Goudie *et al.* 1993, Pedley 2009, Domínguez-Villar *et al.* 2011). The evidence presented by Mediterranean vegetation records through the last ~130 ka (figure 2.7) highlight the transition from extensive wooded conditions of interglacials to steppic conditions associated with glacial and stadial periods. During these transitions, the reduction in forest conditions is thought to be sufficient for tufa formation to cease. Therefore, tufa records provide evidence of warm, moist climates, within a stable land system (e.g. Goudie *et al.* 1993).

Rose *et al.* (1999) produced, to date, one of the best chronologically constrained records of Western Mediterranean landscape response to the climatic evolution of stage 5 (figure 2.13, table 2.1), through the compilation and analysis (sedimentology, stable isotopes and OSL dating) of multiple sediment exposures on Mallorca. Rose *et al.* (1999) found that warm sub-stages (5e, 5c, 5a) were characterized by general land surface stability, with soil development and minimal river activity. The study was able to constrain the development of the red soil to stage 5e, indicating extensive and prolonged landscape stability in order to enable such a soil to develop (e.g. Yaalon 1997). Sedimentological and morphological (electron microscopy of calcite cements) evidence supported the development of soils during the interstadials of stage 5. However, Rose *et al.* (1999) state that soil development during these periods was limited, arguing that landscapes were less stable during these periods. In the case of 5c, Rose *et al.* (1999) argue that the composition of the sediments provides evidence for loess deposition during this time, with

sediment supply at high enough levels to reduce soil formation. Rose *et al.*(1999) argue that despite evidence for increased moisture availability during these periods (5e, 5c, 5a), river activity was minimal due to the effects of increased vegetation and soil cover stabilising ground and preventing sediment input and bank erosion.

Table 2.1 From Rose et al. (1999); compilation of evidence of climate induced shifts in sediment deposition.

Landform, sedimentary and soil properties	Biological evidence	OSL ages (ka)	MAT (°C)	Moisture regime	Environment	OIS
Sandy loam with increasing upwards clay, humus, MS and Fe values	Terrestrial mollusc fauna			Moist	Slopewash transporting soil materials from adjacent hillside slopes	1
Thick beds of sands and gravels and well-sorted, cross-bedded sand	Derived marine molluscan fragments and terrestrial mollusc fauna	30-23 ± 5-3	13.4-6.3	Very dry	Fluvial deposition of large alluvial fans and extensive aeolian dunes beyond influence of the rivers	2
Yellowish brown silt, with weak soil development at surface. Far travelled mineral composition. Low MS, moderate Fe value	Terrestrial mollusc fauna	67-55 ± 11.5-7	14.6-9.9		Loess deposition from distant sources	3
Gravels with brown sandy matrix, and sands with increasing-upwards clay content, moderate MS and Fe value	Derived fragmented molluscs	61-55 ± 12-8	8.2-4.9		Fluvial gravels and aeolian sand, weathered at surface	4
Reddish yellow, well-sorted medium and coarse sand. Brown soil with high MS, Fe and clay values	Marine molluscan fauna	90-73 ± 17-10	17.9-10.3		Coastal deposition of beach ridge	5a
Sub-angular gravel and sands. Low MS and Fe value		94 ± 17	10.8-6.7		Fluvial deposition of material eroded from adjacent hillslopes	5b
Brown, clayey soil on silty parent material. Moderate MS and high Fe value. Local Fe pan			17.9-13.6		Loess with temperate soil formation	5c
Well-sorted sands and bimodal sands and gravels. Low MS and Fe value except at base	Derived fragments mollusca	109 ± 17	13.6-8.2		Aeolian sand and fluvial sands and gravels	5d
Red, clayey soil, with high MS and Fe values and chemically fretted $CaCO_3$ fragments		135 ±17	19.5-11.3	Moist	Mediterranean type soil formation	
Pale brown medium and coarse sand	Marine molluscan fauna	154-129 ± 25-22	19.5-17.9	Moist	Coastal deposition of ridges and beaches	5e
Erosional platform					Shoreline erosion	5e
Bright brown, well sorted, cross-bedded sand		140 ± 30	10.2	Very dry	Aeolian deposition of dunes	6

During the cold climate events of stage 5, Rose *et al*. (1999) identified increased river activity, with erosional and depositional episodes recorded. They believe that, despite reduced moisture availability during these stages, this increased river activity was a function of reduced vegetation cover allowing for increased surface runoff and increased sediment supply to the river systems.

The work of Macklin *et al.* (2002) appears to provide support for the scheme of landscape evolution through stage 5 proposed by Rose *et al.* (1999); of landscape stability during warm stages and river activity during cold events. However, the high uncertainties associated with ages of fluvial sediments make it difficult to derive strong conclusions regarding the timing of fluvial incision of depositional events during stage 5 (Macklin *et al.* 2002). Therefore, this study will be discussed in further detail within section 2.4.3, where chronological uncertainties are less problematic.

2.4.3 Last glacial

As recorded by the vegetation records of the last glacial through the Mediterranean (figure 2.14) the last glacial was a period marked by reduced tree cover, with glacial interstadial values

generally being comparable to values during the decline of stage 5a. As discussed in section 2.3, the last glacial was a period punctuated by millennial scale fluctuations between stadial and interstadial events; such events are well represented within numerous Mediterranean records (section 2.3.4), with pronounced reductions in % tree cover associated with stadial events. Reductions in tree cover associated with the arid stadial events indicate a dramatic change in landsystem resulting in: 1. increased bare ground cover, 2. reduced soil formation, and 3. increased sediment availability.

Macklin *et al.* (2002) compiled a review of Mediterranean river systems (figures 2.14, 2.17) and associated alluviation or valley fill events. Chronological controls on the timing of alluviation and incision events are derived from U-series and OSL age estimates, Macklin *et al.* (2002) argue that the focus within the review has been upon rivers whose Pleistocene evolution is well researched. The authors correlate periods of alluviation with HEs; however, no single river system studied provides evidence for response to all six HEs.

This study is particularly useful at highlighting river response in the Mediterranean on sub-Milankovitch timescales, since within each river system there are too many geomorphic changes occurring over the last 130 ka to be explained by Milankovitch forcing alone. However, although at the time of publication this study presented a collection of 'well dated' records, the chronological techniques used (particularly luminescence techniques) have improved considerably and would allow for both more accurate and more precise dating to be undertaken. The errors associated with the timing of the alluviation events, even within the last glacial, are often far larger than the duration of the climatic event that the alluviation episode is being correlated with. Therefore, although it is clear that fluvial systems within the Mediterranean are responding to shorter climatic cycles, it is not clear what the relationship is between the events witnessed within Greenland and the North Atlantic and Mediterranean rivers.

Recently, Candy *et al.* (2004a) have identified complications with the interpretation by Macklin *et al.* (2002) of the Rio Aguas sequence. Candy *et al.* (2004a) were able to demonstrate that the formation of the terrace coincident with the timing of the Younger Dryas (H0) event, resulted from internal karstic system processes, as opposed to climatically induced hydrological changes. Whilst the formation of the H0 terrace of the River Aguas resulted from non-climatic changes, Candy *et al.* (2004a) do assign other terrace formation events to climatic changes. The U-series chronology of Candy *et al.* (2004a) therefore demonstrates complications within the work of Macklin *et al.* (2002) and suggests that stronger chronological constraints on fluvial records may be needed to fully understand sub-Milankovitch response of Mediterranean rivers.

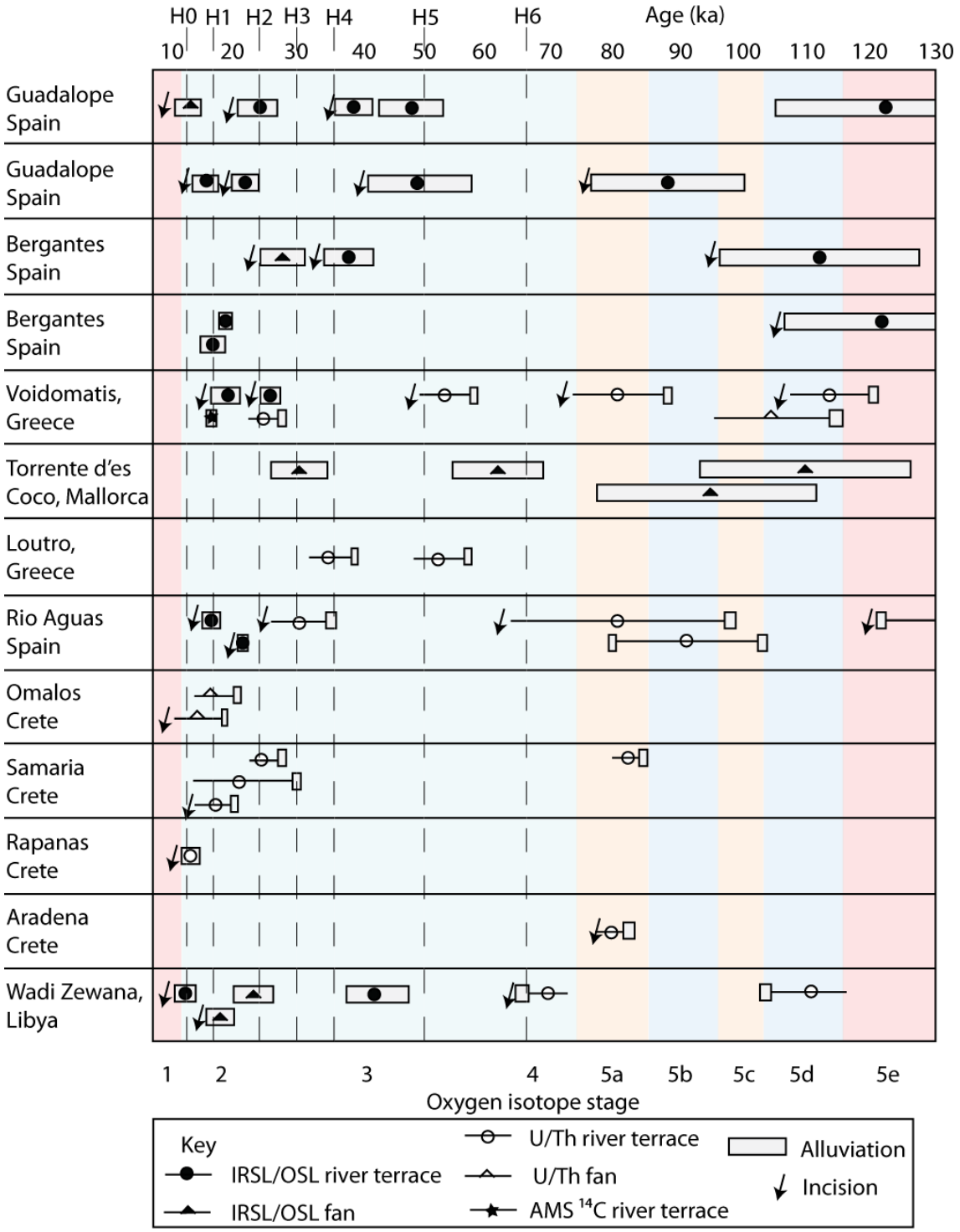

Figure 2.16 Composite of Mediterranean fluvial changes during the last 130 ka, from Macklin et al. (2002).

A less utilised, but arguably as useful record for interpreting Mediterranean landscape response to Quaternary climate changes is through the analysis of loess records, which offer the opportunity to build chronologically constrained, multi-proxy records (chapter 4). The loess preserved within Southern Spain is restricted compared to the loess fields of Northern Europe and China. Günster *et al.* (2001) attempted to correlate loess sections within the Granada basin in order to build a composite regional loess stratigraphy. Günster *et al.* (2001) present a

composite stratigraphy starting from last interglacial soil formation and covering the entire last glacial. However, as with the work of Padul (Pons and Reille 1988), Günster *et al.* (2001) correlate changes in loess deposition to the European Würmian stratigraphy, in which only a few of the Greenland stadials/interstadials are recognised (figure 2.17). As discussed previously (section 2.3), recent palynological evidence from within the Mediterranean has indicated a much more complex terrestrial history. This could cause major problems with the loess-palaeosol stratigraphy proposed by Günster *et al.* (2001), as correlation is based upon relative stratigraphic position alone. If the region's climate is fluctuating on a Greenland D-O timescale then correlation with Northern European stratigraphy is incorrect as the European stratigraphy does not contain evidence of all of the D-O stadial-interstadial transitions.

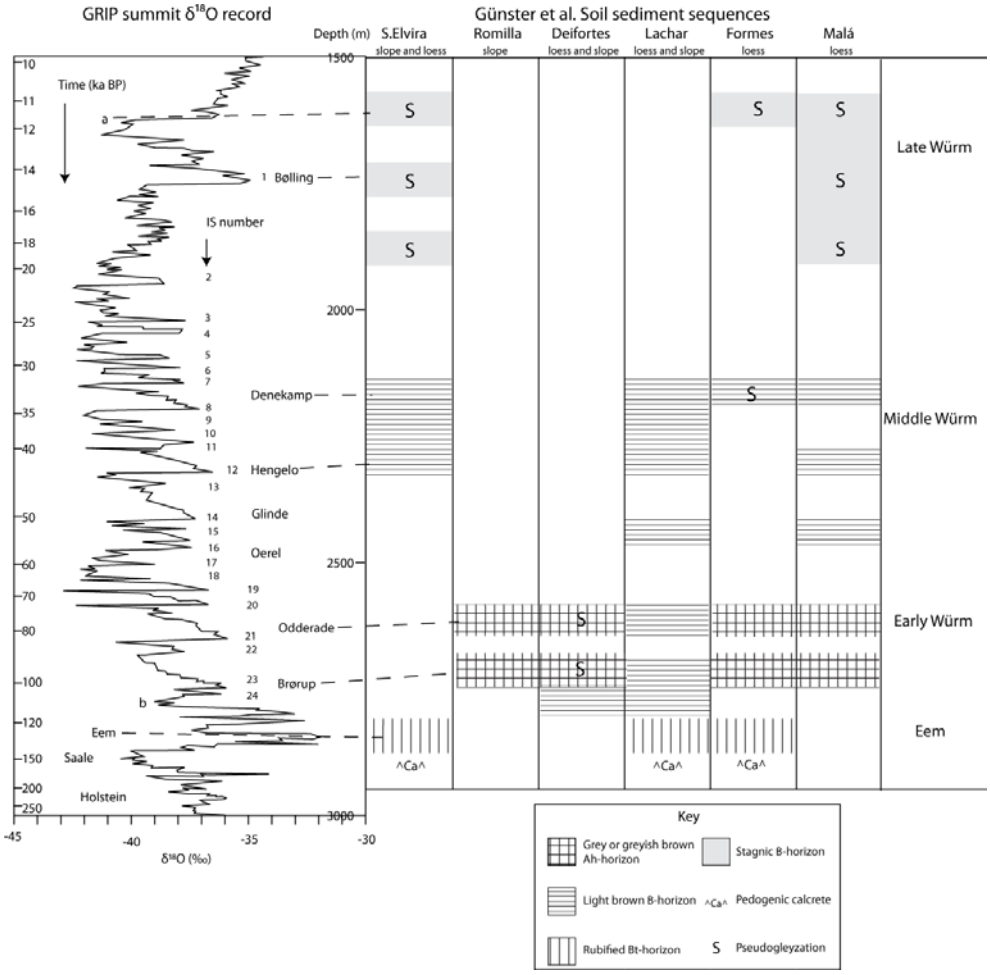

Figure 2.17 GRIP chronology with European stage correlation (adapted from Lowe and Walker 1997) compared with the loess stratigraphy of the Granada Basin proposed by Günster et al. (2001).

The basis of the Günster *et al.* (2001) study is the recognition of Eemian type soils at the base of each sediment exposure. This is argued to anchor the loess-palaeosol sequences within the last glacial. However, as demonstrated by Rose *et al.* (1999), the region has been subjected to loess deposition within stage 5, and as such the assumption of Günster *et al.* (2001) of loess being a

purely glacial phenomenon may not be appropriate within a Mediterranean context. Another problem with the Günster *et al.* (2001) stratigraphy is that the correlations between sections are based upon bulk sedimentological properties, soil characteristics and relative stratigraphic position; palaeosols thought to be characterised by similar properties being correlated as the same interstadial soil within the constraints of the European Würmian stratigraphy. Since no radiometric dating was performed on the sections studied by Günster *et al.* (2001), their interpretations are open to re-evaluation in the light of new chronological data.

A reassessment of the loess-palaeosols within the Granada basin based upon sedimentology, micromorphology and stable isotopic evidence combined with geochronology is necessary for investigating the assumptions made by Günster *et al.* A reassessment of the sections, including the development of a robust chronology; could provide evidence of sub-Milankovitch forcing on Greenland timescales, with the potential to correlate with the Iberian marine cores.

2.4.4 Summary

Patterns of geomorphic response of the Mediterranean through the climate changes of the last ~125 ka appear to suggest that widespread landscape stability occurred during times of interglacial warmth, whilst extensive modification of land-systems occurred under glacial climates. However, investigation of the terrestrial records indicates a more complex relationship, involving large scale landscape changes occurring on both Milankovitch and sub-Milankovitch timescales.

Through MIS 5e regional stability is reported coinciding with the period of extensive interglacial forest coverage, with evidence for extensive well developed soil formation, tufa precipitation and stability within river systems. As shown in the vegetation records of the region, there is a suggestion that near full interglacial vegetation recovers during the following stage 5 interstadials (5c, 5a). This appears to be corroborated by the geomorphological evidence belonging to these climate episodes, with a return to tufa precipitation, soil formation and river stability (e.g. Rose *et al.* 1999, Martín-Algarra *et al.* 2003, Domínguez-Villar *et al.* 2011). The stadial episodes of stage 5 (5d, 5b) appear to reflect the reduction in forest conditions and the shift towards steppic vegetation recorded for the region; where increased mobilisation of sediments and a reduction in vegetation stabilising landscapes is reflected by regional alluviation episodes and increased fluvial deposition.

The climate of the last glacial within the western Mediterranean is characterised by rapid climate events, probably correlated to the D-O cycles of the North Atlantic region. Such cycles within the Mediterranean are expressed as cold, arid stadials with a near total loss of forest vegetation, and more humid interstadials associated with increasing forest conditions. Within the western

Mediterranean the geomorphic response to the stadial environments appears to be recorded as increased fluvial deposition events, with regional alluviation events corresponding to stadial events. Despite evidence suggesting much drier conditions, it appears that the landscape instability produced through the substantial loss in vegetation cover produces significant sediment mobilisation to affect river sedimentation. There is also regional evidence for loess accumulation during stadial episodes, with suggestions of both locally derived and far travelled loess provenance (chapter 3), again supporting the idea of widespread steppic vegetation conditions, where sediment mobilisation rates are high.

The interstadial events of the last glacial are marked by reduced fluvial deposition and, potentially, through the establishment of weakly developed soil horizons within loess deposits. However, evidence for the degree of soil development indicates that such episodes are short-lived and less pronounced than the interstadials associated with Milankovitch timescales seen in stage 5.

The existing evidence for geomorphic response to climate fluctuations through the past 125 ka indicate that the region is highly sensitive, showing pronounced landsystem shifts associated with climate shifts on both Milankovitch and sub-Milankovitch timescales. It seems likely that the amplitude of vegetation shifts seen within the region, associated with the pronounced shifts in effective precipitation through the period in question, is a key driver for such geomorphic shifts.

2.5 Holocene

2.5.1 High latitude records of Holocene climate

The Holocene begins after the Younger Dryas cooling event ~11.7 ka according to the GICC05 timescale (e.g. Vinther *et al.* 2006), with the Holocene thermal maximum beginning at around 9 ka (Vinther *et al.* 2009). Although the timing of peak Holocene conditions varies significantly between Greenland Ice Sheet records, it is thought that GRIP and NGRIP provide reliable records of Holocene climates (Vinther *et al.* 2009).

Within North Atlantic records, SST reconstructions place the timing of peak interglacial warmth slightly earlier, at ~10.2 ka (Mayewski *et al.* 2004) (figure 2.19). Despite discrepancies over timing, which, in part, may be linked to differences in core chronologies, polar ice core records and North Atlantic records show closely correlating climate evolution through the Holocene. Since the thermal maximum, there has been a general trend towards cooler temperatures within mid to high latitudes, associated with the decreasing insolation levels (figure 2.18). Records indicate that

Holocene climate has so far been relatively stable when compared to other climatic periods of the last 125 ka.

Although muted in comparison to other parts of the Quaternary, Holocene records from Greenland and the North Atlantic do contain evidence for pervasive climate cycles and rapid cooling events. There is an apparent pacing of events within the Holocene operating at 2800-2000 and 1500 yr intervals (Mayewski *et al.* 2004 and references therein), there is strong evidence for these low amplitude oscillations within Greenland ice cores (O'Brien *et al.* 1995, Vintner *et al.* 2006) and north Atlantic marine cores (Bond *et al.* 1997).

Mayewski *et al.* (2004) introduce the term 'Rapid Climate Change' to describe climatic shifts within the Holocene where geographically broad records document the change. Through the compilation of ~50 palaeoclimate records with a broad geographical distribution and comprising of varying proxy records, Mayewski *et al.* (2004) identified that most Holocene rapid climate events were characterised by cooling in the high latitudes and tropical aridity. However, the event occurring at ~9-8 ka (which contains the 8.2 ka event) was characterised by cool polar conditions and wetter tropics (Mayewski *et al.* 2004, Fletcher and Zielhofer 2011).

It is thought that this change in characteristic relates to the mechanisms responsible for the climate events; Mayewski *et al.* (2004) state that although the mechanisms responsible for rapid climate changes within the Holocene remain unknown, there appears to be a relationship between the events and solar variability. However, they argue that the ~8-9 ka event occurred during a time when ice sheet dynamics, similar to those through the last glacial, remained in place, and therefore the bipolar mechanisms responsible for rapid changes through the last glacial could be the cause for this event.

The global review by Mayewski *et al.* (2004), however, contains only one Mediterranean record, and does not necessarily provide a good insight into the climate of the region or the environmental or geomorphological responses (Fletcher and Zielhofer 2011).

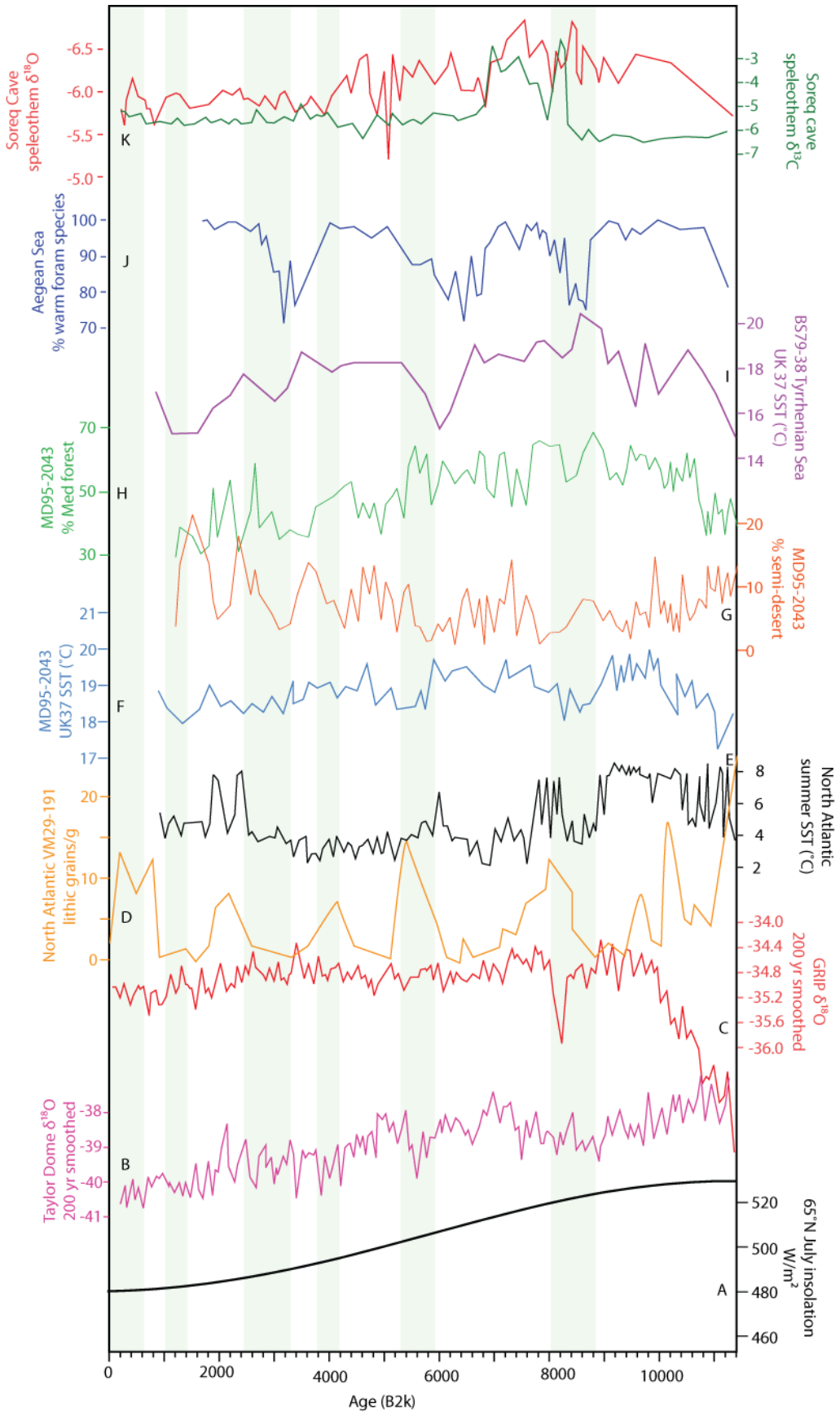

Figure 2.18 Compilation of key records of Holocene climate changes. A. Insolation curve(Laskar et al. 2004), B. Taylor Dome C oxygen isotope (Steig et al. 2000), C. GRIP isotope record from Johnsen et al. (1992), D. North Atlantic Lithics (Bond et al. 1997) and E. N.A SST (Mayewski et al. 2004), F. MD95-2043 SST (Cacho et al. 2001, 2002) and G. pollen (Fletcher and Sánchez Goñi 2008), H-I, Aegean Sea foram record (Rohling et al. 2002), J. Soreq cave speleothem isotopic record (Bar-Matthews et al. 1999). Grey bars indicate position of Holocene rapid climate events (Mayewski et al. 2004).

2.5.2 Mediterranean records of Holocene

This section will discuss the Holocene climate of the Mediterranean with reference to the events discussed for the North Atlantic, Greenland and northern Europe. This discussion will focus on the sites shown in figure 2.19.

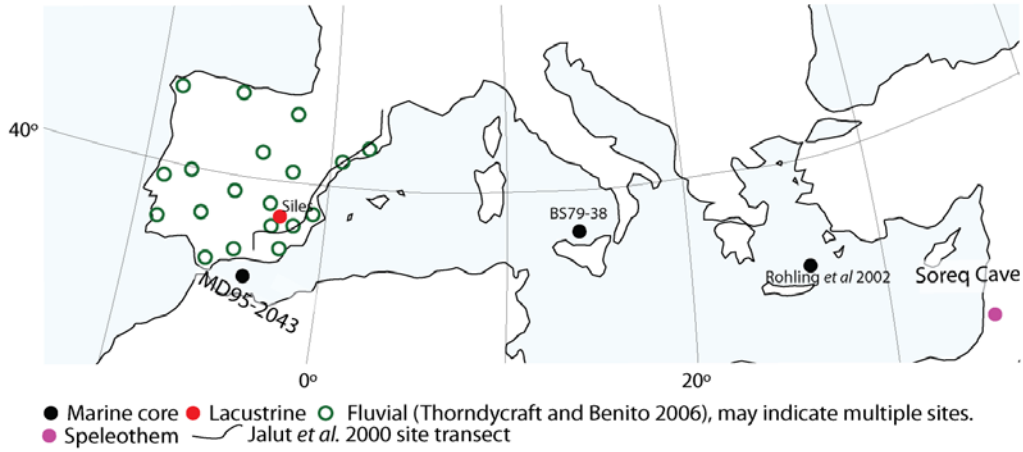

Figure 2.19 Map of Mediterranean Holocene records discussed

2.5.2.1 Mediterranean Sea

As shown in figure 2.18, the Mediterranean Sea appears to be experiencing the same climate variability through the Holocene as recorded within North Atlantic sediments. This is shown by reductions in Alboran SSTs broadly correlating with the Holocene rapid climate events noted by Mayewski *et al.* (2004) (shown in grey bars figure 2.18). However, there do appear to be significant differences within regional records of Holocene Mediterranean Sea conditions.

Cacho *et al.* (2001) produced a transect from the North Atlantic (Gulf of Cadiz), western Mediterranean Sea (Alboran) and central Mediterranean Sea (Tyrrhenian); within these records Cacho *et al.* (2001) argue for a discrepancy in the timing of peak interglacial conditions, arguing that the North Atlantic experiences peak interglacial warmth first, followed by the western Mediterranean and central Mediterranean Seas respectively. Cacho *et al.* (2001) report that the arrival of maximum Holocene SSTs was at 11.5-10.2 ka BP, 10-9 ka BP and 8.9-8.4 ka BP within the Gulf of Cadiz, Alboran Sea and Tyrrhenian Sea, respectively. Despite differences in the arrival of peak interglacial warmth, the records go on to show a general trend towards cooling after peak conditions, punctuated by events which appear to correlate broadly with the rapid climate events noted by Mayewski *et al.* (2004).

Cacho *et al.* (2001) argue that the apparent west-east gradient associated with the onset of peak Holocene conditions indicates the importance of North Atlantic inflow waters in communicating northern hemisphere climates. However, Cacho *et al.* (2001) also highlight the role of the

Mediterranean basin in modifying North Atlantic signals, noting that the Tyrrhenian Sea record demonstrates an amplified response to Holocene rapid climate events when compared with more westerly records. This, Cacho *et al.* (2001) argue, indicates a Mediterranean basin-induced amplification, possibly induced by increased winds. Such an amplified easterly response appears to be corroborated by the foraminiferal record of Rohling *et al.* (2002) (figure 2.18).

Previous discussion of the last glacial climate within the Mediterranean basin detailed the evidence for a period exhibiting greater aridity than presently experienced within the Mediterranean. Oceanic records indicate that during the early Holocene, through the thermal maximum, the region experienced a positive water balance (Thunnel and Williams 1989). Thunnel and Williams (1989) examined the oxygen isotopic composition of foraminifera from eastern and western Mediterranean Sea cores, and through corrections for shifting temperatures and ice volumes were able to extract a record of salinity (due to differential dissolution of ^{18}O in varying salinities). The salinity record of Thunnel and Williams (1989) has been interpreted as a record of effective moisture availability, with periods of high rainfall correlated with low salinity and high aridity with increasing salinity levels. Salinity level reconstruction of Thunnel and Williams (1989) is interpreted as showing that the mid-Holocene (~8 ka) as a period of significantly enhanced water availability compared to the late Holocene, although all Holocene values indicate higher levels of moisture availability when compared to the last glacial (Thunnel and Williams 1989).

2.5.2.2 Mediterranean terrestrial climate records

Through the compilation of Holocene pollen records within Europe, Davis *et al.* (2003) produced regional Holocene reconstructions, using key species as indicators of temperature and/or precipitation regimes. Reconstructions of southern European climate suggested an absence of a mid-Holocene thermal maximum (Davis *et al.* 2003), indicating that conditions through the Holocene were slightly cooler than at present, contrary to the evidence based on SST reconstructions. Davis *et al.* (2003) suggest that southern European temperatures peaked during the early Holocene (~10 ka) but then dropped sharply, around ~8.2 ka, and recovered steadily to present day levels. Davis *et al.* (2003) argue that this temperature regime was accompanied by regional drying through the Holocene.

Evidence from the eastern Mediterranean supports the idea of increasing aridity through the Holocene after the early Holocene climatic optimum. The record of $\delta^{18}O$ and $\delta^{13}C$ variations through Soreq Cave speleothems (Bar-Matthews and Ayalon 2011), indicates there is a general trend towards increasing $\delta^{18}O$ values from the Holocene climatic optimum through to the late

Holocene. As ^{18}O is negatively correlated to precipitation levels, the record at Soreq indicates progressive drying post Holocene climatic optimum (Bar-Matthews and Ayalon 2011). However, unlike the record compiled by Davis *et al.* (2003) which suggests a very minor, or absent expression of Holocene rapid climate events post 8.2 ka; Soreq indicates that rapid climate events during the Holocene are expressed within Mediterranean records. The record indicates that these rapid climate events can be correlated with wetter conditions in the Mediterranean; this is supported by increased $\delta^{13}C$ values, indicating increased weathering under moister conditions (Bar-Matthews and Ayalon 2011).

It is possible that the record of Davis *et al.* (2003) may not clearly express Mediterranean response to Holocene rapid climate events, as through the correlation of records it may be possible that the evidence has become obscured by issues associated with resolution and/or chronology. Therefore, the regional pollen record contained within core MD95-2043 may be quite useful as it enables direct comparison with the marine proxy records, suggested by Davis *et al.* (2003) to be opposed to terrestrial climate evidence.

Fletcher and Sánchez Goñi (2008) state that the regional record obtained from MD95-2043 indicates that the early to mid-Holocene (11.7-5.4 ka) is associated with forested conditions, indicating relatively moist conditions, followed by a shift towards increasing steppic vegetation (5.4 ka onwards), supporting the suggestion of Holocene aridification. The findings of Fletcher and Sánchez Goñi (2008) are comparable with the findings of Jalut *et al.* (2000) and Magny *et al.* (2002), who compiled terrestrial pollen records through the western Mediterranean and suggest a mid-Holocene transition to warmer drier conditions. The concept of Holocene aridity is supported through the compilation of southern Spanish pollen records, which record a shift to xerophytic (dry adapted) vegetation around 5.4 ka (Carrión *et al.* 2010).

However, the Mediterranean region experienced extensive anthropogenic alteration through the Holocene. It is argued, (Magny *et al.* 2002, Jalut *et al.* 2000, Fletcher and Zielhofer 2011, Pantaleon-Cano *et al.* 2003) that there is no evidence within western Mediterranean pollen records that humans were responsible for the shift to steppic taxa, and it must, therefore, be climatically induced. Pantaleon-Cano *et al.* (2003) and Carrión *et al.* (2010) suggest that significant human modification of Iberian vegetation occurs ~2 ka.

Within the MD95-2043 record, Fletcher and Zielhofer (2011) suggest that periods of aridification (through forest decline) correlated with SST reductions can be seen to correlate with the Holocene rapid climate events. This is contrary to evidence from Soreq, which suggests that the eastern Mediterranean experiences wetter phases associated with rapid Holocene events.

Comparison of the pollen record with lake level records of Iberia (figure 2.20) indicate that often Holocene rapid climate events are associated with desiccation events, although these are not regionally synchronous (Fletcher and Zielhofer 2011); this pattern of response is also proposed by Magny *et al.* (2002).

2.5.3 Mediterranean geomorphic response through the Holocene

The onset of the Holocene marks the transition from the rapid climate instabilities, which characterise the last glacial period, to a stable climate marked by low-amplitude climate fluctuations. This return to warm, stable, forested conditions is marked by the return to tufa precipitation within southern Spain and an associated return to soil development and landscape stabilisation (Pedley 2009, Martín-Algarra *et al.* 2003, Domínguez-Villar *et al.* 2011).

The model proposed by Vita-Finzi (1969) suggested that river systems of the Mediterranean experienced one episode of alluviation occurring towards the end of Roman occupation (Macklin and Woodward 2009), termed the 'Younger fill' (figure 2.15). Vita-Finzi (1969) argued that this alluviation event occurred due to increased flooding and erosion in response to a cooler, wetter climate. However, with increased geomorphic understanding of the Mediterranean, and improved chronological techniques, it became evident that Vita-Finzi's model was an oversimplification (Macklin and Woodward 2009).

Compilation of alluviation events and flood event histories (figure 2.20), ^{14}C dated using AMS techniques, is beginning to unravel the differing impact of climate and human influences on Holocene Mediterranean rivers. There is evidence to support human induced changes in fluvial systems, particularly for the latter part of the Holocene, surrounding the Medieval and modern civilisations (Benito *et al.* 2008). However, it is suggested that such studies still suffer from chronological issues which make distinctions between human and climate influences difficult (Mackling and Woodward 2009). Through a probability based assessment of ^{14}C ages of flood deposits within Spanish river systems, Thorndycraft and Benito (2006) have attempted to produce more robust event stratigraphies. Thorndycraft and Benito (2006) suggest that through the late Holocene flood events can be largely correlated with episodes of climatic cooling within the North Atlantic, whereas the mid-Holocene, a period of forested conditions (figure 2.19, Fletcher and Sánchez Goñi 2008), is represented by stable channel conditions. Within the late Holocene (<~2.5 ka), Thorndycraft and Benito (2006) argue that there remains evidence for increased flooding during cold North Atlantic episodes, but there is also evidence to human induced alluviation events (Benito *et al.* 2008).

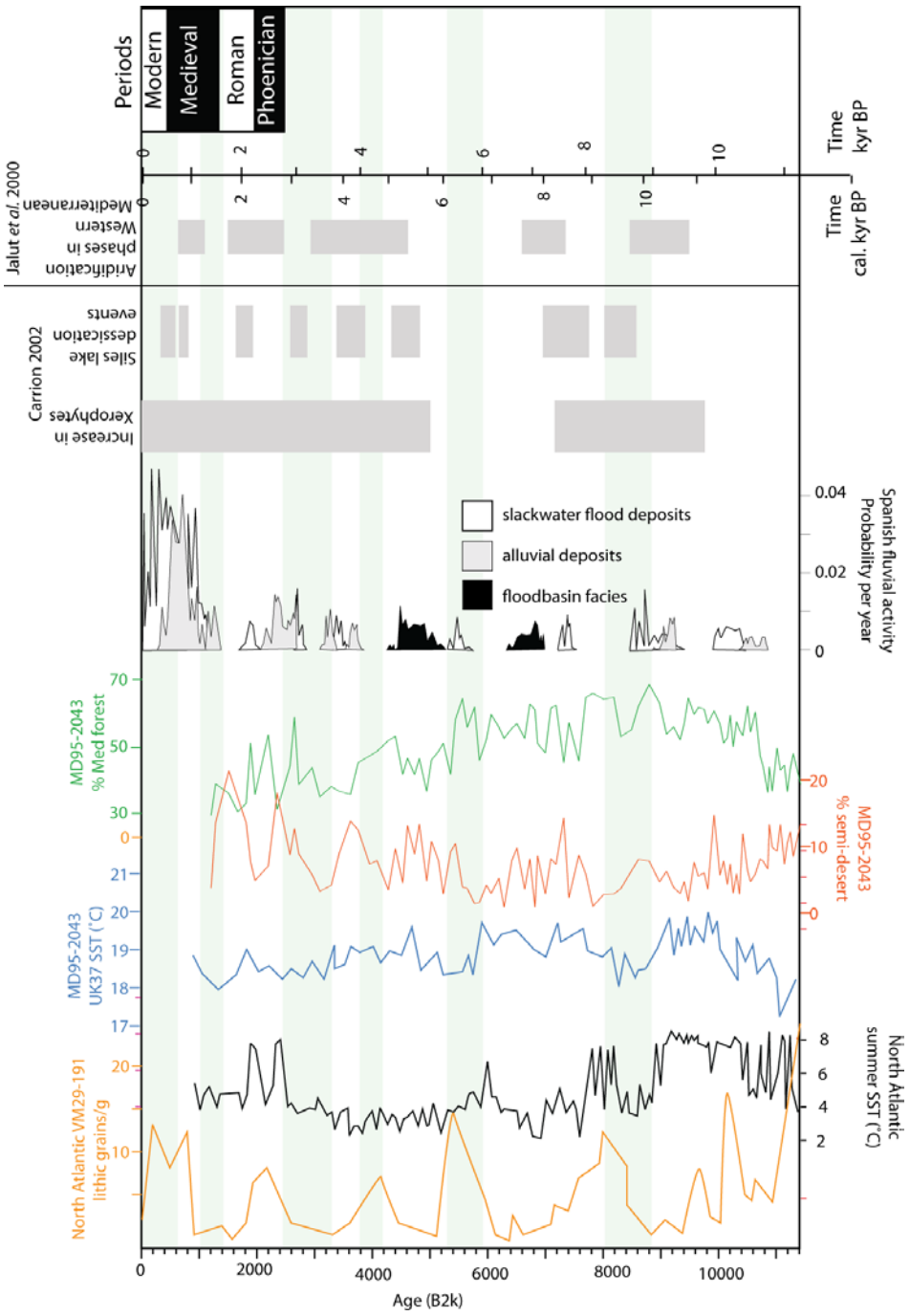

Figure 2.20 Compilation of North Atlantic records of Holocene climate, compared to Iberian records of terrestrial response. North Atlantic Lithics (Bond et al. 1997) and SST (Mayewski et al. 2004), MD95-2043 SST (Cacho et al. 2001, 2002) and pollen (Fletcher and Sánchez Goñi 2008), Spanish Fluvial activity (Thorndycraft and Benito 2006), Lake Siles (Spain) desiccation events and shift to xerophytic plants (Carrión 2002), Western Mediterranean aridification events from pollen records (Jalut et al. 2000). Grey bars indicate position of Holocene rapid climate events (Mayewski et al. 2004).

2.5.4 Summary

Climatic records of the Holocene from both the North Atlantic and the Mediterranean regions indicate that the period has experienced low frequency, sub-Milankovitch climate variability, potentially related to solar activity levels. Mediterranean Sea records and terrestrial pollen studies

indicate that through the Holocene the Mediterranean has experienced subtle cooling, post early Holocene optimum conditions, associated with increasing regional aridity. Through this general trend, the region appears to have been subjected to periodic aridification phases, which some authors have suggested are correlated to the Holocene rapid climate cooling events seen within North Atlantic records.

Compilations of regional records of terrestrial response appear to support palynological interpretations of aridification phases, with some correlations apparent between steppic taxa increases and lake desiccation events (figure 2.20). However, evidence from Spanish river systems indicate that alluviation events, relating to aridity through increased sediment supply, provide a less clear correlation in terms of both Iberian and North Atlantic correlations.

Importantly, both the palynological records and fluvial records of Iberia indicate that anthropogenic influence on climatic signals is minimal through the early and mid-Holocene. However, both records demonstrate that, through the late Holocene it becomes increasingly difficult to unravel climatic vs. human modification of ecosystems and geomorphic processes.

Chapter 3 – Loess as a palaeoclimatic archive

This chapter aims to introduce the current understanding of loess-palaeosol sequences and their accumulation and potential for reconstructing Quaternary climate changes within the Mediterranean. A summary of our current ideas will be outlined through the discussion of:

1. Current suggestions for defining aeolian silt deposits as loess
2. Outline the mechanisms of silt formation within various climatic and environmental settings
3. The distribution of loess deposits and the timing of their deposition
4. The chronological, biological and sedimentary techniques commonly applied to the analysis of loess-palaeosol sequences
5. The potential of the study of Mediterranean loess sequences for enhancing our understanding of terrestrial response to Quaternary climate changes

3.1 Defining loess

"Loess can be defined simply as a terrestrial clastic sediment, composed predominantly of silt-size particles, which is formed essentially by the accumulation of wind-blown dust." (Pye 1995 page 653).

As loess is deposited from suspension it most commonly occurs as a massive deposit, although it occasionally contains subtle bedding structures. It is the massive, well sorted nature of loess that makes it readily distinguishable from aeolian sands and fluvial sediments. Pecsi (1990) outlines 10 criteria for the definition and recognition of loess deposits: (1) A homogenous, porous, well sorted, pale yellow deposit, composed primarily of silt (10-50 μm), (2) composed primarily of quartz (40-80%), feldspars, calcite and dolomite, (3) loess horizons are usually unstratified, but may contain pedogenic horizons, (4) clay and sand is a minor component (5-25%) with clay minerals illite and montmorillonite being dominant, (5) variable carbonate content (1-20%), (6) loess is permeable to water, although it may contain evidence of cementation between grains, (7) commonly forms steep, stable 'loess walls', (8) easily eroded by surface waters,(9) typically contains remnants of flora and fauna, (10) deposited wind-blown silts require transformation to loess via stabilisation by vegetation and/or some diagenesis.

This has not been universally accepted, as the very nature of loess is dependent upon source region and transport pathways, which can lead to a significant degree of variation in the composition of loess deposits. This is highlighted in the work of Pye (1984) which outlines the varying characteristics of key loess deposits from different geographical locations.

Pye (1995) identifies three fundamental requirements for the formation of loess: (1) continual source of dust, (2) sufficient wind energy to enable the transportation of dust, and (3) a site suitable for accumulation, generally a vegetated depression and/or an area with sufficient rainfall to cause deposition.

Silts which have accumulated via sub-aerial deposition are referred to as primary loess. However, as loess is an easily erodible, soft sediment, it can be reworked by slope or fluvial processes and is then referred to as secondary loess (Pye 1995).

3.2 The origin of loess

There are two modes of formation of the silt required for loess; these are glacial processes and desert processes, seen in figure 3.1. The majority of loess deposits are linked to glacial stages and glacial system landscapes. Initially, it was hypothesised that glacial abrasion resulted in the production of large amounts of silt-sized material which could then be deflated and accumulated elsewhere as loess. However, laboratory reconstructions of glacial grinding have produced contradictory evidence. Wright *et al.* (1998) indicated that on its own this mechanism may not produce significant silt sized material. However, Smalley *et al*. (2005) argue that when a repeat experiment was undertaken they were able to produce large amounts of silt by using quartz containing natural crystal defects.

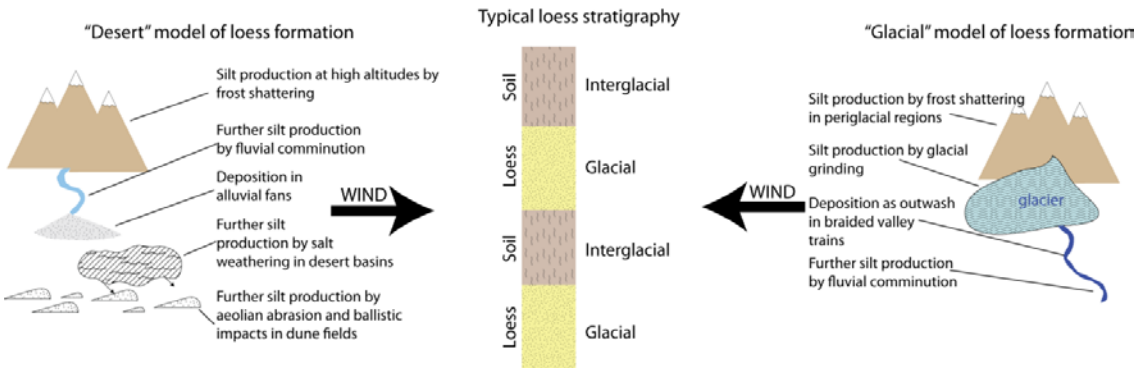

Figure 3.1 Adapted from Muhs and Bettis (2003) on the production mechanisms of silt sized particles.

Additionally, it has been demonstrated that other glacial and non-glacial processes can be responsible for the production of large amounts of silt sized material (Wright 2001, Muhs and Bettis 2003, Iriondo and Kröhling 2007). Predominantly, the responsible mechanisms are believed to be physical weathering processes (frost shattering and salt weathering) (Pye and Sperling 1983), abrasion during fluvial transport (Wright *et al.*1998) and aeolian induced grain abrasion (Whalley *et al.* 1982).

In order for aeolian dust to become loess it must be deposited and accumulate on the land surface. Primary loess is formed through sub-aerial accumulation of silt. In order for loess to accumulate, Tsoar and Pye (1987) argue that there exists a critical rate of dust deposition of 0.5 mm/a, below this rate all deposited dust is incorporated in the soil by bioturbation and rain action. Two primary factors are believed to be responsible for the deposition and accumulation of loess: rain and vegetation. The primary mechanism for removal of dust form the atmosphere is via rain out, which is a commonly observed phenomenon widely studied within the Mediterranean (e.g. Avila *et al.* 1996, Loÿe-Pilot and Martine 1996, Fiol *et al.* 2005) where dirty rain or red rain occurs. Dirty rain describes the phenomenon where, in the Mediterranean, Saharan dust outbreaks result in dust particles within the high atmosphere which act as nuclei for moisture formation, trapping the dust within resulting precipitation (Loÿe-Pilot *et al.* 1986). Dust deposition may also occur through 'dry' deposition in distal regions via loss of wind energy (Pye 1995). It is argued that Saharan dust may be a main constituent of Mediterranean red soils (Muhs *et al.* 2010), where a moderate supply enables a recognisable contribution, but does not result in as thick an accumulation of dust as loess.

Once dust is deposited onto the land surface it requires trapping in order to accumulate. Vegetation, primarily grasses and shrub type vegetation, is thought to be the primary trapping mechanism (e.g. Pye 1995, Tsoar and Pye 1987, Pye and Tsoar 1987, and references therein). Supply of dust is an important factor controlling loess formation; however, Tsoar and Pye (1987) argue that a dust trap is equally important. Tsoar and Pye (1987) argue that desert loess tends to be found on the semi-arid margins of desert regions where there is suitable and sufficient vegetation to trap silt.

It is argued that the primary diagnostic characteristics of loess (cohesion and texture) may be the product of 'loessification' (Pecsi 1990, Iriondo and Kröhling 2007). 'Loessification' describes the action of syn-depositional weathering (occurring at the time of deposition), and it is argued that it is this weathering and the resulting cemented nature of the loess through the precipitation of carbonates (primarily) that results in the characteristic appearance of many loess deposits (Iriondo and Krohling 2007). However, Pecsi (1990) does recognise that the process of 'loessification' is not responsible for the formation of silt sized particles, and that the alteration of silt deposits by this process is not uniform, but is dependent upon aspects of climate and depositional rates.

However, again, there is no consensus within the loess community, with some arguing that the process of loessification is key to the identification/definition of loess and others arguing for a

simpler 'Pye type' definition in which loess formation occurs through the aeolian deposition of silt (see Smalley *et al.* 2011).

3.3 Distribution

The global distribution of widely recognised loess deposits can be seen in figure 3.2 (Pecsi 1990). There is a clear link between the distribution of these major loess centres and the distribution of areas of high relief/and or LGM ice extent (Smalley and Vita-Finzi 1968, Smalley and Krinsley 1978) thereby defining the majority of major, thick loess accumulations as cold climate processes (Smalley and Vita-Finzi 1968). Iriondo and Krohling (2007) assign the existence of the North American and North European loess to glacial processes and the Chinese and Central Asian deposits to cold climate weathering processes.

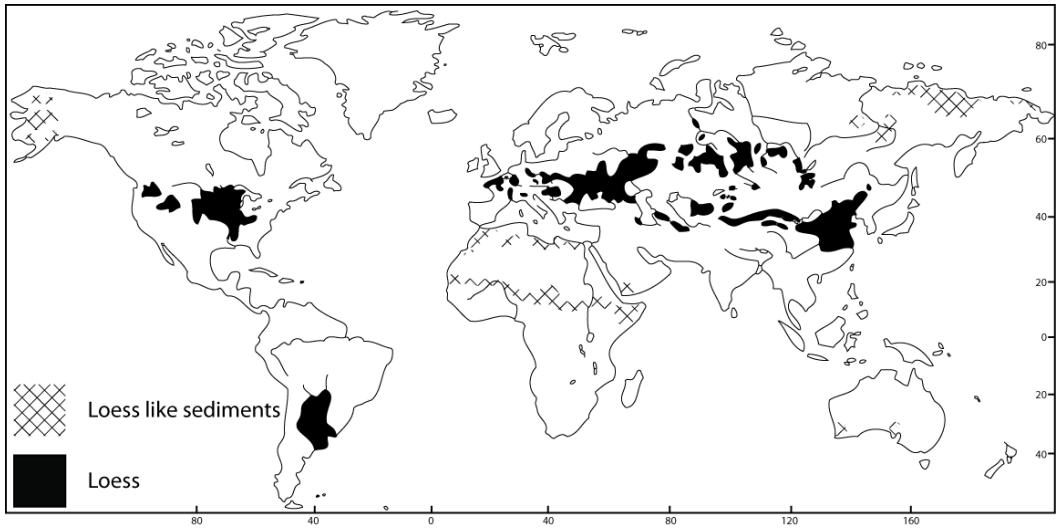

Figure 3.2 World loess and loess like sediment distribution map taken from Pecsi 1990. Pecsi (1990) has allocated 'loess like' deposits to areas where they believe sufficient classification work has yet to be carried out.

The distribution of loess within Northern Europe is shown in Figure 3.3 (Haase *et al.* 2007) and clearly shows that most European loesses are found within the flat, lowland regions of Northern Europe.

However, as many of the major loess deposits of the world are thought to result from cold climate or glacial processes, this has sometimes affected the very definition of loess, with those deposits outside of cold climate systems being disregarded (e.g. Smalley and Vita-Finzi 1968) or misidentified and neglected in terms of study. For example, Smalley *et al*. (2005) suggest that most North African loess is produced by deflation from lacustrine basins due predominantly to grain size characteristics, and Chinese desert loess is produced from high mountain regions affected by glaciation. Smalley and Vita-Finzi (1968) argue that true loess, according to the original German definition of loess, must be glacial in origin. They therefore argue that desert

deposits are loess-like, but do not consider them true loess. This stance appears to have been disregarded by recent work, with the acceptance that loess of desert origin is able to satisfy numerous existing identification criteria regardless of the mode of production. Importantly, the alternative mechanisms of silt formation within different environments (glacial, peri-glacial, desert) result in significant differences in the composition and grain textures of the resulting accumulations (chapter 6).

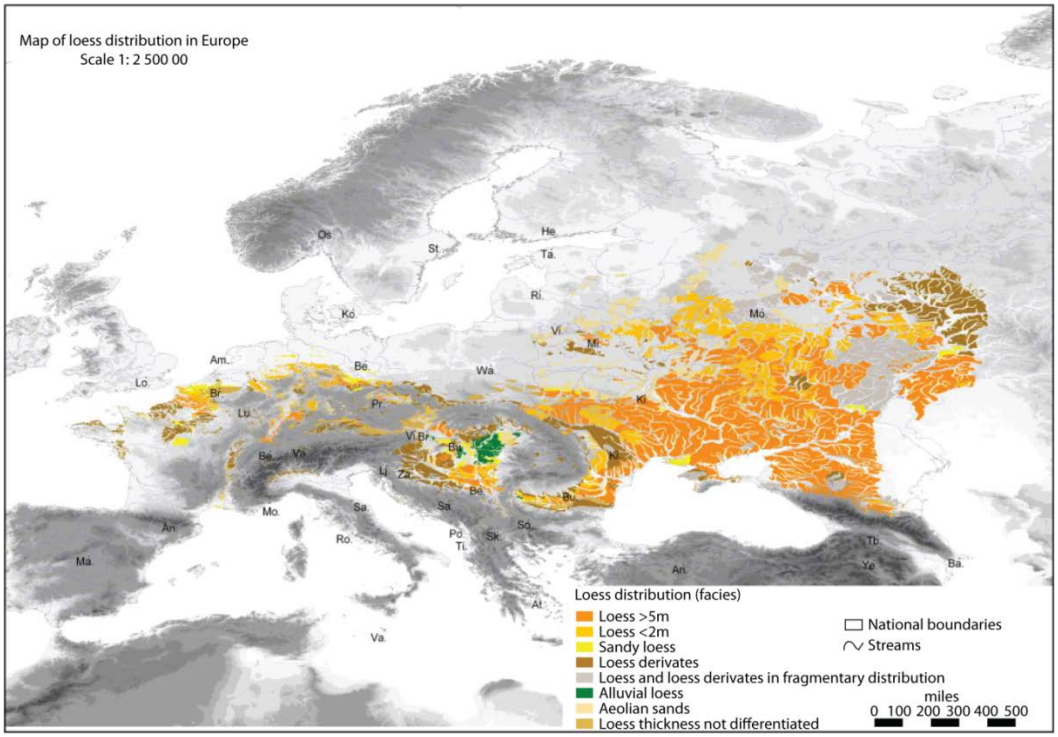

Figure 3.3 Map showing distribution of loess in Europe, collated from published data by Haase et al. (2007)

3.3.1 The Mediterranean

Compared to the northern European loess deposits, deposits within the Mediterranean region have received little attention. Coude-Gaussen (1991) compiled a basic map outlining the existence of loess around the Mediterranean Sea, based upon the limited published studies (see figure 3.4).

Coude-Gaussen (1991) argues that the loess within the northern Mediterranean exhibits grain size and mineralogical characteristics which indicate a local origin, suggesting that cryogenic processes during glacial periods are responsible for the formation of the silt and fine sand material (Bonifay 1965, Cremaschi *et al.* 1990).

Figure 3.4 Map showing distribution of loess around the Mediterranean. Compiled by Coude-Gaussen (1991) based upon published studies.

The northern and central Spanish loess deposits are characterised as reworked loess (secondary) and/or gypsic derived silts (Coude-Gaussen 1991) with similarities in composition to local materials (Garcia *et al.* 2011). Recently, there have been publications detailing the location of loess or loess like deposits from central Spain (Garcia *et al*. 2010, Garcia *et al.* 2011). As with other Northern Mediterranean loess deposits, the grain size and mineralogical assemblages present suggested a local origin, with deflated alluvial silts reasoned to be the most probable source (Garcia *et al.* 2011).

Importantly, all of the Northern Mediterranean loess sequences so far reported share similar depositional histories, with limited loess preservation from MIS 6, soil development during stage 5e, and a return to loess deposition during stages 4-2, with varying degrees and stages of pedogenic alteration occurring throughout this period (Coude-Gaussen 1991, Garcia *et al.*2010, 2011, Bonifay 1965, Mücher *et al*. 1991, Günster *et al.* 2001). Generally, these deposits are not independently dated, but are assigned an age based on their relationship to soils of inferred Eemian age. Additionally, most of the deposits (except those reported by Rose *et al.* 1999), particularly those located in the Northern Mediterranean, are reported to be predominantly coarse grained silts (argued to support predominantly local provenance), typically secondary in nature and have been subject to only limited study (for example; Coude-Gaussen 1991, Cremaschi *et al.* 1990, Bonifay 1965, Mücher *et al*. 1991).

Although it is often considered that loess deposits may be extensive within North Africa, to date, the few publications dealing with loess south of the Mediterranean Sea tend to focus on the deposits of Tunisia. Coude-Gaussen (1987) provides a brief overview of what little is known about

the deposits of North Africa, and states a number of shared characteristics, shared sedimentary origin (desert loess), frequent reworking by slope or fluvial processes and a young (Upper Pleistocene) age. As the formation of silt sized material results from the 'desert' mode of formation (see figure 3.1), the timing of depositional events is not necessarily tied to glacial stage processes in the same way as Northern European sites.

Coude-Gaussen (1987, 1991) argues that the most likely time of loess deposition within North Africa is during moderate pluvial (humid) events, where rainfall and vegetation are sufficient to trap atmospheric silt. However, Dearing *et al.* (2001) produced arguably the most detailed study of any North African loess sequence, including radiometric dating of the Matmata sequence in Tunisia. Dearing *et al.* (2001) argue that the timing of loess deposition is from ~240-~110 ka, correlating episodes of loess deposition with marine isotope glacial stages (MIS 6) and palaeosol development with marine isotope interglacial stages. However, the independent chronology built for this site is dependent upon the combination of a number of OSL/TL methods, with the older ages for the site being supplied by additive dose OSL and TL methods; both of these methods have been demonstrated to be problematic (Roberts 2008 and references therein), with OSL regenerative techniques being the standard, and preferred OSL dating method. The ages derived from the OSL regenerative ages for Matmata are significantly younger, and could suggest a last glacial age for the sequence (Dearing *et al.* 2001).

Not all loess within Spain share the characteristics of the majority of Mediterranean loess deposits. Rose *et al.* (1999) identified the existence of loess on the Balearic Island of Mallorca. Based upon the complex mineralogy and fine texture of the deposits, the authors attribute the deposits to far-travelled atmospheric dust; however, no source region is suggested. Additionally, Rose *et al*. (1999) were able to place geochronological constraints upon the timing of loess accumulation on Mallorca, with deposition occurring within stage 5c as well as during the later glacial stage. Therefore, it is both the timing of deposition of loess on Mallorca prior to MIS 4 and far-travelled provenance distinguishes Mallorcan loess from other Mediterranean loess deposits.

All previous studies have constrained timing by ascribing a last interglacial age to the main soil horizon or through geomorphological constraints. In addition to the deposits on Mallorca, a number of deposits in southern Spain have been identified (Günster *et al*. 2001) which are argued to be loess or loessic in nature. Günster *et al.* (2001) argue that these deposits are local in origin, being derived from weathering of local bedrock, although no data is put forward to support this conclusion. Günster *et al.* (2001) detail five, predominantly secondary (reworked) loess sequences which, through the identification of an Eemian soil at the base of each sequence, they attribute loess accumulation to the last glacial period. Within each of the sequences a number of

weak to moderate soil horizons are noted, which Günster *et al.* (2001) correlate with sub-orbital variation present within the last glacial period.

The paper outlines substantial XRD, micromorphological and grain texture work, however, no result, summary or account of such analysis is presented in order to support the suggested interpretation of the sediments. As such, the work of Günster *et al.* (2001) fails to further understanding of the loess deposits that exist within the region.

The existence of loess within Southern Spain and the Balearics, in addition to their distinctive characteristics (Rose *et al.* 1999), raises a number of key questions. Is there a transitional zone within the Mediterranean region, where the process of silt formation shifts between a North African (desert) model and a Northern European (glacial) model? To date, with the exception of Mallorcan loess, it is argued that the deposits of the northern Mediterranean are derived from local processes. However, it has been demonstrated that varying amounts of North African desert silt reaches the Mediterranean region (e.g. Loÿe-Pilot and Martin 1996, Prospero 1996, Goudie and Middleton 2001). Are there climatic periods within the Quaternary where this silt supply becomes a dominant geomorphological process?

A number of studies have documented the existence of a North African dust component within soils (e.g. Muhs *et al.* 2010, Andreucci *et al*. in print), as a major component of Canarian loess (Suchodoletz *et al.* 2009) and a large body of work exists on modern dust transport to the Mediterranean (for example see Prospero 1996 and references therein). However, from such studies it is unclear whether climatic conditions have ever prevailed that would allow North African dust to be a dominant input to Southern Spain to the extent required to allow loess deposition to dominate.

The physical geography of Iberia results in high levels of erosion, reducing the preservation potential of terrestrial deposits. Therefore, much of our understanding of the region is derived from local marine records, which in this region may offer the most complete sequences for interpreting terrestrial response to Quaternary climate changes. Marine core records from the Iberian Peninsula may offer clues about the shifting sediment supply from North Africa, which in turn may allow inferences to be made about conditions optimum for dust supply to Southern Spain. Figure 3.5 shows the results from Moreno *et al.* (2002) from MD95-2043 located off the southern coast of Spain within the Alboran sea.

Moreno *et al.* (2002) have used a variety of proxy records in an attempt to assess North African dust flux to the Mediterranean basin during the last glacial. They suggest that through this period dust flux was driven by D-O climate cycles, with episodes of high dust deposition associated with

arid stadial periods (figure 3.5). Moreno *et al.* (2002) have identified this pattern of response principally from grain size and mineralogical data. End member modelling of the sediments within the core has enabled Moreno *et al.*(2002) to identify the existence of three grain size populations (EM1, 2, 3), on the basis of modern day grain size relationships, they assign EM3 to fine grained fluvial input, EM2 to coarse grained fluvial input and EM1 to North African aeolian input. Additionally, Moreno *et al.* (2002) have used the Si:K ratio as an indicator of shifting dominance of aeolian and fluvial inputs, respectively. Silica inputs have been assigned as indicators of North African aeolian origin on the basis of the mineralogical composition of modern dust sources in the region, indicated as being rich in quartz (Guieu and Thomas 1996), and Moreno *et al.* (2002) argue that the potassium signal is dominated by the fluvial transport of potassium rich clays (e.g. Illite). Variations in these proxy records are shown in figure 5.3, and there is a clear correlation between peaks in aeolian indicator proxies used by Moreno *et al.* (2002) in association with stadial events through the last glacial. This pattern of response has also been suggested to exist in the record of ODP977A, also located in the Alboran Sea (Bout-Roumazeilles *et al.* 2007, 2012). Bout-Roumazeilles *et al.* (2007, 2012) use clay mineralogy as a tracer of sediment inputs and source arguing that the presence of palygorskite can only be associated with aeolian transport from North African sources. The record of palygorskite occurrence also indicates peak aeolian inputs associated with the stadial events of the last glacial.

Moreno *et al.* (2002, 2004, 2005) and Bout-Roumazeilles *et al.* (2007, 2012) have used this apparent relationship between stadial climates and increased dust flux to reconstruct variations in atmospheric circulation with stadial and interstadial climates (figure 5.3). It is suggested that a sustained, positive NAO type atmospheric scenario exists during stadial climates, produced by a strengthened climatic gradient between the Icelandic and Azores pressure centres. Thus, during a positive NAO circulation, the jet stream is displaced northwards resulting in sustained regional aridity during stadial climates.

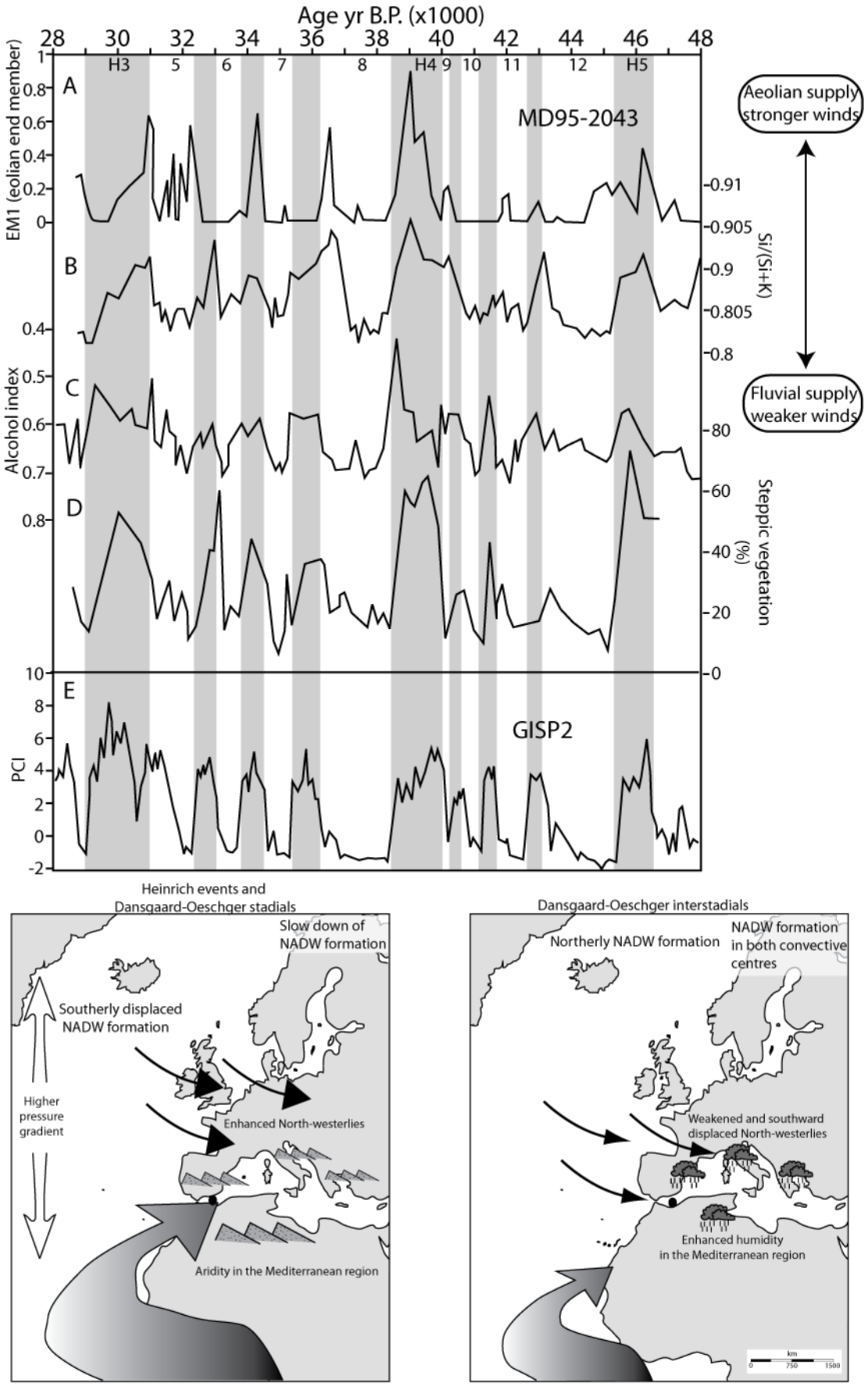

Figure 3.5 Upper: proxy data from MD95-2043 (Moreno et al. 2002). (a) proportional contribution of the aeolian end-member, (b) Si/(Si+K) ratio, (c) alcohol index (deep water formation proxy) n-hexacosanol/(n-hexacosanol+n-nonacosane) from Cacho et al., (2000), and (d) % steppic vegetation Sanchez-Goni et al. (2002) compared with (e) the Polar Circulation Index (PCI) calculated in GISP2 ice core (Mayewski et al., 1994). Lower: Suggested atmospheric conditions during glacial stadial/interstadial events (Moreno et al. 2004)

There are however, a number of issues with these correlations. Firstly, Moreno *et al.* (2002) correlate peaks in aeolian indicators with peaks in steppic vegetation cover (from the same core) as indicating regional aridity. However, if the core is recording substantial shifts in sediment source, it follows that pollen supply must also be shifting, and as such, the pollen record could be showing a shift between Spanish and North African input dominance. It is stated that the occurrence of *cedrus* pollen is an indicator of North African origin (Fletcher and Sánchez Goñi 2008, Carrion 2004); it follows that during times when *cedrus* is reaching the core location, other North African origin pollen would be reaching it too. It is therefore possible that the climatic record within the core is not one of Iberian aridity/humidity with stadials/interstadials, but rather one of shifting air masses or winds in response to the climate cycles of the last glacial.

Secondly, the employment of an Si:K ratio to indicate aeolian input by Moreno *et al.* (2002) appears flawed. Moreno *et al.* (2002) cite Guieu and Thomas (1996) to back up their assertion that North African dust is rich in quartz. However, that study analysed in-situ sediment exposures which were a potential source of dust emission. Studies analysing the composition of North African dust through the Mediterranean indicate varying quartz content, with a substantial Illite component (e.g. Avila *et al.* 1996, Chester *et al.* 1984). This suggests that Moreno *et al.* (2002) are incorrect to assume that fluvial systems must supply the greatest potassium rich sediments to the core.

Finally, the data of Moreno *et al.* (2002) is all proportional and so a change in one component will appear to drive a change in another. This could be particularly problematic when interpreting the shifting dominance of Si:K, and the inferred shift between high fluvial activity and high aeolian activity. It is possible, for example, that the source of quartz (Si) to the site is constant and one is actually recording a switching on and off of potassium rich source sediments, or vice versa. The record of MD95-2043 will be discussed in detail in chapter 12.

3.4 Analysis of loess

3.4.1 Chronology

As loess is an extensive, and sometimes near-continuous terrestrial deposit, understanding and accurately assessing the timing of deposition and pedogenic alteration would enable a detailed understanding of terrestrial response to climate changes over wide geographical areas throughout the Quaternary. Roberts (2008) provides an overview of the application of luminescence within loess studies and discusses the impact recent advances in the technique have had upon previously published dates.

Much of the development within luminescence has been based upon experiments using loess deposits. Primarily this is due to the suitability of the material; luminescence deals primarily with quartz and feldspar which are both abundant within most loess deposits and because of the nature of deposition and transport of loess the luminescence signal is usually fully 'zeroed' prior to deposition.

Luminescence signals are formed from the exposure of grains to ionising radiation (principally the decay of uranium, thorium and potassium in the sediment, and from cosmic radiation) in the environment. This signal builds up steadily over time following the deposition and subsequent burial of the grain, as long as the grain remains buried and is not bleached by re-exposure to sunlight, the luminescence charge will continue to build up with time. Measurement of the stored luminescence charge in the laboratory is then used to calculate the total amount of radiation the sediments had been exposed to since deposition termed equivalent dose (De), given in Grays (Gy). Dividing 'equivalent dose' (De) by the rate at which dose was delivered during burial, the so-called 'dose rate' (Dr) (Gy/ky), gives the luminescence age estimate. Age (ky) = De/Dr

TL dating was the first technique applied to loess in the 1980s (e.g. Wintle 1981). However, there has been a move away from TL dating within recent years due to a number of issues with the technique. The TL signal derives predominantly from feldspar, but also from quartz, with both minerals displaying varying behaviours in terms of emission, bleaching and signal stability. The relative contributions of the minerals were difficult to assess and made it difficult for standard techniques and behaviours to be produced and tested and therefore making ages difficult to compare and reproduce. Roberts (2008) highlights that TL dating requires long light-exposure times to remove unwanted signal and importantly, that an un-bleachable TL signal exists, leading to additive radiation levels and incorrect establishment of equivalent dose.

Huntley *et al.* (1985) were the first to produce an OSL signal from quartz. However, TL remained the primary dating technique for loess until around 2000 when the SAR protocol was introduced (Murray and Wintle 2000). The SAR protocol is a single aliquot, regenerative dose technique meaning that establishment of the natural signal and subsequent laboratory induced signals are undertaken on a single sample (aliquot), allowing for multiple aliquots of each sample to be run using standardised criteria. The introduction of this technique resulted in a significant increase in the precision of ages produced (e.g. 5-10% errors) (Roberts 2008).

The standardisation of the technique also facilitated laboratory comparisons to be made and allowed for correlation between ages and/or sites to be made with confidence. This therefore,

advanced loess studies, enabling high resolution studies to reconstruct deposition rates (e.g. Stevens *et al.* 2006, 2007, Lai *et al.* 2007) and therefore, small scale climatic features.

3.4.2 Sedimentary characteristics

Pye (1984) supplied basic sedimentary characteristics from literature detailing loess profiles within the USA, Europe, China, Asia, South America and New Zealand. Based on geographical location, Pye (1984) assigns each loess profile as either originating from glacial processes (e.g. Europe) or non-glacial process loess (e.g. South America). From this Pye was able to state that the typical composition of deposits recognised as loess are; 50-80% silt (4-63μm), up to 20% clay in unweathered loess and typically 10% sand (although this can be up to 40% of mass in loess classified as 'sandy'). Pye states that the median grain size is typically in the range of 20-40μm, or 15-35μm in weathered loess, although obviously both of these ranges are dominated by influence of wind strength, provenance and proximity to source and degree of pedogenic alteration. Pedogenic alteration of loess produces a reduction in grain size, which is often used as a proxy to strengthen field observations of pedogenic horizons.

Within the Chinese loess plateau grain size has been used as both a correlative tool (for example; Lu and Sun 2000, Vandenberghe *et al.* 1997, Nutgeren and Vandenberghe 2004) and as a palaeoclimatic indicator (for example; Porter and Zhisheng 1995, Xiao *et al.* 1995). However, the use of grain size as an indicator of atmospheric circulation (wind strength and aridity) is dependent upon an understanding of the provenance of material. Again, attempts have been made to model mixing populations of grains in order to unravel transport history (Prins *et al.* 2007). Such an approach has not been applied extensively elsewhere, although Vandenberghe *et al.* (1998) do represent one example of its application in Europe. Vandenberghe *et al.* (1998) argue that there is a correlation between deposited grain size and climate, with finer grain sizes and lower sedimentation rates occurring during warmer periods.

However, there are a number of problems with this approach, which are highlighted by this particular study. Firstly, often the chronologies for such sequences are not strong enough to make robust inferences regarding rates of deposition (see Stevens *et al.* 2006, 2007). In particular, the study presented by Vandenberghe *et al.* (1998) is marred by serious chronological issues with the authors rejecting ^{14}C dates they view as too young in favour of TL dates which support their palaeoclimatological interpretation of the grain size record. Additionally, if no independent record of provenance can be established, it is particularly difficult to draw strong conclusions regarding the relative importance of atmospheric circulation or climate as it is impossible to untangle such influences.

Recent work has introduced the use of mineralogy and isotopes as tracers of dust sources; again much of this work has focussed on the Chinese loess plateau (e.g. Stevens *et al.*2010, 2011, Sun 2002), but there is also work relating to dust sources within the Mediterranean (e.g. Muhs *et al.* 2010) which may be applicable to loess within the region.

Strontium and Neodymium isotopes have been used as genetic fingerprints to identify source regions of loess (e.g. Smith *et al.* 2003, Jahn *et al.* 2001, Sun 2002). The Sr and Nd isotopic composition of mantle and crustal derived rocks is significantly different, allowing an isotopic distinction to be made between these rock types and, therefore, between the sediments derived from them (Grousset and Biscaye 2005). Within bedrock it has been demonstrated that weathering of the rocks does not alter the Nd composition, although Sr can vary according to weathering history (e.g. Cole *et al.* 2009, Hemming 2007). Grousset *et al.* (1992, 1998) and Grousset and Biscaye (2005) have attempted to construct isotopic 'fingerprints' of sediments from within the North African dust supply regions and local bedrock. Such an isotopic database can be used to discriminate between source regions of sediment accumulations supplied by the region (Grousset *et al.* 1998 and refs therein). This has been used to trace dust storm events within the Mediterranean (e.g. Frost *et al.* 1986), the North Atlantic (e.g. Grousset *et al.* 1988) and beyond (e.g. Grousset *et al.* 1998, Grousset *et al.* 1992). Commonly, this technique is used to trace dust input into oceans and ice cores, but less frequently as a tracer of dust source for loess accumulation.

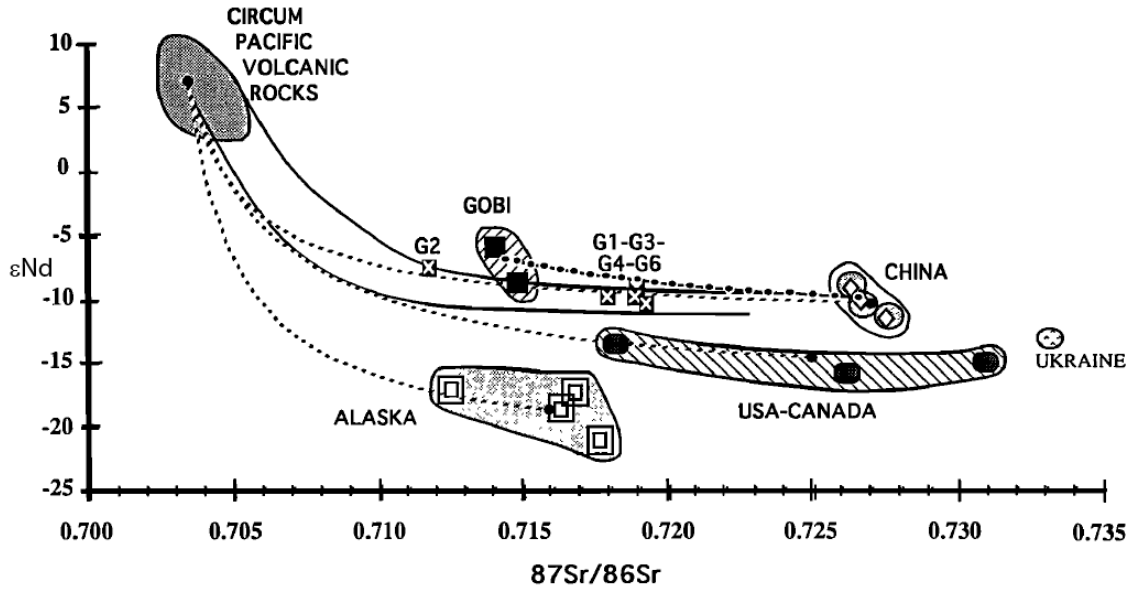

Figure 3.6 Sr vs. Nd plot from Biscaye et al. (1997). Plot used to demonstrate Asian origin of dust in Greenland ice cores (x marks).

Often such work is accompanied by either XRD (X-ray diffraction) data giving 'whole rock' composition and/or trace mineral composition (for example see Smith *et al.* 2003). This allows a secondary line of evidence allowing correlations to be made between deposits and source regions. However, within the Mediterranean, this combination (and even the use of mineralogy alone) has been used primarily as a tracer for modern (e.g. Kubilay and Saydam 1995) and palaeo dust supply (e.g. Erel and Torrent 2010, Muhs *et al.* 2010, Frumkin and Stein 2004), but not as a tracer for the sustained dust source supply enabling loess to accumulate within the region. Both of the previous methods are based upon bulk analysis of sediments, which can, where a mixed provenance is present, identify the proportional input of sources and/or the source itself.

Recently, Stevens *et al.* (2011, 2010) have suggested that the use of heavy minerals and in particular U-Pb dating of zircon grains may aid identification of individual source regions. Although a preliminary investigation of the technique, Stevens *et al.* (2010) were able to identify the multiple source regions giving rise to certain areas of the loess within the Chinese plateau and determine their fluctuating relative inputs allowing for palaeoclimatic interpretations to be made about the varying strengths of wind systems in the region. However, a major issue with the use of heavy minerals is that often identification is undertaken on minerals >63 μm, which results in the identification of sand sources, but not necessarily representative of the far-travelled aeolian silt.

3.4.3 Biological proxies

Biological proxies are relatively rare within loess deposits, as the porous and calcareous nature of the sediments is not well suited for preservation of many organic substances (Muhs 2007). However, molluscs are frequently found within loess deposits, and these have been used extensively to provide reconstruction of the local environment in order to derive climatic information. Molluscan records are constructed by sieving for a large number of individuals from specific horizons or depths of the profile; counts on individual species are then used to construct an assemblage (e.g. Rousseau and Kukla 1994, Moine *et al.* 2008). By combining the environmental conditions preferred by each species present within the population, and accounting for relative abundances, it is possible to infer the local vegetation community and, to some extent, moisture availability. Shifting vegetation and/or moisture availability can then be used to reconstruct shifts in climate (e.g. Rousseau *et al.* 2002).

Examples of the utilisation of molluscan based reconstructions from loess profiles are primarily concerned with loess from the USA (e.g. Rousseau and Kukla 1994) and Europe (e.g. Moine *et*

al. 2008), relatively few studies focus on malacological assemblages from Chinese loess (Rousseau 2001). Malacological assemblage studies of loess were initially focussed on defining the number of climatic cycles recorded within the sequence, through the recognition of interglacial and glacial stage assemblages. However, there is an increasing focus on high resolution molluscan loess studies, in order to identify rapid climate shifts (e.g. Dansgaard-Oeschger cycles) recorded within loess sequences and demonstrate the impact of such climate events on both the terrestrial system and ecological assemblages (e.g. Moine *et al.* 2008).

Predominantly, however, molluscan records provide a localised reconstruction only, and it can be difficult to understand the regional applicability. Additionally, vegetation shifts, on the large scale, are often between shrubby grasslands during times of loess accumulation, towards increased tree or moisture requiring vegetation during times of palaeosol development; often such vegetational shifts can be inferred through understanding the processes required for loess accumulation and alteration. In addition to producing primarily broad climatic inferences (Ložek 1990), the resolution of molluscan studies within loess sequences is low due to the volume of material required, as such, molluscan studies are arguably most useful as biostratigraphic markers (Rousseau 2001) enabling local to regional scale correlation

3.5 Palaeosol evidence

Palaeosols are often recognised during the field investigation of loess sequences, through a shift in sedimentary characteristics, such as grain size and colour. However, particularly when dealing with weak pedogenic horizons, it is necessary to provide evidence that such changes were induced by soil forming processes, as such it is rare that grain size alone is used as an indicator of pedogenesis. As such, a variety of techniques are commonly utilised to aid palaeosol identification, these techniques will be discussed below.

3.5.1 Magnetic susceptibility

Magnetic susceptibility has been used extensively on sequences from the Chinese loess plateau as both a tool for identifying palaeosol development (e.g. Zhou *et al.* 1990, Verosub *et al.* 1993), as a tool for correlation of sequences within the plateau (e.g. An *et al.* 1991), alignment to global climate signals (Kukla *et al.* 1988, Heller and Tung-Sheng 1982, Balsam *et al.* 2005) and as a tool for establishing chronology and sedimentation rates (e.g. Ding *et al.* 2002).

However, the origin of the magnetic susceptibility (primarily thought to relate to the amount of ferromagnetic minerals present) signal within loess-palaeosols is not fully understood, and there are a number of different hypotheses suggested, which affect how the signal should be used and interpreted. Kukla *et al.* (1988) and Kukla and An (1989) proposed that the signal was related to

sediment supply, where a constant supply of ferromagnetic minerals was diluted by increased sediment supply during loess accumulation episodes. The favoured hypothesis was introduced by Verosub *et al.* (1993) which distinguished between lithogenic and authigenic magnetic minerals. Verosub *et al.* (1993) found that there was an increase in authigenically produced magnetic signal within palaeosols; this view was supported by interpretations of Zhou *et al.* (1990) and Maher (1998). However, Meng *et al.* (1997) have suggested that decomposition of vegetation also plays a significant role in the magnetic enrichment of palaeosol layers within the Chinese loess plateau.

The prevailing hypothesis is that, during periods of soil formation, vegetation decomposition and pedogenic processes led to the enrichment of superparamagnetic minerals. These minerals give palaeosols an enhanced high frequency signal relative to lithogenic loess. As such, the frequency dependent signal should be used to express the shifts between sediments dominated by low (un-altered) frequency magnetism and high (pedogenic) magnetism (Sun and Liu 2000). However, as the magnetic susceptibility signal is dependent upon the lithogenic component, areas with perhaps more complex depositional histories, may display more complex magnetic susceptibility signals (e.g. Schellenberger *et al.* 2003, Sun and Liu 2000).

Outside of China, magnetic susceptibility is less commonly used as a tool for dating and/or correlation without additional independent age control (e.g. Rousseau *et al.* 1998) and is more commonly used alongside a wide range of sedimentological techniques to aid palaeoclimatic interpretation (e.g. Rousseau *et al.* 2002, Antoine *et al.* 1999). It is possible this might reflect the more complex provenance and depositional histories of loess outside the Chinese loess plateau.

3.5.2 Carbonate content

Carbonate content of loess sequences is used to suggest pedogenic alteration, typically thought to reflect a ‘top down’ model of modification (Jenny 1941). In this model, development of a stable land surface leads to leaching of carbonate from the upper horizons and redistribution to the lower horizons, with removal and subsequent accumulation being progressive as a feature of time, climate and parent material (Jenny 1941).

Percentage carbonate content is typically used within loess-palaeosol sequences as a supplementary method of pedogenic horizon identification and classification (e.g. Chen *et al.* 1997, Antoine *et al.* 1999). The morphology and distribution of carbonate features throughout loess sequences can be studied on a micro scale and has formed the basis of a wide range of micromorphological studies of loess-palaeosol sequences (e.g. Kemp 1995, 1999, 2001). Additionally, the typical ‘top down’ model (Jenny 1941) of soil development is not always

applicable within loess systems; this has been explored via the use of micromorphology (Kemp 1995, 1999, 2001).

Additionally, it has been demonstrated that the presence of secondary carbonate can dampen magnetic signals (Kemp *et al.* 2004), complicating the interpretation of pedogenic alteration through magnetic susceptibility records. This dampening effect is a result of the negative magnetism caused by materials such as carbonate, which are part of a group called diamagnetic minerals (see Dearing 1999 p. 6). The study presented by Kemp *et al.* (2004) demonstrates the necessity of producing multi proxy studies of loess-palaeosol sequences to fully determine depositional and alteration history.

3.5.3 Micromorphology

Kemp (1985a) has argued that micromorphology is a vital tool for the identification and examination of palaeosols. Loess researchers (Kemp 1995, 1999, 2001, Kemp and Derbyshire 1998, Jacobs and Mason 2007) have suggested that the pedogenic alteration of loess may not be as simple as the top down model of pedogenesis (Jenny 1941) suited to describing the pedogenic alteration of other depositional systems. The traditional view of loess-palaeosol sequences is one of alternating sedimentation and alteration with cold and warm climates respectively. However, Kemp (1995) argues that pedogenic alteration of loess should be viewed as a continuum, with the balance between pedogenesis and sedimentation constantly shifting. This shifting balance is argued to result in two styles of pedogenic alteration; post-depositional (top-down) and syn-depositional or accretionary pedogenesis (Kemp 1995, Kemp *et al.* 1995b). Such a micromorphological approach has become termed a pedo-sedimentary system (figure 3.7).

Kemp *et al.* (1995) and Kemp (1995, 2001) have predominantly used micromorphology as a tool for recognition of weak pedogenesis within loess-palaeosol sequences. Typically, this has been through the identification of shifting concentrations of minor pedogenic features (typically calcitic), such features are generally not identifiable in the field. As such, this enabled Kemp (1995, 2001) to identify pedogenesis that occurred during deposition of the loess (syn/accretionary pedogenesis) in addition to pedogenesis occurring after deposition. Therefore, if the style of pedogenic alteration is recognised, sedimentary and climatic inferences can be made from periods of accumulation (syn-depositional) as well as post-deposition alteration episodes. The ability to recognise weak pedogenic alteration through micromorphological analysis also enables the identification of short lived pedogenic episodes, such as those occurring during interstadial events.

Micromorphological analysis of loess-palaeosol sequences enables a pedo-sedimentary model to be constructed; this framework can then be used to aid interpretation of proxy records from the sequence, which can be of particular value in constraining the timing of precipitation of carbonate features. Additionally, micromorphological analysis can provide information on the types of carbonate features present, which aids material selection for isotopic analysis, and can provide a means of assessing diagenetic modification of material (Budd *et al.* 2002).

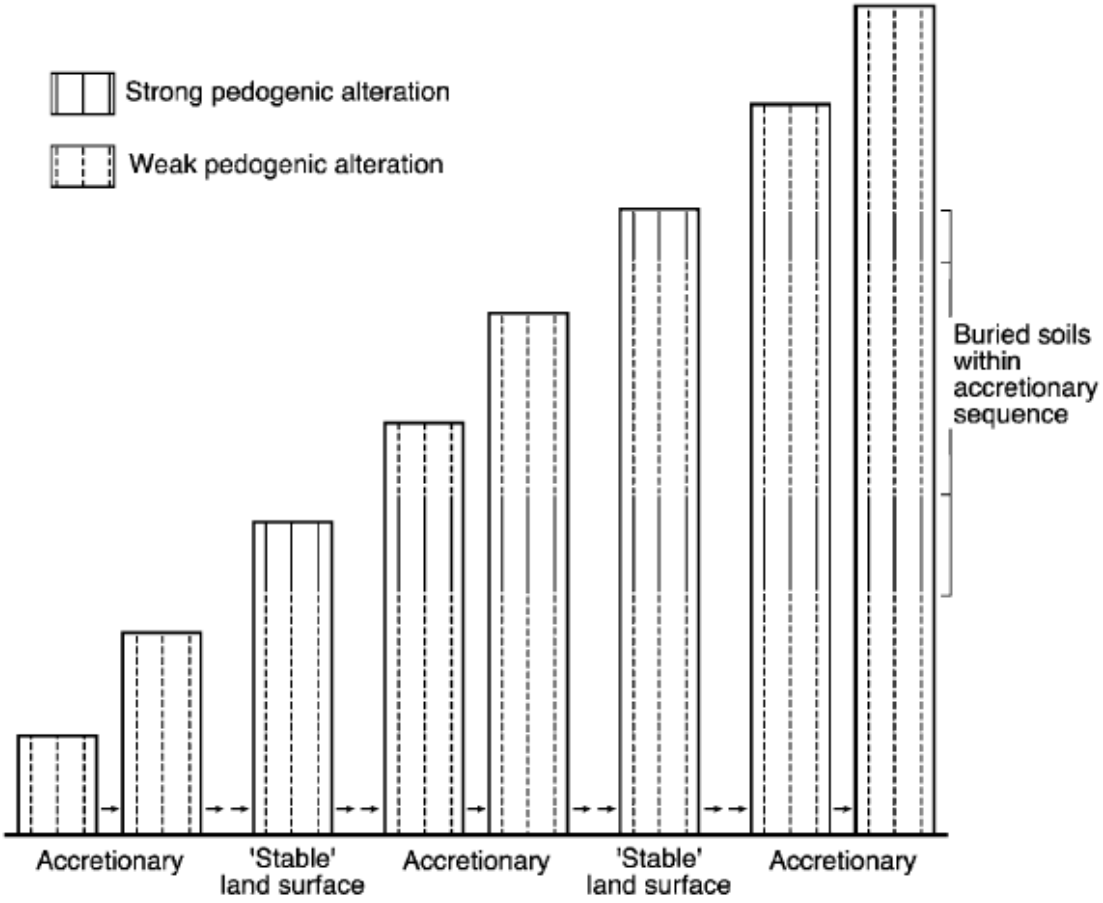

Figure 3.7 Schematic model showing the development of a loess-palaeosol sequence in response to changing dominance of sediment input and pedogenic processes (Kemp 2001). Accretionary alteration of sediments associated with rapid accumulation and weak pedogenic alteration, alternate with periods of strong pedogenic alteration associated with reduced dust inputs and a stable land surface.

3.6 Isotopic composition of soil carbonates

Loess-palaeosol sequences typically contain secondary carbonates (Jiamao *et al.* 1997). The isotopic composition of such carbonates can be used as palaeoenvironmental proxies (e.g. Cerling and Quade 1999). In order that the isotopic composition of soil carbonates (such as those found within some loess-palaeosol sequences) can be considered as a proxy for past climate, certain criteria must be satisfied (Jiamao *et al.* 1997): Firstly, the signal is not inherited or influenced by the parent material, secondly, that the carbonates form in equilibrium with the soil

atmosphere and water; and finally, that no isotopic exchange has occurred since formation. Studies analysing the composition of soil carbonates formed on varying parent material demonstrated that the isotopic composition of the soil carbonates was related to the soil environment, and not the composition of the parent material (Quade *et al.* 1989, Cerling 1984, Cerling and Quade 1993). Cerling (1984) analysed the composition of modern soil carbonates and found a strong relationship between their isotopic composition and that of the local meteoric water and the soil CO_2 composition. Cerling therefore concluded that, where diagenetic alteration has not occurred, soil carbonates are a reliable proxy record for both palaeoclimatic and palaeoecological information. The composition of soil carbonates and their use as proxy records within loess deposits will be discussed in detail in Chapter 4.

3.7 Interpreting loess-palaeosols in the Mediterranean

Loess deposits located within the Mediterranean differ from those which form the basis of the majority of loess studies. Predominantly, studies focus on the thicker, cold-climate sequences of Northern Europe and China. It is unlikely that similar extensive, thick loess deposits could form or be preserved within the Mediterranean. The region is removed from areas of glacial silt production, and secondly, the region is one of high erosion potential. There is therefore a lower preservation potential for any dust accumulation within the region.

Studies on loess within Spain have always assumed a last glacial age, and therefore a cold climate depositional history. However, no direct dating has been undertaken on such deposits, and it is generally an assumption that loess would be deposited during the last glacial. However, the supply sources of loess within southern Spain (either local or North African), and the complex mosaic of vegetation that exists throughout the region (e.g. Tzedakis *et al.* 2003), would not necessarily constrain the timing of deposition to the coldest climate episodes. Understanding the timing of loess deposition within southern Spain and determining its provenance will enable understanding of the terrestrial climate in a region lacking in terrestrial sequences.

The nature of the loess deposits within Spain is generally thought to be secondary (reworked) in nature and are generally relatively limited exposures. However, as detailed in this chapter the numerous techniques which may be applied to the study of loess-palaeosol sequences mean that it is possible to produce detailed palaeoclimatic information, even from limited, and/or secondary loess profiles. In particular the employment of micromorphology and stable isotopic composition of secondary carbonates allows the nature and timing of pedogenic alteration to be understood, and for this to be placed within a palaeoclimatic context.

Chapter 4 – Stable isotopic composition of soil carbonates

Stable isotopes are a key technique for understanding Quaternary climates. The use of this technique within marine and ice cores has demonstrated the validity of the Milankovitch theory of orbital forcing as the key mechanism that drives glacial/interglacial cycles and has led to the recognition of sub-Milankovitch abrupt climate events (McCrea 1950, Emiliani 1955, Shackleton 1967, 1987, Imbrie *et al*. 1984, Stuiver *et al*. 1995; Hughen *et al*. 1996; Rasmussen *et al*. 2008). The stable isotopic composition of soil carbonates has been shown to be a valuable palaeoenvironmental proxy, aiding reconstruction of palaeoclimatic changes on both Milankovitch and sub-Milankovitch timescales (e.g. Cerling and Quade 1993, Andrews *et al.* 1997, Candy *et al.* 2011, 2012, Gallant *et al.* in prep.). Although pedogenic carbonates are common in loess-palaeosol sequences the analysis of their isotopic composition is not a technique which is routinely applied. There are however, a number of environmental factors which can drive and modify the isotopic composition of soil carbonates. Furthermore different mechanisms of carbonate precipitation may lead to the modification of the isotopic signal in different ways. Therefore, an understanding of the environmental factors influencing and controlling the isotopic composition of soil carbonates, as well as an understanding of the mechanisms of their formation, is required in order to correctly interpret the stable isotopic record. This chapter will firstly, introduce the mechanisms, morphology and significance of the style of pedogenic carbonate formation and, finally, discuss the environmental controls on both $\delta^{13}C$ and $\delta^{18}O$ values of soil carbonates.

4.1 Formation of carbonates within loess-palaeosol sequences

4.1.1 Basic chemistry

Isotopic analysis of soil carbonates uses the relative abundances of the light and heavy stable isotopes of carbon (^{12}C and ^{13}C respectively) and oxygen (^{16}O and ^{18}O respectively) to derive palaeoenvironmental data. Although the isotopes of each element will behave in chemically similar ways, their different atomic masses lead to differential bond strengths meaning that they will respond to the effects of temperature, evaporation and phase changes at different energies and rates (Clark and Fritz 1997). This results in fractionation, or separation of the isotopes on the basis of their mass. It is the degree to which fractionation has occurred that enables stable isotopes to be used as palaeoenvironmental proxies.

The oxygen and carbon isotopic ratios of carbonates are measured against, and reported in comparison to, a carbonate standard, Pee Dee Belemnite (PDB and VPDB). Isotope value ratios

(e.g. $^{18}O/^{16}O$) are compared to the isotopic composition of the standard and given as δ values. A negative δ value indicates the sample was depleted in the heavy isotope (e.g. ^{18}O) (or isotopically "light") relative to the VPDB standard, and a positive δ value indicates that the sample was enriched in the heavy isotope relative to the standard. δ values are calculated by:

$$\delta^{18}O = 1000 \times (^{18}O/^{16}O_{sample} - ^{18}O/^{16}O_{standard})/(^{18}O/^{16}O_{standard})$$

Isotope values stated in this thesis are given relative to VPDB for carbonate (or SMOW (standard mean ocean water) for water, where stated).

4.1.2 Formation

This study deals primarily with pedogenic carbonates, which are authigenic carbonates formed *in-situ* by soil processes. Within pedogenic carbonates ($CaCO_3$) the carbon and oxygen are derived from different sources: carbon is derived from the CO_2 of the soil atmosphere, fed through biological processes and atmospheric exchange, and oxygen is derived from meteoric waters (Cerling 1984). Exposure of sediments that are rich in detrital carbonate (e.g. loess) to weathering mobilises Ca^{2+} through dissolution of calcium carbonates, which combines with carbonic acid (H_2CO_3) present in waters to precipitate calcium carbonate ($CaCO_3$). This process can be summarised by the equation below, given in Candy *et al.* (2011):

$$Ca^{2+} + 2HCO_3^- \leftrightarrow CaCO_3 + CO_2 + H_2O$$

The basis of interpreting the isotopic composition of soil carbonates is, therefore, understanding the origin of the oxygen and carbon in the bicarbonate. Bicarbonate forms through CO_2 dissolution in water, where bicarbonate supplies both the oxygen and carbon to the precipitation of calcium carbonate, outlined by the reaction equations below:

$$CO_2 + H_2O \leftrightarrow H_2CO_3$$

$$H_2CO_3 \leftrightarrow H^+ + HCO_3^-$$

$$HCO_3^- \leftrightarrow H^+ + CO_3^{2-}$$

$$CO_3^{2-} + Ca^{2+} \leftrightarrow CaCO_3$$

Therefore, the carbon is derived from the soil atmosphere CO_2 and oxygen from meteoric water in the soil environment. As such, the $\delta^{13}C$ value of soil carbonate reflects the $\delta^{13}C$ value of CO_2 in the soil atmosphere. The $\delta^{18}O$ of soil carbonates preserves a record of the ^{18}O of the water, which in soil systems is fed by local precipitation (Clark and Fritz 1997).

The dissolution of carbonates is enhanced by the acidic nature of rainwater and the uptake of soil organic acid during percolation through the soil profile (Kemp 1985a). Leaching of bicarbonate by soil water occurs in humid environments where the annual soil moisture surplus results in removal of bicarbonate from the profile (Kemp 1985a, 1985b, Decampo 2010). However, in more arid environments there is a soil moisture deficit. Consequently, higher levels of evaporation and degassing from soil profiles in such environments leads to the supersaturation of soil Ca^{2+} in the water. This supersaturation drives the precipitation of calcium carbonate (Tucker and Wright 1991, Decampo 2010, Alonso-Zarza and Wright 2010). Soil carbonates also form in temperate regions, where the presence of highly calcareous sediments or bedrock can result in supersaturation of soil waters with calcium.

The timescales over which pedogenic carbonates form is highly varied, as many factors exert significant influence over the rate of their formation, e.g. parent sediment, climate (moisture and temperature), and vegetation. It has been demonstrated that the formation of well-developed calcrete horizons requires 10^5 to 10^6 years to develop (Machette 1985, Candy *et al.* 2004b, 2005). However, the limited redistribution of carbonate and minor calcite precipitation is likely to occur over much shorter timescales.

4.1.3 Morphology

It has been suggested that the morphology and structure of pedogenic carbonates can aid the interpretation of pedogenic processes and past environments (Kemp 1985a, 1995, 1999, 2001) as well as aiding the interpretation of the isotopic composition of soil carbonates (e.g. Łącka *et al.* 2009, Gallant *et al.* in prep). Barta (2011) has recently provided a review of the literature surrounding the morphologies of secondary carbonates within loess-palaeosols, although there is no consensus or rigid terminology within the literature. I will therefore define the carbonate forms that are significant to this study on the basis of appearance and believed mechanism of formation.

4.1.3.1 Earthworm granules

Distinct granules comprised of intercalated spar crystals are found within some buried soils (figure 4.1a). It has been demonstrated that these originate from the calciferous glands of earthworms and are excreted at the land surface (Canti 1998). Their presence is therefore indicative of a stable land surface, with relative abundance being somewhat indicative of the duration of landscape stability. Recently, work has been undertaken to assess the validity of using the stable isotopic composition of earthworm granules as a palaeothermometer (Canti 2009, Versteegh *et al*. 2011). However, this work is very much in the preliminary stages and

methods for the identification of species from granule morphology may have to be strengthened, as it is possible that species will fractionate isotopes differently.

4.1.3.2 Root pseudomorphs

Within the literature these are referred to with perhaps the widest range of names, including (but not limited to) rhizoliths, rhizoconcretion, rhizomorph, root cast, root tubules (Becze-Deak *et al.* 1997, Barta 2011, Łącka *et al.* 2009). All terms refer to the preservation of root structure through the precipitation of carbonate, typically forming elongate, tubular shapes (Barta 2011) (figure 4.1b). Klappa (1980) provides a review of the formation mechanisms and morphology of root pseudomorphs.

4.1.3.3 Needle fibre calcite

Describes a calcitic form related to microbial processes the calcite appears as needle or rod shaped crystals and is commonly found within pore spaces (figure 4.1c) (Verrecchia and Verrecchia 1994, Loisy *et al.* 1999). The isotopic composition of such forms is most likely to relate to the fractionation processes governed by the microbial agents responsible for precipitation. There has been little work carried out on how the isotopic composition of needle-fibre calcite relates to meteoric waters and as such it is a form that is often left out from isotopic studies of soil carbonates. There has been relatively little work carried out on the isotopic composition of needle fibre calcite. It is thought that microbial precipitation of calcite results in fractionation of both carbon and oxygen, meaning that their isotopic composition is not directly comparable with that of other soil carbonates (Strong *et al.* 1992, Bajnóczi and Kovács-Kis 2006).

4.1.3.4 Hypocoatings

Hypocoatings within thin section are identified as areas of groundmass enriched with calcite around voids (Kemp 1985a) (figure 4.1d). They are formed as soil solutions travel through the pore network and penetrate into the soil matrix (Kemp 1995, Durand *et al.* 2010), but may also be related to the rapid precipitation of calcite due to root metabolism (Wieder and Yaalon 1982). As such, they can form in response to biogenic and/or non-biogenic processes. The formation of such features is thought to be rapid as they are primarily composed of micrite (Kemp 1985a). Often hypocoatings are associated with pore coatings or infillings where micrite, microsparite or spar has precipitated from the calcitic concentration in the groundmass around the void, or through persistent presence of water in the void (Kemp 1985a).

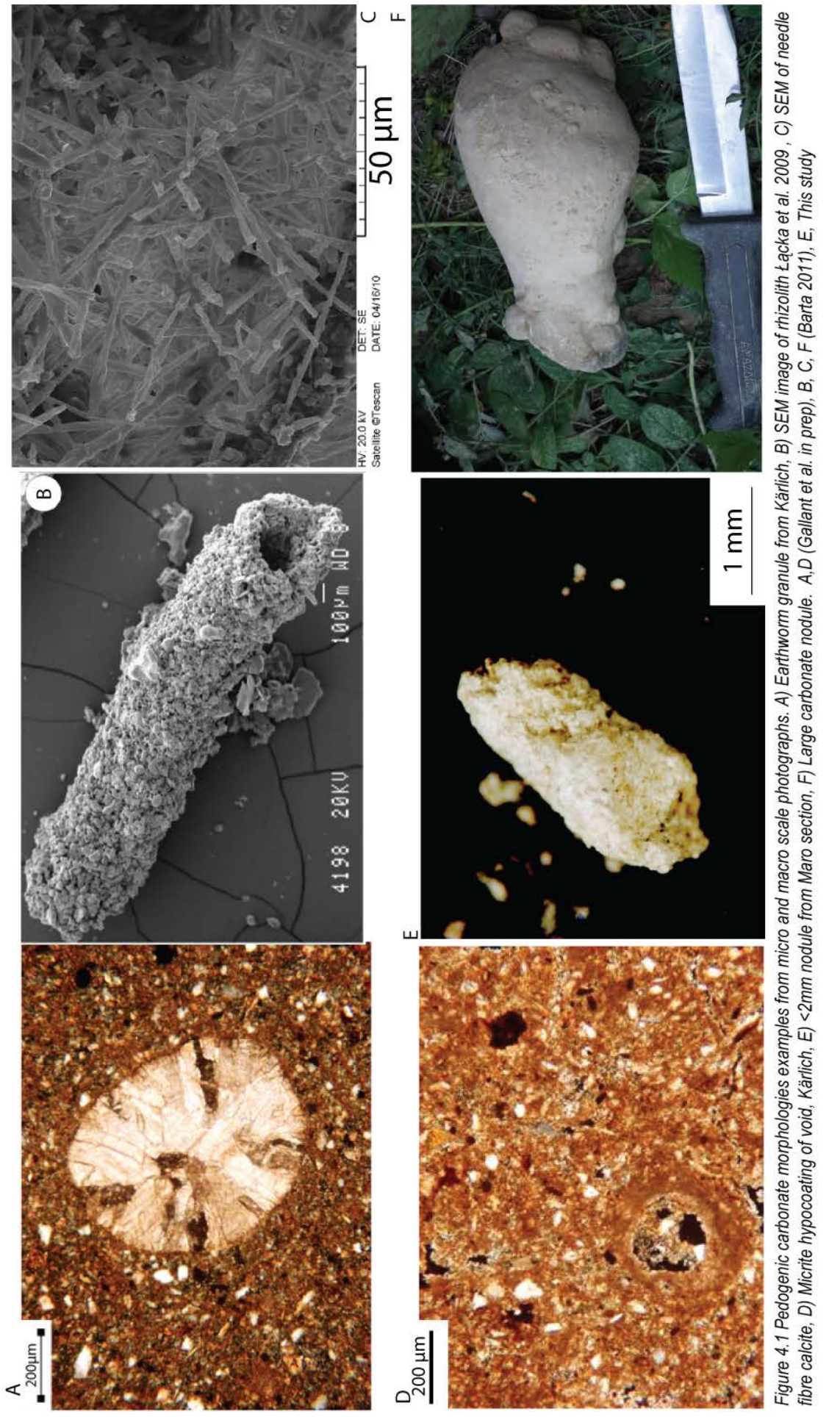

Figure 4.1 Pedogenic carbonate morphologies examples from micro and macro scale photographs. A) Earthworm granule from Kärlich, B) SEM image of rhizolith Łącka et al. 2009 , C) SEM of needle fibre calcite, D) Micrite hypocoating of void, Kärlich, E) <2mm nodule from Maro section, F) Large carbonate nodule. A,D (Gallant et al. in prep), B, C, F (Barta 2011), E, This study

4.1.3.5 Nodules

Primarily within loess-palaeosol studies, the discussion of nodules deals with those typical of calcic soils; these are large, densely cemented carbonates (figure 4.1f), generally located beneath a decalcified zone. Their occurrence relates to extensive decalcification beneath a stable land surface. Their isotopic composition has been studied by numerous authors (e.g. Rowe and Maher 2000, Wang and Zheng 1989). However, within such studies their micromorphology is rarely studied and it is often suggested that such carbonates are subject to reprecipitation and isotopic overprinting through diagenesis (e.g. Deutz *et al.* 2002).

This study will focus on small nodules (<2 mm) (figure 4.1e); such nodules are typical of syn-depositional alteration of sediments (Kemp 1995). Gallant *et al.* (in prep) and Candy *et al.* (2012) demonstrated that such carbonate concretions have the ability to produce high resolution climate records of both accretionary and weakly pedogenically altered loess. As such they offer the potential to develop isotopic studies on loess-palaeosol sequences through both loess accumulation and large scale pedogenic profile development. This technique, therefore, has the potential to investigate climate change during glacial/interglacial and stadial/interstadial periods.

4.1.4 Vertical distribution

The distribution of microscopic pedogenic features through loess-palaeosol profiles have been used to reconstruct pedo-sedimentary models of formation (e.g. Kemp 1995, 1999, 2001, Kemp *et al.* 1995). Although differences in the style of pedogenic alteration affects the distribution of all pedogenic features, only the effects on the morphology and distribution of calcitic features will be discussed, as it is the origin of these features which determines the interpretation of their isotopic composition. Kemp (1995) identified that loess palaeosol sequences can be modified by different styles of pedogenic alteration; accretionary and post-depositional. Accretionary pedogenesis or syn-depositional alteration is the pedogenic alteration of actively accumulating sediments and is thought to be associated with moderate to low rates of sediment input and is dominated by localised mobilisation and reprecipitation of calcium carbonate (Kemp 1995). Post depositional alteration occurs at a stable land-surface and is associated with vertical leaching of calcite and accumulation of reprecipitated carbonate at depth (Kemp 2001).

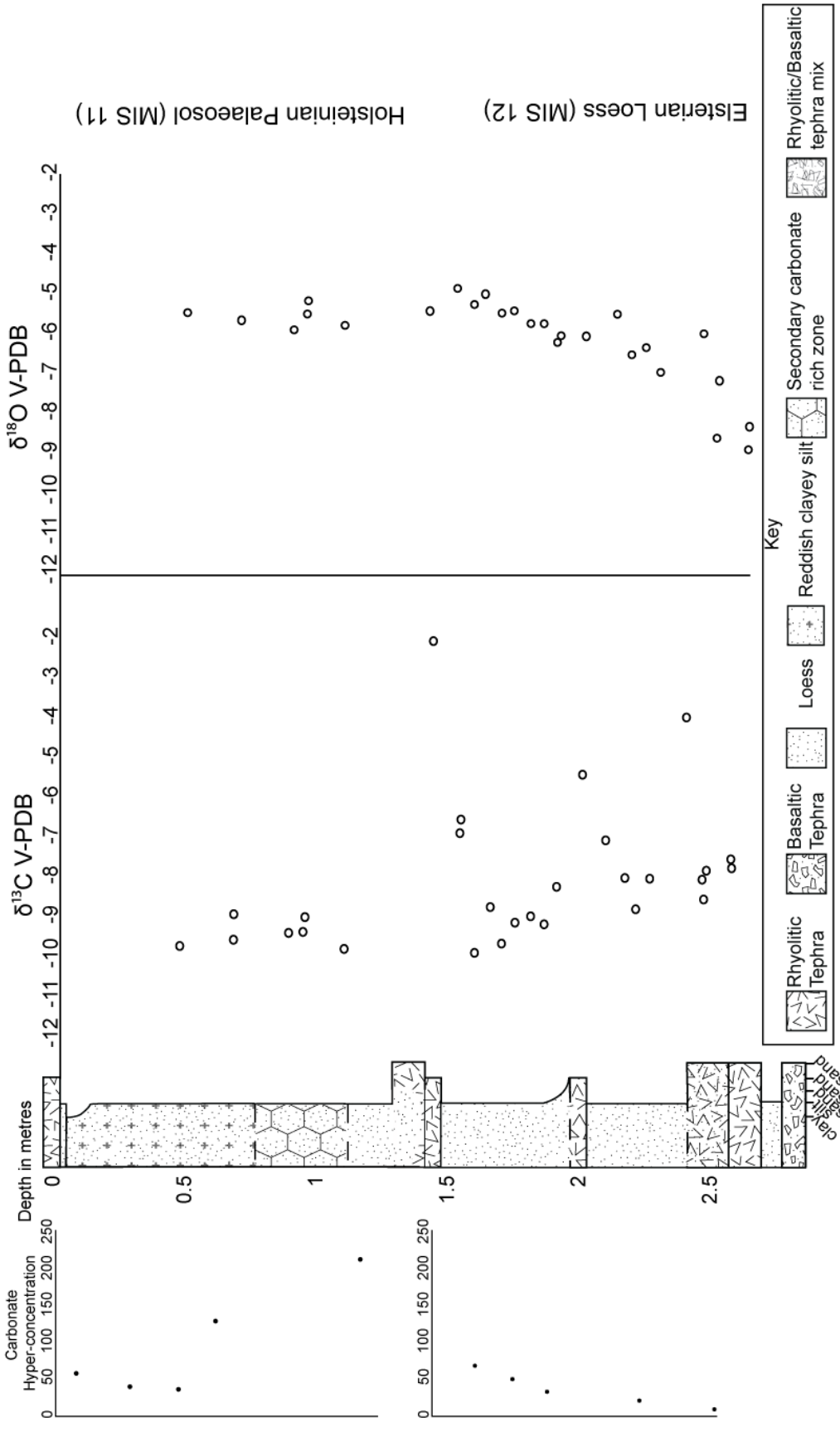

Figure 4.2 Distribution of carbonate pedo-features through loess-palaeosol sequence from Kärlich (adapted from Gallant et al. in prep). Sequence records syn-depositional alteration of accumulating loess during glacial and post-depositional alteration of sediments during the interglacial. This is highlighted by the upwards increasing calcite occurence associated with syn-depositional alteration and the increasing with depth calcite profile associated with post-depositional alteration.

The relationship between the style of pedogenic alteration and the interpretation of the isotopic composition of pedogenic carbonates is highlighted by Gallant *et al.* (in prep) (figure 4.2). Gallant *et al.* (in prep) identified that the accumulation of loess at Kärlich during the Elsterian was associated with increasing accretionary pedogenic modification, marked by the increasing occurrence of carbonate features upwards (lower profile figure 4.2), whereas the interglacial sediments were subject to sustained pedogenic alteration at a stable land-surface, resulting in strong vertical leaching and redistribution of carbonate (upper profile figure 4.2). Therefore, the composition of glacial pedogenic carbonates was identified as recording climate during sediment accumulation through the glacial, whereas the interglacial carbonates recorded an homogenised interglacial signal (figure 4.2).

It is therefore suggested that the distribution and formation mechanism of pedogenic features should be analysed in order to understand the origin of their isotopic composition. This is different to previous studies, which have previously only used the micromorphological analysis of soil carbonates as a tool for identifying the authigenic, unaltered nature of the carbonates analysed (e.g. Łącka *et al.* 2009).

4.2 Carbon isotopes

The $\delta^{13}C$ content of soil carbonates is controlled by the carbon isotopic composition of the soil atmosphere. Soil atmosphere CO_2 is primarily derived from the respiration of plants (Quade and Cerling 2007). During photosynthesis plants preferentially take up $^{12}CO_2$ over $^{13}CO_2$. It has been demonstrated, however, that C3 (e.g. trees and shrubs) and C4 (e.g. CAM grasses) plants preferentially select (fractionate) the light and heavy isotope of carbon to different degrees (Cerling *et al.* 1989) (figure 4.3). Plant respired CO_2 in a C3-photosynthetic pathway-dominant environment has a typical $\delta^{13}C$ of -25.4 ±3 ‰ , whereas C4-photosynthetic pathway plant-respired CO_2 is around -12.4 ± 3‰ (Cerling *et al.* 1989, Cerling and Quade 1993). Through diffusion of CO_2 from the soil atmosphere (+4.4 ‰) and fractionation during calcite precipitation (+9 to 12 ‰), there is an enrichment that occurs during the precipitation of soil carbonate of around 16.4 to 13.4 ‰ at 0-25 ˚C with respect to the $\delta^{13}C$ of plant respired CO_2 (Cerling and Quade 1993). Therefore, soil carbonates will typically have $\delta^{13}C$ of -12 to -9 ‰ under C3-photosynthetic pathway vegetation and 1 to 4 ‰ under C4-photosynthetic vegetation (Cerling and Quade 1993) (figure 4.3).

Much of the literature dealing with the isotopic composition of secondary carbonates within loess-palaeosol sequences therefore aims to use the carbon isotopic composition of soil carbonates as a method of reconstructing relative dominance of C3 vs. C4-photosynthetic pathway plants at the

time of formation (Frakes and Jianshong 1994, Wang and Zheng 1989, Sun *et al.* 2012, Yang *et al.* 2012). In southern Spain however, there is no evidence to suggest the presence of C4 plants throughout the Pleistocene (Quade *et al.* 1994, Cerling *et al.* 1997, Woodward *et al.* 2004) and so, the $\delta^{13}C$ values of soil carbonates in the region should reflect the dominance of C3-photosynthetic vegetation. There are, however, a number of factors which can influence the $\delta^{13}C$ of soil carbonates within a semi-arid region such as southern Spain and these require discussion.

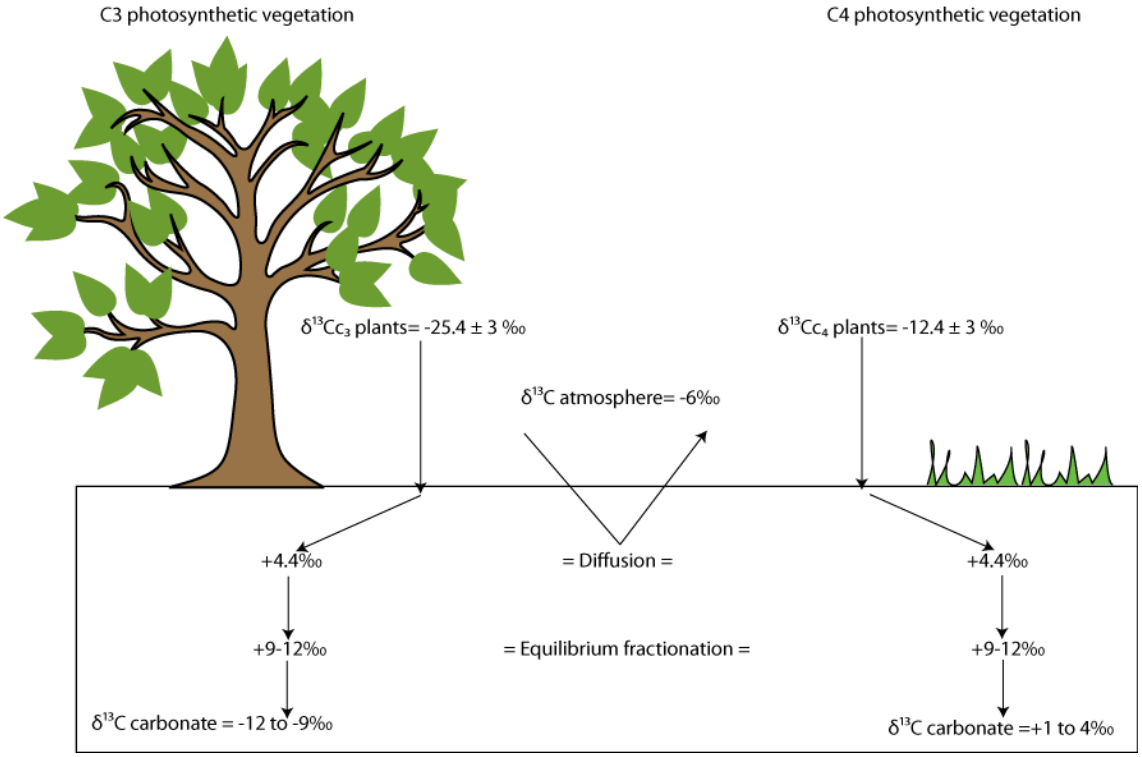

Figure 4.3 Fractionation of stable carbon isotopes by C3 and C4-photosynthetic pathways, adapted from Quade and Cerling (2007) ($\delta^{13}C$ VPDB).

Candy *et al.* (2012) have recently demonstrated that in regions where evaporation rates are high, a significant modification of the typical $\delta^{13}C$ of soil carbonates occurs, through two primary mechanisms. Dever *et al.* (1987) demonstrated that evaporation of soil moisture leads to a reduction in dissolved CO_2 through degassing which preferentially removes the lighter $^{12}CO_2$. Additionally, increased aridity leads to a reduction in biomass, increasing the input of atmospheric CO_2 relative to plant-respired CO_2 (Quade *et al.* 1989b). The isotopic composition of pre-industrial atmospheric CO_2 is around -6‰ (Friedli *et al.* 1986) and as such is significantly enriched in ^{13}C relative to soil CO_2 derived from C3 plants. Therefore, soil carbonates forming under conditions of low vegetation density, where atmospheric CO_2 contributes significantly to soil CO_2, will have enriched $\delta^{13}C$ values. Therefore, a number of processes exist that lead to soil carbonates forming in arid conditions having enriched $\delta^{13}C$ values.

4.3 Oxygen isotopes

Cerling and Quade (1993) demonstrated that the oxygen isotopic composition of modern soil carbonates is directly related to the composition of local meteoric water. It has been shown (e.g. Rozanski *et al.* 2003), particularly within high to mid-latitudes, that the primary control on the composition of meteoric water is air temperature. As such, the composition of soil carbonates can be used as a proxy for palaeotemperature. In practice, however, there are a number of modifying factors which may be hard to quantify and, as such, the employment of soil carbonates as 'palaeothermometers' is often, at best, suggestive rather than quantitative.

This section will therefore discuss (1) the controls on the $\delta^{18}O$ of precipitation, and, (2) the controls on the $\delta^{18}O$ of soil carbonates.

4.3.1 Oxygen isotopic composition of precipitation

4.3.1.1 Temperature and latitude

Dansgaard (1964) first documented the relationship between mean annual temperature (MAT) and $\delta^{18}O$ of precipitation (figure 4.4), identified through the compilation of data from more than 200 International Atomic Energy (IAEA) and World Meteorological Organisation (WMO) stations. Such a relationship between MAT and isotopic composition of precipitation occurs as a result of the different atomic masses of ^{18}O and ^{16}O.

As an air mass cools, precipitation is formed, preferentially forming ^{18}O enriched water as less energy is required to keep ^{16}O in a vaporised state. This results in progressively ^{18}O-depleted precipitation at cooler temperatures (Mook 2006).

This temperature relationship is intrinsically related to the latitude effect. The majority of precipitation is sourced from the tropics (Rozanski *et al.* 2003), as this vapour travels into the higher latitudes, ^{18}O is preferentially rained out. Theoretically, this system is often simplified to one of a non-recycling or closed system (Rayleigh model) so that the water vapour is not recharged, in order that the reservoir is increasingly depleted in ^{18}O through the effects of latitude and temperature.

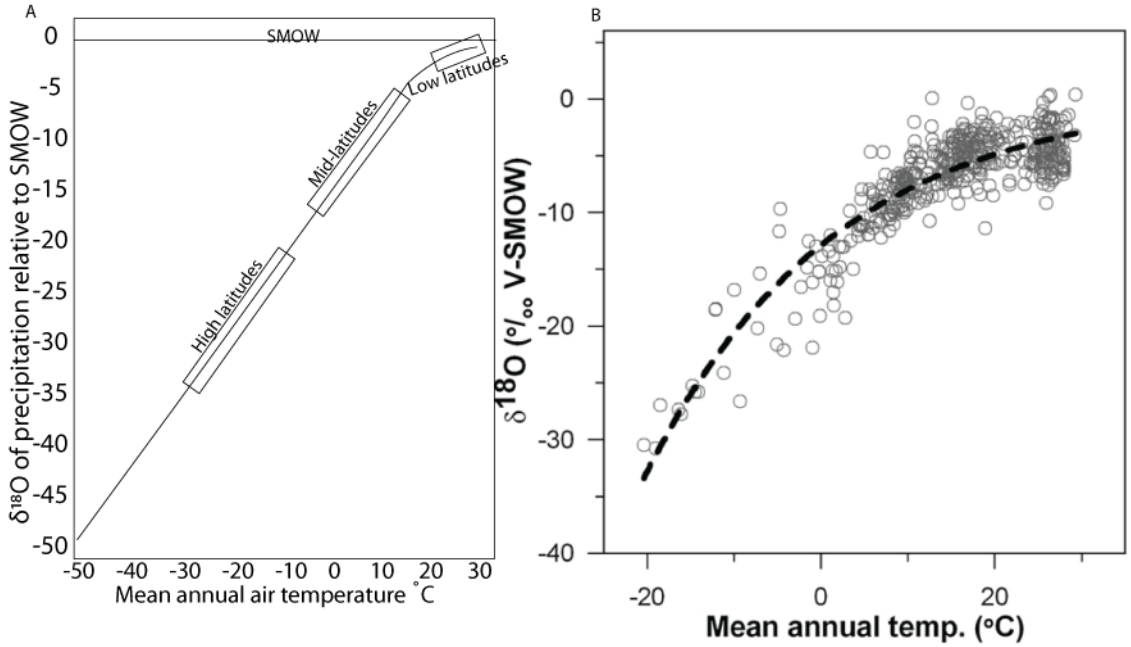

Figure 4.4 Relationship between mean annual temperature and ^{18}O of precipitation (SMOW). A Schematic of relationship (Dansgaard 1964), B. Relationship obtained from worldwide data (van der Veer et al. 2009).

4.3.1.2 Rain out/continental effect

The effects of both rain out and contintentality result in the progressive depletion of ^{18}O in precipitation, due to the preferential rain out of $H_2{}^{18}O$ from cloud moisture (figure 4.4). Rozanski *et al.* (2003) demonstrated progressive ^{18}O depletion in precipitation with increasing continentally, for example in Europe the continental gradient is around -2‰ $\delta^{18}O$ per 1000km. This is also referred to as the distance from coast effect, precipitation falling over ocean, island or coastal stations varies only slightly from the composition of the first condensate of the moisture, whereas stations located with increasing distance from the coast record precipitation progressively depleted in ^{18}O with increasing distance from source (figure 4.5). Again, this is a result of preferential rain out of $H_2{}^{18}O$ due to greater energy required to maintain this heavier water molecule within a gaseous state.

Figure 4.5 demonstrates the initial fractionation of ^{18}O from ocean sources where $H_2{}^{16}O$ is more readily evaporated (kinetic fractionation). Initial rainfall is much less depleted than the initial water vapour as $H_2{}^{18}O$ is preferentially precipitated. This further depletes the remaining water vapour, which acts as a closed system, resulting in increasingly ^{18}O-depleted precipitation with distance from the source (Hoefs 1997).

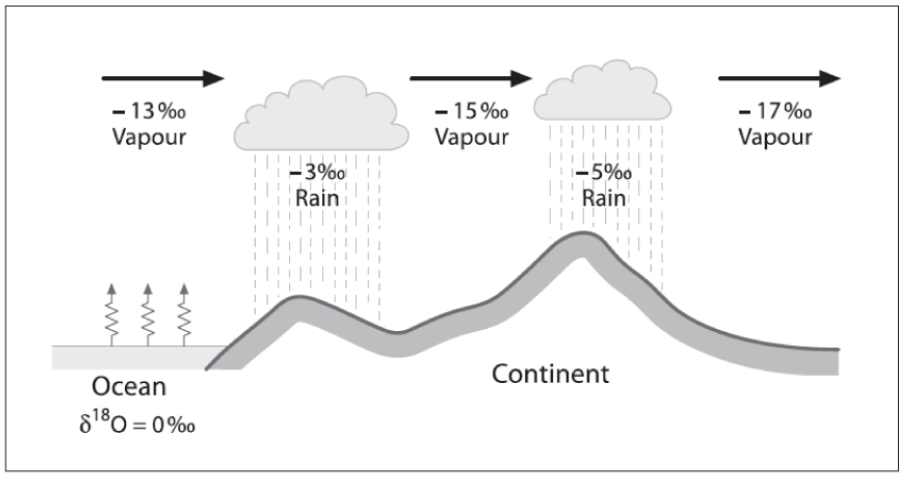

Figure 4.5 Schematic demonstrating the effects of rain out and increasing contintentality on the $\delta^{18}O$ of precipitation (Hoefs 1997)

4.3.1.3 Altitudinal effect

The effects of altitude are driven by the same processes controlling the relationship between rain out/continentality and the isotopic composition of precipitation, where there is an increasing depletion of $\delta^{18}O$ with distance from the first precipitation event. Increasing altitude drives rising air masses and leads to adiabatic cooling, driving rainout (Clark and Fritz 1997), and therefore increasing altitude results in the progressive depletion of ^{18}O through prefential rain out of $H_2{}^{18}O$. The global relationship between altitude and the composition of precipitation is that $\delta^{18}O$ decreases by 2.8 ‰/km (Poage and Chamberlain 2001); however, there is significant variation in local relationships between altitude and the isotopic composition of precipitation (Quade *et al.* 2007) (figure 4.6).

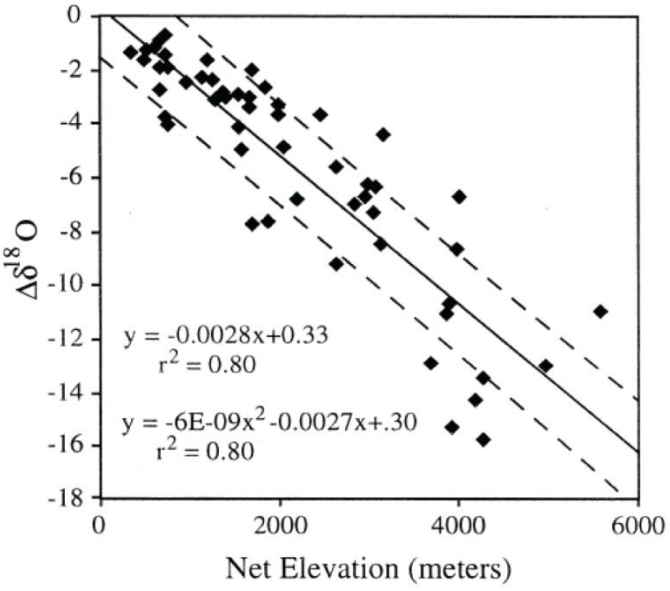

Figure 4.6 Relationship between $\delta^{18}O$ and altitude. Poage and Chamberlain (2001) precipitation data versus altitude, compiled from sites in Europe, North, South and Central America.

4.3.1.4 Amount effect and seasonality

This effect was first noted by Dansgaard (1964) and describes the relationship between the amount of monthly rainfall and its isotopic composition. It is thought that the relationship between precipitation amount and isotopic composition is primarily due to levels of evaporation from the cloud base and falling precipitation (Rozanski *et al.* 1993, Hoefs 1997). During months of low rainfall, evaporative enrichment of falling precipitation occurs through preferential removal of $H_2{}^{16}O$, whereas during high rainfall months there is reduced potential for evaporative enrichment of the $\delta^{18}O$ of falling precipitation (Rozanski *et al.* 1993). This effect is well documented within tropical regions (Mook 2008, Rozanski *et al.* 1993), where precipitation amount can become the dominant control on the isotopic composition of precipitation (figure 4.7).

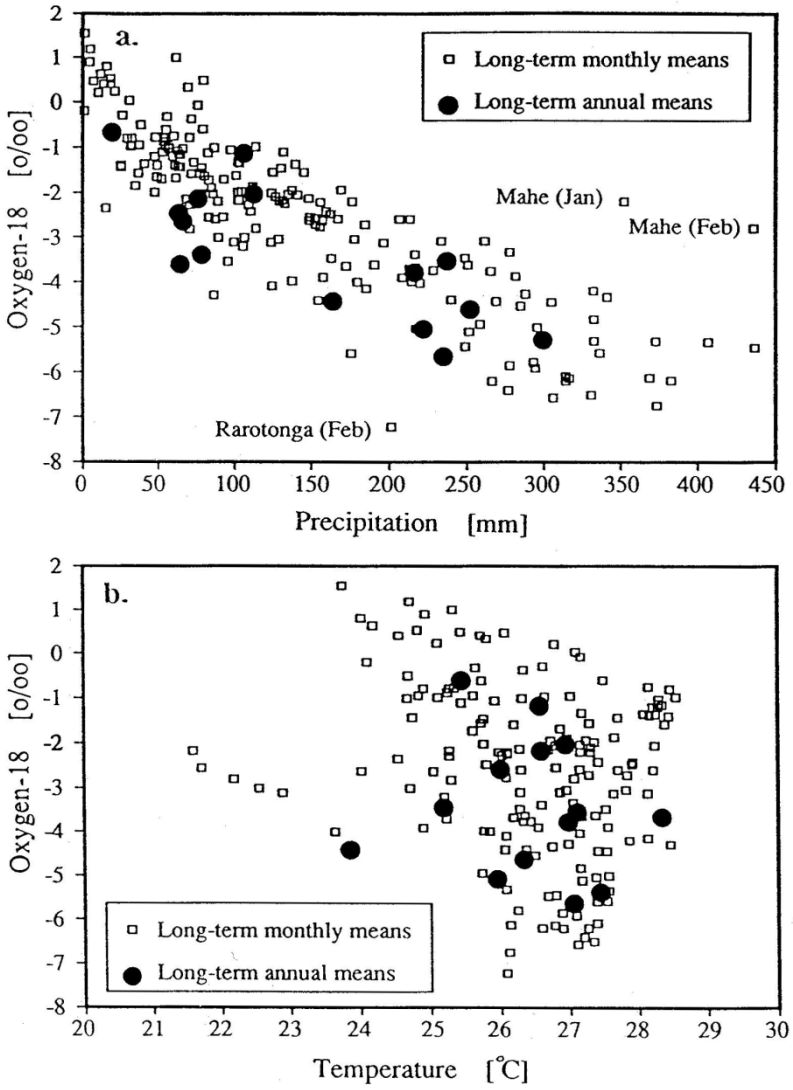

Figure 4.7 The amount effect as the dominant control on $\delta^{18}O$ of precipitation (Rozanski et al. 1993). Long term monthly and mean annual $\delta^{18}O$ values for tropical island stations plotted as a function of; A. Mean monthly precipitation, B. Mean monthly temperature.

Although the amount effect is not a dominant control on the isotopic composition of precipitation in temperate mid-latitude climates, Rozanski *et al.* (1993) demonstrated the existence of seasonal variation of $\delta^{18}O$ of precipitation. Rozanski *et al.* reported relatively enriched $\delta^{18}O$ values for summer precipitation, which they argue is a result, primarily, of increased evaporation from the cloud base. Such evaporative processes, would result in preferential evaporation of lighter $H_2{}^{16}O$, resulting in relative enrichment of $\delta^{18}O$ in the remaining precipitation. This relationship can be modified however, by a seasonal amount effect (Higgins and MacFadden 2004) (figure 4.8). Where environmental temperatures rise above 20˚C and there is significant precipitation, there is a decrease in $\delta^{18}O$ of precipitation, this is due to preferential evaporation of $H_2{}^{16}O$ from rainfall (Rozanski *et al.* 1993, Higgins and MacFadden 2004).

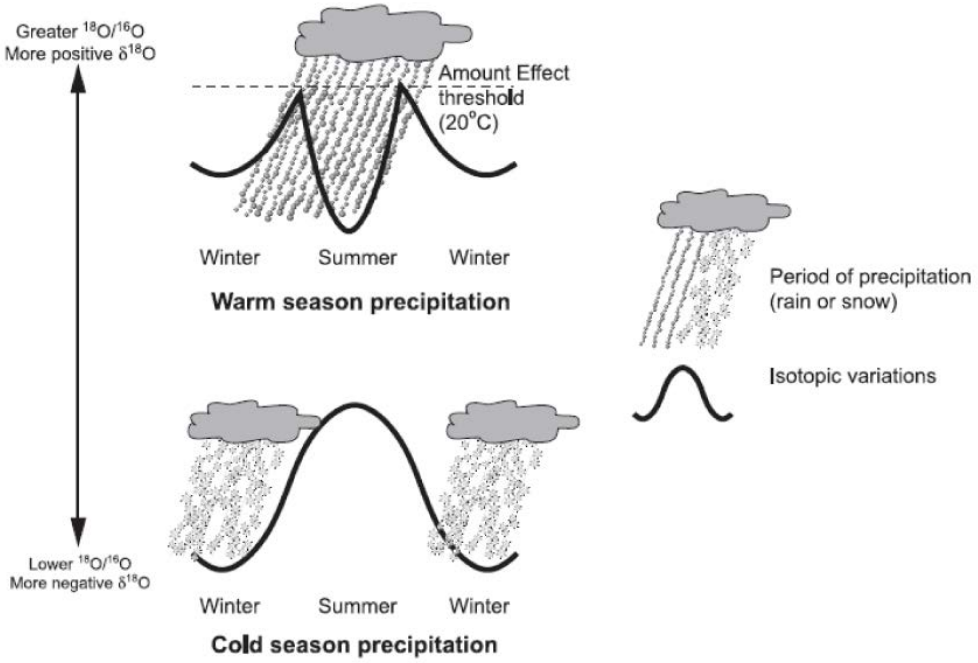

Figure 4.8 Relationship between seasonality and $\delta^{18}O$ of precipitation (Higgins and MacFadden 2004).

4.3.2 Composition of soil carbonates

In most mid-latitude regions, it is argued that the $\delta^{18}O$ value of precipitation is driven primarily by MAT, as soil carbonates form from meteoric waters; it follows that their oxygen isotopic composition should also be driven by MAT. Cerling (1984) identified a close relationship between the composition of soil carbonates ($\delta^{18}O$ VPDB) and the composition of local meteoric waters (figure 4.9), which have been demonstrated to be closely related to MAT (Dansgaard 1964, Rozanski *et al.* 1993). However, MAT is not the only control on the composition of soil carbonates, with fractionation of oxygen isotopes during calcite precipitation also being a controlling process.

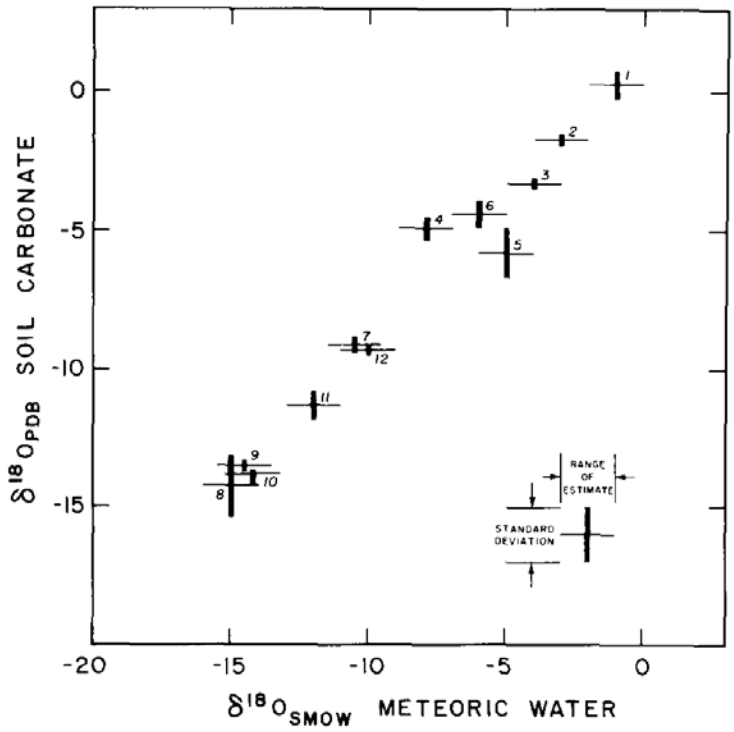

Figure 4.9 Relationship between $\delta^{18}O$ of modern soil carbonates and $\delta^{18}O$ of precipitation (Cerling 1984). Data from Europe, N.America and Africa.

4.3.2.1 Fraction during precipitation of calcite

The precipitation of calcite displays temperature-dependent fractionation of oxygen isotopes (Hays and Grossman 1991, Kim and O'Neil 1997). This relationship is described as a shift in $\delta^{18}O$ of -0.3‰ per +1°C (Craig 1965, Hays and Grossman 1991, White et al 1999, Leng and Marshall 2004). This is due to the thermodynamic behaviour of the isotopes, where it is more likely that in an equilibrium reaction, the heavy isotope (e.g. ^{18}O) is preferentially precipitated into a solid at lower temperatures (Clark and Fritz 1997).

Therefore, it is both the temperature dependent isotopic composition of meteoric waters and the temperature-dependent fractionation of calcite that controls the oxygen isotopic composition of soil carbonates. The relationship between air temperature and the $\delta^{18}O$ value of rainfall is around +0.6‰ per +1°C (Rozanski et al., 1993). This combined with the effect of calcite fractionation (-0.3‰ per +1°C), produces an overall relationship of around +0.3‰ per +1°C in the $\delta^{18}O$ value of a soil carbonate.

4.3.2.2 Evaporation

Evaporation of soil moisture results in enrichment of $\delta^{18}O$ through preferential removal of lighter $H_2{}^{16}O$ (Dever *et al.* 1987, Quade *et al.* 1989); modern analogue studies have confirmed the effects of evaporation (Cerling and Quade 1993, Ufnar 2008), but have been unable to constrain

a fractionation relationship. Candy *et al.* (2012) have recently demonstrated that within Mediterranean soil carbonates evaporation can be the dominant process controlling both $\delta^{18}O$ and $\delta^{13}C$ values. Candy *et al.* (2012) argue that where covariance of $\delta^{18}O$ and $\delta^{13}C$ values occurs, the isotopic composition of soil carbonates is being driven by evaporative processes.

4.4 Applications in loess research

4.4.1 Carbon Isotopes

Carbon isotopes have been used extensively within the Chinese loess plateau to reconstruct levels of C3 and C4 vegetation as a means for inferring monsoonal shifts and associated aridity/humidity (Frakes and Jianzhong 1994, Wang and Zheng 1989 Sun *et al.* 2012, Yang *et al.* 2012). The technique has been applied within the context of European loess; however, it is predominantly to demonstrate C3 dominance (Pustovoytov and Terhorst 2004, Gocke *et al.* 2011).

Within the Mediterranean, it has been demonstrated that, in modern climate conditions, there is a very limited occurrence of C4 plants (Woodward *et al.* 2004, Cerling and Quade 1993) (<10% cover in N.W. Africa and S. Iberia), thought to be limited by the absence of a wet growing season (Tzedakis 2009). Studies have shown that throughout the Quaternary there is no evidence to suggest the existence of C4 plants within the region (Quade *et al.*1994, Cerling *et al.* 1997). However, the resolution (both temporally and spatially) of such studies is low. Therefore, it is thought that the $\delta^{13}C$ composition of soil carbonates within southern Spain will primarily reflect a C3 vegetation. However, $\delta^{13}C$ may not be limited to confirming vegetation composition, but may be a useful indicator of fluctuating aridity (e.g. Candy *et al.* 2012).

4.4.2 Oxygen Isotopes

The majority of studies analysing the stable isotopic composition of pedogenic carbonates formed within loess profiles focus on the carbon isotopes, this is presumably due to the complex controls on $\delta^{18}O$ values. However, there are a number of studies from China (e.g. Jiamao *et al.* 1997, Rowe and Maher 2000, Wang and Zheng 1989, Li *et al.* 2007) and Europe (e.g. Łącka *et al.* 2009, Pustovoytov and Terhorst 2004, Gocke *et al.* 2011) that have utilised oxygen isotopic composition of loess carbonates as palaeoenvironmental proxies.

A number of studies have measured the $\delta^{18}O$ of loess formed carbonates, but have not drawn conclusions regarding the isotopic composition of precipitation or temperature (e.g. Rowe and Maher 2000, Wang and Zheng 1989, Jiamao *et al.* 1997) instead using them to draw broad climatic inferences to support the interpretation of $\delta^{13}C$ values.

However, a number of workers have attempted to draw more quantitative conclusions from $\delta^{18}O$. Li *et al.* (2007) used the composition of soil carbonates to reconstruct composition of precipitation across the Chinese loess Plateau from Holocene through to MIS 5 sediments in order to investigate shifting monsoonal patterns. Łącka *et al.* (2009), using the equations of Dworkins *et al.* (2005), attempted to reconstruct MAT from soil carbonates formed within eastern European loess sequences, identifying limited climate changes from MIS 2-4.

There are a number of issues with these quantitative approaches: the authors do not place the soil carbonates within a pedo-sedimentary framework (through micromorphology) and are unable, therefore, to directly link the timing of formation of the carbonates to climatic events. Additionally, there is no evidence presented to demonstrate that no diagenetic alteration has occurred. Attempting to reconstruct precipitation composition or in particular temperature, in an absolute, rather than relative fashion, ignores the importance of a number of factors which can contribute to the composition of soil carbonates and therefore introduces errors into the methods.

Gallant *et al.* (in prep) have demonstrated that through the establishment of a pedo-sedimentary framework, it is possible to assess compositional changes relative to the timing of their formation (e.g. post-depositional/syn-depositional). This approach enabled the identification of glacial and interglacial climate signals, as well as the identification of a short lived climatic amelioration.

Chapter 5 – Methodology

The aim of this chapter is to explain the rationale behind the selection of the sites and the analysis of the sediments exposed at each site. The methodologies applied to each site are described and the rationale for their application is discussed. In general terms the research has three main objectives; 1) analysis to record changing sedimentary processes within each profile, 2) analysis of characteristics which can provide palaeoenvironmental information, and 3) dating of the sequences in order to place the evidence generated through stages 1 and 2 into a chronological framework. To this end, the methodology is divided into the follows sections:

1) Rationale for site selection and field techniques
2) Rationale for the laboratory techniques chosen
3) Laboratory analysis methods
4) Geochronological techniques and methods

As such, this chapter contains three sections. Firstly, site selection and field techniques are discussed. Secondly, the rationale for the employment of a suite of standard sedimentological and geochemical techniques is introduced and an outline of the methodologies is given. Finally, the technique of optically stimulated luminesce dating (OSL) is introduced and the methodology outlined. OSL dating requires tailoring of the methods used based upon experimental outcomes, and therefore, primary data is provided to illustrate steps taken to produce age estimates for the samples studied.

5.1 Site selection

A number of loess sites in Southern Spain have been detailed in Günster *et al*. (2001); the locations of these sites can be seen in figure 5.1. The exact location of a number of sites could not be ascertained from details given in Günster *et al*. (2001), however, by field walking the areas described by Günster *et al.* (2001) and comparing outcrops with published sediment descriptions it was possible to identify the position of three of the sites listed and identify three new sites (see figure 5.1).

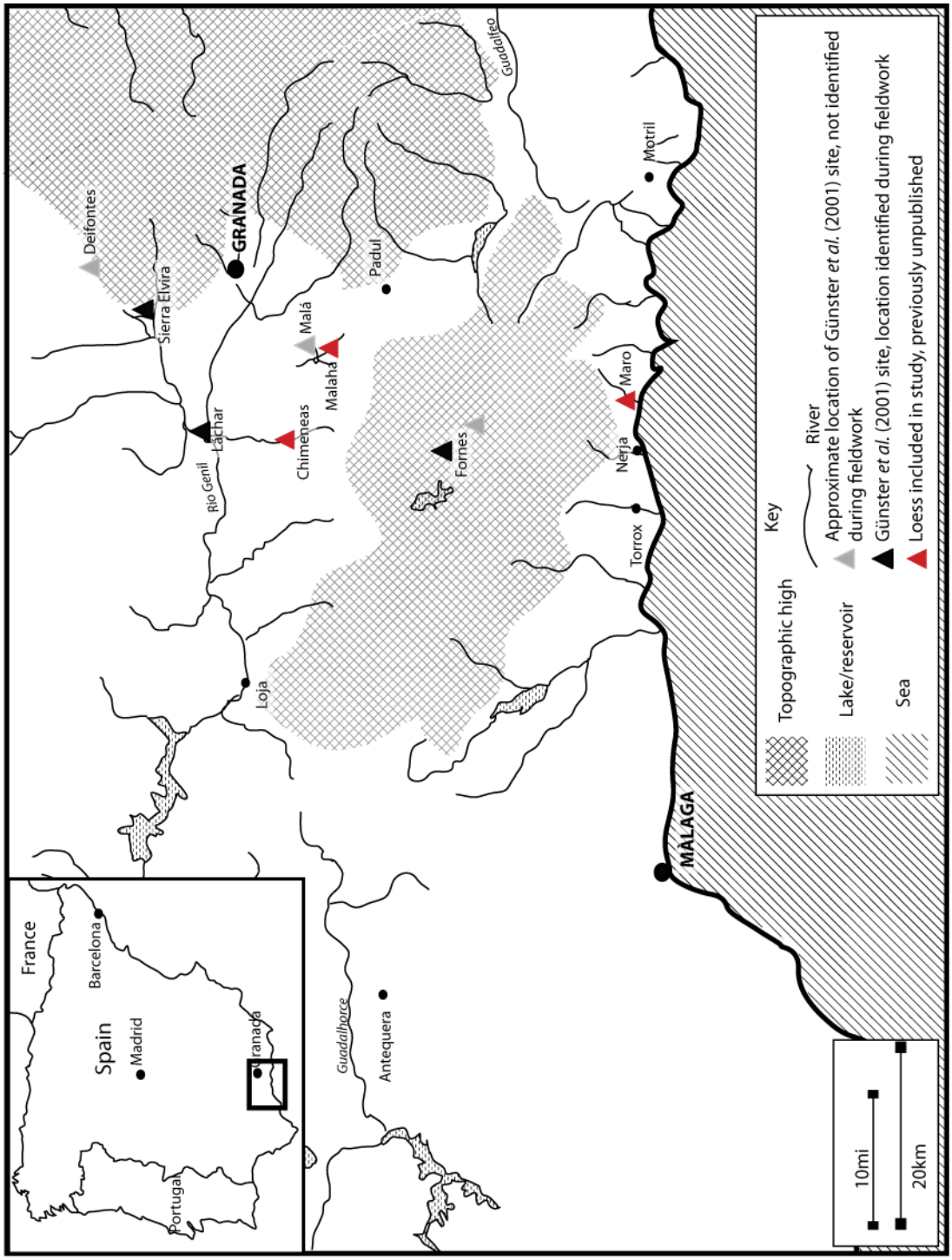

Figure 5.1 Location of sites listed in Günster et al. (2001) and those included within this thesis.

5.2 Field techniques

5.2.1 Logging

Sediment sections were logged, described and sketched to determine their structural (e.g. bedding, unit contacts) and textural characteristics (e.g. colour, sorting, grain size) using standard methods (e.g. Jones *et al.* 1999). Where possible, a single vertical log was constructed to capture the lithological variations within a sediment section, i.e. where only one or two units with little lateral variability were present. Where this was not possible, and sequences were more complex and laterally variable, multiple logs were taken to account for this variability. Photographs were also taken to support field sketches and descriptions. Site specific logging and sampling strategy is detailed in the site chapters (chapters 7-9).

5.2.2 Bulk sampling

Samples for bulk sediment analysis were taken from each site. Vertical transects were placed through the exposure at locations where sediment logs had been recorded. Incremental bulk samples were taken at 5 cm intervals along vertical transects, with each sample consisting of 5 cm by 10 cm by 10 cm of material (Height x Width x Depth). The height of bulk samples was modified where necessary to ensure that samples were not placed across lithological boundaries.

5.2.3 Thin section sampling

Orientated, undisturbed blocks of sediment were removed using Kubiena tins for micromorphological analysis. At each site the position of Kubiena sampling was based on 1) taking samples in order to characterise the sedimentary variability within each unit, and 2) sampling across the boundaries of sedimentary units. An increased density of samples was taken from units that exhibited potential pedogenic characteristics in the field.

5.2.4 OSL sampling

OSL sampling was undertaken at each site, with blocks of 10 cm x 10 cm x 10 cm cut and removed from the section and double bagged in black, light proof bags ready for subsampling in dark room conditions. At all three sites, OSL samples were taken to; 1) constrain the beginning and end of deposition, and 2) to establish the age of major sedimentary units within each section.

5.3 Technique rationale – reconstructing depositional environment

Sedimentological analysis of the deposits was undertaken for three reasons. Firstly, in order to characterise the loess like sediments, and potentially differentiate between loess and other fine

grained sediment deposits present within the region. Secondly, in order to further observations made in the field by quantifying both composition and variability of the sediments both within and between units. And finally, to aid the palaeoenvironmental and pedo-sedimentary interpretation of the sediment sequences studied.

5.3.1 Particle size

Particle size analysis (PSA) quantifies particle size and sorting of the sediments, which aids characterisation of units and deposits. Different depositional environments and transport mechanisms have varying abilities to carry and sort sediments (e.g. Gale and Hoare 1992, Miall 1992). In addition to being a useful indicator of depositional origin, PSA can aid identification of pedogenic horizons where sustained pedogenic alteration results in an increased clay content (Retallack 2005).

5.3.2 Calcium carbonate

Calcium carbonate concentration measurements were undertaken to strengthen distinctions between the sedimentary units identified in the field, but also to strengthen identification of pedogenic horizons, with leaching of calcium carbonate being related to increased pedogenic activity (e.g. Kemp 1985b).

5.3.3 Magnetic susceptibility

Dual frequency magnetic susceptibility measurements enable a measure of total magnetic mineral content (low frequency) and a measure of pedogenic magnetic mineral content (difference between low and high frequency (%cfd)) (Dearing 1999). As such, magnetic susceptibility measurements can aid identification of pedogenic horizons where a large proportion of magnetic susceptibility is produced by superparamagnetic minerals formed through pedogenic processes (high %cfd) (Dearing 1999). Changes in low frequency measurements reflect changes in total magnetic susceptibility, where pedogenic alteration can be excluded as a mechanism driving the low frequency signal (e.g. no change in %cfd, sedimentology or micromorphology), changes can be interpreted as reflecting a shift in the magnetic content of supplying sediment bodies. Therefore, measurement of magnetic susceptibility can be used to discriminate between deposits of different origins and to identify pedogenic horizons (Dearing 1999).

5.3.4 Organic carbon

Identification of pedogenic horizons may also be strengthened through the analysis of bulk organic carbon content. Palaeosol horizons may be recognised due to their elevated organic carbon content. Often, however, palaeosol horizons are associated with only fractional increases

in organic carbon (Retallack 2005). It is thought that palaeosol organic carbon content is reduced by mobilisation due to water and microbial decomposition (Retallack 1991).

5.3.5 Micromorphology

Micromorphological analysis of the sediments of each section can further strengthen distinctions between units and aid interpretation of depositional process by providing further qualitative information for example texture, sorting, and roundedness. One of the key uses of micromorphology is the recognition and description of pedogenic processes (chapter 3). This is particularly useful in loess-palaeosol sequences where pedogenic processes are often viewed as a continuum (Kemp 1995, 1999, 2001), and incipient soils are common. Quantitative micromorphological data of pedogenic features (often not visible at the macro scale) is vital for both the recognition of palaeosols and identification of pedogenic style (accretionary or post-depositional (Kemp 1995)).

5.3.6 Isotopic composition of pedogenic carbonates

The isotopic composition of pedogenic carbonates can be used to reconstruct the vegetation and climate of the environment in which they formed (Candy et al. 2011); the controls on isotopic composition are discussed in chapter 4. $\delta^{13}C$ values reflect the relative proportion of vegetation with a C3 or C4 photosynthetic pathway in the surrounding area (Cerling 1984, Cerling *et al.* 1991, Wang and Greenberg 2006) and $\delta^{18}O$ values are typically thought to reflect the temperature of the region (Cerling 1984, Candy *et al.* 2011), although where there is strong covariance between carbon and oxygen isotopic values it has been suggested that the isotopic system is recording environmental aridity (e.g. Candy *et al.* 2012).

Although carbonate precipitates in loess profiles are common (e.g. Becze-Deak 1997, Jiamao *et al.* 1997), only small (<2 mm) amorphous carbonate concretions (chapter 4) were selected for analysis. These were selected because (1) they were the most commonly occurring form present in the sediments from each site and (2) unlike other carbonate forms their formation does not appear restricted to episodes where pedogenesis is dominant (Gallant *et al.* in prep). Analysis of the isotopic composition of such carbonates should aid palaeoenvironmental reconstruction of the conditions present at the time of sediment accumulation and/or alteration.

5.4 Technique rationale – Identifying loess

The site selection process described previously in section 5.1 outlined the sedimentary characteristics used to identify loess like sediments at study sites. Although depositional processes that are capable of depositing silt-dominated deposits are rare (loess, some overbank

settings, lacustrine) it is important that the presence of loessic material is identified on more than just appearance and basic sedimentology. At each site, silt dominant material was sampled from the modern rivers and slopes (Chimeneas and Malaha) close to the study sites (table 5.1). Along with the palaeofluvial sediments present at each site, comparison of the characteristics of these sediment samples with those from the loess like sediments will enable distinctions to be made.

Table 5.1 Sediment samples selected for defining characteristics of different depositional settings.

	Sample	Location	Sediment type
Modern river and slope sediments	3331	Maro- upstream of schist	River sediments
	3332	Maro- schist and marble catchment	River sediments
	3736	La Malaha	River silt
	3737	La Malaha	Slope material
	3738	Chimeneas- upstream from sequence	River silt
	3739	Chimeneas-at sequence location	River silt
	3740	Chimeneas	Slope material
Palaeo fluvial sediments	3380 (5-10cm)	Maro- section 2	Silty - overbank
	3411 (10-15cm)	Maro- section 1	Silty - overbank
	3443 (342-247cm)	Maro- section 1	Silty - overbank
	3646 (30-35cm)	La Malaha	Sandy silty - overbank
	4031 (0-5cm)	Chimeneas	Sandy silty - overbank
	3953 (130-135cm)	Chimeneas	Sandy silty - overbank
	3956 (160-165cm)	Chimeneas	Sandy silty - overbank
	4035 (470-475cm)	Chimeneas	Sandy silty - overbank
Loess sediments	3369 (60-65cm)	Maro- section 2	Predominantly silt
	3361 (96-98cm)	Maro- section 2	Predominantly silt
	3357 (113-118cm)	Maro- section 2	Predominantly silt
	3453 (390-395cm)	Maro- section 1	Predominantly silt
	3456 (405-410cm)	Maro- section 1	Predominantly silt
	3466 (445-450cm)	Maro- section 1	Predominantly silt
	3638 (70-75cm)	La Malaha	Predominantly silt
	3624 (140-144cm)	La Malaha	Predominantly silt
	3991 (235-240cm)	Chimeneas	Predominantly silt
	3974 (248-253cm)	Chimeneas	Predominantly silt
	4014 (358-363cm)	Chimeneas	Predominantly silt
	4018 (377-382cm)	Chimeneas	Predominantly silt
	4026 (417-422cm)	Chimeneas	Predominantly silt

The landscape of Southern Spain means that, beyond loess processes, overbank deposits are the most likely units to be silt dominated. However, although superficially similar, because loess and fluvial silts have different provenances, transport pathways and transport dynamics, many of the sedimentary and geochemical characteristics may be very different. In order to differentiate between depositional mechanisms producing silt rich deposits, sedimentological characteristics (PSA and $CaCO_3$ content), mineralogical information (XRD data), grain shape and texture (SEM) and isotope geochemistry (Sr-Nd isotopes) were analysed for the samples listed in table 5.1 (SEM and Sr-Nd not carried out on all samples, chapter 6). Theoretically, it should be possible to

differentiate between loess(ic) sediments and overbank sediments using the following techniques;

1) PSA
2) $CaCO_3$
3) Mineralogy (XRD)
4) SEM analysis of grain surface textures
5) Sr and Nd isotopes

5.4.1 Particle size

Overbank or fluvial deposition is unlikely to result in a silt peak as pronounced as those seen in typical loess sequences (see chapter 3); this is due to mixed energies being present in both systems and also sorting processes that occur during sediment settling e.g. in an overbank environment a silt peak would be overlain by settled clay. Fluvial systems (including overbank environments) have the ability to transport a coarse sediment fraction (e.g. sands and gravels), which aeolian transport of dust does not have. Additionally, PSA should distinguish aeolian silts from colluvial slope deposits, due to the different levels of sorting present in the two systems.

5.4.2 Calcium carbonate

Loess deposits are typically rich in carbonates (Pye 1984), whereas deposits derived from a fluvial transport system are likely to contain much less carbonate. Calcium carbonate is a highly soluble compound and so is easily dissolved during fluvial transport, whereas aeolian transport mechanisms are less likely to remove and reduce the carbonate content of the eroded material. As such, aeolian systems have a greater potential to retain a high carbonate content. However, this signal can be modified by pedogenic alteration and may change according to sediment source.

5.4.3 Mineralogy (XRD)

In the study region fluvial and slope processes work over relatively short distances. In the Sierra Nevada short, seep-sided catchments are common and are the topographic setting of all of the study sites. In contrast, aeolian silts can be transported over great distances in the high atmosphere. As a regional example it has been shown that Saharan derived sits are regularly transported to the Canaries (Suchodoletz *et al. in press*), Southern Spain (Lyamani *et al.* 2005) and the Balearic Isles (Muhs *et al.* 2010). Undertaking XRD analysis of the sediments will allow us to determine the mineralogical composition of the samples, with the fluvial and slope samples

providing a locally derived signal for each site and the loess like sediments having the potential to have a non-locally derived mineralogy.

5.4.4 SEM grain surface textures

SEM analysis of grain shape and surface textures has been suggested to be a useful technique for discriminating between different depositional processes (e.g. Krinsley and Doornkamp 1973). The majority of the literature deals with the morphology of sand sized quartz grains (Krinsley and Smalley 1972, Krinsley and Doornkamp 1973, Bull 1981), and examples of loess grains typically refer to glacially derived silts (e.g. Cegla *et al.* 1971). At present, therefore, there is no accepted system for the identification of the source of silts within arid and semi-arid regions. For this reason, SEM analysis has been used to investigate if differences in morphology and/or surface texture exist between fluvial and loess like sediments, but palaeoenvironmental inferences are not made based upon identified characteristics.

5.4.5 Sr-Nd isotopic composition

5.4.5.1 Rationale

It may be possible to differentiate between depositional environments on the basis of their Sr and Nd isotopic ratios, due to the localised sediment supply of fluvial and slope systems and the potential for aeolian dust to travel over much larger distances. The Sr and Nd isotopic composition of sediments relates to the rocks from which they derive, with mantle and crustal derived materials having different isotopic compositions (e.g. Faure 1986) (figure 5.2). As such, sediments deriving from different areas and different transport pathways will inherit their Sr and Nd composition from a unique mix of sediments. This has been previously demonstrated within the Mediterranean where the technique was employed to differentiate between Nile terrigenous sediments and North African aerosol input in the eastern Mediterranean basin (Weldeab *et al.*2002).

Therefore, within this study the isotopic composition of sediments from modern slope and river systems along with and palaeo-fluvial deposits should be distinguishable from those of loessic deposits. Loess deposition will typically contain a far-travelled component, whereas fine grained sediments within other terrestrial systems (e.g. fluvial) will be dominated by local systems (e.g. the Sierra Nevada). In addition, comparison of the isotopic composition of the aeolian sediments with published data from North African dust sources may help to identify possible source regions of the loess deposits included within this study.

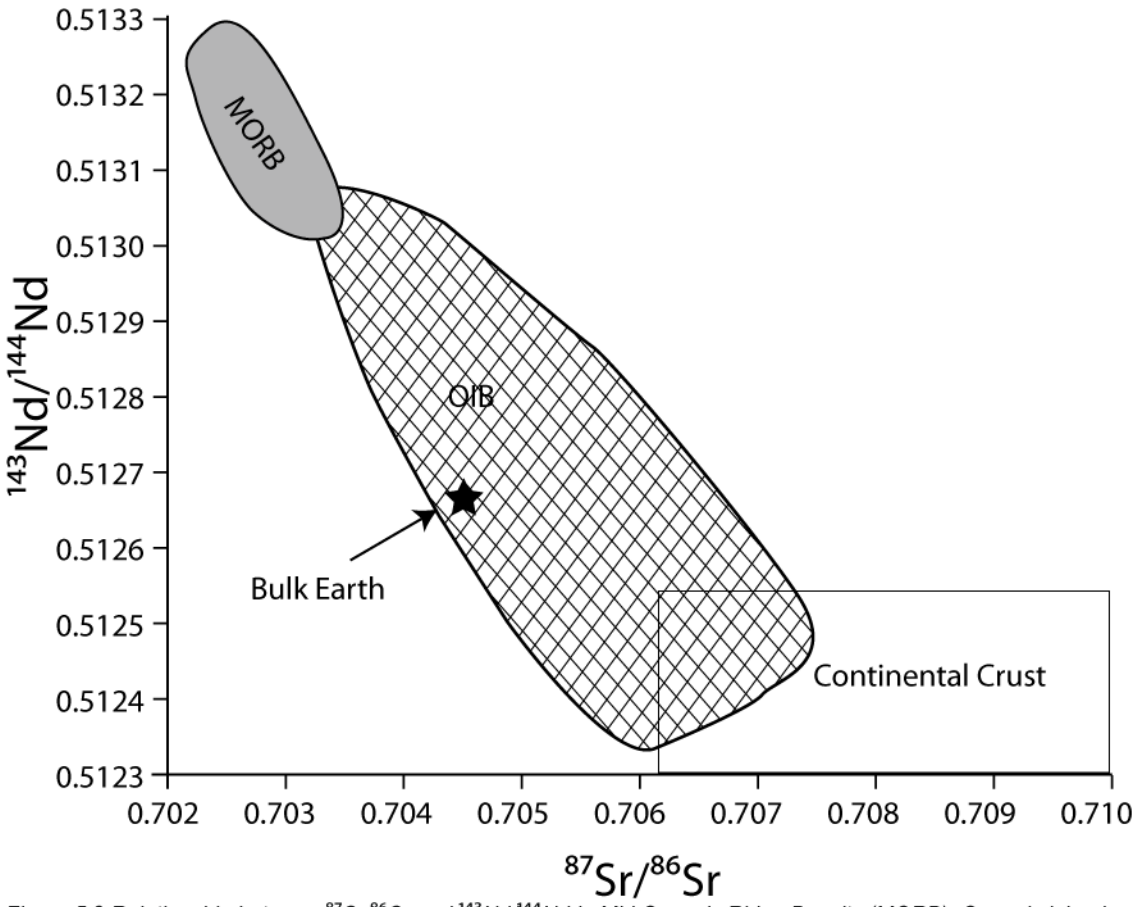

Figure 5.2 Relationship between $^{87}Sr/^{86}Sr$ and $^{143}Nd/^{144}Nd$ in Mid Oceanic Ridge Basalts (MORB), Oceanic Island Basalt (OIB) and Continental crust (adapted from Albaréde 2003)

5.4.5.2 Controls on isotopic composition

Neodymium ratios are given as $^{143}Nd/^{144}Nd$, where ^{144}Nd is unradiogenic and ^{143}Nd is a radiogenic isotope produced by the decay of ^{147}Sm (Faure 1986). Rocks of a crustal origin have lower $^{143}Nd/^{144}Nd$ ratios than mantle derived rocks. This is because Nd is a more incompatible element than Sm, meaning that melts have lower Sm/Nd ratios than the source and hence evolve to lower $^{143}Nd/^{144}Nd$ values (Albaréde 2003). This initial fractionation is the most important control on the $^{143}Nd/^{144}Nd$ ratio of old rocks, as the half-life of ^{147}Sm is very long ($T_{1/2}$ = 1.06 x 10^{11} y) (Faure 1986) and so only alter the $^{143}Nd/^{144}Nd$ ratio of rocks of a great age (i.e. that which formed the crust), which may help differentiate between very young and very old geological sources (e.g. Cole *et al.* 2009). Both Sm and Nd are unaffected by weathering (Goldstein et al.1984; Taylor et al. 1983) and so, $^{143}Nd/^{144}Nd$ is always a reflection of the geological source of sediments.

Strontium ratios are given as $^{87}Sr/^{86}Sr$, where ^{86}Sr is unradiogenic and ^{87}Sr is a radiogenic isotope produced by the decay of ^{87}Rb (Faure 1986). Crustal rocks have higher $^{87}Sr/^{86}Sr$ ratios than mantle rocks, as ^{87}Rb is a highly incompatible element (readily crystallises from mantle) (Albaréde 2003). The mantle is therefore, relatively depleted in ^{87}Rb and so has evolved to lower $^{87}Sr/^{86}Sr$ than the crust. As such, the $^{87}Sr/^{86}Sr$ ratio of sediments can be used to differentiate

between different deposits sourced from different sediment compositions and sources (e.g. Grousset and Biscaye 2005). However, the Sr isotope system is more affected by weathering than the Nd isotope system. In systems affected by long term weathering the sediments show elevated $^{87}Sr/^{86}Sr$ values, due to the behaviours of Sr and Rb (Hemming 2007). Rubidium has a similar ionic radius to potassium, which enables Rb to substitute for K in K-bearing minerals, such as clays (Faure 1986). Strontium has a somewhat similar ionic radius to calcium and so can substitute for Ca in minerals such as calcium carbonate (Faure 1986). Therefore, in weathering environments where clays are produced and calcium carbonates can be removed sediments become relatively enriched in ^{87}Rb, ultimately increasing the $^{87}Sr/^{86}Sr$ ratio. Additionally, as Rb is a better substitute for K than Sr is for Ca (Faure 1986), Sr is more readily removed by weathering processes (Hemming 2007). However, this weathering induced increase in $^{87}Sr/^{86}Sr$ ratio is reversed in sediments which have only undergone recent weathering (Hemming 2007). In environments where Rb enrichment is recent, there is lower ^{87}Sr (through removal and lack of radiogenic decay) and ultimately a lower $^{87}Sr/^{86}Sr$ ratio (Hemming 2007). It has been shown that acid pre-treatment of sediment samples can eliminate the contribution to Sr ratios from weathering derived materials (Nobre Silva *et al.* 2010), enabling the Sr ratio of unaltered sediments to be analysed (figure 5.3).

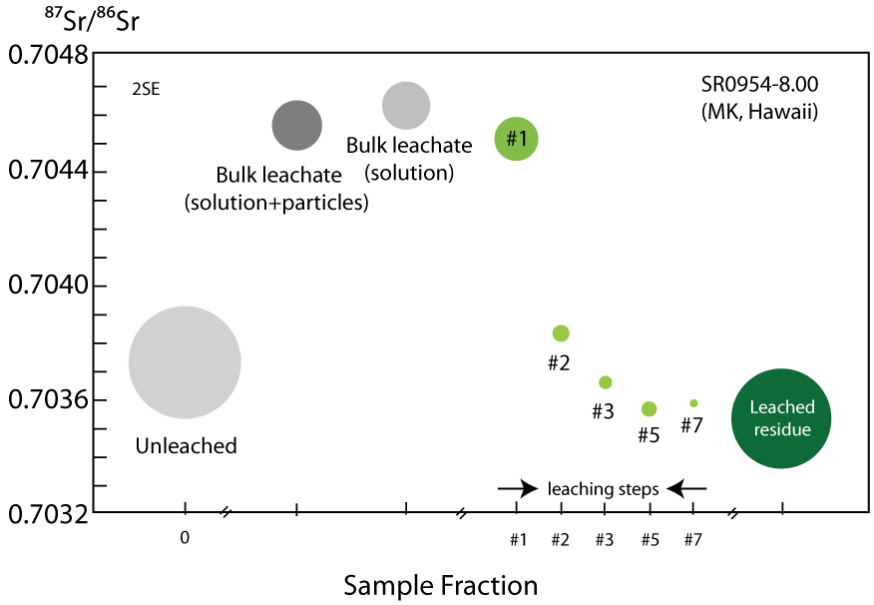

Figure 5.3 Effect on Sr composition of acid leaching (pre-treatment) (Nobre Silva et al. 2010). Unleached bulk sample records mixed Sr composition between leached residue and leachate, where leachate has a high Sr ratio due to the effects of weathering.

5.4 Methods of analysis

All bulk samples were air-dried and prepared according to the quality control laboratory procedures of the Departments of Geography and Earth Sciences, Royal Holloway, University of

London. Repeat samples and/or laboratory and international standards (isotopic analyses) were run alongside analysis of samples, demonstrating in all cases that the analytical error (precision and accuracy) was negligible.

5.4.1 Particle size, calcium carbonate content, magnetic susceptibility and organic carbon

PSA was undertaken on all bulk samples collected from all sites, following the methodology outlined in Gale and Hoare (1992), seen in figure 5.4. The >63 μm fraction was measured using a dry sieve stack and the <63 μm was measured on a Micrometrics Sedigraph 5200 PSA system. No chemical pre-treatment, such as hydrogen peroxide or acetic acid was used during sample preparation. Calcium carbonate content of the bulk samples was determined using a Bascomb Calcimeter (Avery and Bascomb 1974). Organic carbon content was calculated using the Walkley-Black method (Hesse, 1971). Magnetic susceptibility of each sample was measured using a Barington MS2 meter on low and high frequencies, following Dearing (1999).

5.4.2 Micromorphology

Thin sections were prepared following the method set out in Palmer et al. (unpublished). Descriptions were made following Kemp (1985a) and Bullock *et al.* (1985). Each thin section was divided into six areas, with full descriptions being made on each area, in order that variability of features could be placed in a stratigraphic context. General characteristics, sorting, void occurrence and coarse:fine (c:f) composition was noted. Void occurrence data were measured as a visual estimate of slide coverage as outlined in Bullock *et al.* (1985). Further information relating to relative dominance of void types was noted for each section of the thin section, using terminology outlined in Kemp (1985a): Predominant >70%, dominant 50-70%, frequent 30-50%, common 15-30%, few 5-15%, very few 2-5%, rare 0.5-2%, very rare <0.05%, where percentages relate to proportion of total voids. This descriptive process was followed for categorisation of organics, redoximorphic and crystalline concentration/depletion features. For each, total area of slide coverage was noted, with proportion of individual features recorded. For example, a description noting 5% void cover, with dominant vughy, common vesicle and common channel voids indicates that 5% of the total area of the slide was composed of void spacing; where 50-70% of those voids are vughy, 15-30% vesicle and 15-30% channels.

5.4.3 Isotopic composition of pedogenic carbonates

Pedogenic carbonates were hand-picked under a microscope from the <2 mm material retained from the initial sieving stage (see figure 5.4). Once picked, samples were powdered using an agate mortar and pestle. The stable isotopic composition of the carbonate was measured using a

VG Prism series 2 mass spectrometer. Samples were immersed in phosphoric acid at 90˚C, the CO_2 liberated through the subsequent reaction was analysed to give the $\delta^{18}O$ and $\delta^{13}C$ isotopic composition of the sample. Internal (RHBNC-PRISM) and external (NBS-19) standards were analysed every 10 samples to ensure accuracy and reproducibility (data in appendix).

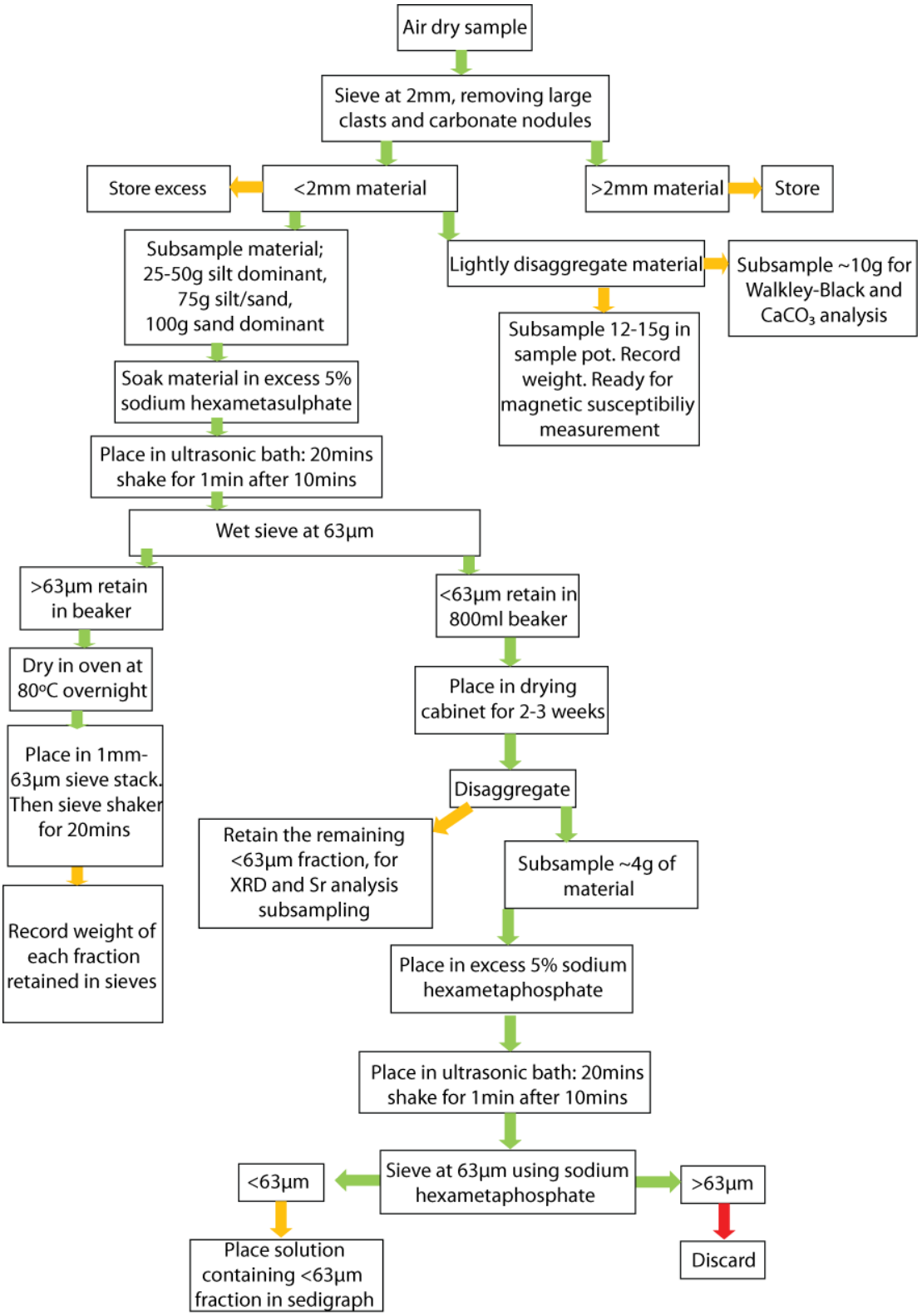

Figure 5.4 Procedure followed for PSA and Walkley-Black, magnetic susceptibility and calcium carbonate content subsampling.

5.4.4 Mineralogy, SEM and strontium-neodymium isotope ratios

Samples (table 5.1) used for XRD analysis of mineralogical composition were sieved to <30 μm to be consistent with the median grain size of the sediments and to be consistent with the fraction used to measure Sr-Nd isotope values. Powdered samples were applied to a glass slide and mineralogical composition was measured on a Philips PW1830/3020 spectrometer using copper Kα X-rays. Dr D. Alderton (Earth Sciences, RHUL) led analysis of the XRD data, with mineral peaks identified from the ICDD Powder Diffraction File database and quantitative analysis of mineral composition carried out using Rietveld analysis.

SEM images were taken of modern fluvial and loess like sediments from each site, using both a bulk <2 mm fraction and a chemically pre-treated <30 μm fraction. The <2 mm fraction (figure 5.2) was spread over a flat surface, carbon discs were then placed adhesive side down into the sediments. The <30 μm fraction was pre-treated following the methods outlined in Mazzullo *et al.* (1992) for the separation of quartz for shape and surface texture analysis. As drying of these sediments may have caused flocculation of the fine particles, these samples were dry sieved using a 30 μm mesh directly onto the adhesive face of the carbon discs. Images were taken using a Hitachi TM-1000 tabletop microscope (desktop SEM).

The analysis of the Sr-Nd isotopic composition of North African dust within the literature is carried out on the <30 μm fraction. This is done in order to be consistent with the median grain size of the sediments and to minimise the effect of grain size on Nd and Sr values (Grousset and Biscaye 2005). Dasch (1969) states that the $^{87}Sr/^{86}Sr$ ratio is size fraction dependent due to the mineralogical differentiation of different grain sizes, where finer fractions are relatively enriched with radiogenic Sr rich clays, although the exact effect of grain size on Sr and Nd composition is not fully understood (e.g. Feng *et al.* 2009). Therefore, in order to be consistent with published data, the <30 μm fraction was analysed.

Analysis of the samples followed the technique outlined in Grousset and Biscaye (2005), with the exception of pre-treatment to remove carbonate carried out using dilute acetic acid instead of sodium acetate. This was under the recommendation of Prof. M. Thirlwall (Earth Sciences, RHUL) and is the standard method followed in the RHUL Earth Sciences laboratory. Leaching of the samples to remove weathering products followed the protocol outlined below:

1. 250-300 μg of material was immersed in 5 ml of 10% acetic acid
2. Mixture was placed in an ultrasonic bath for 15 minutes
3. Sample was settled, and leachate pipetted off

4. Sample immersed in distilled water and left to settle, and then water removed

5. Process repeated until no reaction between sample and acetic acid (four repeats).

Leaching of samples through acid pre-treatment (outlined above) has been shown to be an effective method of removing any Sr component derived from weathering (Nobre Silva *et al.* 2010). This should remove the influence of differential weathering on the Sr ratios of samples, and mean that the original lithic Sr ratio should be obtained.

Leached samples were dissolved in a mixture of hydrofluoric acid (HF) and Nitric acid (HNO3) and Sr and Nd separated through chromatographic columns. Samples were analysed on a VG354 thermal ionisation mass spectrometer, with measurements made using multiple Faraday cups. Both Sr and Nd samples were run on Rhenium (Re) filaments, with Sr being loaded with a Tantalum Fluoride (TaF) activator. Sr isotopes were run using the multi-dynamic procedure of Thirlwall (1991a). Nd isotopes were run as an oxide using the multi-dynamic procedure of Thirlwall (1991b). Sr and Nd standard solutions of SRM987 and dilute Aldrich, respectively, were run in each turret and gave values of 0.710252 ± 10 (SRM987), 0.710255 ± 13 (SRM987) and 0.511404 ± 7 (D.Aldrich). Long term means up to January 2011 gave values of 0.710248±10 for SRM 987 and 0.511405±6 for Dilute Aldrich. The standards analysed alongside samples in this study lie within error of these values.

5.5 Chronology

Two techniques were used to produce age estimates in this thesis, namely U-series and OSL. U-series dates were produced following standard techniques presented in this section. OSL age estimates require analytical procedures to be modified according to sample behaviour and so require further discussion (sections 5.6-5.7)

5.5.1 U-series

At Maro, there is a bed containing tufaceaous material (oncoids) beneath the silt unit. A few tufaceous carbonates were picked out from the sediments in order to provide a minimum age constraint of the overlying silt sediments.

One U-series date was calculated from a tufa sample from Maro following the guidelines of Sharpe *et al.* (2003). The sample was prepared and run by Ian Candy using the MC-ICP-MS unit at RHUL Earth Sciences.

5.6 OSL sample preparation

5.6.1 Sample preparation and pre-treatment

Samples collected in the field remained in light proof bags until they were under sodium lamp (non-bleaching) conditions. The light exposed outer 2 cm of sediment was removed from the blocks. A small amount of the material removed was retained for measurement of moisture content and radioisotope concentration. Roughly 1/3 to 1/2 of the cleaned block was then processed for dating using the steps outlined in Roberts (2008), detailed in figure 5.5.

5.6.2 Water content

The water content of the samples affects the overall dose rate experienced by the sample, lessening the amount of radiation received by the sample from the surrounding sediments (Rhodes 2011). The attenuation factors suggested by Aitken (1985) were used to calculate the effect of the water contents of each sample.

Water content of each sample was calculated and is listed in table 5.2 (% water content = mass of water/mass of dry sediment). This value represents the water content of the sediments at the time of sampling. However, water content is likely to have been affected by numerous factors during the sediment's history; this is particularly evident when assessing the difference between water contents measured for Maro section 1 (sheltered from direct sunlight) and section 2 (exposed to direct sunlight) (table 5.2).

At each site, the silt units have been overlain by fluvial deposits indicating that at least for short periods, the silt units were likely to have had high moisture contents, likely at, or close to saturation. Each site has then undergone subsequent fluvial down-cutting as at each site the modern river is lower than each of the silt units, resulting in a reduced moisture content within each silt unit. At both Chimeneas and Maro section 2, the sediments are exposed to sunlight throughout a large part of the day; it is believed that this has been the case for some time. The silt unit at each site therefore, has a complex moisture content history not necessarily reflected in present day moisture levels of the sediments.

5.6.2.1 Estimating past water content

Saturated water content of all samples was measured (table 5.2), in order that a maximum water content value could be established. Dried sediment was inserted into a syringe (of known weight), containing wire wool at the base, water was added to the sediment until in excess then excess water removed (the wire wool preventing sediment leaving the syringe during water extraction). The weight of the saturated sediment was recorded, then the samples were dried and the

difference between wet and dry weights providing the total amount of water the sample holds at saturation.

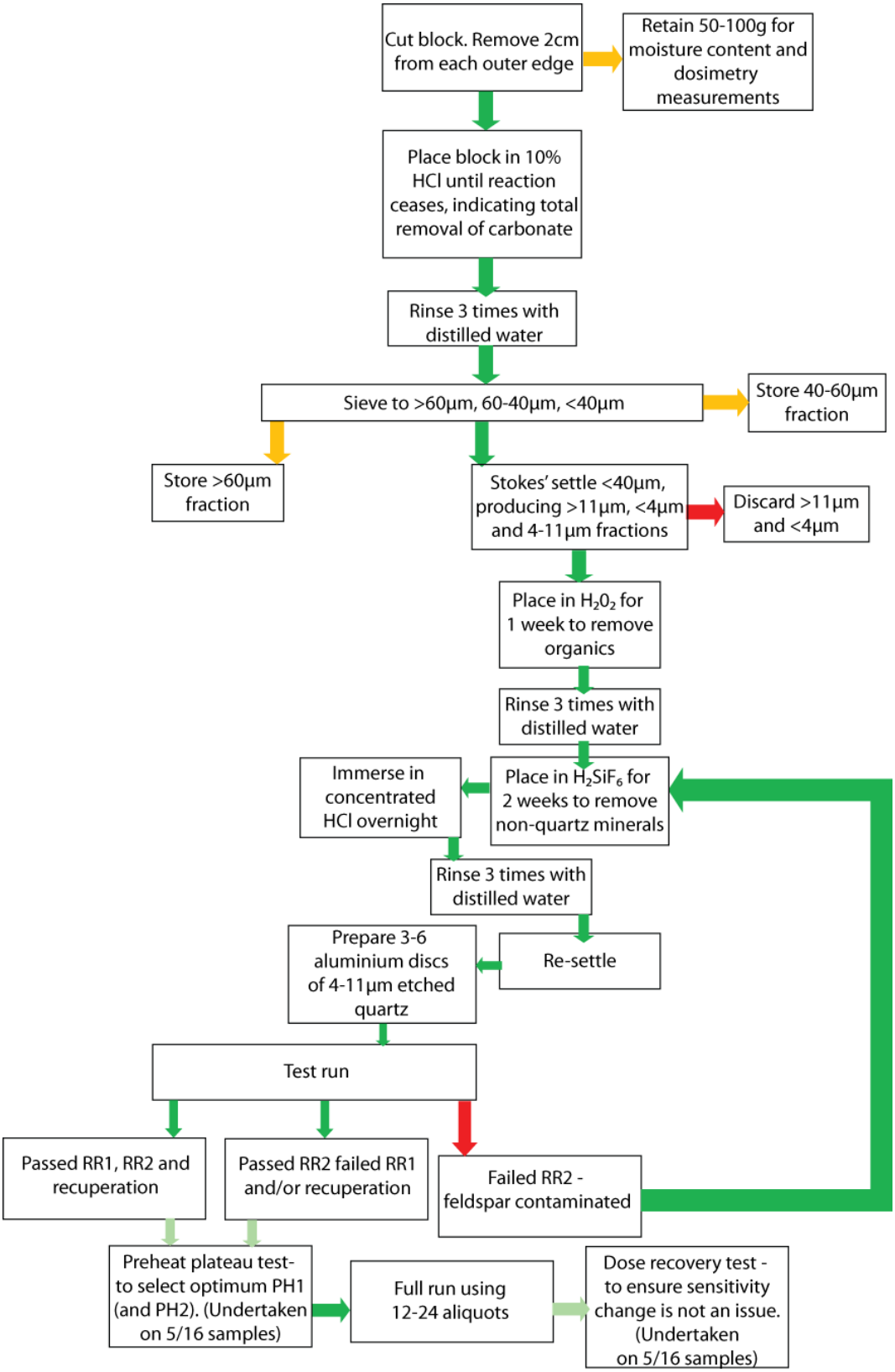

Figure 5.5 OSL sample preparation following Roberts (2007), (2008). RR1 - recycling ratio (Murray and Wintle 2000), RR2 - IR depletion ratio (Duller 2003)

Given the climate of Southern Spain, it is unlikely that samples were saturated for the majority of the time since their deposition. Therefore, it would not be appropriate to apply saturated water content values to any of the samples. The situation of samples MAL1, MAL2, RDM083 and RDM084 make them the most sheltered from exposure to evaporative effects, their water content ranges from ~10-20%. For the purposes of this study a water content of 15% will be assumed for all samples, with an error of +/-5%. This produces a range of 10-20% water content, the range of values recorded by sites protected from evaporation.

Table 5.2 Sample present day moisture content and saturated water content (mass of water/mass of dry sediment)

Sample	Sample moisture content (%)	Saturated water content (%)
chim2	0.55	33.12
chim3	3.36	34.59
chim4	4.26	23.80
chim5	4.94	28.39
chim6	5.37	33.27
chim7	7.31	41.01
mal1	17.25	45.13
mal 2	19.46	47.39
rdm091	16.92	35.83
rdm092	0.83	26.89
rdm093	1.33	30.81
rdm094	4.15	30.56
rdm083	10.10	28.27
rdm084	12.28	32.94
rdm085	4.76	29.67
rdm086	7.10	26.91
rdm0822	7.13	37.69

5.6.3 Grain size

Of the grain size fractions typically used for OSL dating, the 4-11 μm fraction is commonly used for dating of loess deposits (e.g. Roberts, 2008 and references within) as it often the grain size fraction most closely related to the mean grain size of the deposits. In addition to the 4-11 μm fraction being representative of the sediments being dated, the size fraction has a number of advantages. Firstly, it is a narrow size fraction range, which means that laboratory beta dose rate will not vary greatly (Armitage and Bailey 2005). Secondly, 4-11 μm grains are effectively alpha thin, which means that it can be assumed that uniform alpha radiation was received through the grain (Rhodes 2011). For these reasons, the 4-11 μm fraction was used for dating all samples.

5.6.4 Dosimetry

OSL is a measure of radiation received by the sediment since burial, with radiation inputs coming from the surrounding sediment and cosmic rays. The number of electrons stored in luminescence

traps is relative to both the environmental radiation levels and burial time, therefore if luminescence signal can be measured and radiation levels can be estimated (given as dose rate (Dr): Gy/ka), it is possible to produce an estimate of burial age (OSL age) through establishing the level of laboratory induced radiation necessary to reproduce the natural luminescence signal of the sample; referred to as equivalent dose (De).

5.6.4.1 Cosmic ray radiation

Cosmic ray dose rates were calculated from sample altitude, burial depth and location (Prescott and Hutton 1988, 1994) using the Cosmic programme. An error of 10% was assumed.

5.6.4.2 Surrounding sediment dosimetry

Sediment contribution to the dose rate experienced by grains comes from the levels of radionuclides present (^{40}K and isotopes within the decay series of ^{238}U, ^{235}U and ^{232}Th). For each sample material removed during block processing was analysed via ICP-AES to establish levels of radionuclides present. This method assumes that no radioactive disequilibrium is present and that the deposit behaved as a closed chemical system since deposition (Olley *et al.* 1996), and that total radiation emitted is equal to radiation received (infinite matrix assumption).

5.6.4.3 Total dose rate

The total dose rate received by a particle is therefore a combination of cosmic ray contribution and radionuclide contribution, calculated as Gy/ka per ppm (following Adamiec and Aitken 1998). Where total dose rate from radionuclide and cosmic rays are modified according to grain size (Bell 1980, Mejdahl 1979), alpha efficiency (Rees-Jones 1995) and water content (Aitken 1985).

5.7 OSL - measurement

Sample preparation for dating is outlined in figure 5.4, following the procedure detailed in Roberts (2007, 2008), using Hydrofluorosilicic acid as a means to attempt to remove all but quartz from the original polymineral 4-11 μm fraction. Dating of samples was undertaken using the Single-Aliquot regenerative dose (SAR) protocol outlined in Murray and Wintle (2000) (see figure 5.6), with 4-11 μm material settled onto aluminium discs.

5.7.1 Reader specification

OSL measurements were undertaken using a Risø TL/OSL-DA-15 automated dating system. Single aliquots are stimulated using blue (470 μm) light emitting diodes (LED), with a total power of 40mW/cm^2 (Bøtter-Jensen *et al.* 2003). Infra-red (IR) stimulation of aliquots used an IR (870 μm) laser diode with a power density of 132 mW/cm^2. OSL passed through 7.5mm of Hoya U-340

filter and detected using a photomultiplier tube (Electron Tubes Ltd 9235QB). Samples were irradiated using a 40 mCi $^{90}Sr/^{90}Y$ beta source giving ~6 Gy/min, calibrated relative to the National Physical Laboratory, Teddington ^{60}Co γ-source (Armitage and Bailey 2005).

5.7.2 SAR protocol

SAR is the most commonly applied OSL dating method (Preusser *et al.* 2009). The technique exposes single aliquots to irradiation and measurement cycles in order to construct a growth curve from which equivalent dose may be calculated (Murray and Wintle 2000) (figure 5.6). After initial measurement of the natural luminescence signal, the aliquot is subjected to varying, known laboratory doses in order to establish the relationship between given dose and luminescence signal.

5.7.2.1 Recycling ratio (RR1)

Within the SAR protocol each cycle contains a standard test dose, which allows the OSL sensitivity of the sample to be monitored throughout the cycles, allowing natural and regenerative OSL signals to be modified or sensitivity corrected (Murray and Wintle 2000). Sensitivity changes occur when the thermal or radioactive treatment of a sample produces changes within the grains, altering the amount of OSL emitted per unit of dose absorbed (Wintle and Murray 1999, Armitage *et al.* 2000). As a further check on the behaviour of the sample and to ensure that the standard test dose is correctly modifying output, Murray and Wintle (2000) suggest using the recycling ratio. Recycling ratio is calculated by using two low βx (see figure 5.6) doses of the same strength at the start and end of the SAR protocol. If the OSL signal of these two doses is within +/-5% of each other, then any sensitivity change is assumed to have been adequately accounted for.

5.7.2.2 IR depletion ratio (RR2)

A second internal check was suggested by Duller (2003) to ensure that the OSL signal was derived primarily from quartz. Although chemical pre-treatment should remove most other minerals, it is necessary to assess if pre-treatment was sufficient to achieve this (see figure 5.5). The majority of the OSL signal will be derived from quartz and feldspar (Duller 2003), however the luminescence properties of the two minerals are very different and make dating of mixed compositions difficult, due to the fading characteristics of feldspars and their ability to retain luminescence charge at higher temperatures (Duller 2003). It is therefore beneficial to ensure that the OSL signal is determined from only one mineral, and for the majority of OSL dating, this will be quartz. Duller (2003) demonstrated that by introducing an additional SAR cycle at the end of the SAR protocol outlined in Murray and Wintle (2000), where an infrared stimulated luminescence (IRSL) step is introduced it is possible to check for feldspar contamination.

Following delivery of the regeneration dose (usually the same as the first regeneration dose forming the regenerative dose response curve) and preheat, the aliquots are exposed to IRSL. This stimulates a luminescence response from feldspar but not quartz, the aliquots then undergo OSL stimulation using standard blue diodes (Duller 2003).

Therefore, if an aliquot 'loses' a proportion of its luminescence signal via IR stimulation, that aliquot contains feldspar. Contamination is significant enough to cause aliquot rejection if the OSL signal lost during the IRSL SAR cycle is > 5% different to the OSL signal gained from the same regeneration dose.

7.2.2.3 Recuperation

During the SAR protocol (after growth curve construction) a 0 Gy dose is given as one of the βx doses (see figure 5.6), if the OSL signal measured from the zero dose is >5% of the natural signal then recuperation is deemed to be excessive for that aliquot (Roberts 2008). Murray and Wintle (2003) state that recuperation is caused by charge remaining in a light insensitive trap after step 6 of the SAR cycle. The relatively low test dose cut-heat step (step 5, PH2) is not sufficient to eliminate this charge, however, the preheat 1 (step 2, PH1) is sufficient to transfer some of this charge to optically sensitive traps. Therefore where 0Gy is used as the laboratory dose, any luminescence signal measured must derived from a recuperated signal.

5.7.3 SAR test behaviour

5.7.3.1 Pre-treatment test

A small number of aliquots (6-12) were run for at least one sample from each site after initial chemical treatment. Aliquots were run under standard SAR conditions (220˚C PH1 and 160˚C PH2), using RR2 values to assess remaining levels of feldspar presence (Duller 2003). Samples with feldspar contamination required additional pre-treatment (figure 5.5).

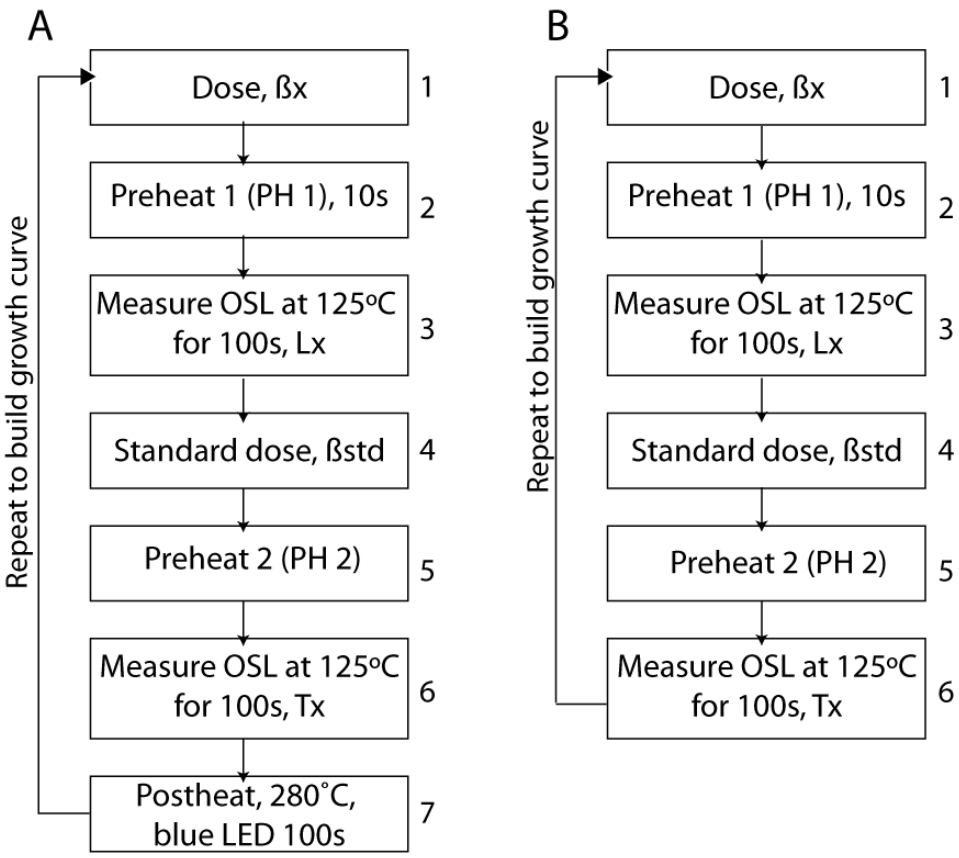

Figure 5.6 SAR protocol after Murray and Wintle (2000). A. protocol for Maro samples, modified after Murray and Wintle (2003), B. protocol for La Malaha and Chimeneas samples.

5.7.3.2 Pre-heat and dose recovery test

Where no evidence of feldspar contamination was present, a selection of samples were put through a preheat plateau sequence using a range of commonly used PH1 (160-280˚C) and PH2 (160 ˚C, raised 220 ˚C) regimes (Murray and Wintle 2000, Bailey 2000, Wintle and Murray 2006). A combined preheat plateau, dose recovery test was used.

Wintle and Murray (2006) state that the major shift in luminescence sensitivity is thought to occur when the samples is first heated. Wallinga *et al.* (2000) and Roberts *et al.* (1999) suggest that by using a previously unheated, zeroed sample and giving it a known laboratory dose it is possible to assess the ability of the SAR protocol to measure the test dose. Samples were bleached (zeroed) using two 200 second exposures to blue LEDs, with a pause of 12000 seconds between each bleaching. Samples were then given a laboratory dose close to their natural signal and the SAR protocol is followed. The ratio of the measured dose to the known dose is calculated (dose recovery ratio) and the preheat regime providing the best dose recovery ratios was chosen for dating the relevant samples.

5.7.3.3 Malaha SAR procedure

Sample behaviour was measured using MAL 1 (figure 5.7) using the criteria set out in table 5.3. Dose recovery was acceptable for samples using a PH1 of 160, 240 and 260 ˚C. Samples using a PH1 of 280 ˚C recorded elevated recovered doses. Samples with a PH1 of 180 and 200 ˚C are not shown in figure 5.6a due to failed RR1/RR2 ratios. For MAL 1 a PH1 of 260 ˚C was chosen as this provided acceptable dose recovery, and good RR1/RR2 ratios. An elevated PH2 of 220 ˚C was chosen to avoid issues of recuperation seen in samples using a PH2 of 160 ˚C (e.g. Murray and Wintle 2003). A PH1 of 280 ˚C was used for MAL 2 as this gave a higher proportion of acceptable RR1 values.

Table 5.3 La Malaha SAR protocol

Sample	Aliquots	PH 1 (˚C)	PH 2 (˚C)	Given doses (Gy)
Mal 1	16	260	220	9, 18, 27, 35, 0, 9, 9
Mal 2	22	280	220	9, 18, 27, 35, 0, 9, 9

5.7.3.5 Chimeneas SAR procedure

Dose recovery preheat plateau tests were conducted on two samples from Chimeneas (figure 5.8). These tests indicated that both samples produced the best dose recovery and recycling ratios using a PH1 of 240 ˚C. There was no evidence of recuperation in the samples from Chimeneas, and so a 160 ˚C PH2 was used (table 5.4).

Table 5.4 Chimeneas SAR protocol

Sample	Depth in log (cm)	Aliquots	PH 1 (˚C)	PH 2 (˚C)	Given doses (Gy)
CHIM 7	460	18	240	160	105, 210, 315, 420, 510, 0, 105, 105
CHIM 6	404	12	240	160	105, 210, 315, 420, 510, 0, 105, 105
CHIM 5	360	13	240	160	105, 210, 315, 420, 510, 0, 105, 105
CHIM 4	270	20	240	160	105, 210, 315, 420, 510, 0, 105, 105
CHIM 3	172	16	240	160	105, 210, 315, 420, 510, 0, 105, 105
CHIM 2	130	14	240	160	105, 210, 315, 420, 510, 0, 105, 105

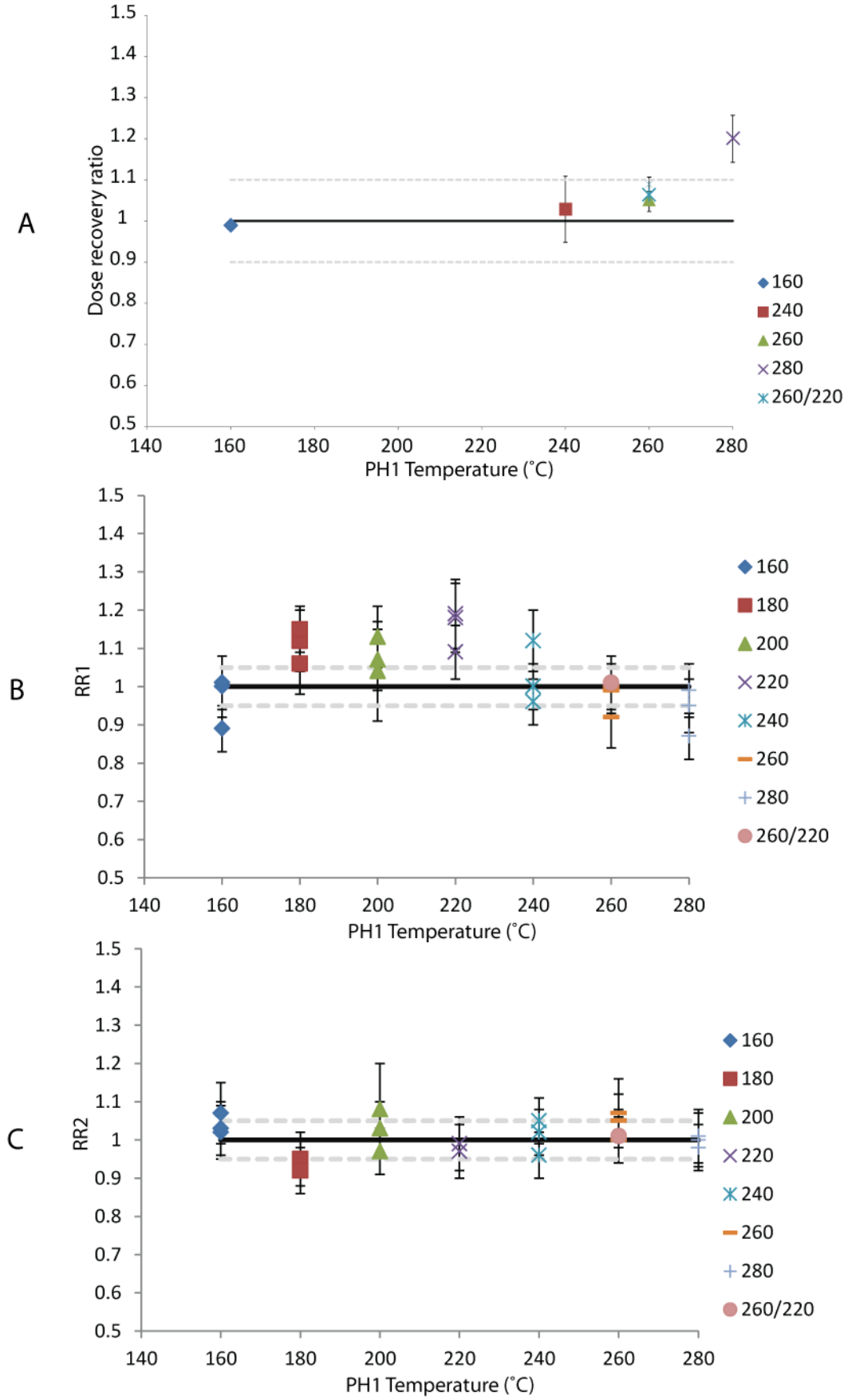

Figure 5.7 Dose recovery and preheat behaviour for MAL1. A Dose recovery ratio with preheat, B. RR1 variation with preheat, C. RR2 variation with preheat. All PH2 temperatures at 160 °C, except for where stated (220°C).

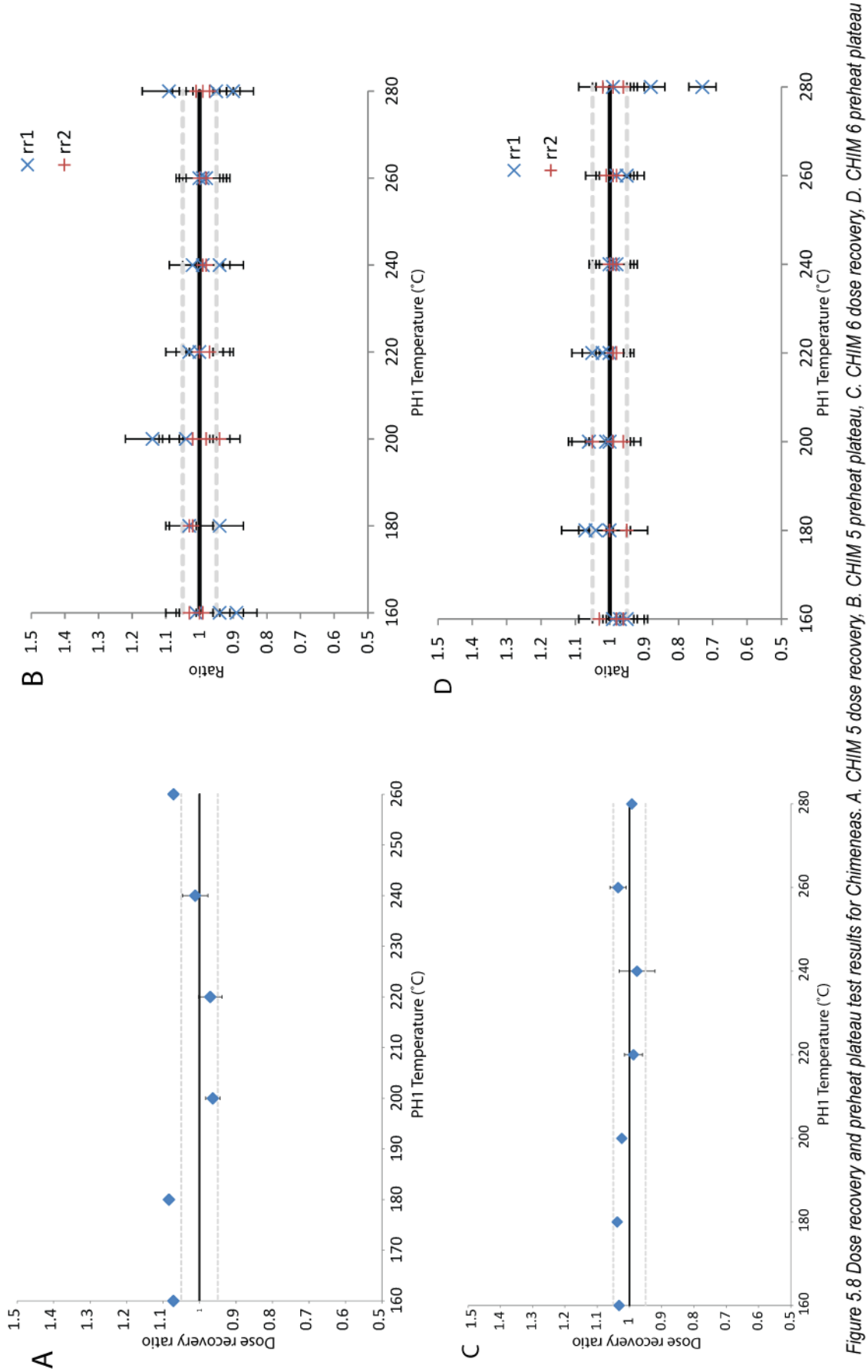

Figure 5.8 Dose recovery and preheat plateau test results for Chimeneas. A. CHIM 5 dose recovery, B. CHIM 5 preheat plateau, C. CHIM 6 dose recovery, D. CHIM 6 preheat plateau

5.7.3.6 Maro SAR procedure

The samples from Maro required a modified SAR protocol due to recuperation. Initially, samples were run using standard SAR preheat conditions (PH1 260 ˚C, PH2 160 ˚C), PH2 was raised to 220 ˚C to attempt to minimise recuperation; however as shown in figure 5.9a recuperation remained an issue. Dose recovery preheat plateau tests including the use of a 280 ˚C post heat (figure 5.9) showed that a modified SAR protocol (PH1 260 ˚C, PH2 220 ˚C, post heat 280 ˚C) (figure 5.6a) would produce reliable OSL age estimates for the samples from Maro.

Table 5.5 Maro SAR protocol

Section	Sample	Aliquots	PH 1 (˚C)	PH 2 (˚C)	Post heat (˚C)	Given doses (Gy)
1	Rdm091	17	260	220	280	9, 19, 45, 90, 180, 358, 0, 9, 9
	Rdm092	15	260	220	280	9, 19, 45, 90, 180, 358, 0, 9, 9
	Rdm093	24	260	220	280	9, 19, 45, 90, 180, 358, 0, 9, 9
	Rdm094	23	260	220	280	9, 19, 45, 90, 180, 358, 0, 9, 9
2	Rdm083	11	260	220	280	19, 58, 93, 193, 290, 385, 0, 19, 19
	Rdm084	12	260	220	280	19, 58, 93, 193, 290, 385, 0, 19, 19
	Rdm085	12	260	220	280	19, 58, 93, 193, 290, 385, 0, 19, 19
	Rdm086	12	260	220	280	19, 58, 93, 193, 290, 385, 0, 19, 19
3	Rdm0822	12	260	220	280	19, 57, 96, 192, 288, 385, 0, 19, 19

Murray and Wintle (2003) demonstrate that the addition of a high (280˚C) post heat under blue LED illumination (step 7 in figure 5.6) minimises the effect of recuperation. It is thought that this persistent recuperation component derives from the medium component (Wintle and Murray 2006), where charge remains in a light insensitive trap after SAR stage 6 (figure 5.6) and the subsequent preheat (stage 2) thermally transfers some of this charge into an optically sensitive trap resulting in a measureable OSL signal (Murray and Wintle 2003). Optical stimulation of the sample under elevated temperatures has been shown to remove the charge as soon as it is transferred to OSL centres, thereby eliminating the effect of thermally transferred recuperation on OSL ages (Murray and Wintle 2003).

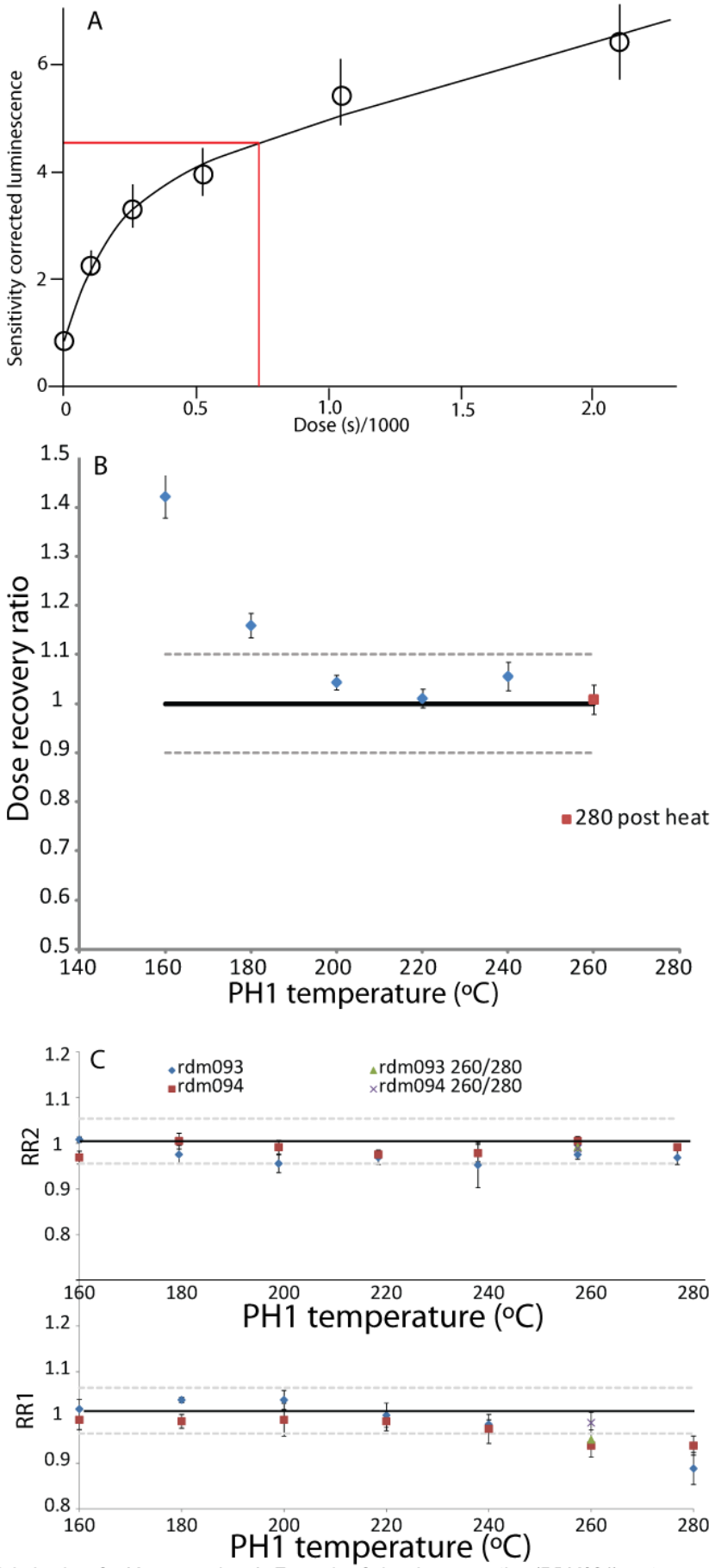

Figure 5.9 OSL behaviour for Maro samples. A. Example of signal recuperation (RDM081), note zero dose point does not plot at zero on y-axis, B. Dose recovery preheat plateau for RDM094, C. RDM093 and RDM094 preheat effects on RR1 and RR2

Chapter 6 – Defining loess in southern Spain

This chapter aims to characterise loess deposits in southern Spain and to differentiate them from other silt depositing environments. Sedimentological, mineralogical and geochemical data from each loess deposit (Malaha, Chimeneas and Maro) will be presented and compared and contrasted to site specific silt deposits produced by modern river and slope processes as well as palaeofluvial systems. The aim of this chapter is not to discuss the study, interpretation and environmental significance of the three loess deposits identified, but in order to discuss the origin of the loess sediments some primary data from each sediment sequence studied will be presented for the first time within this chapter.

6.1 Introduction

At each study site, loess was identified according to previously published criteria (e.g. Pecsi 1990). Present at each study location was an exposure of homogenous, silt dominant, cohesive, buff coloured sediment was present, which was identified in the field as being loess or loessic in nature. However, there are a number of depositional systems within the Mediterranean which may produce silt dominant deposits, such as lakes, certain fluvial environments (e.g. ponding areas, overbank) and colluvium. As there is no previous data regarding the nature of loess in southern Spain, it is necessary to provide a comprehensive review of the composition and nature of the loess as well as to provide multiple lines of evidence regarding the depositional origin of the sediments regarded as loess within this study.

Sediments were sampled from the modern river, slope surfaces and palaeofluvial material at each study site (where available), in order to compare and contrast local sediment systems producing silt with the studied loess material. No lake sediments were sampled as there was no modern lake present, neither was there evidence to suggest that a lake may have existed at any study site during the Late Quaternary.

6.2 Sampling strategy

At each study site, sediments thought to be loess-like in nature were bulk sampled for sedimentological analysis (chapters 7, 8 and 9). From this, individual bulk samples representative of the exposures were selected for characteristic and provenance analysis, in order to attempt to clarify the depositional origin and source of the sediments at each site (figure 6.1, table 6.1). At each site, the loess-like sediments were underlain (and overlain, at Chimeneas) by sediments thought to be non-loess. These sediments were also sampled for comparison (figure 6.1, table 6.1). Additionally, modern analogue samples were taken from each site (table 6.1). Samples were

taken from modern river beds at each site, where possible these were sampled in overbank or ponding areas where silt rich sediments were located (figure 6.2). At Chimeneas and Malaha slope sediments were also sampled (figure 6.2).

Table 6.1 Sample data for modern analogue and palaeo sediments

	Sample	Location	Sediment type
Modern river and slope sediments	3331	Maro- upstream of schist	River sediments
	3332	Maro- schist and marble catchment	River sediments
	3736	La Malaha	River silt
	3737	La Malaha	Slope material
	3738	Chimeneas- upstream from sequence	River silt
	3739	Chimeneas-at sequence location	River silt
	3740	Chimeneas	Slope material
Palaeo fluvial sediments	3380 (5-10cm)	Maro- section 2	Silty - overbank
	3411 (10-15cm)	Maro- section 1	Silty - overbank
	3443 (342-247cm)	Maro- section 1	Silty - overbank
	3646 (30-35cm)	La Malaha	Sandy silty - overbank
	4031 (0-5cm)	Chimeneas	Sandy silty - overbank
	3953 (130-135cm)	Chimeneas	Sandy silty - overbank
	3956 (160-165cm)	Chimeneas	Sandy silty - overbank
	4035 (470-475cm)	Chimeneas	Sandy silty - overbank
Loess sediments	3369 (60-65cm)	Maro- section 2	Predominantly silt
	3361 (96-98cm)	Maro- section 2	Predominantly silt
	3357 (113-118cm)	Maro- section 2	Predominantly silt
	3453 (390-395cm)	Maro- section 1	Predominantly silt
	3456 (405-410cm)	Maro- section 1	Predominantly silt
	3466 (445-450cm)	Maro- section 1	Predominantly silt
	3638 (70-75cm)	La Malaha	Predominantly silt
	3624 (140-144cm)	La Malaha	Predominantly silt
	3991 (235-240cm)	Chimeneas	Predominantly silt
	3974 (248-253cm)	Chimeneas	Predominantly silt
	4014 (358-363cm)	Chimeneas	Predominantly silt
	4018 (377-382cm)	Chimeneas	Predominantly silt
	4026 (417-422cm)	Chimeneas	Predominantly silt

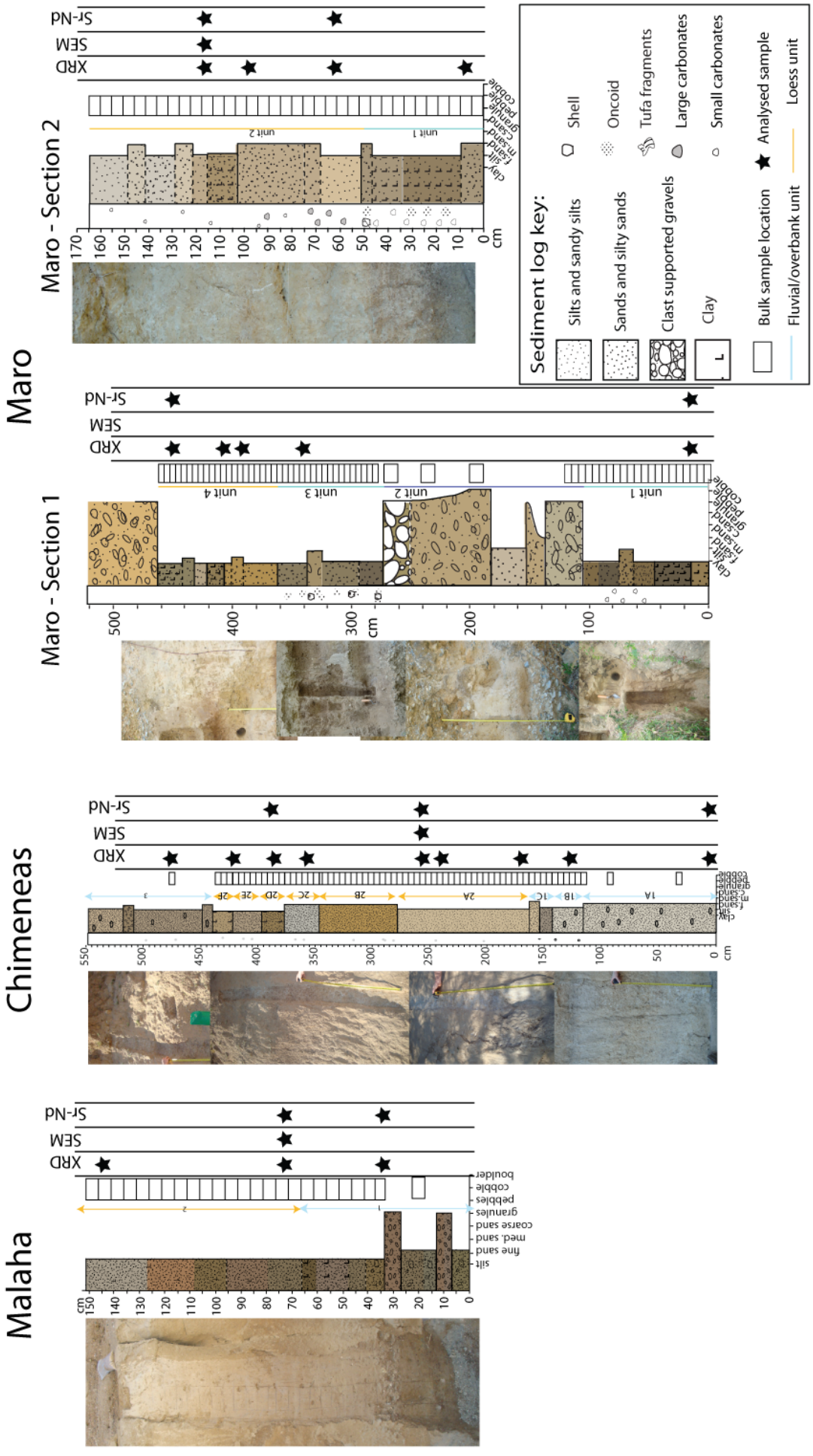

Figure 6.1 Site logs and photographs showing sampling locations for sedimentological, mineralogical and geochemical data presented throughout chapter

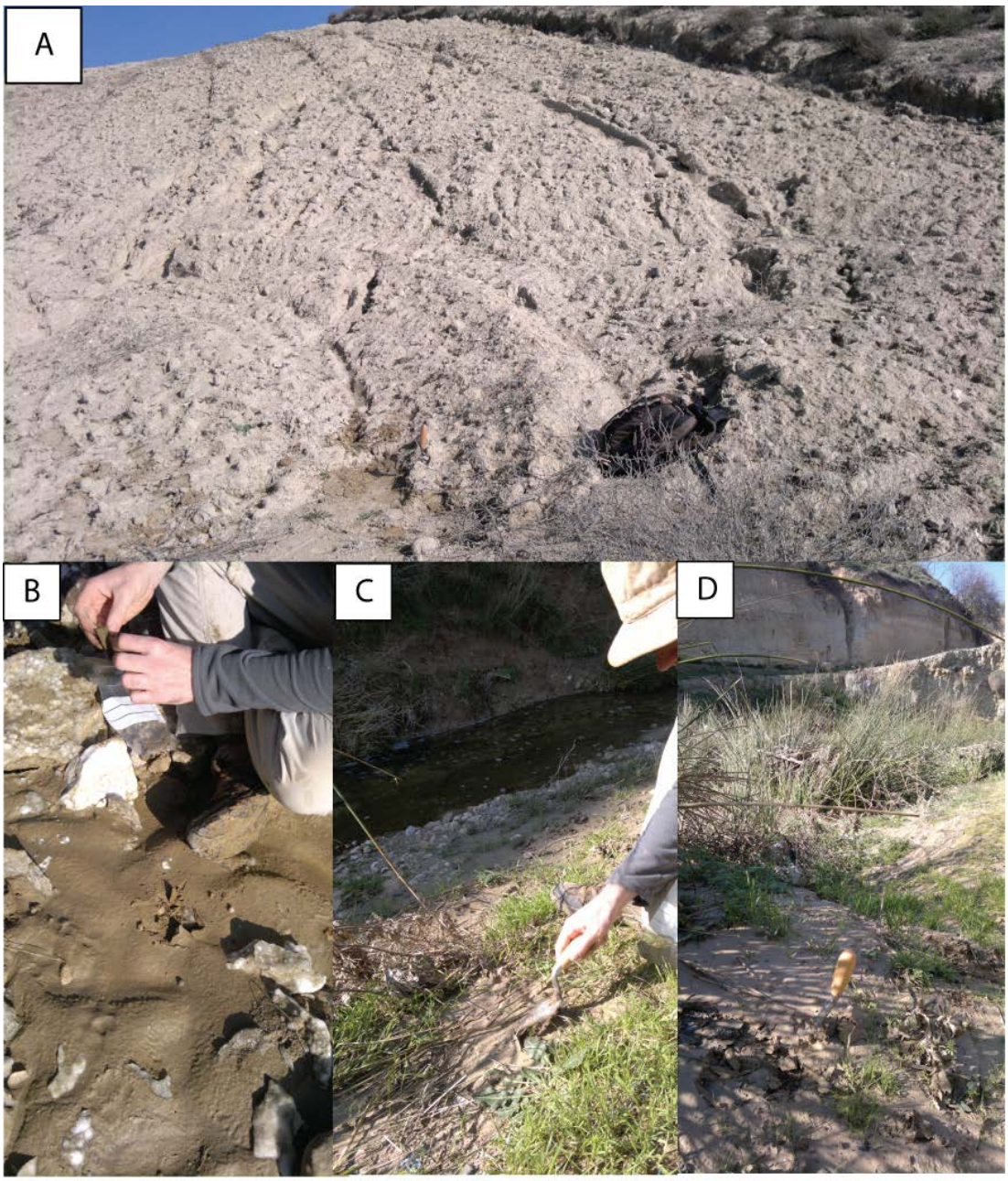

Figure 6.2 Examples of sampling of modern analogue sediments. A. Slope above Malaha valley, B. Silt rich sediments from ponded river setting at Malaha, C. Upstream of Malaha loess exposure, D. Sampling of silt rich river sediments at Chimeneas

6.3 Sedimentological characteristics

Different depositional mechanisms resulting in fine grained sediment deposition (e.g. colluvial, aeolian, alluvial and fluvial) will have different system energies, different sorting potential and different sediment supply systems. Aeolian silts form well sorted, silt dominant deposits and have a much higher sorting potential than overbank or colluvial environments. PSA may help identify differences in median grain size and sorting characteristics. As it is likely that fluvial, colluvial and aeolian deposits will be sourced from different areas, it is possible that differences may be identified within $CaCO_3$ and magnetic mineral content. However, it is important to remember that grain size, $CaCO_3$ content and magnetic susceptibility may be altered significantly by pedogenic

processes (e.g. Kemp 1985b, Dearing 1999). Grain size is given in μm or % total weight, calcium carbonate content is given in % total weight and low frequency (lf) values are given in 10^{-8} m^3 kg^{-1} (raw data in appendix).

6.3.1 La Malaha

Composition of sediment samples from La Malaha are shown in figures 6.3, 6.4 and table 6.2. The loess-like sediments at Malaha have a lower gravel content than the other sediments sampled and are better sorted, being composed almost entirely of silt and clay. However, $CaCO_3$ and magnetic susceptibility values of the loess-like samples and the underlying palaeofluvial samples are similar.

6.3.2 Chimeneas

Composition of sediment samples from Chimeneas are shown in figures 6.3, 6.4 and table 6.2. PSA of the sediments indicates that the loess-like sediments have a different composition from those of the modern analogue samples, but are somewhat similar in terms of composition and sorting to the palaeofluvial sediments. The modern analogue sediments have a higher $CaCO_3$ content than the palaeofluvial and loess-like samples, but there is a wide range of magnetic susceptibility values through all sediment types.

6.3.3 Maro

Composition of sediment samples from Maro are shown in figures 6.3, 6.4 and table 6.2. The loess-like sediments at Maro do not contain any gravel component, unlike the majority of other samples. The modern river sediments contain a significant gravel component, high sand content and low clay content, showing a very different composition to the loess-like sediments. However, the modern river samples were taken from within an active channel, as there was no obvious area of ponding or floodplain deposition associated with the channel. The palaeofluvial sediments indicate that fine-grained sediment deposition can occur within the valley, and the composition of these sediments is not hugely different to that of the loess-like sediments. $CaCO_3$ content and magnetic susceptibility do not show any significant differences between the depositional settings.

6.3.4 Summary

PSA identifies that the loess-like sediments at each site have a consistently lower gravel content than the modern analogue samples, and frequently lower gravel content than the palaeofluvial sediments. However, PSA highlights the ability of fluvial and slope systems to produce silt

dominated sediments at each location. $CaCO_3$ content and magnetic susceptibility do not show significant variations between the different deposits and hence cannot be regarded as diagnostic.

Table 6.2 PSA, $CaCO_3$ and magnetic susceptibility data for sediments sampled from Malaha, Chimeneas and Maro

	Sediment	Sample #	% Gravel	% Sand	% Silt	% Clay	Median (μm)	% $CaCO_3$	LF (10^{-8} m^3 kg^{-1})
Malaha	Modern river	3736	0.49	2.85	68.72	27.93	11.74	11.39	24.10
	Modern slope	3737	1.74	8.72	46.29	43.25	2.70	15.73	10.98
	Palaeofluvial	3646	32.14	6.56	31.82	29.49	10.44	21.63	65.94
	Loess	3638	0.41	1.20	54.02	44.37	2.63	24.11	76.[87]
	Loess	3624	0.19	1.06	56.58	42.17	2.96	20.50	63.62
	Mean loess	n/a	0.18	1.17	55.12	43.53	2.74	22.76	63.09
Chimeneas	Modern river	3738	0.31	2.07	63.95	33.68	7.13	44.84	32.02
	Modern river	3739	0.00	4.21	69.35	26.44	10.91	45.16	2.08
	Modern slope	3740	0.47	4.04	60.73	34.76	6.02	61.48	28.30
	Palaeofluvial	4031	30.39	57.43	8.79	3.38	1175.36	45.13	8.00
	Palaeofluvial	3953	0.00	38.44	38.97	22.59	40.94	24.19	5.30
	Palaeofluvial	3956	0.00	27.61	48.72	23.67	46.69	24.95	16.10
	Palaeofluvial	4035	3.08	13.89	47.99	35.04	5.24	39.27	58.70
	Loess	3991	0.00	40.65	33.36	26.00	22.63	36.81	25.30
	Loess	3974	0.00	18.71	51.38	29.91	11.06	26.11	20.90
	Loess	4014	0.00	21.38	46.47	32.16	6.48	33.25	23.60
	Loess	4018	0.00	15.90	49.20	34.90	5.16	35.96	29.00
	Loess	4026	0.00	13.72	54.79	31.49	6.59	42.10	45.60
	Mean loess	n/a	0.00	23.84	45.62	30.54	10.41	32.21	29.72
Maro	Modern river	3331	10.19	53.80	31.18	4.83	88.70	n/a	n/a
	Modern river	3332	4.11	69.35	22.21	4.33	114.76	12.17	48.14
	Palaeofluvial	3380	20.30	41.74	25.40	12.57	120.38	34.89	4.13
	Palaeofluvial	3411	0.00	12.13	58.70	29.17	9.45	11.56	8.03
	Palaeofluvial	3443	0.15	17.38	52.62	29.85	10.36	19.37	7.10
	Loess section 2	3369	0.00	15.88	61.16	22.97	13.90	18.09	11.55
	Loess section 2	3361	0.00	59.52	28.38	12.10	81.74	11.53	7.98
	Loess section 2	3357	0.00	24.85	52.23	22.92	18.41	19.00	10.38
	Loess section 1	3453	0.00	58.98	30.11	10.91	80.12	23.73	5.23
	Loess section 1	3456	0.00	27.99	47.60	24.41	14.81	16.84	5.88
	Loess section 1	3466	0.00	29.63	50.17	20.19	21.95	15.96	7.88
	Mean loess 2	n/a	0.00	41.40	40.02	18.58	41.62	16.68	11.39
	Mean loess 1	n/a	0.00	39.06	41.54	19.40	34.00	17.92	5.79

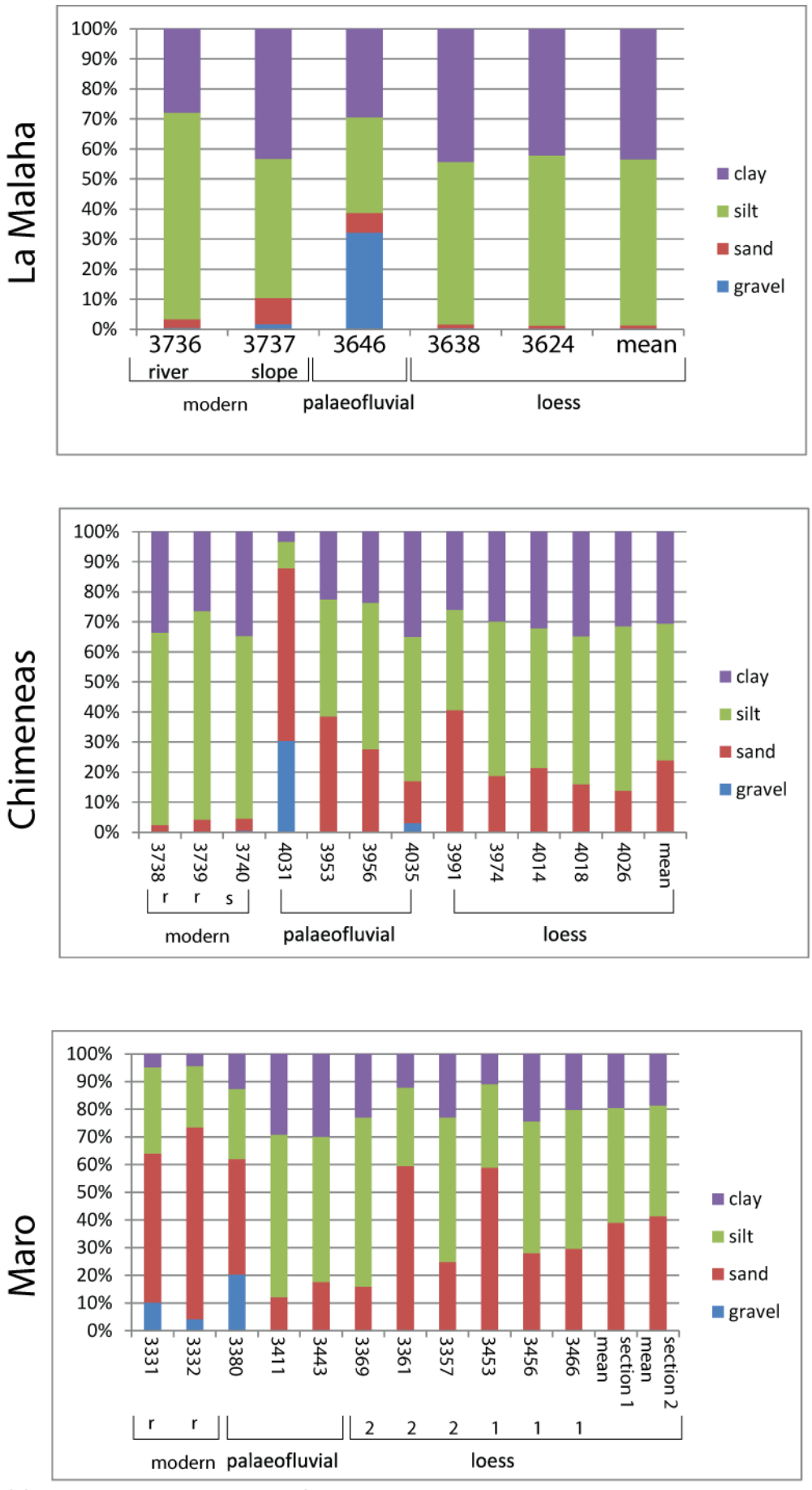

Figure 6.3 Particle size composition data for each location showing modern river and slope sediments, palaeofluvial (overbank) sediments and loess(ic) sediments.
r=river, s=slope, means calculated from full dataset

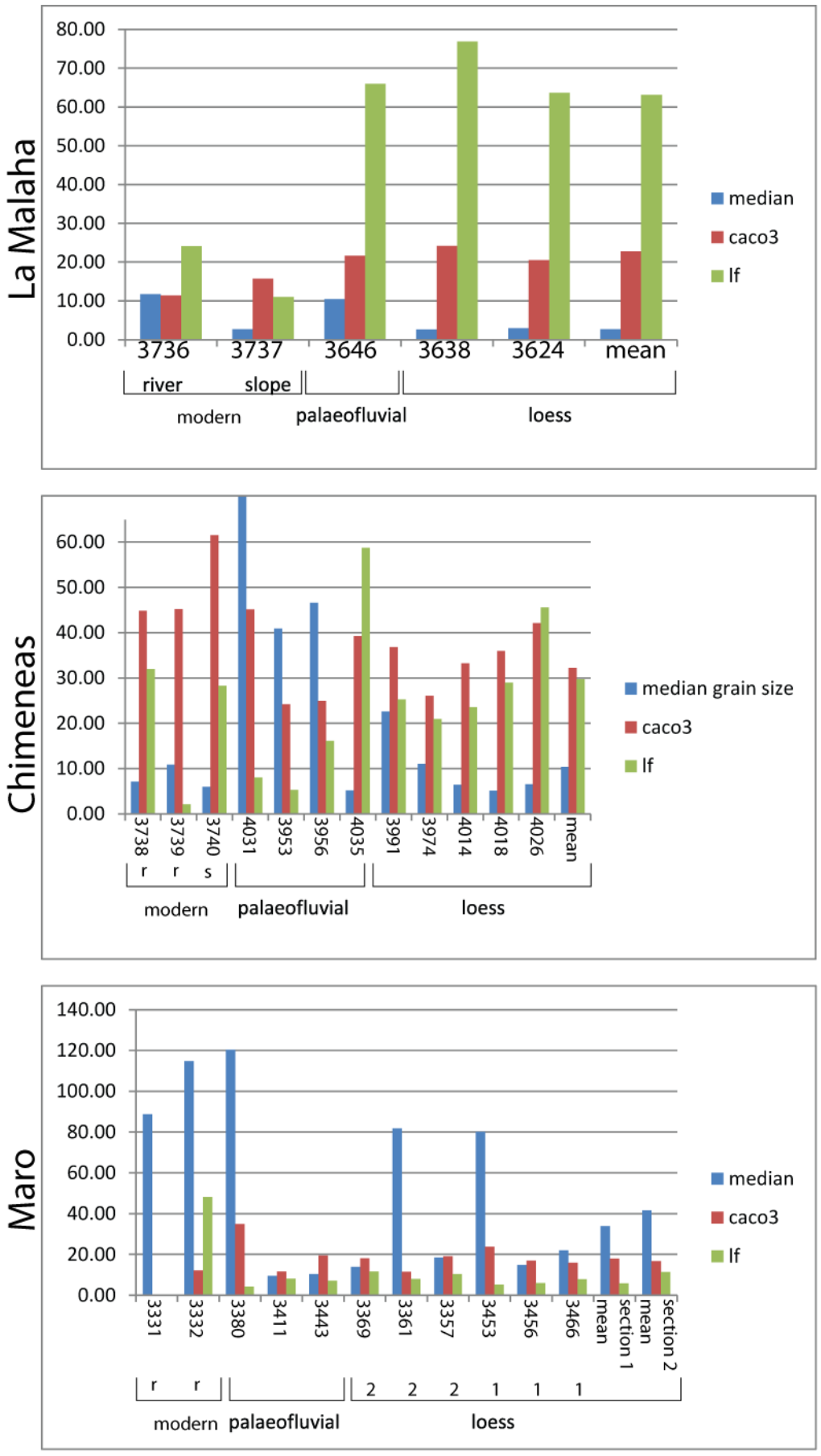

Figure 6.4 Plots showing median grain size (µm), Calcium carbonate content and total magnetic susceptibility (low frequency - lf). r=river, s=slope, mean values calculated from entire dataset for site

6.4 Mineralogy

Fluvial systems and slope processes in the region studied contain locally sourced sediments from the Sierra Nevada range and the Granada basin, whereas loess deposits can contain a far-travelled dust component. Differences in sediment source may be reflected by different mineralogical compositions, and has been demonstrated to be a useful tool in tracing and distinguishing sediments in the Mediterranean (e.g. Woodward *et al.* 1992, Suchodoletz *et al.* in press). XRD analysis was used to identify the mineralogical composition of the bulk sediments, analysis was undertaken on the <30 μm fraction in order that the data gained reflected the fine silt dominated sediments sampled.

6.4.1 La Malaha

The two samples from the loess-like sediments at Malaha have a very similar mineralogical composition (table 6.3), dominated by clay minerals, calcite and quartz. The loess-like sediments differ in composition to the palaeofluvial sediments (dominated by feldspar, calcite and clays), modern fluvial sediments (high quartz content) and the modern slope sediments (calcite dominant, presence of gypsum). These apparent differences are not picked up in clay composition (figure 6.5b, table 6.3), where the loess-like sediments are very similar to the modern river sediments.

6.4.2 Chimeneas

There is no discernible difference in whole rock or clay composition of the sediments sampled at Chimeneas (figure 6.5 and table 6.3). The sediments do show a significant difference to those of the other sites, with a much higher calcite component than is seen at Malaha or Maro (figure 6.5a)

6.4.3 Maro

As with Chimeneas, the sediments from Maro do not show deposit specific differences in whole rock or clay composition (figure 6.5 and table 6.3).

6.4.4 Summary

XRD analysis has identified that all sites contain the same suite of minerals in varying quantities. Mineralogical composition of the sediments has not proven to be a useful sediment discriminator.

Table 6.3 Mineralogical composition of sediments from all sites based on Rietveld Quantitative Analysis of wavelength data (performed by D. Alderton RHUL)

Site	Sediment	Sample #	Whole rock								Clays			
			% amphibole	% feldspar	% dolomite	% calcite	% quartz	% clays	% gypsum	% pyrite	% illite	% smectite	% kaolin	% chlorite
Malaha	Modern river	3736	0	8.5	4.6	12.3	26.8	47.8	0	0	40.3	0.1	6.2	1.2
	Modern slope	3737	1	14.9	5.3	46.3	10.3	15	7.2	0	14.6	0	0.4	0
	Palaeofluvial	3646	0	23.4	4.5	16.9	9.6	45.6	0	0	38	0	2.8	4.8
	Loess	3638	0	6.9	2.5	21.3	11.5	57.8	0	0	48.7	0.3	8.2	0.6
	Loess	3624	0	8.1	2.3	14	15	60.7	0	0	50.1	0.3	8.1	2.2
Chimeneas	Modern river	3738	0.1	7.6	8.7	60.8	9.8	11.9	1.2	0	11.4	0	0.2	0.3
	Modern river	3739	0.1	1.9	8.4	59.7	10.6	19.1	0	0	17.8	0	1.3	0
	Modern slope	3740	0	8.6	0	78.3	6.7	5.9	0.6	0	5.7	0	0.2	0
	Palaeofluvial	4031	2.9	10.7	8.4	54.2	9.6	13	1.1	0	11.7	0.8	0.1	0.4
	Palaeofluvial	3953	2.1	9.6	8.5	37.8	5.8	8.6	27.6	0	8	0.3	0.3	0
	Palaeofluvial	3956	4.7	15.3	5	38.7	8.2	13	15	0	11.5	0	0.1	1.4
	Palaeofluvial	4035	1.5	9	0.1	66.4	10.4	11.6	1	0	11.2	0	0.3	0.1
	Loess	3991	2.4	8.7	6	53.4	12.7	16	0.7	0	14	0.5	0.1	1.4
	Loess	3974	5	13.8	5.7	41.7	9.2	15.5	9	0	12.4	1.3	0.1	1.7
	Loess	4014	2.8	9.6	6.4	58.6	10.7	11.8	0.2	0	11.6	0	0.2	0
	Loess	4018	2.2	11.5	6.5	55.9	9.7	13.4	0.6	0	12.5	0	0.2	0.7
	Loess	4026	0.5	6.9	9.2	61.2	9.6	12	0.7	0	10.9	0	0.3	0.8
Maro	Modern river	3331	1	12	9.1	6.4	33.8	37.6	0	0	34.7	0	2.9	0
	Modern river	3332	3.4	12.2	10.9	6.6	29.9	37	0	0	32.4	1.3	3.3	0
	Palaeofluvial	3380	1.6	3.9	8.2	57.3	10.7	18.2	0	0	7.5	1.4	6.5	2.8
	Palaeofluvial	3411	0.4	5.8	9.6	8.7	13.8	61.5	0.3	0	42.9	0	11.3	7.3
	Palaeofluvial	3443	3.2	8	13.1	19	15.3	40.8	0.6	0	27.2	0	8.9	4.7
	Loess section 2	3369	1.4	7.5	12.8	14.7	15.1	48.4	0	0	34.4	1.7	8	4.3
	Loess section 2	3361	1.3	9.4	13.7	6.1	20.9	48.5	0	0	35.1	2.5	8	2.9
	Loess section 2	3357	2.2	7.1	21.9	15.2	19.3	34.4	0	0	25	1.7	6.8	0.9
	Loess section 1	3453	2.9	8.4	6.7	17.1	11.4	51.8	1.3	0.3	31.5	0	14.4	5.9
	Loess section 1	3456	3.5	12.2	11.7	6.8	12.6	52.5	0.6	0.2	39.3	0	9	4.2
	Loess section 1	3466	2.2	10	17.5	13.8	13.5	42.8	0.1	0.2	31	0	9.3	2.5

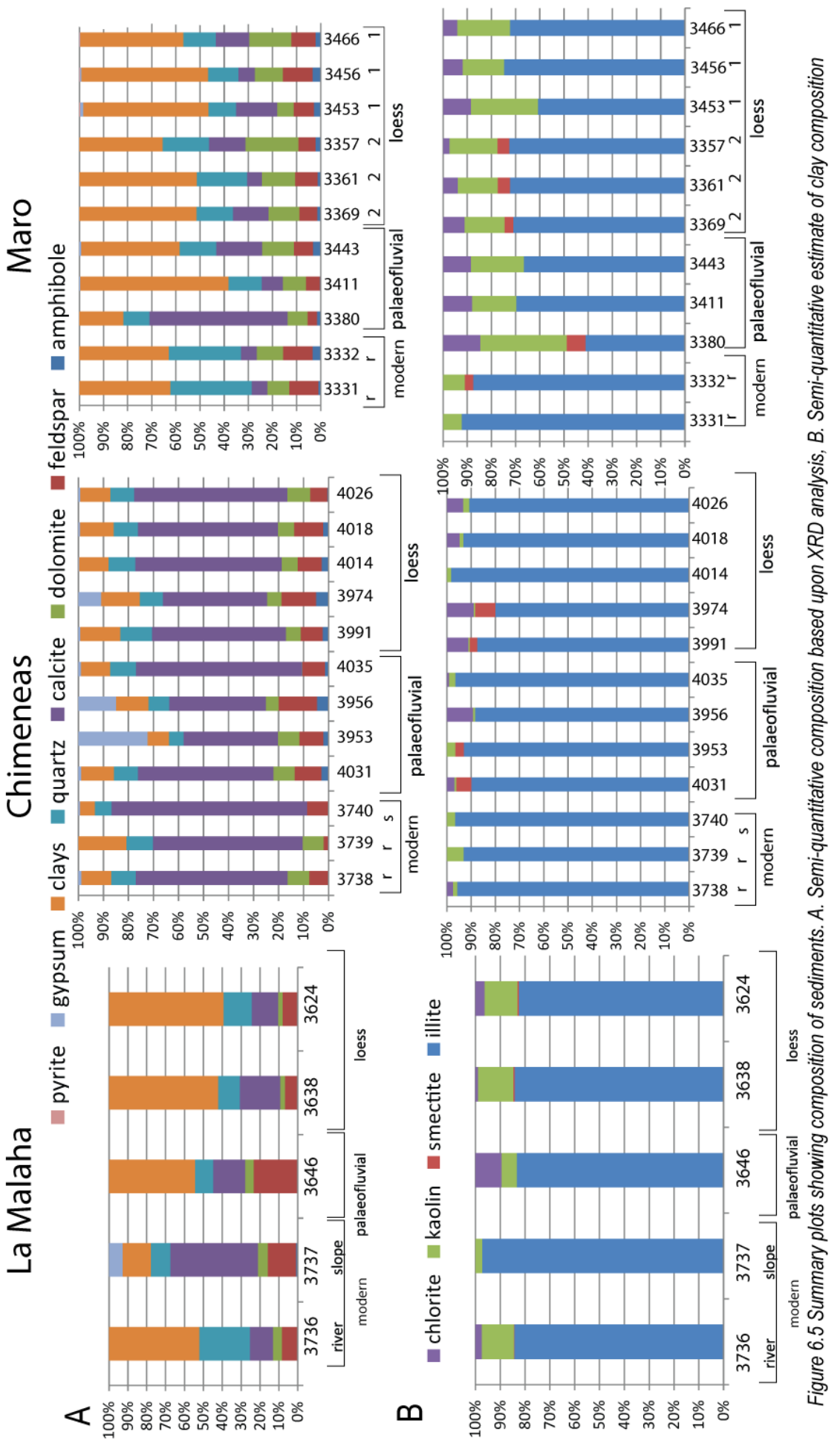

Figure 6.5 Summary plots showing composition of sediments. A. Semi-quantitative composition based upon XRD analysis, B. Semi-quantitative estimate of clay composition

6.5 Grain textures

SEM analysis of grain shape and surface textures has been suggested as a method of distinguishing between depositional environments and processes (e.g. Krinsley and Smalley 1972, Krinsley and Doornkamp 1973, Bull 1981, Mazzullo *et al.* 1992). The majority of the existing literature deals with the textural properties of sand sized quartz and the identification of loess particles is generally based upon analysis of glacially derived silts (e.g. Cegla *et al.* 1971). There is some suggestion however, that loess may be identified on the basis of chemical alteration of grain surfaces and fine material adhering to particle surfaces (Cegla *et al.* 1971, Krinsley and Doornkamp 1973). SEM analysis was therefore undertaken in order to investigate whether differences in grain shape and texture existed between the modern fluvial system and the loess-like sediments.

SEM analysis was undertaken on a <30 μm quartz separated fraction produced following the methods outlined in Mazzullo *et al.* (1992), in order to compare the characteristics of quartz grains representative of the mean grain size produced in the two environments. Additionally, SEM images were taken from bulk samples from each environment in order to assess any gain surface coatings that may have been removed through chemical pre-treatment.

6.5.1 La Malaha

There is no notable difference in grain shapes between the modern fluvial system and the loess-like sediments (figure 6.6). Grain surface texture images (figure 6.7) indicate that there may be some difference between grains sampled from the two sediment settings. The chemically pre-treated quartz shows a platy, but somewhat irregular surface in the fluvial sediments, whereas the quartz from the loess-like sediments again shows a platy structure, but with a smoother appearance. The platy structure is interpreted as cleavage fractures (Krinsley and Doornkamp 1973), the irregular surface of the fluvial quartz may be produced by multiple conchoidal fractures or pitting produced through surface dissolution associated with chemical weathering (Krinsley and Doornkamp 1973). Images of the bulk sediments from the two environments indicate that grains from the loess-like sediments may have more material adhering to their surfaces.

6.5.2 Chimeneas

Again, there is no notable difference in grain shapes between the modern fluvial system and the loess-like sediments (figure 6.6). Unlike La Malaha, the grain surfaces (figure 6.7) from the modern fluvial and loess-like sediments have a very similar appearance. In both environments, the separated quartz fraction shows heavily fractured and pitted grain surfaces.

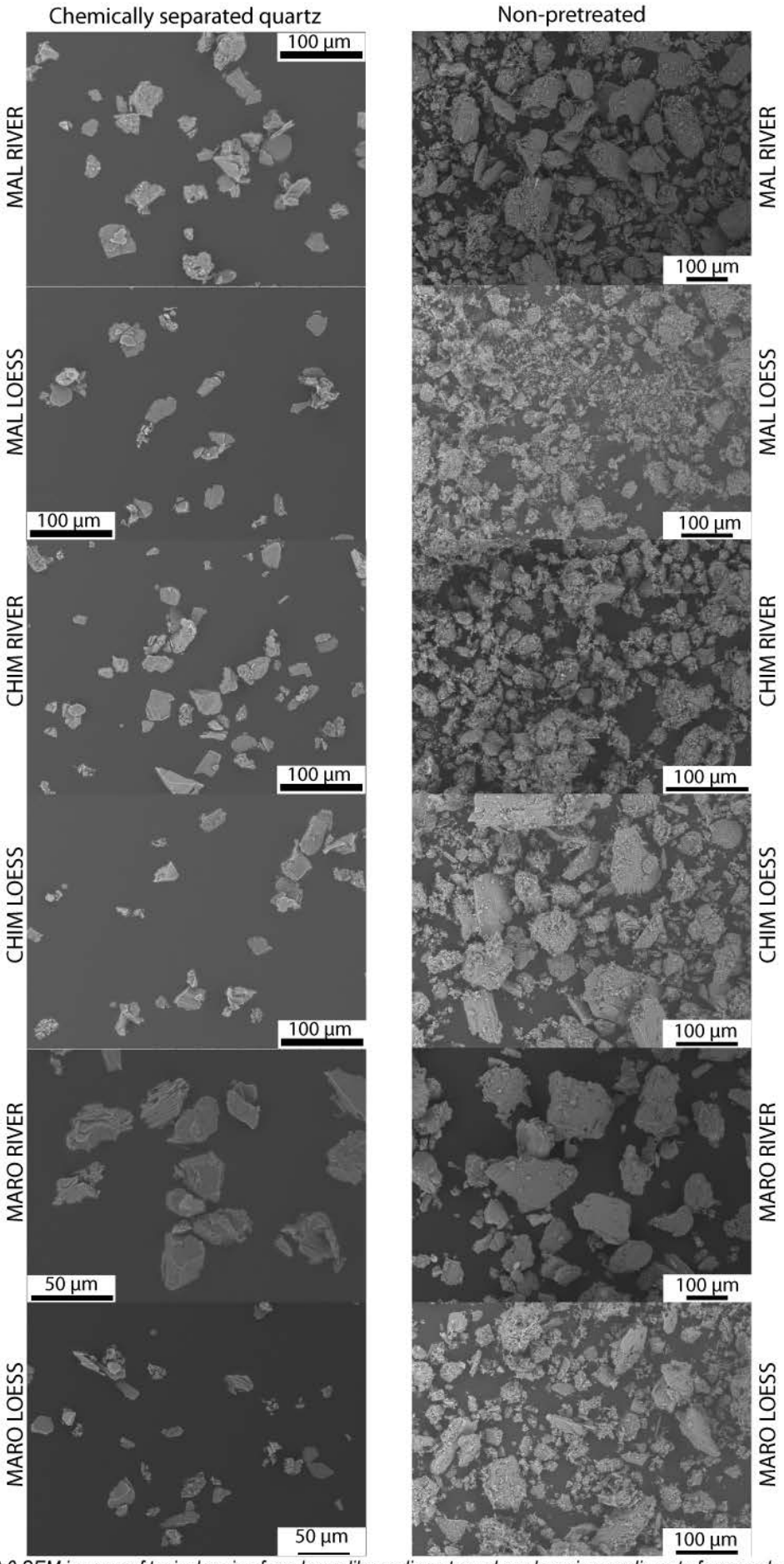

Figure 6.6 SEM images of typical grains from loess like sediments and modern river sediments from each site. Left chemically separated quartz (<30 µm) from all sites, right bulk, un-pretreated sediments (<2 mm)

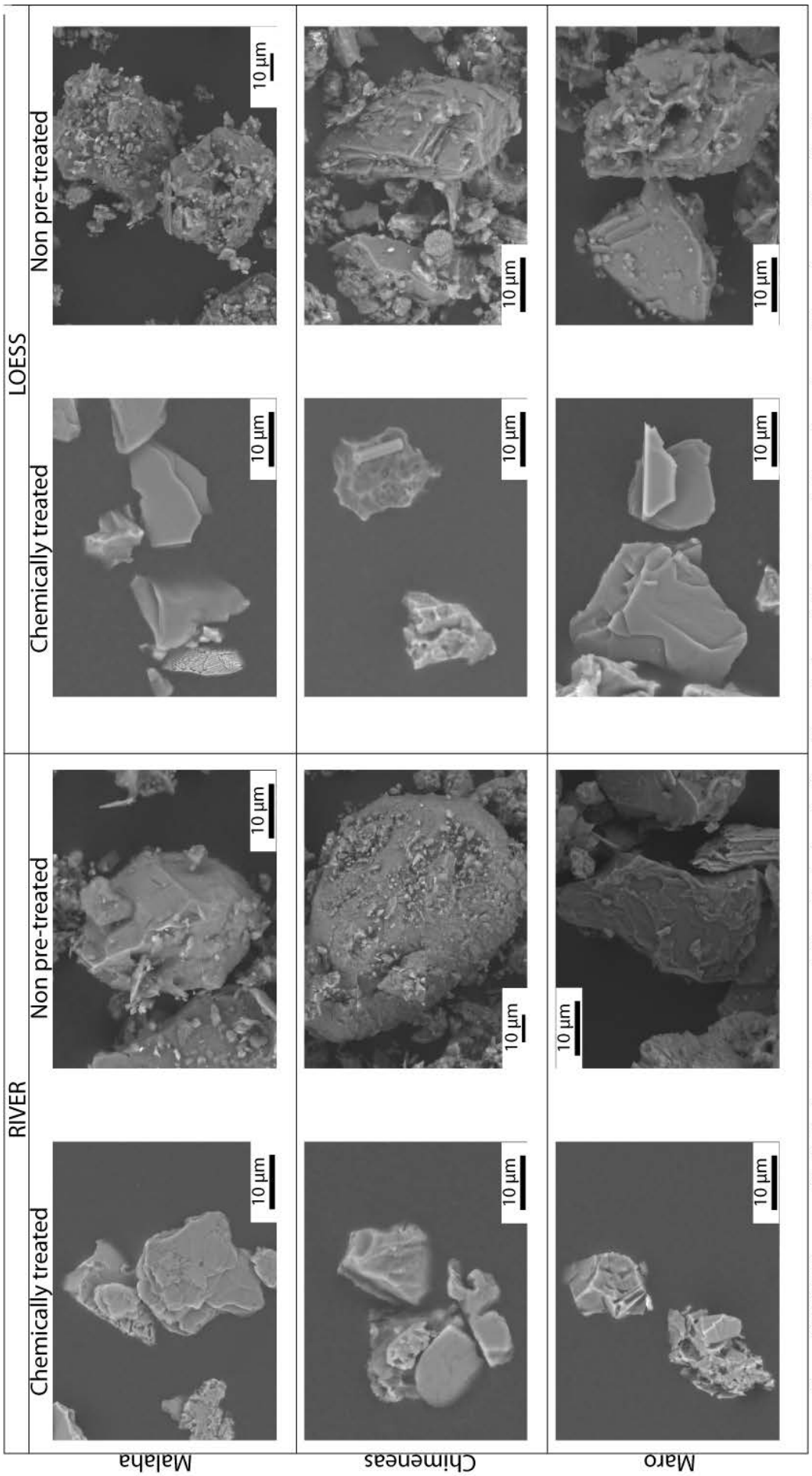

Figure 6.7 SEM images of individual grains, representative of typical grains found in each deposit. Grains from both modern river and loess type sediment bodies. Chemically treated (<30 µm) and bulk sediments (<2 mm)

6.5.3 Maro

There are no discernible differences between grain shapes for the two environmental settings (figure 6.6). As with La Malaha, there appears to be some differences between quartz grain surfaces from the two deposits. Again, the fluvial quartz shows a heavily fractured, pitted surface, whereas quartz from the loess-like deposit displays a platy, smoother surface with less pitting and conchoidal fracturing. Again, as with La Malaha grain surfaces from the bulk sediment fraction of the loess-like deposit shows greater fine particle adhesion than grain surfaces from the fluvial deposit.

6.5.4 Summary

SEM images of grains from the fluvial deposits and loess-like sediments at the three sites may help to distinguish between depositional environments. However, any distinctions made are based upon qualitative interpretation of images taken of only a few grains. This analysis has not been used to attempt to reconstruct depositional environment on the basis of textural features, only to suggest differences which may exist between grains from the two deposit types sampled. Images from La Malaha and Maro appear to indicate some differences between grains deposited in the two environments, with quartz grains from the loess-like deposits having a smooth, platy appearance and those from fluvial settings having a heavily fractured, pitted appearance. Such differences may indicate different transport mechanisms and/or degrees of mechanical and chemical alteration. Grain surfaces from the bulk fraction at La Malaha and Maro show that there may be greater fine particle adhesion to grains from the loess-like sediments than in the fluvial sediments. This may record clay or precipitate adhesion and may relate to the cohesive nature of the loess-like sediments. At Chimeneas, however, grain textures (both bulk and quartz) appear to be the same from the fluvial and the loess-like sediments.

6.6 Sr-Nd isotopic composition

As with mineralogical data obtained via XRD analysis, neodymium and strontium isotope ratios were used to attempt to differentiate the deposits sampled. $^{87}Sr/^{86}Sr$ and $^{143}Nd/^{144}Nd$ ratios are considered to be useful tools for the provenancing of sediments, as Sr and Nd ratios are controlled primarily by origin (mantle vs. crust) and age (e.g. young volcanic vs. old continental) (Faure 1986). Therefore it may be possible to discriminate between locally derived sediments (e.g. fluvial and slope) and those with a far travelled component (e.g. loess) using Sr and Nd isotopic compositions.

Strontium and neodymium isotope ratios have been used as tracers of dust source to both marine and continental settings (Biscaye et al 1997, Grousset et al 1992, Grousset *et al.* 1988, Grousset and Biscaye 2005, Chen *et al.* 2007, Ujvari *et al.* 2012). As North Africa is a potential dust source for southern Spain (e.g. Moreno *et al.* 2002), it is possible that the existing North African data set could help to provenance any non-local dust input (e.g. Grousset and Biscaye 2005).

The results presented are a limited dataset produced to investigate whether the technique could be a useful method for discriminating between the depositional settings and potentially identifying source regions for the sediments. Analysis was undertaken on the <30 μm fraction in order to be consistent with previous datasets that exist for the region (e.g. Grousset and Biscaye 2005). It is worth noting that most of the Nd values obtained to date have large uncertainties. This is due to an on-going issue affecting the precision of the TIMS unit at RHUL, so that affected samples have low ratio values (table 6.4).

6.6.1 La Malaha

The modern fluvial, modern slope and palaeofluvial sediments from La Malaha all have relatively low Sr ratios (0.710630, 0.708457, 0.710484, respectively), whereas the loess sample has a significantly higher Sr ratio (0.714322) (figure 6.8). Due to the large errors associated with the Nd data, it is not possible to draw conclusions from the current dataset (table 6.4). Although Sr ratios can be modified by weathering (e.g. Cole *et al.* 2009, Hemming 2007), it is not likely that this shift is due to post-depositional (geologically modern) weathering of sediments, as recent weathering produces a shift towards lower $^{87}Sr/^{86}Sr$ ratios (Hemming 2007). Additionally, the chemical pre-treatment of the sediments (leaching) should have removed any weathering signal. As such it is likely that the shift in Sr ratio values associated with the loess-like sediments at La Malaha represents a shift in source.

6.6.2 Chimeneas

All of the samples from Chimeneas record low Sr ratios (0.708623 to 0.709551, table 6.4). The loess samples record an apparently similar Nd composition (considering large uncertainties) and Sr composition to the modern slope material sampled. The modern fluvial sample has a similar Sr ratio to the other Chimeneas sediments (loess, modern slope), but has a significantly lower Nd ratio. The close relationship between Chimeneas loess-like samples and slope samples indicates that they are likely to have been sourced from the same sediments. Additionally, these values plot closely with those from the fluvial and slope sediments at La Malaha. As both of these locations are within the Granada basin, these values appear to correspond to sediment sourced locally within the basin.

6.6.3 Maro

The sediment samples from Maro show intermediate Sr ratios, between the high Malaha loess value and the Granada basin sediments (figure 6.8). The large Nd errors mean it is not possible to differentiate between Maro sediments and other sediments on this basis. However, the Maro loess samples do have significantly lower Sr ratios than the palaeofluvial and modern fluvial sediments from the site. This may indicate a shift in sediment source.

Table 6.4 Sr Nd isotope values for each site

Site	Sediment	Sample #	$^{87}Sr/^{86}Sr$	2σ	Ratios	$^{143}Nd/^{144}Nd$	2σ	Ratios
Malaha	Modern river	3736	0.710630	0.000010	105	0.512062	0.000021	18
	Modern slope	3737	0.708457	0.000010	105	0.512062	0.000005	84
	Palaeofluvial	3646	0.710484	0.000013	105	0.512040	0.000027	10
	Loess	3638	0.714322	0.000010	110	0.512055	0.000013	11
Chimeneas	Modern river	3739	0.708656	0.000011	130	0.512025	0.000022	11
	Modern slope	3740	0.709551	0.000011	105	0.512054	0.000004	105
	Loess	3974	0.708623	0.000010	105	0.512050	0.000005	103
	Loess	4014	0.709399	0.000015	130	0.512060	0.000018	14
Maro	Modern river	3331	0.713348	0.000010	105	0.512051	0.000009	35
	Modern river	3332	0.713103	0.000010	105	0.512040	0.000005	63
	Palaeofluvial	3411	0.712639	0.000010	105	0.512024	0.000005	105
	Loess section 2	3369	0.710895	0.000009	105	0.512027	0.000004	105
	Loess section 2	3357	0.711844	0.000009	110	0.512039	0.000013	9
	Loess section 1	3466	0.712194	0.000009	105	Fail	fail	fail

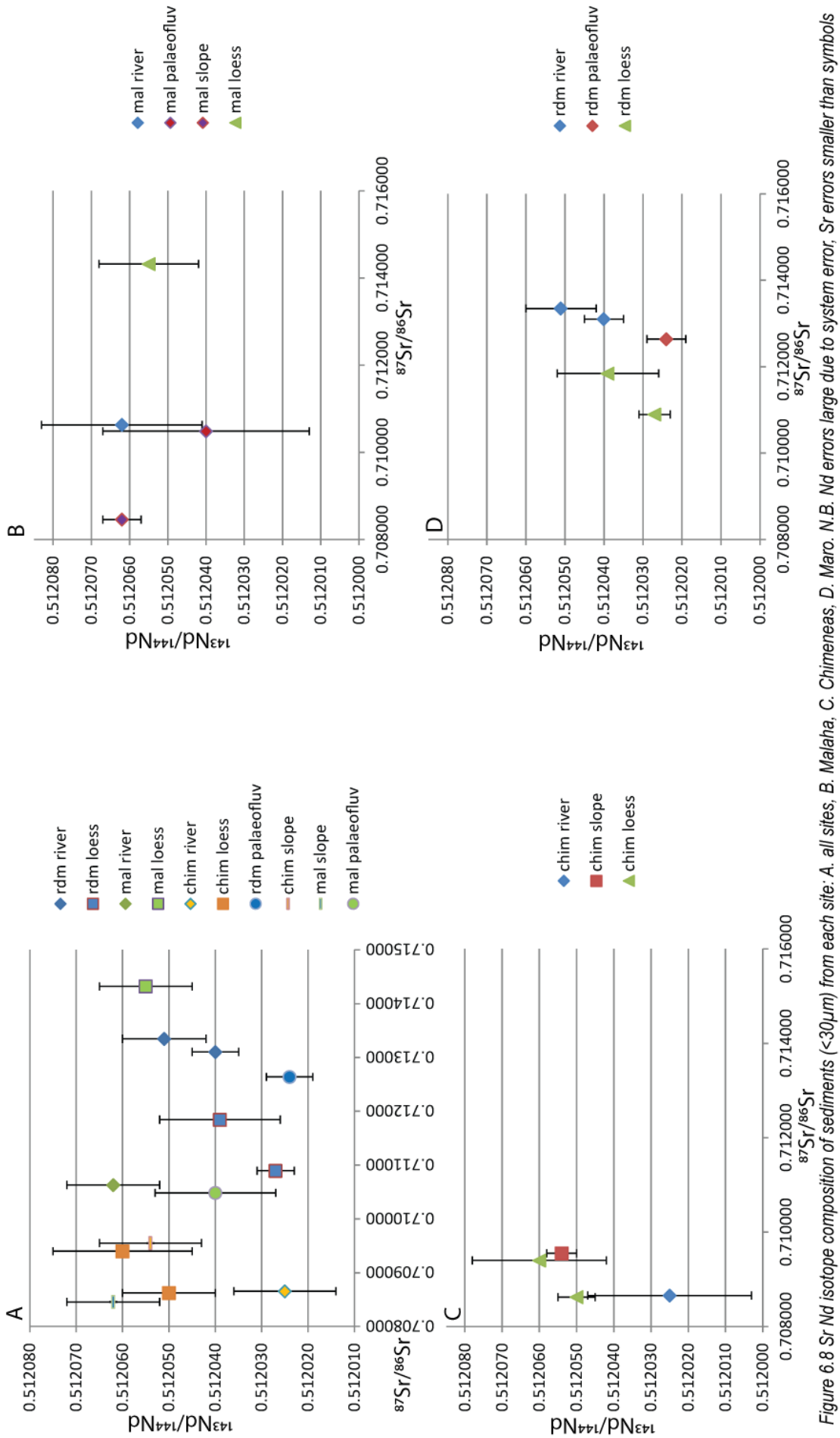

Figure 6.8 Sr Nd isotope composition of sediments (<30μm) from each site: A. all sites, B. Malaha, C. Chimeneas, D. Maro. N.B. Nd errors large due to system error, Sr errors smaller than symbols

6.6.4 Summary

The Sr-Nd ratios obtained for the sediments sampled in southern Spain show a range of values from high Sr (e.g. Malaha loess) to low Sr (e.g. Malaha slope material) (figure 6.6). Unfortunately, due to system issues, the errors associated with Nd values are too large to enable discrimination of data using this proxy. The results from this study are compared to potential regional end members in figure 6.9, with two volcanic sources (Iberian and Moroccan) providing low Sr-high Nd sources (Gomez-Pugnarie *et al.* 2000, Gill *et al.* 2004) and North African dusts providing a potential high Sr-low Nd end member (Grousset and Biscaye 2005 and references therein). Mixing hyperbolas are shown in figure 6.9, and were calculated from representative volcanic and dust data using the equations of DePaolo, incorporating both elemental concentrations and the isotopic composition of the end members (Langmuir *et al.* 1978, DePaolo and Wasserburg 1979).

The samples from Maro and the Malaha loess all have high Sr values and so trend towards North African aerosol composition, indicating that it is a possible sediment source for the deposits. In particular, the Malaha loess sample is very close in isotopic composition to the North African aerosol samples and so is likely to contain a high North African dust component. It does, however, not show an identical isotopic composition to North African dust and therefore, Malaha loess would require a small input from a low Sr component to contribute to its isotopic composition. There is limited data available regarding the isotopic composition of aerosols from specific North African regions, so it is not currently possible to state a specific source region from the data currently available. The isotopic composition of the samples from Chimeneas and the fluvial and slope samples from Malaha do not appear to contain such a large proportion of the North African dust component. These samples have low Sr-high Nd contents, suggesting an increased volcanic input.

This data indicates a possible North African component to sediments from Maro (all samples) and La Malaha (loess). The close correlation between North African aerosol data and that of the Malaha loess sample indicates that North African dust is a large component of this sediment. Although limited in its scale, this data set has identified differences between locally derived sediments and those with a far travelled component. Additionally, there appear to be important differences in the provenance of loess-like sediments within southern Spain and, with a more extensive database for comparison and further analysis of Spanish sediments, it may be possible to identify specific source regions for locally derived and far travelled sediment components.

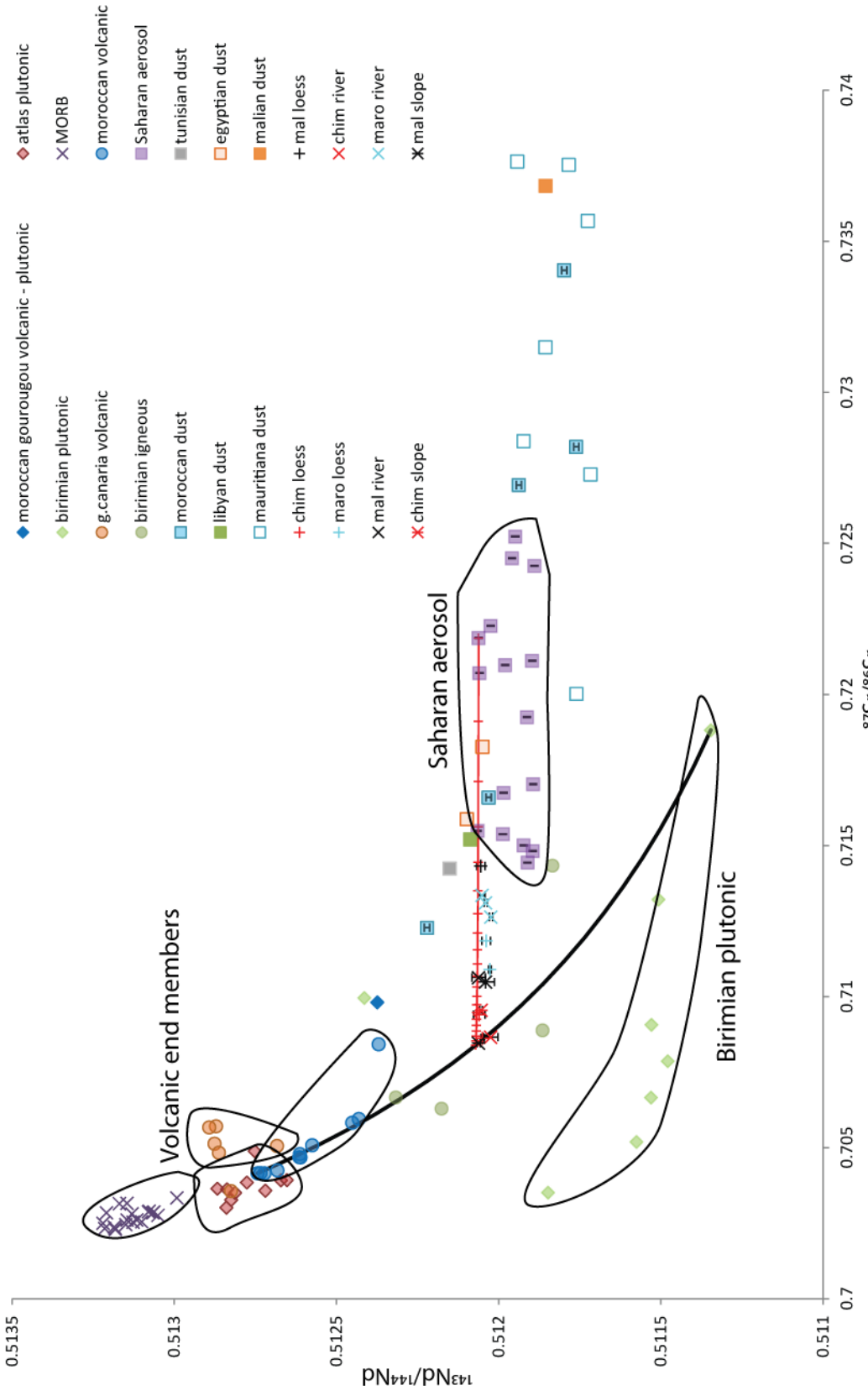

Figure 6.9 Comparison of Sr and Nd ratios of sediments from Maro, Malaha and Chimeneas with potential regional sources. N.African data from Grousset et al 1998 and Grousset and Biscaye 2005, Moroccan volcanics data from Gill et al 2004, Sierra Nevada Igneous data from Gomez-Pugnarie et al. 2000, Birimian data from Taylor et al. 1992. Sr errors smaller than data points, Nd errors shown for data produced in this project

6.7 The identification and nature of loess in southern Spain

Loess-like sediments were identified in the field on the basis of their well sorted, homogenous nature, buff colouration and cohesive nature (e.g. Pecsi 1990). Median grain size of loess-like sediments in southern Spain ranges from ~3-42 μm, with mean $CaCO_3$ content ranging from ~17-32% (Table 6.2). Loess-like sediments are composed of clays (dominantly illite), calcite, quartz, feldspar and dolomite. In terms of grain size, $CaCO_3$ and mineralogical composition loess-like sediments are not readily distinguishable from other fine grained sedimentary environments.

SEM analysis of grain surfaces indicates differences in grain surface characteristics between fluvial sediments and loess-like sediments at Maro and La Malaha (figure 6.7); there is, however, no discernible difference between grain surfaces at Chimeneas.

Sr-Nd isotopic composition of the sediments provides perhaps the most useful discriminatory tool. The loess-like sediments at Chimeneas have an indistinguishable isotopic composition compared to the local sediment systems (fluvial and slope), and are therefore referred to as locally derived sediments. At Maro, there is some difference in isotopic composition of the sediments, with the loess-like sediments having lower Sr values than the fluvial sediments, possibly suggesting a different sediment source. At Malaha, there are clear differences in isotopic composition between the local sediment systems (fluvial and slope) having low Sr values and that of the loess-like sediment with a high Sr value. The isotopic composition of the loess-like sediment from Malaha is closely comparable with North African aerosol data, and it is suggested that the loess-like sediments at Malaha have a large North African dust component.

On this basis, it is suggested that the loess-like sediments at Malaha are a far-travelled loess sediment. Although the origin of the Sr-Nd signal of the Maro samples is less clear, on the basis of SEM grain analysis indicating the loess-like sediments at Maro to be very similar in nature to those of Malaha, Maro is also identified as loess. The coarser nature of the loess sediments at Maro compared to Malaha may indicate a greater degree of reworking or local sediment input. Evidence from Chimeneas indicates a locally derived sediment, similar in geochemical, mineralogical and grain characteristic terms to that of the local sediments systems. This does not, however, mean that the loess-like sediments at Chimeneas cannot be loessic in nature. Last glacial loess in the Mediterranean is often described as heavily reworked, locally sourced sediment (e.g. Günster *et al.* 2001, Garcia *et al.* 2010, 2011). It is therefore, suggested that, due to the cohesive, homogenous nature of the loess-like sediments at Chimeneas, which distinguishes them from the other fine grained sediment deposits in the region, the loess-like sediments represent heavily reworked, locally derived loess.

Chapter 7 – La Malaha

This chapter presents the work undertaken at La Malaha. Firstly, an introduction to the geography of the surrounding area will be presented. Secondly, the results from La Malaha will be presented, with a synthesis of the results will presented through a pedo-sedimentary depositional model and palaeoenvironmental interpretation of the sequence.

7.1 Site introduction

This sediment exposure is located 1.5 km south of the town of La Malaha, which lies 14 km southwest of Granada (Figure 7.1). Geologically the site is situated at the contact zone of the internal and external zones of the Betic Cordillera and lies within the confines of the Granada basin, a Neogene basin comprising marine marls, limestones and gypsum as well as continental sands, silts and conglomerates (Figure 7.2). To the south lie the basement ranges consisting of Triassic dolomites, limestones and marbles (Figure 7.2). The La Malaha sequence, studied as part of this research, is exposed in the wall of a ~4 metre deep gorge cut by the Arroyo del Salado, a southeast to northwest draining tributary of the Rio Genil. The exposure is shown in figure 7.3. The base of the studied section, which occurs in the west wall of the Arroyo, is found 2 metres above the modern river channel. The lowermost 1.5 metres of the section consists of a massive, silt-dominated unit and is overlain by 2.5 metres of fluvial sands and gravels. In the field the well-sorted, massive nature of the silt-dominated unit met the published criteria for loess or loessic material. Consequently, only the silt-dominated unit is described here.

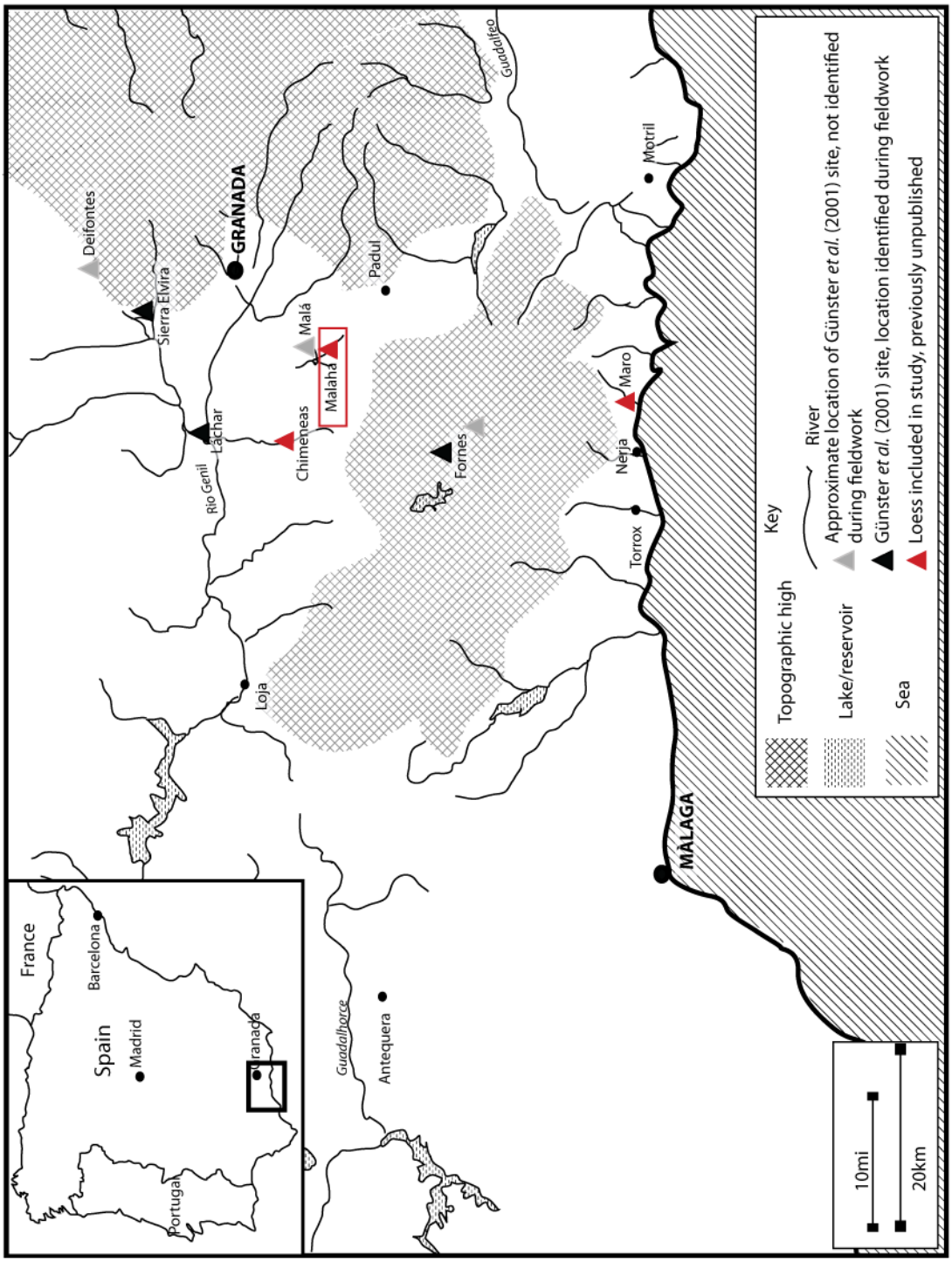

Figure 7.1 Map showing the location of the La Malaha exposure, with key towns and loess sites for reference.

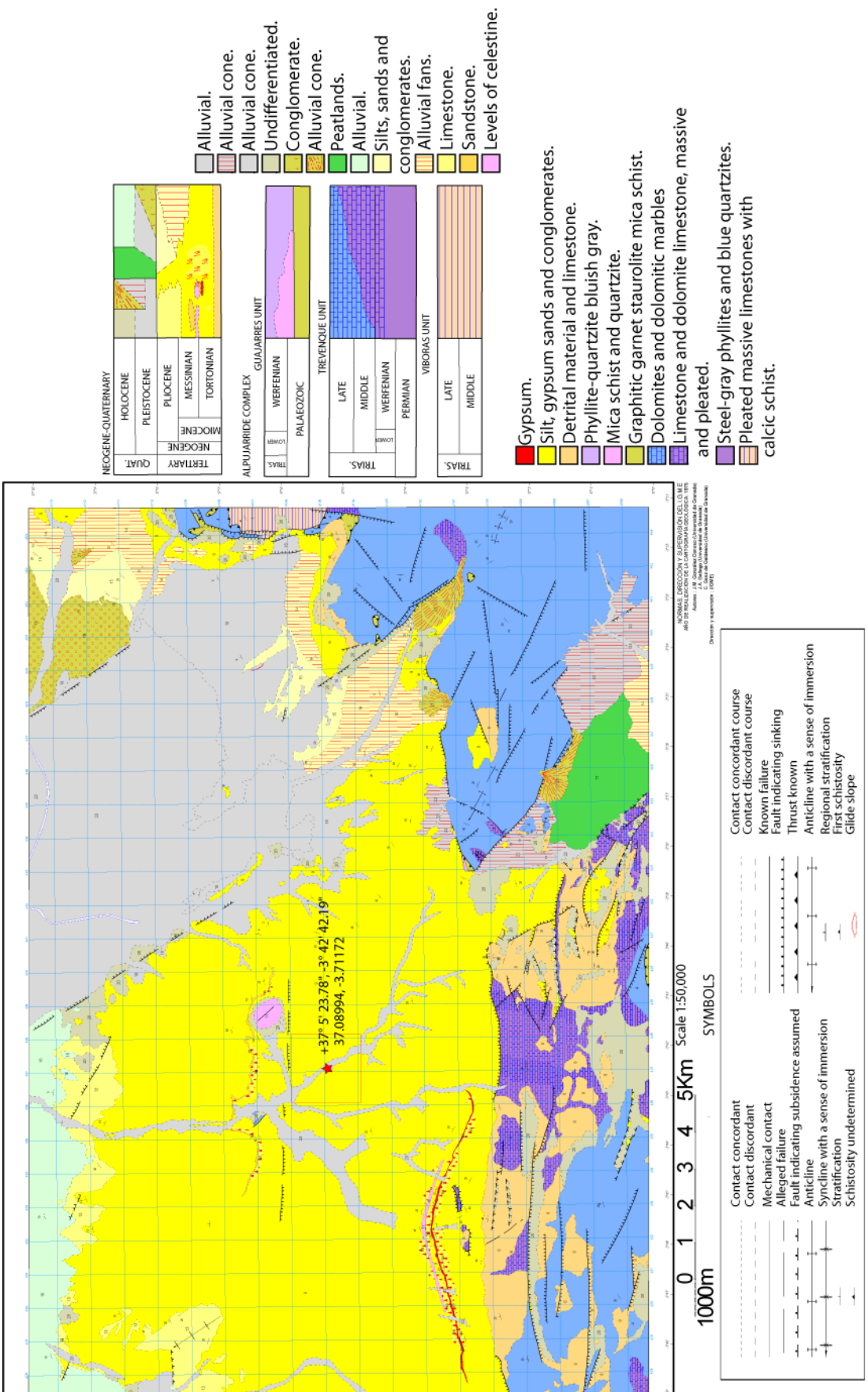

Figure 7.2 Geological map of the region around La Malaha. Adapted from the geological map of González et al. (1985).

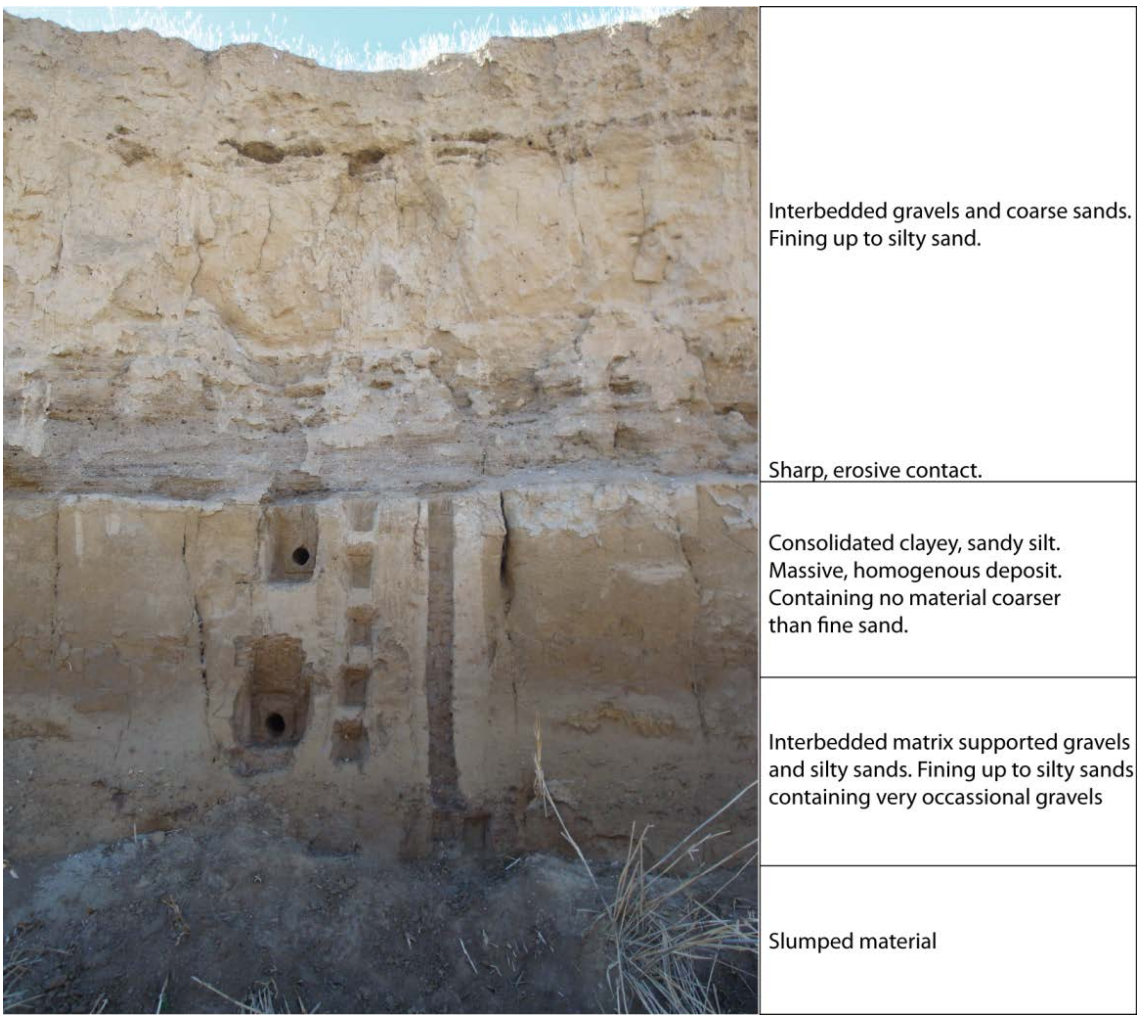

Figure 7.3 Photograph showing the exposure at La Malaha. Showing the situation of the studied section and the underlying and overlying sediments. Photograph taken by author.

7.2. Field descriptions and sampling

The section at La Malaha consists of two main units (figure 7.4). Unit 1 (0-67 cm) is a moderately to poorly sorted sediment consisting of clayey silts and sands with occasional gravel clasts interspersed with gravel lenses. Unit 2 (67-154 cm) is a cohesive, better sorted silt-dominant deposit. Clear colour variations occur through unit 1 and powdery carbonates are found throughout (figure 7.5).

Unit 2 was identified as sharing many of the sedimentary characteristics of loess deposits (chapter 3); therefore the majority of samples were taken from this unit. The lower unit was also sampled in order to characterise the processes operating at La Malaha prior to the accumulation of unit 2. Sampling locations are shown in figure 7.6.

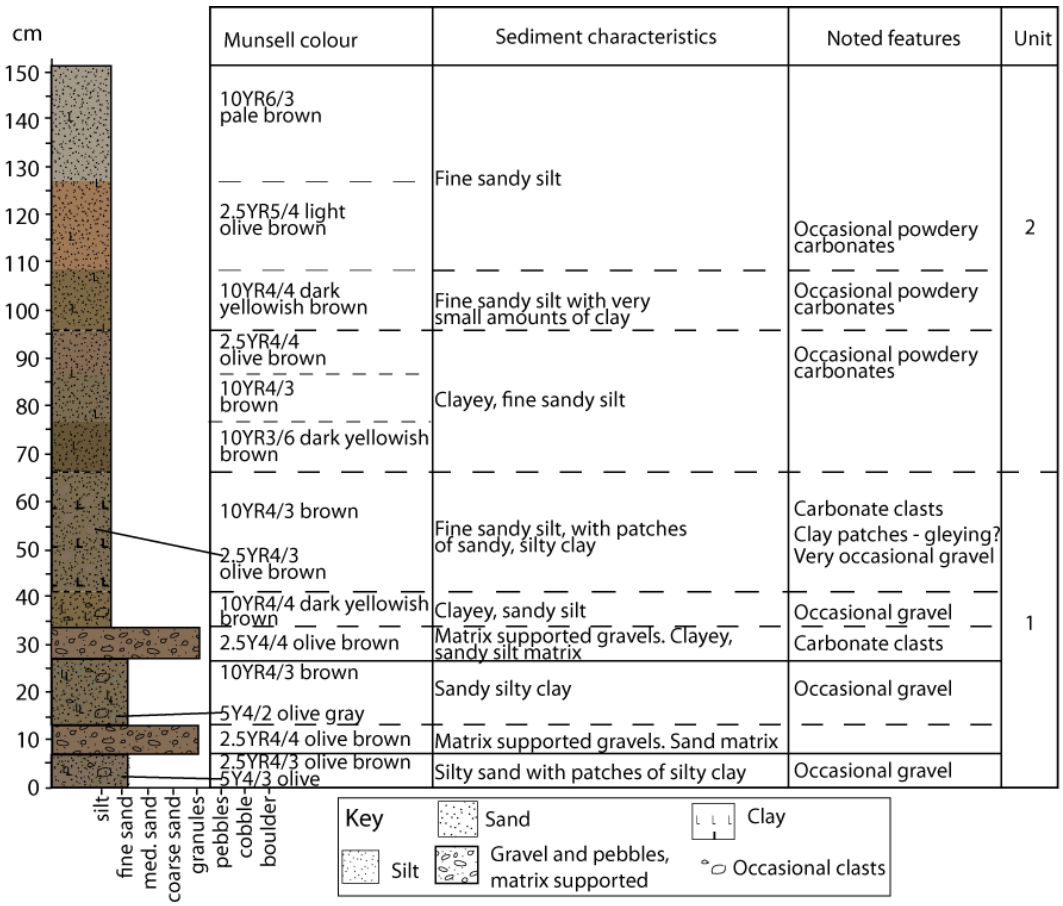

Figure 7.4 Field log of La Malaha with descriptions of noted sedimentological changes. Graded shifts between sedimentological changes are marked with a dashed line. Sharp contacts between beds of sedimentologically distinct beds are marked with a solid line. Colours assigned to the sediment log are recreations of Munsell colours.

Figure 7.5 Carbonate (example circled in red) within a gravel bed of unit 1 and less common carbonates within a fine grained bed of unit 1 at La Malaha. Photograph taken by author.

Figure 7.6 La Malaha sampling locations

7.3 Results

7.3.1 Particle size analysis

All results are given in % total weight. PSA was undertaken following the methods outlined in chapter 5. As discussed in chapter 5, no pre-treatment (e.g. HCl) was undertaken on the sediments prior to PSA, as aeolian sediments are often rich in carbonate (Pye 1984, Pécsi 1990) and, as such, represents material of interest within this study.

Table 7.1 Summary statistics for sedimentological variations present at La Malaha. Median grain size for each group is the mean calculated from the median grain sizes calculated from each bulk sample.

	Depth (cm)	Median (μm)	St dev (μm)	90% C.I. (μm)
Unit 2	0-84	2.73	0.21	0.09
Unit 1 fine	84-109	2.85	0.24	0.23
Unit 1 coarse	109-139	5.77	4.05	6.83

Through unit 2, grain size varies very little, with the entire unit being comprised predominantly of fine, silt material (table 7.1, figure 7.7). There is a negligible gravel component ranging from 0 to 0.19% weight, sand content varies from 0.73 to 1.40% weight, silt content ranges from 52.04 to 58.02% weight and clay ranges from 40.65 to 46.28% (raw data in appendix). The average median grain size of the bulk samples from unit 2 is 2.73μm. Within unit 2, the depth of increased clay content occurs at the same level as sediments noted in the field to be darker in colouration and where powdery carbonates occur (~30 cm depth) (figure 7.4).

In the fine grained beds of unit 1 there is again, very little variation in grain size. As with unit 2, the unit consists primarily of fine silts (table 7.1, figure 7.7), with the average median grain size of the bulk samples being 2.85 μm. Gravel content ranges from 0.30 to 1.60% weight, sand content varies from 1.57 to 5.90% weight, silt content ranges from 47.79 to 56.24% weight and clay ranges from 41.37 to 45.91% (raw data in appendix).

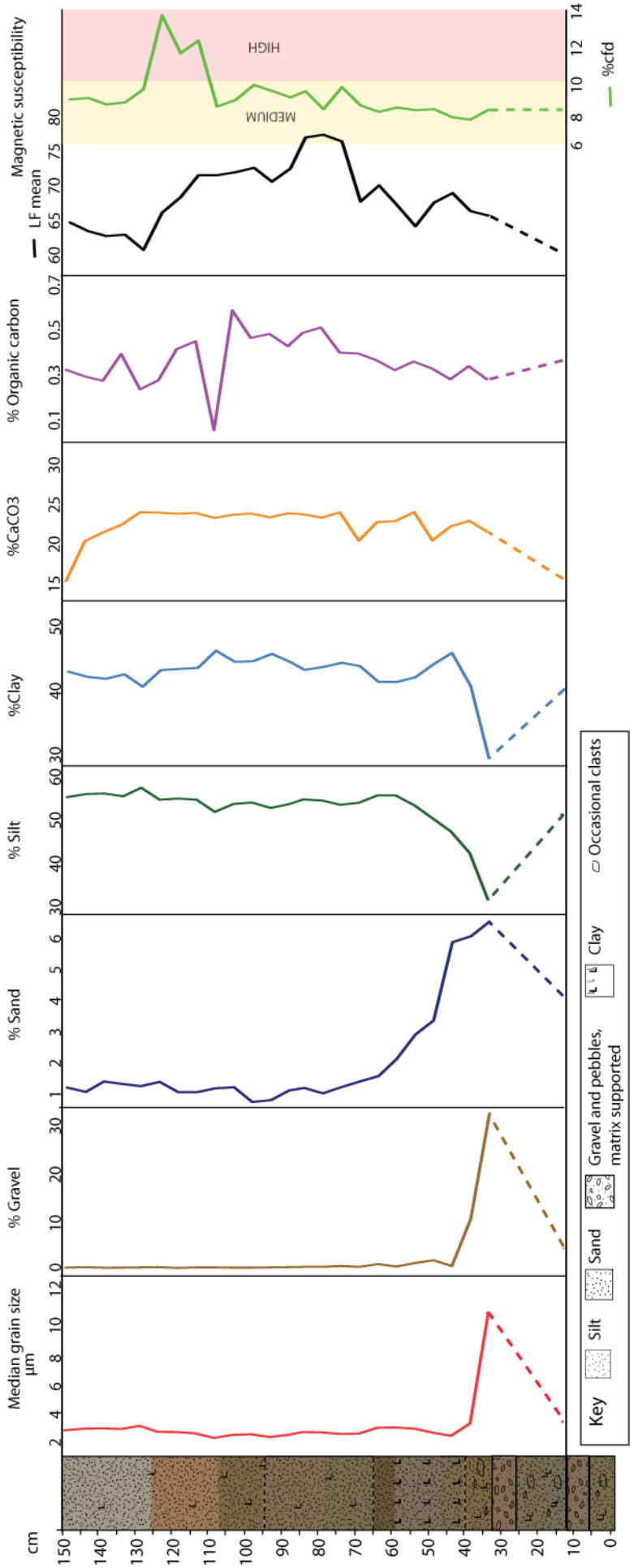

Figure 7.7 Bulk sedimentological analysis data from La Malaha against stratigraphy. The dashed line indicates inferred sediment shift due to discontinuous sampling strategy used to characterise grain size of unit 1

The gravel beds of unit 1 show a greater variation in grain size between bulk samples (table 7.1) relating to the relative dominance in gravels between beds. The average median grain size of bulk samples from this section of the sequence is still silt (5.77 μm). However, as shown by the population parameters in table 7.1 and figure 7.8, there is an increased coarse component within these sediments. Gravel content ranges from 4.19 to 32.14% weight, sand content varies from 4.15 to 6.56% weight, silt content ranges from 31.82 to 51.60% weight and clay ranges from 29.49 to 40.74% (raw data in appendix).

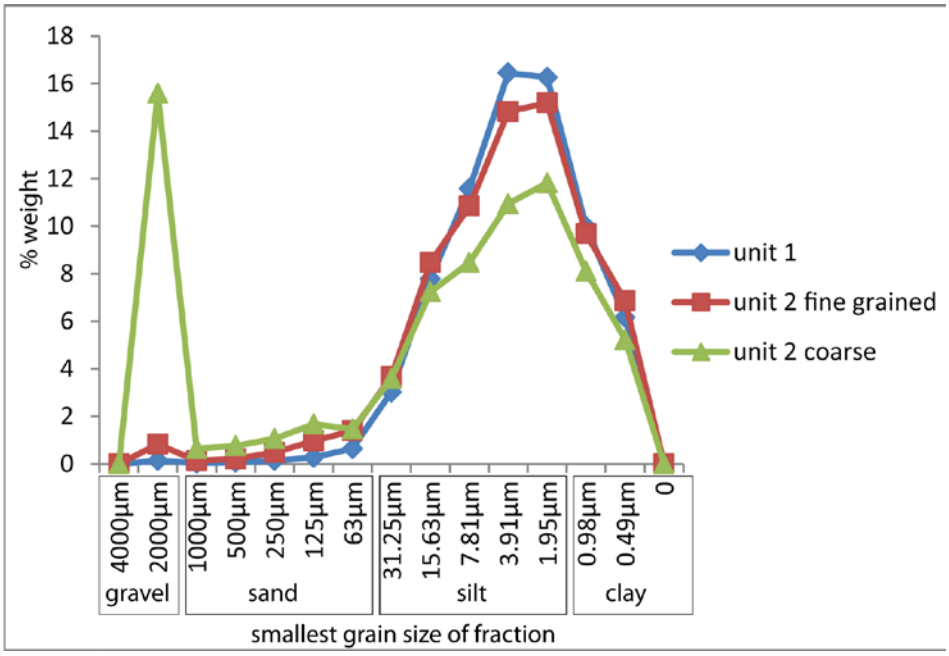

Figure 7.8 Average % weight of each size fraction from PSA, for all bulk samples belonging to the three sediment types present at La Malaha.

As shown in figure 7.8, the section at La Malaha becomes coarser with depth, with a reduction in both silt and clay content from unit 2 to unit 1.

7.3.2 Calcium carbonate content

In both units at La Malaha, there are only small shifts in $CaCO_3$ content, ranging from ~15-25% (figure 7.7). Unit 2 shows the largest variations, with the top of the sequence having a calcium carbonate content of 15.46%, increasing to 24.15% at 134-129 cm depth. Average content is 22.76% with a standard deviation of 2.24%.

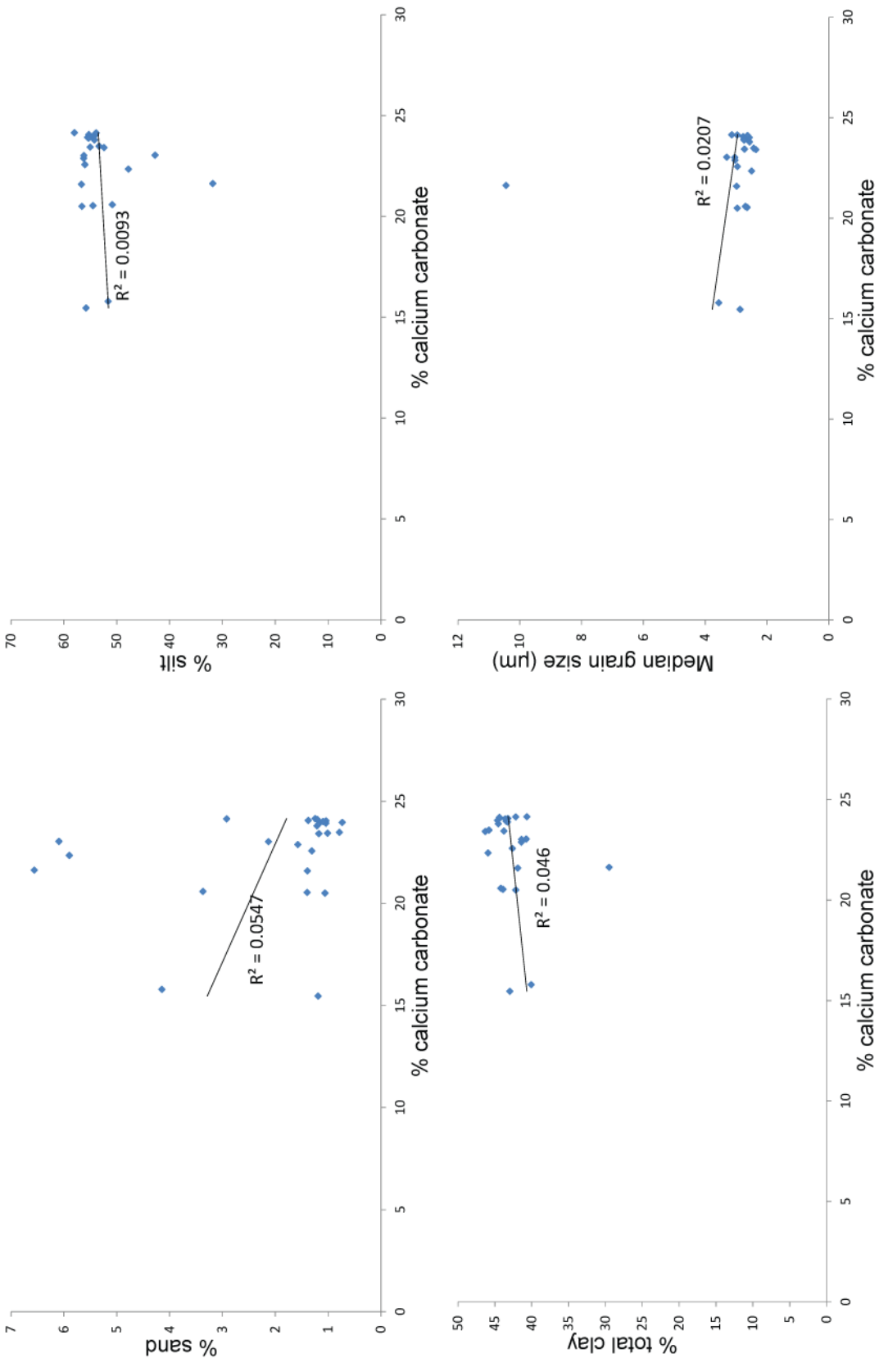

Figure 7.9 Calcium carbonate content plotted against various grain size parameters, showing lack of correlation between the two measurements.

The finer sediments of unit 1 have a similar average $CaCO_3$% content to that of unit 2 (22.59%), however, there is less variation in this unit, with values from 20.58 to 24.14%. There is greater variability in carbonate content through the coarse beds of unit 1, with values ranging from 15.79 to 23.04%, and the lowest value occurring in lowest bulk sample taken, beneath one of the gravel rich beds. Raw data can be found in appendix.

A concern with producing accurate grain size measurements when not using an acid pre-treatment is that there may be interference in grain size resulting from disaggregation of calcium carbonate during analysis. Within the sequence at La Malaha, there is no correlation between the carbonate content and the grain size; this suggests that the calcium carbonate content is not affecting the grain size (figure 7.9).

7.3.3 Magnetic susceptibility measurements

As outlined in chapter 5, magnetic susceptibility is measured on two frequencies (high and low). The difference between readings taken at the two frequencies is a measure of the abundance of ultrafine (<0.03 μm) superparamagnetic (SP) minerals which occur as a result of soil processes (Dearing 1999). Dearing (1999) states that in samples where SP minerals are present, high frequency magnetic susceptibility readings will be lower than those for low frequency magnetic susceptibility; giving a high combined frequency difference reading (%cfd). All measurements are mass and volume corrected to 10^{-8} m^3 kg^{-1} (raw data in appendix).

Table 7.2 Summary of magnetic susceptibility measurements from the sediments at La Malaha. LF=low frequency, HF = high frequency, Cfd= % combined frequency difference.

		χLF				χHF				χCfd %			
Sediments	Depths (cm)	min	max	mean	St dev	min	max	mean	St dev	min	max	mean	St dev
Unit 2	0-84	60.88	77.85	69.93	5.36	55.24	71.56	63.09	5.04	8.08	13.62	9.40	1.53
Unit 1 fine	84-109	64.40	70.42	67.89	0.24	59.24	64.84	62.49	1.30	7.59	8.19	7.96	2.27
Unit 1 coarse	109-139	60.36	66.64	64.31	3.44	55.50	61.66	59.26	3.30	7.47	8.07	7.86	0.34

All of the units are characterised by relatively low levels of magnetic susceptibility (table 7.2) for both low and high frequency susceptibility, indicating relatively low levels of magnetic minerals. As shown by figure 7.7, the variations in %cfd do not correlate with lf values. %cfd values are relatively stable throughout the section, varying between 8 and 9%, except at depths 124-114 cm, where there are raised %cfd values of 11.40-13.60%. The peak in %cfd occurs where there is a

darkening of the sediments, and around the area where powdery carbonates first occur in the section.

7.3.4 Organic carbon content

The sediments contain very small quantities of organic carbon, with values consistently <0.6% (figure 7.7, table 7.3). Values as low as this do not indicate any significant accumulation of organic carbon, so will not be discussed further.

Table 7.3 Summary statistics for organic carbon content through La Malaha sediments

	Depths	Max (%)	Min (%)	Mean (%)	St dev
Unit 2	0-84	0.59	0.05	0.38	0.13
Unit 1 fine	84-109	0.36	0.28	0.33	0.03
Unit 1 coarse	109-139	0.36	0.28	0.33	0.04

7.4 Micromorphology

7.4.1 Groundmass and Skeleton grains

All thin sections were initially described in terms of their general characteristics (figure 7.10); texture, composition and structure. Texture is given as the ratio between coarse (>20 μm) skeleton grains and fine (<20 μm) groundmass components stated as c:f (Kemp 1985a, King 2000, Bullock *et al.* 1985). C:f ratios of unit 1 are 1:1 and unit 2 are 1:2, all showing open porphyric structure (Bullock *et al.* 1985). At Malaha, sediments with high proportions of coarse-grained sediments also contain high proportions of sub-angular rather than angular material. No quantitative assessment of mineralogy was undertaken via thin section analysis.

Groundmass was described in terms of homo/hetero-geneity (texture and colour) and preferred orientation of groundmass components give in terms of birefringence fabrics (Kemp 1985a, Bullock *et al.* 1985). The sections from Malaha record undifferentiated and crystallitic birefringence (figure 7.10), where crystallitic fabrics occur where groundmass is micrite enriched (Kemp 1985a, Bullock 1985, Stoops 2010). The majority of void types recorded in the La Malaha sequence are vughy, channel or vesicle voids, thought to relate to biological activity within the sediments (Kemp 1985a, King 2000, Stoops 2010).

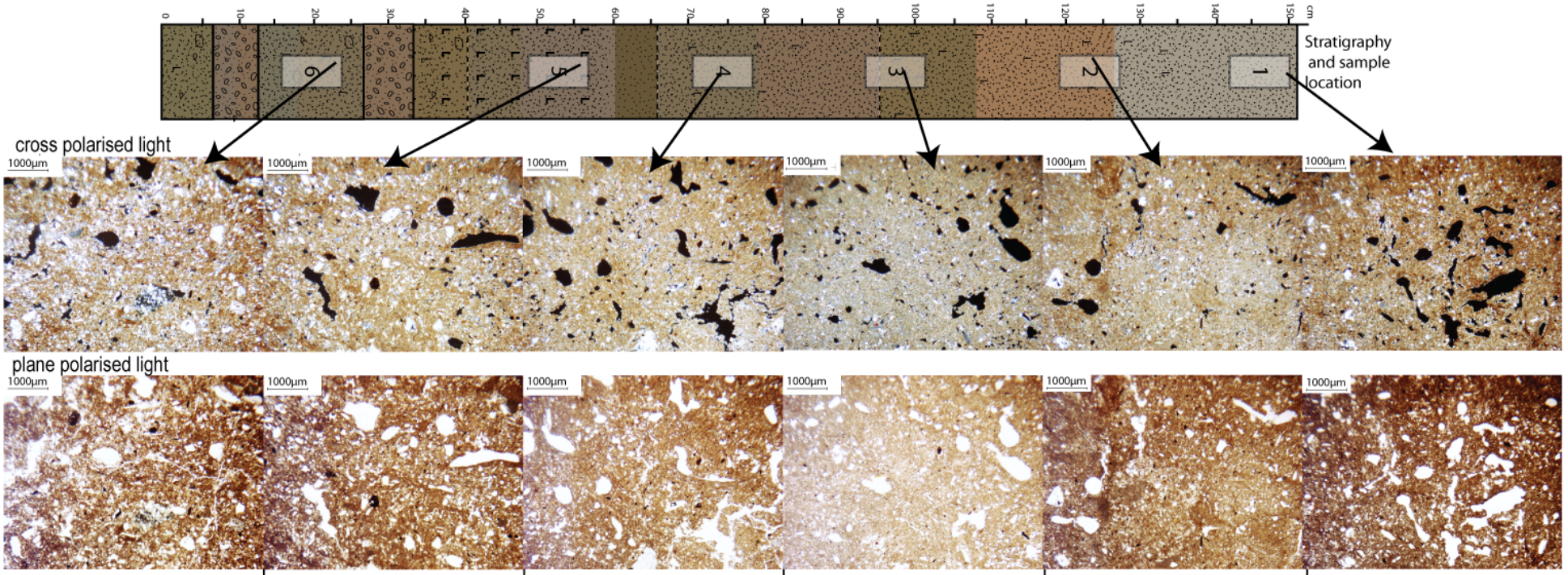

Groundmass: Homogeneous: c:f 1:1. Poorly sorted gravel, sand, silt and clay. Skeleton grains up to fine gravel, increased coarse and medium silt content compared to MAL 4-1. Grains are dominantly sub-rounded to sub-angular, equant, medium silt.Micromass is dominantly composed of an undifferentiated b-fabric. Structure: Massive, 5% voids: dominant meso-vughy, frequent meso-channel, rare mesoto micro-vesicle.	Groundmass: Homogeneous: c:f 1:1. Moderately sorted sand, silts and clay. Increased skeleton grain content. Skeleton grains up to fine sand, increased coarse and medium silt content compared to MAL 4-1. Grains are dominantly sub-rounded to sub-angular, equant, medium silt. Micromass is dominantly composed of an undifferentiated b-fabric. Structure: Massive, 5% voids: dominant meso-channel, frequent meso-vughy.	Groundmass: Homogeneous: c:f 1:2. Well sorted silts and clay. Very rare coarse silt, fewer skeleton grains than MAL 3. Skeleton grains are dominantly angular to sub-anglular, equant, medium silt with rare coarse silt. Common prolate fine silt grains. Micromass is equally composed of an undifferentiated b-fabric and crystallitic b-fabric. Structure: Massive, 15-20% voids: frequent meso-planar, frequent meso-vughy and common meso-vesicle.	Groundmass: Homogeneous: c:f 1:2. Well sorted silts and clay. Rare coarse silt, fewer skeleton grains that MAL 2. Skeleton grains are dominantly angular to sub-anglular, equant, medium silt with rare coarse silt. Common prolate fine silt grains. Micromass is equally composed of an undifferentiated b-fabric and crystallitic b-fabric. Structure: Massive, 10% voids: dominantly meso-channel, frequent meso-vughy.	Groundmass: Homogeneous: c:f 1:2. Well sorted silts and clay. Slightly increased skeleton grain content compared to MAL 1. Skeleton grains are dominantly angular to sub-anglular, equant, medium silt with some coarse silt. Common prolate fine silt grains. Micromass is equally composed of an undifferentiated b-fabric and crystallitic b-fabric. Structure: Massive, 20% voids: dominantly meso-vughy, frequent meso-vesicle, few meso-channels.	Groundmass: Homogeneous: c:f 1:2. Well sorted silts and clay. Skeleton grains are dominantly sub-anglular, equant, medium silt with rare coarse silt. Common prolate fine silt grains. Micromass is dominantly composed of an undifferentiated b-fabric, with common crystallitic b-fabric. Structure: Massive, 20-25% voids: dominantly meso-vughy, frequent meso to micro-channels, very rare meso-vesicles.

Figure 7.10 Images of typical groundmass of each thin section, images taken at 20x magnification in both cross polar, and plane polarised light. Origin of arrows on schematic of Kubiena tin samples, indicates approximate location of photomicrographs. Images are accompanied by a description of the groundmass and structure of the thin sections.

7.4.2 Concentration/depletion features

There are only rare occurrences of preserved organic material within thin sections from La Malaha. These are found as amorphous blackish to reddish brown staining of groundmass or around voids (figure 7.13, 7.16). These amorphous organics are typically significantly decomposed, preserving little or no cellular structure (class 3/4 of Stolt and Lindbo 2010).

Calcitic pedofeatures can form through localised or substantial dissolution, leaching and reprecipitation of calcite (Kemp 1985a). The distribution and morphology of such features is key to understanding the mechanism of their formation (e.g. Kemp 1995, 1999). Features are described in terms of their morphology and crystalline form, where micrite <4 μm, microsparite 5-20 μm and spar >20 μm (Bullock *et al.* 1985, Durand *et al.* 2010). Calcitic pedofeatures at Malaha occur primarily as hypocoatings, void linings, void infillings and nodules (figure 7.11). Calcitic nodules are identified as '*in situ*' if they have a diffuse, irregular contact with the groundmass (Durand *et al.* 2010) (figure 7.12). At Malaha, such features occur as densely cemented micritic to microsparite features, typically <1 cm in size. Hypocoatings are weakly to densely cemented micrite to microsparite formed in the groundmass around voids and, at times, are very extensive features (figure 7.12, 7.14).

There are very rare occurrences of redoximorphic features, present as weakly to strongly impregnated iron/manganese staining of the groundmass (figures 7.16). Redoximorphic features form in relation to soil wetting and drying leading to the mobilisation and oxidation of iron/manganese compounds (Kemp 1985a, King 2000, Lindbo *et al.* 2010).

The morphology of textural and pedogenic features from each thin section is shown in figures 7.11-7.16.

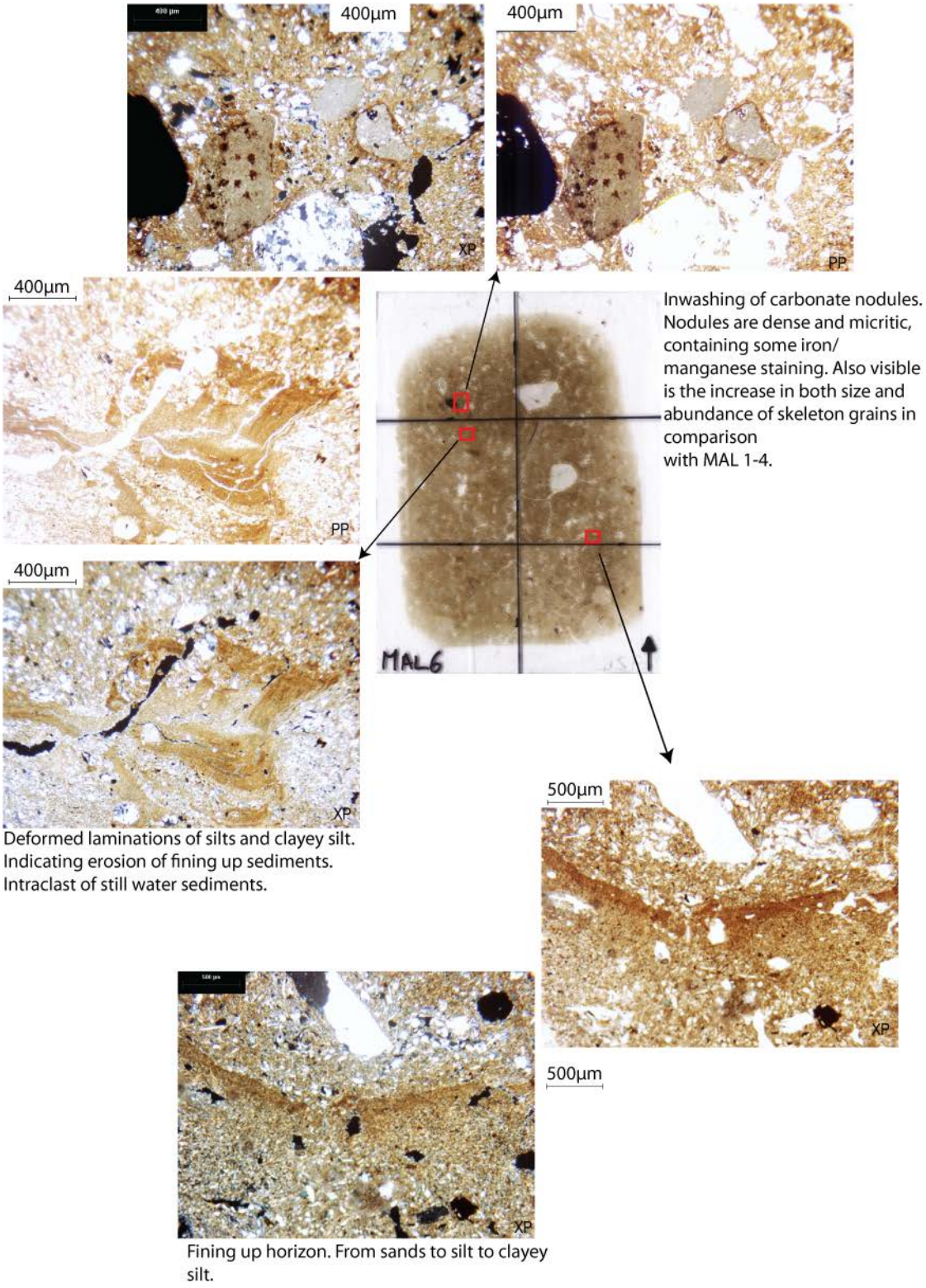

Figure 7.11 Photomicrographs of key features within MAL 6. Xp notates cross polarised light, pp notates plane polarised light. Scale bar present on each photomicrograph, all images orientated correctly.

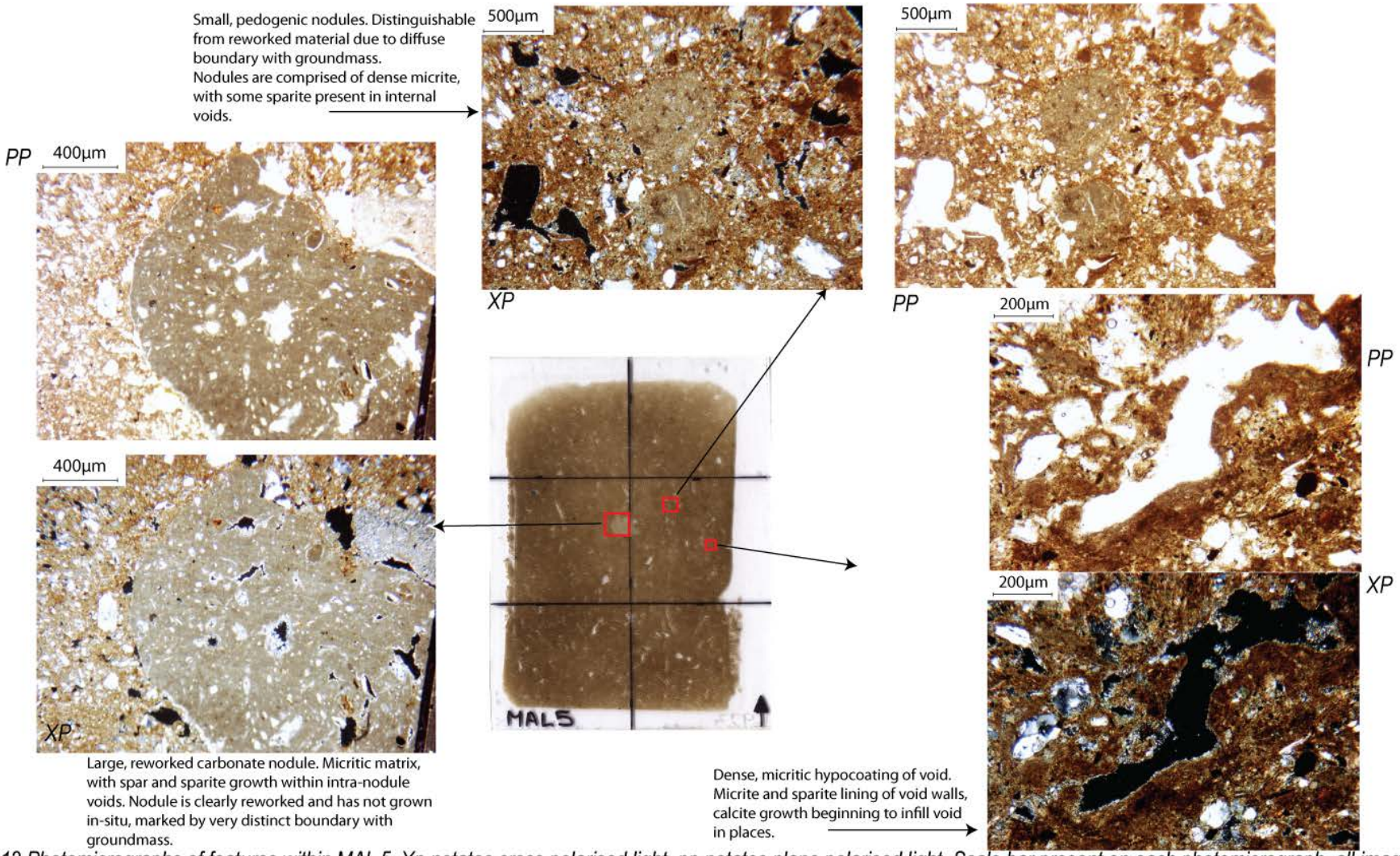

Figure 7.12 Photomicrographs of features within MAL 5. Xp notates cross polarised light, pp notates plane polarised light. Scale bar present on each photomicrograph, all images orientated correctly.

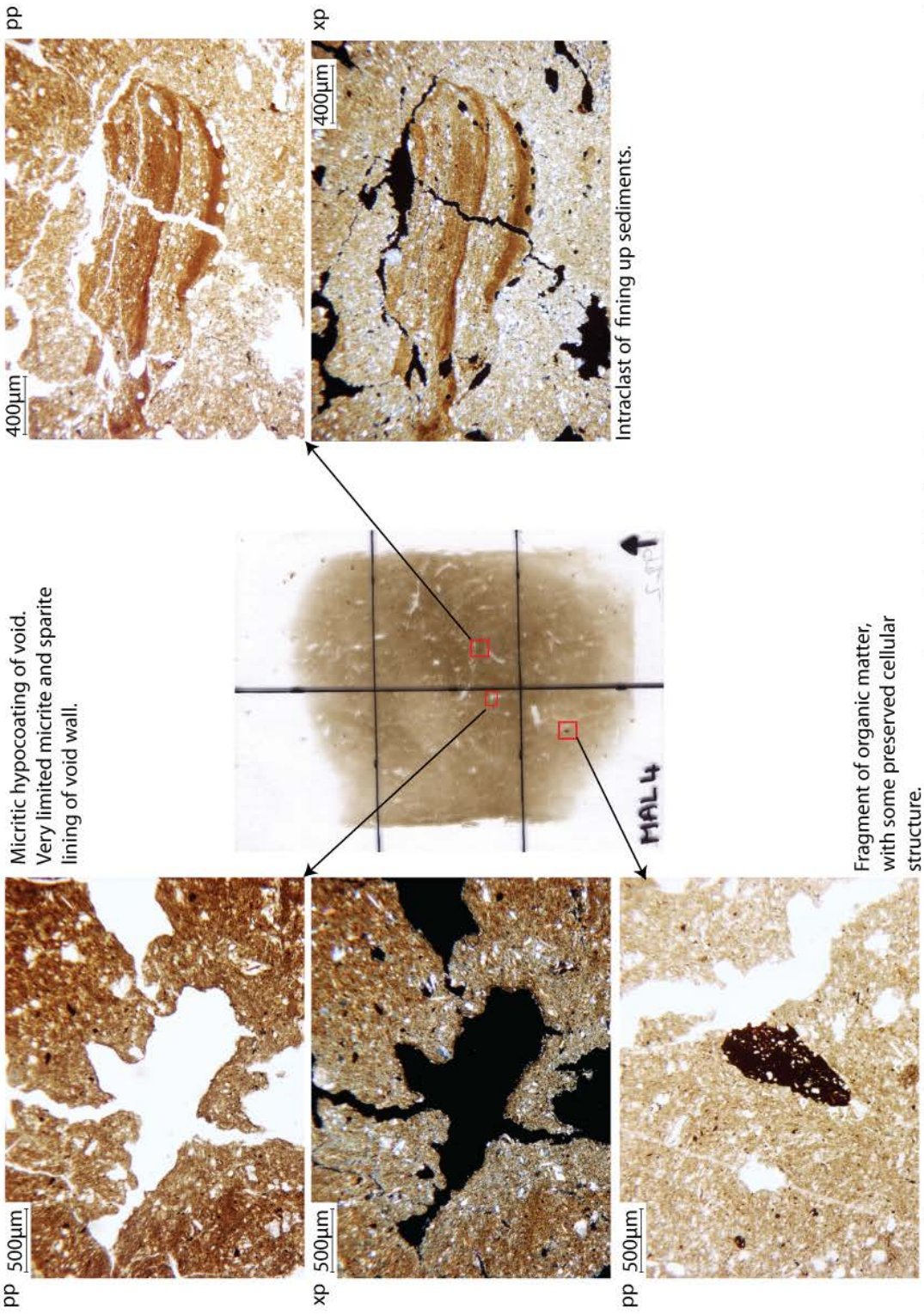

Figure 7.13 Photomicrographs of features within MAL 4. Xp notates cross polarised light, pp notates plane polarised light. Scale bar present on each photomicrograph, all images orientated correctly.

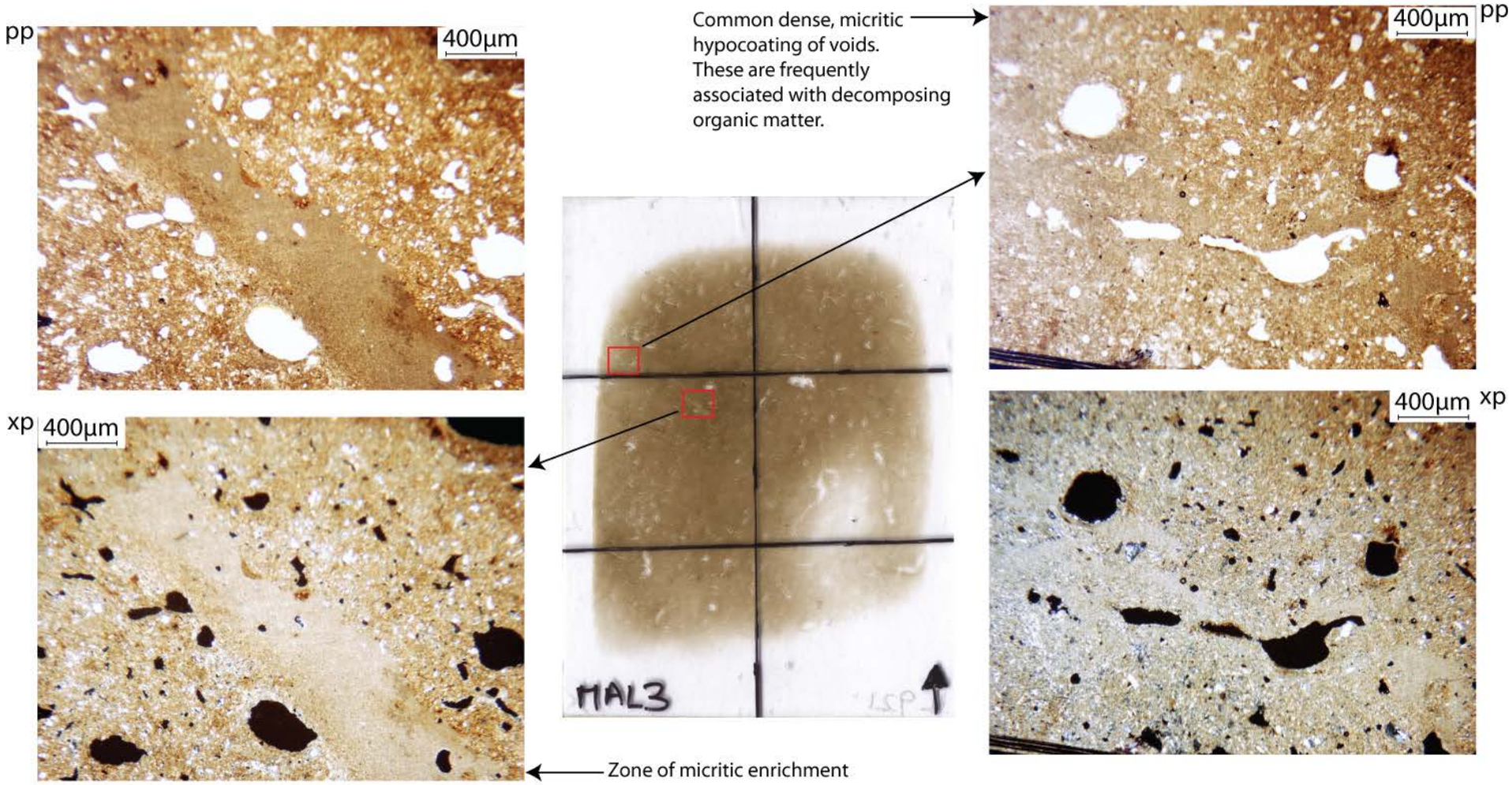

Figure 7.14 Photomicrographs of features within MAL 3. Xp notates cross polarised light, pp notates plane polarised light. Scale bar present on each photomicrograph, all images orientated correctly.

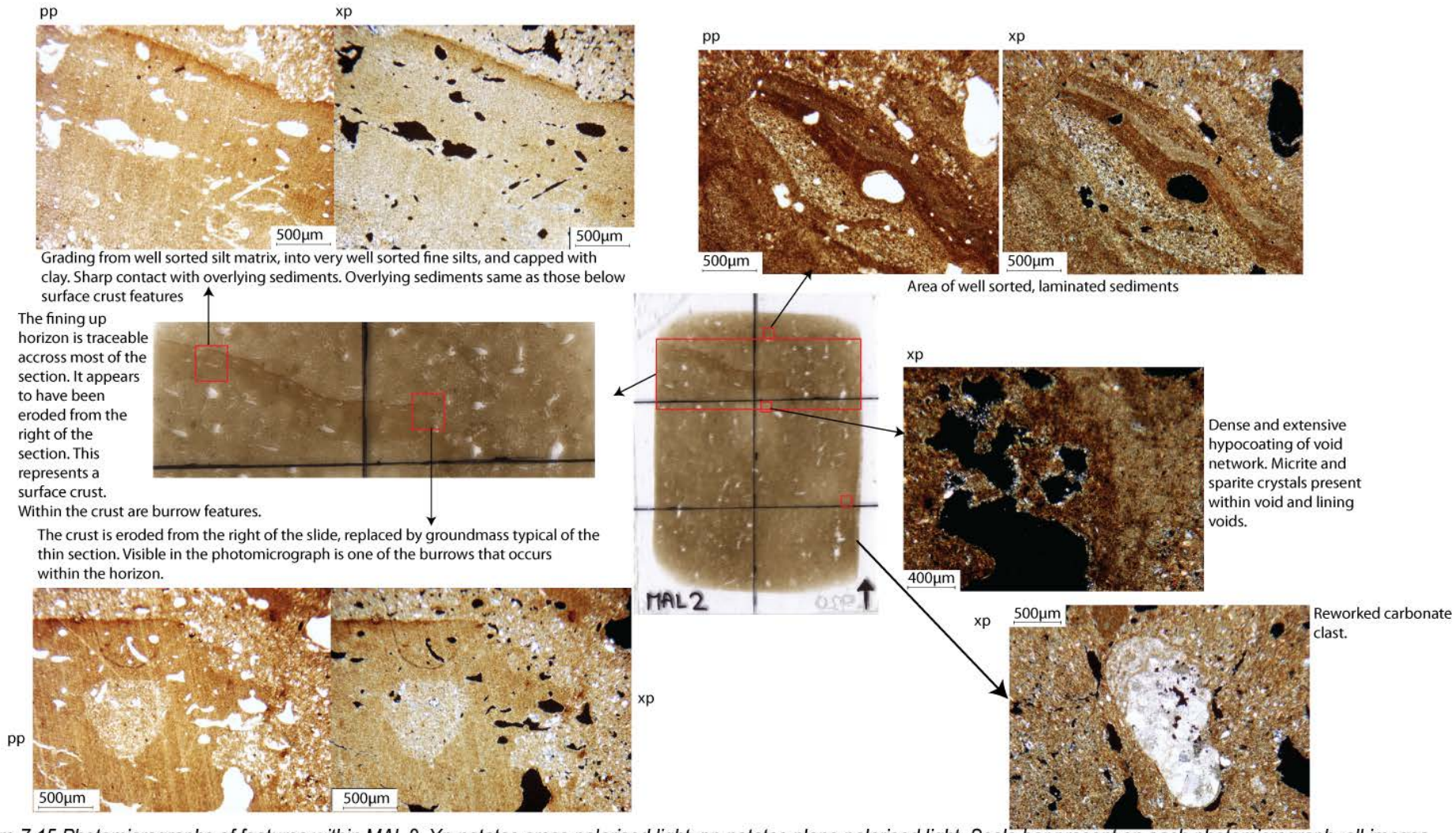

Figure 7.15 Photomicrographs of features within MAL 2. Xp notates cross polarised light, pp notates plane polarised light. Scale bar present on each photomicrograph, all images orientated correctly.

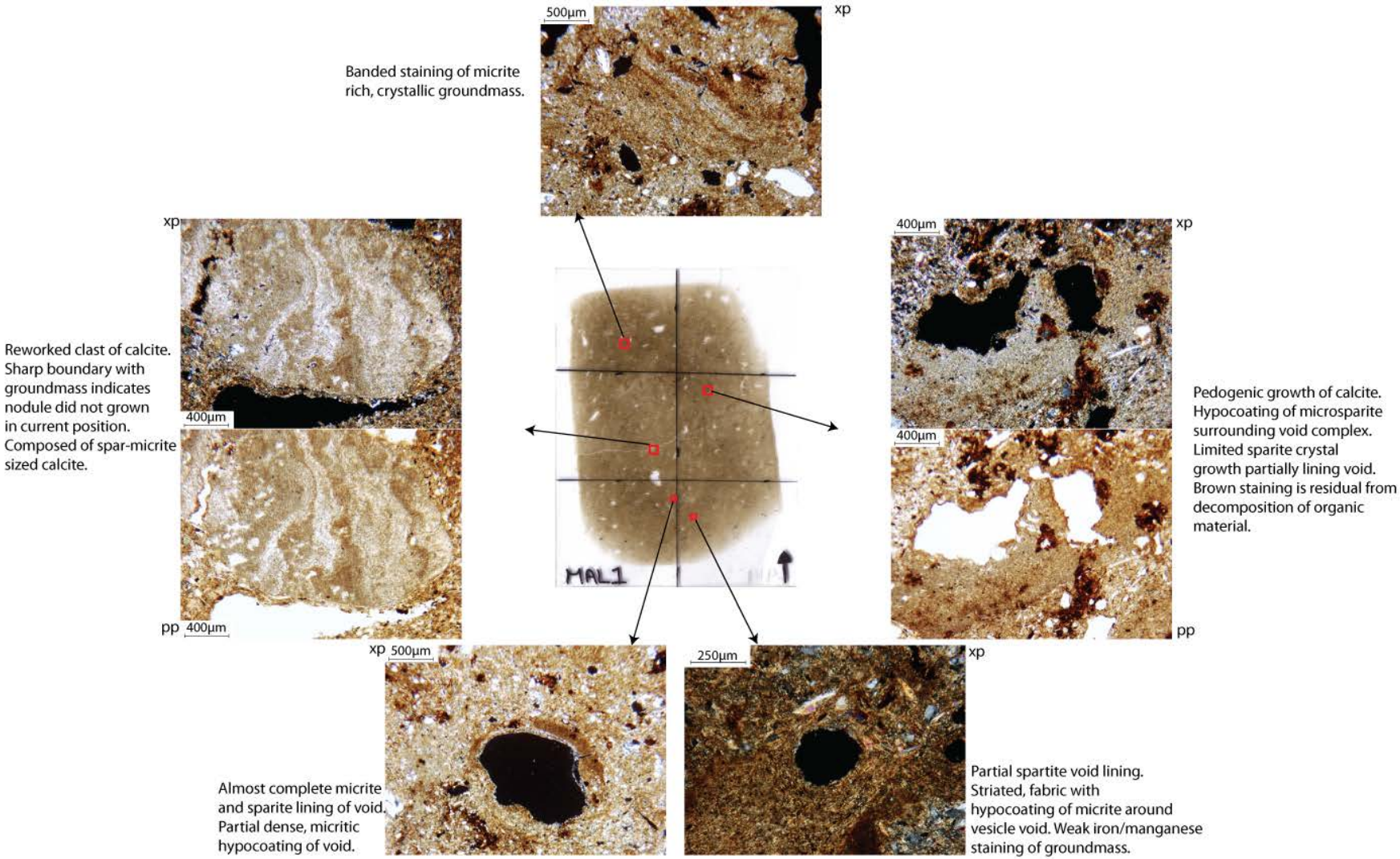

Figure 7.16 Photomicrographs of features within MAL 1. Xp notates cross polarised light, pp notates plane polarised light. Scale bar present on each photomicrograph, all images orientated correctly.

7.4.3 Vertical distribution

7.4.3.1 Unit 1

Unit 1 is identified in thin section as being moderately sorted, with an increased skeleton grain content (relative to unit 2), with grains being up to gravel in size (figure 7.11). Skeleton grains within MAL 6 and MAL 5 are typically sub-rounded, equant to oblate. The texture of MAL 5 records finer sediments than those seen in MAL 6. Additionally, the sediments in MAL 5 are massive, whereas there is evidence of fining sequences and laminations within MAL 6 (figure 7.11). The laminated sediments present (figure 7.11) occur as clearly defined, distinct patches, grading from very well sorted coarse to medium silt to silty clay. The laminations do not occur as continuous horizontal features. The laminated sediments have a clear structure and distinct, sharp boundaries with the groundmass. This suggests that these features are rip up clasts, laminated sediments entrained by tractional currents and laid down when flows wane. Deformation may occur during transport but implies some degree of moisture content within those intra-clasts. The fining-up horizon within MAL 6 is horizontally discontinuous and thin. It records a clear sequence of sorted deposition from fine sands to silty clay. Such a feature may represent deposition under still water conditions, or fining due to surface crusting.

Figure 7.17 shows the distribution of micromorphological features and characteristics through the sediment sequence at La Malaha. There is a progressive fining and increased sorting upwards through the section and also a shift towards increasingly angular skeleton grains. Organic and redoximorphic features are low in abundance throughout the sequence and there is no discernible pattern in their distribution.

Carbonate forms are present within both MAL 6 and MAL 5. Within MAL 6, carbonates are restricted to reworked clasts/nodules and a micritic groundmass (figures 7.10, 7.11). However, within MAL 5, there is evidence for the dissolution and reprecipitation of carbonate as hypocoatings, void linings and small, very rare diffuse pedogenic nodules within the groundmass (figure 7.12).

7.4.3.2 Unit 2

Thin sections MAL 1-4 (figure 7.13-7.16) typically have a high groundmass content, with few skeleton grains (compared to MAL 5 and 6); the skeleton grains present being up to medium silt in size and typically angular to sub-angular (figure 7.17). MAL 1-4 consist of a much finer, better sorted material containing more angular skeleton grains than MAL 5 and 6. As with MAL 5 and 6,

there are only rare occurrences of both organic and redoximorphic features, meaning that there is no discernible pattern in their distribution.

Sections MAL 4-2 record a significant increase in the precentage cover of calcitic pedofeatures upwards through the sequence (20-40 %), and a slight reduction percentage cover recorded in MAL 1 (20 %). This increasing percentage cover is highlighted by the increased abundance of pedogenic nodules, hypocoatings and void linings (figure 7.17). Increasing abundance of calcitic pedofeatures upwards through unit 2 (up to ~125 cm) is consistent with increased localised mobilisation and reprecipitation of carbonate associated with accretionary pedogenic alteration (e.g. Kemp 1995, 1999, 2001). The rates of accretionary pedogenic alteration are thought to be linked to sediment input and/or climate, and it is therefore possible that the pattern of pedogenic modification recorded through unit 2 is consistent with a decreasing sediment input and/or a climatic warming/wetting enabling increased effectiveness of pedogenic processes (e.g. Kemp 1995, 1999, 2001).

There are textural concentration features present within the thin sections of unit 2 (figures 7.13, 7.15, 7.16). Within MAL 2 there is a nearly horizontally continuous textural feature (figure 7.15). This feature grades from the typical groundmass, to a very well sorted fine silt, into a silty clay capping; again with a distinct boundary marking the return to typical groundmass deposition. Within this sediment band are ‘pockets’ of groundmass sediments and a reduced void occurrence compared to the rest of the sediments in MAL 2. As the feature fines upwards out of the groundmass, it is interpreted as being *in-situ*, most likely formed through surface crusting processes (e.g. Belnap 2008). Below this surface crust, there is only one textural feature recorded (figure 7.13) which, as it is distinctly laminated and displays reverse grading, is interpreted as being a rip-up clast feature. Above the surface crust of MAL 2, MAL 1 records a reduction in pedogenic carbonate features and the return to reworked carbonate clasts/nodules (figure 7.16).

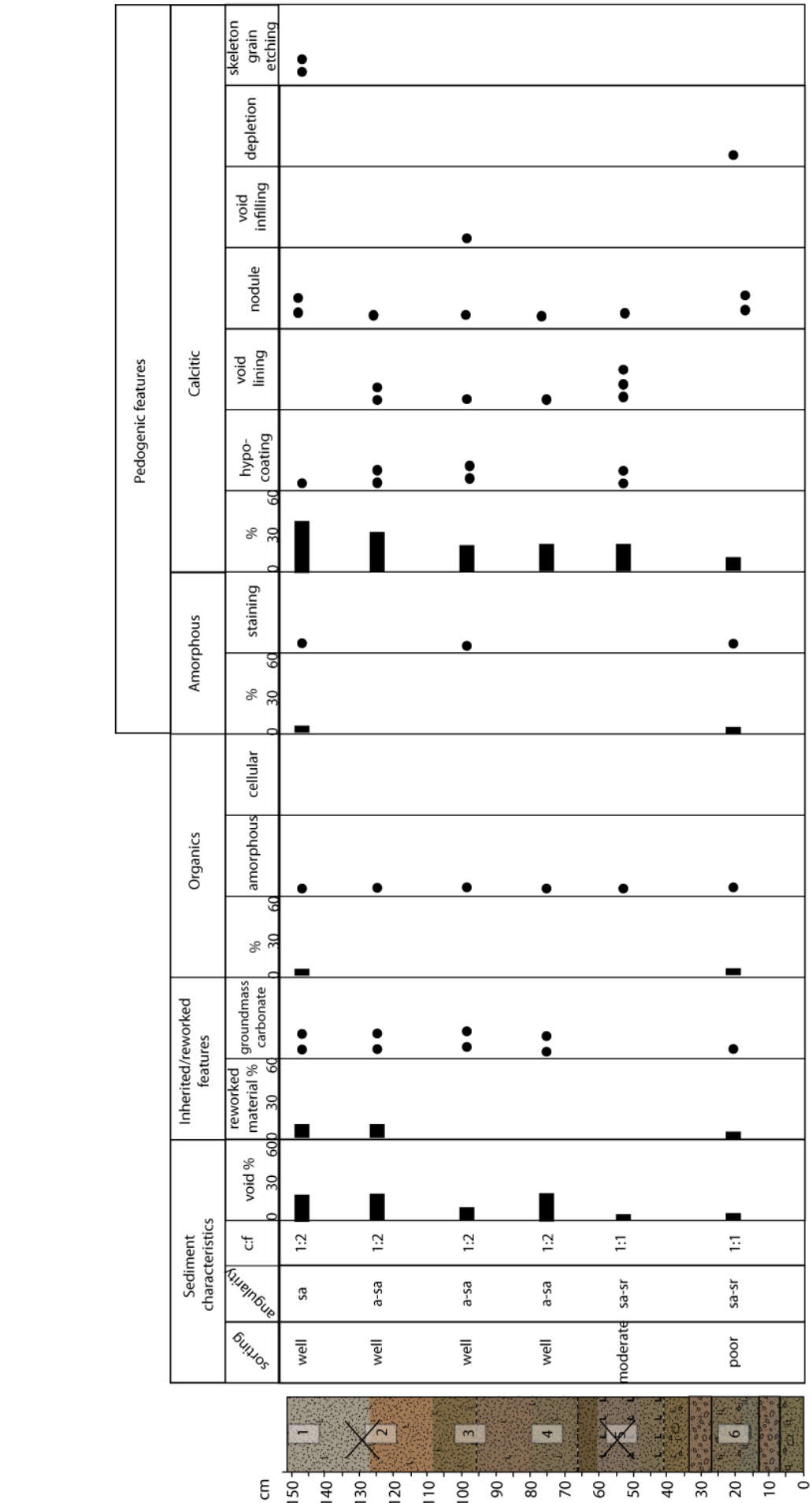

Figure 7.17 Compilation of visual estimates of micromorphological features assessed from thin sections taken at La Malaha.

7.5 Isotopic geochemistry of pedogenic carbonates

Despite the recognition of carbonates present in the field, it was not possible to recover any from the bulk samples. Therefore there is no record of the isotopic composition of carbonates at La Malaha.

7.6 Site chronology

As shown in figure 7.6, 2 OSL samples were taken at La Malaha, located at 133 cm and 55 cm (to middle of block). Sample treatment and dating runs were carried out following the methods detailed in chapter 5. Sample run conditions and dosimetry data are given in tables 7.4 and 7.5.

Table 7.4 Summary table of Malaha dating runs, full details in chapter 5

Sample	Aliquots	PH 1 (˚C)	PH 2 (˚C)	Given doses (Gy)
Mal 1	16	260	220	9, 18, 27, 35, 0, 9, 9
Mal 2	22	280	220	9, 18, 27, 35, 0, 9, 9

Table 7.5 Summary of dosimetry and dating results

Sample	Radionuclide concentration			Sample depth (m)	Cosmic dose rate (Gy/ka)	Total dose rate (Gy/ka)	Water content (%)	Equivalent dose, De (Gy)	Age (ka)
	K (%)	U (ppm)	Th (ppm)						
Mal 1	2.00	2.60	11.0	3	0.165	3.40	15	4.6	1.4 ±0.1
Mal 2	1.98	2.46	11.1	3.7	0.152	3.33	15	7.3	2.2 ±0.2

Growth curves were formed using the SAR protocol outlined in chapter 5. All growth curves were fitted with a saturating exponential plus linear curve, as in all cases this proved to be the line of best fit. The laboratory induced equivalent dose for both OSL samples MAL 1 and MAL 2 occurs on the saturating exponential part of the dose response curve (figure 7.18), where there is a definite increase in sensitivity corrected OSL intensity with increasing regeneration dose. This demonstrates the sample is not saturated, and therefore a geologically meaningful De may be calculated.

Estimates of equivalent doses for each sample were calculated from >12 aliquots (table 7.4). The spread of equivalent doses gained from each aliquot display a unimodal, narrow distribution (figure 7.19). The test behaviour of the aliquots for each sample, together with the

stratigraphically consistent age estimates (figure 7.20), indicates that there is no reason to doubt the OSL age estimates for the sequence at La Malaha.

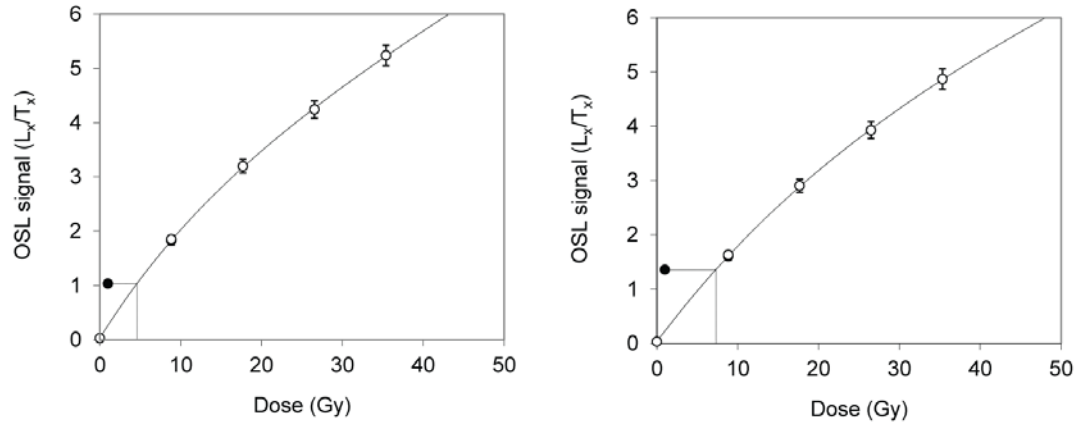

Figure 7.18 The sensitivity corrected dose response curves for a single aliquot of Mal 1 (left) and Mal 2 (right). The curves were fitted using a saturating exponential and linear function, both curves are representative of all aliquots from each sample. The black dot represents the natural, with an intercept of 4.62 Gy for Mal 1 and 7.31 Gy for Mal 2. The recycling point is located at 10Gy.

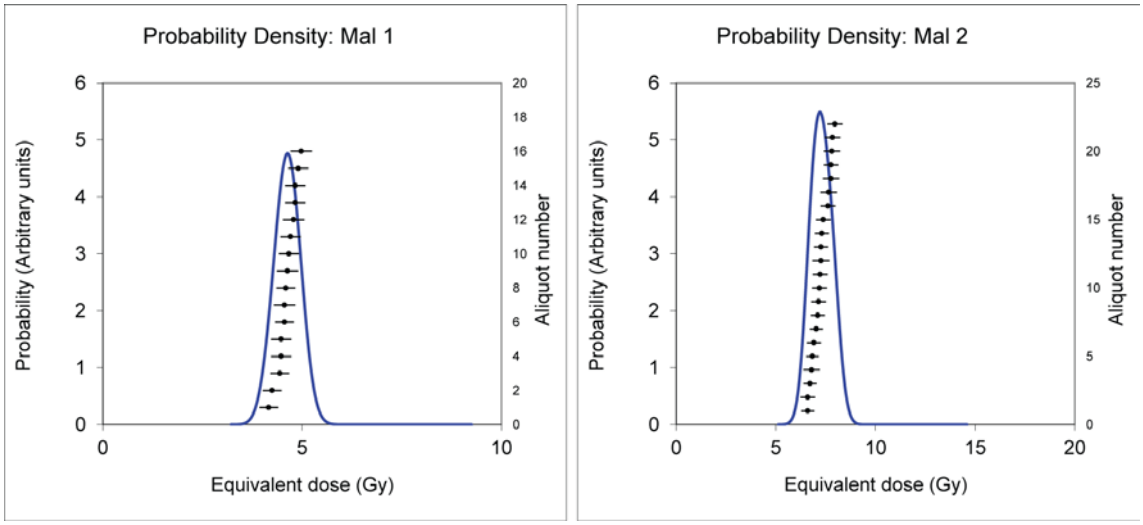

Figure 7.19 D_e *distributions shown as probability density functions and with individual* D_e *values shown with error bars in order of increasing value*

7.7 Sedimentological Interpretation

7.7.1 Unit 1 sedimentology

Unit can 1 be characterised as a predominantly massive silt unit, containing a significant proportion of sand, varying quantities of gravel (up to ~32%) and a significant proportion of silt (up to ~41%) (table 7.1). The unit generally consists of a massive sandy, clayey silt bed containing occasional fine gravels within this are two beds of sub-rounded, matrix supported gravels (figure 7.20).

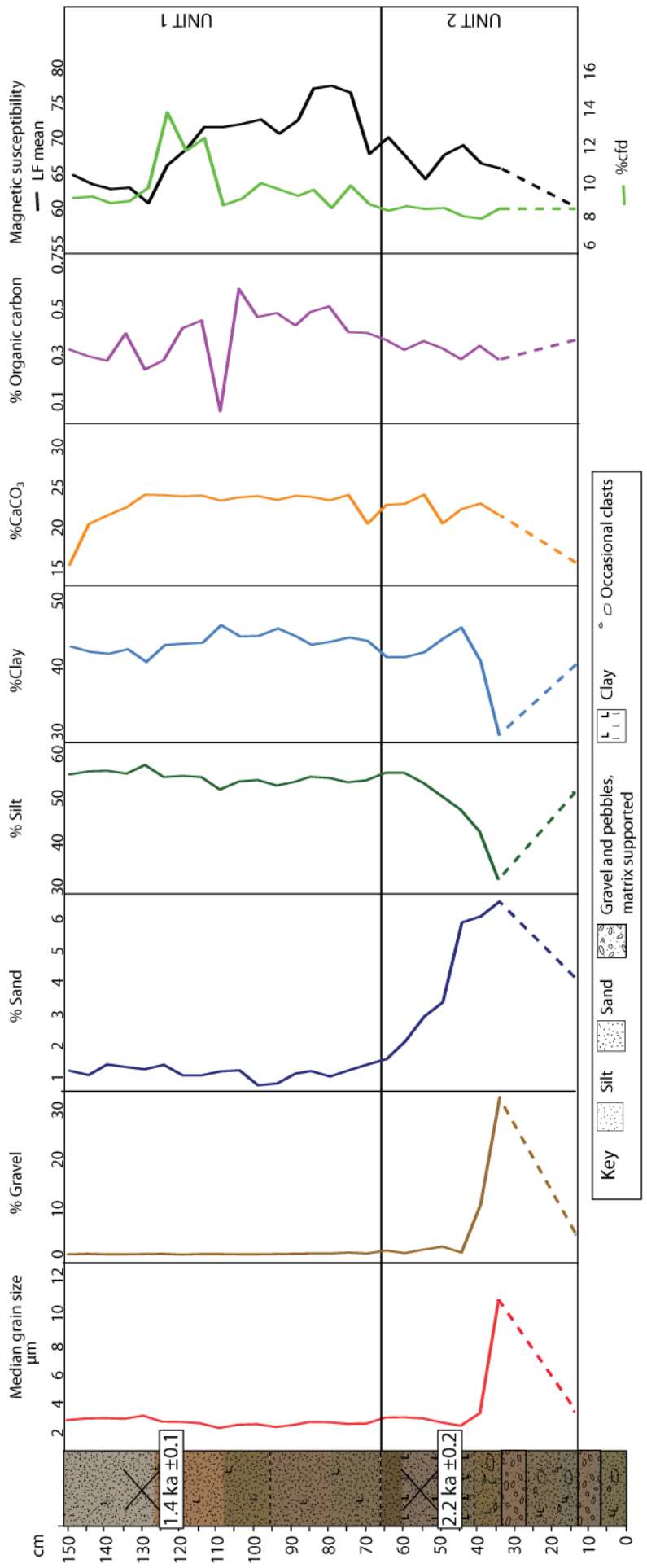

Figure 7.20 Compilation of sedimentological data for La Malaha with OSL age estimates.

The massive, fine grained sediments within the unit are typical of sediments deposited by still water conditions, enabling the deposition of silts and clays. The unit is typical of the model of sedimentation of floodplain sediments outlined by Miall (1992). The matrix-supported gravels indicate that both the fine and coarse material were deposited together, either as a debris flow, hyper-concentrated flow, or high-energy flood event that underwent rapid deposition (Miall 1992). However, the lack of grading within the coarse beds may indicate sudden deposition through a hyper-concentrated flow event (Costa 1988, Mulder and Alexander 2001). If such a flow rapidly loses energy, for example in an overbank setting, then a poorly sorted, matrix-supported gravel may occur (Costa 1988). It is therefore proposed that unit 1 at La Malaha represents floodplain sedimentation, under variable sediment load regimes associated with varying flow dynamics.

The sediment analysis records no evidence for pedogenic alteration of the sediments. The calcium carbonate content of the unit is relatively stable (~15-20%) (figure 7.20) and as such, does not provide evidence for the pedogenic redistribution of carbonate that is indicative of processes operating on a stable land surface (e.g. Kemp 1985b) (chapter 5). The magnetic susceptibility record through unit 1 (figure 7.20, table 7.2) shows that the sediments have undergone only minor post depositional alteration. The low frequency magnetic record, indicating both ferromagnetic and superparamagnetic minerals (Dearing *et al.* 2001) of the sediments, shows little variability in unit 1 (60-66 10^{-8} m^3 kg^{-1}). The frequency dependent (% cfd) (difference between high frequency and low frequency) magnetic record, used as a proxy of pedogenic alteration of minerals (Dearing 1999), ranges between 7.5 and 8% for unit 1. Dearing (1999) classifies such values as indicative of sediments containing a moderate amount of minerals produced through pedogenic process (see table 7.6). However, such concentrations are not considered substantial enough for the unit to be characterised as a palaeosol on the basis of its magnetic susceptibility record (Dearing 1999, Dearing *et al.* 2001).

Table 7.6 Dearing's (1999) interpretation guide for magnetic susceptibility measurements.

χfd	% χfd	Cause
Low	<2	Virtually no (<10% SP grains)
Medium	2-10	Admixture of SP and coarser non-SP grains, or SP grains <0.005μm
High	10-14	Virtually all (>75%) SP grains
Very high	>14	Rare values, erroneous measurement, anisotropy, weak sample or contamination

7.7.2 Unit 1 micromorphology

Micromorphological evidence from unit 1 highlights the poor sorting (figures 7.11, 7.12, 7.21) within the sediments, as well as the sub-rounded nature of the grains. The sub-rounded nature of the skeleton grains (up to gravel in size) could be indicative of transport and deposition within a fluvial system (Bridgland 1986, Krinsley and Doornkamp 1973). Furthermore, the poor to moderate sorting of the sediments is characteristic of rapid deposition, supporting the suggested fluvial origin of this unit.

Present within thin section MAL 6 are areas of laminated sediments with a sharp contact with the groundmass (figure 7.11). Their well-sorted nature and sharp contact with the surrounding groundmass identifies that they were originally deposited under conditions different to those responsible for the deposition of unit 1. As such, they are identified as rip-up clasts, eroded from previously deposited sediments. Comparison of the sediment structures present within these rip-up clasts with sediments deposited in ponded water in active ephemeral systems in the Mediterranean (thin section from Libya provided by I. Candy, unpublished) indicates (see figure 7.22), that this is a likely depositional environment for these types of sediments at La Malaha. These finely laminated sediments are very well sorted, grading from fine sands into silty clay and represent sediment facies typical of ponded sediment deposits (Miall 1992).

As such, they are likely to represent deposition under still water conditions within abandoned or periodic flow regime channels within a braided system. These deposits have then been eroded and incorporated into bedload during the high flow events that have resulted in the massive, silt dominant beds of unit 1. Such a system currently runs through the Malaha valley, where ponded sediment settling still occurs.

Thin section MAL 5 (figures 7.12, 7.21) records an increase in the occurrence of calcitic concentration features. Within this section, they are primarily micritic hypocoatings around voids. Such features indicate rapid precipitation of calcite, usually associated with root networks during localised dissolution and reprecipitation of carbonate within the sediments (Kemp 1985a). The presence of small (<1 mm), diffuse micritic nodules is also indicative of pedogenic alteration of the sediment, but neither is indicative of sustained pedogenic alteration (Kemp 1995).

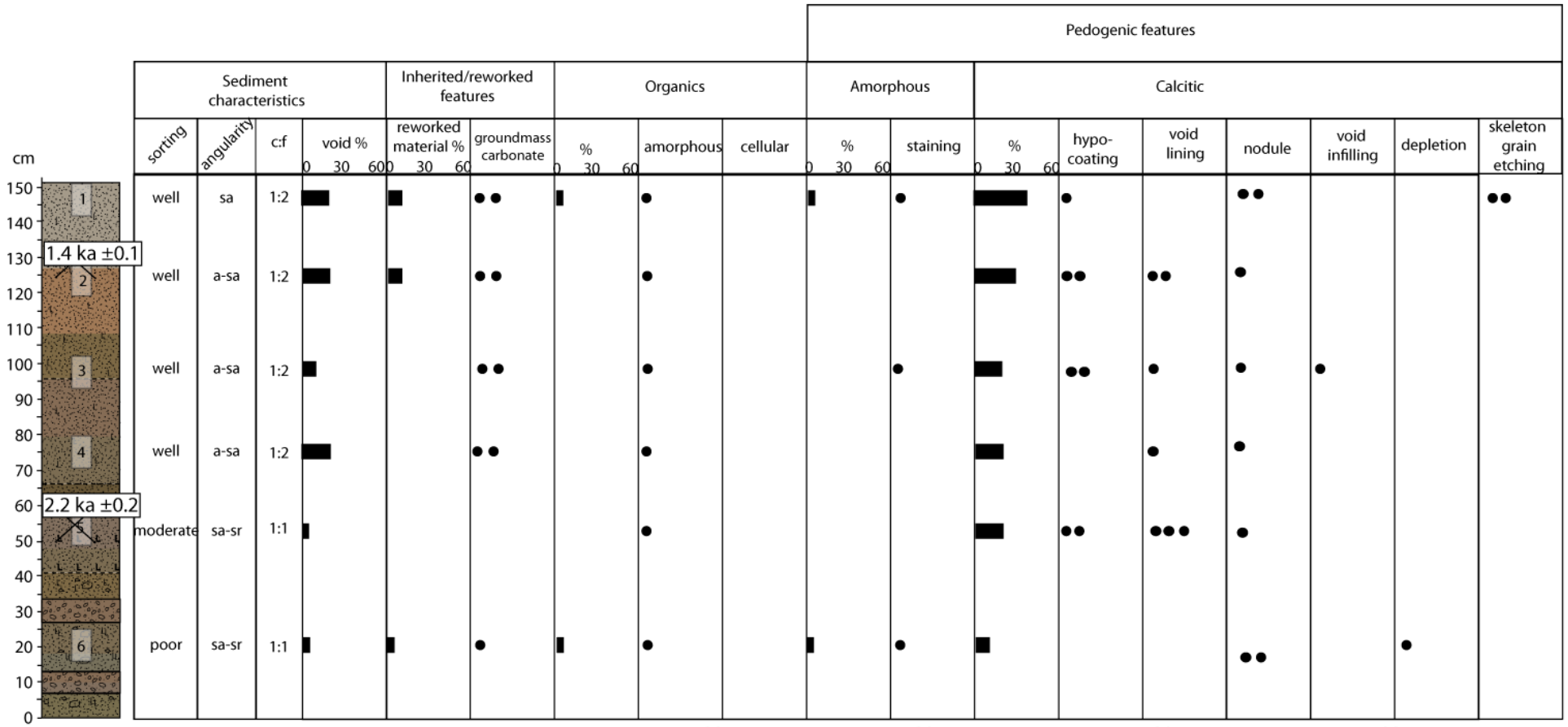

Figure 7.21 Vertical distribution of micromorphological features and OSL age estimates

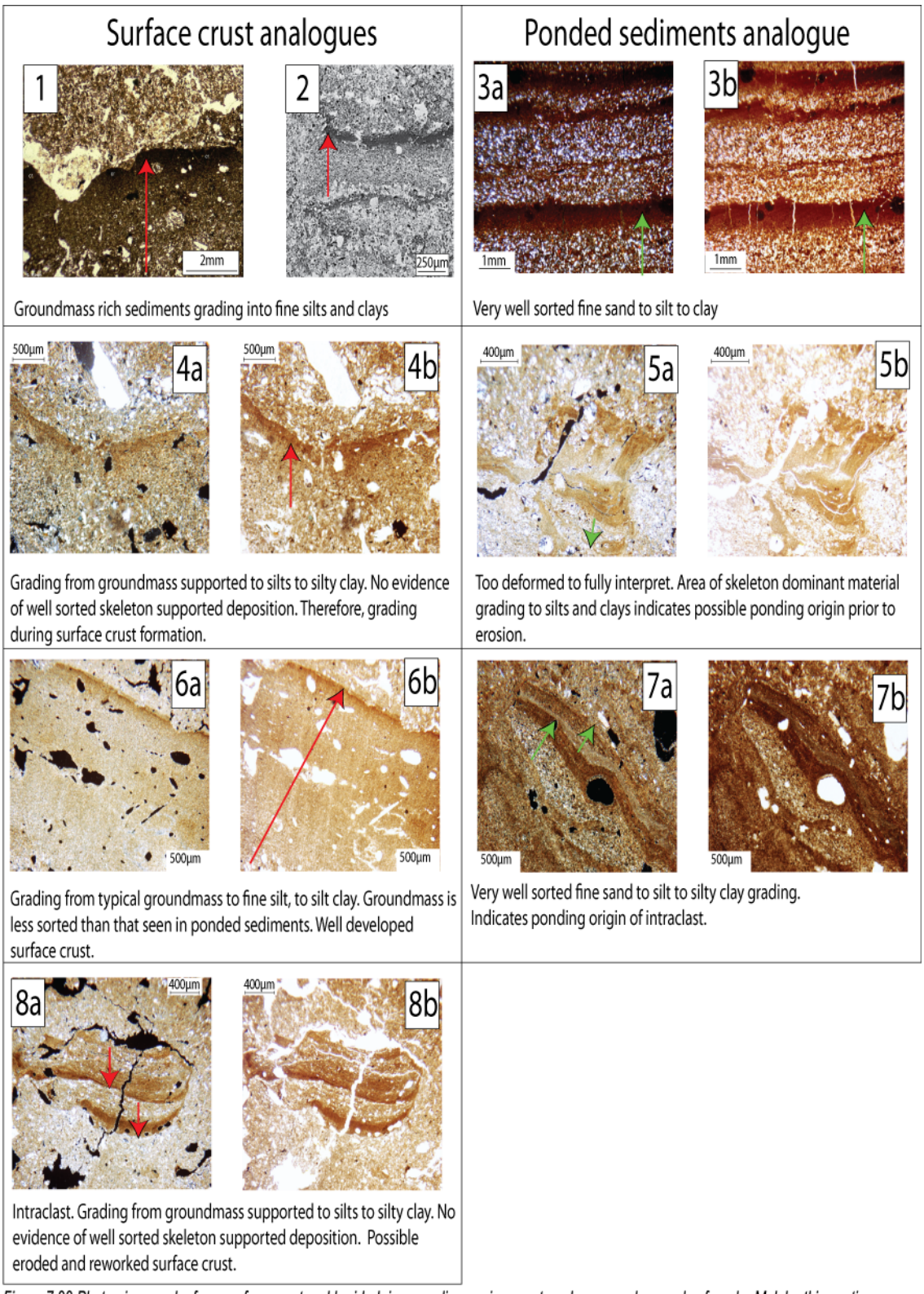

Figure 7.22 Photomicrographs from surface crust and braided river ponding environment analogues and examples from La Malaha thin sections. 1) Photomicrograph of crust within loess profile. Showing fining of material capped by dense silty clay coating. Evidence of biological activity present. Plane polarised light. Taken from: www.soil.ncsu.edu/lockers/lindbo/soil%20photos/micromorphology%20slides/Stoops%20collection/docs/ch8_cmp.html 2)Remnant of disrupted crusts within Chinese loess profile. Kemp (1999) states it is formed by infrequent, high magnitude rainfall events on a sparsely vegetated land surface. Black and white, plane polarised. 3-8 a)plane polarised light, b) cross polarised light. 3) Modern laminated sediments from ponding environment, braided river system, Libya. 4) MAL 6. 5) MAL 6. 6)MAL 2. 7) MAL 2. 8) MAL 4.

Both authigenic and allogenic carbonate nodules are present within section MAL 5. There is a clear distinction between authigenic (grown in-situ) and in-washed carbonates (figure 7.12).

Allogenic nodules have a distinct boundary with the groundmass and are typically densely cemented, whereas authigenic nodules are typically weakly to densely cemented, with a diffuse boundary with surrounding groundmass. The difference in contacts with the groundmass indicates reworked (sharp), or in-situ growth (diffuse) (Durand *et al.* 2010).

Micromorphological analysis of sediments from unit 1 supports the PSA results, which record fining upwards of a poorly to moderately sorted sediment. The increased occurrence of calcitic pedofeatures towards the top of unit 1 indicates localised redistribution of carbonate through dissolution and reprecipitation, most likely occurring through accretionary pedogenesis.

7.7.3 Unit 2 sedimentology

PSA from unit 2 (figure 7.20) demonstrates that the unit is a sandy clayey silt, with very little variability within the grain size characteristics through the unit. There are very small quantities of gravel present through unit 2 (0-0.41% weight), small amounts of sand (0.73-1.40% weight), high content of clay (40.65-46.28% weight) and a high silt content (52.40-58.02% weight). As shown in figure 7.8, unit 2 contains a smaller fraction of sands and gravels and a higher silt content than the sediments within unit 1.

Unit 2 was identified as loess-like on the basis of field descriptions (cohesive silt body) and PSA. As discussed in chapter 6, unit 1 is distinguishable from local fluvial and slope sediments on the basis of grain textures (SEM) and Sr-Nd composition. The Sr-Nd composition of the sediments indicates a non-local source for the silt, and suggests a significant North African dust component to the deposit. On this basis, unit 2 is interpreted as a deposit of loess and is consistent with the existing descriptions of loess within the literature as stated in chapter 3. However, primary loess will not contain even occasional gravel clasts. It is therefore likely that the unit is comprised of secondary loess, where aeolian silts are locally reworked within fluvial or slope systems.

Fluvially reworked loess sediments often maintain much of the original sediment characteristics. However, it can sometimes be possible to identify them in the field as there is often evidence for bedding structures (e.g. Gardner 1977). Unit 2 is a massive, structureless body of sediment, typical of the field descriptions of loess deposits (e.g. Pécsi 1995). Whilst the unit's appearance is in keeping with primary loess, the small sand and gravel content indicates that either the aeolian silt was reworked, or sediment mixing with limited input of coarser sediments was occurring.

The calcium carbonate content of the unit is consistently around 24%. Hhowever, towards the top of the unit (154-134 cm) there is a progressive decrease to ~15%. There are two possible explanations for the shift in carbonate content. Firstly, it could be due to the downward dissolution

of carbonate under a stable land surface (Kemp 1985b). This dissolution has not resulted in the total removal of calcium carbonate from the upper section of unit 2, nor has it resulted in a horizon significantly enriched with calcium carbonate at depth. Therefore, this scenario would suggest establishment of a relatively short lived land surface (e.g. Kemp 1995, Kemp *et al.* 2004). Secondly, it could be the result of a shift in sediment source and therefore a shift in sediment composition. However, the progressive nature of the shift makes this unlikely.

It has been demonstrated that calcium carbonate content has a dampening effect on total magnetic susceptibility of a sample (Kemp *et al.* 2004, Dearing 1999). It is therefore important to ensure that there is no correlation between the two values. As shown in figure 7.20, there is very little variability in the $CaCO_3$ record of La Malaha, and so shifts in carbonate content alone cannot explain the variability seen within the magnetic susceptibility record. The low frequency magnetic susceptibility record from unit 2 shows that from 114-~70 cm the unit contains raised levels of magnetic minerals, when compared to the values from the rest of the section. This may be indicative of a shift in sediment source (e.g. Grimley *et al.* 1998), where the sediments comprising unit 2 (114-70 cm) have a higher total magnetic mineral content. The %cfd of unit 2 indicates a zone of significant superparamagnetic mineral enrichment. Between depths of 124-134 cm, %cfd values are above 10% (11.4-13.6%), according to Dearing (1999) (table 7.6) values as high as these represent sediments comprising of ~75% or more superparamagnetic minerals.

Current understanding of magnetic susceptibility as a proxy for pedogenic alteration is that the fine superparamagnetic minerals identified by the % difference between high and low frequency readings are produced by the weathering of iron bearing minerals to superparamagnetic magnetite or maghemite (Dearing *et al.* 2001, Zhou *et al.* 1990).

Dearing (1999) produced a record of mineral magnetics through the study of rocks, sediments and soils in England (figure 7.23, table 7.6). According to the values recorded at La Malaha, the sediments located between 124-134 cm are significantly enriched in superparamagnetic minerals, which suggests that they can be classed as soils according to Dearing's (1990) scale. Malaha results are plotted in blue in figure 7.23. Despite having lower overall magnetic concentrations, according to Dearing (1999), the samples are not in the range considered as having low magnetism, and therefore, the results should be fully comparable with those gained by Dearing (1990).

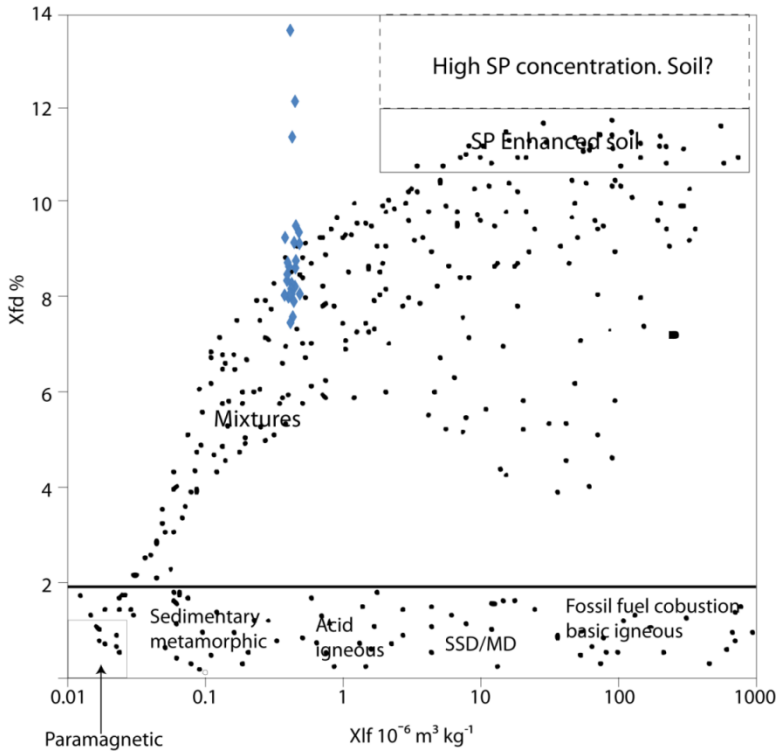

Figure 7.23 Comparison of magnetic susceptibility values from La Malaha with those compiled by Dearing (1999). Blue diamonds represent La Malaha data.

7.7.4 Unit 2 micromorphology

The thin sections taken through unit 2 (MAL 4-1) show a shift in sorting characteristics, c:f ratio and roundedness characteristics of skeleton grains compared to sections from unit 1. Through unit 2, most of the sediments are well sorted, ranging from medium silts to clays with very little in the way of coarser material being present. There is an increase in total cover of groundmass (fine silts and clays) and a shift towards sub-angular skeleton grains.

This summary of the main bulk characteristics present in thin sections from unit 2 support the sedimentological interpretation of a shift in depositional process occurring from unit 1 to unit 2. Textural and micromorphological characteristics support the interpretation of a shift from floodplain deposition (unit 1) to loess or loessic accumulation (unit 2). A shift towards better sorting and a shift towards dominant silt deposition support a transition towards aeolian silt deposition. This is supported by the increased in angularity of skeleton grains (e.g. Krinsley and Doornkamp 1973).

Associated with this shift in depositional process is an increase in micromorphological evidence for pedogenic processes (figure 7.27). Through unit 2 there is increasing % cover of calcitic pedo-features upwards through the sediments, marked by increasing occurrence of hypocoatings and

void linings. Within typical soil horizons the processes leading to the dissolution and reprecipitation of calcite result in a downward enrichment of pedogenic carbonates (e.g. Kemp 1985a,1985b). At La Malaha, however, micromorphological evidence is of increased pedogenic alteration upwards, associated with only minor changes in bulk carbonate content. Whilst untypical of pedogenesis occurring at a stable land surface, Kemp (1995, 1999) has identified similar profiles within loess accumulations, arguing for aggradational pedogenic formation.

It is common for surface crusting to occur in arid regions (Belnap 2008). The process occurs when infrequent, intense rainfall occurs on sparsely vegetated land surface. This results in the disaggregation of soil peds into fine particles (Kemp 1995, Belnap 2008). Belnap (2008) states that water ponding on the soil surface allows fine particles to rise to the surface and form a crust upon drying or for fine particles to be redistributed and concentrated by rain splash. The process leads to the progressive fining of the groundmass, resulting in an upward fining sequence (figure 7.22). In more arid climates, chemical crusts can occur (Belnap 2008). Such crusts form from evaporites, displaying a compositionally distinct horizon, which would be clearly identifiable in thin section. There is no evidence from La Malaha of chemical crusting.

Interpretation of the evidence from the thin sections of unit 2 shows evidence of surface crusting in sections 4-2; however, some of these features appear as intraclasts or eroded material. As such, some of the features are deformed or inverted, and were not easy to interpret. On the basis of a lack of very well sorted basal sediments, they are interpreted as disrupted soil crusts (figures 7.22).

Micromorphological evidence from unit 2 indicates the deposition of sorted, predominantly fine silt material, containing angular to sub-angular clasts, supporting the idea of loess deposition. Within the thin sections, there is some evidence for reworked material through disrupted and incorporated surface crust fragments, showing some localised reworking of material. Above the surface crust horizon present in MAL 2, there is a shift towards slightly increased roundedness of skeleton grains, incorporation of carbonate clasts and possible evidence for rip up clast material. This suggests that the top of the sequence may record an increase in localised reworking of sediments or possibly, a return to fluvial deposition.

7.8 Palaeoenvironmental interpretation

7.8.1 Pedo-sedimentary reconstruction

Stage 1 - The basal sediments consisting of beds of matrix supported, sub-rounded gravel rich material were deposited through rapid deposition, likely to have occurred within a floodplain

setting or a low-energy channel environment. The upwards fining of the unit records a transition to a lower energy, possibly a more distal position within the floodplain setting. The upper section of unit 1 contains evidence for increasing effects of pedogenic alteration, through the occurrence of calcitic features. Such features taken together with the bulk carbonate content indicate that this was weak, short lived pedogenic alteration which may have been occurring through accretion of the sediments, possibly in response to decreasing sediment input (figure 7.24).

Stage 2 - The transition to aeolian silt deposition is marked by increased sorting of the sediments, identified in both thin section and bulk PSA, and also supported by increased angularity of skeleton grains typical of aeolian silt transportation (e.g. Krinsley and Doornkamp 1973). Micromorphological analysis indicates the increasing occurrence of calcitic pedo-features upwards through the profile, which together with the stable bulk carbonate content, indicate only localised, weak pedogenesis. The distribution of such features indicates that pedogenic alteration increases upwards through the unit, which is consistent with accretionary pedogenesis during decreasing sediment input (Kemp 1995, 2001). Increasing magnetic susceptibility values (%cfd) also support the interpretation for increasing pedogenic alteration towards the top of the unit.

Stage 3 - The occurrence of a near complete, relatively thick soil crust surface within MAL 2 is not linked with increased pedogenic alteration, as such a feature can occur over a short time period (Belnap 2008). However, it does appear to mark a shift towards less sorted sediments, containing coarser skeleton grains and increased evidence for reworking of sediments. Therefore, the sediments at the top of unit 2 are interpreted as heavily reworked loess, either through fluvial or slope processes. The shift in total magnetic susceptibility values (lf) may support the interpretation of a shift in sediment origin, as values return to similar levels recorded through the deposition of unit 2.

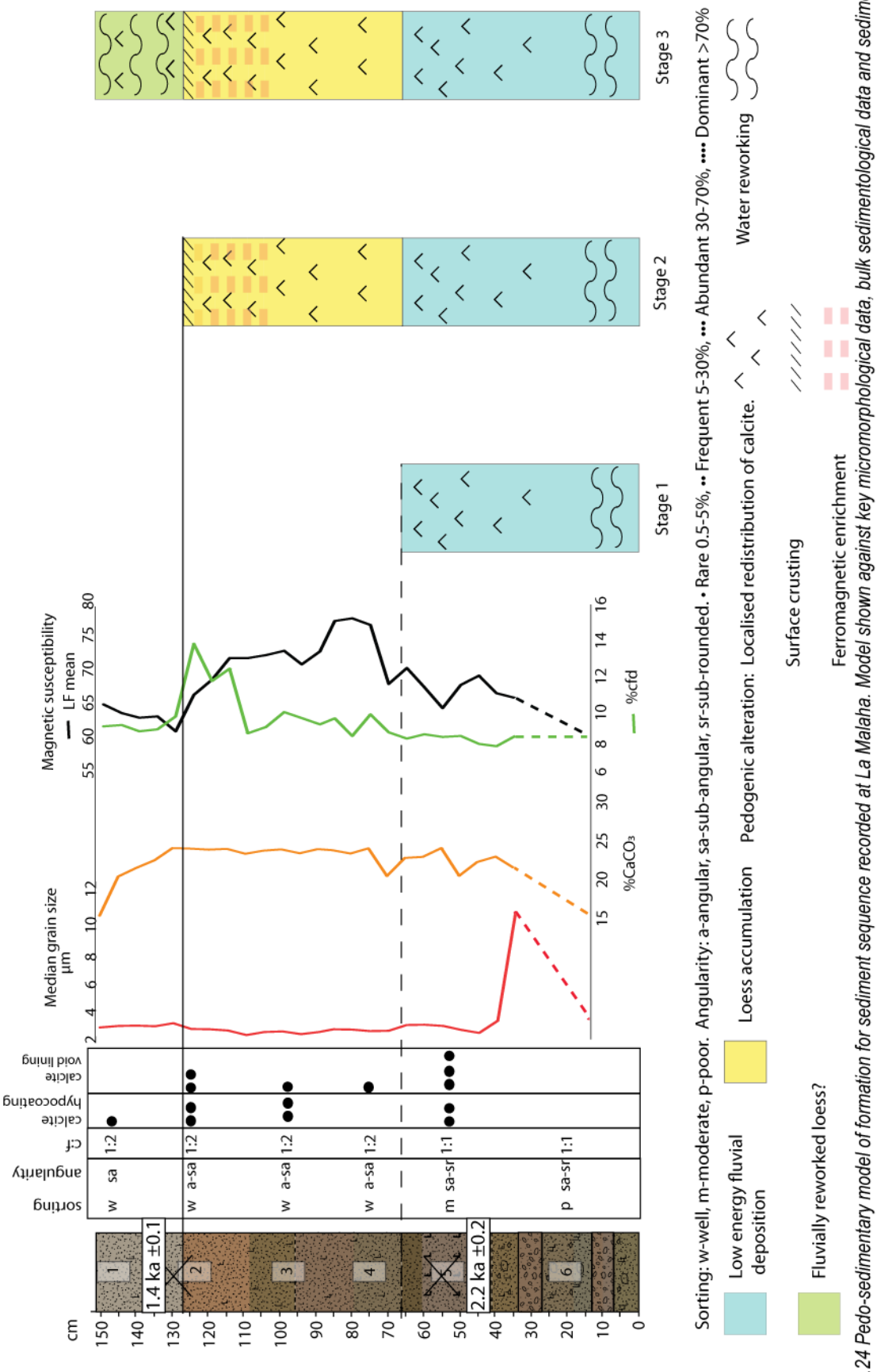

Figure 7.24 Pedo-sedimentary model of formation for sediment sequence recorded at La Malaha. Model shown against key micromorphological data, bulk sedimentological data and sediment stratigraphy.

7.8.2 Palaeoenvironmental significance

The deposition of overbank sediments (unit 1) in southern Spain is not climatically significant. This is due to the existence of a highly seasonal rainfall regime through the late Quaternary (chapter 2) (e.g. Prentice *et al.* 1992, Harding *et al.* 2009). Within a highly seasonal rainfall regime, such as Mediterranean climates, intense rainfall events can result in overland flow and surface sediment erosion (e.g. Thornes 2009). This can result in rivers with a high sediment load, bursting banks and producing overbank sedimentation.

Pedogenic alteration of the sediments increases upwards through the unit, indicating an accretionary style of pedogenic alteration. Such alteration can be the product of a climatic amelioration and/or reducing sediment input. The fining upwards of the unit may imply channel migration, placing the sediments at a more distal position to channelized flow, reducing sediment input thereby increasing the effectiveness of pedogenic alteration.

As discussed in chapter 6, it is possible to distinguish the sediments of unit 2 from locally derived slope and fluvial sediments on the basis of Sr-Nd composition. Together with differences in roundedness characteristics of the sand and silt grains and a shift in magnetic mineral content, it enables the classification of unit 2 as loess. The existence of some gravel and a significant sand component to the deposit indicates a localised input to the loess, possibly through slope processes. As such, the deposit is referred to as a secondary loessic deposit.

The onset of loess deposition at La Malaha occurs after 2.2 ka ±0.2 until sometime after 1.4 ka ±0.1, this period is correlated with Roman occupation and significant anthropogenic landscape alteration within the region. The period is often correlated with significant sediment mobilisation in response to widespread land clearance for agricultural purposes (e.g. Pantaléon-Cano *et al.* 2003 and references therein). This, therefore, could be both a potential source of dust and a mechanism for vegetation cover reduction allowing loess to accumulate. However, Sr-Nd composition of the sediments indicates a non-local origin of the loess and suggests a strong North African component (chapter 6). It is therefore unlikely that Roman land clearance of the region could explain the significant far travelled sediment input.

As shown in figure 7.25, the period of loess accumulation at La Malaha also correlates to a period of regional aridity, recorded through palynological records (e.g. Jalut *et al.* 2000) and lake desiccation events (e.g. Carrion 2002), as well as periods of sediment mobilisation within North Africa (Swezey 2001) and increased North African dust flux (deMenocal *et al.* 2000, Cole *et al.* 2009). It is therefore likely that the loess accumulation at La Malaha corresponds to a period of

increased North African dust mobilisation during a period in which vegetation levels were reduced through southern Spain in relation to a climatic and/or anthropogenic forcing.

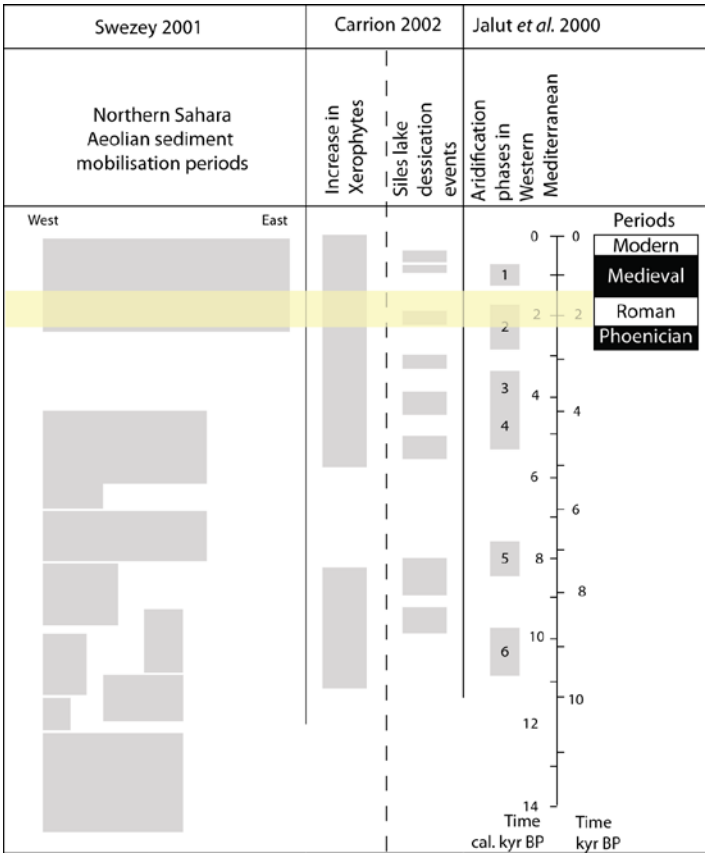

Figure 7.25 Compilation of regional aridity signals through the Holocene

The accumulation of loess at La Malaha, albeit locally reworked at least in part, records increasing pedogenic alteration upwards through the section. The increasing effects of accretionary pedogenesis records a diminishing sediment input, possibly in association with a climatic warming/wetting.

The regional implications of the palaeoclimatic information interpreted from the loessic accumulation at La Malaha will be discussed in further detail in chapters 11 and 12.

Chapter 8 - Chimeneas

This chapter presents the work undertaken at Chimeneas. Firstly, an introduction to the geography of the surrounding area will be presented. Secondly, the results from the work undertaken at the site will be discussed and the interpretation of the sediment sequence at Chimeneas will be presented.

8.1 Site introduction

The exposures at Chimeneas are located <1 km west of the town of Chimeneas, 21 km west-south-west of Granada (figure 8.1). As with La Malaha (chapter 7), Chimeneas is located within the Granada basin, a Neogene basin containing limestones, gypsums and continental sands, silts and conglomerates (figure 8.2). Triassic dolomites, limestones and marbles lie to the south of the basin (figure 8.2). The sediment sequence at Chimeneas is exposed in a valley cut by the Barranco de las Zarzas, a south to north flowing tributary of the Rio Genil. Sediments are exposed on both sides of the valley; in addition, there are sediments exposed by a road cutting which runs perpendicular to the valley, in an east-west direction (figures 8.3). Sediments on both valley sides were logged down to the level of the modern river channel. At the base of the sequence lies 6-7 m of fluvial sands, silts and gravels, overlain by up to 2.5 m of cohesive, silt dominated sediments which, in turn, are overlain by ~2 m of fluvial sands and gravels. Field description of the sequence identified the silt dominant unit as being consistent with the published criteria for loess or loessic sediments; consequently, this chapter focuses on this unit.

Figure 8.1 Map showing the location of the Chimeneas sections, with key towns and loess sites for reference.

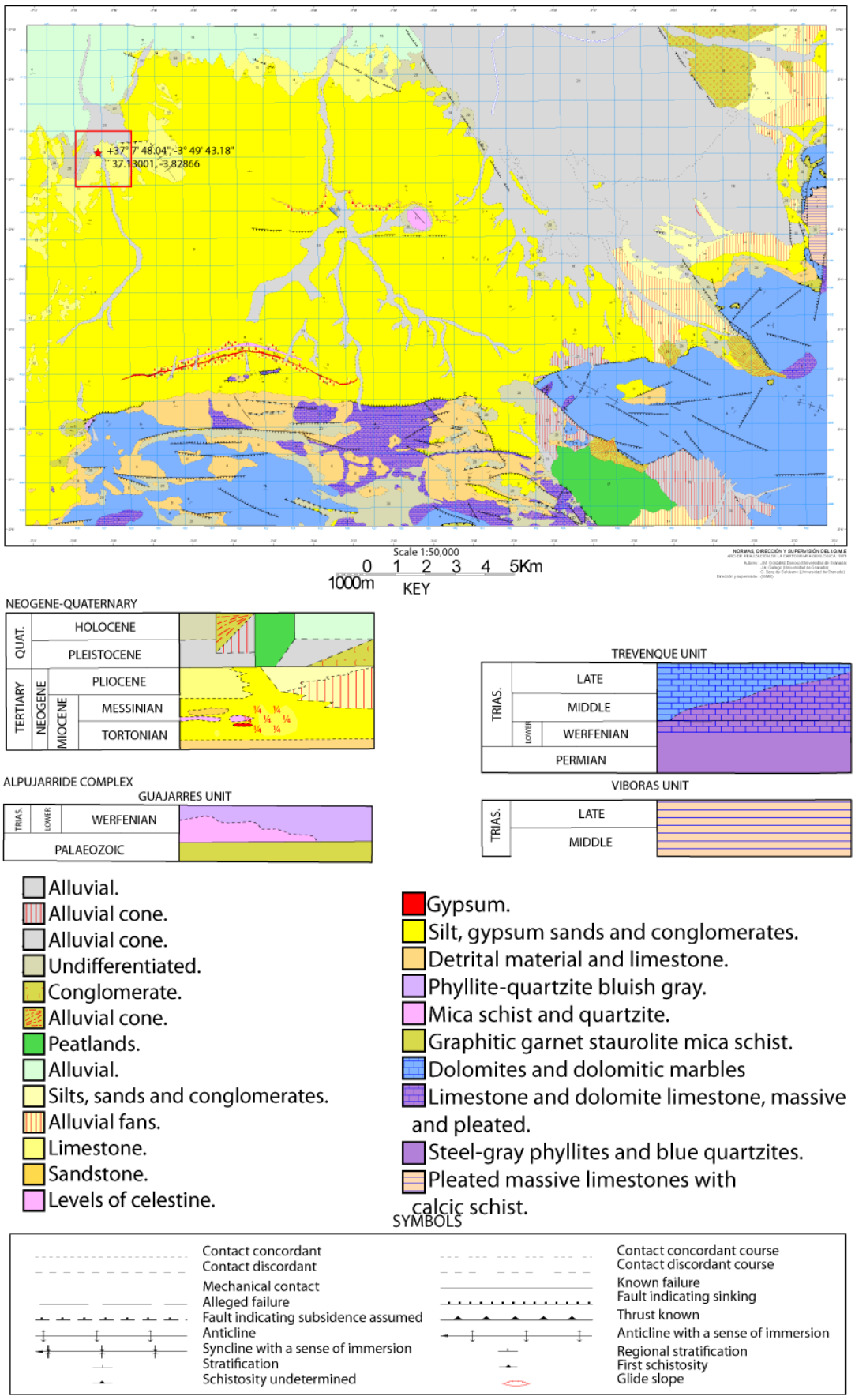

Figure 8.2 Geological map of the region around Chimeneas. Adapted from the geological map of González et al. (1985)

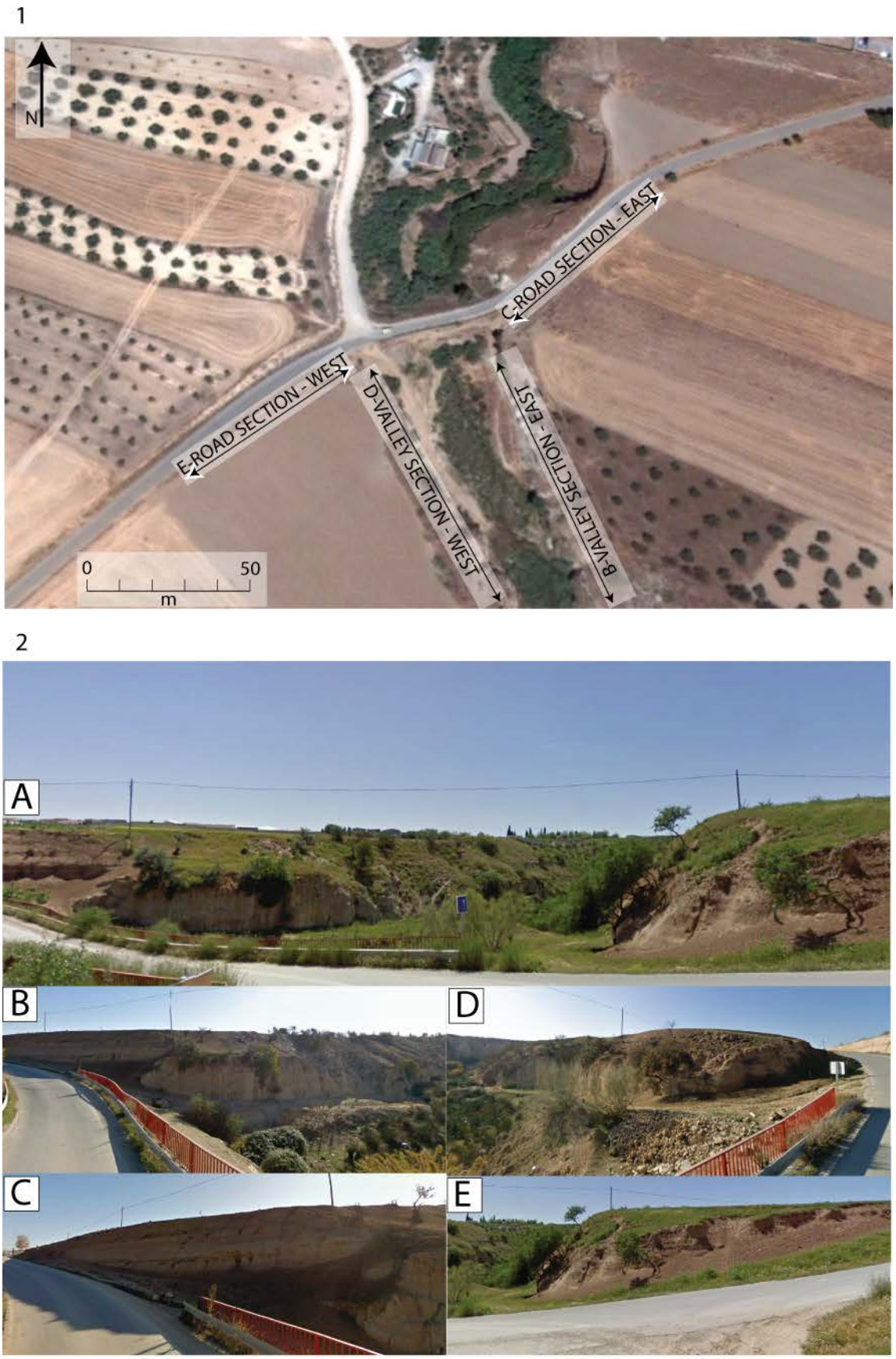

Figure 8.3 Satellite image of Chimeneas, with sediment exposures labelled. Photographs showing the valley and sediment exposures at Chimeneas: A. view of site, B-E sediment exposures, locations indicated on satellite image. Images taken from Google street view and Google Earth.

8.2 Field observations

In order that a sampling strategy could be devised, logging of all available exposures on both sides of the valley was undertaken. This section will provide the exposure schematics, logs and panoramic photographs for each exposure followed by a basic description of the sediments present. These observations will form the basis of the sampling strategy; detailed sedimentology of the sediments included within the sampling areas will be presented and discussed.

8.2.1 Eastern valley sediments: Field descriptions

The sediments from the eastern side of the valley can be seen in figure 8.4. Initial field observations identified two main units present on the eastern valley side. There was no exposure of marl bedrock present on the eastern side of the valley. The lowest unit visible was an extensive accumulation of fine material (sands and silts) containing occasional gravels and interbedded gravel/pebble horizons. These sediments are covered by logs 1-5 and represent much of the sediments infilling this side of the valley. Overlying the basal unit are the sediments contained within logs 6-7, covering the road cutting section of the sequence. These sediments appear similar in composition to those of the lower unit; however, they appear to be better sorted (lack of occasional gravel) and with a higher clay content. In addition to fewer gravel clasts, the fine grained beds of the upper unit are cohesive in nature and appear as massive deposits. There is gravel present within the road cut sections; however, this typically occurs as interbedded gravel rich, matrix supported horizons.

8.2.2 Western valley sediments: Field descriptions

At the base of the sediments infilling the valley is marl bedrock (figure 8.5, log 1), which is overlain by sorted sands and gravels. Predominantly, this material consists of matrix dominated sands containing small amounts of gravel sized material, but it is interbedded with distinct beds of matrix supported, gravel rich sediments. Present throughout the sands and gravels are small, powdery, crystalline nodules of gypsum. The beds of sands and gravels are then capped by a distinct white horizon (177-196 cm log 5, 115-143 cm log 6), overlain by darker, finer sediments (143-163 cm log 6). These sediments represent unit 1 and appear to describe most of the sediments making up the exposure on the western side of the valley cutting sequence (figure 8.7). Above the distinct white horizon are the sediments of unit 2, representing the majority of the sediments exposed in the road cut section. These sediments are contained within logs 7 to 9 (figure 8.6). The sediments are predominantly fine grained, well sorted, cohesive bodies of sandy silt interbedded with darker horizons. This unit is the largest body of sediment in the valley consistent with criteria for the recognition of loess(ic) sediments, and so it was this unit that was the focus of the sediment logging and sampling undertaken in the valley.

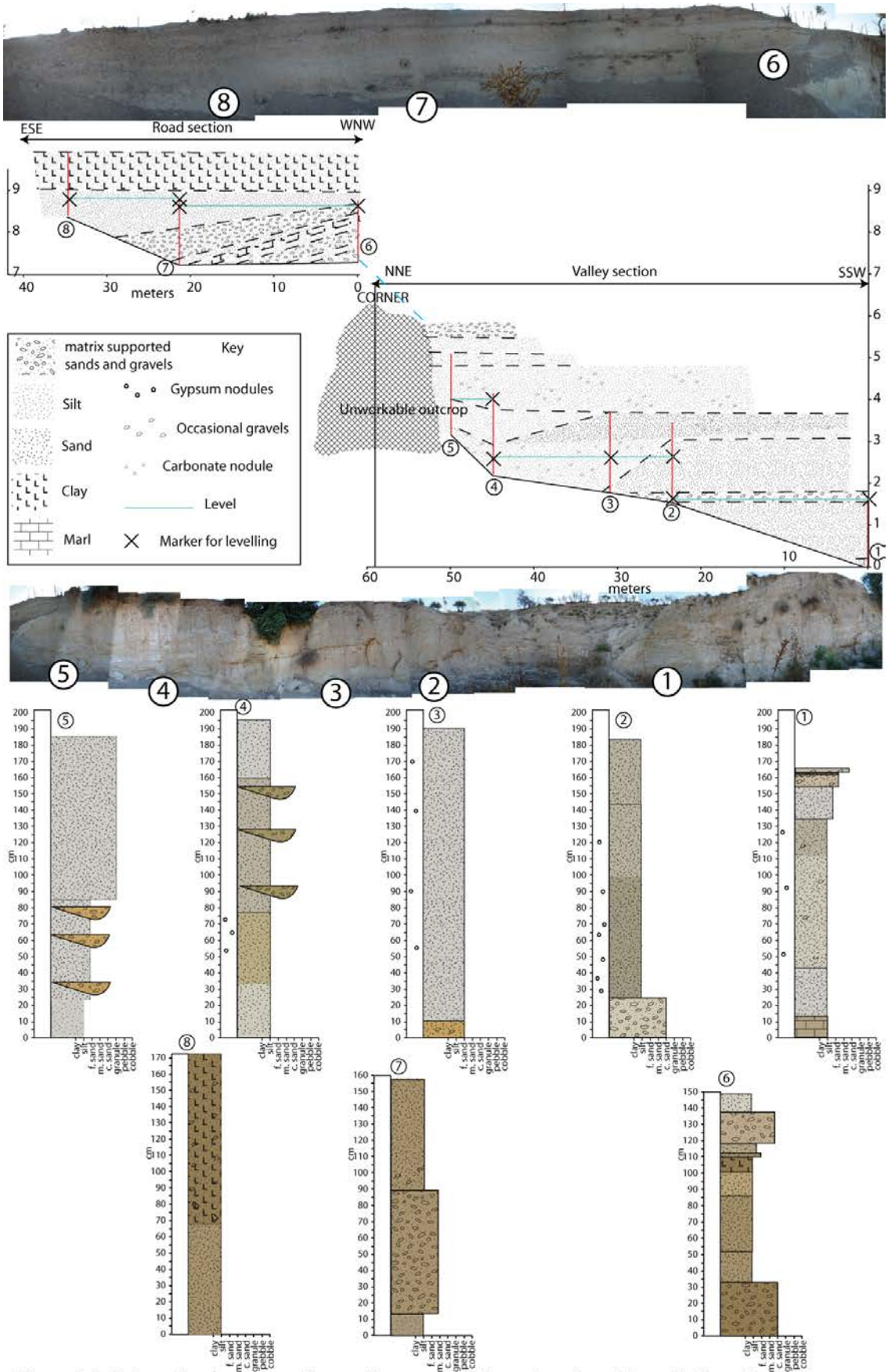

Figure 8.4 Schematic of eastern valley section compiled through sediment logs. Sediment logs were levelled relative to each other and distributed to capture all major sedimentological changes present.

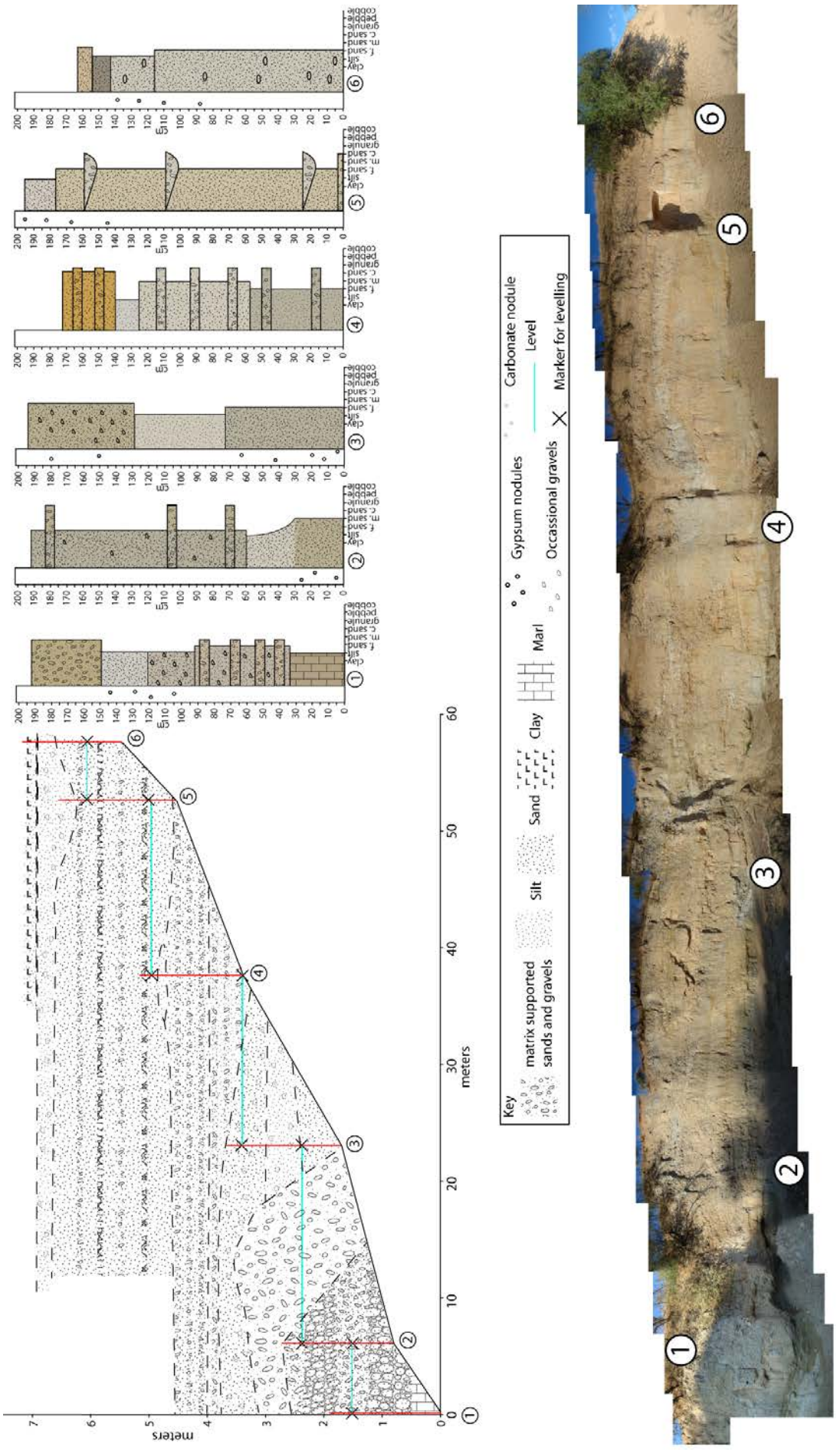

Figure 8.5 Western valley exposures, showing schematic of exposure, panoramic photograph (taken by author) and sediment logs.

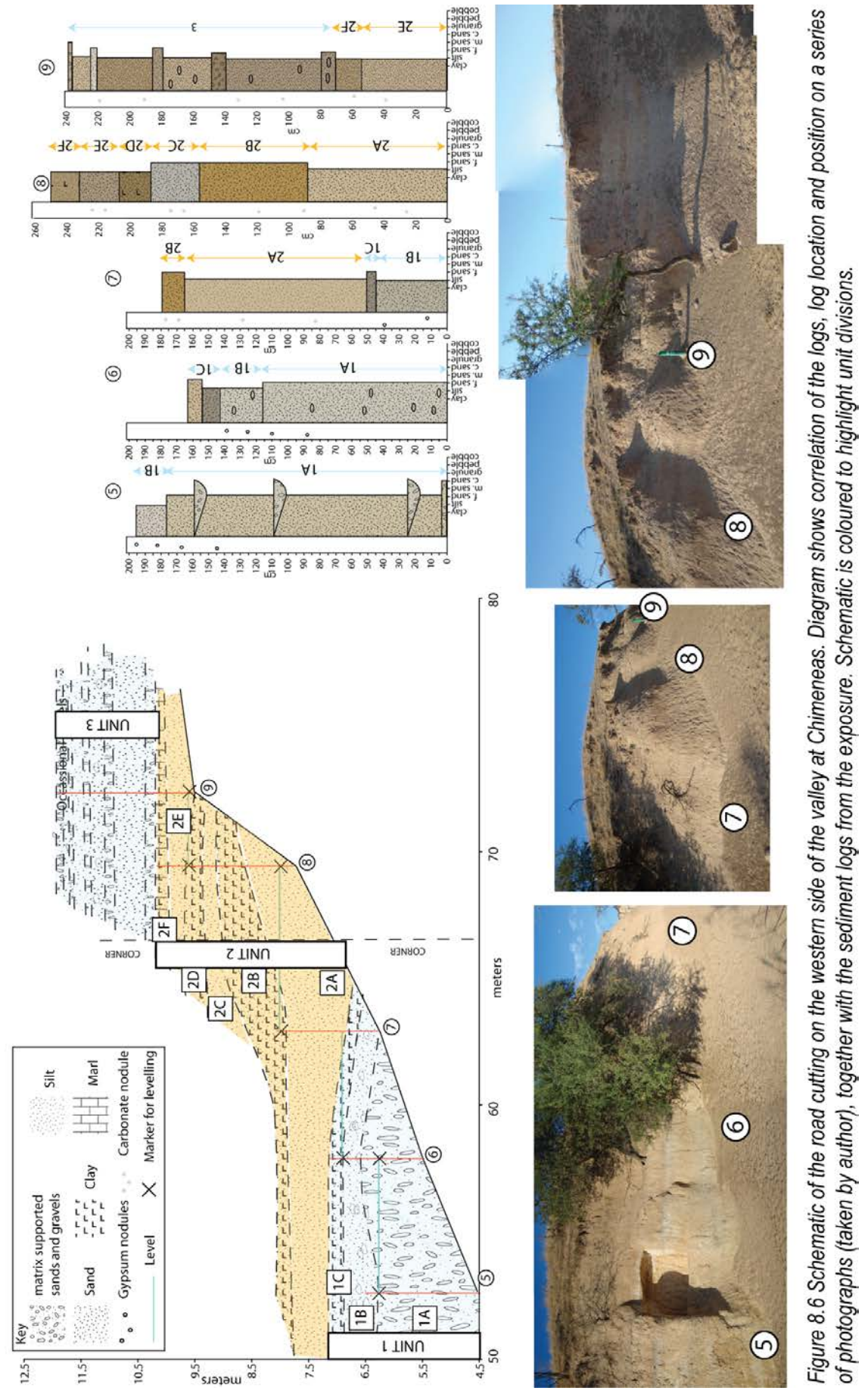

Figure 8.6 Schematic of the road cutting on the western side of the valley at Chimeneas. Diagram shows correlation of the logs, log location and position on a series of photographs (taken by author), together with the sediment logs from the exposure. Schematic is coloured to highlight unit divisions.

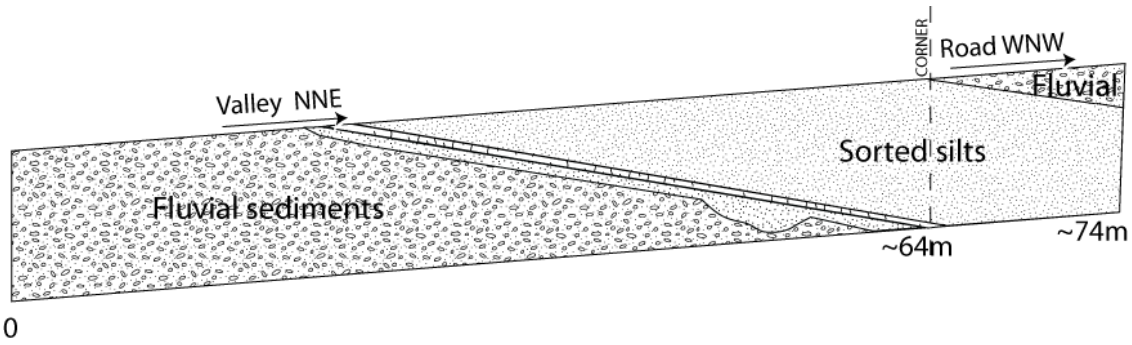

Figure 8.7 Schematic diagram showing how valley and road cutting sediments relate to each other.

8.3 Composite log

8.3.1 Detailed sedimentology

The unit divisions outlined previously describe the bulk, shared properties of each sediment body. There were however, distinct horizontally continuous sedimentological changes contained within each unit, for this reason units were further subdivided (figures 8.8 and 8.9). Log 6 records the top of the fluvial sediment sequence (unit 1), the base of the log (1A 0-115 cm) is a silty, fine sand bed containing occasional gravels, with gravel content appearing to decrease upwards through the bed. Above bed 1A (1B 115-143 cm) the sediments appear similar in composition but with a higher silt content and frequent gypsum nodules, the sediments have a distinctive white-ish colouration (5Y8/1 white) which make it a distinct, horizontally traceable bed. The sediments forming the top of log 6 (1C 143-153 cm and 1D 153-163 cm) appear to be darkened horizons with varying silt and fine sand content. As with 1B, these sediments provide a distinct horizontally continuous horizon for linking logs.

Logs 7 and 8 record well sorted, silt sized material, which appears to containing varying quantities of carbonate nodules and varying cohesion. From the base of log 7 to the top of log 8, there are 4 horizons of darkened, finer sediments, often associated with small, powdery nodules (1C-D, 2B, 2D, 2F). In the field, nodules identified as powdery with indistinguishable crystals were noted as carbonates and those with a yellowish colouration and visible crystal structure were noted as gypsum (Porta 1998). The silt beds within logs 7 and 8 (2A, 2C, 2E) are cohesive, carbonate rich, homogenous and appear to lack bedding structures. Such a description is consistent with the definitions that enable sediments to be interpreted as loess (chapter 3). Each of the darkened horizons (1C, 2B, 2D, 2F) provides a continuous traceable horizon for linking of logs together and helping to build a composite stratigraphy (figures 8.8, 8.9).

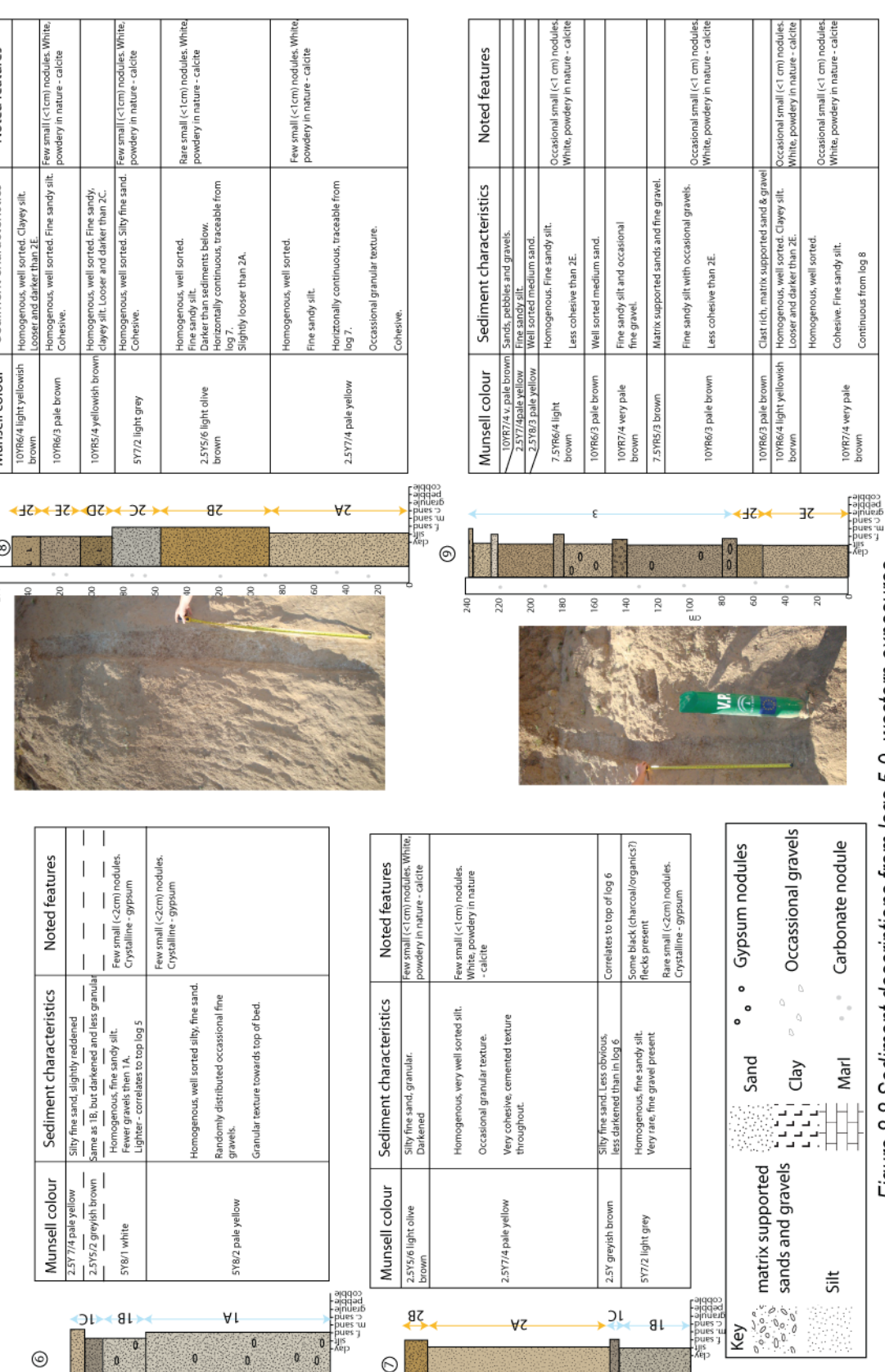

Figure 8.8 Sediment descriptions from logs 5-9, western exposures.

The darkened horizon (2F) from the top of log 8 (232-250 cm) is recorded within log 9 (54-70 cm), the sediments occurring above mark a return to gravel deposition, with alternating beds of sands, silts, and gravels occurring through the rest of log 9. Although the pattern of alternating fine beds and gravel beds continued above log 9, these sediments were not included in this study as they were very close to the land-surface where field ploughing may have disrupted the sediments.

8.3.2 Constructing the composite log

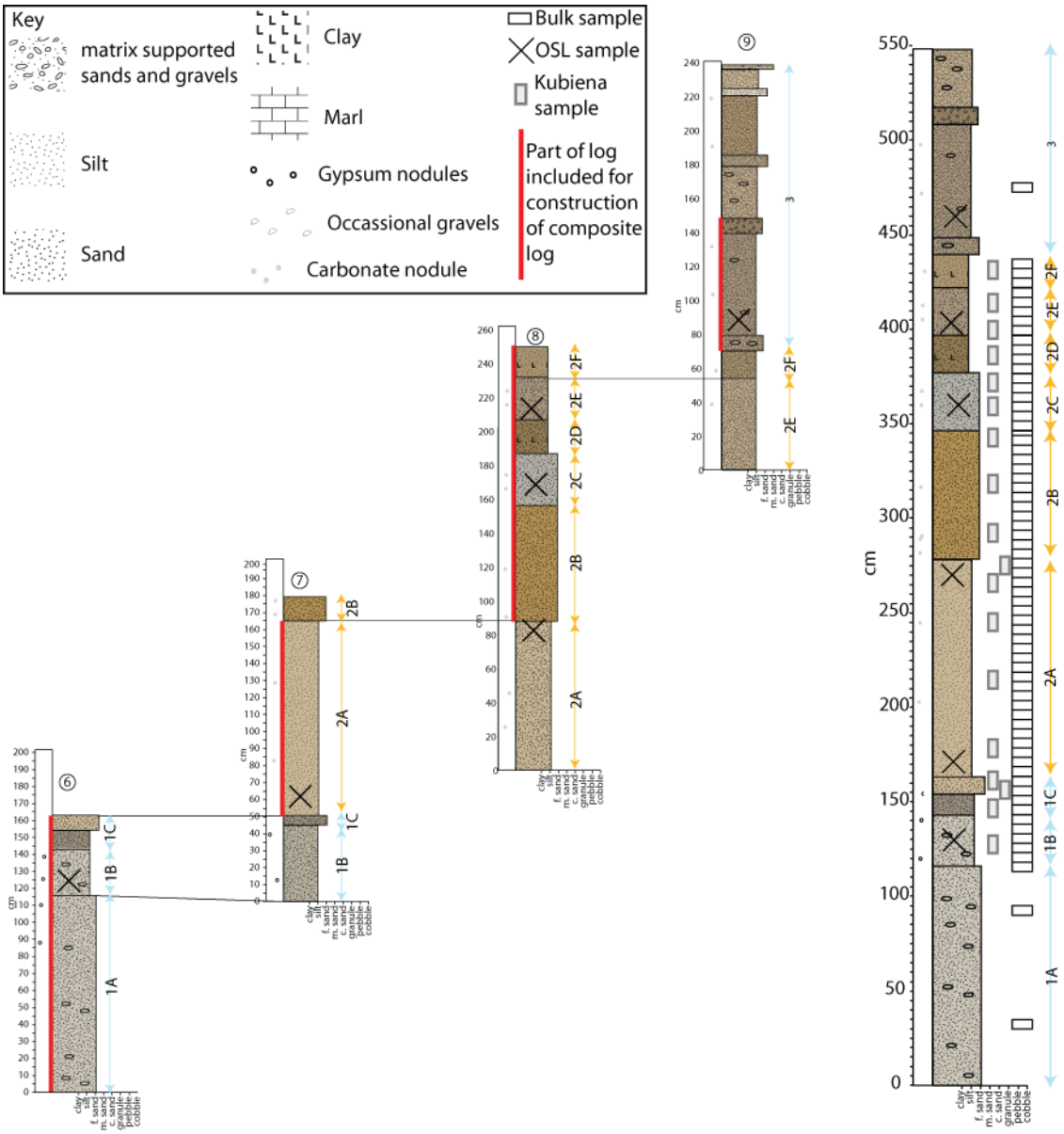

Figure 8.9 Sediments logs 6-9 showing linking beds (black lines). Some sub-units were included within multiple sediment logs, but only included once within the composite. Red bars next to sediment logs indicate section included in composite.

As mentioned above, the darkened horizons provided useful marker beds from which it was possible to link sediment logs. These correlations were used to ensure that only one example of each sub-unit of sediments were included within the composite stratigraphy (figure 8.9). The

composite log includes all sub-units contained within sediment logs 6-9 and was used as a basis for deciding sample locations.

8.3 Sampling

Sampling locations are shown in figure 8.9 placed according to the sampling strategy outlined in chapter 5.

8.4 Sedimentology

Raw data from sample analyses can be found in the appendix.

8.4.1 Particle size analysis

Particle size data (figure 8.10, table 8.1) from unit 1 shows that it is a sandy, clayey silt containing occasional small gravels. The average composition of the sediments is ~48% silt, ~30% sand, ~21% clay and <1% gravel (table 8.1). The sub-units (1a, 1b and 1c) do not vary greatly in their composition compared to the composition of the unit as a whole.

Unit 2 contains no gravel component; PSA identifies it as a clayey, sandy silt with an average composition of ~30% clay, ~46% silt and ~24% sand. There is some variability within the sub-units of unit 2, with sand content reducing upwards through the unit and clay content increasing upwards, silt content is relatively consistent throughout.

The PSA results for unit 3 are from only one sample. The results indicate that, as noted in the field, the unit marks the return to the deposition of gravels at Chimeneas. The sampled sediment is described as a clayey, sandy silt with some fine gravels, composition is listed in table 8.2.

When plotted according to depth (figure 8.10) the PSA results identify a marked shift in sedimentology. Through unit 1 and sub-unit 2A there are fluctuations of up to 15% in sand and silt content through the sediments. Above sub-unit 2A, however, variability in composition is greatly reduced. In addition to a transition to a more stable composition, the sequence also records a fining upwards, which appears to be driven by increasing clay content upwards through the sediments.

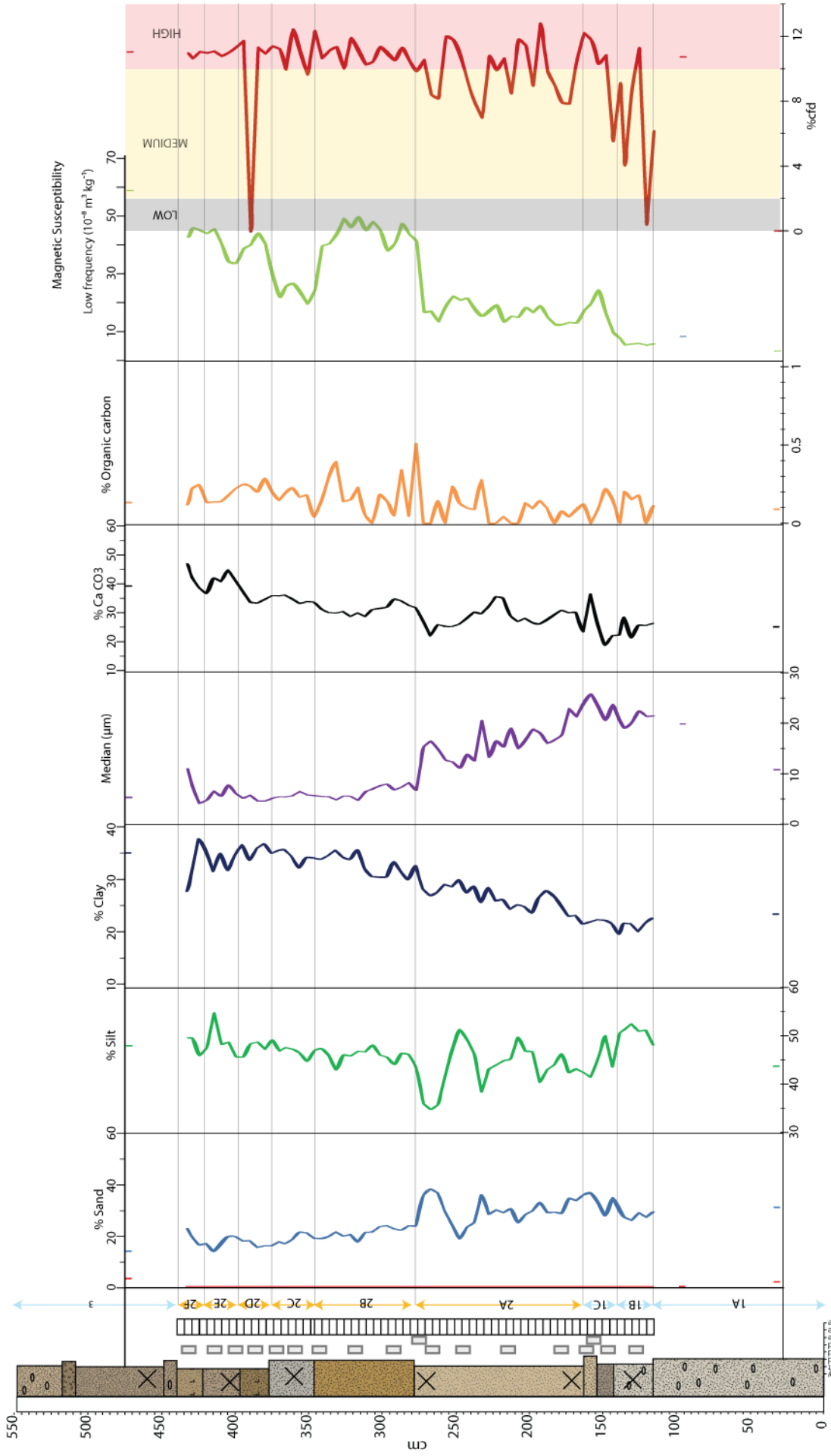

Figure 8.10 Bulk sedimentological data results from the analysis of sediments included within the composite log constructed for Chimeneas.

Table 8.1 Summary statistics of particle size data for all units within composite log. Median grain size given in μm, all other data in % total weight.

Unit	Statistic	gravel %	sand %	silt %	total clay %	fine clay %	median
1	Mean	0.15	30.24	48.33	21.27	13.85	20.68
	Standard Deviation	0.53	3.28	3.81	1.72	2.70	3.65
	Minimum	0.00	25.90	41.42	16.90	8.18	10.77
	Maximum	1.83	36.67	52.54	23.35	18.44	25.77
1a	Mean	0.91	31.47	47.50	20.12	9.72	15.29
	Standard Deviation	1.29	0.54	5.31	4.56	2.19	6.39
	Minimum	0.00	31.09	43.74	16.90	8.18	10.77
	Maximum	1.83	31.85	51.25	23.35	11.27	19.81
1b	Mean	0.00	27.70	50.80	21.50	14.23	20.83
	Standard Deviation	0.00	1.43	1.61	0.92	0.60	1.34
	Minimum	0.00	25.90	48.16	20.01	13.77	18.95
	Maximum	0.00	29.28	52.54	22.56	15.13	22.43
1c	Mean	0.00	32.30	46.20	21.51	15.12	22.67
	Standard Deviation	0.00	3.65	4.08	1.14	2.80	2.27
	Minimum	0.00	27.69	41.42	19.53	10.89	20.41
	Maximum	0.00	36.67	50.72	22.33	18.44	25.77
2	Mean	0.00	23.84	45.62	30.54	18.45	10.41
	Standard Deviation	0.00	6.48	3.63	4.26	2.23	5.69
	Minimum	0.00	13.72	34.78	21.49	14.07	4.14
	Maximum	0.00	38.33	54.79	37.75	22.15	23.97
2a	Mean	0.00	30.11	43.63	26.25	16.94	16.54
	Standard Deviation	0.00	4.93	4.41	2.21	2.01	3.40
	Minimum	0.00	18.71	34.78	21.49	14.07	11.06
	Maximum	0.00	38.33	51.38	29.91	21.30	23.97
2b	Mean	0.00	21.62	45.73	32.65	18.24	6.47
	Standard Deviation	0.00	1.97	1.42	2.01	1.63	1.17
	Minimum	0.00	17.48	42.96	29.90	15.97	4.69
	Maximum	0.00	23.94	48.15	35.65	20.37	8.24
2c	Mean	0.00	18.99	46.77	34.24	20.47	5.69
	Standard Deviation	0.00	1.71	0.97	1.17	0.87	0.37
	Minimum	0.00	16.73	44.74	32.16	19.42	5.40
	Maximum	0.00	21.38	47.63	35.64	22.15	6.48
2d	Mean	0.00	16.30	48.39	35.30	20.61	5.02
	Standard Deviation	0.00	1.17	0.86	1.36	1.00	0.57
	Minimum	0.00	15.30	47.19	33.63	19.52	4.57
	Maximum	0.00	17.99	49.20	36.78	21.92	5.76
2e	Mean	0.00	17.53	48.61	33.86	20.13	6.21
	Standard Deviation	0.00	2.46	3.73	2.21	1.73	1.03
	Minimum	0.00	13.72	45.62	31.49	17.52	5.15
	Maximum	0.00	19.68	54.79	36.57	22.11	7.79
2f	Mean	0.00	18.88	48.17	32.94	19.94	6.82
	Standard Deviation	0.00	2.94	1.78	4.56	1.92	3.13
	Minimum	0.00	16.30	45.95	27.66	17.29	4.14
	Maximum	0.00	22.75	49.62	37.75	21.76	10.99
3	Value	3.08	13.89	47.99	35.04	20.09	5.24

8.4.2 Calcium carbonate content

Table 8.2 Bulk sedimentological properties of all units from composite log. $CaCO_3$ and organic carbon given in % total weight. Magnetic susceptibility values given in $10^{-8} m^3 kg^{-1}$, lf=low frequency, hf=high frequency, cfd=c % combined frequency difference

Unit	Statistic	%CaCO3	Organic carbon	lf	hf	cfd
1	Mean	25.54	0.11	9.91	9.03	7.37
	Standard Deviation	4.52	0.08	6.68	5.85	4.15
	Minimum	18.74	0.00	3.42	3.42	0.00
	Maximum	36.53	0.22	24.46	21.96	11.71
1A	Mean	26.84	0.09	5.93	5.48	5.33
	Standard Deviation	2.37	0.00	3.55	2.91	7.54
	Minimum	25.17	0.08	3.42	3.42	0.00
	Maximum	28.52	0.09	8.44	7.54	10.66
1B	Mean	25.51	0.13	5.75	5.39	6.11
	Standard Deviation	2.62	0.08	0.28	0.09	4.21
	Minimum	21.33	0.00	5.40	5.28	0.37
	Maximum	28.54	0.20	6.06	5.54	11.22
1C	Mean	25.03	0.09	15.67	14.10	9.45
	Standard Deviation	6.84	0.10	6.95	6.08	2.41
	Minimum	18.74	0.00	7.72	7.02	5.49
	Maximum	36.53	0.22	24.46	21.96	11.71
2	Mean	32.21	0.14	29.72	26.63	10.28
	Standard Deviation	5.27	0.11	12.93	11.54	1.89
	Minimum	22.04	0.00	12.50	11.46	-0.05
	Maximum	46.99	0.51	49.68	44.20	12.72
2A	Mean	28.30	0.08	16.65	14.99	9.85
	Standard Deviation	3.28	0.08	2.92	2.52	1.67
	Minimum	22.04	0.00	12.50	11.46	6.93
	Maximum	35.63	0.28	22.36	19.74	12.72
2B	Mean	31.21	0.19	44.40	39.62	10.75
	Standard Deviation	1.87	0.15	3.67	3.27	0.61
	Minimum	28.67	0.00	37.86	33.74	9.78
	Maximum	34.77	0.51	49.68	44.20	11.83
2C	Mean	34.14	0.16	25.93	23.08	10.98
	Standard Deviation	1.70	0.06	6.51	5.82	1.08
	Minimum	31.21	0.04	19.64	17.76	9.57
	Maximum	36.18	0.23	39.70	35.50	12.36
2D	Mean	34.44	0.23	38.33	35.18	8.34
	Standard Deviation	1.15	0.04	6.52	6.56	5.60
	Minimum	33.37	0.20	28.96	25.68	-0.05
	Maximum	35.96	0.29	44.10	39.92	11.33
2E	Mean	41.26	0.18	38.44	34.17	11.11
	Standard Deviation	2.66	0.05	4.93	4.42	0.36
	Minimum	37.49	0.14	33.62	29.84	10.71
	Maximum	44.86	0.25	45.58	40.56	11.65
2F	Mean	41.08	0.18	44.32	39.52	10.83
	Standard Deviation	4.56	0.06	1.41	1.30	0.19
	Minimum	36.59	0.12	42.60	37.96	10.56
	Maximum	46.99	0.25	45.84	41.00	10.98
3	Value	39.27	0.30	58.72	52.28	10.97

Calcium carbonate content of the bulk sediments samples are shown in figure 8.10, summary statistics given in table 8.2, full data listed in the appendix.

Carbonate content through unit 1 varies from 18.74 to 36.53%, with the mean content being 25.54%. The sub-units 1a and 1b show only minor fluctuations of ~±3% around this average value. Sub-unit 1c shows a greater amount of variation, with the lower fine grained darkened horizon having the lowest content (18.74%) and the upper, coarser horizon having the highest content (36.53%).

The average carbonate content of unit 2 is 32.21%, however this value masks the obvious depth trend shown in figure 8.10. There is an increasing carbonate content upwards through the sediments, with the lower sub-unit (2A) having an average $CaCO_3$ content of 28.30% increasing to an average carbonate content of 41.08% in the upper sub-unit (2F). In addition to the overall trend towards increasing carbonate content, there is some intra-unit variability.

Through 2A carbonate content is relatively stable there is, however, a notable peak in carbonate content at 218-233 cm, peaking at 35.63% before returning to levels around the average content for the sub-unit. There is then a jump in content associated with the base of sub-unit 2b (278-308 cm) with values peaking at 34.77%, there is then a slight reduction in content down to ~29% before values begin steadily increasing upwards through the remainder of 2B reaching ~31%. 2C records steadily increasing carbonate content from 31.21% at the base up to 36.18% at the top of the bed. 2D records a slight reduction in carbonate content from 35.96% at its base down to 33.37% towards its top. 2E contains a higher carbonate content that 2D below it, with content increasing from 37.49% at its base up to 42.10% at the top. The transition to 2F records a drop in carbonate content to 36.59% at the base, steadily increasing upwards through the bed to 46.99% at the top. Only one sample was taken from unit 3, containing 39.27% carbonate.

8.4.3 Magnetic susceptibility

Magnetic susceptibility measurements are shown in figure 8.10, summary statistics are given in table 8.2, full data in appendix. Low frequency readings, indicating overall magnetic mineral content are relatively low throughout the section at Chimeneas, ranging from 3.42 to 58.72 10^{-8} m^3 kg^{-1}. There is a clear pattern evident within the sediments however, with those of the darkened horizons (1C, 2B, 2D, 2F) recording peaks in magnetic mineral content relative to the surrounding sediment beds.

The %cfd record, indicative of pedogenic magnetic mineral content (e.g. Dearing 1999), is less clear. Values throughout the section are typically around 8-12% (table 8.2), with no pattern

appearing to relate to stratigraphic boundaries. There is a general trend towards more stable, higher %cfd values upwards through the sediments.

However, repeat measurements (given in appendix) of both low and high frequency readings indicate there could be up to a 10% error associated with the technique. Such large differences in readings would not alter the pattern of low frequency shifts seen at Chimeneas, but could have a large effect on %cfd values.

8.4.4 Organic carbon content

Organic carbon results are shown in figure 8.10, summary statistics given in table 8.2, full data in appendix. Throughout the sediments at Chimeneas organic carbon content is extremely low; therefore the results will not be discussed further.

8.4.5 Sedimentological interpretation

The lower units exposed on both sides of the valley comprise of fine silty sand beds with occasional gravels interbedded with clast rich, matrix supported gravels. Based on field observations, these sediments are identified as being alluvial sediments. Their poor sorting characteristics and the matrix supported nature of the sediments indicates rapid deposition within a low energy environment, typical of floodplain sediment sequences (Miall 1992).

On the western side of the valley, these sediments are capped by a white coloured (5Y 8/1 white) horizon which forms a distinct, traceable sediment body. This, in turn, is overlain by a body of darkened sediments. These sediments are interpreted as representing a possible soil horizon associated with a weak decalcification of the upper horizon and subsequent leaching downwards through the sediments. This weak decalcification is likely to reflect only a short lived episode of post-depositional alteration at a stable land-surface. The occurrence of this short-lived land-surface stability marks the transition to loess(ic) accumulation at Chimeneas.

The sediments of unit 2 are well sorted clayey sandy silts and appeared consistent with criteria for the recognition of loess sediments (chapter 3), these sediments are interbedded with horizontally continuous darkened sediments interpreted in the field as weak palaeosol horizons. PSA results from unit 2 indicate a general fining of sediments upwards, with a steadily declining median grain size appearing to be driven by increasing clay content (figure 8.11), which could indicate increasing pedogenic alteration of sediments or a reducing transport energy. There is a general trend towards increasing bulk carbonate content upwards through the sediments of unit 2, which suggests that increasing clay content is not pedogenic in origin. Pedogenic chemical

weathering of particles to clay sized material occurs over a relatively long time scale which would most likely included sustained leaching of carbonate, this is not seen in this sequence. As such, the increasing clay content is likely to be a feature of accumulation rather than alteration, it is therefore suggested that the clay content could result from increased incorporation of local surface soils through reworking or through increased transport of flocculated clays as silt sized material. If increasing clay content through unit 2 is reflective of increasing incorporation of local surface soils it would be one explanation for the consistently high %cfd values which are evident through the sediments (figure 8.11).

The darkened horizons interbedded within the loess sub-units do not record large shifts in particle size, but they do indicate some degree of decalcification occurring with each darkened bed. This adds some support to the field interpretation that these darkened sediment beds represent weak palaeosols.

Above the cohesive silt sediments is a return to less cohesive, less well sorted sediments (unit 3). These sediments although still predominantly fine, have a clear gravel component present throughout. Due to the similar textural characteristics between these sediments and those infilling the valley, they are interpreted as marking a return to floodplain accumulation.

8.5 Micromorphology

8.5.1 Groundmass and Skeleton grains

Sedimentological characteristics of thin sections were noted in terms of texture (c:f), composition (homogeneity) and structure (bedding and voids) following the guidelines of Bullock *et al.* (1985) and Kemp (1985a). Thin section description of mineralogy was not carried out, as mineralogy of sediments was assessed via XRD. Large quantities of gypsum were present in the thin sections from Chimeneas. *In-situ* gypsum growth is a displacive process (Poch *et al.* 2010) which would result in disruption of sediment structure, therefore structural features (for example % void cover) may have been altered considerably and so should be considered with caution. All thin sections show apedal macro-structure (Kemp 1985a) and are generally massive, homogenous sediments although some textural concentration features are present in sections from the top of the sequence.

8.5.2 Concentration/depletion features

There is some preservation of organics (0-5% slide coverage) within the sediments of Chimeneas. The cellular structure of the organics present is only rarely preserved; typically the

organics are highly degraded (Stolt and Lindbo 2010). The degraded organics appear as reddish brown to blackish amorphous staining usually occurring in association with a void.

Calcitic pedofeatures are common within loess-palaeosol sequences (Jiamao *et al.* 1997). Such features relate to the localised or sustained dissolution and subsequent reprecipitation of carbonate from soil waters. The presence and distribution of such features within loess-palaeosol sequences have been used to identify the pedogenic history of the sediments. Kemp (1995, 2001) has suggested that the balance between pedogenic processes and sediment input controls the style of pedogenic alteration. Sustained pedogenic alteration during low sediment accumulation episodes results in a top down style of alteration which is associated with removal of carbonate from upper horizons and subsequent reprecipitation in the form of large carbonate nodules at depth (Kemp 1985b, Kemp 1995). Accretionary pedogenic alteration describes pedogenic alteration of sediments during active accumulation which is associated with localised carbonate redistribution (Kemp 1999).

The calcitic concentration features present in thin sections from Chimeneas are small nodules (<1 cm), hypocoatings and void linings, there are no void infillings preserved in the sections. These features are noted in terms of their abundance (% slide cover) and crystal morphology (micrite <4 μm, microsparite 5-20 μm and spar >20 μm (Bullock *et al.* 1985, Durand *et al.* 2010). All calcitic nodules noted had diffuse boundaries with surrounding groundmass consistent with authigenic growth (Durand 2010). Hypocoatings and nodules were moderately to strongly impregnated micrite to microsparite occurring around voids (hypocoatings) and within the groundmass (nodules).

Redoximorphic concentration features comprise growth features of iron or manganese. These features relate to the mobilisation of iron/manganese in saturated (reducing) environments and subsequent oxidation induced precipitation (Kemp 1985a, King 2000, Lindbo *et al.* 2010). There are very few (<1% coverage) redoximorphic concentration features recorded within the sediments of Chimeneas. The few that are present occur as small (<100 μm) moderately impregnated, blackish amorphous stains within the groundmass. It is not possible to visually distinguish between iron and manganese concentrations within thin section (Kemp 1985a).

Gypsum nodules were identified during field description of the sediments at Chimeneas. Within thin sections gypsum is present within the groundmass of some thin sections and also as a void infilling feature throughout the sequence. The presence of gypsum as an inherited or pedogenic feature is linked with arid climates as evaporation is key to its precipitation and because it is easily leached from soils under humid climates (Poch *et al.* 2010). Gypsum crystals can be

transferred via aeolian processes, or can form in sediments where there is a high concentration of Ca^{2+} and SO^{2-}_4 ions present formed through the dissolution of calcium sulphate bearing rocks or derived from limestone and biogenic carbonates (Poch *et al.* 2010).

The origin of pedogenic gypsum is related to movement of waters rich in Ca^{2+} and SO^{2-}_4 ions. This can be through *per ascensum* processes where water rises up through sediments from the water table by capillary rise or by incomplete wetting of sediments by downwards movement of waters (*per descensum*) (Jafarzadeh and Burnham 1992, Nash and Ullyot 2007). *Per ascensum* processes are dominant in very arid climates, whereas *per descensum* is typical of moderately arid climates (Jafarzadeh and Burnham 1992). However, where gypsum bedrock is present, such as at Chimeneas (figure 8.2), groundwaters may become supersaturated with Ca^{2+} and SO^{2-}_4 ions. Although evaporation is required to draw water up through the sediments via capillary rise, a hyper-arid environment is not required to promote precipitation via evaporation. Lenticular gypsum is the most common crystal form found within soils (Porta and Herrero 1988, Amit and Yaalon 1996, Poch *et al.* 2010).

Rare to common lenticular gypsum crystals are found within the groundmass of some Chimeneas thin sections. This gypsum is typically ~100 μm in length and 3:1 to 2:1 length:width. Rarely the edges of some crystals appear irregular. Lenticular crystals are located within voids throughout the thin sections at Chimeneas. The crystals are often interlocking and completely line or infill the void. Average crystal length ranges from ~100-300 μm, with a length:width ratio of 3:1 to 2:1.

8.5.3 Distribution of micromorphological features

Throughout the section at Chimeneas the sediments studied through thin section (figure 8.12) were well to moderately sorted, with groundmass being the dominant component of the sediments. This dominance of groundmass, indicated by c:f ratios is reflective of the very fine grained nature of the sediments identified through PSA. The % coverage of voids is noted, however, this estimate of coverage was particularly difficult due to the presence of large amounts of gypsum. *In-situ* gypsum growth is a displacive process (Porta and Herrero 1990, Poch *et al.* 2010), which could have significantly affected the void morphologies and size, therefore voids will not be discussed as soil features relating to biological activity.

There are low levels of organics preserved throughout the sediment sequence with increasing occurrence upwards (figure 8.12), from <1% occurrence at the base of the sequence up to 5% slide coverage observed towards the top. Very rare occurrences of iron/manganese staining occurs, at its maximum accounting for <1% of slide area.

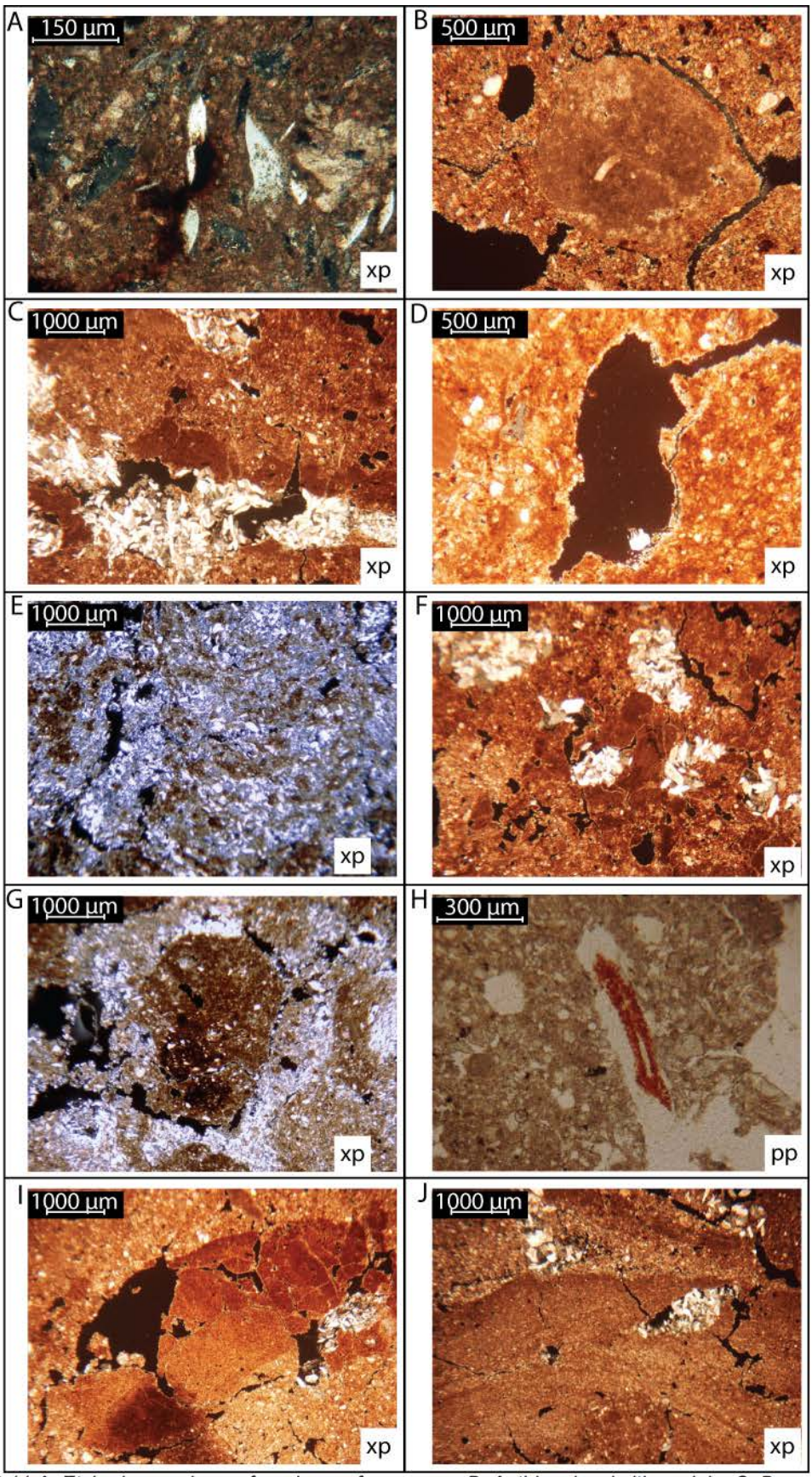

Figure 8.11 A. Etched groundmass from base of sequence, B. Authigenic micritic nodule, C. Dense micritic hypocoating disrupted by gypsum infill, D. Micritic hypocoating and microspar void lining preserved in void free of gypsum, E. Gypsum saturated groundmass, close to isle fabric distribution from base of sequence, F. Interlocking gypsum filling voids from upper sediments, G. Micritic nodule split by displacive gypsum growth, H. Preservation of cellular organic material, I. Disrupted surface crust, J. Textural concentrations of laminated clayey silts and sands produced by flow.

Gypsum occurs in groundmass through the base of the sequence, part way up through unit 2A, associated with occasional gyprock fragments. These gypsum crystals appear as fine grained (~50 μm average) grains incorporated in the groundmass, some grains have uneven edges indicating some dissolution has occurred (Porta and Herrero 1990). Gyprock clasts are identifiable due to the tabular morphology of the interlocking crystals and the sharp boundary with the groundmass (Porta and Herrero 1990). Almost all voids present in every thin section are completely or partially infilled by lenticular gypsum crystals, commonly interlocking. There is a general trend towards smaller crystal sizes and less area coverage of gypsum upwards through the sequence (figure 8.12).

The depth profile of calcitic pedofeatures is complex (figure 8.12). However, if broken down into sub-unit variations there are clear patterns present. 1C was identified in the field as a potential soil horizon. These sediments are associated with a low % cover of calcitic features a decrease in bulk carbonate content and a very slight clay enrichments (figure 8.10). Beneath 1C is sub-unit 1B which records an increase in % calcitic pedofeature occurrence marked by an increase in occurrence of hypocoatings and small nodules. Decalcification in the upper horizons resulting in the accumulation of carbonate in the sediments below is consistent with pedogenic alteration of sediments at a stable land-surface (Kemp 1985b). The upper horizon being partially decalcified suggests that either land-surface stability was not a long term occurrence, or that the sediments have been recalcified by an overlying sediment body.

Through unit 2A there is an upwards increase in the occurrence of calcitic pedofeatures, although hypocoatings and nodules are present throughout, their total area coverage increases. This increase in pedofeatures is not associated with major changes in bulk carbonate content (figure 8.10), which indicates that calcite dissolution and reprecipitation was a localised phenomenon representative of accretionary pedogenic alteration (Kemp 1995, 1999).

2B was identified in the field as a possible soil horizon. Micromorphological analysis of the sediments identifies increasing calcitic pedofeature occurrence with depth through the sub-unit, which is consistent with the bulk carbonate depth profile of the bed (figure 8.10). The occurrence of calcitic features throughout the bed indicates that all sediment has been altered by reprecipitation of calcite, indicating that it is likely that accretionary pedogenic alteration occurred during accumulation and subsequent post-depositional partial decalcification of the upper sediments occurred during a short lived stable land surface.

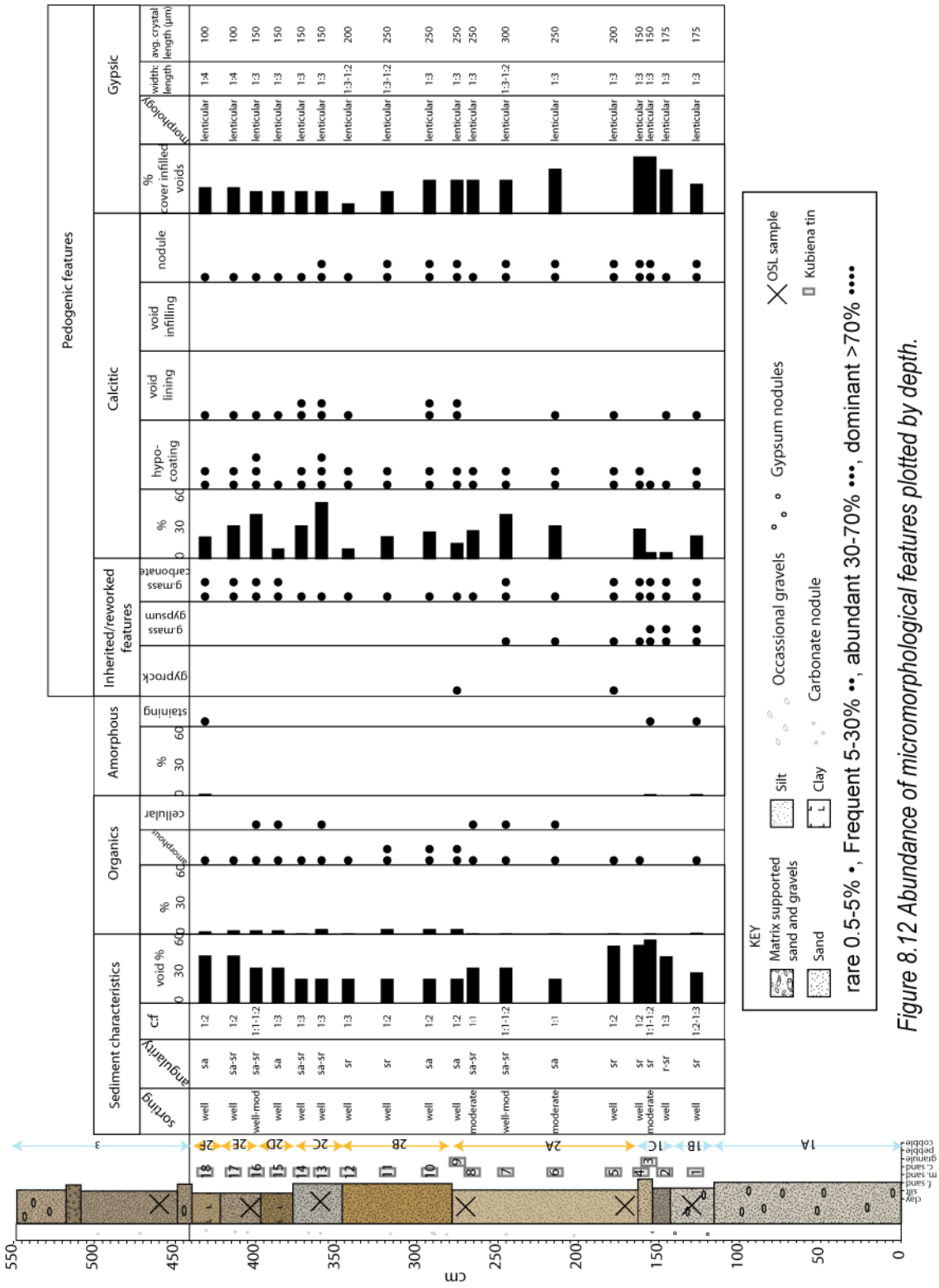

Figure 8.12 Abundance of micromorphological features plotted by depth.

2C was noted in the field as a loess or loessic sediment capped by a possible weak soil horizon (2D). As with 1C and 1B, 2D is a partially decalcified horizon (figure 8.10) containing low levels of calcitic pedofeatures, the lower sediments (2C) are relatively enriched in calcitic features with abundant hypocoatings and frequent small nodules. This is consistent with post-depositional alteration during existence of a short-lived stable land-surface (Kemp 1999, King 2000). This pattern of calcitic pedofeature distribution and bulk carbonate content is observed within the overlying sediments, with 2E being relatively enriched in bulk carbonate and calcitic features compared with the overlying horizon 2F.

The pattern of alternating loess accumulation and soil forming intervals is also associated with increased reworking of sediments upwards through the sequence. From sub-unit 2C upwards thin section analysis identified a number of disrupted surface crusts and very well sorted textural concentration features occurring as rare bands of fine to medium sand (figure 8.11). Both the disruption and erosion of surface crusts together with textural concentrations consistent with deposition by flow (see figure 7.24 previous chapter) indicate increased input of non-aeolian sediments and localised reworking of sediments. Micromorphological analysis therefore indicates that deposition at Chimeneas becomes increasingly loessic in nature upwards through the sequence.

Present through each thin section taken from Chimeneas are extensive growths of lenticular gypsum crystals, primarily in the form of interlocking crystal linings and infillings of voids. The displacive nature of the crystal growth is evident through the presence of large planar voids emanating from void expansion through gypsum crystal growth. This displacive growth can be identified in places as causing disruption to calcitic pedofeatures (figure 8.11), indicating that the phase of gypsum growth relating to the presence of interlocking crystal features occurred as a later overprinting feature after the deposition and initial pedogenic alteration of the sediments at Chimeneas. Despite recognition of gypsum precipitation being a subsequent phase of alteration of the sediments, it is not possible to constrain when this alteration occurred.

Towards the base of the section there is a much greater abundance of gypsum, both as interlocked crystal growths in the groundmass and within voids, but also as individual grains which appear to be forming part of the groundmass. In places, the basal sediments consist of >50% lenticular gypsum growths and appear to be approaching isles fabric (Porta and Herrero 1988), where gypsum growth is so extensive it is the dominant constituent of the sediments containing only peds of original host sediment. The abundance of gypsum reduces up profile, and

gypsum growth becomes confined to within voids. Within these sediments, gypsum more commonly occurs as a partial void filling feature.

An absence of gypsiferous sediments overlying the sequence at Chimeneas, together with the depth profile of accumulation suggests that the gypsum is related to a *per ascensum* mode of formation (Jafarzadeh and Burnham 1992, Candy and Black 2009), where groundwater or meteoric water is moved upwards through the profile via capillary rise in response to strong evaporation at the ground surface (Goudie 1983, Gutierrez Elorza 1995, Watson 1985).

8.6 $\delta^{18}O$ and $\delta^{13}C$ composition of carbonates

8.6.1 Results

Pedogenic carbonates (<2mm) were handpicked from bulk sediments as outlined in chapter 5. Isotopic composition of all pedogenic carbonates measured from the sediments at Chimeneas are given in table 8.3.

$\delta^{13}C$ values range from -4.61 to -7.99‰, mean -6.09‰. The mean $\delta^{13}C$ value of each sub-unit lies close to the mean value for the data set as a whole (table 8.4). $\delta^{18}O$ values range from -4.77 to -6.84‰ (mean -5.35‰). However, there are distinct differences in the range of oxygen isotopic values from pedogenic carbonates originating from different sub-units; with all sub-units recording <1‰ range of values except 2A where the range is almost 2‰ (table 8.4).

8.6.2 Co-variance

Candy *et al.* (2012) identified that strong covariance within the isotopic composition of meteoric carbonates indicates that both the carbon and oxygen isotopic composition is being driven by aridity. Figure 8.13 indicates that there is no significant covariance between $\delta^{13}C$ and $\delta^{18}O$ values for pedogenic carbonates at Chimeneas.

8.6.3 Interpretation of isotopic composition of pedogenic carbonates

$\delta^{13}C$ values from the pedogenic carbonates of Chimeneas range from -7.99 to -4.61‰. As discussed in chapter 4, carbon isotopic composition of soil carbonates is often used as a proxy for vegetation composition, with C3 and C4 photosynthetic pathway plants respiring CO_2 into the soil of different isotopic compositions (-27±1.5‰ and -11.8±1.4‰) , respectively (Cerling and Quade 1993, Quade and Cerling 2007). The $\delta^{13}C$ value of the soil environment becomes enriched by gaseous exchange (diffusion), with further enrichment occurring due to fractionation during calcite precipitation. The combined effects of fractionation and diffusion result in an overall

enrichment of 14.8±1.6‰ of $\delta^{13}C$ of soil carbonates relative to plant respired CO_2 (Cerling and Quade 1993, Quade *et al.* 1989a).

Table 8.3 Isotopic composition of pedogenic carbonates sampled from Chimeneas

Sub-unit	Depth	$\delta^{13}C$ (‰)	Error (1σ)	$\delta^{18}O$ (‰)	Error (1σ)
2F	440	-6.58	0.04	-6.23	0.03
2F	437	-5.45	0.07	-5.42	0.03
2E	427	-5.75	0.01	-4.82	0.02
2E	417	-5.94	0.00	-4.87	0.07
2E	412	-6.35	0.04	-5.22	0.04
2E	402	-6.38	0.03	-5.27	0.04
2D	397	-6.18	0.00	-5.24	0.03
2D	392	-6.48	0.00	-5.37	0.01
2D	387	-6.57	0.02	-5.20	0.01
2C	373	-6.03	0.01	-5.03	0.02
2C	368	-5.97	0.02	-5.05	0.00
2C	358	-6.11	0.02	-5.04	0.01
2C	353	-6.28	0.05	-5.16	0.07
2B	348	-6.09	0.01	-4.97	0.09
2B	333	-6.42	0.00	-4.95	0.02
2B	323	-5.19	0.01	-4.77	0.06
2B	318	-5.14	0.03	-4.90	0.02
2B	308	-6.48	0.01	-5.35	0.01
2B	303	-4.61	0.03	-4.94	0.07
2A	278	-6.15	0.04	-4.96	0.11
2A	263	-5.95	0.04	-5.07	0.09
2A	248	-6.03	0.02	-5.48	0.06
2A	233	-6.25	0.01	-5.30	0.04
2A	218	-6.03	0.03	-5.88	0.00
2A	203	-5.82	0.02	-5.87	0.03
2A	188	-7.99	0.03	-6.84	0.07
2A	173	-6.25	0.01	-6.20	0.02
1C	163	-5.66	0.01	-5.52	0.00
1C	153	-6.43	0.02	-6.10	0.02
	Mean	-6.09	0.02	-5.35	0.04
	Minimum	-4.61	0.07	-4.77	0.11
	Maximum	-7.99	0.00	-6.84	0.00

Table 8.4 Summary of isotopic composition of pedogenic carbonates from each sub-unit

Sub-unit	Measurement	Mean	Min.	Max.
1c	$\delta^{13}C$ (‰)	-6.05	-6.43	-5.66
	$\delta^{18}O$ (‰)	-5.81	-6.10	-5.52
2a	$\delta^{13}C$ (‰)	-6.31	-7.99	-5.82
	$\delta^{18}O$ (‰)	-5.70	-6.84	-4.96
2b	$\delta^{13}C$ (‰)	-5.65	-6.48	-4.61
	$\delta^{18}O$ (‰)	-4.98	-5.35	-4.77
2c	$\delta^{13}C$ (‰)	-6.10	-6.28	-5.97
	$\delta^{18}O$ (‰)	-5.07	-5.16	-5.03
2d	$\delta^{13}C$ (‰)	-6.41	-6.57	-6.18
	$\delta^{18}O$ (‰)	-5.27	-5.37	-5.20
2e	$\delta^{13}C$ (‰)	-6.11	-6.38	-5.75
	$\delta^{18}O$ (‰)	-5.05	-5.27	-4.82
2f	$\delta^{13}C$ (‰)	-6.02	-6.58	-5.45
	$\delta^{18}O$ (‰)	-5.82	-6.23	-5.42

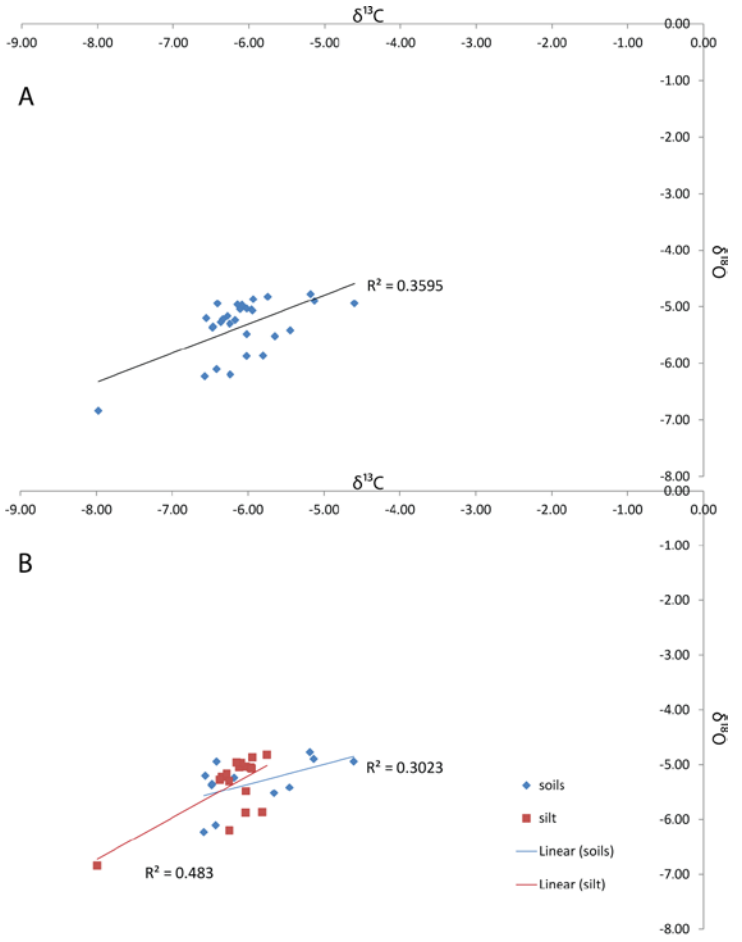

Figure 8.13 A. δ¹³C vs. δ¹⁸O for all samples. B. δ¹³C vs. δ¹⁸O plotted according to stratigraphic association

The $\delta^{13}C$ values of soil carbonates at Chimeneas are too enriched to be consistent with a soil CO_2 derived purely from C3 photosynthetic vegetation, which would produce soil carbonates with $\delta^{13}C$ values of 8 to -12‰ (Cerling and Quade 1993, Wang and Greenberg 2006). Values enriched in ^{13}C could indicate a mixture of C3 and C4 photosynthetic vegetation, with soil carbonates formed under C4 dominant soil environments having $\delta^{13}C$ values of 1 to 4‰ (Cerling and Quade 1993, Wang and Greenberg 2006). There is however, no evidence to suggest the existence of C4 photosynthetic vegetation in southern Spain through the Quaternary (Quade 1994, Cerling *et al.* 1997, Woodward *et al.* 2004) and the values recorded at Chimeneas are not enriched enough that it is necessary to suggest C4 vegetation as a cause (Candy *et al.* 2012). In soil systems where there is a low vegetation cover, a significant proportion of the soil CO_2 is derived directly from the atmosphere (Quade *et al.* 1989b), which has an isotopic composition of around -6‰ at pre-industrial levels (Friedli *et al.* 1986). As such, atmospherically derived CO_2 is significantly enriched in ^{13}C relative to soil CO_2 derived from C3 photosynthetic plants and, therefore, pedogenic carbonates forming within such a soil system would also be enriched in ^{13}C.

However, a lack of covariance between $\delta^{13}C$ and $\delta^{18}O$ values from Chimeneas soil carbonates ($r2 = 0.3592$, p-value = 0.169838) indicates that the two isotopic systems are driven by different mechanisms. Therefore, although the $\delta^{13}C$ values indicate a significant atmospheric component thought to be linked with low levels of vegetation, $\delta^{18}O$ values do not indicate that, at the time of calcite precipitation, the soil environment was strongly controlled by evaporative processes.

Where strong evaporation can be excluded (as with this study) the $\delta^{18}O$ value of soil moisture is a reflection of the composition of local precipitation (Candy *et al.* 2012), with a strong linear relationship existing between air temperature and the $\delta^{18}O$ value of rainfall existing in mid-latitude regions (Dansgaard 1964, Rozanski *et al.* 1993). This relationship is in the order of +0.6‰ per +1°C (Rozanski et al., 1993). The $\delta^{18}O$ value of soil carbonates is derived from the $\delta^{18}O$ value of soil moisture and therefore $\delta^{18}O$ of soil carbonates is controlled by air temperature (Cerling and Quade 1993). The $\delta^{18}O$ value of soil carbonates is further modified by the relationship between temperature and the fractionation of oxygen isotopes during carbonate precipitation of -0.3‰ per +1°C (Craig 1965, Hays and Grossman 1991, White et al 1999, Leng and Marshall 2004). As these two controls work in opposite directions, the combined effect is that a 1°C rise in temperature should result in an increase of ~0.3‰ in the $\delta^{18}O$ value of a soil carbonate.

There is a progressive enrichment in $\delta^{18}O$ values recorded upwards through unit 2A (figure 8.14), this enrichment is marked by a shift from -6.84‰ at the base up to -4.96‰ at the top of the sub-unit; an enrichment of 1.88‰. This enrichment occurs through sediments affected by accretionary pedogenic alteration, where soil carbonates form in response to localised carbonate redistribution during accumulation (Kemp 1995). As such, variations in the oxygen isotopic composition of the soil carbonates reflect temperature changes during accumulation. Due to the numerous factors capable of influencing $\delta^{18}O$ values of soil carbonates, their use as palaeothermometers is flawed. However, given the known relationship between mean annual temperature and the composition of precipitation and the fractionation of calcite discussed previously, it is possible to suggest that in a soil system where the $\delta^{18}O$ value of pedogenic carbonates is a function of air temperature an oxygen isotopic enrichment of 1.88‰ could represent a climatic amelioration of ~6°C.

Through sub-units 2B-2E there is very little variation recorded within $\delta^{18}O$ values (range: -4.77 to -5.37‰, average -5.09‰). This homogeneity of values indicates similar conditions at the time of formation. Bulk and micromorphological characteristics of these sediments indicate a succession of loess-palaeosol horizons, where formation of carbonates is linked to post-depositional alteration of sediments under stable-land surface conditions. As such, carbonates found within 2B relate to that soil forming interval, carbonates within 2C-2D relate to the formation of the 2D soil

and carbonates within 2E and the lower part of 2F relate to the formation of 2F. Again, there is no evidence of covariance between $\delta^{13}C$ and $\delta^{18}O$ values through this section and therefore, $\delta^{18}O$ values are thought to be driven by temperature. The similarity between the values gained through 2B-lower part of 2F and those from the top of 2A indicate that temperatures during the soil forming intervals were similar to those reached at the peak of the climatic amelioration recorded during the accumulation of 2A.

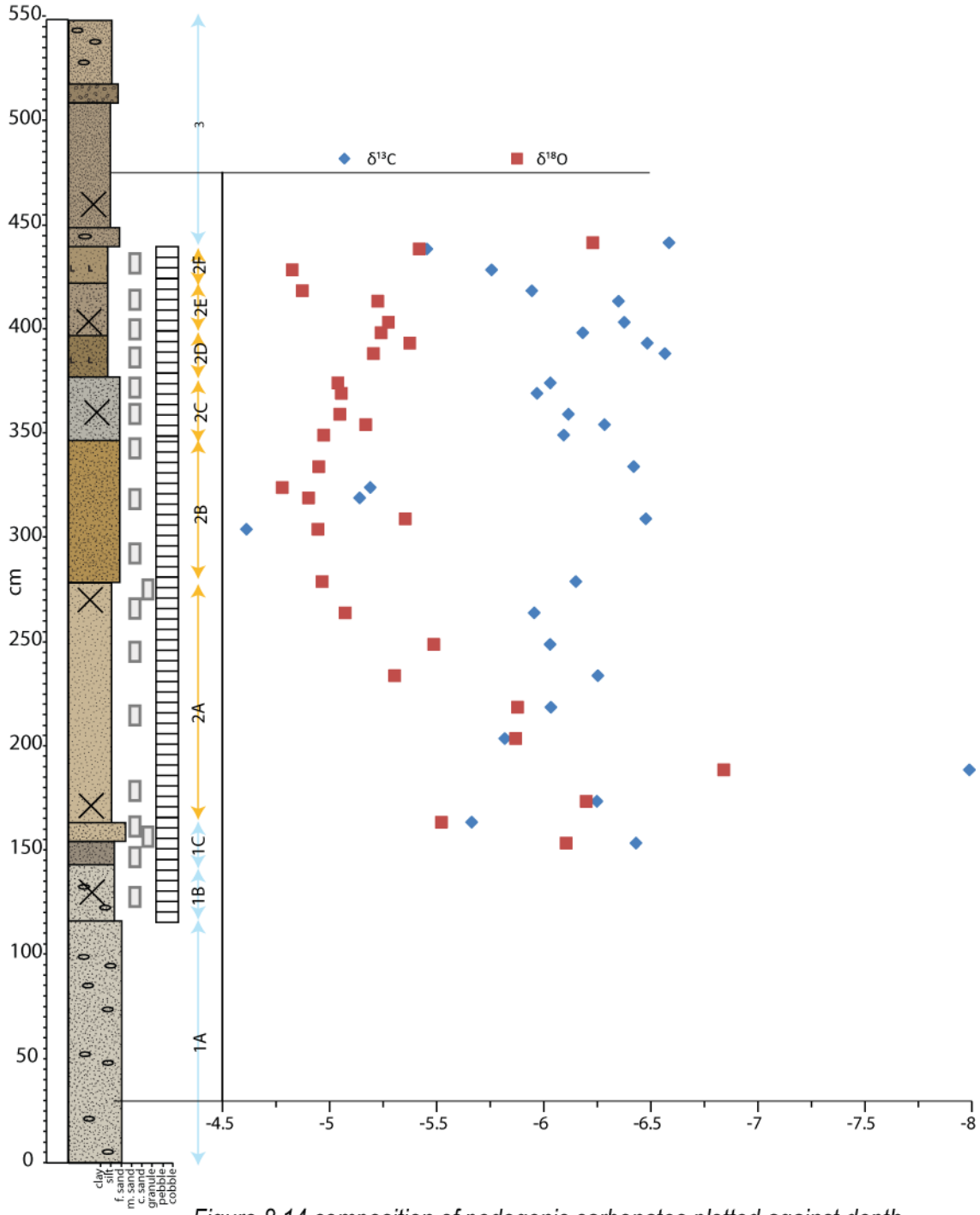

Figure 8.14 composition of pedogenic carbonates plotted against depth.

The sediments at the very top of 2F record a peak in bulk carbonate values (figure 8.10) which is inconsistent with micromorphological evidence which suggests that the horizon below (2E) was enriched with carbonate during alteration of 2F at a stable land-surface. It is possible, however, that this peak in carbonate reflects a re-calcification of the sediments, possibly by unit 3 or by an eroded sediment body. Therefore, the origin of the pedogenic carbonates at the very top of 2F is uncertain, but they do record a $\delta^{18}O$ depletion of 1.41‰. The scale of this depletion is similar to that of the enrichment seen through sub-unit 2A. If this depletion is the result of changing temperatures, then it could relate to a shift in the region of -5˚C.

8.7 OSL site chronology

Six OSL samples were taken through the sequence at Chimeneas (figure 8.9). A minimum of 12 aliquots were used to produce equivalent dose estimates from which an age estimate was calculated using the method outlined in chapter 5. Sample run conditions are given in table 8.5, sample dosimetry data is given in table 8.5.

Table 8.5 Run conditions for OSL samples from Chimeneas

Sample	Depth in log (cm)	Aliquots	PH 1 (˚C)	PH 2 (˚C)	Given doses (Gy)
CHIM 7	460	18	240	160	105, 210, 315, 420, 510, 0, 105, 105
CHIM 6	404	12	240	160	105, 210, 315, 420, 510, 0, 105, 105
CHIM 5	360	13	240	160	105, 210, 315, 420, 510, 0, 105, 105
CHIM 4	270	20	240	160	105, 210, 315, 420, 510, 0, 105, 105
CHIM 3	172	16	240	160	105, 210, 315, 420, 510, 0, 105, 105
CHIM 2	130	14	240	160	105, 210, 315, 420, 510, 0, 105, 105

Growth curves (figure 8.15) were generated using increasing laboratory induced luminescence, curves were fitted using a saturating exponential plus linear relationship. In all cases, the natural luminescence signal intercepts the growth curve where there is a strong monotonic increase in sensitivity corrected OSL intensity with increasing regenerative dose (figure 8.15). Therefore, the sample is not saturated and a geologically meaningful De may be calculated.

Table 8.6 Summary of dosimetry and dating results for Chimeneas

Sample	Depth in log (cm)	Radionuclide concentration			Sample depth (m)	Cosmic dose rate (Gy/ka)	Total dose rate (Gy/ka)	Water content (%)	Equivalent dose, De (Gy)	Age (ka)
		K (%)	U (ppm)	Th (ppm)						
CHIM 7	460	0.82	1.89	4.4	1.5	0.104	1.77	15	22.07	12.5 ± 1.1
CHIM 6	404	0.83	1.89	4.5	1.5	0.180	1.77	15	24.45	13.8 ±1.2
CHIM 5	360	0.85	1.81	4.4	1.75	0.154	1.76	15	28.97	16.5 ±1.5
CHIM 4	270	0.82	1.69	4.5	2	0.163	1.70	15	31.74	18.6 ±1.7
CHIM 3	172	0.54	1.20	3.1	3	0.104	1.20	15	27.80	23.2 ±2.0
CHIM 2	130	0.46	1.19	2.5	4	0.180	1.06	15	19.27	18.2 ±1.7

Estimates of equivalent doses for each sample were calculated from >12 aliquots (table 8.5). The spread of equivalent doses gained from each aliquot display a unimodal, narrow distribution (figure 8.16). Test behaviour (RR and IR ratios) and narrow distribution of De values generated for each sample indicate that all samples were behaving well and therefore, should provide reliable OSL age estimates.

Calculation of the environmental dose rate assumes closed system behaviour in the uranium and thorium decay chains (Olley *et al.* 1996). However, the presence of a later over printing of gypsum in the sequence indicates a geochemically active environment involving the fluctuation of water and solutes which is thought to be a principle mechanism responsible for disequilibrium (Olley *et al.* 1996). The timing of gypsum overprinting cannot be assessed; it is only possible to say that it is a later feature. As such, the likely introduction of U-series disequilibrium decay and the absorption of radiation by the presence of gypsum cannot be accounted for (e.g. Nathan and Mauz). Consequently it is possible that the measured present day dose rate does not truly reflect the dose rate during the entire burial period.

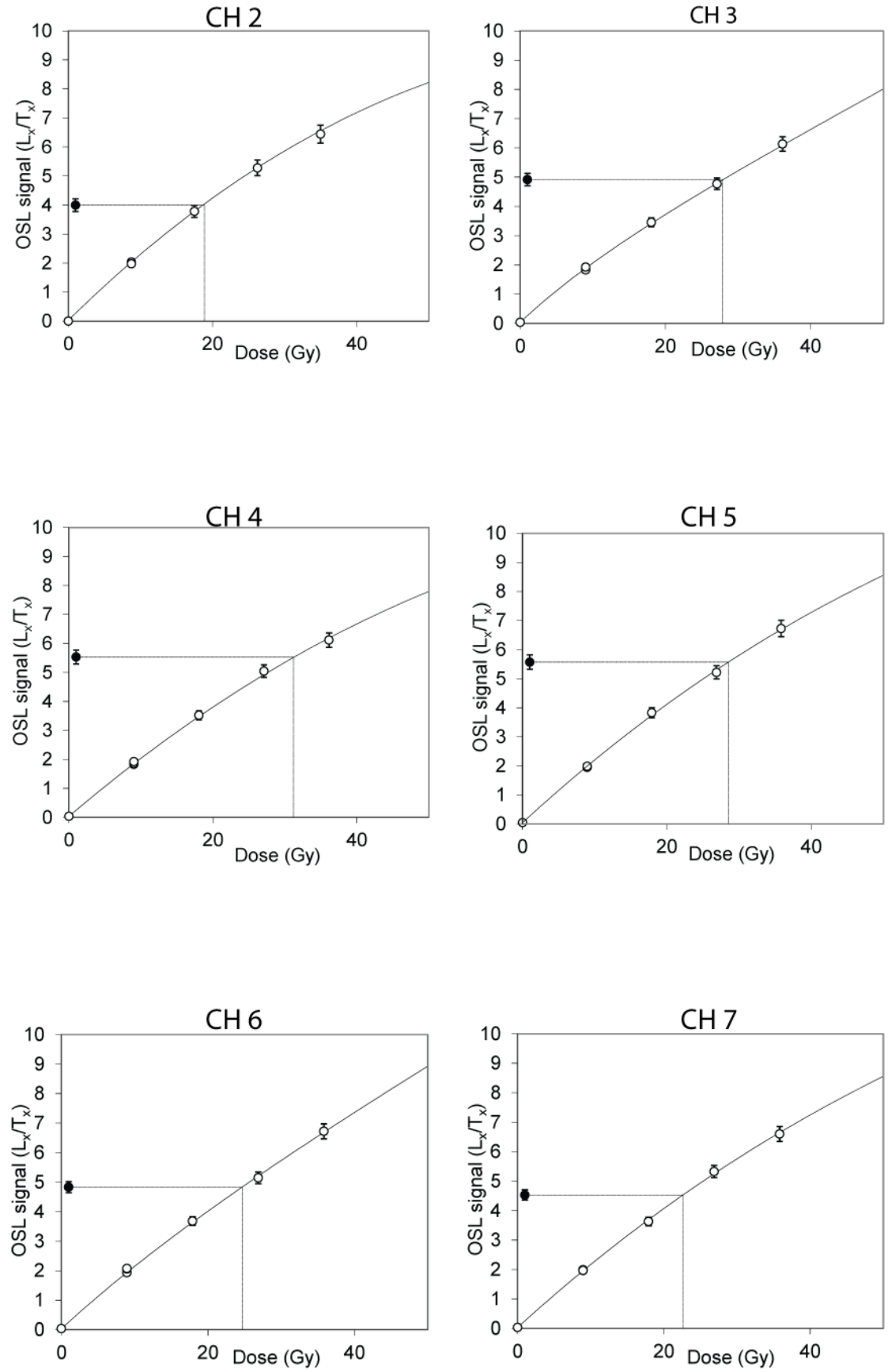

Figure 8.15 Typical growth curves produced from a single aliquot for each OSL sample. Black dot on y-axis indicates natural signal, lines intercepting growth curve indicate equivalent laboratory dose.

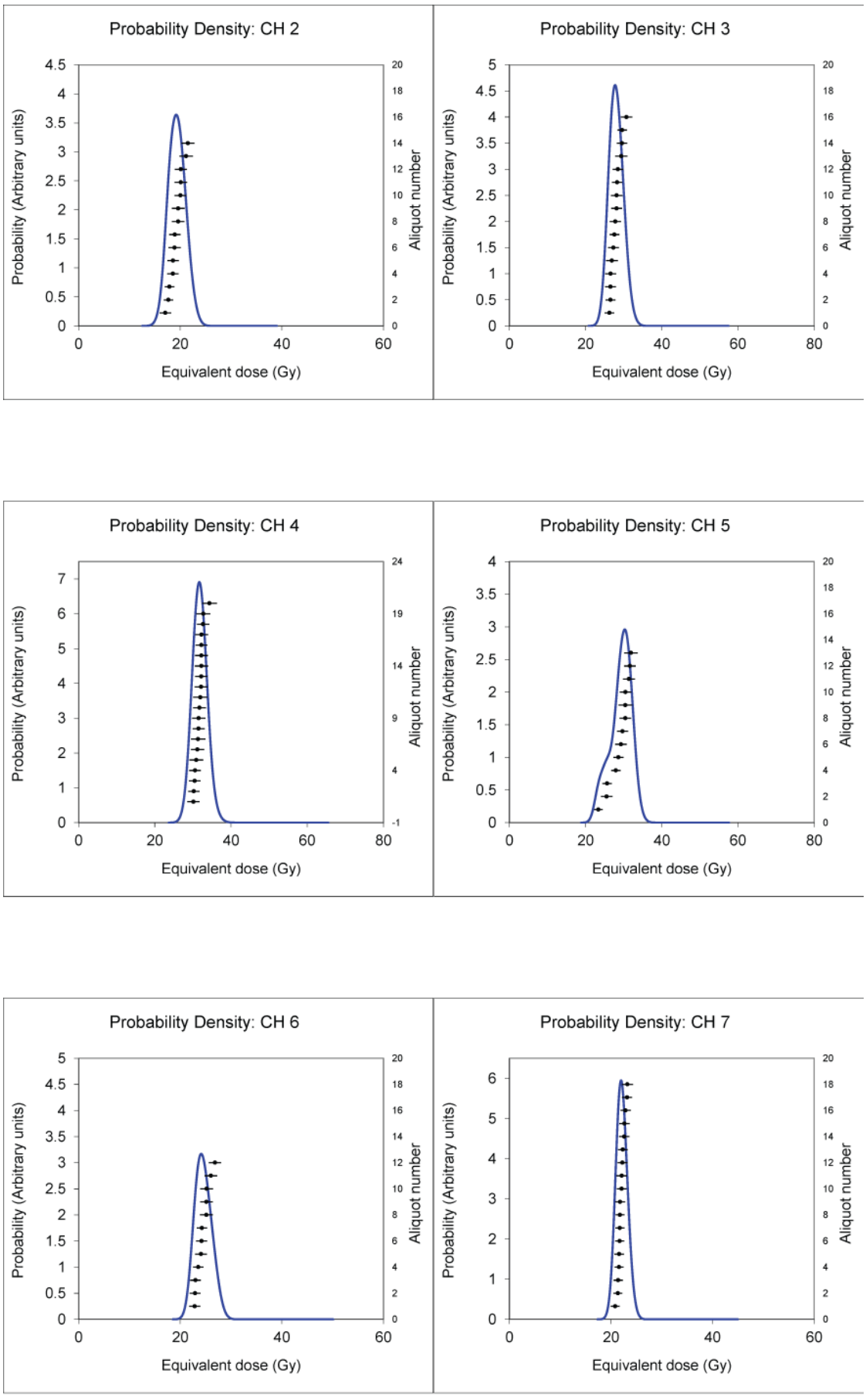

Figure 8.16 *D_e distributions shown as probability density functions, individual D_e values shown with error bars in order of increasing value*

8.8 Pedo-sedimentary depositional models

Stage 1: Only sub-units 1B and 1C were sampled, and therefore, only their formation and alteration is discussed. 1C was identified in the field as a potential soil horizon as a darkened, horizontally continuous feature. Bulk carbonate content indicates that the upper sediments of 1C are partially decalcified. Micromorphological evidence identifies calcitic pedofeatures present throughout, but increasing in abundance beneath the partially decalcified sediments. Evidence from these sediments is consistent with post-depositional pedogenic alteration at a stable land surface, partial decalcification of the upper horizons and accumulation of only small (<1cm) carbonate nodules at depth indicates only a short-lived episode of stability (Kemp 1985b, Kemp 1995, Kemp 1999).

Stage 2: Bulk carbonate content is relative stable through sub-unit 2A indicating no substantial dissolution and movement of carbonate. This is consistent with the distribution of calcitic pedofeatures which increase in abundance upwards through the bed. Interestingly, the pattern of calcitic pedofeature abundance seems to mirror the changes in median grain size, where coarser sediments are associated with fewer pedofeatures and fine sediments associated with increasing abundance. It is often assumed that dust input rates are proportional to grain size; where increased wind power results in accumulation of coarser material at greater rates (Lui and Ding 1993, Xiao *et al.* 1995, Lu *et al.* 1999). Median grain size decreases upwards, associated with increasing occurrence of calcitic pedofeatures indicating that the sediments have been subjected to increasing localised redistribution of carbonate through accretionary pedogenic alteration associated with reduced sediment input. The oxygen isotopic composition of pedogenic carbonates derived from these sediments indicates that this decreasing sediment input was associated with a climatic warming. At the very top of 2A, there is an increase in median grain size associated with a slight decline in abundance of pedogenic calcite, isotopic evidence indicates that this increased sediment accumulation rate occurred within a still warming climate.

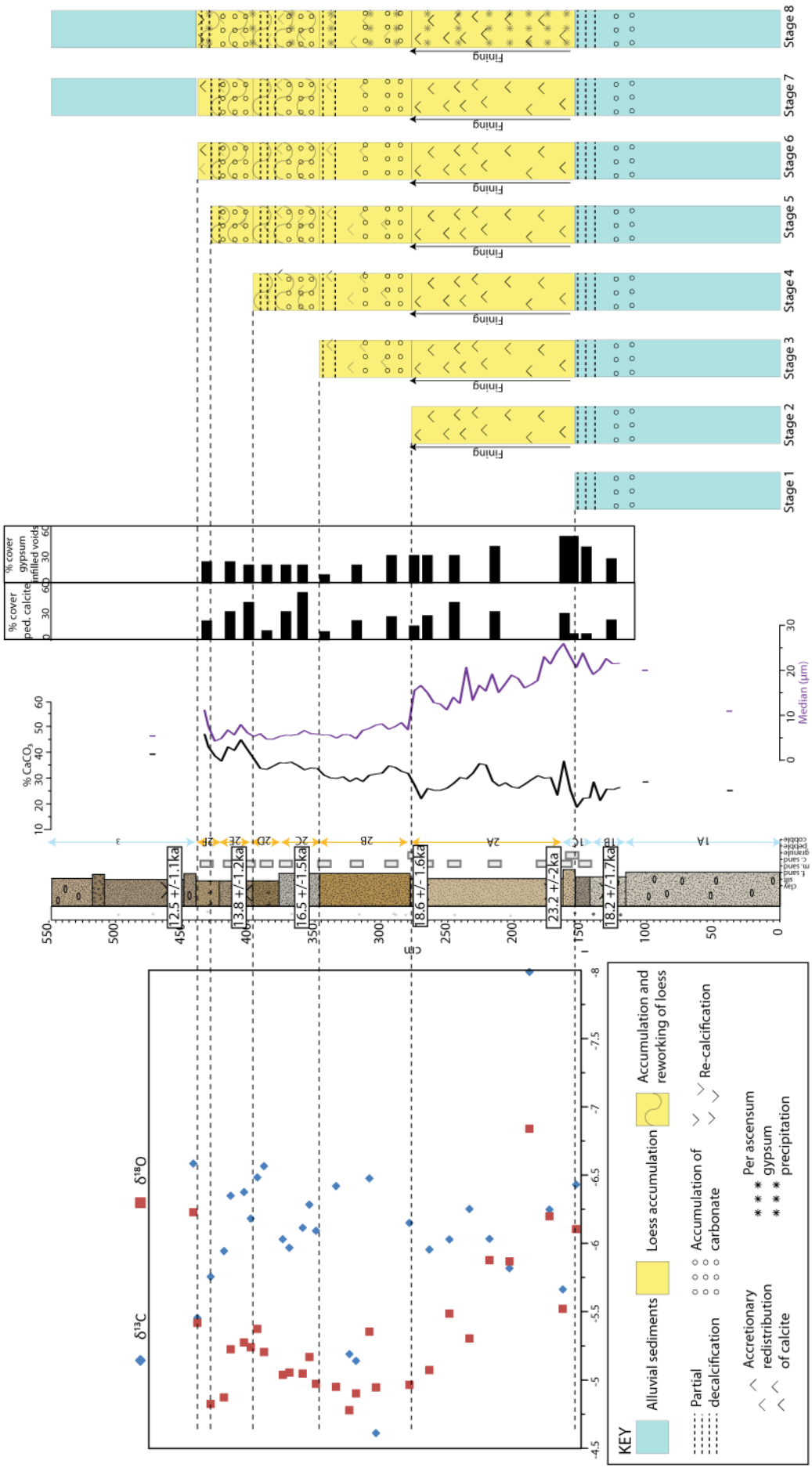

Figure 8.17 Pedosedimentary model of formation of the sediment sequence at Chimeneas

Stage 3: Calcitic pedofeatures occur throughout 2B suggesting that the unit may have undergone accretionary pedogenic alteration during accumulation. There is, however, an increase in the abundance of calcitic features towards the base of the sub-unit, associated with a progressive increase with depth in bulk carbonate content. Such a depth carbonate relationship indicates a degree of carbonate down-washing during stable land-surface conditions, resulting in increasing occurrence of pedogenic carbonates with depth. Pedogenic alteration of the sediments during the short-lived land surface is the dominant period of alteration of the sediments, and therefore the isotopic composition of carbonates formed during this period dominate the values gained through this sub-unit.

Stage 4: Calcitic pedofeatures occur throughout 2C and 2D, again suggesting that the unit may have been subject to some degree of pedogenic alteration during accumulation. However, post-depositional alteration of the sediments has resulted in the partial decalcification of 2D and the accumulation of calcitic pedofeatures at depth (2C). As the majority of soil carbonates are formed in response to the post-depositional alteration episode, the isotopic composition of the carbonates sampled from these sediments will be dominated by carbonates formed during this period.

Stage 5: Sub-units 2E and 2F record the same pattern of alteration recorded through 2C-D.

Stage 6: The very top of 2F records a peak in bulk carbonate content associated with a distinct coarsening. Both features could represent a return to loessic accumulation after the alteration of 2F and 2E below, or these upper sediments could have been recalcified by overlying sediments. It is suggested that as the shift in carbonate content is associated with a definite coarsening of sediments that this represents a return to loessic accumulation, and therefore 2F should be split into two distinct sub-units; with the base representing post-depositional alteration during a stable land-surface and the upper part representing a return to loess accumulation.

The oxygen isotopic composition of the soil carbonates contained within the lower and upper part of 2F reflect the different conditions during the time of their formation. The carbonates within lower 2F formed during a relatively warm climate associated with pedogenic alteration during the existence of a short lived stable land-surface. Whereas the oxygen isotopic composition of soil carbonates from upper 2F appear to record a progressive depletion in $\delta^{18}O$ values, indicating a temperature shift of around -5˚C. This apparent marked temperature decline is associated with increasing grain size of the accumulating sediment, indicating increasing wind power and accumulation rates (Lui and Ding 1993, Xiao *et al.* 1995, Lu *et al.* 1999, King 2000)

Stage 7: Marks the return to the accumulation of fluvial sands and gravels.

Stage 8: Throughout the sediments at Chimeneas micromorphological analysis revealed the extent and distribution of gypsum throughout the sequence. As shown in figure 8.11 and discussed previously, gypsum crystals appear within voids throughout and within the groundmass of the lower sediments. Where growth of interlocking gypsum crystals has occurred within the groundmass and within voids, it appears to have disrupted and broken up existing calcitic pedofeatures. This therefore, identifies that gypsum growth is a later overprinting feature associated with the movement of Ca^{2+} and SO^{2-}_{4} enriched water. The distribution of gypsum appears similar to that suggested to occur via a *per ascensum* mode of formation (Candy and Black 2009), where groundwater is drawn upwards via capillary rise (Goudie 1983), likely to occur within the existing void network.

8.9 Palaeoenvironmental significance

The sequence at Chimeneas represents the first independently dated last glacial loess-palaeosol sequence in southern Spain. Mineralogy and geochemistry indicates that, at Chimeneas, last glacial loess was derived from local sediment sources (chapter 6). Despite evidence for local reworking of loess material, the accumulation of a thick, locally derived loessic sediment sequence indicates that during accumulation the surrounding area was significantly different to present. The fluvial sediment sequence at the base of Chimeneas ceased accumulating prior to 18.2 ka ±1.7, providing a stable land surface upon which loess accumulation could occur.

The sediment sequence at Chimeneas records alternating stages of loess accumulation and pedogenic alteration. Episodes of loess accumulation require the aeolian mobilisation and transport of large amounts of fine grained sediments originating from the area local to Chimeneas. Such a mobilisation would require a reduced vegetation cover in order that sediments were not prevented from being eroded by winds. Within the Mediterranean, it is suggested that vegetation type and cover is predominantly controlled by the volume of effective precipitation (e.g. Tzedakis 2003). Records of Mediterranean vegetation indicate a reduced vegetation cover through the last glacial, with steppic vegetation dominating (Sánchez Goñi *et al.* 2008). It is unclear however, if this reduced vegetation cover is the result of an overall decrease in precipitation or increased seasonality limiting the growing season (Prentice *et al.*1992). The occurrence of multiple short-lived soil horizons within the sequence at Chimeneas indicates regular reductions or cessations in loess accumulation, linked to a reduction in wind energy and/or increased sediment stability due to an increase in vegetation cover.

Micromorphological analysis of the sequence has enabled the origin of the isotopic composition of soil carbonates to be assigned to different periods and different styles of pedogenic alteration.

Oxygen isotopes through the lowest loess unit record a significant climatic amelioration ($\delta^{18}O$ enrichment of 1.88‰) during accumulation of ~6˚C associated with increasing modification through accretionary pedogenesis. Isotopic composition of the soil carbonates above this horizon (up to mid 2F) relate to two separate periods of post-depositional alteration, with $\delta^{18}O$ values indicating climatic conditions similar to those reached at the peak of the climatic amelioration recorded in the lower loess unit. At the very top of the sequence (upper 2F), it is suggested that there is a return to loessic accumulation subject to accretionary pedogenic alteration. The oxygen isotopic composition of soil carbonates formed within this small sediment horizon indicates a significant temperature drop in the region of -5˚C ($\delta^{18}O$ depletion of 1.41‰).

The lack of covariance between carbon and oxygen isotope values recorded within the soil carbonates at Chimeneas is in itself significant. It has been suggested previously (Candy *et al.* 2012) that aridity is the main factor controlling the composition of soil carbonates within the Mediterranean, and as such a strong covariance between $\delta^{13}C$ and $\delta^{18}O$ should be evident. Despite elevated $\delta^{13}C$ values from Chimeneas suggesting an increased atmospheric input to the soil environment linked to low vegetation cover (Quade *et al.* 1989a), the $\delta^{18}O$ values do not indicate that the reduced vegetation cover was associated with strong evaporation of soil moisture during the formation of the carbonates. As discussed previously (chapter 2), there is strong evidence for enhanced aridity during the last glacial, so it is somewhat surprising that in a region where relatively humid periods (interglacials) produce soil carbonates whose isotopic composition is driven by aridity (Candy *et al.* 2012), the soil carbonates of the last glacial at Chimeneas are not.

Candy *et al.* (2012) found significant covariance between $\delta^{13}C$ and $\delta^{18}O$ values of meteorological carbonates formed during the last glacial within both the Sorbas and Carboneras basins, located ~160 km east of Chimeneas. Despite being relatively close geographically, there are significant differences which may explain the differences in the controls on the isotopic composition of soil carbonates from the two areas. Chimeneas is situated at an elevation of ~800 m.a.s.l whereas the Sorbas and Carboneras basins are much closer to sea level (~400 and ~100 m.a.s.l respectively). This difference in elevation results in a variation in the climate of the two regions, in terms of precipitation amount and temperature; total precipitation 361 mm, 15.2 °C average temperature at Chimeneas, and 196 mm total precipitation and an average temperature of 18.7 °C for the region around Sorbas and Carboneras (data from Agencia Estatal de Meteorologia for nearest weather stations; Granada and Almeria respectively).

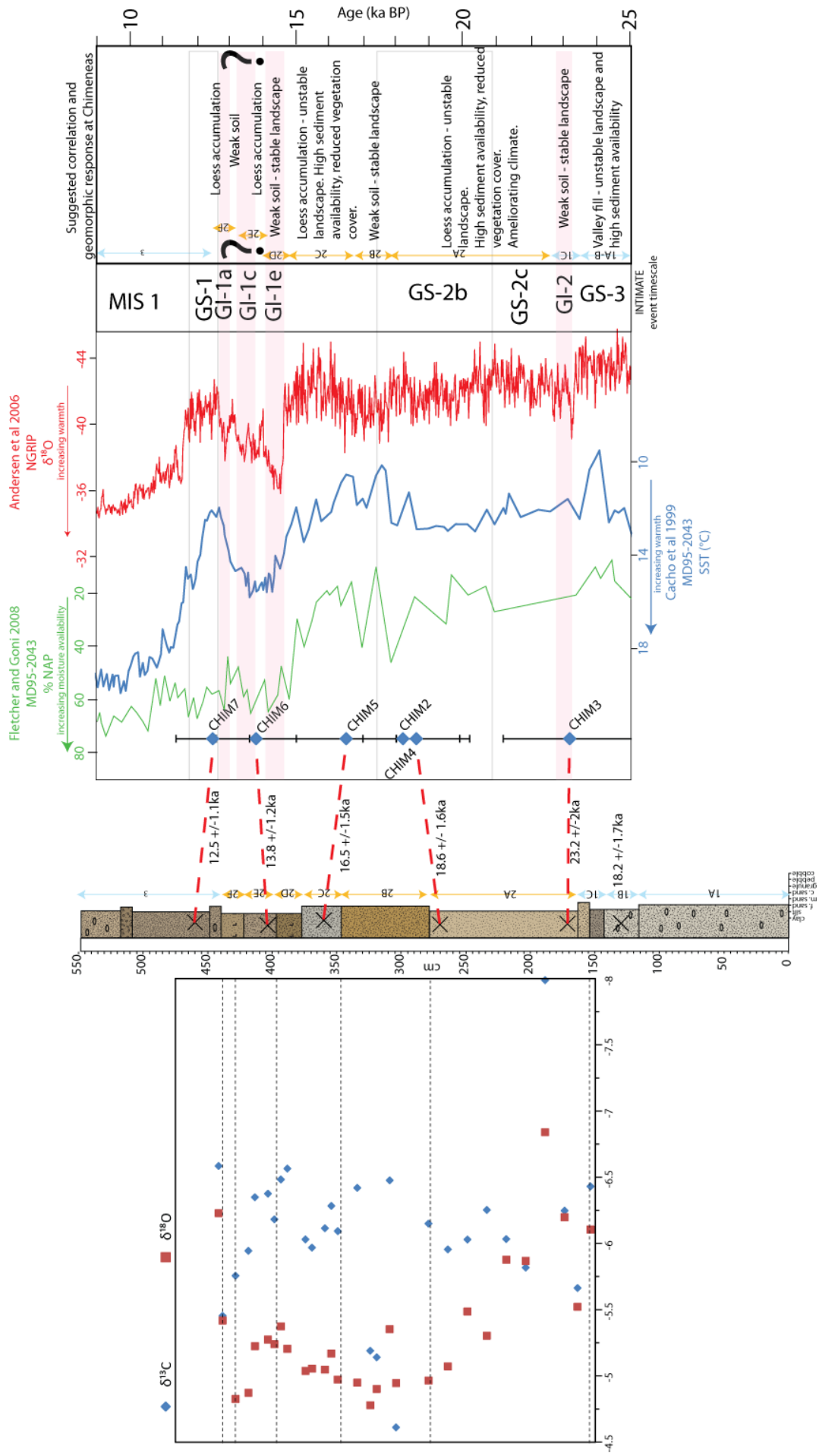

Figure 8.18 Comparison of Chimeneas sediment and isotope record with regional vegetation and sea surface temperature records (MD95-2043) and $\delta^{18}O$ values from Greenland

The last glacial is thought to be a more arid, cooler period within southern Spain (e.g. Sánchez Goñi *et al.* 2008, Fletcher and Sánchez Goñi 2008). The evidence for increased environmental aridity does not reveal whether the period is subject to an overall decline in annual precipitation, or a reduction in the length of the wet period resulting in reduced effective moisture availability (Prentice *et al.* 1992, Allen *et al.* 1999, Tzedakis 2003). Soil carbonates in regions where a winter rainfall regime exist usually form at the end of the wet period where soils began to dry out encouraging the precipitation of carbonate (e.g. Breecker *et al.* 2009). If, during the last glacial, there was a reduction in the length of the winter rainfall period, then it is likely that soil carbonates would be forming earlier in the year during colder months. If the modern day difference between temperatures at Chimeneas and Sorbas/Carboneras remained, or was exaggerated during the last glacial, then soil carbonates at Chimeneas would be forming at lower temperatures, and therefore, within soils experiencing lower rates of evaporation than those of the warmer, coastal basins.

The dating of the sequence suggests a remarkable similarity in the timing of climate changes recorded at Chimeneas and those seen within the proxy records of MD95-2043 and Greenland (figure 8.18). The correlations indicated in figure 8.18 are suggested on the basis of geomorphological interpretation of the sediment sequence; where loess accumulation occurs under reduced vegetation conditions associated with cooler, arid periods and soil formation occurs during relatively humid episodes under increased vegetation cover, these correlations are broadly supported by the OSL chronology produced for the sequence.

The vegetation variations witnessed through the region during the last glacial are predominantly discussed in terms of shifts in aridity, with water availability being the dominant control on the region's vegetation (Tzedakis 2003). However, the record at Chimeneas indicates that vegetational shifts were also associated with large temperature changes. This is evident through sub-unit 2A, where the isotopic composition of soil carbonates appears to reflect the climatic amelioration associated with increasing Greenland air temperatures and Iberian forest cover through Greenland Stadial 2, approaching the Greenland Interstadial 1 complex.

The increasing dominance of pedogenic alteration upwards through the sequence recorded through both the bulk sedimentology and micromorphological analysis of the sediments is thought to reflect the warm, moist, forested conditions coincident with the timing of the Greenland Interstadial 1 complex. At the very top of the loess-palaeosol sequence at Chimeneas, there is a marked oxygen isotopic depletion in soil carbonate values, it is suggested that this may relate to the climatic cooling at the onset of Greenland stadial 1 (Younger Dryas).

Chapter 9 – Maro

This chapter outlines the geological and geomorphological setting of the valley containing the Maro sediment exposures. Firstly, an introduction to the local geological setting of the site will be presented. This will be followed by a plan schematic of the valley, indicating the three sediment exposure locations. A brief overview of the sediments contained within section 3 will be presented with an interpretation of the sequence. The remainder of the chapter will discuss the work undertaken at sections 1 and 2. The results of the work undertaken at the two sections will be discussed and pedo-sedimentary models of the formation of the sediment sequences contained within sections 1 and 2 will be presented. Finally, the palaeoenvironmental significance of the sediment sequences presented will be discussed.

9.1 Site introduction

9.1.1 Location

Figure 9.1 shows the location of the site. The sediment sections are located ~53km east of Malaga, 2.5km east of the village of Maro. The site is located within a steep sided, north-south orientated valley where the Rio de la Miel joins the Mediterranean Sea. Located within the valley are three sediment exposures all studied; all were described and logged and each exposure was sampled for OSL dating. Only the sections containing a significant silt deposit (section 1 and 2) were studied in detail for sedimentology, micromorphology and stable isotopes (figure 9.1).

9.1.2 Geological setting

The sequences at Maro are located within the steep sided valley of Rio de la Miel. The landscape of the region is dominated by large-scale topographic features formed during the tectonic evolution of the Betic Cordillera. The Betic Cordillera is divided into Internal and External zones; with divisions based primarily upon composition and origin (Sanz de Galdeano and Andreo 1995). Maro is located within the Herradura units of the Alpujaride tectonic complex (Azañón *et al.* 1998) which forms part of the Internal zone. The sediment exposures at Maro are located close to the mouth of the Rio de la Miel, which flows into the Mediterranean Sea. The upper reaches of the river flow through predominantly marble bedrock, with a transition to schist bedrock occurring just prior to the location of the sediment exposures in the valley (figure 9.2). The Rio de la Miel is a perennial stream fed by spring located directly upstream at the study area (figure 9.1b).

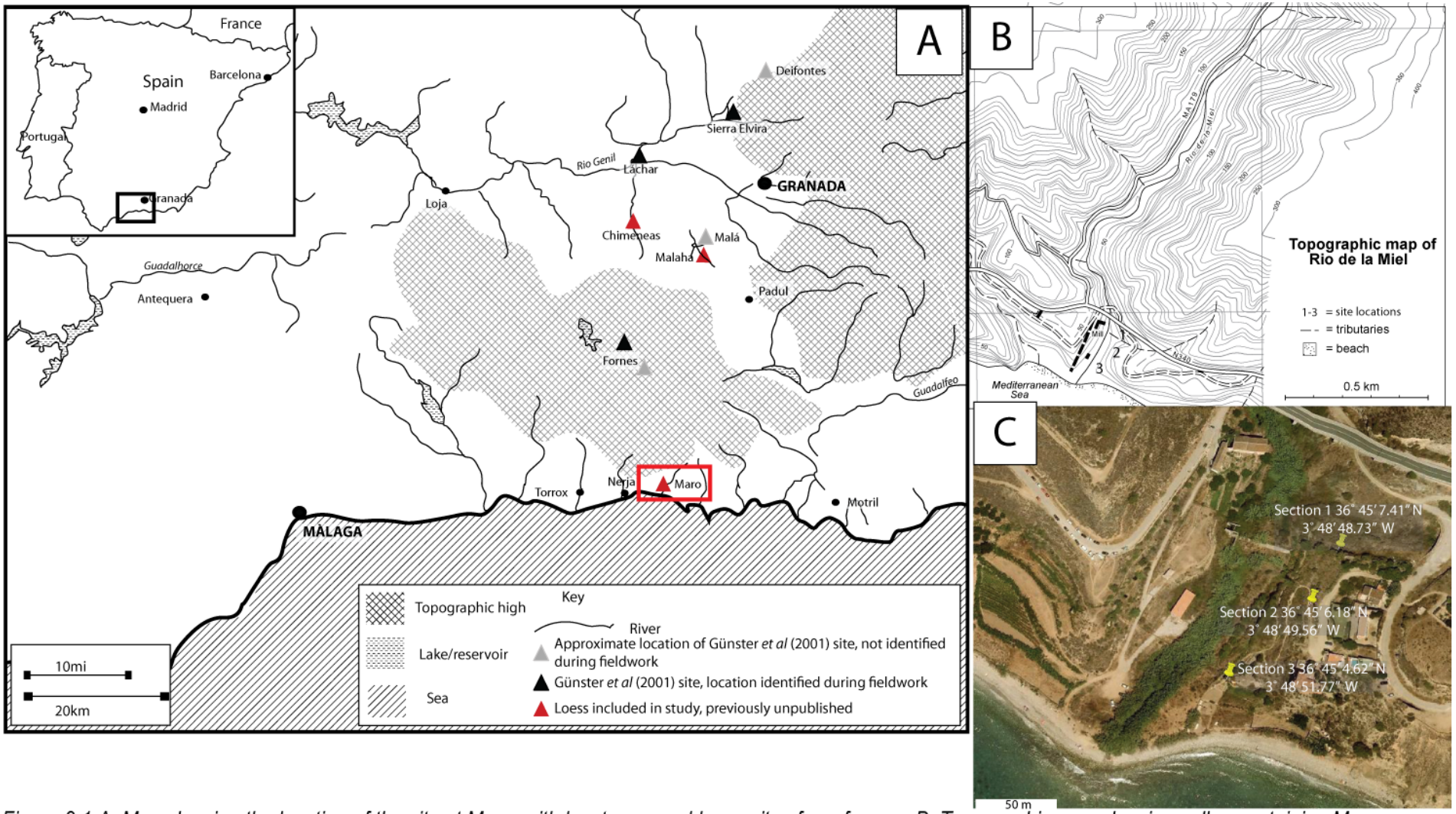

Figure 9.1 A. Map showing the location of the site at Maro, with key towns and loess sites for reference.B. Topographic map showing valley containing Maro sequences C. Satellite image of the Rio de la Miel valley (from Google Earth)indicating the locations of the three Maro sequences.

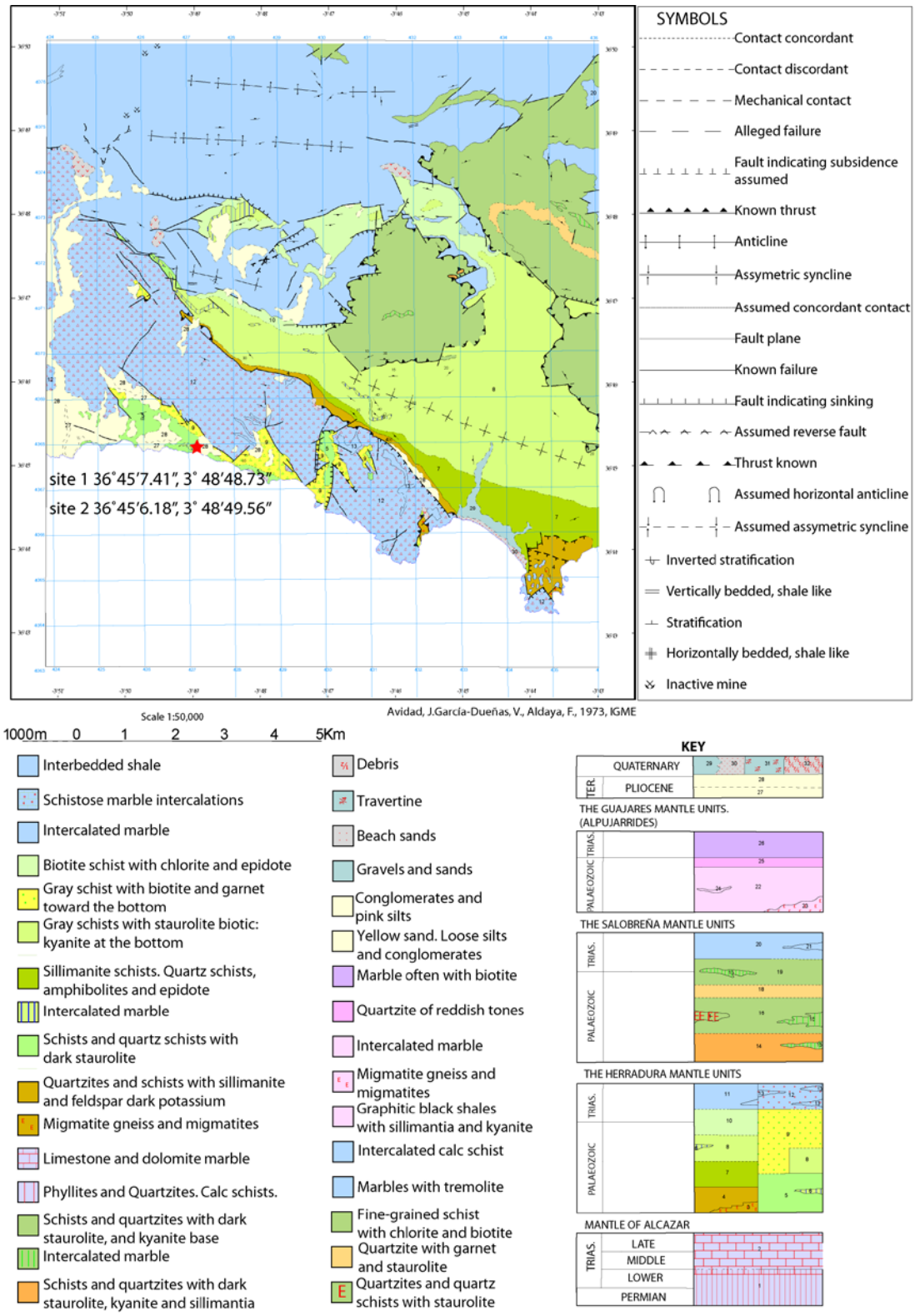

Figure 9.2 Geological map of the region around Maro. Adapted from the geological map of Martin et al. (1977).

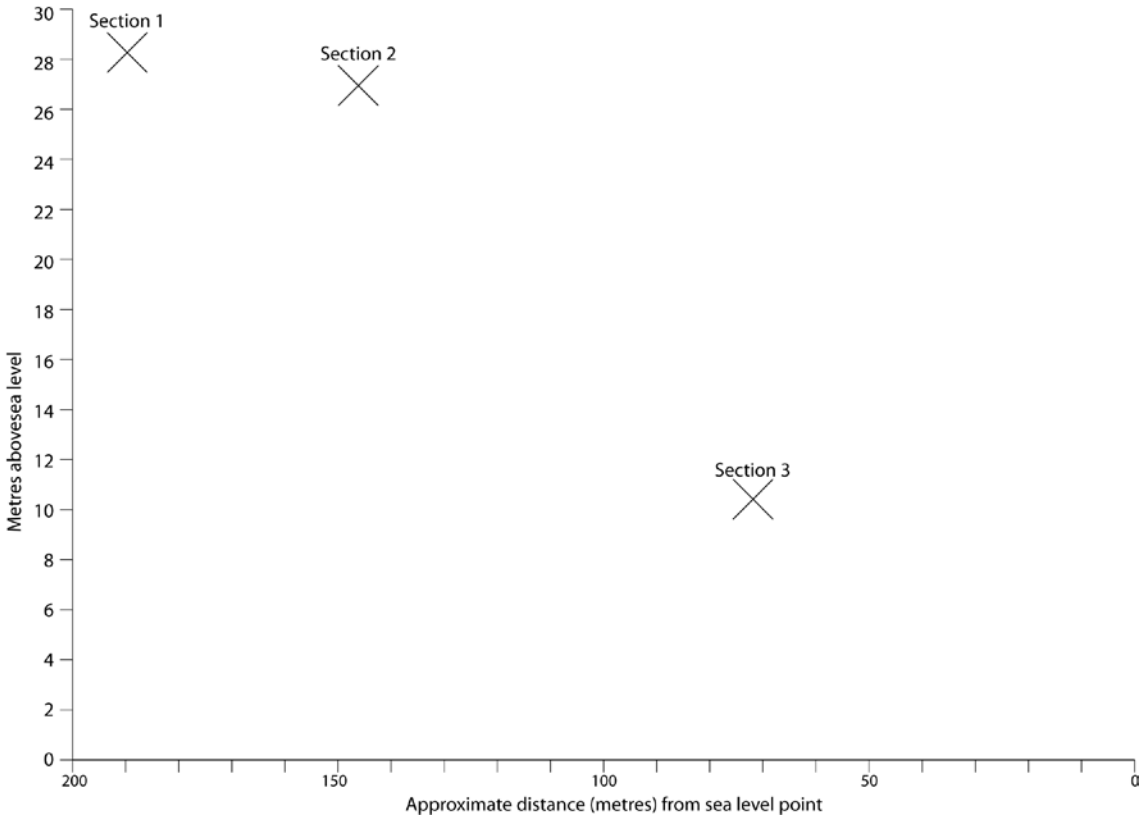

Figure 9.3 Schematic showing height above sea level of sections 1-3, indicating approximate distance from 0m levelling point.

Due to the complex tectonics of the region, rates of uplift vary greatly along the southern coast of Spain (Zazo *et al.* 1999). Based on the dating (U-series) of sea levels relating to the MIS 5e high stands, Zazo *et al.* (1999) have provided a summary of high stand positions along the southern coast. The sites at Maro are located within 'zone G' of the Zazo *et al.* (1999) study, where the uplift history of the section is interpolated from only one high stand record. The raised shoreline within zone G is located at 1.5m above modern sea level. Zazo *et al.* (1999) have assumed a +6m MIS 5e sea level (Chappell and Shackleton 1986), which implies that this coastal section has subsided ~4.5 m since MIS 5e. If the one site included within the study by Zazo *et al.* (1999) is truly representative of the stretch of coastline in question and estimates of MIS 5e sea levels are reasonable; it follows that the coastline around Maro is subsiding at a rate of ~0.36 mm/year assuming constant rates. Therefore at Maro, it is possible that over the last 125 ka sea level was up to 4.5 m higher than at present.

9.2 Section 3 results

Currently within the Rio de la Miel valley there is a tufa actively forming around a spring line (figure 9.4). The tufa can be classified as a cascade tufa according to Pedley (1990). On the opposite side of the valley is an exposure located at 10.15 m above sea level (figure 9.3), which due to the presence of cemented stem structures appeared also to be tufaceous. This section

(section 3) was logged and one OSL sample was taken to establish the depositional process responsible for its accumulation and its age.

Section 3 is located above the Holocene terrace of the Rio de la Miel system, but below sections 1 and 2 (figure 9.3). Understanding both the timing and depositional formation of the deposit may help further understanding of the Quaternary landscape of the valley.

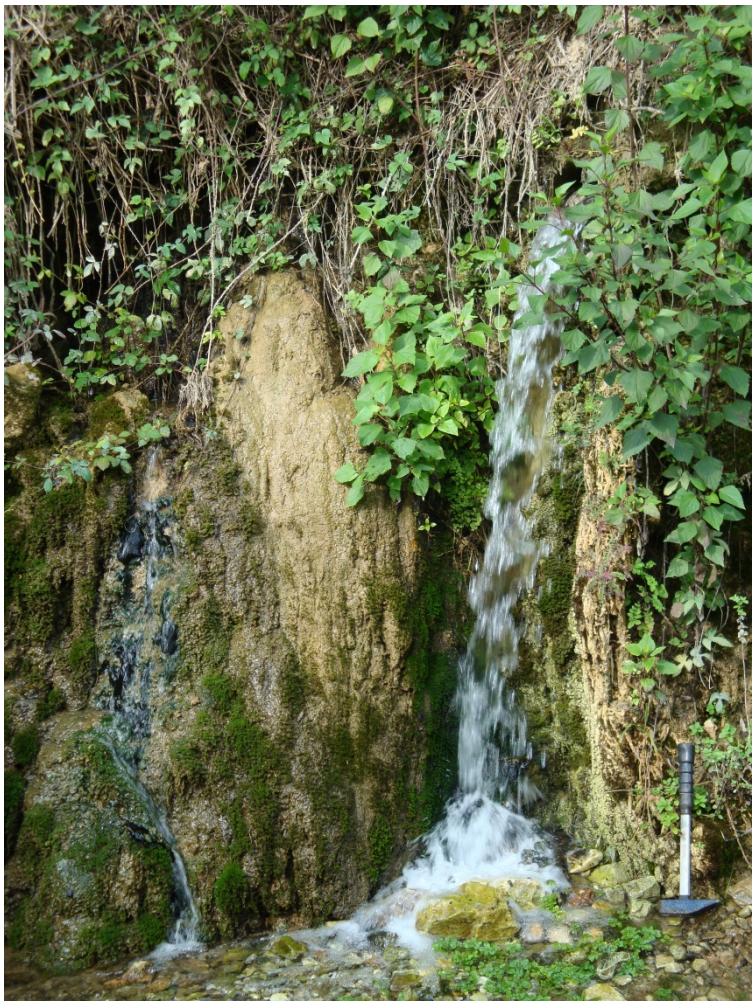

Figure 9.4 Photograph of active tufa formation from around springlines and contained drainage pipes. Photograph taken by author, geological hammer ~30 cm.

9.2.1 Section 3 Field logging

Two sediment logs were constructed for section 3 (figure 9.5); log 1 on the western face and log 2 on the southern face (pictured above). These were positioned in order to fully characterise the changes occurring within the deposit. The entire of log 1 and the lowest ~1m of log 2 (figure 9.6) were comprised of a very fine grained material, with subtle colour variations and occasional coarser sediment pockets. Applying HCl to the sediment within the field indicated a high

carbonate content throughout the two logs. The upper part of log 2 was comprised of a darker coloured material in which it was possible to identify laminated calcified stem structures.

Figure 9.5 Photograph (taken by author) of cemented outcrop. Log 2 is located on the south face pictured; Log 1 is located on the west face.

9.2.2 Section 3 sampling

Detailed laboratory analysis of the sediments was not undertaken as sections 1 and 2 are the focus of work within the valley. However, one OSL sample was taken from log 1 in order to constrain the timing of the formation of the deposit (figure 9.6).

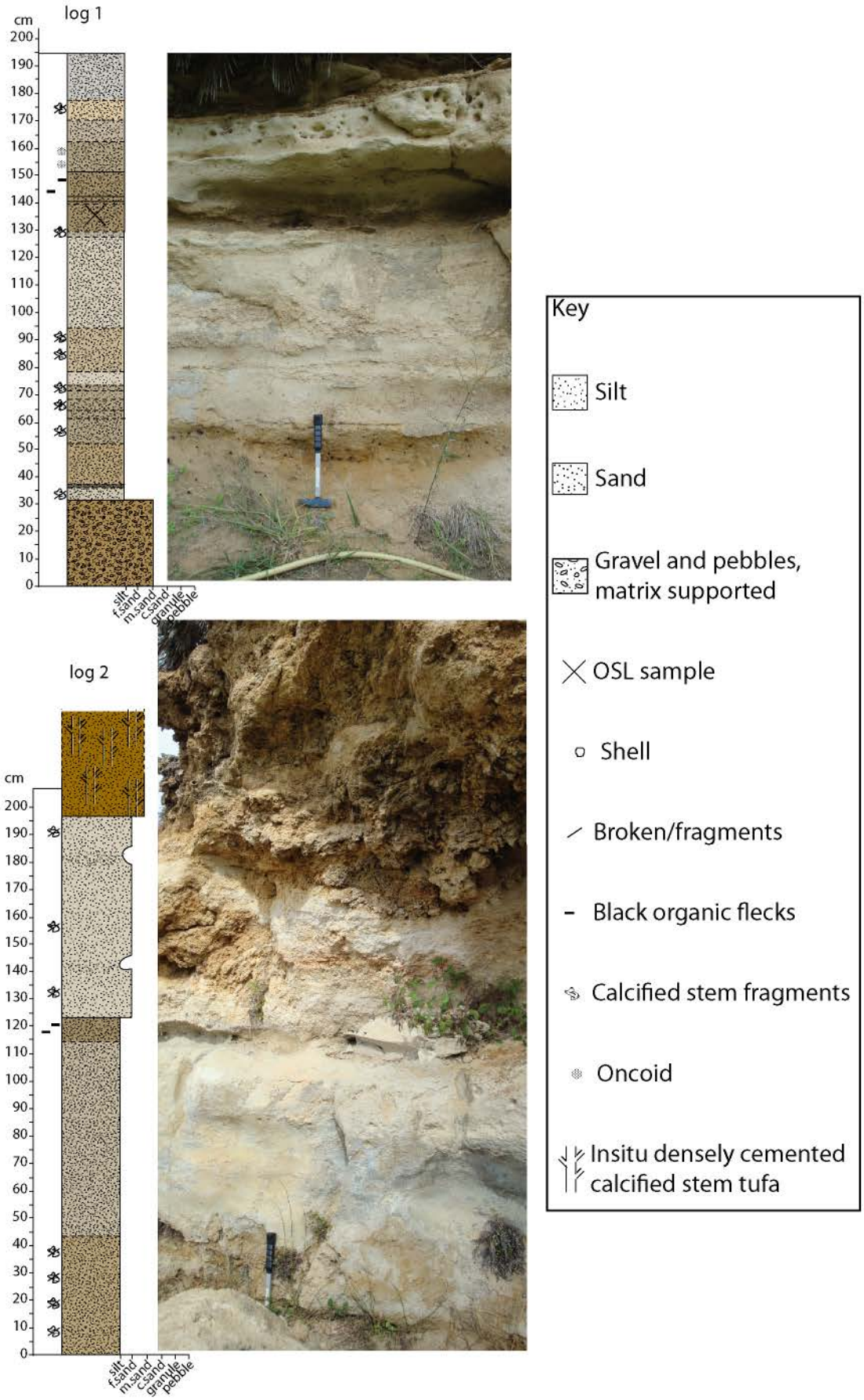

Figure 9.6 Field logging of section 3 at Maro. Photographs taken by author, geological hammer for scale ~30 cm.

9.2.3 Section 3 interpretation

Based upon the apparent composition of the unit, the cemented structures present and the apparently very high carbonate content the exposure is described as tufaceous. The lower part of the exposure which is comprised of very fine material appears to fit with Pedley's (1990) description of microdetrital tufa which forms through the precipitation of calcite in still water environments such as lakes and ponded areas. The mechanisms for this type of precipitation are thought to relate to photosynthetic processes of algaea (Pedley 1990). The material occurring towards the top of unit 2 can be classified as a phytoclastic tufa, where there has been significant carbonate deposition around roots and stems (Pedley 1990). The structure of the tufa deposit indicates deposition within a paludal or braided system (Pedley 1990). The transition from microdetrital deposition to calcified stems indicates deposition occurring within a shallow ponded area which becomes increasingly shallow and infilled by vegetation resulting in the deposition of phytoclastic tufa.

9.3 Section 1

Figure 9.7 Photograph (taken from Google street view) of section 1 within the valley. The section consists of the buff coloured sediments facing the camera, behind the post to the left of centre

This section is located at ~28m above sea level, with the sediment exposure orientated perpendicular to the modern river channel. Due to the heavily vegetated valley sides it is not possible to assess how the sedimentary exposure fits in with other valley sediments.

9.3.1 Section 1 Field descriptions

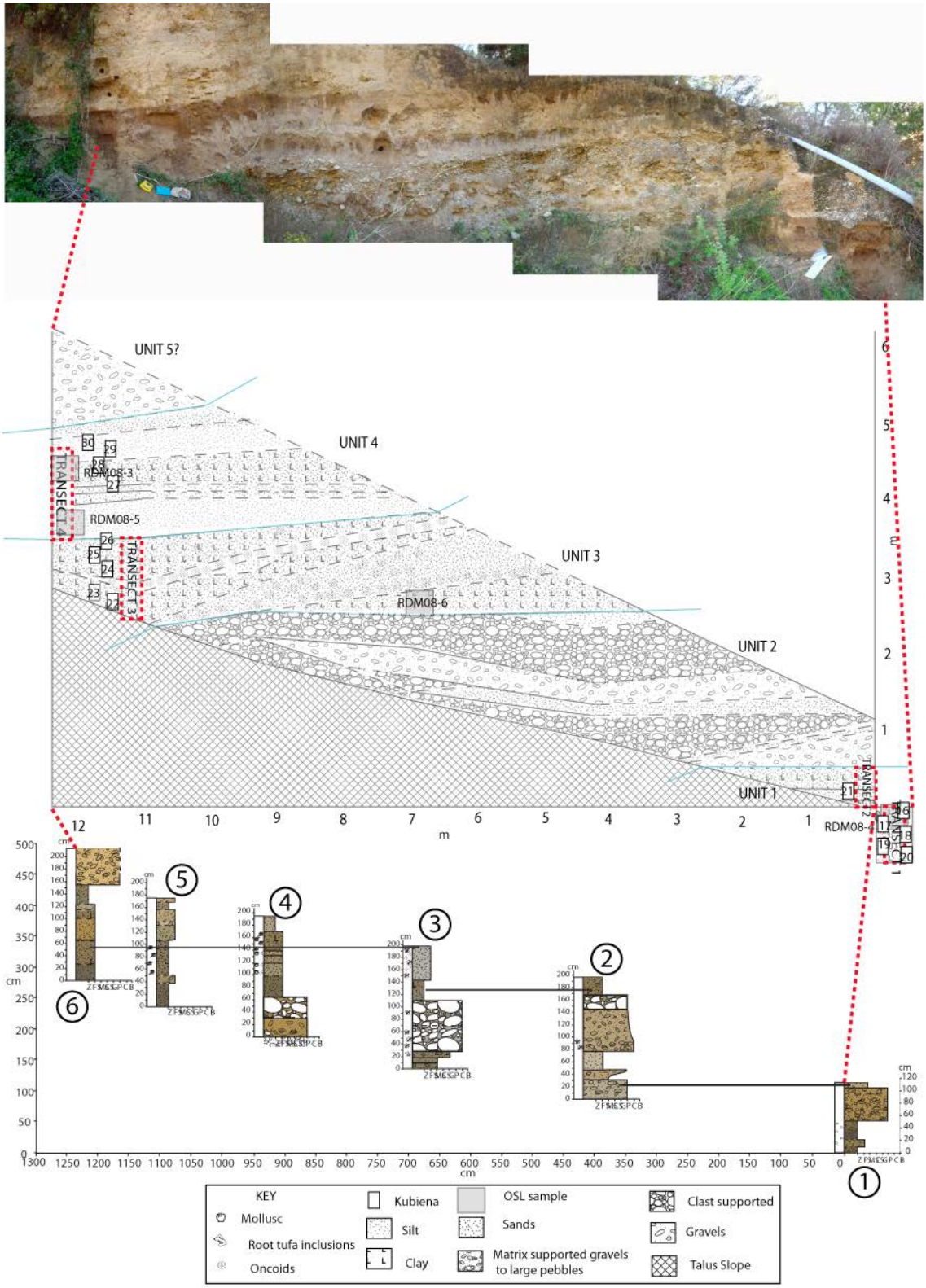

Figure 9.8 Photograph of section 1, with section schematic showing unit division, and sediment logs. Black lines between sediment logs indicates levelling tie points. Sampling locations are indicated on the section schematic.

Logs 1 and 2. A predominantly fine grained bed, comprised primarily of clayey silts, containing varying quantities of fine sand. Within the unit, there are very occasional fine granule sized clasts present. Changes in textureare marked by subtle changes in sediment colour (figure 9.9). Towards the top of the unit (0-42 cm) a few small (<1 cm), soft carbonate nodules are present.

Logs 2, 3 and 4. Unit 2 is distinct from unit 1 due to the coarser texture of the sediments. The unit is comprised of beds of clast rich and matrix dominant sediments. Within the unit are frequent, discontinuous, very well sorted sand beds.The matrix supported beds vary from granule to pebble sized clasts within a coarse sand matrix, up to clast supported cobble units. In places, the clast supported cobble beds contain cobble sized fragments of tufaceous material. Additionally, the clast bearing beds contain some imbricated clasts and evidence of grading

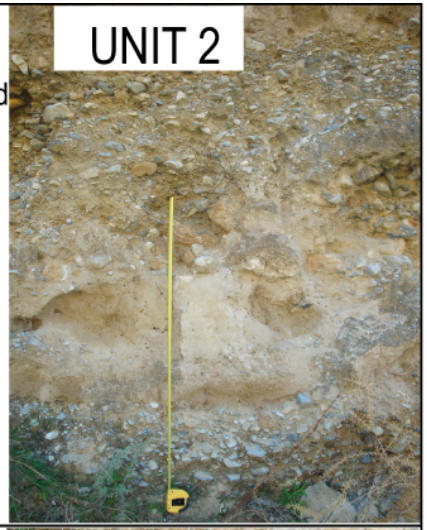

Logs 3, 4, 5 and 6. Unit 3 is comprised of clayey, sandy, silt with the textural components varying subtly throughout the unit. Towards the base of the unit (38-51 cm log 5), the sediment grades into a clast supported bed. This bed contains pebble sized carbonate coated shells, clasts and detritus. This horizon fines upwards, returning to clayey, sandy silt. However, unlike the base of the unit,the material above the clast supported bed contains occasional carbonate coated, pebble sized material.

Logs 5 and 6. This unit is marked by a shift towards buff coloured sediments. Texturally, the unit is similar to unit 3 being comprised of silty sand. However, it appears to have a lower clay content, contains no gravel sized material and is more cohesive in nature. Although initially appearing massive there are subtle changes in both colour and texture present through the unit (figure 9.9). There are occasional increases in sand content and a band of slightly darkened, fine grained sediments occurring roughly half way up the unit and a more subtle darkened horizon towards the top of the unit.

Figure 9.9 Unit descriptions for the sediments of section 1. Photographs (taken by author) of each unit accompany descriptions, trowel or 1m of tape included for scale.

Initial field observations enabled the division of the sediments within section 1 to be divided into units on the basis of distinct shifts in sediment composition. Unit divisions were assigned on the basis of definite, sustained shifts in texture and/or colour; within section 1 4 units were identified (figure 9.8). The section was logged extensively with logs levelled relative to each other in order that all major sedimentological changes within the section were included. As the main units within the section are horizontally continuous, logs were placed through sediments characteristic of the unit as a whole, but were not aimed at recording all intra-unit sediment variability.

As shown in figure 9.8, the base of the section 1 occurs at unit 1, where slope material and vegetation prevented further excavation. Topping the sequence, above unit 4, is a gravel bed (figures 9.8, 9.19).These sediments were too high to be accessible and so were not included within the study.

Sediment sampling was based upon the construction of a composite sediment log (figure 9.10) that would include the four unit divisions of section 1 and typical intra-unit variation. Sampling locations can be seen in the schematic diagram of figures 9.8, 9.11.

9.3.2 Interpretation of field observations – section 1

Field description of unit 1 identifies it as a poor to moderately sorted unit consisting primarily of clay to sand sized material, with very rare occasional fine gravel in places. The unit is unconsolidated, but relatively cohesive due to the apparently high clay content. The unit is lacking bedding structures. There are however clear colour changes identified within the field which in places correspond to a subtle shift in texture. The sorting of the unit indicates rapid deposition and appears similar in composition to the massive alluvial fines model suggested by Miall (1992). However, the dark, slightly-reddened colouration of the unit, clay rich nature of the sediments and presence of small (<1 cm), soft carbonate nodules may suggest that the unit has undergone pedogenic alteration.

Unit 2 is identified as a well sorted deposit of interbedded clast supported and clast rich beds with sand lenses. The clasts contained within unit 2 are typically sub-rounded and consist of predominantly marble, quartzite and schist (although no quantitative analysis was undertaken in this study), a composition reflective of the surrounding geology (figure 9.2). This unit appears typical of sediments described by Miall (1992) as gravel bars and bedform sediments, consisting of stratified and crudely bedded clasts interbedded with sandy bedforms. Changes in grain size within the sediments relate to varying energy relating to stream power or proximity to channelised flow.

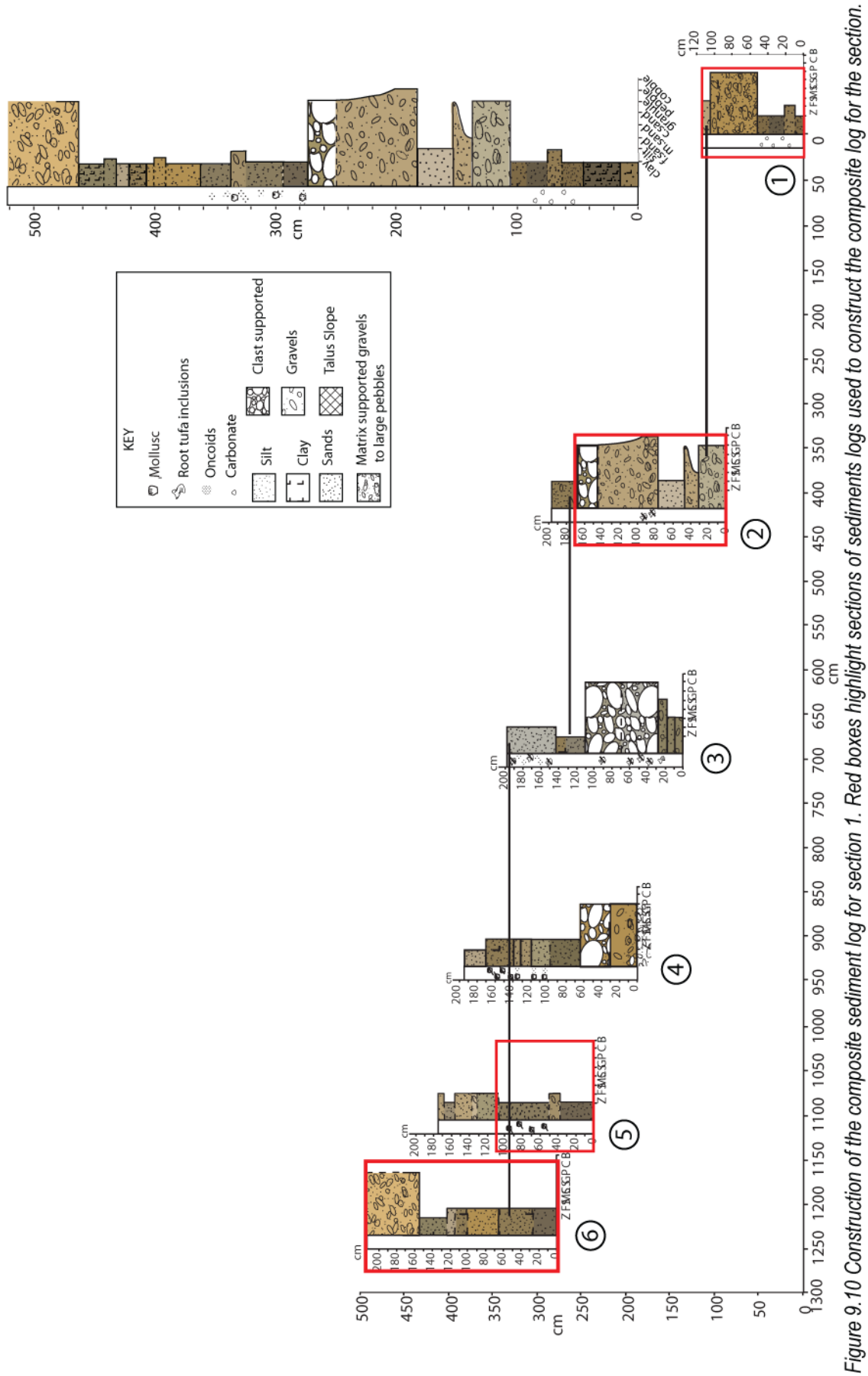

Figure 9.10 Construction of the composite sediment log for section 1. Red boxes highlight sections of sediments logs used to construct the composite log for the section.

Unit 3 is similar in texture to unit 1, but distinctive due to the presence of two horizons of carbonate coated clasts, shells and stems. These carbonate forms are consistent with the description of oncoids (Pedley 1990) (figure 9.11), a form of tufa which occurs in slow flowing, stable channels (Pedley 1990). On the basis of field descriptions the fine grained sandy, clayey silts are interpreted as being deposited by floodplain processes. The lower oncoid bed, which appears as clast (oncoid) supported at the base is interpreted as being an *in-situ* channel deposit due to the well sorted nature of the deposit. The upper oncoid bed, is matrix (sandy, clayey silt) dominated and as such represents a poorly sorted sediment. This deposit may have been formed during proximal, or higher energy alluvial deposition incorporating previously deposited oncoids or through disruption of the oncoid bed via biological reworking through root growth.

Figure 9.11 Photograph of oncoids removed from unit 3, photograph taken by author.

Unit 4, is identified as a primarily silt deposit containing varying quantities of fine sands and clays. The unit is cohesive in nature and as such, appears to fulfil the requirements outlined in chapter 3 to be identified as a loess or loessic sediment. The unit contains one horizon of well sorted fine sand, indicating a shift to higher energy deposition, potentially via channelized flow, aeolian deposition or slope wash. Within unit 3, it was possible to identify two horizons of slightly darkened sediments (405-412 cm and 440-463 cm) which were highlighted as possible weak soil horizons. The lower horizon appeared more darkened in nature and was a more readily horizontally traceable feature.

9.3.3 Section 1 sampling

The section was sampled for bulk sedimentology using continuous transects, Kubiena tins of undisturbed sediment were taken for micromorphological analysis and blocks removed for OSL dating. Sampling was undertaken at four transects through the sediment in order that each unit could be characterised (figure 9.8, 9.12)

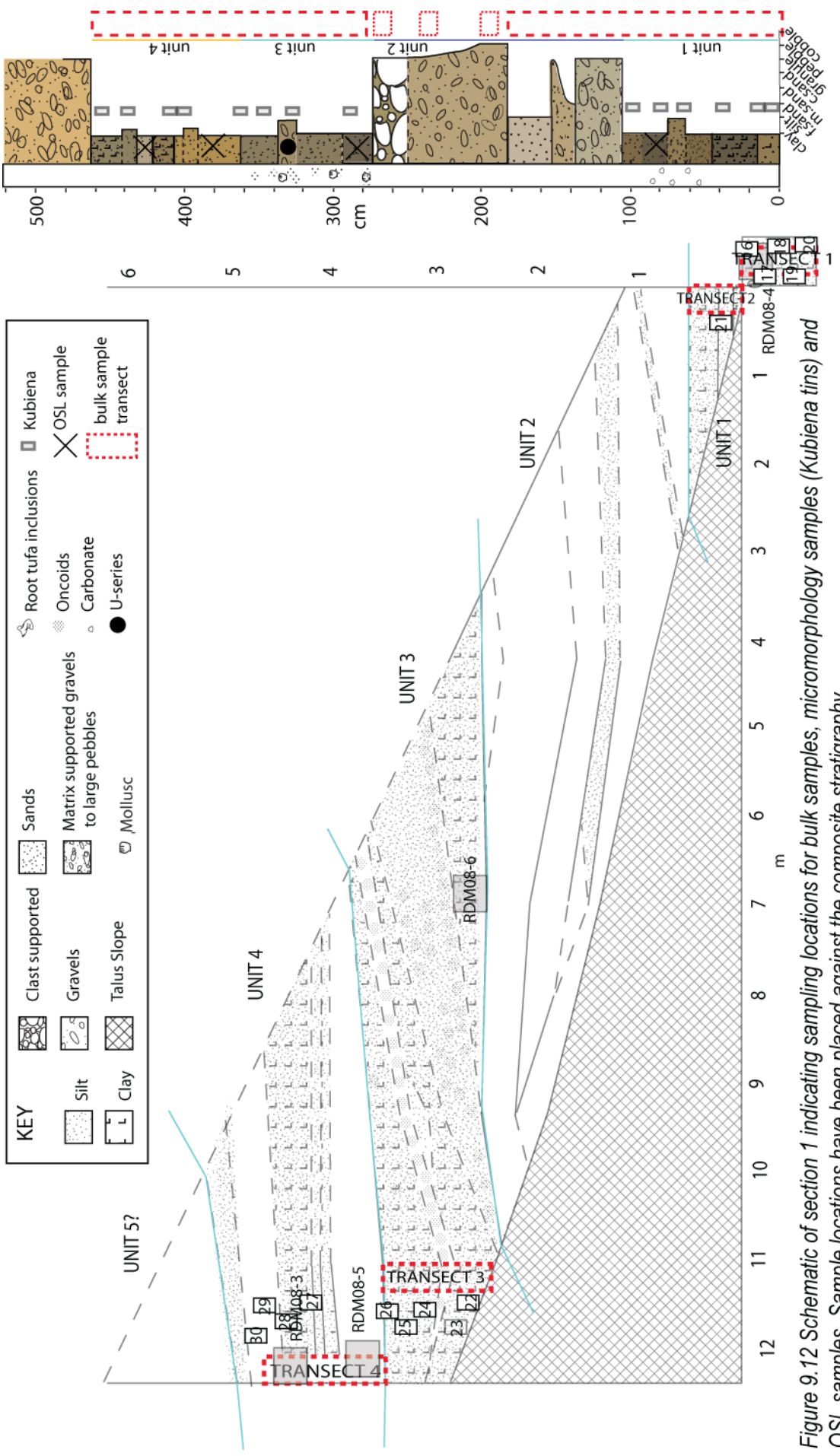

Figure 9.12 Schematic of section 1 indicating sampling locations for bulk samples, micromorphology samples (Kubiena tins) and OSL samples. Sample locations have been placed against the composite stratigraphy.

9.3.3.1 Bulk sampling

Continuous bulk sampling transects were taken through units 1, 3 and 4 (figure 9.13). Each transect was 10 cm wide with each sample being up to 5cm high. Sample heights were modified in line with sedimentological changes noted in the field. Three bulk samples (lower, middle and upper positions) were taken from unit 2 in order to characterise the sediments.

9.3.3.2. Micromorphology sampling

Kubiena tins were used to extract undisturbed sediment samples for micromorphological analysis as described in chapter 5. Fifteen kubiena tins were distributed through units 1, 3 and 4. Kubiena tins were placed in order to characterise intra-unit variability and horizons noted as possible soils.

9.3.3.3 OSL sampling

OSL samples were retrieved using the methods outlined in chapter 5. Four samples were taken from section 1; one from unit 1, one from unit 3 and two from unit 4. Sample locations were selected in order that an age estimate could be established for each unit. The two samples in unit 4 were taken towards the base of the unit, and above sediments identified as the lower possible soil horizon, in order that the age of the unit could be established and to attempt to constrain the timing of the potential soil forming interval. Unit 2 was not sampled directly due to the coarse nature of the unit making sampling difficult and because a minimum and maximum age of the unit could be established from the ages produced from the units above and below.

9.3.3.4 U-series sampling

Within unit 3 were abundant carbonate features identified in the field as oncoids. A selection of oncoids were removed from the lower (clast supported) oncoid bed.

9.3.4 Particle size analysis

All size fraction results are given in % total weight. PSA was undertaken following the methods outlined in chapter 5.

Silt is the dominant particle size throughout unit 1, with the average median grain size of the unit being medium silt (~17 μm). The unit consists of varying quantities of sand, silt and clay and occasionally fine gravels (table 9.1), supporting the interpretation of the unit as a moderately to poorly sorted sediment.

Table 9.1 Summary of PSA results for each unit of section 1. Unit 2 results given as averages refer to one bulk sample only, all other results relate to all bulk samples from continuous transect sampling. Gravel data through unit 3 includes oncoids.

		Unit 1	Unit 2	Unit 3	Unit 4
.Gravel (% weight)	Max	27.30	88.63	15.50	0.00
	Min	0.00	73.60	0.00	0.00
	Avg	2.27	79.13	1.96	0.00
	St dev	6.31	8.27	4.55	0.00
Sand (% weight)	Max	46.49	20.03	39.29	66.37
	Min	12.09	8.22	6.98	16.41
	Avg	24.85	14.36	22.44	39.06
	St dev	9.48	5.92	8.76	11.92
Silt (% weight)	Max	61.71	6.92	56.40	55.25
	Min	34.03	2.12	30.94	24.31
	Avg	50.15	4.57	44.66	41.54
	St dev	8.32	2.40	6.96	7.65
Clay (% weight)	Max	30.24	3.09	42.87	28.34
	Min	14.24	1.03	20.00	9.31
	Avg	22.73	1.94	30.94	19.40
	St dev	3.80	1.06	6.65	4.84
Median (μm)	Max	45.05	17580.39	36.73	95.10
	Min	9.29	5542.19	4.76	10.15
	Avg	21.33	12778.44	13.31	34.00
	St dev	9.65	6377.61	8.59	24.25

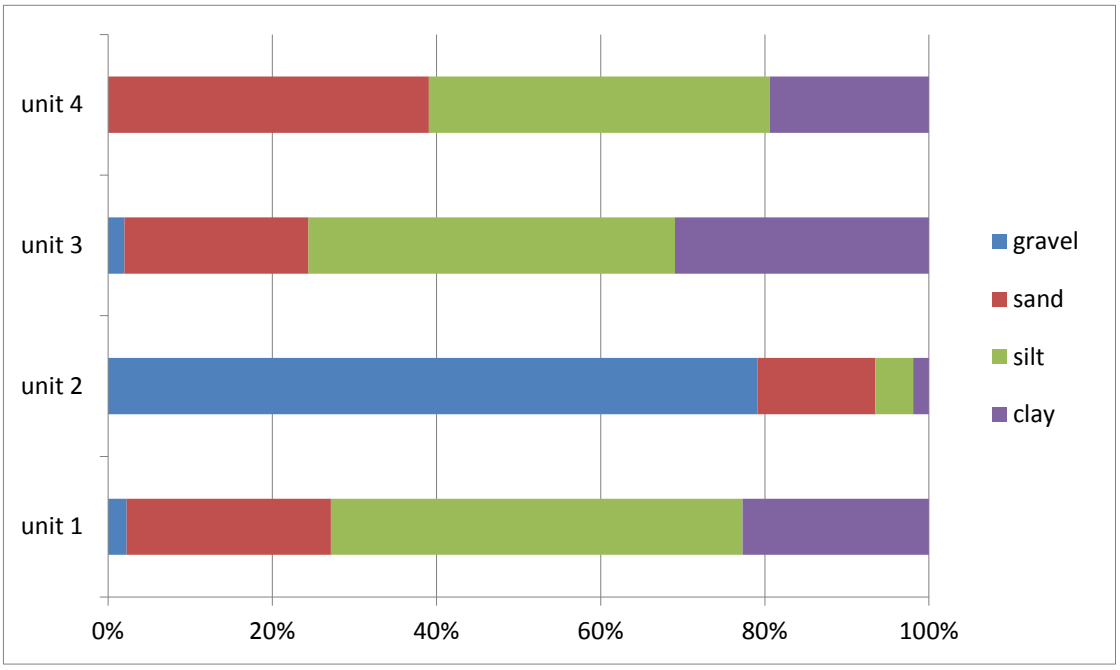

Figure 9.13 Average % weight composition of each unit from section 1.

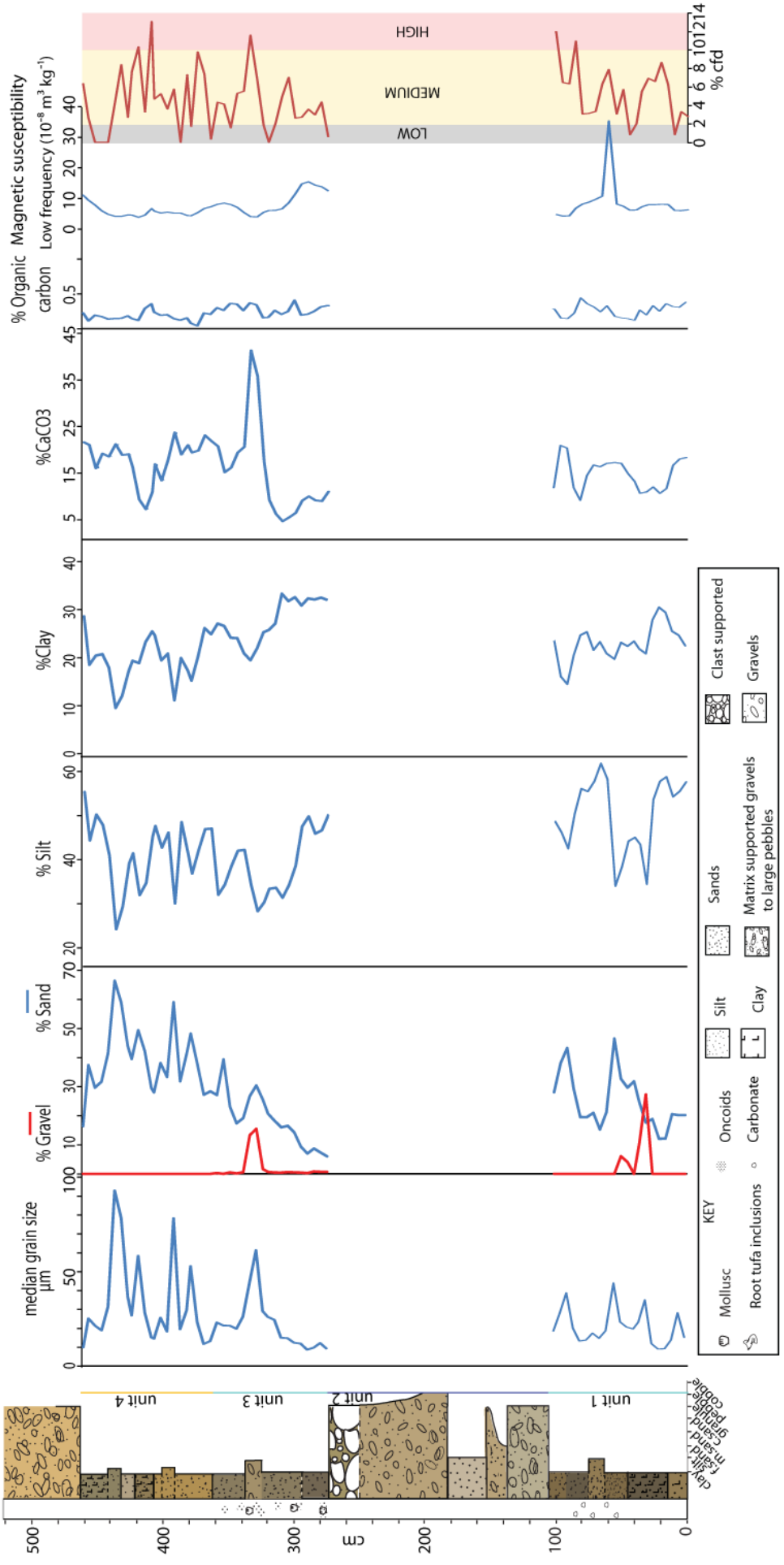

Figure 9.14 Bulk sedimentology results against section 1 composite log.

9.3.5 Calcium carbonate content

Calcium carbonate content of unit 1 varies between 20.91 % and 9.02 % (table 9.2), with the areas of lowest carbonate content appearing to correspond to the darkest, clay enriched sediments (figure 9.14).

Table 9.2 Summary of bulk carbonate content of sediments in section 1, Maro

Unit	maximum	minimum	average	Standard deviation
1	20.91	9.02	14.70	3.46
2	43.46	29.08	38.08	7.84
3	41.48	4.50	16.75	10.18
4	23.73	7.09	17.92	4.38

The calcium carbonate content of unit 2 follows a similar pattern as the median grain size through the unit; with a peak in both values occurring with the onset of oncoid deposition. Elevated carbonate content remains within the upper part of the unit alongside the occurrence of occasional oncoids (figure 9.14).

Calcium carbonate content through unit 1 is generally around 20 %, however there is a significant depletion (to 7.09 %) which occurs in association with the darkened, clay enriched horizon beginning at ~410 cm. Above this horizon, carbonate content returns to ~20 % and remains relatively stable through the remainder of the unit.

9.3.6 Magnetic Susceptibility

Table 9.3 Summary of magnetic susceptibility measurements through section 1 at Maro

Unit	Proxy	maximum	minimum	average	Standard deviation
1	LF	35.18	4.25	8.50	6.33
	HF	32.40	3.98	8.02	5.81
	% cfd	11.98	0.81	5.32	3.03
2	LF	22.45	2.00	10.23	10.79
	HF	22.15	1.85	9.99	10.73
	% cfd	7.50	1.34	4.41	3.08
3	LF	15.40	3.98	7.73	3.20
	HF	14.85	3.63	7.41	3.16
	% cfd	11.59	0.00	4.53	3.14
4	LF	11.05	3.88	5.79	1.80
	HF	10.35	3.48	5.52	1.75
	% cfd	13.06	0.00	4.74	3.75

Low frequency magnetic susceptibility measurements through section 1 records relatively low values according to Dearing (1999); ranging from 2.00 to 35.18 10^{-8} m^3 kg^{-1} (table 9.3). %cfd values are dominantly within the medium range according to Dearing's (1999) classification (indicated on figure 9.14). However, towards the top of units 1 and 3 %cfd values are just above 10 % and as such can be classified as containing a high volume of superparamagnetic grains (Dearing 1999). A subsequent high %cfd section occurs in association with the darkened sediments occurring towards the middle of unit 4.

9.3.7 Organic carbon

Organic carbon content is consistently below 0.5 % with no significant enrichment occurring anywhere within section 1 (figure 9.14, table 9.4). Therefore, the organic carbon content of section 1 will not be discussed further.

Table 9.4 Summary of organic carbon content of the four sediment units within section 1, Maro

Unit	maximum	minimum	average	Standard deviation
1	0.43	0.12	0.25	0.09
2	0.17	0.08	0.12	0.04
3	0.40	0.04	0.25	0.09
4	0.35	0.04	0.17	0.07

9.4 Section 2

Figure 9.15 Photograph (taken by Mark Hardiman) of section 2 within the valley. The section consists of the buff coloured sediments in the centre of the photograph.

This section is located at ~27m above sea level, with the sediment exposure running parallel with the modern river channel. Vegetation cover and slope deposits means that it is not possible to identify how the sediments correlate with other exposures within the valley.

9.4.1 Section 2 Field descriptions

Section 2 contains three distinct sediment units. At the base is a fine grained, darkened unit (unit 1) which is overlain by a cohesive, buff coloured silt unit (unit 2), and a pocket of clast supported sediments (unit 3) occurring to the right of the section (figure 9.16).

UNIT 1: Is primarily a fine sandy, clayey silt containing very occasional gravels and oncoids. The unit is up to 45 cm high from the base of the exposure. The base of the unit is a darkened, slightly clay enriched sediment containing regular oncoids. The top of the unit is a siltier, paler coloured sediment containing fewer oncoid clasts.

UNIT 2: Is a cohesive, buff coloured fine sandy silt appearing to be free from gravels and oncoids. There is some intra-unit textural and colour variability (figure 9.16), with a darkened band of material approximately halfway up the exposure and areas of sand dominant material present. Towards the base of the unit is a zone of large (>10 cm) carbonate nodules. It was not possible to reach sediments of this unit above head height and therefore, the full extent of the unit is not known.

UNIT 3: Is a lens of clast supported cobbles overlain by clast supported oncoids. There is a lens of the material on the right and left of the exposure at the same height. Only the right hand side lens was included within the logging and sampling.

Although there is some minor lateral variation within the sediments of section 2, the main sedimentological units and their intra-unit variability is contained within transect 1 (figure 9.17). As such, transect one provides a composite log for the section, enabling for sampling positions to be placed against log 6 which was taken through the same sediments as transect 1.

9.4.2 Interpretation of field observations – section 2

Unit 1 and unit 2 of section 2 share the same basic sedimentological characteristics as units 3 and 4 (respectively) of section 1. Therefore, because of their shared characteristics and similar height within the valley (figure 9.3); unit 1 (section 2) is interpreted as being a continuation of the oncoid rich, floodplain sediments forming unit 3 of section 1 and unit 2 (section 2) is interpreted as being a further deposit of the loessic material of unit 4 from section 1.

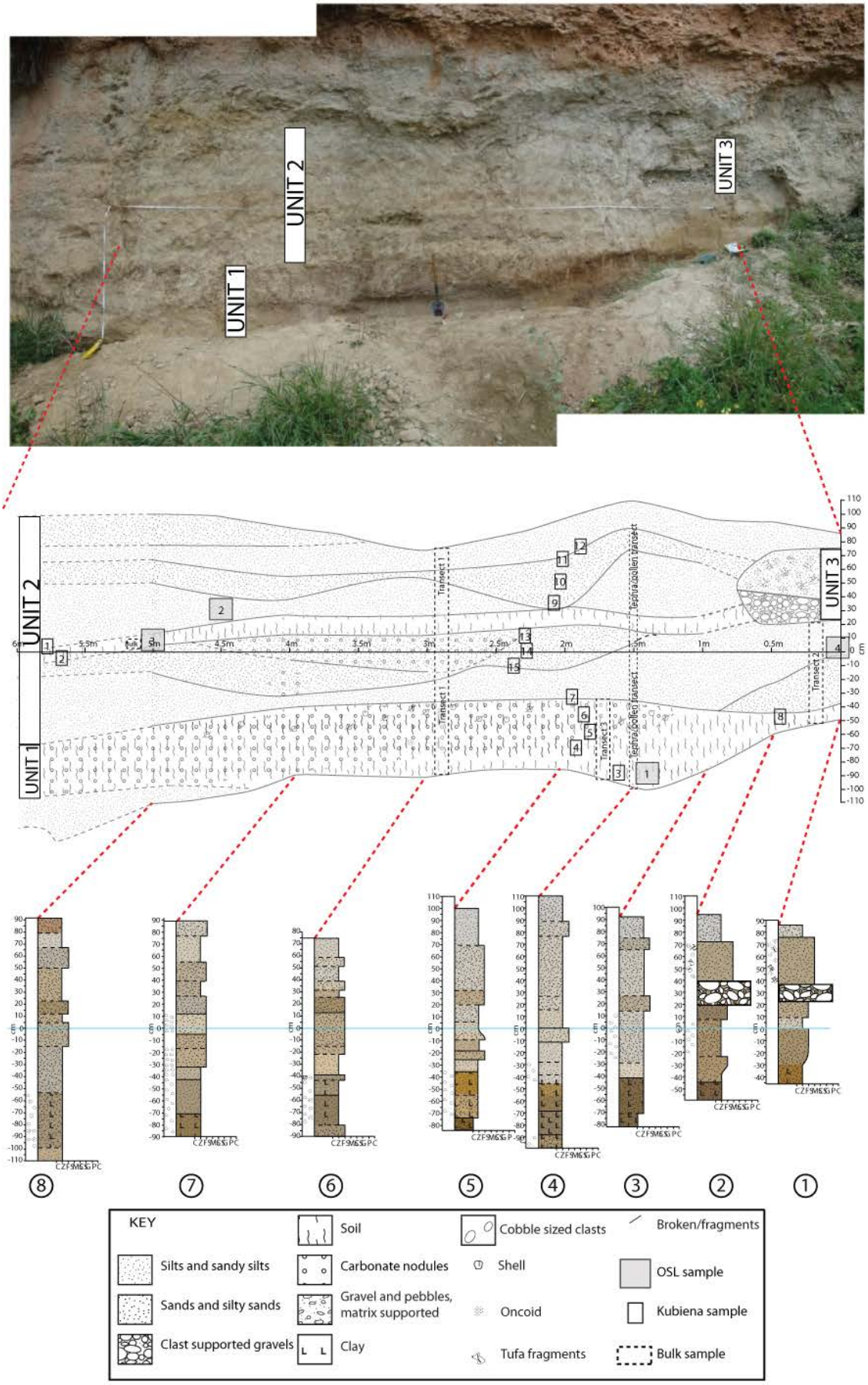

Figure 9.16 Photograph of section 2 with section schematic showing sediment logs and sampling locations. Blue line between sediment logs indicates levelling line.

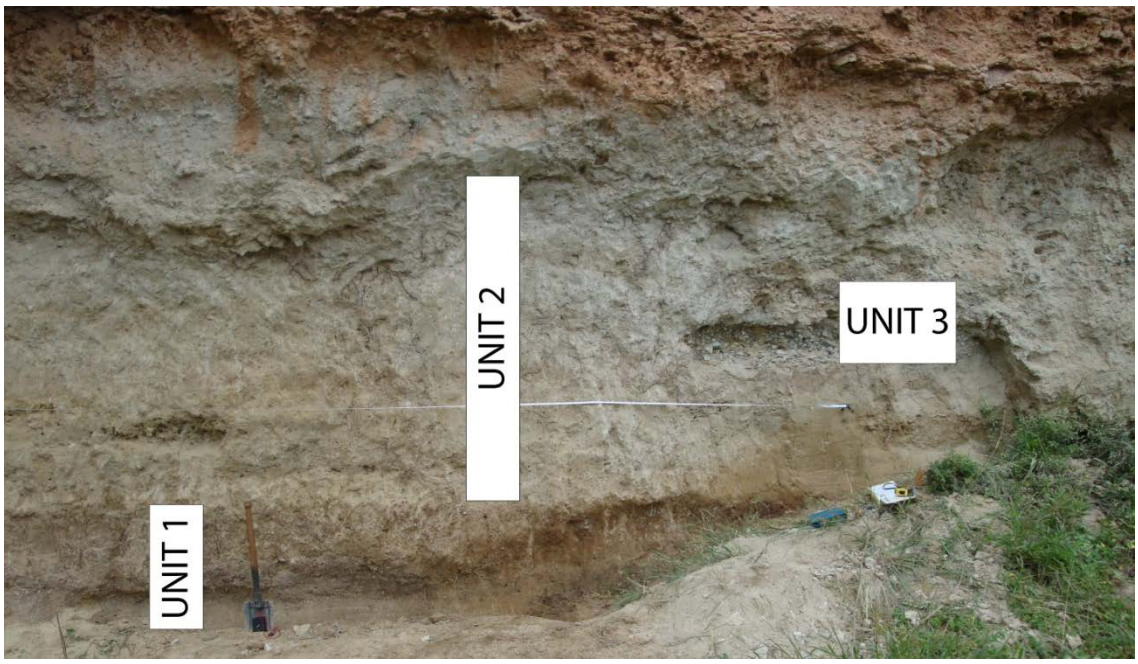

Figure 9.17 Photograph (taken by author) of Maro section 2 labelled with unit numbers

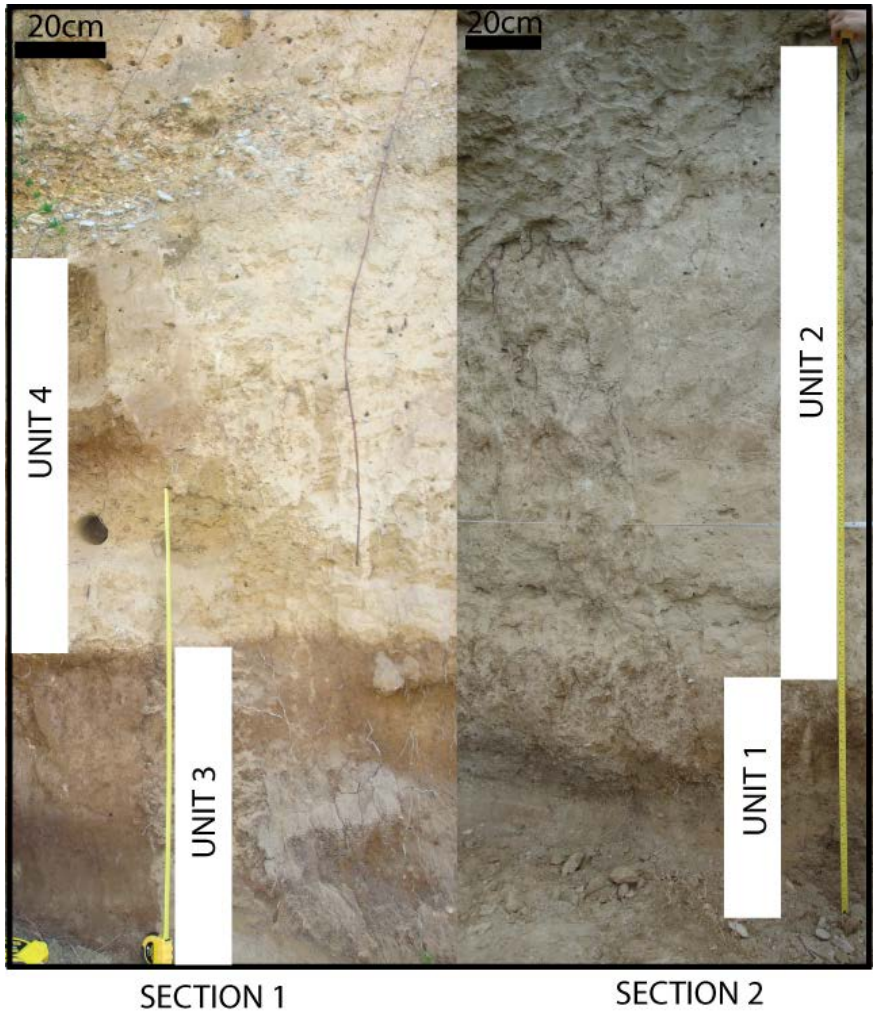

Figure 9.18 Proposed correlation of sediment from Maro sections 1 and 2

9.4.3 Section 2 sampling

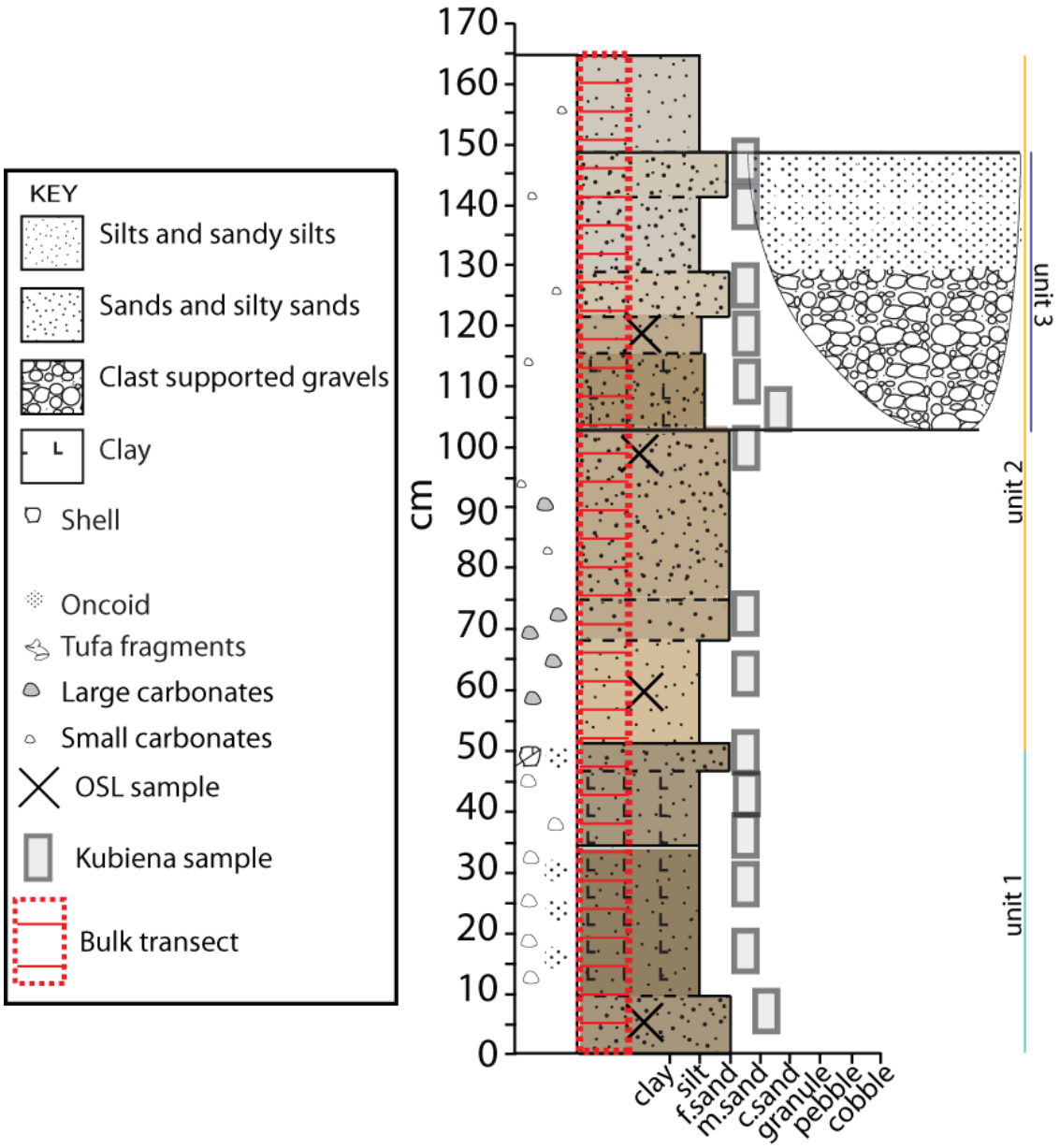

Figure 9.19 Section 2 composite log and sample locations

9.4.3.1 Bulk sampling

Bulk sampling transects were located within logs 1, 4 and 5, bulk sedimentological results in appendix. As the continuous sampling transect from log 6 was representative of the intra-unit variability present at the section, only these results are presented in full.

9.4.3.2. Micromorphology sampling

Fifteen kubiena tin samples were taken for micromorphological analysis. Six tins were evenly distributed through unit 1. Nine tins were placed through unit 4, in order to fully characterise the sediments with a focus on the darkened horizon running through the middle of the sediments.

9.4.3.3 OSL sampling

Four OSL samples were taken from section 2. One located at the base of unit 1, one located at the base of unit 2 and two samples placed above and below the darkened horizon. This sampling strategy was used in order to gain age estimates for each unit and to attempt to constrain the timing of formation of the possible soil horizon.

9.4.4 Particle size analysis

All results are given in % total weight. PSA was undertaken following the methods outlined in chapter 5.

The base of unit 1 contains some (up to 20 %) gravel sized material, predominantly made up of oncoids (table 9.5). The unit then fines rapidly from 15 cm upwards to a clayey sandy silt containing very occasional fine gravels and oncoids. The transition from unit 1 into unit 2 was not clearly defined in the field and is not identifiable by a clear shift in grain size.

Table 9.5 Summary of PSA data, section 2 Maro. Gravel data through unit 1 includes oncoids.

		Unit 1	Unit 2	Unit 3
.Gravel (% weight)	Max	20.30	0	83.93
	Min	0.00	0	71.17
	Avg	5.04	0	77.55
	St dev	6.19	0	9.02
Sand (% weight)	Max	43.06	59.75	26.86
	Min	18.53	15.88	12.76
	Avg	29.48	41.40	19.81
	St dev	9.75	11.68	9.96
Silt (% weight)	Max	54.81	61.16	2.39
	Min	25.40	24.99	1.29
	Avg	41.63	40.02	1.84
	St dev	8.97	8.64	0.78
Clay (% weight)	Max	31.37	27.29	0.92
	Min	12.57	12.10	0.68
	Avg	23.85	18.58	0.80
	St dev	6.59	3.73	0.17
Median (µm)	Max	120.38	82.66	0.67
	Min	8.35	13.90	0.47
	Avg	33.63	41.62	0.57
	St dev	38.26	22.84	0.14

Unit 2 is also defined as a mix of clay, sand and silt (table 9.5). However, as shown in figure 9.20, unlike unit 1, unit 2 contains no gravel sized material. Both the summary data (table 9.5) and PSA plotted by depth (figure 9.21) highlight the textural variability through unit 2. As with the silt unit previously discussed at section 1, the sediments within unit 2 contain regular inputs of sand;

ranging from 61 to 25 % silt and 60 to 16 % sand. The highest clay content (27 %) occurs where the darkened horizon was noted in the field.

Unit 3 is the gravel lens to the right of the section; this unit is a clast supported unit containing 71 to 84 % gravel within a predominantly sandy matrix (20 % average).

Comparison of the average composition of the sediments from each unit of section 2 (figure 9.20) highlights the differences between the units; with unit 2 having no gravel component, unit 1 minimal gravel and a higher clay content and unit 3 comprising almost entirely of gravels and sand. It is also useful to compare PSA from units correlated from sections 1 and 2 on the basis of field characterisation of the sediments. In both sections 1 and 2 the buff coloured, cohesive sediments (unit 4 and 2, respectively) appear to have a very similar average textural composition. The fine grained, oncoid containing sediments of unit 3 (section 1) and unit 1 (section 2) are also very similar in composition, with a small gravel component and significant clay component.

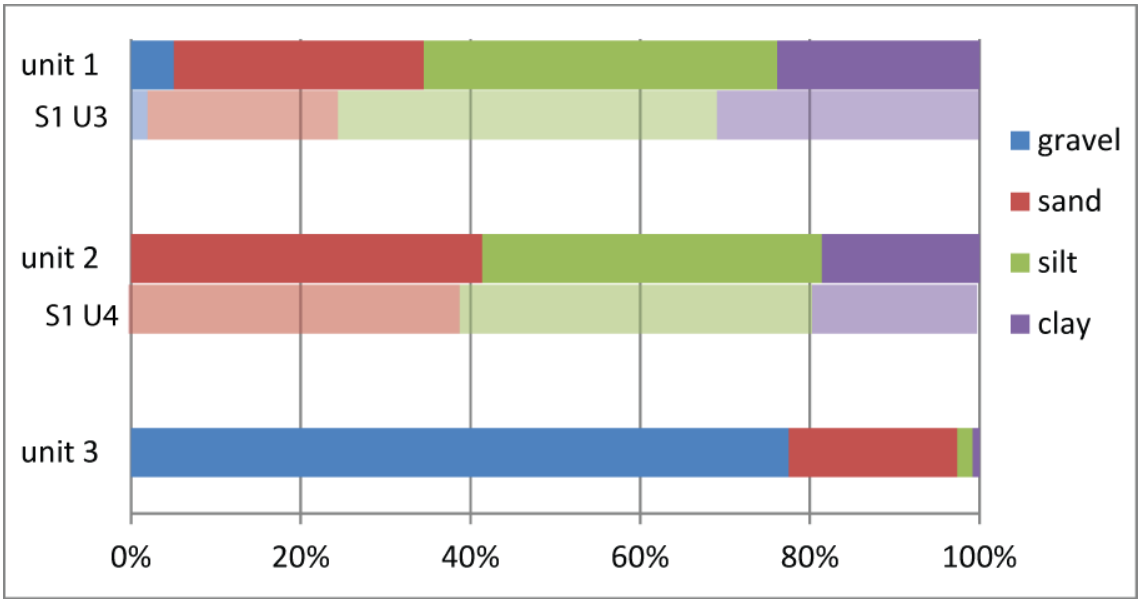

Figure 9.20 Average textural composition of each unit of section 2, Maro. Equivalent data for correlated units in section 1 are given (faded) for comparison

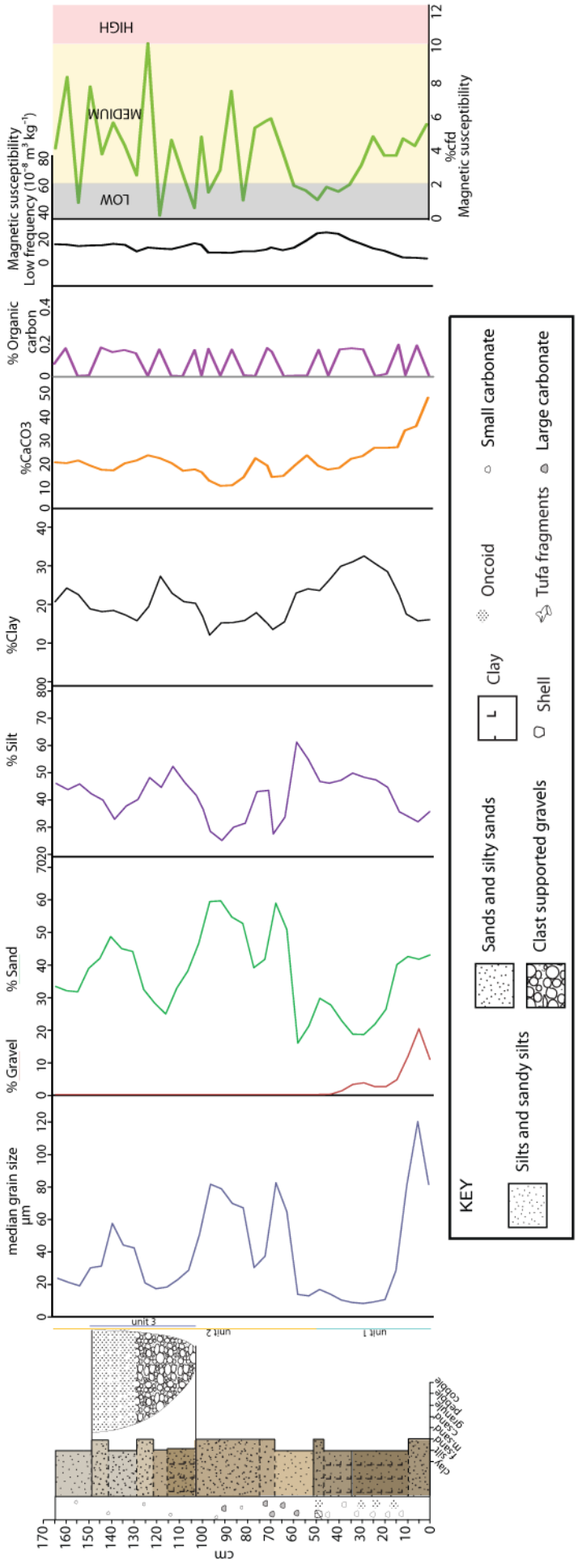

Figure 9.21 Bulk sedimentological data for Maro section 2

9.4.5 Calcium carbonate content

Calcium carbonate content of unit 1 is highest at the base (47 %), where the unit contains the most oncoidal clasts. % carbonate then declines rapidly to 25 % at 15cm, remaining relatively stable at ~20 % through the rest of the unit (table 9.6, figure 9.21).

Unit 2 has a fairly stable bulk carbonate content, averaging at 17 %. However, there are areas of lower carbonate content (~10 %) associated with the sand dominant horizons, particularly with the sandy horizon (81 to 98 cm) located beneath the darkened horizon (103 to 113 cm).

Table 9.6 Summary of calcium carbonate content through section 1, Maro

Unit	maximum	minimum	average	Standard deviation
1	47.22	16.22	25.69	8.94
2	22.32	9.21	16.68	3.70
3	22.89	10.32	16.60	8.89

9.4.6 Magnetic Susceptibility

Through section 2 the sediments record relatively low levels of magnetic susceptibility ranging from 22.73 to 3.65 10^{-8} m^3 kg^{-1} (table 9.7). All but one % cfd values plot within the low to medium range (figure 9.21) (0-10 %); the highest value occurs in association with the darkened horizon of unit 2 (10.13 %). In the sediments above the darkened horizon %cfd values remain elevated plotting mostly within the medium range.

Table 9.7 Summary of magnetic susceptibility values through section 2, Maro

Unit	Proxy	maximum	minimum	average	Standard deviation
1	LF	22.73	3.65	12.76	7.33
	HF	22.30	3.45	12.46	7.27
	% cfd	5.48	1.13	3.16	1.46
2	LF	14.80	7.78	11.39	2.26
	HF	14.70	7.20	10.91	2.16
	% cfd	10.13	0.23	4.15	2.60
3	LF	8.58	7.35	7.96	0.87
	HF	8.38	6.85	7.61	1.08
	% cfd	6.80	2.33	4.57	3.16

9.4.7 Organic carbon

All organic carbon values are extremely low at <0.5 % throughout (table 9.7, figure 9.21). As all values are consistently low organic carbon will not be discussed further.

Table 9.8 Summary of organic carbon values through section 2, Maro

Unit	maximum	minimum	average	Standard deviation
1	0.42	0.04	0.24	0.11
2	0.20	0.04	0.09	0.04
3	0.14	0.07	0.11	0.05

9.5 Sedimentological interpretation of sections 1 and 2

9.5.1 Section 1 Unit 1

The basal unit of the sequence is classified as a poorly sorted unit composed of clay through to gravel sized material. The bulk sedimentological analysis of the sediments supports the interpretation discussed in section 9.3.2, with the unit being typical of deposition within a floodplain environment (Miall 1992). There are two lows within the %carbonate curve which correspond the darkened clay enriched sediments at 15-39 cm and 80-90 cm. These sediments also contain the highest %cfd magnetic susceptibility values. This suggests that there may have been two periods of pedogenesis forming weakly decalcified, clay enriched sediments with a higher superparamagnetic mineral component. The occurrence of floodplain deposition within the valley is not necessarily indicative of a specific climate. If, however, the sediments have undergone pedogenic alteration, micromorphological analysis may aid the formation of a palaeoclimatic interpretation.

9.5.2 Section 1 Unit 2

The bulk sedimentology of unit 2 supports the interpretation offered in section 9.3.2 of deposition within a braided river system (Miall 1992). Within the unit is a bed rich in fragments of phytoclastic tufa and flowstone, these relatively fragile tufa forms are well preserved within the cobble beds. Their preservation within high energy deposits indicates that they are not far travelled and as such most likely represent erosion of a local tufa system. They occur in the bed with the largest clasts, indicating the highest energy flow which could relate to an erosive, high energy storm event. Despite tufa growth being linked to interglacial climates (chapter 2) they may have been eroded from an ancient exposure as opposed to an active tufa system. As such, unit 2 does not provide palaeoclimatic information.

9.5.3 Section 1 Unit 3, Section 2, Unit 1

These sediments have similar bulk properties to the basal sediments of unit 1 and as such are interpreted as deposited by floodplain processes. Within section 1 at 54-64 cm is a clast supported bed of oncoids. Oncoids are a form of tufa, produced within carbonate rich streams by the coating of detritus (clasts, shells vegetation) with precipitating carbonate (Pedley 1990). In

order for oncoids to be produced, the stream must be stable, low energy and with a very low sediment load otherwise full carbonate coating will not occur (Pedley 1990, 2009). As with other tufaceous deposits, oncoid formation occurs within interglacial conditions, where stable land surfaces (through soil formation and vegetation) result in low sediment loads.

The occurrence of a clast supported bed of oncoids suggests they were deposited within a channelized setting. Above the clast supported oncoid bed the sediments of section 1 and the full deposit recorded at section 2 contain occasional oncoid clasts within a sandy, clayey silt matrix. This represents a return to floodplain deposition where high rainfall events leads to increased stream power and sediment load, resulting in floodplain deposition of poorly sorted sediments including the incorporation of the oncoids removed from the channel setting.

Towards the top of the unit in section 1, there is an increase in %cfd which may suggest some pedogenic alteration. No such signal is recorded within the sediments from section 2. The presence of oncoids in the sediments indicates deposition during warm, stable conditions (Pedley 1990, 2009); possibly an interglacial.

9.5.4 Section 1 Unit 4, Section 2 Unit 2

At both sections 1 and 2 these sediments consist of a buff coloured, very cohesive silt unit which in the field lead to a depositional interpretation as loess. However, the sediments at both section contain a substantial sand component; varying from 66.37-16.41 % (section 1) and 59.75-15.88 % (section 2). As discussed in chapter 3 loess typically comprises of ~60 % silt, however at Maro the sediments identified in the field as loess contain 55.25-24.31 % (section 1) and 61.16-24.99 % (section 2) silt. This textural difference from 'typical' loess does not necessarily discount loess accumulation as the depositional mechanism of the sediments but it does highlight a significant coarse addition which cannot be entirely explained by the processes responsible for loess accumulation. It is interpreted that the sediments represent loess deposition with localised reworking of sediments, with peaks in sand content thought to relate to periods in which local sediment input is dominant.

At section 1 the darkened horizon towards the middle of the unit is identifiable within the bulk sedimentological characteristics of the sediments through a peak in clay content and %cfd values and a decline in carbonate content. These sedimentological changes support the field identification of the sediments representing a weak soil horizon, subjected to decalcification and pedogenic alteration of the textural and mineralogical composition. A similar sedimentological shift is recognisable within section 2, where the darkened horizon towards the middle of the

deposit is identified by a clay enrichment and a peak in %cfd. However, the calcium carbonate content is relatively constant through the sediments at section 2.

The constant calcium carbonate content through section 2 is somewhat counter intuitive. Towards the base of the loessic sediments is a horizon of large (>10cm), densely cemented carbonate nodules (figure 9.21). The formation of large carbonate nodules is usually associated with sustained decalcification of the overlying sediments under a stable land surface (e.g. Kemp 1985b). The constant and relatively high calcium carbonate content of the sediments suggests recalcification may have occurred.

9.6 Micromorphology of sections 1 and 2

9.6.1 Groundmass and Skeleton grains

Thin sections are described initially in terms of their general characteristics; texture, composition and structure. Texture is noted by the ratio between coarse (>20 μm), skeleton grains and fine (<20 μm), groundmass components given as c:f (Kemp 1985a, King 2000, Bullock *et al.* 1985). The c:f ratios through sections 1 and 2 range from 3:1 to 1:2, all showing open porphyric distributions (Bullock *et al.* 1985). Quantitative assessment of skeleton grain mineralogy was not undertaken through thin section analysis as bulk composition analysis was undertaken via XRD. However, particle shape, size and roundedness characteristics were noted for each section as a means of identifying shifting depositional processes and energies.

Groundmass is described in terms of homogeneity (texture and colour) and preferred orientation in terms of birefringence fabrics (Kemp 1985a, Bullock *et al.* 1985). Within the sections at Maro, two b-fabric types are present; undifferentiated and crystallitic (figure 9.22b). Undifferentiated b-fabric describes a lack of birefringence within the groundmass, while crystallitic describes the presence of small birefringent crystallites within the groundmass (Kemp 1985a) which may relate to original sediment composition or pedogenic alteration (Stoops 2010). All thin sections show apedal macro-structure (Kemp 1985a). In all cases microstructure consists of vughy, channel or chamber dominant voids within a dense groundmass (Kemp 1985a) (figure 9.22a). The presence of such voids is thought to relate to biological activity within soils (Kemp 1985a, Stoops 2010, King 2000) and therefore, the percentage cover of voids can enable interpretation of relative biological activity levels through a sediment sequence.

9.6.2 Concentration/depletion features

Organics are frequently preserved within thin sections from sections 1 and 2 (figure 9.22c). Commonly, these have the form of amorphous black to reddish brown staining of groundmass or complete or partial infilling of void spaces. Typically, these amorphous organic structures are significantly decomposed with cellular structure absent, and at times, the shape of the original organic structure is no longer discernible appearing similar to class 3 or 4 decomposition (Stolt and Lindbo 2010). However, there are frequent occurrences of class 1 or 2 decomposition, where some cellular structure remains intact (Stolt and Lindbo 2010). The presence of organic material is noted through the estimation of % area coverage.

Calcitic pedofeatures form through the dissolution, redistribution and precipitation of calcite from leachates. This mechanism can occur through localised or substantial redistribution through the sequence, with the mechanism understood through the distribution of features and the bulk calcium carbonate content of the sediments. Calcitic features are described in terms of their morphology and crystalline form. Crystalline form is defined from individual crystal size; micrite <4 μm, microsparite 5-20 μm and spar >20 μm (Bullock *et al.* 1985, Durand *et al.* 2010). Within the thin sections from Maro calcitic concentration features occur in the form of nodules, hypocoatings, linings and infillings and earthworm granules (figure 9.22d-g). Calcitic nodules can be authigenic (*in-situ*) or inherited, with authigenic concentrations identified by their diffuse, irregular outline (Durand *et al.* 2010). At Maro, authigenic carbonate nodules are small (<1 cm), irregular, strongly to moderately impregnated concentrations of micrite to microsparite. The hypocoatings are weakly to strongly impregnated, micrite to microsparite formed in the groundmass around voids. Calcitic linings and infillings consist of microsparite to occasional spar crystals, forming within the interior of voids. Earthworm granules are rare within the sediments from Maro; they are recognisable as granules of spar crystals arranged in a radial, parallel or random pattern (Canti 1998, Durand *et al.* 2010 and references therein).

Redoximorphic concentrations occur as iron or manganese irregular, weakly to strongly impregnated segregations within the groundmass. Such features form via the removal of iron or manganese oxides in a reduced soil environment caused by soil saturation in the presence of organic material. Once the iron/manganese solution moves into an aerobic (oxidising) environment such as dry sediment or an air filled void, precipitation occurs (Kemp 1985a, King 2000, Lindbo *et al.* 2010). These occur only very rarely in the sediments at Maro.

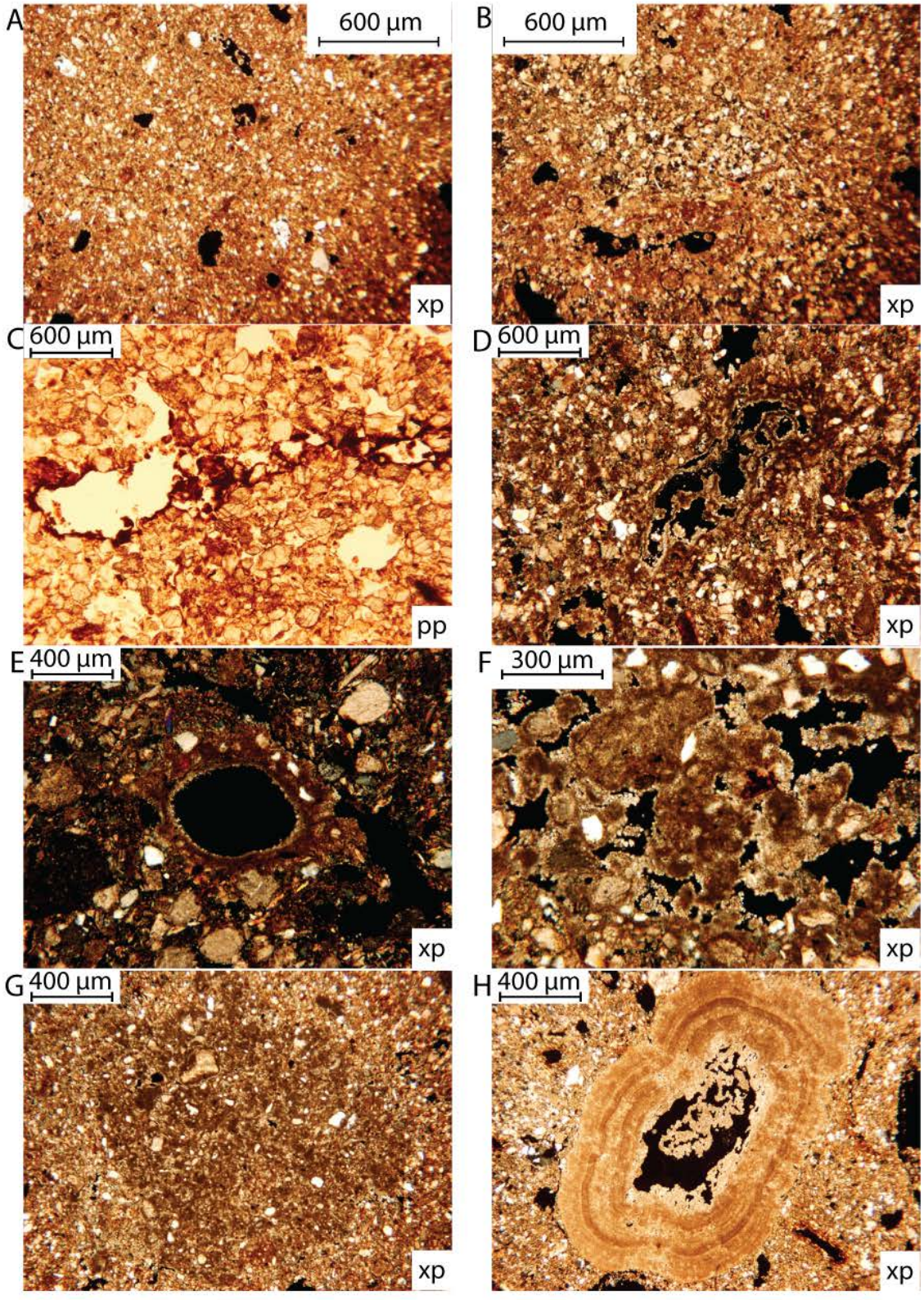

Figure 9.22 A. picture of typical groundmass and void structures, B. Unidfferentiated and crystallitic b-fabric, C. Organic staining of a void network, D. Calcitic preservation of organic structure, with associated hypocoating and microspar void lining, E. Densely cemented, small micritic hypocoating of vesicle void with microspar void lining, F. Complex of hypocoatings and void linings, G. Weakly to moderately cemented micritic nodule with diffuse boundary to groundmass, H. Incorporated tufa fragment showing layered calcite growth and distinct boundary with groundmass.

9.6.3 Distribution of micromorphological features – Section 1

Unit 1- constant low percentage cover of amorphous organics (up to %), presence within and around voids indicating *in-situ* root decay. Void cover appears to correlate to changes in grain size, with increased percentage void occurring at times of lower median grain size (figures 9.14, 9.23). As the void forms found in these sections relates to veg growth, it appears that there is less vegetation growth during coarse sediment accumulation, which may reflect increased sedimentation rates during input of coarse bedload relating to increased stream power.

Although percentage cover of calcitic features is low throughout the unit (up to 10 %), there are two apparent peaks. Firstly at 40cm (section 1, thin section 3 (S1-3)), a peak in percentage cover is associated with abundant hypocoatings (i.e. 30-70 % of voids associated with hypocoatings) and frequent void linings. This peak in calcitic pedofeature occurrence occurs during one of the darkened, clay enriched horizons, but within sediments with a relatively low bulk carbonate content. Thin section analysis highlights the lack of groundmass calcite within this thin section, indicating that primary calcite has been totally re-precipitated in the form of pedofeatures within this area of sediment. This is similar to the processes recorded within the thin section taken from the top of the unit; where a peak in calcitic pedofeatures is associated with an absence of groundmass calcite. The peak in pedofeatures (S2-6) at the top of the unit is also associated with a peak in superparamagnetic minerals (% cfd) (figure 9.14).

Unit 3- There is a peak in calcitic pedofeatures at the base of the unit (S1-7) and again at the top (S1-11) of the unit. At the base of the unit (S1-7) the peak in calcitic pedofeatures occurs beneath an area of sediment with a very low bulk carbonate content (300-310 cm). It is possible that the peak in pedofeatures recorded in S1-7 relates to a period of post-depositional alteration affecting sediments up to 310 cm, prior to the deposition of the overlying clast supported oncoid bed. Leading to the reduced carbonate content of the upper sediments (300-310 cm) and relatively enriched underlying sediments (S1-7). Above the clast supported oncoid bed there is a steady increase in percentage cover of calcitic pedofeatures, reaching a peak of 30 % slide cover at 350 cm (S1-11). This steady increase upwards (from S1-9 to S1-11) is suggestive of accretionary pedogenesis; with pedogenic alteration of sediment increasing in response to a climatic amelioration (warmth and/or moisture) and/or steadily declining sediment input.

Unit 4 – There are two significant reductions in bulk carbonate content through unit 4, at 415 cm and 450 cm, both correlating to darkened, clay enriched horizons. The sediments beneath these horizons are relatively enriched in bulk carbonate and importantly these sediments also record increased percentage cover of pedogenic calcite (S1-13 and S1-14, respectively).

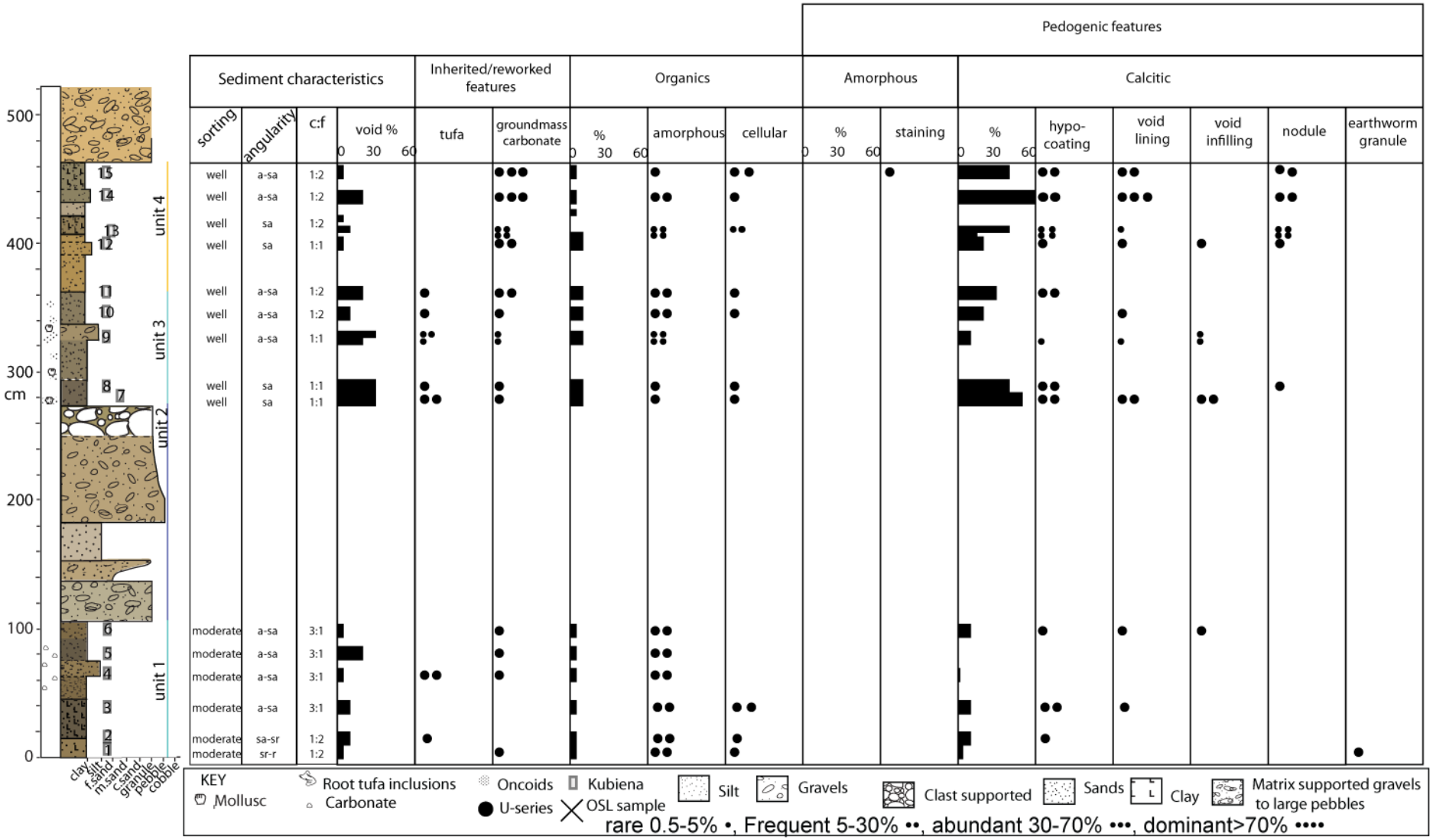

Figure 9.23 Distribution of micromorphological characteristics through section 1, Maro Angularity: s=sub, a=angular, r=rounded.

9.6.4 Distribution of micromorphological features – Section 2

It is suggested that the sediments at the base of section 2 represent floodplain deposition and incorporation of previously deposited oncoids, in this respect, it appears to correlate with the sediments above the clast supported oncoid bed of unit 3, section 1. As with the sediments above the oncoid bed in section 1, micromorphological analysis from section 2 shows a steady increase in the % cover of calcitic features upwards through the sediments (S2-15 to S2-10). This pattern of increasing occurrence of pedogenic calcite upwards indicates increasing effectiveness of accretionary pedogenesis suggesting accumulation under conditions increasingly favourable to pedogenic alteration; e.g. increased warmth and moisture and/or declining accumulation rates.

A correlation between the upper sediments of section 2 and section 1 has been suggested. However, the two sequences record very different distribution of micromorphological features. Unlike section 1, section 2 records increased occurrence of pedogenic calcite with depth (S2-1 to S2-7. Such a profile suggests post-depositional alteration under a stable land surface (Kemp 1985b). Taken together with the occurrence of large carbonate nodules towards the base of the profile, the sediments appear to record sustained down-washing of carbonate towards the base of the sequence. The peak in nodule occurrence is within a sand horizon within the profile. It is likely that the increased pore spacing associated with a sand (as opposed to a silt) bed would provide aerated sediments favouring calcite precipitation from saturated solution. However, the bulk carbonate content of the sediments does not show the same depth/content trend.

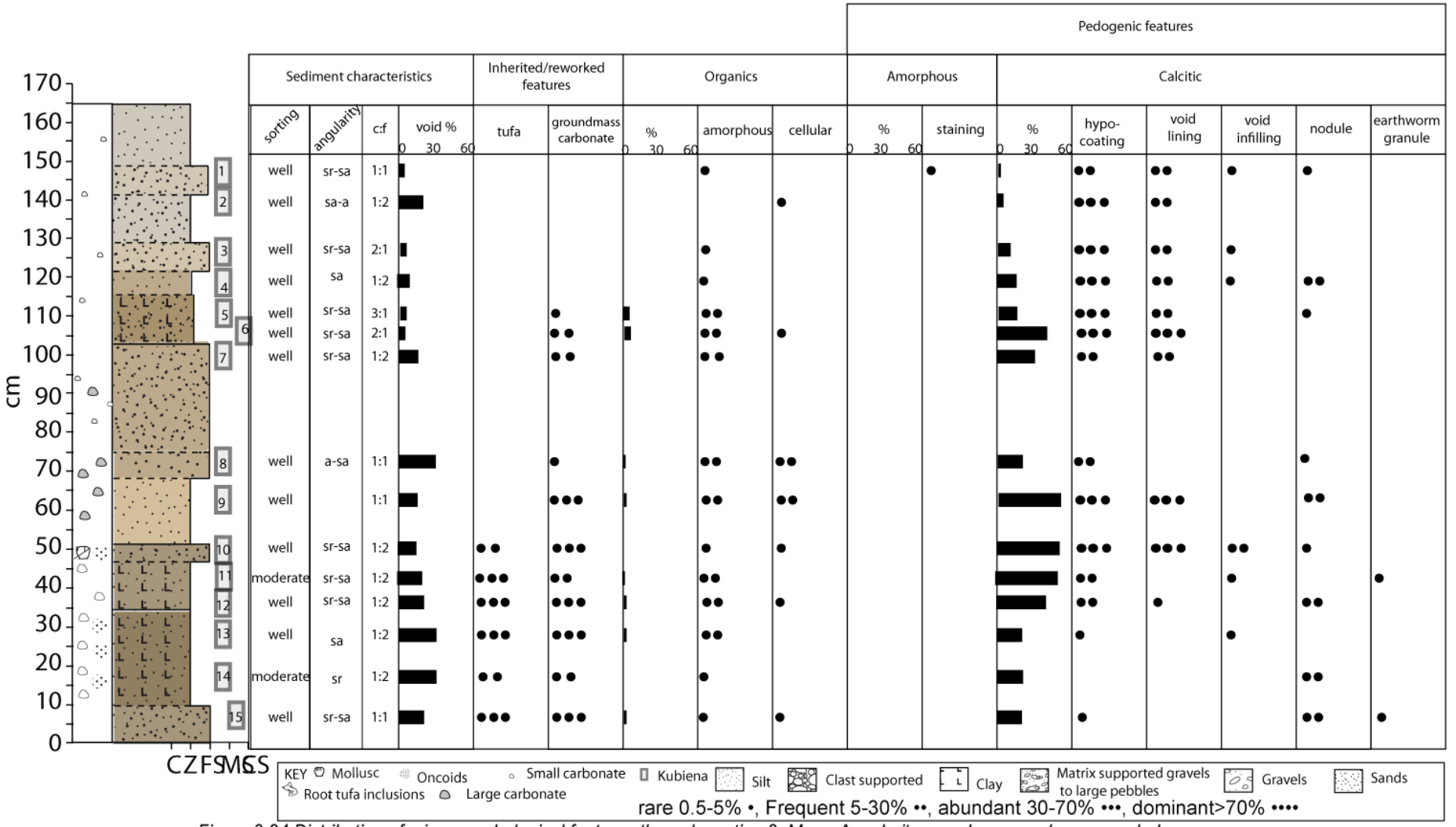

Figure 9.24 Distribution of micromorphological features through section 2, Maro. Angularity: s=sub, a=angular, r=rounded.

9.7 $\delta^{18}O$ and $\delta^{13}C$ composition of carbonates

Samples were taken from the tufa forms located in the valley; modern tufa (figure 9.4), section 3 tufa outcrop (figure 9.6), tufa fragments contained within the clast supported sediments of unit 2, section 1 and oncoids from within unit 3 of section 1. As previously discussed (chapter 2), tufa growth is associated with warm stable climates such as those present during Interglacials. Therefore, the isotopic composition of the tufaceous carbonates should provide a warm climate analogue for comparison.

Micromorphological analysis of the sediments in sections 1 and 2 identified pedogenic carbonate forms present throughout. Samples were hand-picked following the methods outlined in chapter 5. Only samples through the loessic sediments were selected, as thin section analysis identified reworked carbonate forms present throughout the other sediments. Sampling sediments where carbonate forms are authigenic minimises possible complications associated with understanding the origin of the isotopic composition.

All values are quoted in reference to V-PDB. Associated uncertainties for isotopic analysis are 0.02‰ for $\delta^{13}C$ values and 0.06‰ for $\delta^{18}O$ values. Raw data in appendix.

9.7.1 Results

Values obtained from the various tufaceous forms within the valley give isotopic compositions of -7.59 to -10.95 $\delta^{13}C$ and -6.56 to -7.38 $\delta^{18}O$. The variability in the values results from differences between the tufaceous deposits, not from intra-unit variability (figure 9.25). Values measured in pedogenic carbonates from the loessic unit of section 1 range from -3.28 to -10.16‰ $\delta^{13}C$ (average: -6.28‰) and -2.78 to -6.54‰ $\delta^{18}O$ (average: -4.13‰). Isotopic composition of pedogenic carbonates collected from the loessic unit of section 2 show less variation; -3.23 to -6.81‰ $\delta^{13}C$ (average: -5.19‰) and -3.77 to -5.20‰ $\delta^{18}O$ (-4.57‰).

All values are significantly depleted in ^{13}C indicating that they cannot be derived from limestone sources (~0‰; Hudson 1977). All values are within the range of isotopic composition of soil carbonates previously reported from the Mediterranean (Candy *et al.* 2012).

9.7.2 Co-variance

Figure 9.25 demonstrates that there is clear covariance between $\delta^{18}O$ and $\delta^{13}C$ values across the dataset from Maro (r^2=0.63, p=2.05). However, this apparent covariance appears in part to be driven by the strongly depleted values gained from the tufa samples and the relatively enriched values gained from the pedogenic carbonates (figure 9.26 a,b).

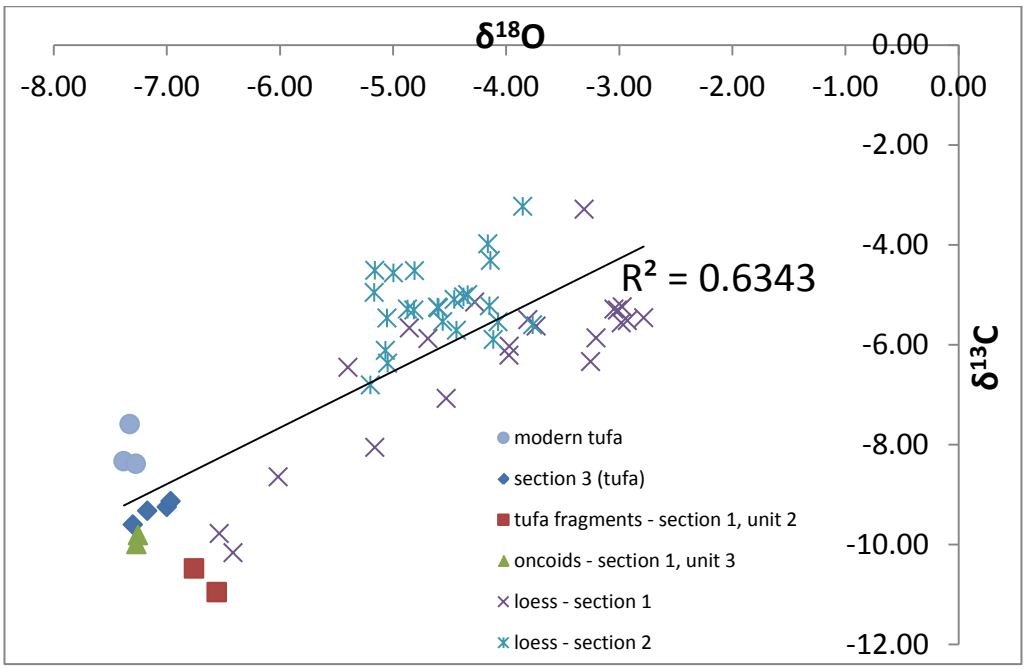

Figure 9.25 Isotopic composition of carbonates sampled from Maro. r^2 value refers to relationship through entire dataset.

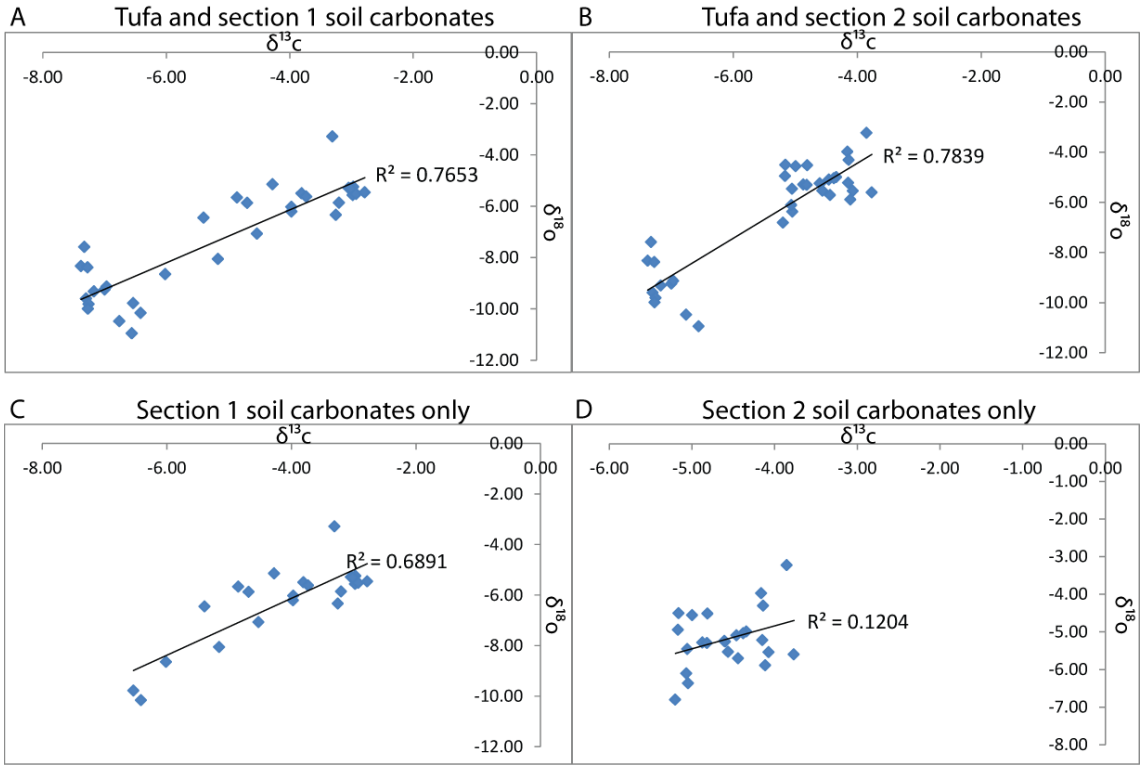

Figure 9.26 Breakdown of covariance within isotopic compositions of carbonates from different sources

9.7.3 Tufa values

The tufa values provide the most depleted $\delta^{13}C$ and $\delta^{18}O$ values from Maro; with $\delta^{13}C$ values averaging -9.35‰ (range -7.59 to -10.95‰) and $\delta^{18}O$ values averaging -7.11‰ (range -6.56 to -7.59‰). There is no covariance present within the tufa dataset.

Tufas form in streams, rivers and lake systems under open air environments and as such can be considered meteoric carbonates. Andrews (2006) outlines the primary controls on the oxygen isotopic composition of tufas as being water temperature and water composition, although modification of the signal can occur through evaporation. In systems driven by evaporation there is strong covariance between oxygen and carbon isotope values, as evaporation results in the preferential degassing of the light isotopes; ^{12}C and ^{16}O (Candy *et al.* 2012, Andrews 2006). The isotopic composition of the tufa samples provides the most depleted $\delta^{18}O$ values, indicating that the tufa carbonates formed in a system with relatively low evaporation rates. Therefore, other factors must be the main drivers of the isotopic composition of the tufa carbonates.

Tufas are typically groundwater fed systems in which the composition of groundwater is controlled by the composition of the recharging meteoric waters (Andrews 2006). A clear relationship exists between mean annual temperature and the composition of meteoric waters exists (Rozanski *et al.* 1993) (chapter 4). It follows, therefore, that the two main controls on the oxygen isotopic composition of tufa (water temperature and composition of precipitation) are controlled by mean annual air temperature.

$\delta^{13}C$ within tufas is primarily a function of dissolved inorganic carbon, from either soil sources or dissolution of limestone (Andrews 2006). The values obtained from tufa samples at Maro are typical of a system deriving its carbon primarily from soil organic matter under vegetation utilising a C3 photosynthetic pathway (Andrews 2006, Candy *et al.* 2012).

There is minimal variation within the $\delta^{18}O$ (<1‰) values from the tufa samples indicating all were formed during periods experiencing similar temperatures. Although there is greater variation within the $\delta^{13}C$ values from the tufas, values are consistent with the potential range of values derived from soil organic matter formed under C3 photosynthetic vegetation (Quade *et al.*1989) and variability seen in modern systems (Andrews *et al.* 1997, Andrews and Brasier 2005, Andrews 2006).

9.7.4 Section 1 – pedogenic carbonates

Comparison of $\delta^{13}C$ and $\delta^{18}O$ values retrieved from pedogenic carbonates within the loessic unit of section 1 shows that there is strong covariance (r^2= 0.69, p=1.49) between the two isotope systems (figure 9.26c). At section 1 this strong covariance occurs whether or not the tufa values are included. This therefore implies that pedogenic carbonates found in section 1 are recording variations in relative aridity.

As discussed in chapter 4 pedogenic carbonates are meteoric carbonates. As with tufaceous carbonate, the $\delta^{18}O$ signal is driven primarily by the temperature and the composition of precipitation and the $\delta^{13}C$ signal driven by vegetation composition (e.g. Cerling and Quade 1993). However, as with tufa systems the isotopic composition of pedogenic carbonates may be significantly modified or even driven by evaporation (Candy *et al.* 2012, Ufnar *et al.* 2008). The strong covariance between $\delta^{13}C$ and $\delta^{18}O$ within the pedogenic carbonates from the loessic material of section 1 demonstrates that they are both are being driven by the same environmental control.

Increasing aridity causes soil moisture evaporation rates to increase. Soil moisture is provided by the local precipitation, the composition of which is primarily temperature driven, evaporation of soil moisture significantly modifies the composition of the water through the preferential loss of light $H_2{}^{16}O$ (Dever *et al.* 1987, Quade *et al.* 1989, Ufnar *et al.* 2008). Preferential removal results in relative enrichment of the soil moisture with $\delta^{18}O$, and therefore any carbonate precipitating from the modified soil moisture will also be enriched with $\delta^{18}O$.

Candy *et al.* (2012) suggest that aridity modifies carbon isotope ratios of soil carbonates through modifying the soil environment in two ways. Firstly, evaporation of soil moisture results in degassing of CO_2 with preferential degassing of $^{12}CO_2$, enriching the soil environment with ^{13}C (Dever *et al.* 1987). Secondly, increased aridity results in reduced vegetation cover allowing more of the soil CO_2 to be derived from atmospheric CO_2, which is more enriched in ^{13}C than plant respired CO_2 (Quade *et al*., 1989; Cerling and Quade, 1993).

As discussed previously, the increasing occurrence of pedogenic calcites upwards through the sediments, together with relatively stable the bulk carbonate values suggest that pedogenic modification has occurred during the accumulation of the sediments. Therefore, the isotopic composition of the pedogenic carbonates provides a record of climate during accumulation of these sediments. There is a general trend towards more enriched values upwards through the sequence (figure 9.27). With the isotopic composition of soil carbonates in this system being driven by aridity, a trend towards increasingly heavy (enriched) isotopic values indicates increasing aridity during sediment accumulation.

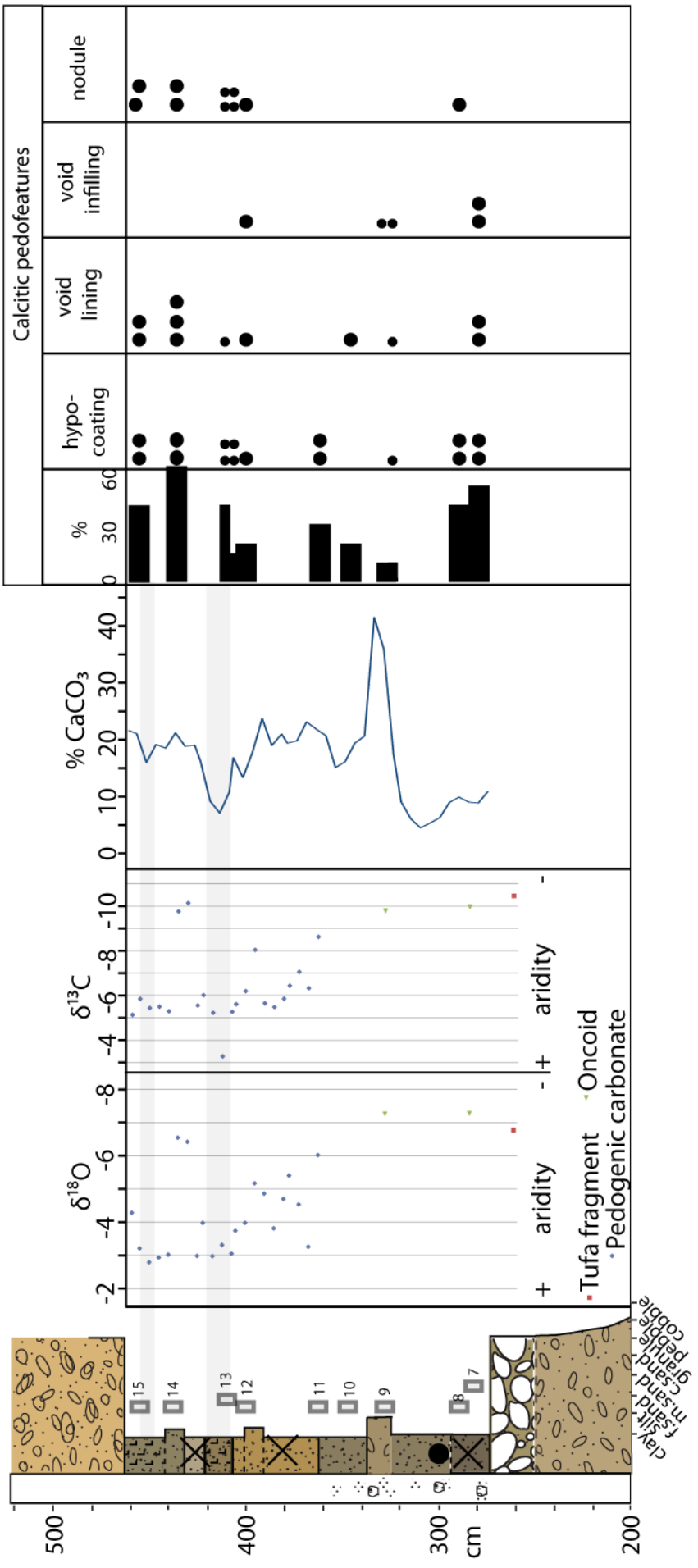

Figure 9.27 Isotopic composition of carbonates from section 1 plotted against depth, bulk carbonate content and distribution of micromorphological calcitic pedofeatures

There are however, two notable fluctuations which oppose the general trend towards heavier isotopic values. At 395-400 cm and 430-440 cm are significantly lighter (depleted) isotopic values ($\delta^{18}O$: -5.16, -6.41, -6.54‰, $\delta^{13}C$: -8.06, -10.16, -9.78‰). These isotopic excursions correlate with the peaks in calcitic pedo-feature occurrences which are located ~15-25cm below each of the darkened horizons. The depleted bulk carbonate values associated with these darkened horizons may indicate that decalcification of these horizons took place during a period of land surface stability (Kemp 1985b). However, the incomplete decalcification indicates a relatively short lived episode of post-depositional pedogenic alteration. The increased occurrence of pedogenic carbonates at a depth of ~15-25cm below the weak soil horizon is consistent with the depth of peak carbonate accumulation beneath soil horizons (Gocke *et al.* 2012). It is therefore likely that the isotopically light values are gained from carbonates likely to have formed in response to the weak post-depositional pedogenic episodes. The depleted isotopic composition ($\delta^{13}C$ and $\delta^{18}O$) of the carbonates suggests that episodes of soil formation occur in association with decreased environmental aridity.

9.7.5 Section 2 – pedogenic carbonates

The isotopic composition of pedogenic carbonates from the loessic material in section 2 is markedly different to those gained from section 1. The average values obtained from section 2 are not dissimilar to those from section 1; however, the variability within values from section 2 is much smaller (figure 9.28). This clumping of values means that when plotted alone, values from section 2 do not display covariance (9.29d) (r^2= 0.12, p=0.11). However, by including the values from the tufa samples in order to supply isotopically light values, there is a strong degree of covariance (r^2=0.78, p=0.89). This apparent covariance, together with the similarity to average values obtained from section 1, suggests that aridity may also be driving the signal from section 2. As discussed previously, the depleted $\delta^{18}O$ composition of the tufas corresponds to formation under less arid conditions. As the values from pedogenic carbonates in section 2 are all significantly more enriched in both $\delta^{18}O$ and $\delta^{13}C$ than the tufa values, it is likely that section 2 pedogenic carbonates formed during a more arid period.

Sedimentological and micromorphological analysis of the sediments from section 2, indicates that there is progressive enrichment of calcitic features towards the base of the sediments, highlighted by the increase in micromorphological calcitic pedo-features and the occurrence of a horizon of large carbonate nodules (>10cm) towards the base of the section. However, the bulk carbonate content of the sediments does not show a progressive enrichment down through the sediments (figure 9.28). This suggests that the overlying sediments may be the source of the carbonate.

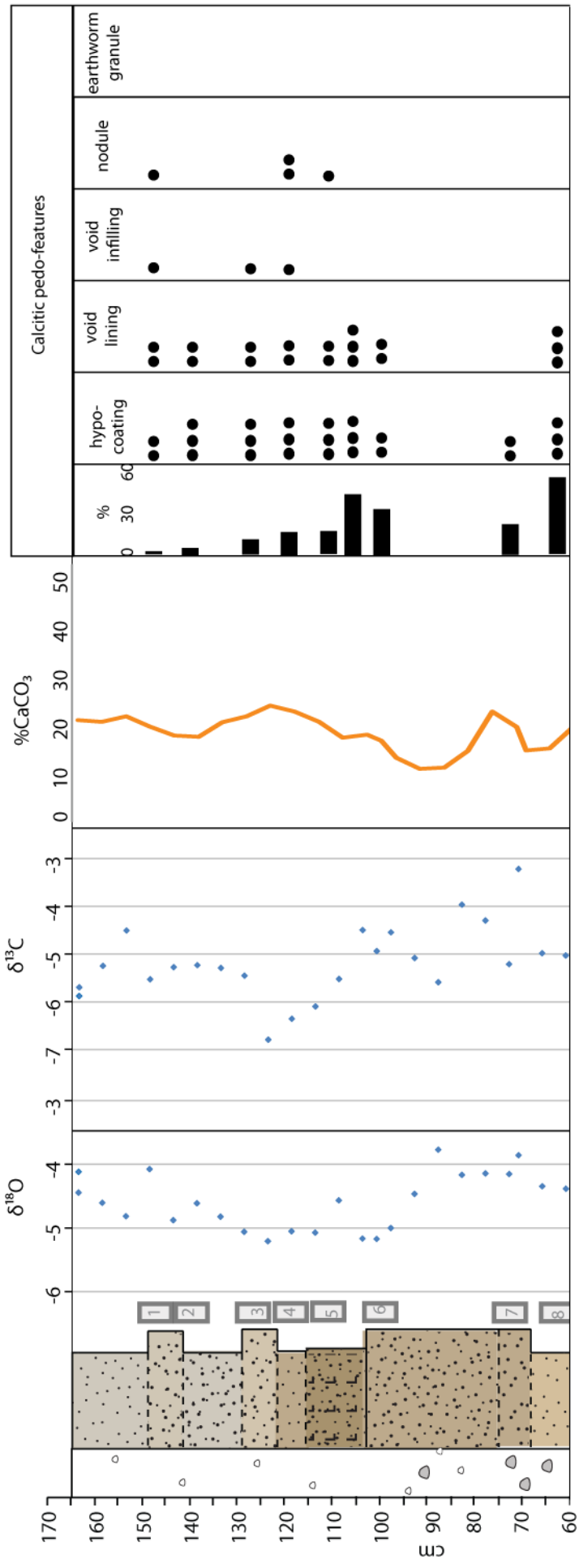

Figure 9.28 Isotopic composition of carbonates from section 2 plotted against depth, bulk carbonate content and distribution of micromorphological calcitic pedofeatures

Unlike section 1 which has ~3 m of sediment overlying it, section 2 is relatively close (~1m) to the land surface sediments. These sediments are not directly accessible, but have the appearance of being overprinted by calcrete development.

If the interpretation of later carbonate overprinting of the sediments is correct, then it is likely that most of the carbonates present within the section will relate to this. If the sediments above are a calcrete horizon, it is likely that this sustained carbonate movement occurred during an interglacial climate (Candy and Black 2009). This potential overprinting is highlighted by the differences in both morphology of carbonates and distribution of pedogenic carbonate features between the loess sediments of sections 1 and 2, where section 2 contains a concentration of large carbonate nodules towards the base of the unit typical of sustained carbonate accumulation and calcrete horizons (Wright 2007, Alonso-Zarza and Wright 2010)

Therefore, the stability of the isotopic signal gained from the pedogenic carbonates present within section 2 reflects their post-depositional formation, most likely to have occurred during an interglacial climate.

9.8 Chronology

9.8.1 OSL dating of sections 1-3

One sample was taken from section 3 (sample location shown in figure 9.6). Four samples were taken from section 1 (figures 9.9, 9.12) and section 2 (figures 9.16, 9.7). A minimum of 12 aliquots were used to produce equivalent dose estimates from which to calculate an age estimate using the methods outlined in chapter 5. Sample run conditions are given in table 9.9, sample dosimetry data is given in table 9.10.

For each aliquot of each sample, growth curves were generated using an exponential plus linear saturating exponential curve, as this proved to be the curve of best fit in all instances. For all samples the laboratory produced equivalent dose plots onto the linear part of the growth curve (figure 9.29), while there remains a steady increase in sensitivity corrected OSL intensity with increasing regenerative dose. Therefore the sample is not saturated and a geologically meaningful De can be calculated.

Estimates of equivalent doses for each sample were calculated from >12 aliquots (table 9.10). The spread of equivalent doses gained from each aliquot display a unimodal, relatively narrow (given the high De values) distribution (figure 9.30). Test behaviour (RR and IR ratios) and narrow distribution of De values generated for each sample indicate that all samples were behaving well and therefore, should provide reliable OSL age estimates.

Table 9.9 Run conditions for OSL samples from sections 1-3, Maro.

Section	Sample	Aliquots	PH 1 (˚C)	PH 2 (˚C)	Post heat (˚C)	Given doses (Gy)
1	Rdm091	17	260	220	280	9, 19, 45, 90, 180, 358, 0, 9, 9
	Rdm092	15	260	220	280	9, 19, 45, 90, 180, 358, 0, 9, 9
	Rdm093	24	260	220	280	9, 19, 45, 90, 180, 358, 0, 9, 9
	Rdm094	23	260	220	280	9, 19, 45, 90, 180, 358, 0, 9, 9
2	Rdm083	11	260	220	280	19, 58, 93, 193, 290, 385, 0, 19, 19
	Rdm084	12	260	220	280	19, 58, 93, 193, 290, 385, 0, 19, 19
	Rdm085	12	260	220	280	19, 58, 93, 193, 290, 385, 0, 19, 19
	Rdm086	12	260	220	280	19, 58, 93, 193, 290, 385, 0, 19, 19
3	Rdm0822	12	260	220	280	19, 57, 96, 192, 288, 385, 0, 19, 19

Table 9.10 Summary of dosimetry and dating results for samples from Maro sections 1-3.

Section	Sample	Radionuclide concentration			Sample depth (m)	Cosmic dose rate (Gy/ka)	Total dose rate (Gy/ka)	Water content (%)	Equivalent dose, De (Gy)	Age (ka)
		K (%)	U (ppm)	Th (ppm)						
1	Rdm091	1.06	1.98	7.3	6	0.104	2.09	15	263.8	125.9 ±12.7
	Rdm092	0.94	2.21	7.6	1.2	0.180	2.15	15	259.8	120.6 ±13.1
	Rdm093	0.76	2.58	6.6	2.5	0.154	2.02	15	281.2	139.3 ±15.3
	Rdm094	0.62	2.08	5.7	2	0.163	1.70	15	253.1	149.1 ±15.7
2	Rdm083	0.92	2.45	8.5	6	0.104	2.20	15	265.5	124.6 ±12.1
	Rdm084	1.07	2.55	8.9	1.2	0.180	2.46	15	268.4	109.3 ±10.5
	Rdm085	0.80	2.60	8.1	6.5	0.098	2.10	15	292.9	139.5 ±14.5
	Rdm086	1.07	2.97	9.1	3	0.145	2.56	15	288.1	112.5 ±11.4
3	Rdm0822	0.4	1.28	2.1	1.6	0.170	1.04	15	118.3	114.2 ±12.3

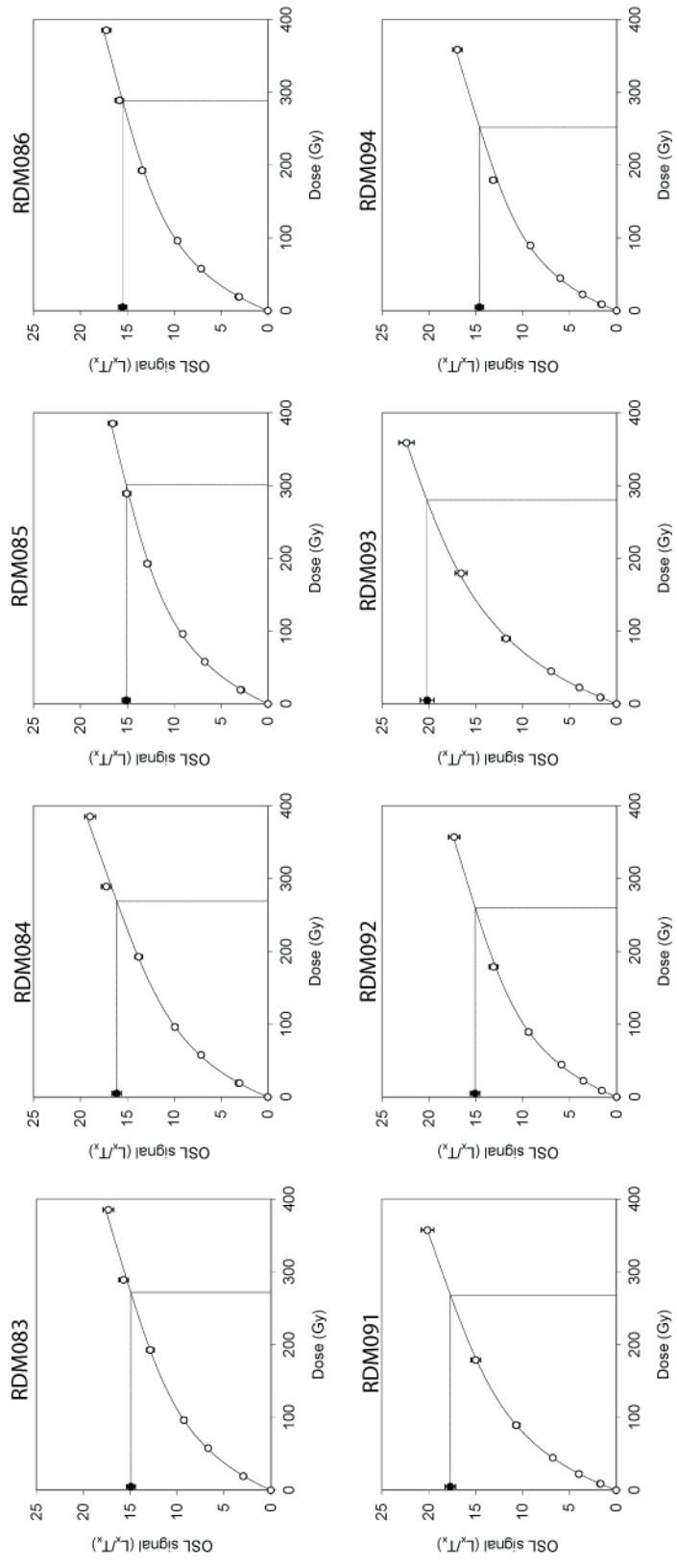

Figure 9.29 Typical growth curves produced from a single aliquot for each OSL sample. Black dot on y-axis indicates natural signal, lines intercepting growth curve indicate equivalent laboratory dose.

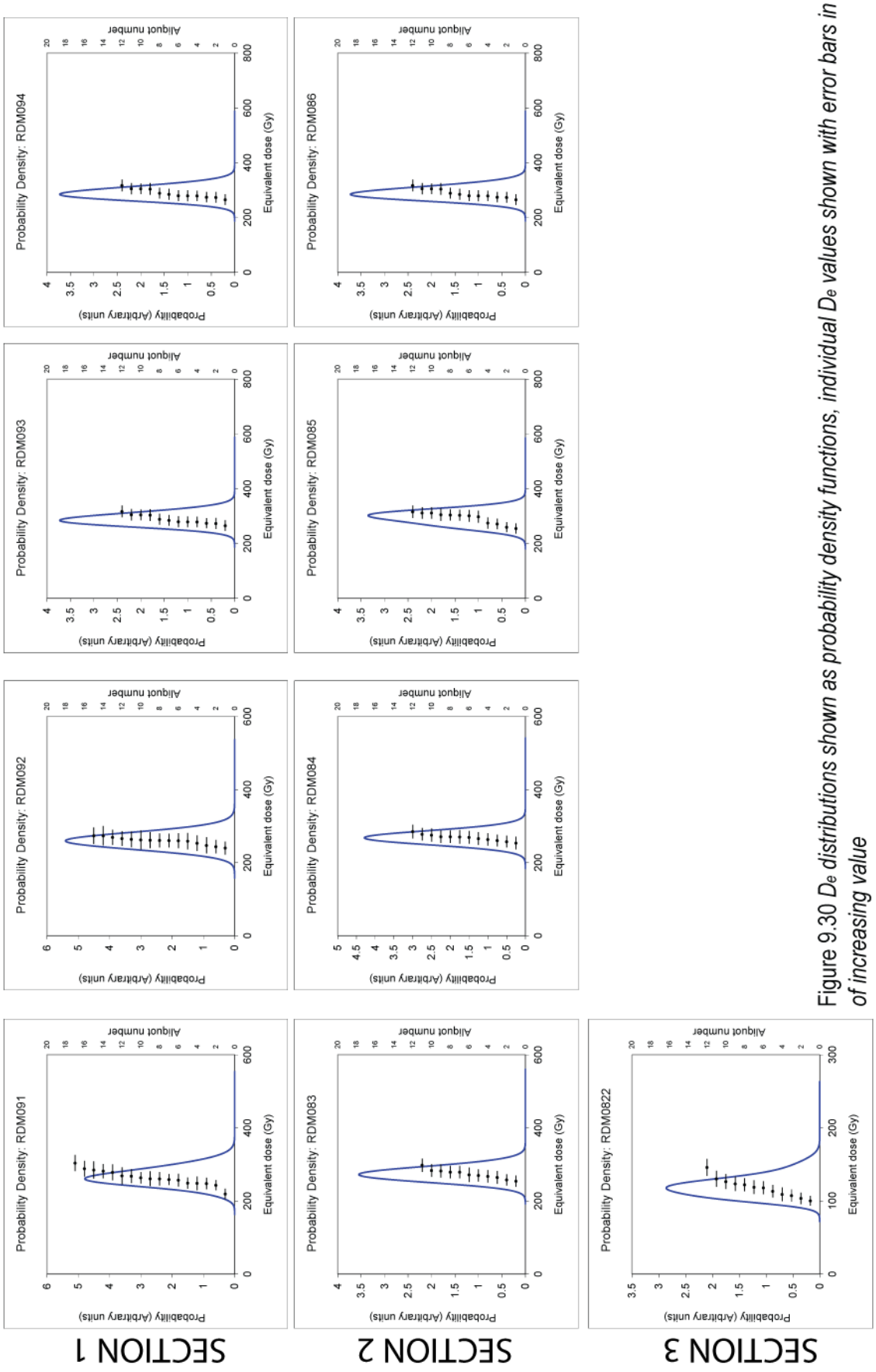

Figure 9.30 *De distributions shown as probability density functions, individual De values shown with error bars in order of increasing value*

9.8.2 U-series dating of section 1

One U-series age was calculated from an oncoid sampled from unit 3 of section 1. The age of 115 ka ±9 was produced by Ian Candy at RHUL. Age estimates are given relative to stratigraphy below.

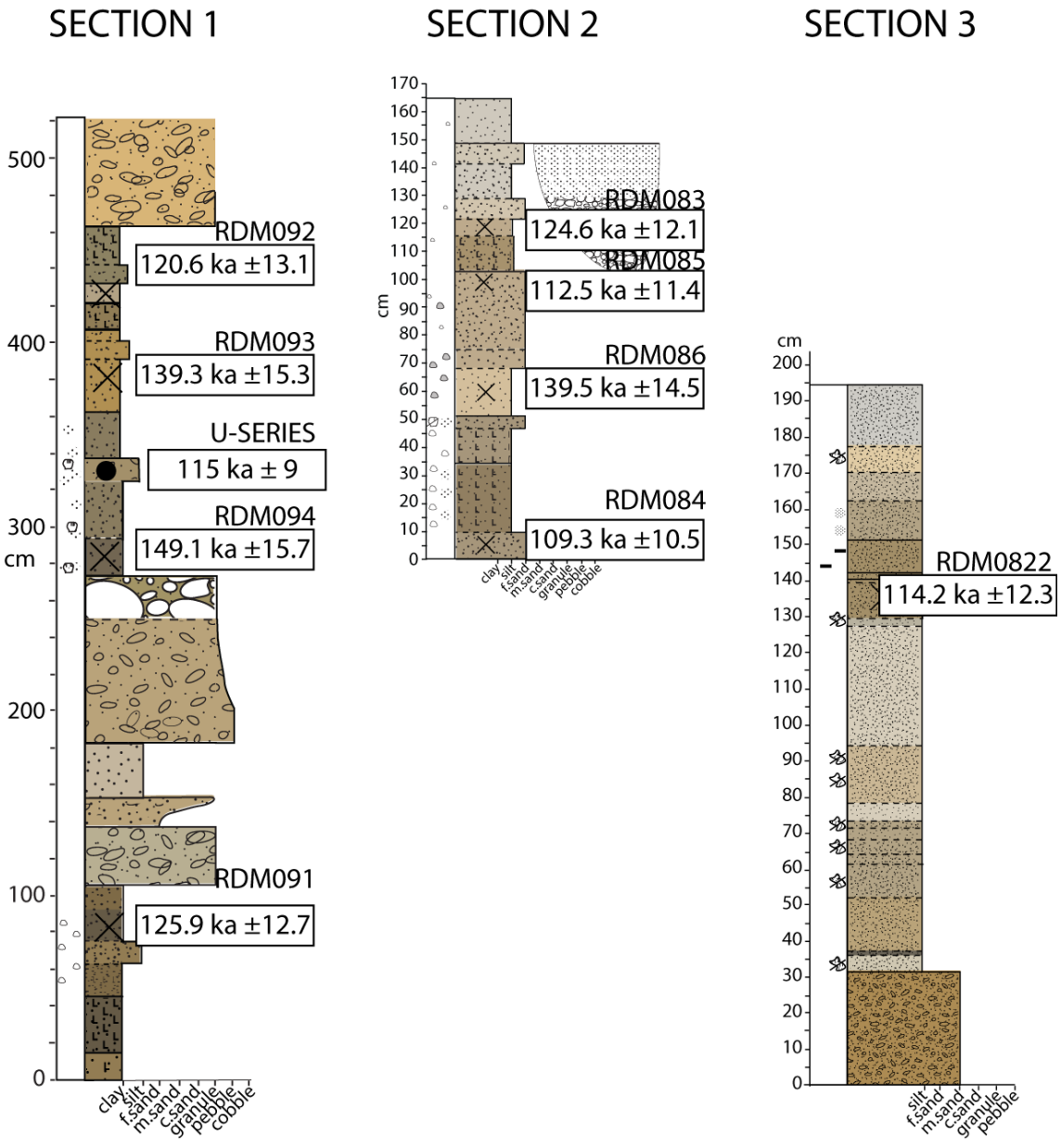

Figure 9.31 Age estimates plotted against stratigraphy for sections 1-3.

9.9 Pedo-sedimentary depositional models

9.9.1 Section 1

Pedo-sedimentary evolution of section 1 sediment sequence shown in figure 9.32.

Stages 1-3: During deposition of unit 1, there is evidence to support three periods of sediment accumulation. Between each accumulation episode a short lived period of land surface stability occurs, allowing for partial decalcification of the upper sediments and redistribution of carbonate downwards, occurring as calcitic pedo-features.

Stage 4: Deposition of fluvial sediments.

Stage 5: A return to floodplain deposition, possibly associated with very partial decalcification of the upper horizon and downward transport of carbonate.

Stage 6: Deposition of the clast supported oncoids bed.

Stage 7: Return to floodplain deposition. Occurrence of calcitic pedo-features increases upwards through the sediments, suggesting accretionary pedogenic modification during deposition.

Stage 8 and 9: Accumulation of loessic sediments. Consistent presence of calcitic-pedo-features in thin sections supports some accretionary pedogenic modification. A decalcified upper horizon marked by darkened, clay enriched sediments indicates pedogenic modification of the sediments occurring at a stable land surface. This decalcification of the upper horizon resulted in significant enrichment in the occurrence of calcitic-pedo-features at 15-25 cm depth below the upper horizon.

Stage 10: Return to loessic accumulation. The presence of calcitic pedo-features indicates accretionary modification during deposition.

9.9.2 Section 2

Pedo-sedimentary model shown in figure 9.33.

Stage 1: Floodplain accumulation of sediments. Occurrence of calcitic pedo-features increases upwards through the sediments, indicating increasing modification of accretionary pedogenesis during accumulation. Increasing accretionary modification could be due to increasingly favourable climatic conditions or due to reducing sediment accumulation rates.

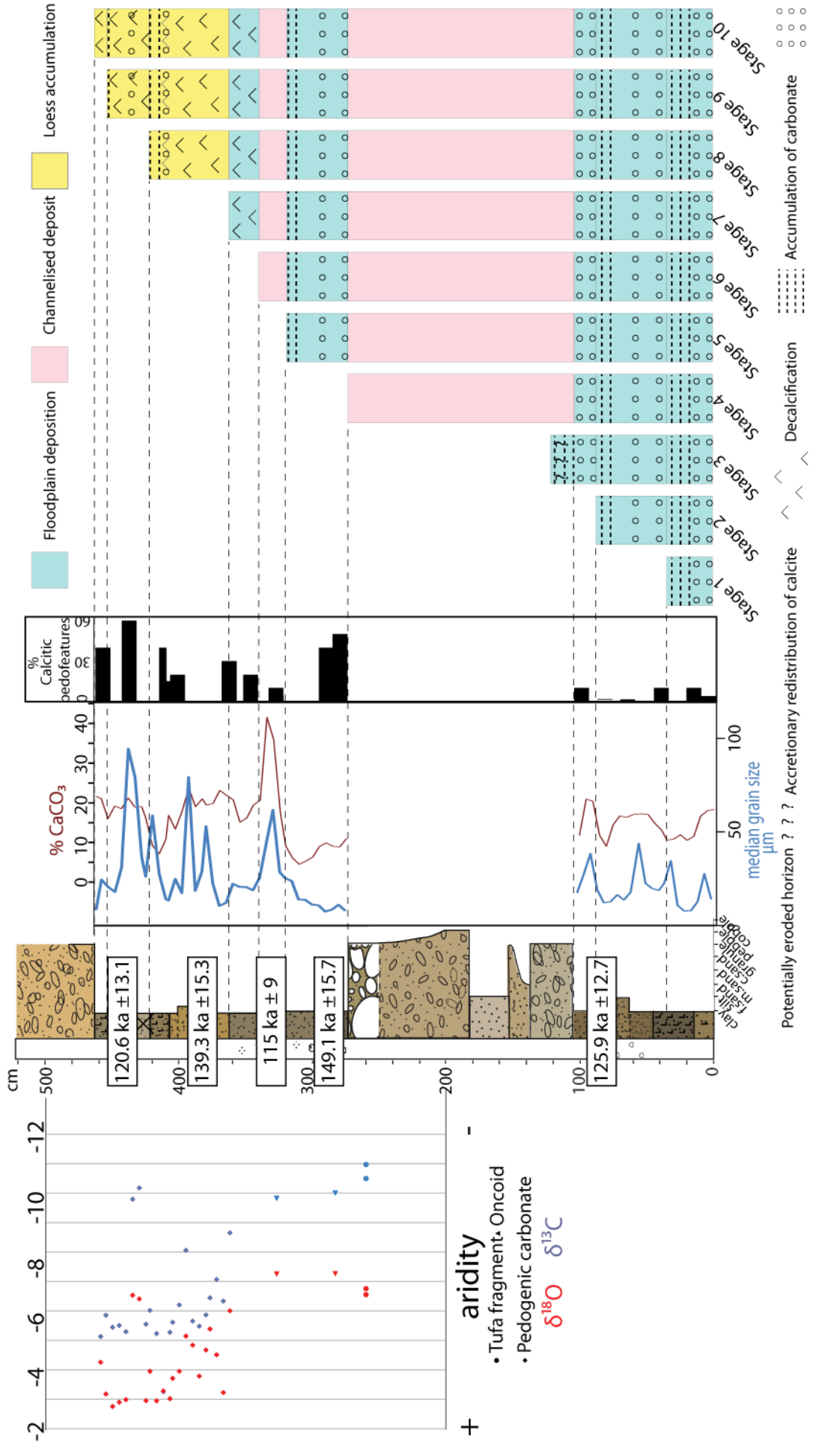

Figure 9.32 Pedo-sedimentary model of deposition and alteration of sediments within section 1

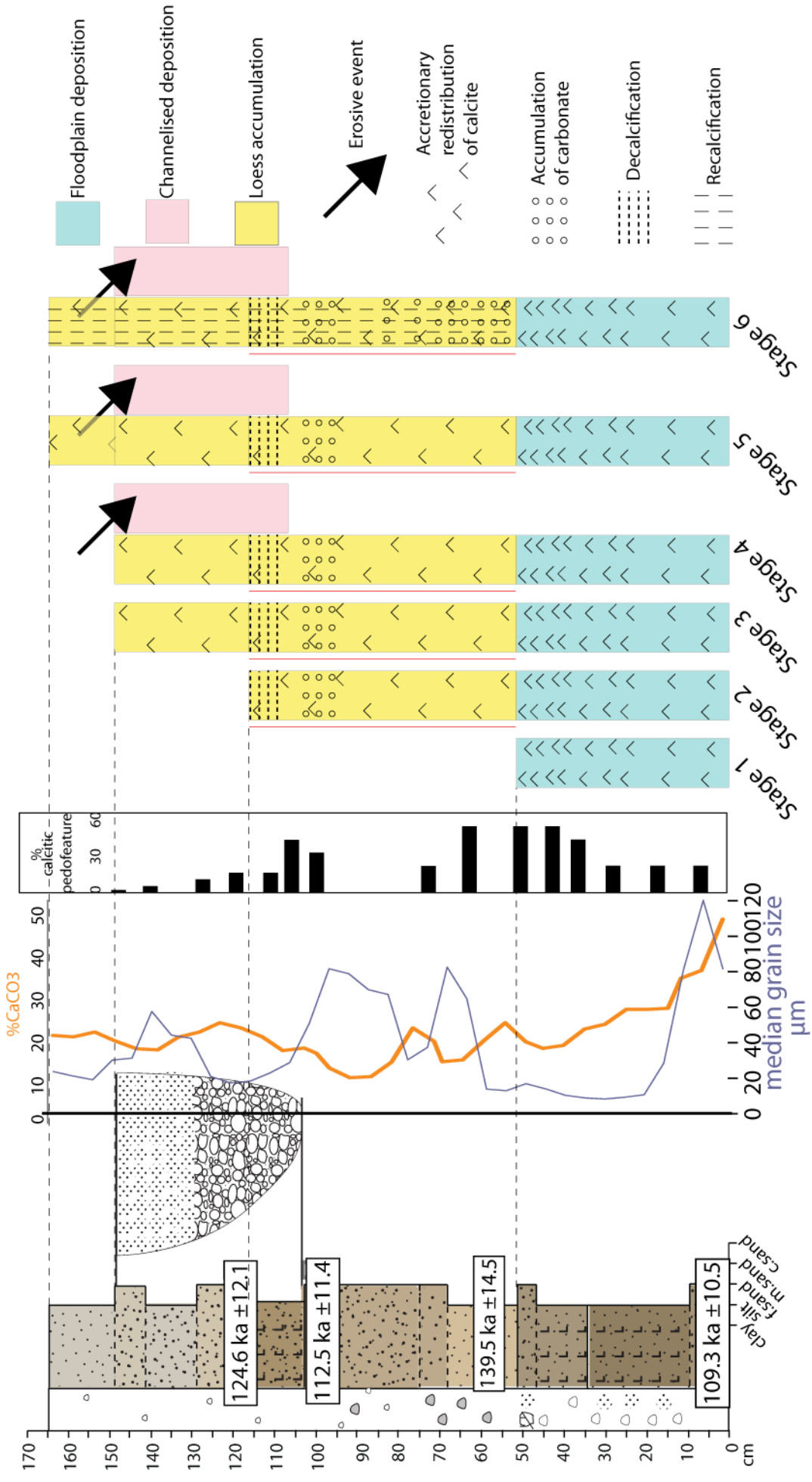

Figure 9.33 Pedo-sedimentary model of deposition and alteration of sediments within section 2. Red line indicates assumed series of events.

Stage 2: Loessic accumulation. As the sediments through section 1 were subject to accretionary pedogenic modification it is assumed that this would also have affected the sediments of section 2. It is also assumed that the darkened horizon (100-115 cm) would have formed during a period of land surface stability, resulting in some decalcification of the upper horizon and redistribution of carbonate below.

Stage 3: Loessic accumulation with assumed accretionary pedogenic modification.

Stage 4: The stratigraphy of the section makes it clear that unit 3 cuts into unit 2. Therefore an erosive event removed sediments to the right of the section, cutting down through unit 2 and resulting in the deposition of unit 3.

Stage 5: A return to loessic accumulation, with assumed accretionary pedogenic modification.

Stage 6. Re-calcification of the sediments from a source above the section. This period of re-calcification is marked by the sustained down-washing of carbonate, resulting in the formation of a nodular horizon towards the base of unit 2 and overprinting the original pedogenic alteration of the sediments.

9.10 Palaeoenvironmental significance

The palaeoenvironmental significance of the sequences at Maro will be discussed only briefly in this section. A full examination of the significance of the sediments and the proxy records derived from them will be dealt with in discussion chapters 10-13.

Due to the large uncertainties associated with the OSL age estimates produced for Maro, the chronologies for each section are not capable of constraining the timing of deposition of individual units or for identifying specific intervals of sediment accumulation. The ages produced however, are all consistent with the sediments at all three sections being of MIS 6 to MIS 5 age (see figure 9.34).

The lowest unit within the valley is section 3. This extensive tufa formation is located south of the loessic sequences, towards the Mediterranean Sea at a height of 10.15 m above current sea level. As previously discussed, tufa formation is often linked with interglacial conditions requiring landscape stability and high vegetation levels (Goudie *et al.* 1993, Domínguez-Villar *et al.* 2011, Pedley 2009, Martín-Algarra *et al.* 2003). Indeed, the isotopic composition of the sediments from section 3 indicates that climate during formation was similar to that recorded by the active tufa system within the valley. Therefore, given the stage 5 OSL age derived from the sediments and the apparent interglacial stable isotopic composition of the tufa, section 3 is interpreted as

representing tufa formation during MIS 5e. The presence of a large tufa system during this period supports the evidence presented by palynological and geomorphological studies which suggest that MIS 5e was marked by forested conditions and stable land systems (e.g. soil formation) within the region (e.g. Sánchez Goñi *et al.* 2008 and Rose *et al.* 1999) (figure 9.35).

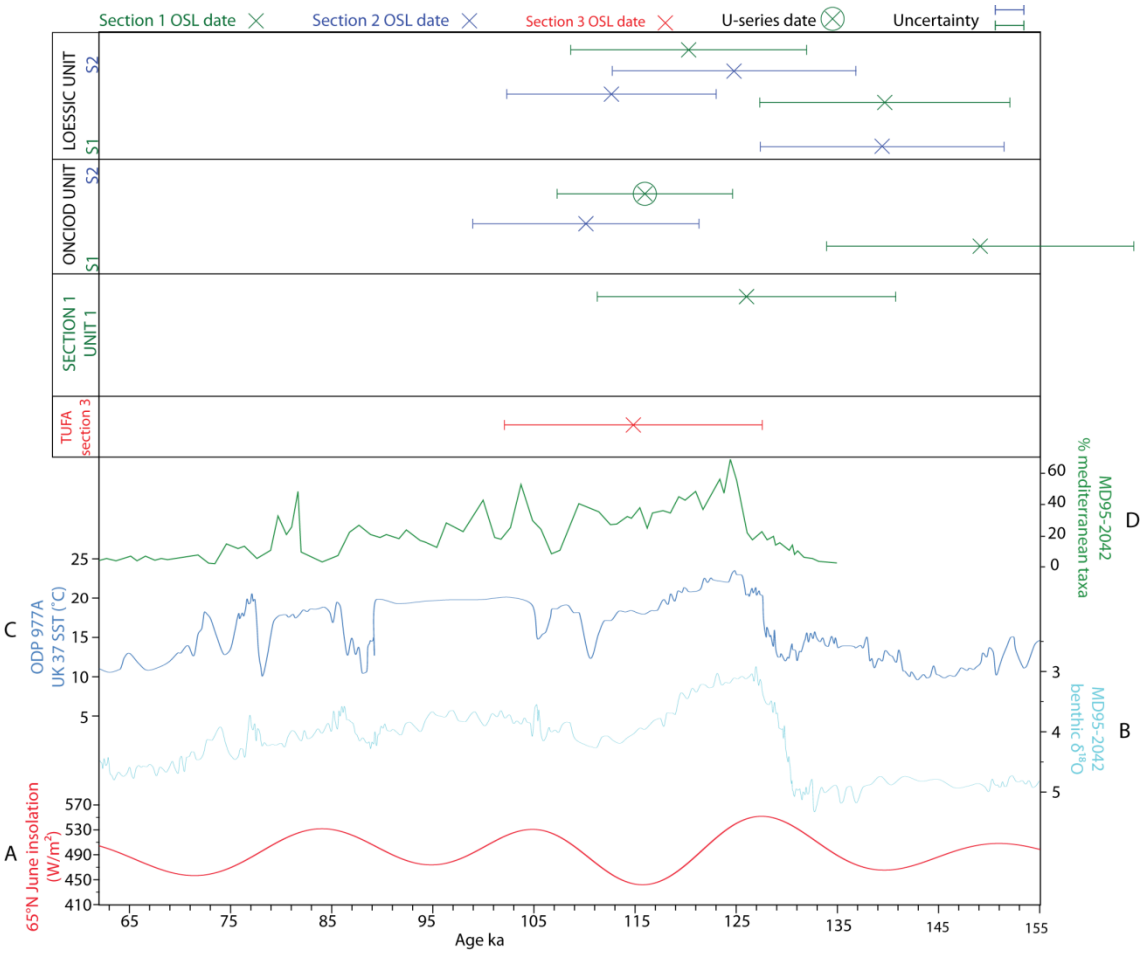

Figure 9.34 Comparison of Maro section chronologies against records of stage 5 insolation, Mediterranean Sea records and western Mediterranean vegetation composition. A. Insolation curve for June 65oN (W/m2) redrawn from Laskar et al. (2004). B. MD95-2042 benthic d18O record redrawn from supplementary data of Martrat et al. (2004). C. ODP-977A alkenone derived SST record from the Alboran Sea, redrawn from supplementary data of Martrat et al. (2004). D. MD95-2042 Portuguese margin record of Iberian pollen variations redrawn from Sánchez Goñi et al. (2008).

The basal units of section 1 (units 1 and 2) are records of sediment accumulation associated with floodplain and active channel conditions. These processes are not restricted to occurring within specific climatic intervals and as such, little palaeoclimatic information can be gained from their analysis. However, the basal floodplain sediments do seem to record repeated episodes of minor pedogenic alteration between depositional events. Such pedogenic activity may be indicative of accretion during a relatively mild climate. The clast supported sediments of unit 2 contain large, well preserved tufa fragments. The presence of these fragments indicates local reworking of interglacial tufa sediments. However, the isotopic composition of the fragments is significantly

enriched with regards to ^{18}O compared to the modern and MIS 5e tufa fragments (figure 9.25). This isotopic enrichment suggests that they formed during different climatic conditions (e.g. Andrews 2006) compared to the other tufas analysed and as such, most likely represent reworking of tufa sediments formed during a previous, unknown interglacial. Given the OSL date calculated for the basal sediments (125.9 ka ±12.7), it is possible that the sediments represent deposition in late MIS 6 or early MIS 5 (figure 9.35).

The oncoidal beds are the first sediments within section 1 and 2 from which there is a clear palaeoclimatic indicator. The presence of an *in-situ* oncoid horizon, noted as the clast supported oncoid bed present within section 1 demonstrates active tufa formation during the accumulation of the sediments. In order for such tufa clasts to form Pedley (1990, 2009) states that the channel is required to be stable, with a low sediment load and of relatively low energy. It is important that there is a low sediment yield as otherwise carbonate coating of clasts would be prevented, additionally it is necessary that clasts can be rolled occasionally to become fully coated but not removed from the system prior to complete coating. Therefore, oncoid formation requires the same landscape stability necessary for the production of larger scale tufa features.

The isotopic composition of the oncoid clasts compare closely with values derived from the MIS 5e tufa (section 3) and from the Holocene tufa supporting an interglacial origin for the sediments. The environmental requirements, isotopic composition and OSL age for the units (figures 9.31 and 9.34) support an MIS 5e correlation for the oncoidal units. Within the thin sections there is however, evidence to suggest only moderate levels of pedogenic modification of the sediments. This is contrary to the evidence of well-developed palaeosol horizons being associated with MIS 5e (e.g. Rose *et al.* 1990). It is suggested that the sediments at Maro were part of an actively accumulating floodplain sequence, subjected to periodic inflows of sediments. This active accumulation prevented significant modification of sediments even during full interglacial conditions (figure 9.35).

The floodplain sediments are overlain by loessic accumulation at both section 1 and section 2. Within the Mediterranean, loess accumulation is often associated with localised silt deflation occurring during the last glacial (e.g. Garcia *et al.* 2011 and Günster *et al.* 2001). At Maro, however, chronological constraints on the timing of accumulation places deposition within stage 5. Additionally, the composition of the sediments (chapter 6) indicates that the sediments are not wholly locally derived, but may have a significant far travelled component. Accumulation of loess during stage 5 indicates a period in which local conditions were very different from those during the full interglacial. As outlined in chapter 3, dust supply needs to be relatively high in order for loess to accumulate (Tsoar and Pye 1987), but vegetation levels are a significant control where

steppic type vegetation would act as a dust trap, whereas dense vegetation would result in dust being incorporated into soils (Tsoar and Pye 1987, Pye and Tsoar 1987, Pye 1995). Full interglacial conditions in Southern Spain are thought to be associated with forested conditions (Shackleton *et al.* 2000), therefore a significant reduction in vegetation cover from interglacial conditions would be required to make the landscape suitable for loess to accumulate.

In order for loess accumulation to occur there would need to be a large shift in conditions from those recorded within the MIS 5e floodplain below. There would need to be a large reduction in vegetation cover in order for sediments to be mobilised and in order for deposited silts to be trapped but not incorporated into soils (chapter 3). Within Mediterranean settings a reduction in vegetation cover is likely to be related to a reduction in effective precipitation (e.g. Prentice *et al.*1992, chapter 2). Therefore, the accumulation of loessic sediments at Maro occurred in association with periods of reduced vegetation cover during stage 5. As shown in figure 9.34, there is a trend towards steppic vegetation cover recorded in Iberia associated with the decline in peak interglacial conditions of MIS 5e, this trend towards declining forest conditions peaks in association with stadial events 5d and again at 5b.

The pedo-sedimentary histories of section 1 and section 2 are very different, however, and this affects that palaeoclimatic information recorded by the two sections. Through section 1 bulk sedimentology and micromorphology indicates predominantly accretionary pedogenic modification, resulting in the isotopic composition of soil carbonated through the section reflecting climate during accumulation of the sediments. The strong covariance of $\delta^{18}O$ and $\delta^{13}C$ values of pedogenic carbonates through section 1 demonstrates an evaporation driven system. The general trend towards isotopically lighter values upwards through the sequence indicates deposition under increasing arid conditions. There are, however, two exceptions to this general trend. Within the sequence there are two weak soil horizons which have resulted in downward leaching of carbonate during stable land surface conditions, resulting in enrichment of carbonate 15-25cm below the soil. The carbonates found within these horizons reflect the climate of the soil forming intervals, with the isotopic composition of the carbonates giving relatively depleted $\delta^{13}C$ and $\delta^{18}O$ values, indicating a less arid climate. Although the chronology of the sequence does not allow for the timing of accumulation or soil forming intervals to be constrained, the sequence does record strong aridity post MIS 5e. This arid, loessic accumulation period was marked by two significant climate variations, during which conditions were significantly less arid. This reduction in aridity appears to have been associated with reduced sediment input resulting in the formation of a stable land-surface and the onset of post-depositional pedogenic alteration.

Through section 2 there is significant overprinting of carbonate through sustained downward leaching from overlying sediments. Therefore, the isotopic record through section 2 reflects a period of alteration occurring sometime after deposition of the loessic sediments. As the overlying horizon appears to be a calcrete forming at the land-surface it is likely that this subsequent alteration occurred during the Holocene. There is however, still important palaeoclimatic evidence contained within section 2. Unit 3 is a clast supported oncoid channel which has cut down through the loessic sediments of unit 2, above the oncoid filled channel feature, deposition returns to loessic accumulation. This sequence of events therefore represents loessic accumulation during arid conditions occurring post MIS 5e, then a shift to less arid conditions. The onset of less arid conditions appears to be marked by the down-cutting of a relatively high energy channel recorded through the deposition of a clast supported pebble bed. The sedimentology then records a shift to oncoid formation, through the preservation of a clast supported oncoid bed, indicating stable land-surface conditions. The sediments of unit 3 and then overlain by loessic sediments, marking a return to arid conditions.

There is evidence within southern Spain that tufa systems can become active again during the interstadials of stage 5 (MIS 5c, 5a) (Domínguez-Villar *et al.* 2011, Martín-Algarra *et al.* 2003), where vegetation must recover close to interglacial values in order to facilitate tufa formation. Sánchez Goñi *et al.* (2008) suggest that Iberian vegetation was unstable during MIS 5c and 5a, although values do recover close to peak interglacial % forest conditions. Therefore, it is likely, that at Maro the second occurrence of oncoid formation represents formation during and interstadial of stage 5.

Section/Unit	Sediments and soil properties	OSL ages (ka)	Climate	Environment	Landscape stability	MIS
unit 2, section 2	Loess accumulation	< ages below	Arid-cool	Return to far travelled loess accumulation	Unstable	MIS 5b?
unit 3, section 2	Clast supported oncoid filled channel feature	< ages below	Warm - moist	Sustained landscape stability with high vegetation cover.	Stable	MIS 5c?
unit 4, section 1 unit 2, section 2	Loess accumulation with accretionary pedogenic alteration. Two episodes of moderate post-deposition alteration present, recorded as partically decalcified, clay enriched horizons.	112.5 ± 11.4 ka 120.6 ± 13.1 ka 124. 6 ± 12.1 ka 139.3 ± 15.3 ka 139.5 ± 14.5 ka	Loess: Arid - cool Soils: Moist-warm	Far travelled loess accumulation during period of aridity and reduced vegetation cover. Punctuated by two episodes of reduced sediment supply associated with moister conditions resulting in soil formation	Loess: unstable Soils: stable	MIS 5d?
unit 3, section 1 unit 1, section 2 section 3	Oncoid beds with moderate pedogenic alteration Tufa	109.3 ± 10.5 ka 115.0 ± 9 ka (U-series) 149.1 ± 15.7 ka 114.2 ± 12.3 ka	Warm - moist Warm - moist	Multiple tufa systems present. Sustained landscape stability with high vegetation cover.	Stable Stable	MIS 5e
unit 1, section 1 unit 2, section 1	Floodplain sediments with minor pedogenic alteration. Overlain by clast supported cobble beds	125.9 ± 12.7 ka		Migration of a bradied river system from distal to proximal position over site of deposition		MIS 6?

Figure 9.35 Compilation of palaeoclimatic data derived from the sediment sequences at Maro

Chapter 10 – The palaeoclimatic potential of the stable isotopic composition of soil carbonates in loess-palaeosol sequences

This discussion chapter outlines both the importance of loess-palaeosol sequences as palaeoenvironmental archives and the potential of analysing the isotopic composition of soil carbonates commonly found within these sequences. An outline of the current understanding of controls on the isotopic composition of soil carbonates within the Mediterranean and mid-latitudes is presented and how the results gained from Maro and Chimeneas fit in with current understanding. The discussion focusses on the importance of the record presented from Chimeneas and how this study changes our understanding of the controls on the isotopic composition of Mediterranean soil carbonates.

10.1 Introduction

Thick loess accumulations are widely used as sedimentary records of Quaternary climate changes and associated geomorphic response over both Milankovitch and sub-Milankovitch timescales (Kukla, 1987, Vandenberghe *et al.* 1998, Rousseau *et al.* 2002, Frenchen *et al.* 2003, Moine *et al.* 2008, Markovíc *et al.* 2011). Bulk sedimentological proxies such as grain size, magnetic susceptibility and calcium carbonate content are commonly used to identify shifts between loess accumulation and pedogenic alteration. Typically periods of loess accumulation are associated with glacial climates and pedogenic alteration occurring during cessation of sediment input in interglacial climates (Dearing *et al.* 2001, Muhs and Bettis 2003, Markovíc *et al.* 2011). However, micromorphological analysis of loess-palaeosol sequences identified a more complex pedo-sedimentary balance (e.g. Kemp *et al.* 1996). Kemp (1995, 1999, 2001) identified the existence of two styles of pedogenic alteration; syn-depositional (alteration during accumulation) and post-depositional (alteration at a stable land surface). The style of pedogenic alteration is often recorded through the distribution and morphology of calcitic pedo-features. As such, the distribution of pedogenic carbonates can provide important information on the pattern and style of loess accumulation. The $\delta^{18}O$ and $\delta^{13}C$ values of soil carbonate are widely used as a palaeoenvironmental indicator; however, this has rarely been applied to loess profiles. The isotopic composition of soil carbonates formed in loess are therefore capable of recording conditions during loess accumulation and/or during alteration at a stable land-surface. The work presented in this thesis highlights the importance of understanding the origin of the signal

contained within soil carbonates of loess-palaeosol sequences through the construction of pedo-sedimentary models developed via micromorphological and bulk analysis of sediment characteristics.

10.2 Controls on isotopic composition of soil carbonates

Soil carbonates are commonly found within loess-palaeosol sequences (Becze-Deák *et al*. 1997, Jiamao *et al.*1997, Kemp 1995) and it has previously been demonstrated that both the oxygen and carbon isotopic composition of soil carbonates are important palaeoclimatic proxies (e.g. Cerling and Quade 1993). All isotope values are reported relative to V-PDB unless otherwise stated. The origin of the carbon and oxygen isotope signal is discussed below.

10.2.1 Carbon isotopes

As discussed previously (chapter 4), $\delta^{13}C$ values of soil carbonates are controlled by the $\delta^{13}C$ composition of the soil atmosphere, which is a product of plant respiration (Quade *et al.* 1989b). The soil atmosphere CO_2 $\delta^{13}C$ values under dominantly C3 or C4 photosynthetic pathways will be -23 to -27‰ or -10 to -13‰ respectively (Cerling *et al*. 1989, Quade *et al.* 1989b, Cerling and Quade 1993). Gaseous diffusion and temperature controlled fractionation during calcite precipitation result in an enrichment of 14-15‰ (Quade *et al.* 1989b, Cerling and Quade 1993). Therefore $\delta^{13}C$ values of soil carbonates under C3 photosynthetic vegetation will be around -8 to -12‰ and those formed under C4 photosynthetic vegetation will be around 1 to 4‰ (Cerling and Quade 1993, Wang and Greenberg 2006).This technique has been used within the Chinese Loess Plateau in order to investigate vegetational shifts occurring in association with monsoonal changes through the Quaternary (Frakes and Jianzhong 1994, Wang and Zheng 1989, Sun *et al.* 2012, Yang *et al.* 2012).

10.2.2 Oxygen isotopes

At mid-latitudes the $\delta^{18}O$ of soil carbonates has been shown to be closely related to mean annual temperature during the time of precipitation (Cerling 1984, Candy *et al*. 2011). $\delta^{18}O$ values of soil carbonates result from the composition of soil moisture and the fractionation of calcite during precipitation, both of which are controlled by temperature (Dansgaard 1964, Rozanski *et al.* 1993, Cerling and Quade 1993, Hays and Grossman 1991). The combined effect of these two controls means that in a system responding solely to mean annual temperature a $1^{o}C$ rise in temperature should result in an increase of ~0.3‰ in the $\delta^{18}O$ value of a soil carbonate (Candy *et al*. 2011).

There are however, a number of factors that can influence the $\delta^{18}O$ of soil moisture and these require further discussion.

10.2.3 Mediterranean soil carbonates

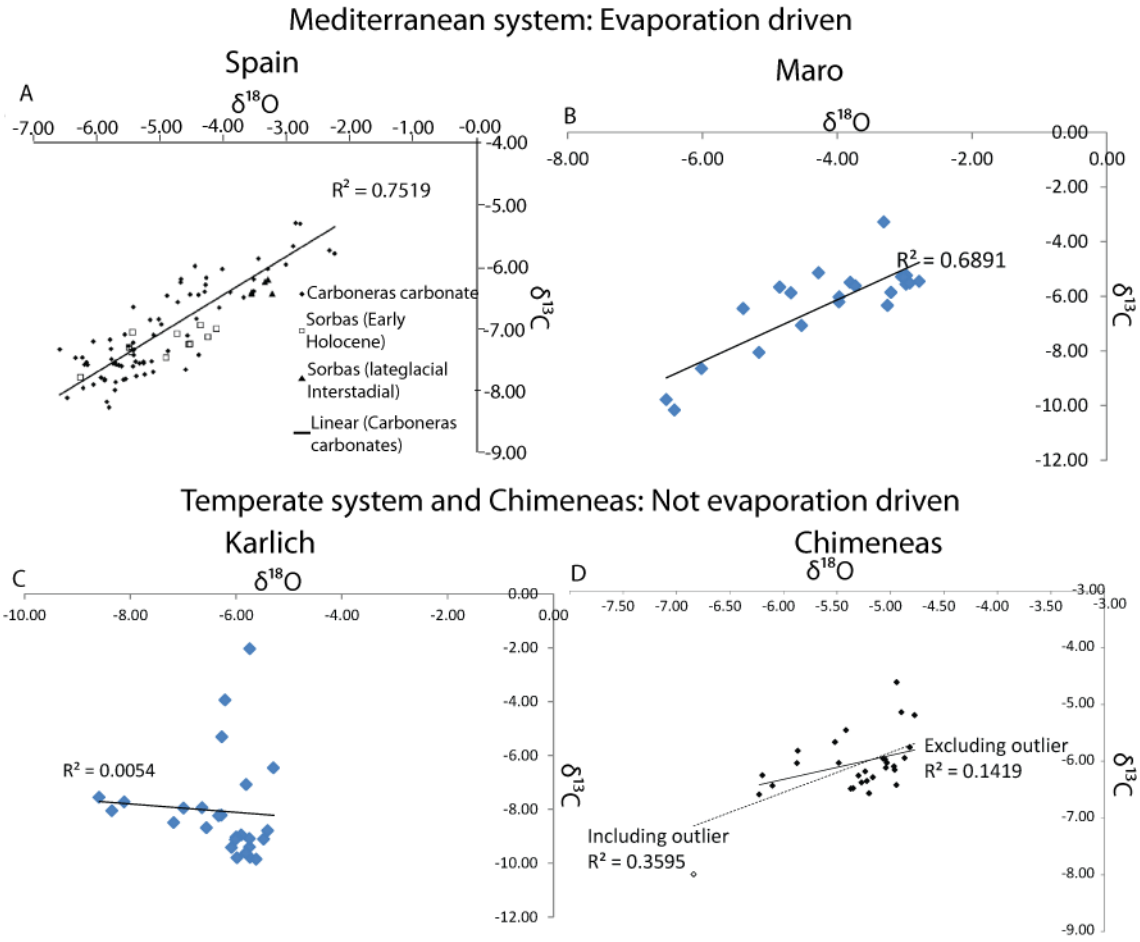

Figure 10.1 Comparison of typical Mediterranean (evaporation driven) and temperate (temperature driven) region $\delta^{18}O$ and $\delta^{13}C$ values with those from Maro and Chimeneas. A. Soil carbonate composition from Sorbas and Carboneras, Spain (Candy et al. 2012), B. Values from Maro (chapter 9), C. Values from the Kärlich loess-palaeosol sequence (Candy et al. 2012, Gallant et al. in prep.), D. Chimeneas values (chapter 8)

It has recently been demonstrated that the isotopic composition of Mediterranean meteoric carbonates is driven by evaporation (Candy *et al.* 2012). Candy *et al.* (2012) compiled an extensive dataset of oxygen and carbon isotope values of meteoric carbonates from the Mediterranean (southern Spain and Greece) and compared them with isotope values from temperate European meteoric carbonates (Britain and Germany). This comparison revealed that carbon and oxygen isotope values of Mediterranean meteoric carbonates forming during glacial (stadial and interstadial) and interglacial periods displayed strong covariance (figure 10.1a), whereas those from temperate climates displayed negligible covariance (figure 10.1c). Candy *et al.* (2012) suggest that the covariance of Mediterranean values demonstrates that both carbon

and oxygen isotope systems are being driven by the same environmental factor; evaporation. Increasing environmental aridity results in increased evaporation of soil moisture leading to enrichment with ^{18}O through preferential loss of light $H_2{}^{16}O$ (Dever *et al.* 1987, Quade *et al.* 1989b, Ufnar *et al.* 2008) and enrichment with ^{13}C via preferential degassing of $^{12}CO_2$ (Dever *et al.* 1987) and increasing atmospheric CO_2 contribution due to reduced vegetation cover (Quade *et al*. 1989b; Cerling and Quade, 1993).

10.3 Maro

As shown in figure 10.1b there is a strong covariance between $\delta^{18}O$ and $\delta^{13}C$ values of soil carbonates at Maro, indicating a typical Mediterranean signal driven by evaporative processes. The record from Maro indicates shifting aridity through Stage 5. With the most depleted values relating to tufa deposition within MIS 5e indicating humid conditions (figure 10.2). The loess-palaeosol sequence at Maro deposited during the sub-stages of MIS 5 indicate increased aridity associated with loess deposition and relative humidity associated with carbonates formed during post-deposition alteration of the sediments at a stable land surface (figure 10.2).

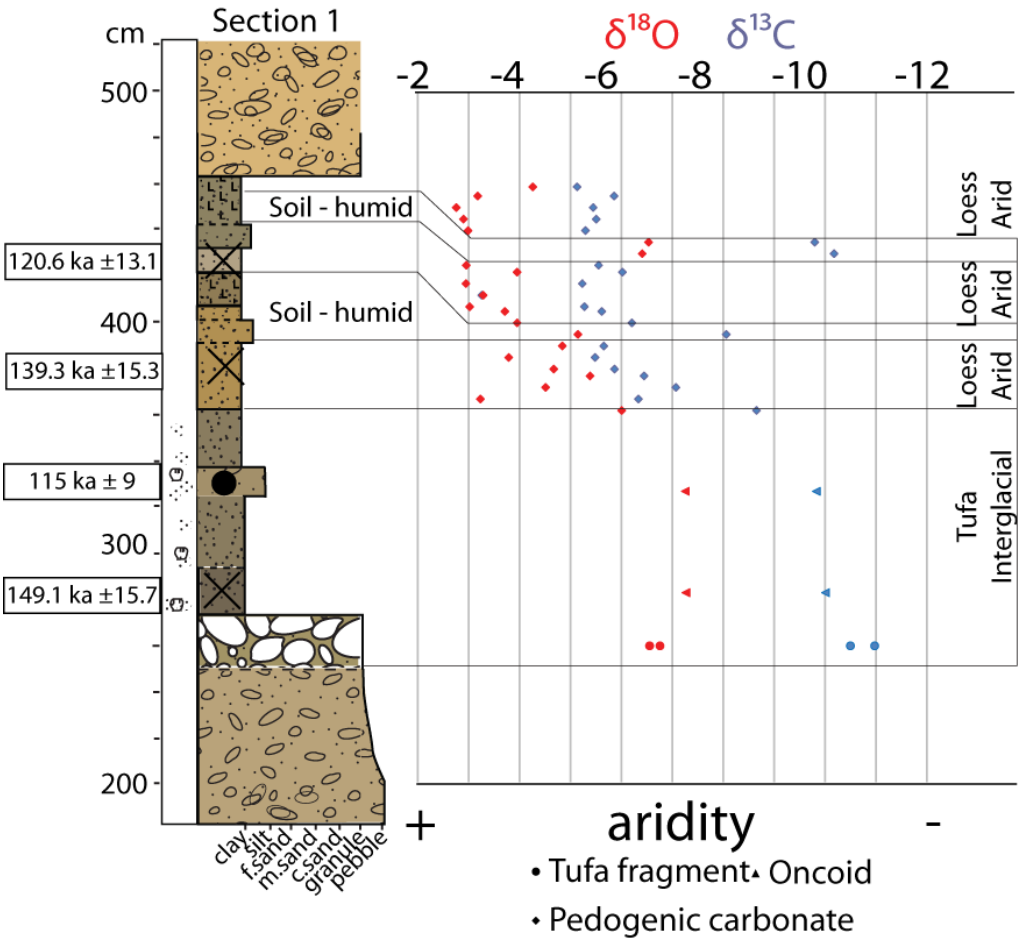

Figure 10.2 Oxygen and carbon isotope values from section 1, Maro

Although stage 5 loess has been identified previously within the western Mediterranean (Rose *et al.* 1999), the isotope record at Maro provides the first proxy record of shifting aridity during stage 5 through loess accumulation and pedogenic alteration.

10.4 Chimeneas

Contrary to our current understanding of environmental controls on the $\delta^{18}O$ and $\delta^{13}C$ values of Mediterranean soil carbonates, this thesis has demonstrated that not all Mediterranean soil carbonates record covariance between oxygen and carbon isotopes. This can be seen in the Chimeneas sequence. The lack of covariance at this site indicates that the two isotope systems are driven by different environmental factors. As such, this thesis provides a unique record of the isotopic composition of Mediterranean soil carbonates in a system where evaporation is not the dominant environmental control.

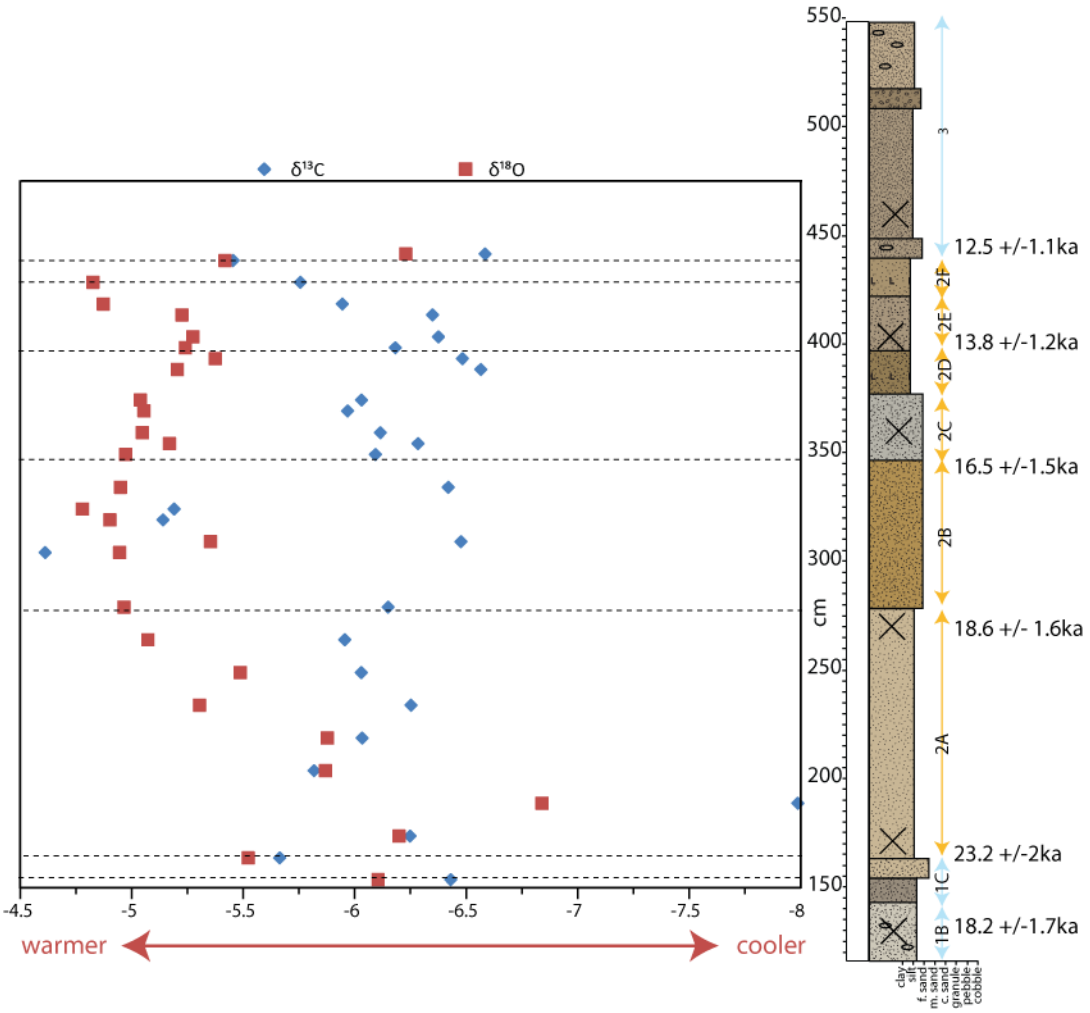

Figure 10.3 Isotopic composition of soil carbonates from Chimeneas

10.4.1 $\delta^{13}C$ composition of soil carbonates

The $\delta^{13}C$ values from Chimeneas range from -7.99 to -4.61‰, which is more enriched than values produced by soil carbonates formed under a purely C3 photosynthetic vegetation (Quade *et al.* 1989b, Cerling and Quade 1993, Wang and Greenberg 2006). There is however, no evidence of C4 photosynthetic vegetation in southern Spain through the Quaternary (Quade 1994, Cerling *et al.* 1997, Woodward *et al.* 2004) and so it is likely that enrichment of $\delta^{13}C$ values relates to an increased contribution of atmospheric CO_2 to the soil environment (Quade *et al.* 1989b, Candy *et al.* 2012). Such values indicate soil carbonates forming under low vegetation levels where there is increased gaseous exchange with the atmosphere (Quade *et al.* 1989b).

10.4.2 $\delta^{18}O$ composition of soil carbonates

The lack of covariance in the isotope values from Chimeneas soil carbonates indicates that oxygen and carbon $\delta^{18}O$ values are not being driven by evaporation. If evaporation is discounted, the $\delta^{18}O$ signal is most likely to be driven by changing soil moisture composition as a result of changing composition of precipitation. There are a number of factors which can influence the $\delta^{18}O$ of soil moisture and soil carbonates which need to be discussed in order to clarify the origin of the $\delta^{18}O$ values recorded at Chimeneas. Firstly, the oxygen isotopic composition of the soil carbonates at Chimeneas will be discussed in terms of factors which can influence the $\delta^{18}O$ of precipitation. Secondly, the site specific conditions which may be responsible for the absence of an evaporation driven signal at Chimeneas will be discussed.

Controls on $\delta^{18}O$ value of precipitation:

- Changes in the ocean isotopic composition
- The ‘amount’ effect
- Change in moisture source
- Temperature

Site specific influences:

- Precipitation (seasonality and amount)
- Temperature
- Altitude

10.5 Composition of precipitation

The oxygen isotope composition of the oceans is known to vary in response to changing ice volume (e.g. Shackleton 1967). Therefore, a period such as the last glacial which experienced significant, and sometimes abrupt changes in ice volume (e.g. Lambeck *et al.* 2000, Clark and Mix 2002), would have also experienced significant changes in oceanic composition. At the last glacial maximum (peak ice volume) composition of the North Atlantic was up to 1‰ enriched in ^{18}O (Schrag *et al.* 2002) compared to Holocene values and the Mediterranean Sea was up to 1.2‰ enriched in ^{18}O (Paul *et al.* 2001). Changes in the composition of precipitation sources for Chimeneas can therefore account for a maximum of 1.2‰ change in $\delta^{18}O$. However, the oceans are enriched in ^{18}O at the last glacial maximum, with steadily decreasing $\delta^{18}O$ values towards the onset of the Holocene; this is the opposite of what is seen at Chimeneas. Therefore, changing composition of the oceans cannot account for the oxygen isotopic shifts recorded in the soil carbonates at Chimeneas.

The amount effect (Dansgaard 1964; chapter 4) describes a phenomenon in high rainfall regions (>2000 mm/yr) such as the tropics where $\delta^{18}O$ values vary with the amount of rainfall (Rozanski *et al.* 1993). This phenomenon has been invoked to explain $\delta^{18}O$ variations in the Soreq cave record (Bar-Matthews *et al.* 2000) based upon the modern relationship between $\delta^{18}O$ values of cave water and precipitation levels (Bar-Matthews *et al.* 1997), where more negative $\delta^{18}O$ values are correlated with higher rainfall. Therefore, warmer, wetter interglacials and interstadials are marked by depleted $\delta^{18}O$ values (Bar-Matthews *et al.* 1997, 2000). Evidence from the western Mediterranean however, indicates that the amount effect is not the primary environmental factor driving $\delta^{18}O$ values of precipitation (Mattey *et al.* 2008), and, unlike the eastern Mediterranean, no clear relationship between amount and $\delta^{18}O$ values exists. Mattey *et al.* (2008) suggest that based upon analysis of modern isotope data from Gibraltar $\delta^{18}O$ values of precipitation are driven primarily by temperature. As such, the amount effect can be discounted as being a driving factor of the record at Chimeneas.

The western Mediterranean weather is dominated by North Atlantic influence (Harding *et al.* 2009); however, precipitation in the region can be sourced from a number of regions (Cruz-San Julian *et al.* 1992). At present, winter precipitation in Iberia is sourced primarily from the North Atlantic and summer precipitation from within the Mediterranean region (Gimeno *et al.* 2010). Each of these source regions produces precipitation over Iberia with very different $\delta^{18}O_{SMOW}$ values; Atlantic precipitation -14.54‰, North African air masses with Mediterranean recharge -7.95‰ and eastern Mediterranean sourced precipitation -6.43‰ (Cruz-San Julian *et al.* 1992). It

has been suggested (e.g. Moreno *et al.* 2002, 2004) that through the Last Glacial there was a shift in precipitation source driven by changing strength of pressure systems in the North Atlantic in response to D-O climate cycles. If this proposed mechanism is correct, it would suggest that precipitation during the last glacial would have different composition during different climatic episodes. However, such changes in source region would not result in a progressive enrichment or depletion of $\delta^{18}O$ values, but rather a sudden shift. Such a response is not captured in the soil carbonate $\delta^{18}O$ record from Chimeneas, and as such, shifting precipitation source cannot be responsible for the isotopic shift recorded at Chimeneas.

As previously mentioned, there is a strong correlation between the $\delta^{18}O$ value of soil carbonates and mean annual temperature in mid-latitude regions (Cerling 1984). This relationship is due to the temperature dependent composition of precipitation and fractionation of soil moisture. There is a strong linear relationship between mean annual temperature and $\delta^{18}O$ of precipitation in mid-latitude regions (Dansgaard 1964, Rozanski *et al.* 1993), where a 1^{o}C increase in temperate results in an enrichment of ^{18}O by 0.6‰ (Rozanski *et al.* 1993). As precipitation is the source of soil moisture, the $\delta^{18}O$ value of the soil environment is also governed by this relationship. The composition of soil carbonates formed from soil moisture is then further modified by the temperature dependent fractionation of calcite during precipitation; where a 1°C temperature increase results in a depletion of $\delta^{18}O$ by -0.3‰ (Craig 1965, Hays and Grossman 1991, White et al 1999, Leng and Marshall 2004). The combined effect of these temperature dependent relationships means that for each 1°C temperature rise soil carbonates are enriched in ^{18}O by 0.3‰. Therefore, at a given study site where evaporation is discounted, soil carbonates formed under higher temperatures should have higher $\delta^{18}O$ values than soil carbonates formed in cooler conditions.

As all other drivers of precipitation composition changes have been discounted, the origin of the shifts in $\delta^{18}O$ at Chimeneas (chapter 8) must result primarily from temperature driven changes. As shown in figure 10.3 the oxygen isotope values from soil carbonates at Chimeneas record a progressive enrichment of 1.88‰ upwards through sub-unit 2A, this could represent a climatic amelioration of around 6°C. The $\delta^{18}O$ values from 2B through to the lower part of 2F provide a record of climate during the weak soil forming intervals, which appear to occur in temperatures similar to those recorded by the carbonates at the top of unit 2A. Soil carbonates from the top of 2F record a depletion of 1.41‰ (figure 10.3), which could indicate a temperature shift of around -5°C.

10.6 Site specific conditions

Candy *et al.* (2012) have previously stated that the isotopic composition of Mediterranean meteoric carbonates formed during both glacial and interglacial periods is driven by evaporation. This thesis has produced an isotopic record of last glacial soil carbonates at Chimeneas which suggests the theory of Candy *et al.* (2012) may not apply to all Mediterranean environments. A comparison of local conditions at Mediterranean sites where evaporative processes drive isotopic composition of soil carbonates with conditions at Chimeneas where composition appears driven by vegetation and temperature may help identify potential reasons for the existence of different controlling factors (table 10.1).

Table 10.1 Chimeneas data from Granada data, Sorbas/Carboneras data from Almeria, Maro data from Malaga (1971-2000, Agencia Estatal de Meteorologia.). Dry months calculated according to Baileys Indices (1979) cited by Dietz et al. (2004).

Site	m.a.s.l	Average temperature (˚C)			Total precipitation (mm)	# Dry months	Evaporation driven ^{18}O ^{13}C?
		Annual	Minimum	Maximum			
Sorbas/ Carboneras	21	18.7	14.3	23.1	196	3	Yes
Maro	16	18	13.1	22.9	524	3	Yes
Chimeneas	690	15.2	8.7	21.7	361	2	No

10.6.1 Precipitation amount and regime

Table 10.1 indicates that a similar precipitation regime exists in the three localities with 2-3 dry months occurring in the summer, where a dry month indicates a period where evaporation potential is greater than the precipitation total received. It is suggested that during the last Glacial the Mediterranean experienced increased seasonality of precipitation with a greater period of summer drought (Prentice *et al.* 1992). Climate models do not suggest that regional variations in precipitation regime were greater during the LGM than at present (Arpe *et al.* 2011). It is therefore assumed that the similarity between modern day precipitation seasonality at the three locations would exist through Late Quaternary changes in precipitation regime.

Modern precipitation levels at Chimeneas are between the extreme low of the Sorbas and Carboneras basins and the high coastal values at Maro (table 10.1). Through the last glacial it is suggested that there may have been an overall increase in the total amount of rainfall received in the region, but over a shorter season (Prentice *et al.* 1992 and references therein). As with changes in seasonality, climate models do not suggest large spatial variability in the total rainfall amounts (Arpe *et al.* 2011), although this could be a product of the coarseness of the models. It

has been suggested that the incursion of cold, arctic air masses into the Mediterranean during the last glacial associated with the southerly position of the polar front (chapter 2) could produce steeper vertical precipitation gradients, favoring precipitation at lower altitudes generally associated with warmer coastal positions buffered by sea temperatures (Kuhlemann *et al.* 2008). If the scenario suggested by Kuhlemann *et al.* (2008) is correct, then it would suggest that Chimeneas may have experienced reduced precipitation levels relative to coastal sites through the last glacial. This site-specific dryness would increase evapotranspiration potential at Chimeneas and means, if correct, that it is even more surprising that the isotope signal is not evaporation driven. As such, there is no evidence to suggest that seasonality and/or amount of precipitation is a viable mechanism for producing the regional variability in the controls on $\delta^{18}O$ and $\delta^{13}C$ values of soil carbonates during the Late Quaternary.

10.6.2 Temperature and Altitude

The greatest differences between the three sites are temperature and elevation, with Chimeneas being the highest and coolest site. These differences are due to adiabatic temperature changes (Barry and Chorley 2003) and increased distance from the Sea. There is a strong relationship between air temperature and evapotranspiration rates (Allen *et al.* 1998, Moratiel *et al.* 2010) and therefore Chimeneas has a lower evapotranspiration potential than the warmer, coastal sites.

During the last glacial, Alboran SSTs were significantly reduced (10-13°C) compared to modern day values (Cacho *et al.* 1999, Kuhlemann *et al.* 2008). These reduced sea temperatures would still have provided warmth to coastal sites compared to the interior regions, such as the glaciated Nevada range (Hughes *et al.* 2006) located close to the Granada basin. It is therefore proposed that Chimeneas would have experienced cooler conditions during the last glacial than the coastal sites contained within Candy *et al.* (2012). Lower temperatures would be associated with reduced evapotranspiration potential (Allen *et al.* 1998, Moratiel *et al.* 2010) and therefore evaporation rates may not have been high enough to be the dominant environmental factor controlling the isotopic composition of soil moisture at Chimeneas.

It is suggested however, that some soil carbonate isotope records from semi-arid regions can reflect seasonal temperature rather than mean annual temperature (e.g. Breecker *et al.* 2009). Breecker *et al.* (2009) identified that in semi-arid climates with highly seasonal rainfall precipitation of carbonate in the soils occurred at the end of the wet season. As southern Spain experiences a strongly seasonal precipitation regime, which is thought to have become increasingly seasonal through the last glacial (Prentice *et al.* 1992) it is likely that soil carbonates

at Chimeneas were formed at the start of the dry season, when soil moisture composition is the result of wet season precipitation. As such, the isotope values from Chimeneas could reflect changing temperatures during the wet (winter) season in southern Spain and therefore the suggested temperature changes within the sequence would reflect changing autumn/winter temperatures not mean annual temperature changes.

It has however, been suggested that the large vegetation changes seen in the Mediterranean during the last glacial occurred in response to the extension and contraction of the length of the wet season (Prentice *et al.* 1992, Tzedakis *et al.* 2001), with warm/wet interstadials having longer wet seasons and cool/dry stadials having shorter wet seasons. This would suggest that during the last glacial the timing of soil drying would have occurred at different times of the spring/summer and therefore, changing the timing of soil carbonate formation. If such seasonal variations significantly altered the timing of carbonate formation at Chimeneas, then variations in $\delta^{18}O$ values of soil carbonates could reflect precipitation during earlier (cooler) months or later (warmer) months, complicating the palaeoclimate signal derived from the soil carbonates.

10.6.3 Control on the $\delta^{18}O$ signal at Chimeneas

The lack of covariance between carbon and oxygen isotope values in the soil carbonate record from Chimeneas indicates that this system is not driven by evaporation, as has previously been suggested for Mediterranean systems (Candy *et al.* 2012). It was therefore important to assess the possible factors which could be driving the strong $\delta^{18}O$ variations captured by the Chimeneas record. Although there are numerous factors which can drive changes in the $\delta^{18}O$ of precipitation, it has been possible to discount the influence of all, except air temperature. It is therefore suggested that the $\delta^{18}O$ fluctuations in soil carbonates at Chimeneas can be used as a semi-quantitative proxy for shifting air temperatures, where a $1^{\circ}C$ temperature rise results in an ^{18}O enrichment of 0.3‰ in the $\delta^{18}O$ of soil carbonates (Craig 1965, Hays and Grossman 1991, White et al 1999, Leng and Marshall 2004, Andrews 2006).

As previously mentioned, during the last glacial the Mediterranean is thought to have experienced higher levels of aridity than during other times of the Late Quaternary (e.g. Prentice *et al.* 1992). It is, therefore, surprising that the $\delta^{18}O$ composition of soil carbonates from the last glacial site at Chimeneas appears to be a temperature rather than an evaporation driven signal. There is, however, a significant geographical difference between Chimeneas and previously studied sites where soil carbonates displayed an aridity driven isotope signal (figure 10.1, table 10.1). The relatively high altitude and inland location of Chimeneas result in it having a much cooler local

climate than the previously studied Mediterranean sites. It is suggested that this cooler climate resulted in a significantly reduced evaporation potential, allowing temperature to be the main driving factor of the oxygen isotopic composition of soil carbonates.

10.7 Significance

This thesis has demonstrated that the isotopic composition of Mediterranean meteoric carbonates is not always driven by evaporation contrary to previous work in the region (Candy *et al.* 2012). It is suggested that in cooler regions of the Mediterranean, i.e. those at higher altitudes, evapotranspiration potential is lower and therefore isotopic composition of soil carbonates is driven by the same environmental factors as those forming in temperate regions, namely vegetation composition ($\delta^{13}C$) and temperature ($\delta^{18}O$). It is unclear, however, within the Mediterranean, if the origin of soil carbonate isotopic signals present a seasonal or annual record of environmental conditions.

The Mediterranean is an extremely diverse region in terms of temperatures, precipitation amounts and precipitation regimes (figure 10.4). This heterogeneity exists as an east-west gradient associated with the strength of North Atlantic influence, as a north-south gradient associated with atmospheric circulation and solar radiation and finally, due to the orographic diversity of the region (Harding *et al.* 2009, Sanchez-Goñi *et al.* 2008). This complexity means that there are likely to be different climatic controls upon meteoric carbonates forming in different areas of the Mediterranean. It is suggested that in regions with high evapotranspiration potential where total rainfall is low and strongly seasonal and temperatures are relatively warm the isotopic composition of meteoric carbonates is likely to be driven by evaporation following the mechanism proposed by Candy *et al.* (2012). However, in regions with lower evapotranspiration potential where there is a higher rainfall total, less seasonality of precipitation and/or lower temperatures, oxygen and carbon isotopes will not be driven by evaporation but by temperature and vegetation respectively. Given the modern day temperature and precipitation gradients that exist within the region (figure 10.4) related both to longitude and latitude but also to altitude, it may be possible to identify isotopic records from meteoric carbonates recording aridity or temperature and vegetation both seasonally and annually.

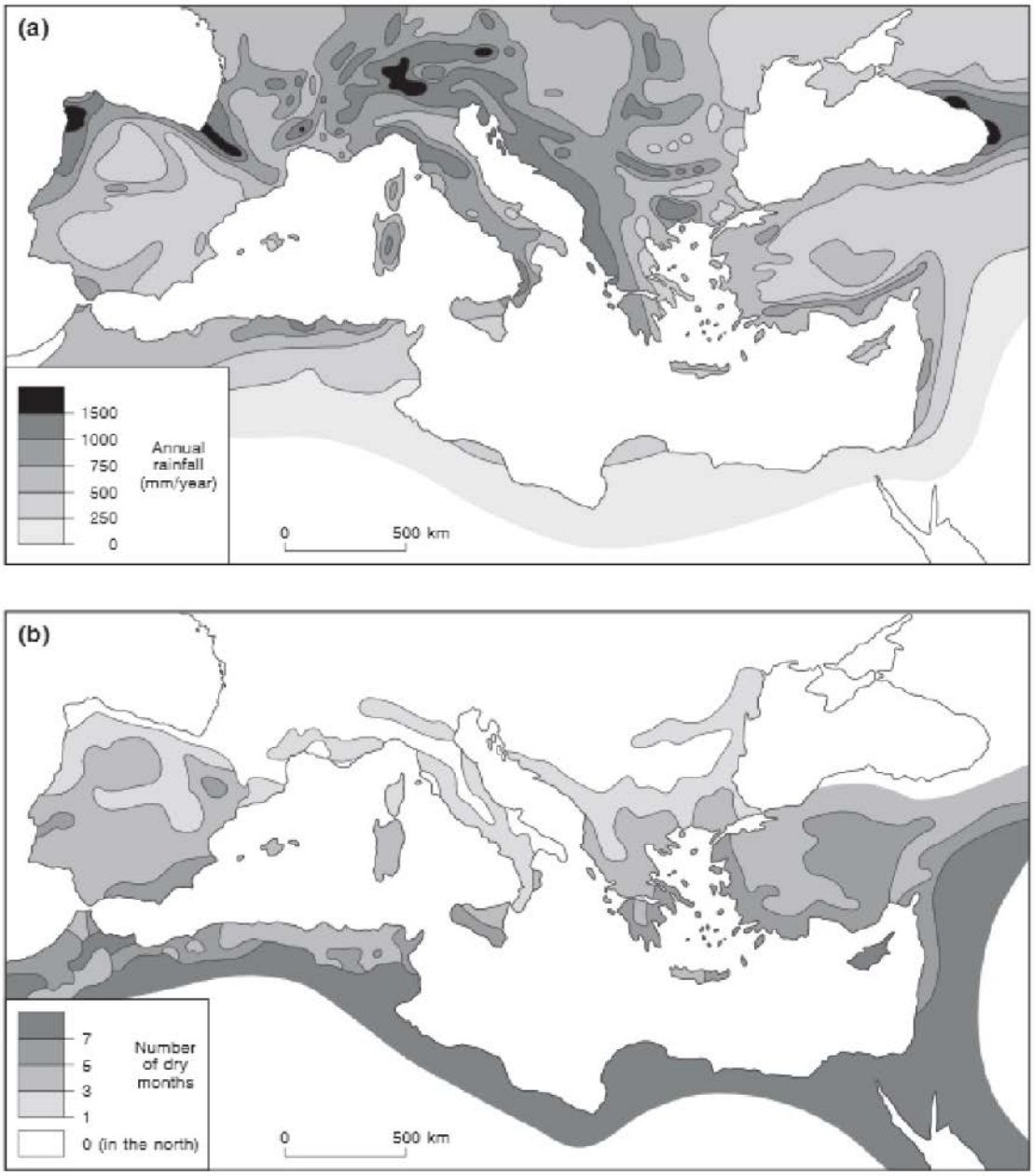

Figure 10.4 Taken from Harding et al. (2009) a) mean annual rainfall (mm), b) rainfall seasonality

Chapter 11- Geomorphic response of landscapes in southern Spain to rapid climate events

The results presented in chapters 7-9 represent the first detailed study of loess in southern Spain and the first time loess deposits in the Mediterranean region have been independently dated. As such, it is now possible to discuss the timing of loess accumulation in southern Spain. Although this study only focuses on three sites, the number of dates and the repeatability of the derived ages means that this is the first study in the region to robustly constrain multiple phases of loess deposition. Consequently, it is felt that a summary of the general characteristics and timing of loess deposition is justified. Furthermore, independently dating episodes of loess accumulation allows for the comparison with regional environmental records in order that the climatic and environmental conditions associated with loess accumulation may be understood. This chapter summarises the sediment sequences at the three sites studied and through comparison with regional records of environmental conditions, compares and contrasts conditions present during loess accumulation events of the Late Quaternary. A regional model of the timing of optimum loess accumulation conditions is presented and its applicability through the Mediterranean is discussed.

11.1 Introduction

Through the late Quaternary the Mediterranean region underwent large scale climate changes (chapter 2) which appear similar in both timing and expression to those witnessed within Greenland and North Atlantic records (Oppo *et al* 2006, McManus *et al.* 2002, Shackleton *et al.* 2000, Martrat *et al.* 2004). Our understanding of how these Milankovitch and sub-Milankovitch climate events affect the landscape of the region is poorly understood and is largely inferred from pollen records contained within western Mediterranean marine cores (Shackleton *et al.* 2000, Sánchez Goñi *et al.* 2000, 2005, 2008, Fletcher and Sánchez Goñi 2008) or central and eastern lacustrine sequences (Allen *et al.* 1999, Tzedakis 2003, 2005, 2009, Tzedakis *et al.* 2001, 2004).

As a semi-arid region the land systems of southern Spain are particularly sensitive to climatic changes and as such the region has been referred to as a 'fragile' landscape (Fletcher *et al.* 2012). As discussed previously, it is thought that through the late Quaternary the region experienced significant changes in precipitation regime, which resulted in large shifts in vegetation type and cover (Prentice *et al.* 1992, Tzedakis *et al.* 2004, Tzedakis 2005, 2009). As discussed in chapter 1, vegetation composition, precipitation volume and seasonality has large impacts upon erosion rates and sediment availability within the region (Thornes *et al.* 2009) and

therefore, it is likely that the region experienced large geomorphic changes through the late Quaternary in association with both Milankovitch and sub-Milankovitch climate changes.

11.2 Western Mediterranean geomorphic response

As shown in figure 11.1 and discussed in chapter 2, there is a clear vegetation response through the Mediterranean in association with interglacial/glacial changes and interstadial/stadial events. During warm climate episodes the region records increased forest cover and during cool climates there is a shift towards steppic conditions. This vegetational response is thought to reflect changing moisture availability through the Late Quaternary, with warmer periods associated with an increase in effective precipitation and cool periods being increasingly arid (e.g. Prentice *et al.* 1992, Bar-Matthews *et al.* 1997, 2000). These changes in water availability are thought to reflect changes in the seasonality of rainfall, with a shortened rainfall season associated with cold climate episodes (Prentice *et al.* 1992). This pattern of vegetational response to climate events is also thought to be reflected within the geomorphic response of the region through the Late Quaternary.

As discussed within chapter 1, vegetational shifts and changes in seasonality of the rainfall received by the region will control the sediment mobilisation and availability within the landscape (e.g. Thornes *et al.* 2009). Through the compilation of fluvial records through the Mediterranean, Macklin *et al.* (2002) identified that episodes of incision and alluviation are generally associated with cold climate events (figure 11.1). This response indicates enhanced stream power and sediment availability during these climate episodes. Rose *et al.* (1999) also identified this pattern of fluvial response in Mallorcan sediment sequences, and additionally constrained periods of soil formation to warm climate episodes (figure 11.1) indicating that warm, humid climates are associated with landscape stability. Evidence of landscape stability during warm climate episodes is also supplied by records of tufa formation through southern Spain (Domínguez-Villar *et al.* 2011, Martín-Algarra *et al.* 2003) where tufa growth is restricted to periods of low sediment supply and high vegetation levels (Goudie *et al.* 1993, Pedley 2009). Within southern Spain tufa precipitation occurs within full interglacial conditions (MIS 5e) and within the warm sub-stages MIS 5c and 5a (Domínguez-Villar *et al.* 2011).

Previous studies of loess in the Mediterranean region have identified deposits as being locally derived sediments which have accumulated through the last glacial (Coude-Gaussen 1991, Garcia *et al.*2010, 2011, Bonifay 1965, Mücher *et al*. 1991, Günster *et al.* 2001). However, contrary to previous studies of Mediterranean loess, Rose *et al.* (1999) identified that loess accumulation on Mallorca was not restricted to MIS 4-2 but occurred also within stage 5.

Additionally, the accumulation of loess on Mallorca was suggested to have derived from far-travelled silts, although no potential source region was identified. Loess is an important geomorphic indicator as it has been shown to record both Milankovitch and sub-Milankovitch climate changes (e.g. Kukla 1987, Moine *et al.* 2008, Markovic *et al.* 2011) and it requires certain conditions in order for accumulation to occur; the most important of which have been suggested to be silt supply, vegetation cover and landscape stability (Tsoar and Pye 1987, Pye and Tsoar 1987, Pye 1995). Firstly, silt supply must be sufficient to enable accumulation on the land surface as a discrete unit rather than incorporation or reworking into underlying sediments via soil processes (Tsoar and Pye 1987). Secondly, vegetation must be sufficient to act as a trap for silt, but not dense enough to incorporate accumulating silt into the soil (Tsoar and Pye 1987, Pye and Tsoar 1987, Pye 1995). Finally, in order for silt deposition to result in an accumulation of loess, the landscape must be stable enough that the sediments are not eroded once deposited. As these factors are directly related to the patterns of environmental change that occur in the Mediterranean during the Quaternary, it is important to constrain the timing, reworking and provenance of loess in southern Spain.

11.3 Stage 5 – Evidence from Maro

The results from Maro are presented and discussed in detail in chapter 9. The sediment sequence records geomorphic response of the landscape to Milankovitch and possibly sub-Milankovitch climate changes through MIS 6-5 (figure 11.2).

At the base of the sequence are overbank sediments dating to late MIS 6. MIS 5e is recorded by the occurrence of oncoids within sections 1 and 2 and by the large tufa lower in the valley (section 3) dated by OSL and U-series. The occurrence of the tufa deposits within the valley indicates a stable landscape with low sediment mobilisation and high vegetation levels, which are conditions reported elsewhere in southern Spain where MIS 5e is also marked by tufa growth (Domínguez-Villar *et al.* 2011, Martín-Algarra *et al.* 2003). Above the oncoidal unit (section 1 unit 3, section 2 unit 1) is the onset of loess accumulation within the valley. The size of the uncertainties associated with the OSL ages are precise enough to show that these deposits record environmental change within MIS 5, but not precise enough to allow robust correlation with individual sub-stages within MIS 5. The following correlation, therefore, uses the stratigraphic succession of the deposits and their environmental significance to generate a tentative correlation with MIS 5e through to MIS 5a. The dating of the loess material is not precise enough to constrain the timing of accumulation to a sub-stage of MIS 5, however, it is unlikely that deposition occurred during the Interglacial where vegetation levels appear consistently high (figure 11.2b). A post-MIS 5e age is supported by the isotopic composition of soil carbonates from the unit, which indicate

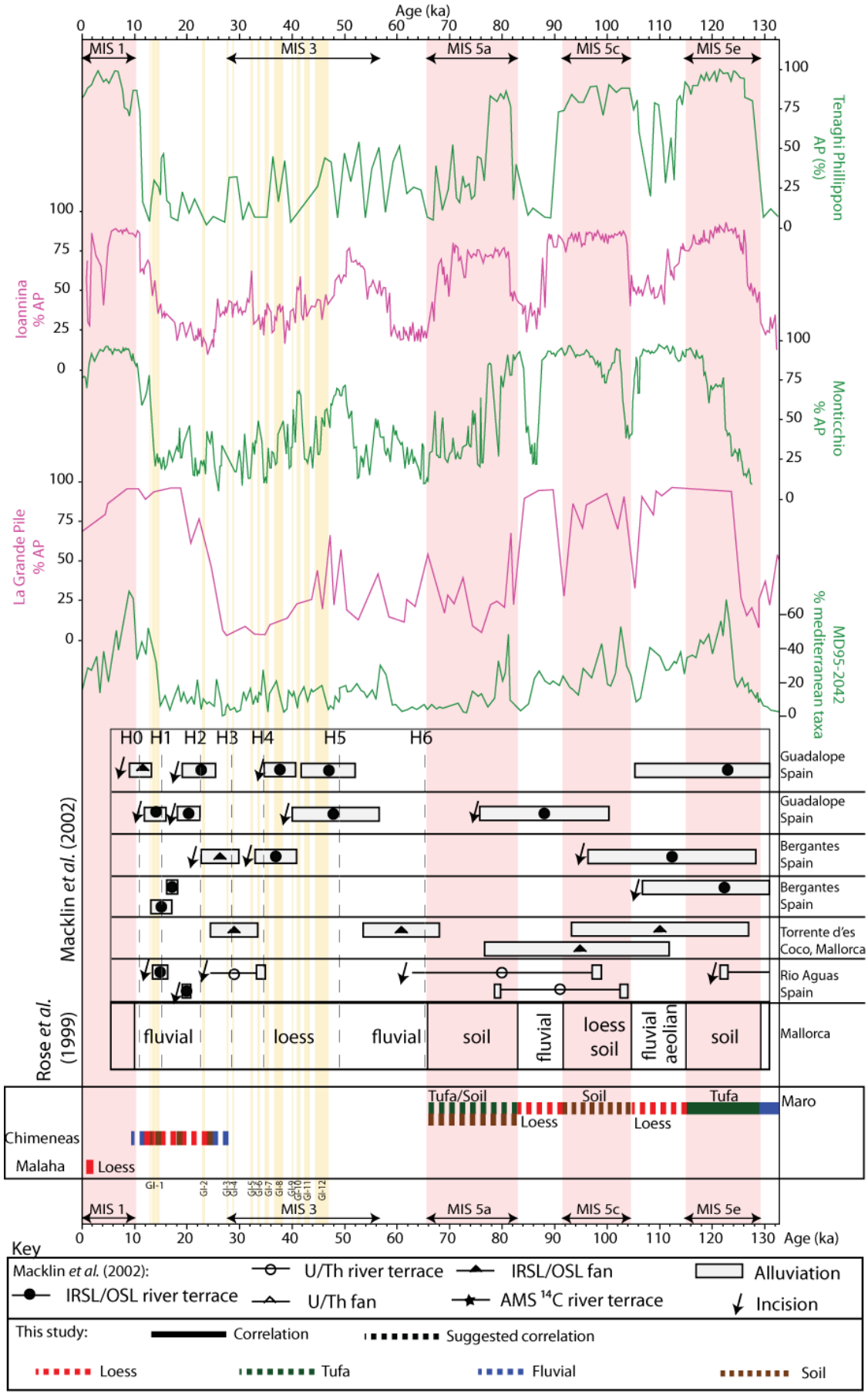

Figure 11.1 Comparison of land scape processes from Maro, Chimeneas and Malaha with previous regional geomorphic records (Macklin et al. 2002, Rose et al 1999) and Mediterranean vegetation records (MD95-2042 (Sánchez Goñi et al. 2000, 2008), La Grande Pile (Woillard and Mook 1987) plotted to Heusser (2000) age model, Monticchio (Brauer et al. 2007), Ionnanina and Tenaghi Phillipon (Tzedakis et al. 2001).

deposition during a period of strong aridity, it is therefore suggested that loess accumulation at Maro occurred during MIS 5d.

Within the loess sediments at Maro there is evidence for development of two weak soil horizons (section 1), indicating two short-lived episodes of landscape stability, possibly associated with a warm sub-stage of intra-stadial variability. Within section 2, however, there is evidence of a sustained episode of landscape stability due to the occurrence of a second *in-situ* oncoid horizon which has cut down through the loess (figure 11.2a). As with the previous tufa deposits at Maro, the occurrence of the second oncoid horizon within late stage 5 indicates a period of landscape stability where sediment supply was sufficiently low and vegetation levels were high enough to support tufa growth (Goudie *et al.* 1993, Pedley 2009, Domínguez-Villar *et al.* 2011). As shown in figures 11.1 and 11.2b, vegetation levels within the Mediterranean recover to near Interglacial levels during sub-stages MIS 5c and 5a and it is therefore likely that the upper oncoid bed occurred during one of these interstadial episodes.

The record from Maro supports the broad geomorphic understanding of the western Mediterranean landscape, with warm climate intervals associated with landscape stability through tufa development and soil formation and cold climate episodes associated with sediment accumulation. Maro also supports the work of Rose *et al.* (1999) in identifying loess accumulation within the Mediterranean as a non-glacial stage process, where accumulation at Maro and Mallorca occurs during a cool (non-Interglacial) period but not during full glacial conditions.

The geochemistry of the loess at Maro (chapter 6) indicates that, as with the Mallorcan loess of Rose *et al.* (1999), stage 5 loess is not locally derived. The geochemistry (figure 11.3) of the loess at Maro indicates that North Africa is a potential source region for a significant proportion of the sediments. However, the loess from Maro records lower Sr ratio values than the modern river and palaeo-fluvial sediments from the same site, and therefore plots further from the North African aerosol data. This indicates that the loess contains a greater proportion of mantle derived sediments, appearing more closely related in composition the fluvial sediments from within the Granada basin. This may indicate that the loess contains a greater proportion of sediments derived from the Spanish interior regions than the fluvial systems at the site.

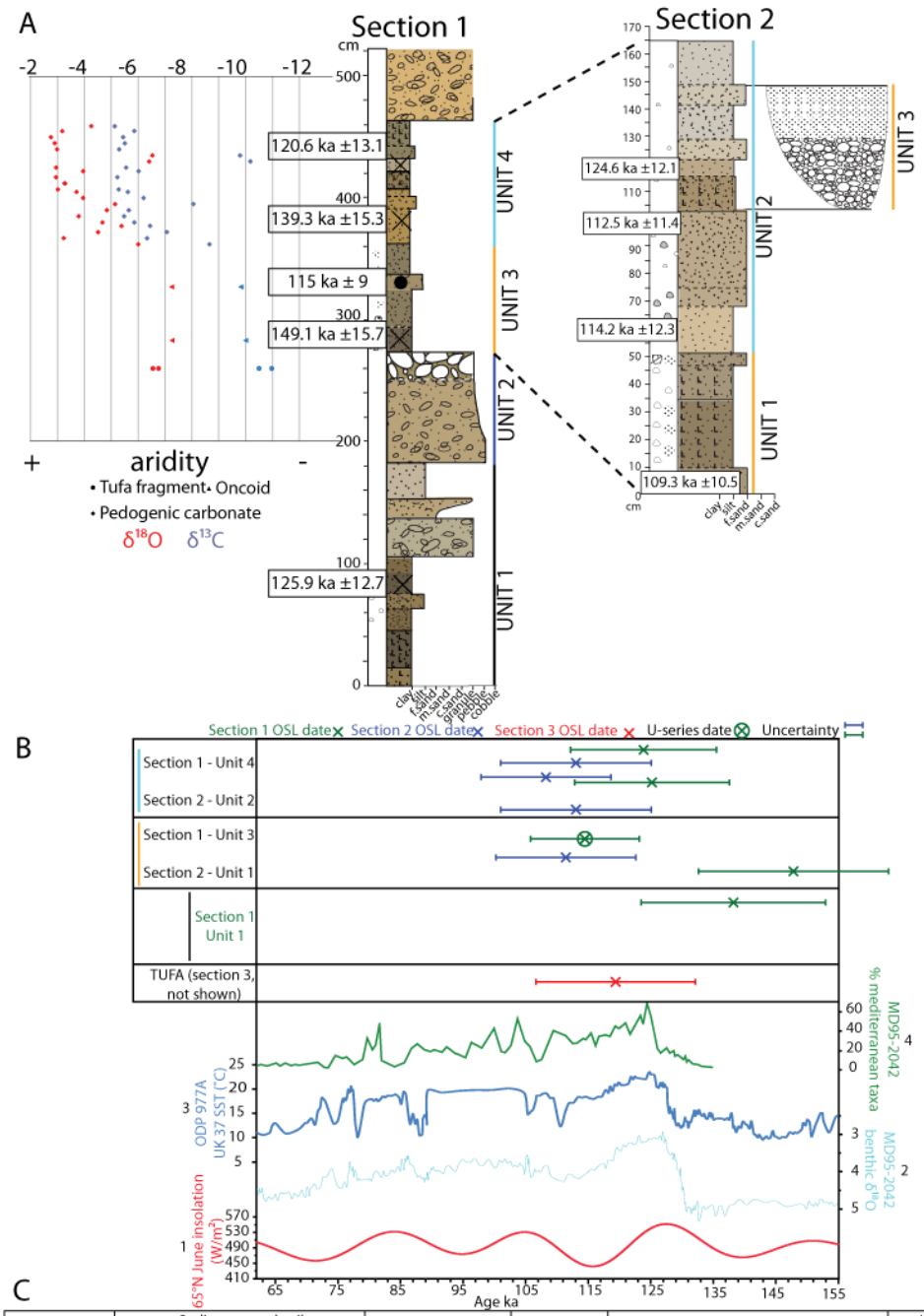

Section/Unit	Sediments and soil properties	OSL ages (ka)	Climate	Environment	Landscape stability	MIS
unit 2, section 2	Loess accumulation	< ages below	Arid-cool	Return to far travelled loess accumulation	Unstable	MIS 5b?
unit 3, section 2	Clast supported oncoid filled channel feature	< ages below	Warm - moist	Sustained landscape stability with high vegetation cover.	Stable	MIS 5c?
unit 4, section 1 unit 2, section 2	Loess accumulation with accretionary pedogenic alteration. Two episodes of moderate post-deposition alteration present, recorded as partically decalcified, clay enriched horizons.	112.5 ± 11.4 ka 114.2 ± 12.3 ka 120.6 ± 13.1 ka 124. 6 ± 12.1 ka 139.3 ± 15.3 ka	Loess: Arid - cool Soils: Moist-warm	Far travelled loess accumulation during period of aridity and reduced vegetation cover. Punctuated by two episodes of reduced sediment supply associated with moister conditions resulting in soil formation	Loess: unstable Soils: stable	MIS 5d?
unit 3, section 1 unit 1, section 2 section 3	Oncoid beds with moderate pedogenic alteration Tufa	109.3 ± 10.5 ka 115.0 ± 9 ka (U-series) 149.1 ± 15.7 ka 114.2 ± 12.3 ka	Warm - moist Warm - moist	Multiple tufa systems present. Sustained landscape stability with high vegetation cover.	Stable Stable	MIS 5e
unit 1, section 1 unit 2, section 1	Floodplain sediments with minor pedogenic alteration. Overlain by clast supported cobble beds	125.9 ± 12.7 ka		Migration of a bradied river system from distal to proximal position over site of deposition		MIS 6?

Figure 11.2 Maro stratigraphy and palaeoenvironmental interpretation A. Stratigraphies from Maro sections 1 and 2 with OSL ages and isotope data from section 1. B. Comparison of OSL ages with regional climate records and insolation (1)Insolation curve for June 65ºN (W/m²) Laskar et al. (2004) (2) MD95-2042 benthic δ¶O and (3)ODP-977A SST data Martrat et al. (2004) (4) MD95-2042 Sanchez-Goni et al. (2008). C. Suggested MIS correlation of Maro sediments and climatic significance.

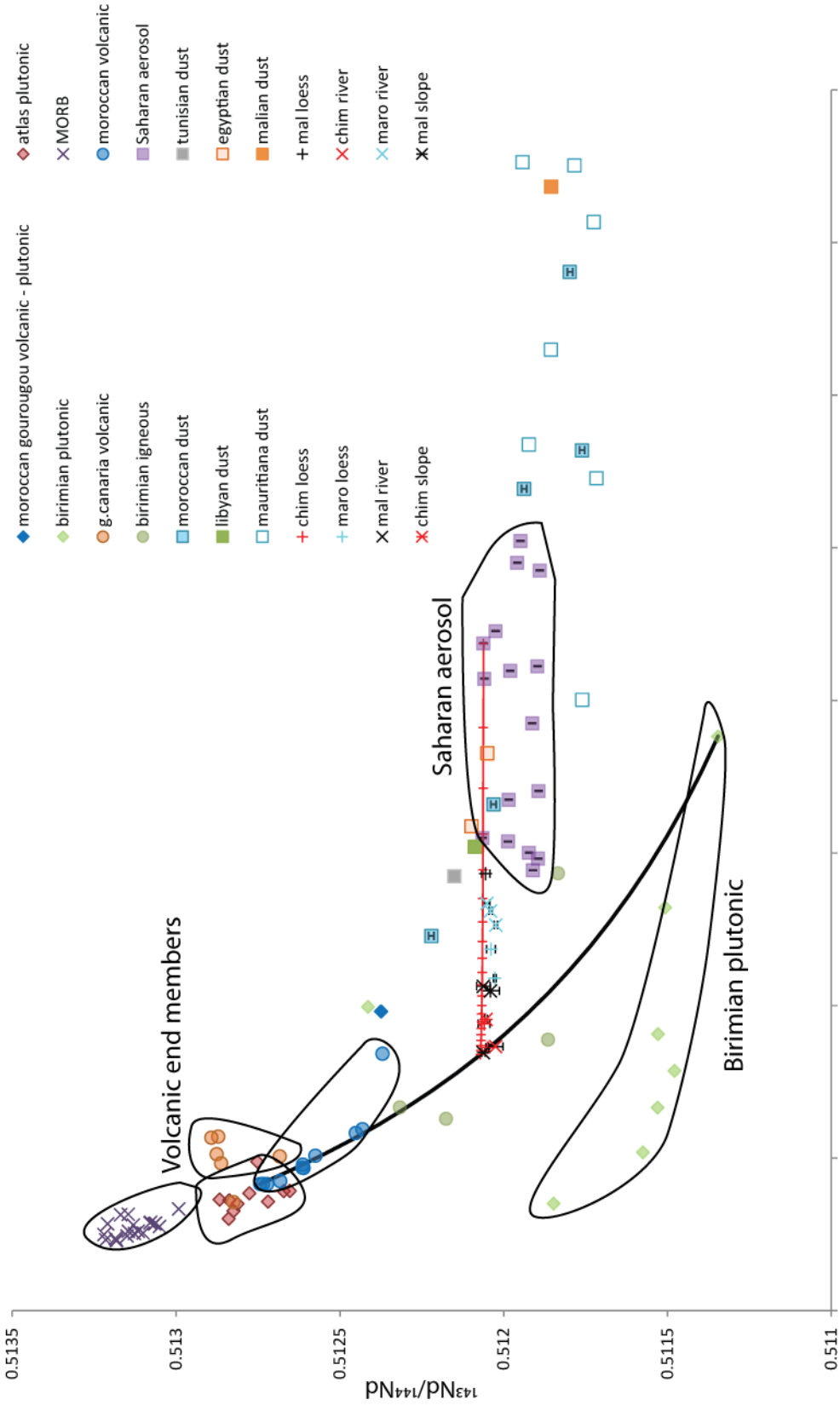

Figure 11.3 Comparison of Sr and Nd ratios of sediments from Maro, Malaha and Chimeneas with potential regional sources. N.African data from Grousset et al 1998 and Grousset and Biscaye 2005, Moroccan volcanics data from Gill et al 2004, Sierra Nevada Igneous data from Gomez-Pugnarie et al. 2000, Birimian data Taylor et al. 1992. Sr errors smaller than data points, Nd errors shown for data produced in this project

11.4 The last glacial – Evidence from Chimeneas

The last glacial is recorded as a period of climatic instability within Greenland and the North Atlantic, marked by oscillation between rapid sub-Milankovitch stadial and interstadial events (Bond et al. 1992, 1993, Dansgaard *et al.* 1993). The pacing and amplitude of these events appears to be recorded within the marine records of the western Mediterranean (e.g. Cacho *et al.* 1999) with the pacing of SST changes apparently near-synchronous to those of the North Atlantic (Shackleton *et al.* 2000, Abreu *et al.* 2003). These rapid oscillations between warm interstadial and cold stadials are recorded within western and eastern Mediterranean vegetation records by increasing forest or steppic conditions respectively (Allen *et al.* 1999, Tzedakis *et al.* 2004, Roucoux *et al.* 2001, Sánchez Goñi *et al.* 2000, 2001, 2008, Combourieu Nebout *et al.* 2002, Fletcher and Sánchez Goñi 2008) (figures 11.1 and 11.4). Prentice *et al.* (1992) suggest that the vegetation changes witnessed in Mediterranean records through the last glacial occur due to changes in effective precipitation; with stadials marked by lower effective precipitation due to increased seasonality of rainfall.

It is suggested that through the last glacial the fluvial systems of the Mediterranean are driven by these sub-Milankovitch oscillations, with stadials associated with alluviation and interstadials marked by channel stability (Macklin *et al.* 2002) (figure 11.1). Although there are issues associated with the dating and correlation of fluvial response through this period (chapter 2), there are too many alluviation events through this period to be driven by Milankovitch forcing alone. Therefore, it appears that the landscape of the Mediterranean demonstrates a strong response to sub-Milankovitch events, with landscape stability during interstadials and increased sediment supply and instability during stadials.

The sediment sequence at Chimeneas records the transition from overbank sedimentation during the last glacial maximum into a loess-palaeosol complex through to the Younger Dryas (GS-1) and then a return to fluvial deposition. The loess at this site appears to be heavily reworked, because both the mineralogy (chapter 6) and geochemistry (figure 11.3) indicate a local source for the sediments. However, the median grain size of the loess (5-20 μm) is very fine which usually indicates a far-travelled silt (Muhs and Bettis 2000, Lui and Ding 1993), in this instance appears to indicate a form of localised sorting. Therefore, on the basis of the composition of the sediments and micromorphological evidence of flow structures, it is suggested that Chimeneas is the most heavily reworked of the three loess deposits detailed in this study.

The loess-palaeosol sequence at Chimeneas records increasing pedogenic alteration upwards through the sediments (figure 11.4), which appears to correspond with regional and Greenland

records that indicate a general climatic amelioration peaking at the GI-1 complex. This climatic amelioration is also recorded by the temperature driven $\delta^{18}O$ signal derived from soil carbonates at Chimeneas (figure 11.4). The OSL dating of the Chimeneas sequence is robust enough correlate to sub-Milankovitch climate events, and the record appears to show a remarkable level of correlation to regional and Greenland climate events. Accumulation of reworked loess at Chimeneas occurs during cold, stadial events with low vegetation levels. Pedogenic alteration of the sediments at Chimeneas occurs in association with increased levels of vegetation, generally associated with interstadial periods.

The sequence at Chimeneas represents the first independently dated last glacial loess in southern Spain. As has been suggested for other last glacial loess deposits in the Mediterranean, it appears that the silt is locally derived, although at Chimeneas it has been heavily reworked prior to deposition. The sequence indicates sediment accumulation during cold climate events and landscape stability during warmer climate events, with geomorphic response in association with sub-Milankovitch climate events.

11.5 The Holocene – Evidence from La Malaha

The Holocene is a period of relative climatic stability, with a return to forested conditions within the Mediterranean (figure 11.1) and the return or tufa precipitation in southern Spain (Domínguez-Villar *et al.* 2011, Martín-Algarra *et al.* 2003). However, there is evidence within Greenland ice cores (O'Brien *et al.* 1995, Vinthner *et al.* 2006) and North Atlantic marine cores (Bond *et al.* 1997) which suggests that the Holocene contains low-amplitude climatic fluctuations. Although muted in comparison to the events of the last glacial, these climatic coolings appear to be paced at 2800-2000 and 1500 yr intervals (Mayewski *et al.* 2004 and references therein).

Evidence indicates that there has been a transition towards increasing regional aridity within the Mediterranean since the mid-Holocene (Jalut *et al.* 2000, Davis *et al.* 2003, Magny *et al.* 2002, Fletcher and Sánchez Goñi 2008, Carrión *et al.* 2010, Bar-Matthews and Ayalon 2011). It is however, suggested that this general trend is punctuated by aridification phases (figure 11.5) associated with Holocene low amplitude cooling events (Fletcher and Zielhoef 2012). Fletcher and Zielhoef (2012) argue that Holocene cooling events in the North Atlantic and Greenland appear to correlate with increased aridity in the western Mediterranean, marked by increases in steppic taxa and lake level drops (Jalut *et al.* 2000, Carrión 2002, Fletcher and Sánchez Goñi 2008).

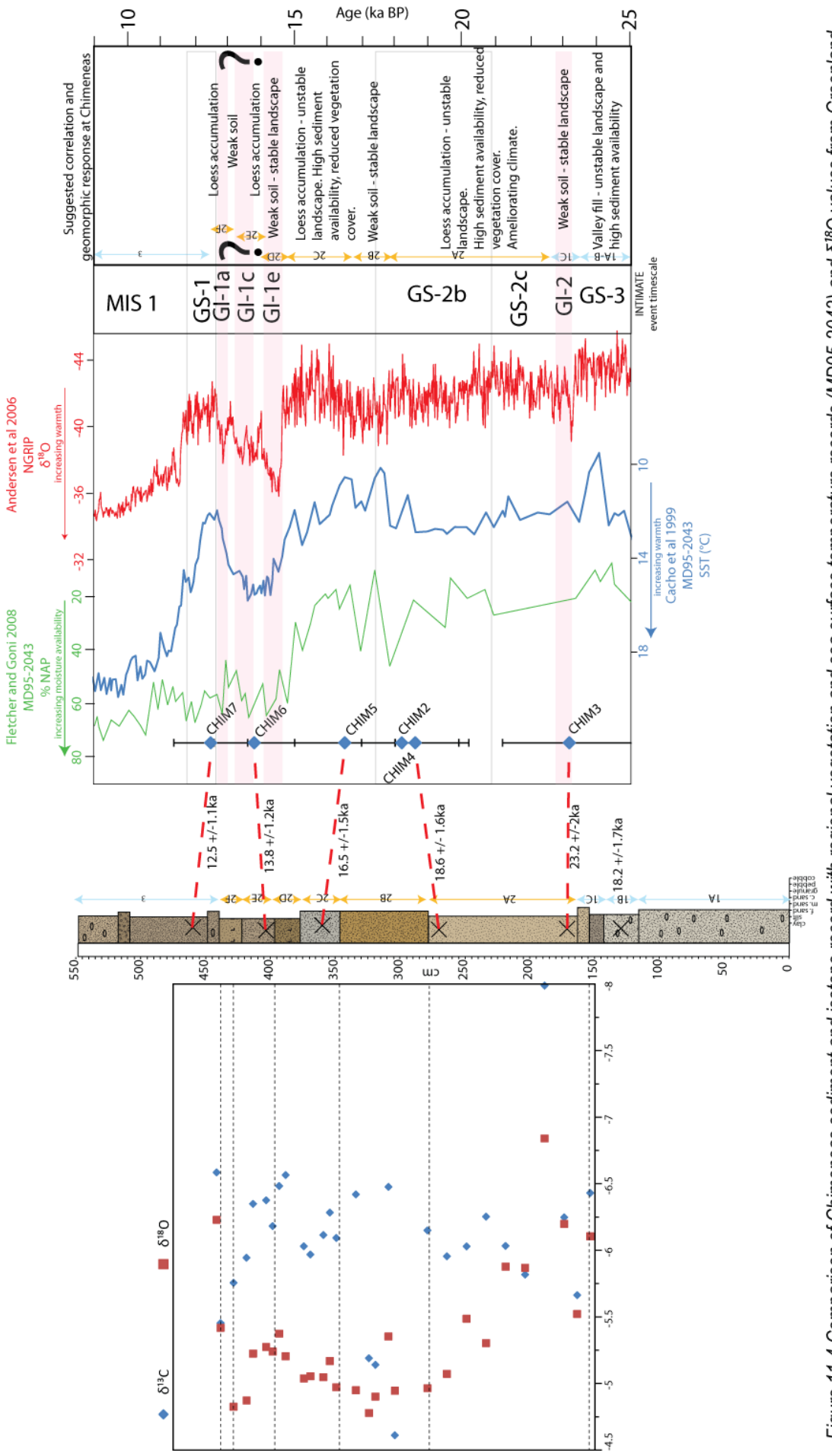

Figure 11.4 Comparison of Chimeneas sediment and isotope record with regional vegetation and sea surface temperature records (MD95-2043) and $\delta^{18}O$ values from Greenland

La Malaha is a short sediment sequence (1.5 m), at the base recording deposition in a floodplain setting overlain by loess. Micromorphological evidence from the sequence indicates increasing pedogenic alteration upwards through the sediments, associated with declining sediment input and/or a climatic amelioration. OSL dating of the sequence identifies that it was deposited between 2.2 ka ±0.2 and 1.4 ka ±0.1. This places the timing of deposition in line with a Holocene cooling event, marked by an increase in steppic taxa associated with aridity (figure 11.5), but also coincident with the Roman occupation of the region. The evidence for climatically driven landscape changes is particularly difficult to resolve during the late Holocene as the period is often correlated with significant sediment mobilisation in response to widespread land clearance for agricultural purposes (e.g. Pantaléon-Cano *et al.* 2003 and references therein).

Importantly, the geochemical composition (chapter 6) of the loess from La Malaha appears to indicate a clear far-travelled origin (figure 11.3). The Sr Nd content of the loess is significantly different to that of locally derived sediments (slope, fluvial and palaeo-fluvial) and plots extremely close to North African aerosol data. It is likely that this short, Holocene loess sequence accumulated via silt transported from North Africa. However, it remains unclear if vegetation levels at La Malaha were low enough to facilitate loess accumulation due to anthropogenic or climatic changes.

11.6 Mediterranean loess as a geomorphic indicator

This study has identified and independently dated loess accumulations in southern Spain deposited during MIS 5, MIS 2 and MIS 1 (figure 11.1).

- The loess at Maro is dated to post-MIS 5e; on the basis of stratigraphy and isotopic evidence from soil carbonates it is suggested to have been deposited during a cool stadial of stage 5 (5d or 5b). Geochemical data from Maro indicates that the loess is not locally derived (figure 11.3), but may have been derived from the Spanish interior, possibly from the continental basins of the Betic-Cordillera. The timing of loess accumulation at Maro is similar to that reported by Rose *et al.* (1999) for loess on Mallorca.
- The last glacial loess accumulation at Chimeneas records heavily reworked, locally derived silts (figure 11.3) and as such, is similar to descriptions of southern and central Spanish last glacial loess (Mucher *et al.* 1991, Garcia *et al.* 2010, 2011).
- The sequence at La Malaha is the first report of Holocene loess accumulation within southern Spain. In order for loess to have accumulated during the Holocene, vegetation levels must have been significantly reduced compared to full Interglacial conditions. The

timing of loess accumulation at La Malaha makes it difficult to assess if vegetation cover was reduced because of climatic or anthropogenic forcing. The geochemical composition (figure 11.3) of the sediments indicates a probable North African origin.

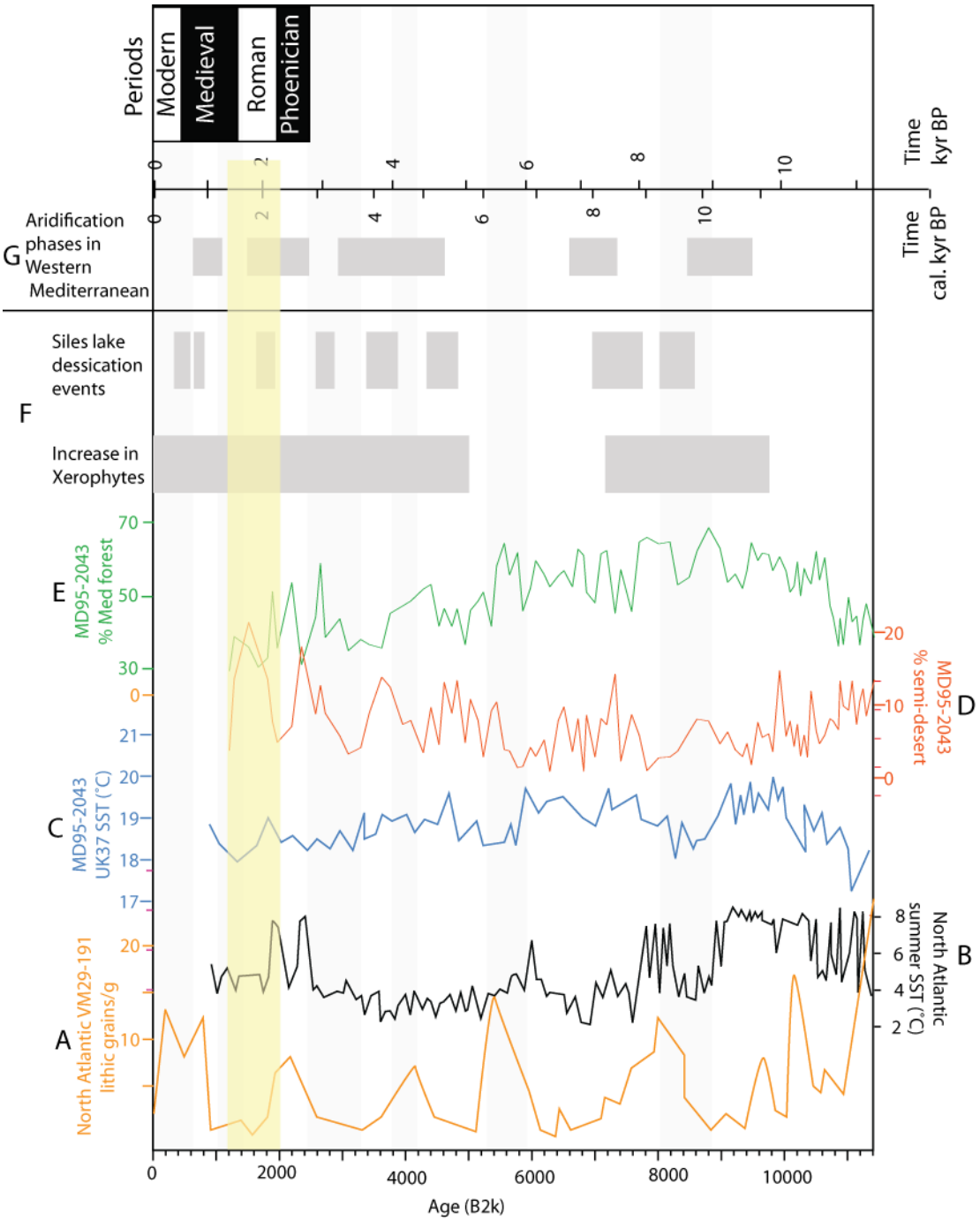

Figure 11.5 Timing of loess accumulation at Malaha (yellow bar) compared to North Atlantic and Iberian records of Holocene climate and environment. A. North Atlantic Lithics (Bond et al. 1997) B. North Atlantic SST (Mayewski et al. 2004) C. MD95-2043 SST (Cacho et al 2001, 2002) D, E. MD95-2043 pollen (Fletcher and Sánchez Goñi 2008) F. Lake Siles (Spain) desiccation events and shift to xerophytic plants (Carrión 2002) G. Western Mediterranean aridification events from pollen records (Jalut et al 2000). Grey bars indicate position of Holocene rapid climate events (Mayewski et al. 2004).

As such, it is suggested that optimum conditions for 'pristine' loess accumulation in southern Spain occur within 'warm isotope-stage stadial' type climates, where vegetation levels are between those of Glacial minima and Interglacial maxima (figure 11.1). Such an environment would have sufficient vegetation levels to act as a sediment trap, but would not be sufficiently vegetated to result in the incorporation of loess into soils. Consequently, relatively thick beds of primary loess are preserved (figure 11.6). At Maro, such an environment is present during the stadials of stage 5, where palynological records indicate warm isotope-stage stadial levels of vegetation cover associated with insolation minima (Sánchez Goñi *et al.* 2000, 2008). Although loess deposition at Malaha occurred within the full Interglacial conditions of the late Holocene, it is suggested that anthropogenic landscape clearance and/or reduced vegetation cover associated with arid conditions occurring after the Holocene optimum and possible enhanced by a late Holocene rapid cooling event, produced an 'warm isotope-stage stadial' type climate effect, facilitating the accumulation of loess.

The sediment sequence at Chimeneas highlights the effects on accumulation during a period associated with Glacial vegetation minimum conditions (figure 11.1). The low vegetation levels of the last glacial period would be associated with the mobilisation of large volumes of sediment within the region. Low vegetation cover would enable silt sized material to be readily removed via deflation from exposed soils and surface sediments (Pye and Tsoar 1987) providing a local silt source, and, it is argued, that there is an increased North African dust supply through the last Glacial (e.g. Moreno *et al.* 2002). Despite the potential for increased supply of dust during this time, the sediment sequence at Chimeneas is heavily reworked compared to the sediments at Maro and Malaha. It is suggested that this increased reworking and remobilisation of loess during the last glacial results from the lack of vegetation, enabling surface sediments to be easily reworked by slope and surface wash processes (figure 11.6) (Pye and Tsoar 1987).

Therefore, it is suggested that loess accumulation in southern Spain should not be thought of as purely a glacial/interglacial process, but also as a warm isotope-stage stadial climate process where moderate vegetation and precipitation levels facilitate accumulation (figure 11.6). This does not mean that loess is not a major part of Mediterranean environments during glacial episodes. However, the mechanisms for its widespread accumulation as a coherent sediment unit are only present during these 'interstadial' climates.

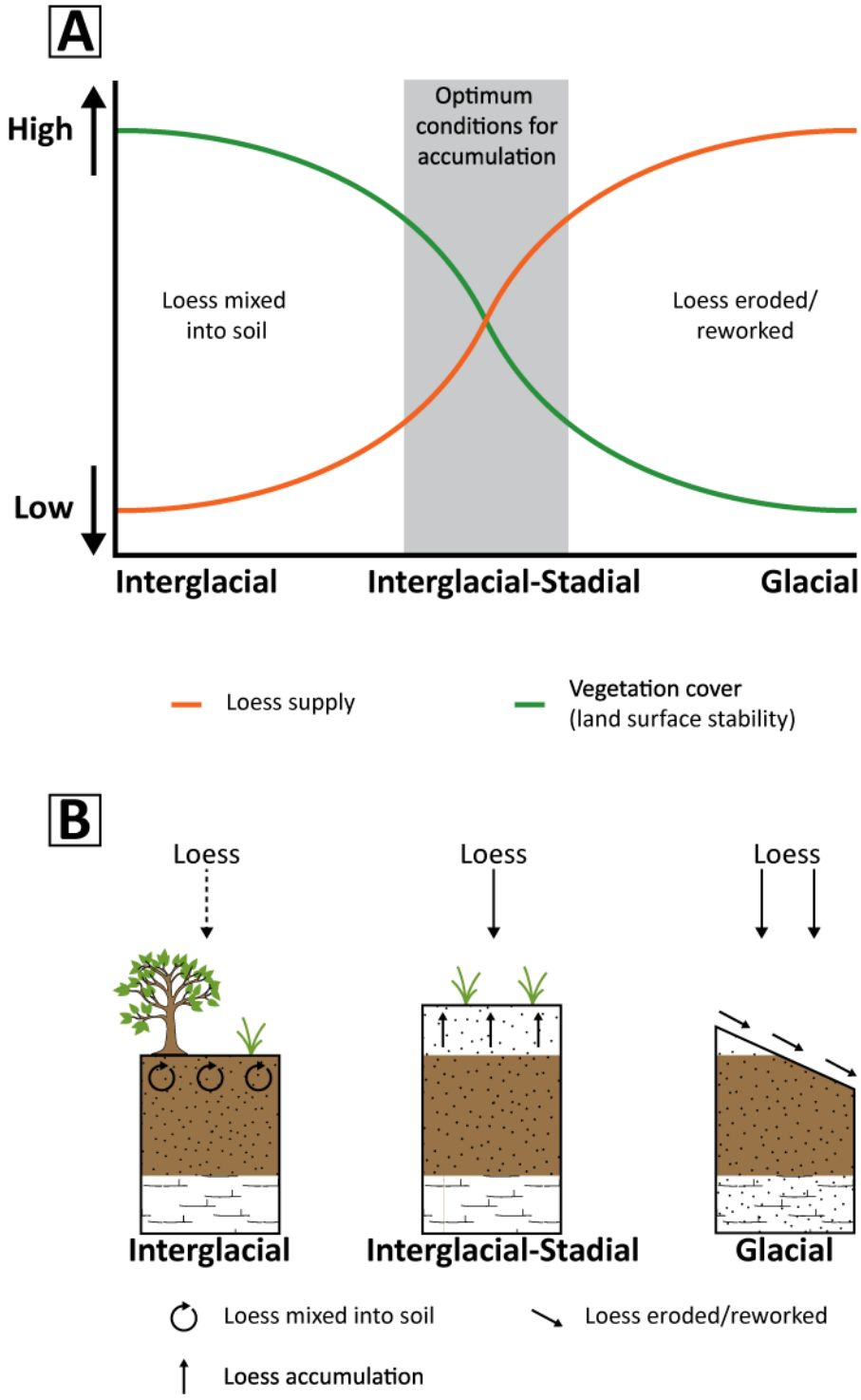

Figure 11.6 Model of climatic optimum conditions for loess accumulation within southern Spain. A. Schematic diagram showing the relationship between climatic periods and landscape stability and vegetation cover and dust supply, illustrating a warm isotope-stage stadial climate provides the best preservation potential for accumulating loess. B. Landscape processes occurring during interglacial, warm isotope-stage stadial and glacial climates and their effect on loess accumulation.

This model of the timing of loess accumulation in southern Spain is contrary to the model suggested by Coude-Gaussen (1990) which stated that loess in the southern Europe accumulates during glacial conditions and loess in North Africa accumulates during 'pluvial' conditions. However, the study by Coude-Gaussen (1990) compiled evidence from all previously identified Mediterranean loess sequences, most of which are from latitudes above 40^{o}N. Mediterranean regions above 40^{o}N are associated with a more typically temperate climate with greater rainfall totals and lower seasonality of precipitation (Sanchez-Goni *et al.* 2008, Harding *et al.* 2009; chapter 10 figure 10.4). The existence of strong latitudinal, longitudinal and altitudinal climate gradients within the Mediterranean region mean that the region displayed a heterogeneous response in terms of the amplitude of vegetational changes in response glacial/interglacial and stadial/interstadial climate changes (chapter 10). Figure 11.1 shows vegetational responses through the Mediterranean to Milankovitch and sub-Milankovitch climate events of the Late Quaternary with changing longitude and latitude. Although latitude and longitude are not the only variations between the site locations shown in figure 11.1, it does demonstrate that vegetation levels and in particular Interglacial maximum and Glacial minimum levels vary significantly through the region. Such regional variation in vegetation cover suggests corresponding variability in sediment availability and preservation potential through the Late Quaternary. As such, it is likely that the timing of the geomorphic optimum conditions for loess accumulation varies through the Mediterranean region according to vegetation, precipitation and silt supply characteristics.

Although this study is somewhat limited, the clearest evidence for a high North African dust input occurs during the Holocene. This study, in addition to existing literature suggests that glacial climates in the Mediterranean are dominated by local dust supply (Coude-Gaussen 1991, Garcia *et al.*2010, 2011, Bonifay 1965, Mücher *et al*. 1991, Günster *et al.* 2001). This is perhaps counterintuitive given the suggested dominance of North African dust supply during the stadial episodes of the last glacial (e.g. Moreno *et al.* 2002). It is clear, therefore, that the factors driving dust supply and those resulting in dust accumulation are poorly understood within the Mediterranean. This study highlights the need for independent dating of Mediterranean loess, rather than an assumption of glacial age. In addition, the characteristics and origin of Mediterranean loess deposits may help further understanding of Mediterranean geomorphic processes.

Chapter 12 – Loess deposition in southern Spain: Implications for understanding palaeoenvironments

This chapter explores the palaeoclimatic significance of the loess studies presented here with particular reference to existing models of regional dust flux. The chapter firstly provides an outline of the palaeoenvironmental interpretation of the three study sites and summarises the timing of loess accumulation, silt sources and degree of local modification. Secondly, the chapter will describe existing records and models of Late Quaternary regional dust flux. Finally the implication of the results from this thesis on such models is discussed. The chapter concludes by discussing the remaining uncertainties associated with understanding the importance of loess within the Mediterranean as well as mechanisms driving dust transport and supply.

12.1 Summary of palaeoclimatic interpretations

This thesis provides the first detailed study of loess deposits in southern Spain. Sedimentological and mineralogical examination of the sediments has highlighted similarities in composition of the deposits between the three study sites. This study has, however, identified significant differences in the timing and style of accumulation (e.g. degree of reworking) as well as differences in the geochemical (Sr-Nd) composition of the sediments indicating differences in provenance.

12.1.1 Chimeneas

The exposure of loess at Chimeneas occurs during the transition from the last glacial maximum towards the onset of the Holocene (23.2 ±2 ka to 12.5 ±1.1 ka). The timing of accumulation at Chimeneas is in keeping with the majority of loess deposits previously identified within the Mediterranean (Bonifay 1965, Coude-Gaussen 1991, Mücher *et al*. 1991, Günster *et al.* 2001, Garcia *et al.*2010, 2011). Unlike the previously documented last glacial loess deposits, the record at Chimeneas has been independently dated rather than assigned a last glacial age on the basis of assumed ages of underlying soil horizons (e.g. Günster *et al.* 2001). Based upon sedimentological characteristics previously identified last glacial loess in the Mediterranean has typically been described as locally derived and heavily reworked. This view is supported by Chimeneas, where Sr-Nd isotope values indicate that silt was sourced from within the Granada basin and micromorphology and PSA indicate that the sediments were heavily reworked by slope and/or fluvial processes (chapters 6 and 8).

The sequence at Chimeneas indicates a strong geomorphic response to sub-Milankovitch climate events of the late last glacial; micromorphological analysis of the sediments supported field

observations of four weak soil horizons present within the sediments. The occurrence of weak soil horizons indicates periods of landscape stability due to a reduced sediment input, typically associated with a warming climate (Kemp 1995a, 1995b, 2001). Vegetation records of the last glacial within the western Mediterranean indicate that the rapid transitions between stadial and interstadial climates were associated with shifts between steppic and increasingly forested conditions respectively (Sanchez Goni *et al.* 2002, 2008). Such changes in vegetation would drastically alter the potential for sediment erosion and mobility (e.g. Thornes 2009), and, as such, it is likely that such vegetational changes are, at least in part, responsible for the change in landscape stability recorded within the Chimeneas sediments. It is also thought that, during the glacial minimum, low vegetation density is responsible for not only increasing sediment availability for aeolian mobilisation, but also for increasing landscape instability enabling increased reworking of the aeolian sediments that were deposited during this period.

The record at Chimeneas highlights that, in southern Spain, such vegetational and landscape changes of the last glacial were associated with large temperature variations. Contrary to previous understanding of the controls on the isotopic composition of soil carbonates within the Mediterranean (Candy *et al.* 2012), the record from Chimeneas provides a temperature, as opposed to an evaporation driven, $\delta^{18}O$ signal. Variations in the $\delta^{18}O$ values of soil carbonates at Chimeneas indicate that soil forming intervals were up to ~6°C warmer than periods of loess accumulation.

12.1.2 Maro

Rose *et al.* (1999) previously identified an accumulation of loess in Mallorca dating to the post-interglacial sub-stages of MIS 5, representing the first Mediterranean loess outside of North Africa to have been dated to before the last glacial. Recognition of the deposit as loess is made on the basis of textural characteristics; Rose *et al.* (1999) do not, however, suggest a source for this silt. Loess that was deposited during the later sub-stages of MIS 5 is identified at Maro (chapter 9). Sub-stage correlation based upon OSL age estimates is not possible due to the large uncertainties associated with each age. The loess at Maro is however, underlain by an MIS 5e tufa deposit, suggesting, if continuity of deposition is assumed, that loess accumulation occurred within MIS 5d. It has not been possible to source the sediments through sedimentological or mineralogical methods (chapter 6). However, Sr-Nd isotope data indicates that there may be a far-travelled dust component within the loess deposits. PSA and micromorphological analysis indicate that the sediments were subject to some reworking and periods of local non-aeolian sediment input (chapter 9).

The occurrence of two soil horizons within the loess exposure of Maro indicates the occurrence of two episodes of short lived land-surface stability, unfortunately it is not possible to constrain the timing of these events as Milankovitch or sub-Milankovitch type changes. The evaporation driven $\delta^{13}C$ and $\delta^{18}O$ record of composition of soil carbonates at Maro indicates that episodes of soil formation were associated with increased environmental humidity; most likely associated with increased effective moisture availability and increasing vegetation cover. Additionally, within the loess at Maro, there is a channel fill feature containing oncoidal forms (tufa), indicating a period of sustained landscape stability and increased vegetation cover (Goudie *et al.* 1993, Pedley 2009, Domínguez-Villar *et al.* 2011), most likely associated with a later warm sub-stage of MIS 5.

12.1.3 La Malaha

The sediment sequence at Malaha is a short (~1.5m) sediment exposure located within a valley cutting. Deposition of loess at the site occurs between 2.2 ± 0.2 ka to 1.4 ± 0.1 ka and, as such, is the first record of Holocene loess reported within southern Spain. The timing of accumulation at La Malaha appears to correspond to a short lived cooling/aridity event (e.g. Fletcher and Zielhofer 2011), but also with the Roman occupation of the region (Pantaléon-Cano *et al.* 2003 and references therein). Both of these events are thought to have resulted in a decline in vegetation cover, and, as such, it is not possible to state if climate or anthropogenic modification of the landscape made it suitable for loess accumulation (e.g. Tsoar and Pye 1987). Importantly however, Sr-Nd isotope data indicate that the loess sediments are significantly different in composition to other Granada basin sediments and appear to have a very high proportion of North African dust (chapter 6). As such, regardless of the mechanisms responsible for modification of the Spanish landscape, a significant increase in supply of North African dust must have occurred during this period.

12.1.4 Summary

This first comprehensive study of loess in southern Spain identifies that deposition can occur within a range of climatic settings, namely Interglacial (Malaha), Glacial (Chimeneas) and warm isotope-stage interstadial (Maro). Additionally, through the use of Sr-Nd isotopes, this study has identified that loess accumulation in southern Spain can be locally-derived or far-travelled, with the far travelled dust component most likely being derived from North African sources. It is clear, therefore, that regional processes responsible for accumulation of loess within this semi-arid region are complex and are not comparable with the classical model of loess accumulation developed for western and central Europe where loess accumulation is routinely a phenomenon of glacial climates (e.g. Muhs and Bettis 2003).

12.2 Dust flux in the Mediterranean

The Mediterranean region currently receives an annual dust flux of 0.2-100 g m^{-2} supplied from the arid and semi-arid regions of North Africa, with southern Spain reported to receive around 23 g m^{-2} annually with a mean grain size of 4-30 μm (Goudie 2009 and references therein). The composition of this dust varies through the Mediterranean, but modern dust of North African origin sampled in northeastern Spain has been reported as being rich in clay minerals, particularly Illite (Avila *et al.* 1996, Chester *et al.* 1984). However, the composition of the resulting dust is dependent upon the precise source region (Avila *et al.* 1996), and it is reported that some potential source regions (e.g. Algeria) may have a quartz dominant composition (Guieu and Thomas 1996), although this difference in composition may be due to sampling of sediment outcrops in potential source regions (Guieu and Thomas 1996) as opposed to atmospheric dust sediments (Avila *et al.* 1996). Transport of North African dust to the western Mediterranean is greatest during the summer months, but occurs throughout the year (Rodriguez *et al.* 2001). The transport of North African dust to southern Spain can be invoked through a number of atmospheric scenarios relating to the position of cyclonic and anticyclonic weather systems in the region (figure 12.1) (Rodriguez *et al.* 2001).

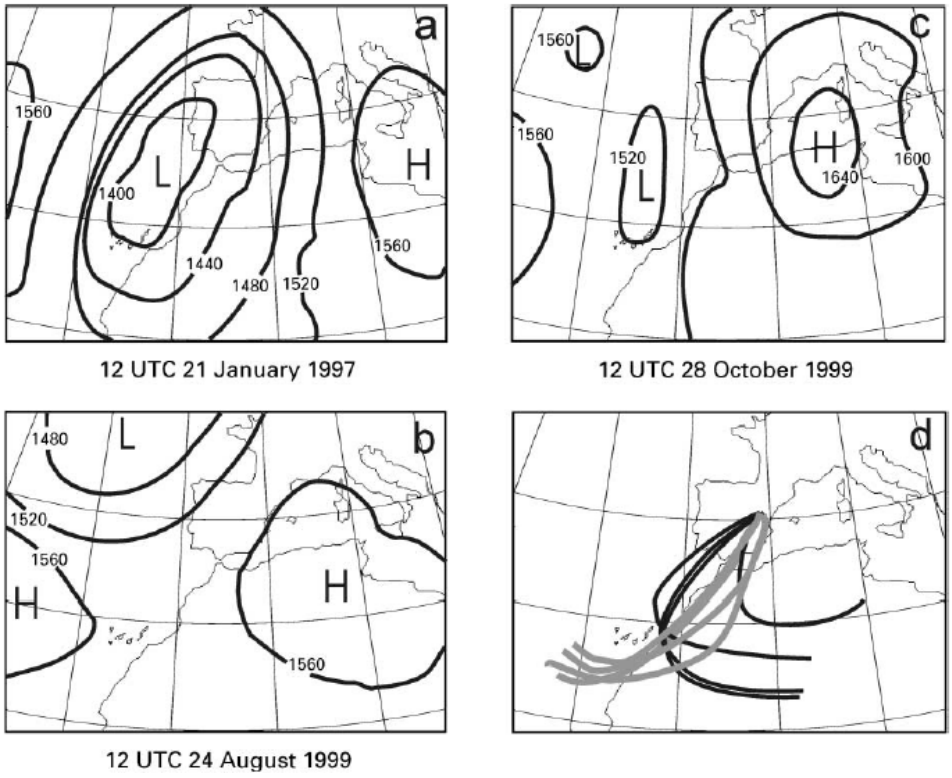

Figure 12.1 Atmospheric scenarios associated with transport of North African dust to southern Spain (Rodriguez et al. 2001). A. Low pressure to the west, B. High pressure south east of Iberia, C. High and low pressure systems to the south east and north west respectively, D. Trajectories of North African dust associated with cyclonic (grey lines) and anticyclonic systems (black lines).

12.2.2 Late Quaternary dust flux

Current understanding of North African dust flux to the Mediterranean during the Late Quaternary is based on only a very limited number of studies which are heavily focussed on the last glacial record of marine sediment cores from the Alboran Sea (figure 12.2) (Moreno *et al.* 2002, 2004, 2005, Bout-Roumazeilles *et al.* 2007, 2012).

Moreno *et al.* (2002) suggested that North African dust flux to the western Mediterranean Basin was driven by D-O cycles, with increased dust deposition within the Alboran Sea being correlated with arid stadial episodes (figure 12.2 a,b,c). This hypothesis is primarily constructed from evidence of changes in grain size and mineralogical composition of the sediments recovered from these cores. Moreno *et al.* (2002) used end member modelling in order to mathematically constrain the number of sediment inputs required to account for the grain sizes present in MD95-2043, stating that a three end member model adequately accounted for the particle size data of the core. EM3 is the finest fraction (<6 μm) and EM1 and EM2 have similar median values, but EM1 has the coarsest modal value. Moreno *et al.* (2002) compared these end member populations (EM1, EM2, EM3) with a sample of modern Saharan aerosol with a modal grain size of 10-15 μm. Moreno *et al.* (2002) state that this comparison identified that EM3, the finest fraction (<6 μm), was too fine to be consistent with Saharan aerosol deposition, but that EM1 and EM2 were closely comparable with the modal grain size of Saharan aerosols. As EM2 was the dominant population present through the core (~60%), Moreno *et al.* (2002) state that if EM2 was Saharan dust, then dust flux would need to be in the order of ≈90 g m^{-2} yr^{-1} in order to account for the sedimentation rate at the site. Moreno *et al.* (2002) argue that as this dust flux value is around four times higher than measurements of the modern dust flux, EM2 cannot represent Saharan aerosol input. EM1 has a similar modal grain size to present day Saharan aerosol and as it only constitutes around 10-12% of core sedimentation, Moreno *et al.* (2002) argue that it is the most likely population to represent Saharan aerosol input.

Additionally, Moreno *et al.* (2002) use the Si:K ratio (Si/Si+K) as a measure of aeolian vs. fluvial input respectively, arguing that Saharan dust has a high quartz content whereas fluvial systems feeding into the Alboran Sea have a high potassium rich (particularly Illite) clay content. Bout-Roumazeilles *et al.* (2007, 2012) also use clay as an indicator of sediment origin within the Alboran Sea, but this time argue that palygorskite can only be transported via aeolian pathways and as such, represents Saharan aerosol deposition at the site (figure 12.2 f).

These records appear to show increases in Saharan aerosol input associated with the very cold, arid stadial episodes of the last glacial and have been used by both Moreno *et al.* (2002, 2004,

2005) and Bout-Roumazeilles *et al.* (2007, 2012) to construct atmospheric scenarios associated with D-O cycle climate events for the Mediterranean (figure 12.3). These articles invoke a positive NAO type atmospheric scenario, where displacement of the jet stream results in increased regional aridity as well as the occurrence of an anticyclonic pressure system to the south east of Iberia (figure 12.3). Such an atmospheric scenario is proposed on the basis of the modern day relationship between NAO phase, regional precipitation and wind regimes.

There are, however, a number of issues associated with the studies of Moreno *et al.* (2002) and Bout-Roumazeilles *et al.* (2007). Firstly, Moreno *et al.* (2002) reference Guieu and Thomas (1996) in support of their statement that North African aerosols have a high quartz content. In fact, Guieu and Thomas (1996) measured the composition of sedimentary exposures within the potential source region of Algeria, but do not discuss actual aerosol composition. As previously mentioned, Saharan aerosols collected from within Spain have shown quartz content to be relatively low and Illite to be dominant. Caquineau *et al.* (1998) also suggest that the quartz content of Saharan aerosol vary greatly with source region, but in all cases the aerosol is reported to be rich in clay minerals. This therefore implies that Moreno *et al.* (2002) were mistaken in their use of Si:K ratio as a tracer of aeolian vs. fluvial input, as it is likely that both Saharan aerosol and local fluvial sediments can be rich in clay minerals. It is likely, therefore, that the close relationship reported by Moreno *et al.* (2002) between EM1 and Si:K ratios exists because EM1 is the coarsest fraction found within the core and would therefore be associated with periods where the input of clay sized material (K rich) was relatively reduced. As such, it is possible that both EM1 and the Si:K ratio reflect periods where there is an increase in the size of material reaching the core site, but not necessarily reflecting increased aeolian content.

Secondly, Moreno *et al.* (2002) state that EM2 could not be aeolian in origin as, due to the proportion of material it represents it would require a much higher dust flux than is currently suggested to exist. However, the rate of dust flux stated by Moreno *et al.* (2002) as being required to explain EM2 as an aeolian product is not much greater than some eastern Mediterranean regions currently receive (Goudie *et al.* 2009). As the record reflects sediment accumulation during the last glacial, a time of vastly reduced vegetation cover (figure 12.3 e), it is likely that there was ~~a~~ greater sediment availability and, therefore, potential for an increased dust flux within the region during this time. This increased potential for aeolian sediment supply to the Alboran Sea means that it is perhaps not justifiable to discount a high sedimentation rate end member on the basis of modern day supply rates.

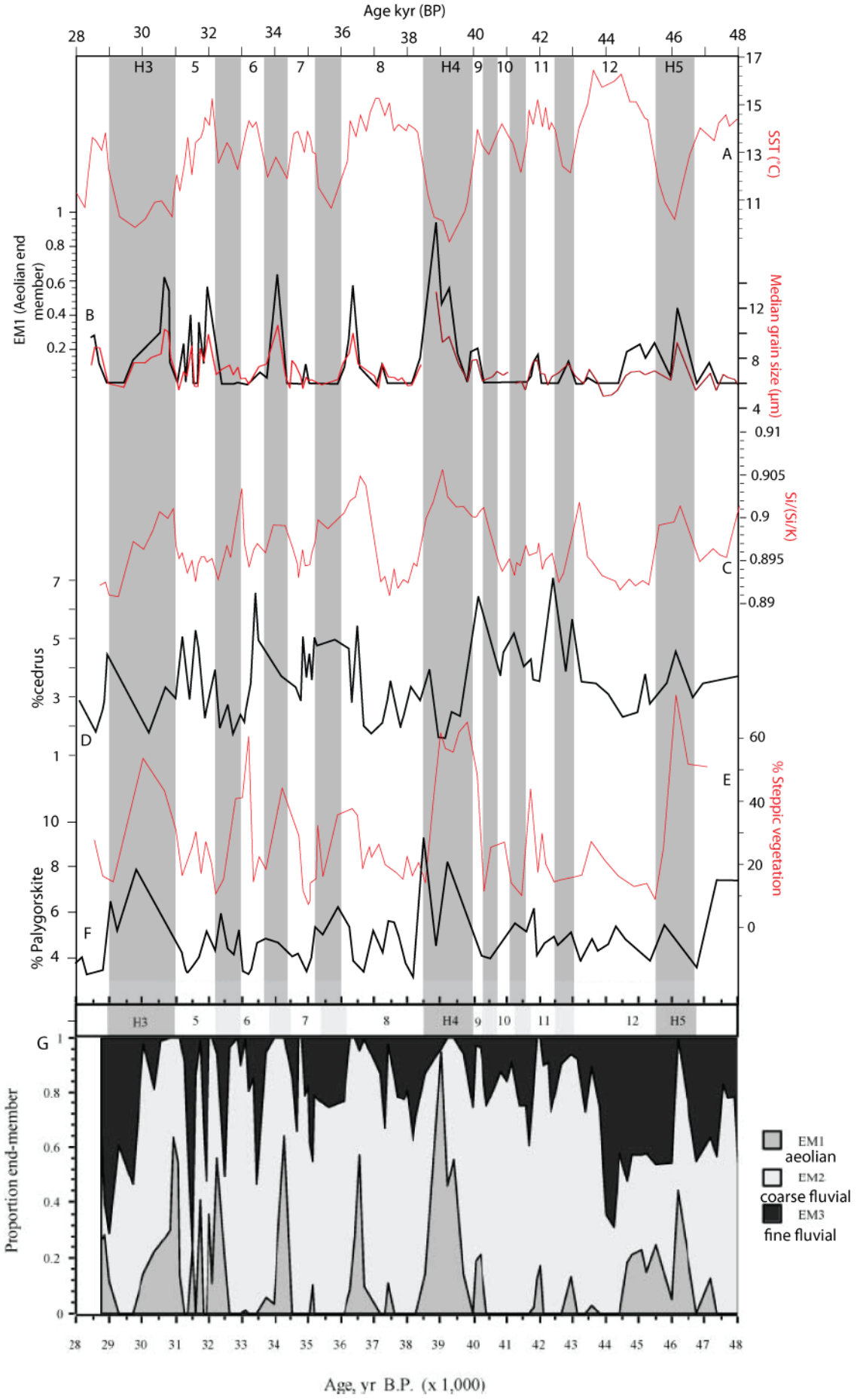

Figure 12.2 Alboran Sea records of dust flux during the last glacial. A-E, G MD95-2043 A. Cacho et al (1999), B,C,G. Moreno et al (2002), D,E. Sanchez Goni et al (2002), F. ODP976 Bout-Roumazeilles et al (2007).

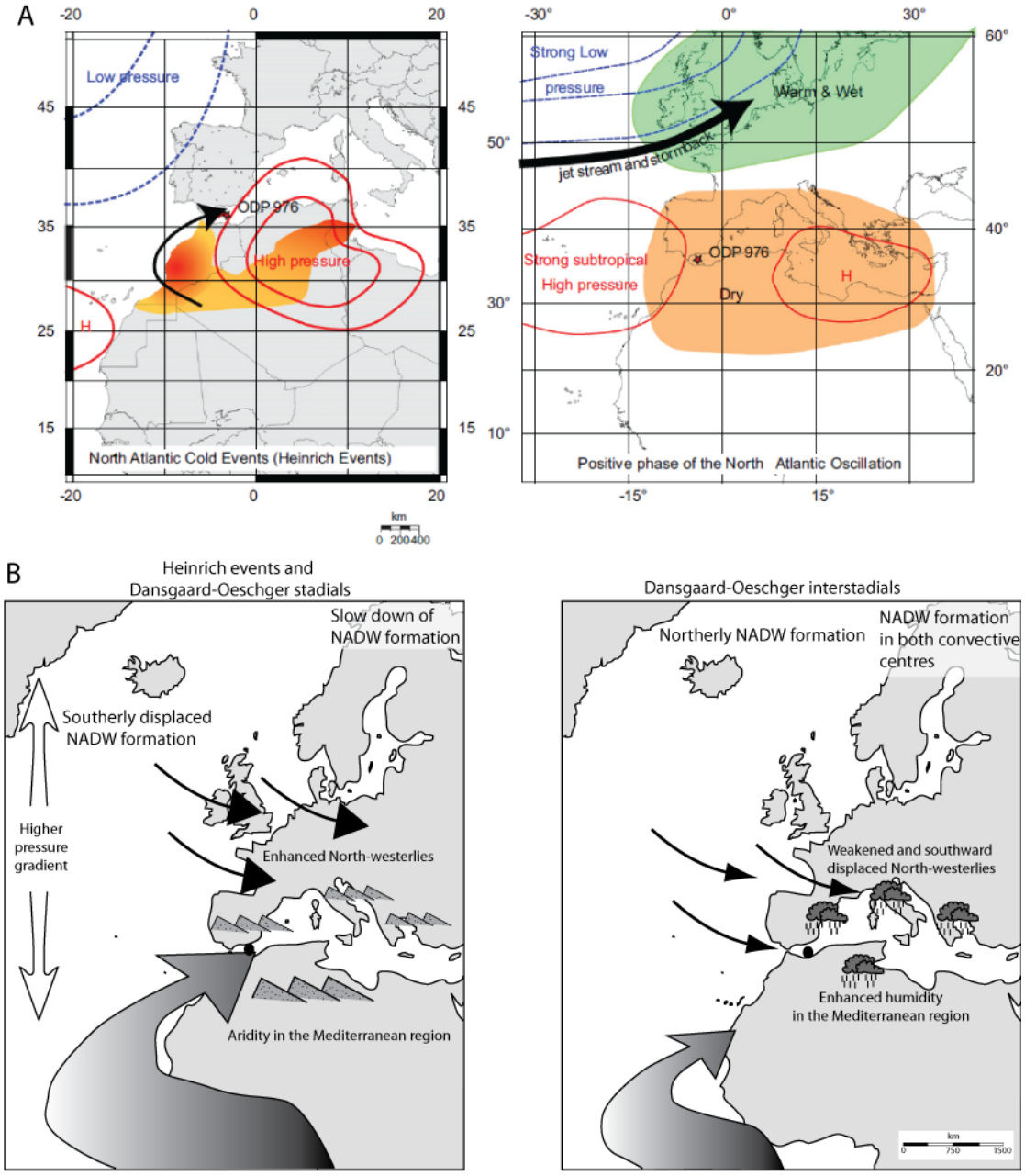

Figure 12.3 Atmospheric models for enhanced North African dust deposition to the Alboran Sea during the last Glacial. A. Bout-Roumazeilles et al (2007), (left) model for dust deposition during stadials compared to atmospheric pattern associated with +NAO phase (right). B. Moreno et al (2004) modelled NAO type atmospheric shifts associated with stadial and interstadial climate events

Finally, Bout-Roumazeilles *et al.* (2007, 2012) use the presence of palygorskite clay within the core to indicate aeolian deposition associated with stadial events. Bout-Roumazeilles *et al.* (2007, 2012) argue that palygorskite is commonly found within North African sediments, but that it can only be transported via aeolian processes. Although there is evidence that some North African deposits are rich in palygorskite (Avila *et al.* 1996, Molinaroli 1996, Avila *et al.* 1997, Bout-Roumazeilles *et al.* 2007), there is also evidence that areas of Iberia have extensive palygorskite deposits, particularly within the continental basins (Lopez-Aguayo and Gonzalez-Lopez 1995,

Sanchez and Galan 1995, Dias *et al.* 1997) and as such North Africa is not the only local source of the clay mineral. Additionally, there is contradictory evidence surrounding the survival of the fibrous clay by differing transport mechanisms (e.g. Aqrawi 1993, Khademi and Mermut 1998), and so it is not clear, if Bout-Roumazeilles *et al.* (2007, 2012) are correct in their assertion that it is a clear aeolian transport indicator.

A further complication comes from the record of *Cedrus* pollen within MD95-2043 (figure 12.2 d) (Sanchez Goni *et al.* 2002). It is suggested that *Cedrus* pollen is an indicator of North African sediment origin, as *Cedrus* occurrence is limited to cool, high areas of North Africa such as the Atlas mountains (Magri and Parra 2002). *Cerus* pollen is present throughout the core and appears to be more closely correlated with post-stadial environments than stadial climates. However, this pattern is driven in part by shifts in pollen composition as well as changes in *Cedrus* population. Importantly, however, the continuous presence of *Cedrus* indicates that sediments of North African origin arrive at the core location throughout the last glacial, contrary to the evidence suggested by the fluctuations in EM1.

12.2.3 Significance of the timing of loess accumulation in southern Spain

Although limited by the number of sites included within this study, loess accumulation has been identified within southern Spain in association with Interglacial, Glacial and warm isotope-stage stadial climates. The occurrence of loess is not restricted solely to the coldest, most arid stadial periods, as might be suggested based upon the evidence of Moreno *et al.* (2002) and Bout-Roumazeilles *et al.* (2007). Additionally, Sr-Nd isotope data from the study sites indicates that loess with a significant North African dust component is associated with warm climate intervals, but not with Glacial conditions (chapter 6). This finding implies that North African dust flux to the region is significantly high outside of the extreme climate conditions of last glacial stadial episode. Importantly, it also highlights the availability of fine silt sized material within southern Spain during the last glacial. The occurrence of large volumes of fine grained silts in southern Spain during this time implies that southern Spain may also be an important source of silts to the Alboran Sea during the last glacial.

Identification of a high North African dust contribution to Holocene loess is perhaps not altogether surprising if considered within the context of North African aridification through the Holocene. The abrupt end of the African Humid Period (AHP) at ~ 5.5 ka BP marks the onset of late Holocene North African aridification recorded through the reduction in lake levels and the mobilisation of large volumes of dust from North Africa (e.g. Gasse and van Campo 1994, deMenocal *et al.* 2000, Cole *et al.* 2009). It is possible that increased North African dust supply during the late

Holocene, coincident with the agricultural and/or climatic reduction in vegetation cover in southern Spain (Jalut *et al.* 2000, Davis *et al.* 2003, Magny *et al.* 2002, Pantaléon-Cano *et al.* 2003, Fletcher and Sánchez Goñi 2008, Carrión *et al.* 2010, Fletcher and Zielhoef 2011) enabled the accumulation of loess at La Malaha.

12.3 Unresolved issues

1. Is dust flux in the Alboran Sea purely North African in origin?

This thesis has documented the existence of a locally sourced last glacial loess deposit within southern Spain. This indicates that during the last glacial North Africa was not the only potential source of dust to the Alboran Sea. As such, it may not be necessary to invoke atmospheric circulation changes to explain an increased dust flux to the Alboran Sea, as it is likely that the regions to the north and the south of the basin had an increased potential to supply dust to the core location. This increase in regional dust availability is directly associated with the regional decrease in vegetation cover during the last glacial (figure 12.2 e).

It may be possible to distinguish between different sources of the dust supplied to the Alboran Sea through the use of Sr-Nd isotopes, which would enable dust to be provenanced and potentially their source pin pointed to specific areas of North Africa or elsewhere in the Mediterranean (e.g. Stumpf *et al.* 2012). Such resolution would enable the generation of source specific atmospheric circulation models. However, it would be necessary to demonstrate that the sediments analysed were aeolian in origin, and that changes in isotopic composition were not related to differential weathering effects (e.g. Cole *et al.* 2009).

2. What are the proxy records of Moreno *et al.* (2002) actually recording?

Firstly, if we assume that Moreno *et al.* (2002) are correct in their assertion that EM1 represents aeolian input and that this is also reflected by increasing Si content, how can we be sure what is driving the relative changes? As all data is given as percentages, a change in one component will drive a change in another. For example, a decrease in potassium content will produce a relative increase in Silica content. It is therefore not possible to identify if there is a true negative correlation between Si and K content, or if the supply of one element is switching on/off whilst the other remains relatively constant.

Secondly, changes in the median grain size through MD95-2043 are shown in figure 12.2b, indicating a definite coarsening of sediments associated with stadial events, which Moreno *et al.* (2002) have taken as primarily representing an increase in aeolian sediment inputs. However, the end member populations are assigned on the basis of similarities to present day sediment supply

to the core site, a relationship which may not be true through the last glacial. Evidence from Mediterranean fluvial sequences indicate that stadial events are correlated with increased sediment transport due to: (1) increased sediment supply because of reduced soil and vegetation cover, (2) increased weathering, (3) increased surface flow events resulting in increased stream power and transport ability due to a reduced precipitation storage potential in vegetation and soils and an increase in seasonality of flow events (Fuller *et al.* 1998, Macklin *et al.* 2002, Candy *et al.* 2004a). This would imply a greater fluvial input to the Alboran Sea during stadial events, which, due to the strongly seasonal high flow events thought to characterise the period, would result in an increase in both fine and coarse sediment supply to the Alboran Sea.

3. What is the Mediterranean record of loess accumulation?

Although limited in its scope to southern Spain, this study has found no relationship between the proposed increase in North African dust flux during the extreme stadials of the last glacial and loess accumulation within southern Spain. Loess deposition in southern Spain during the last glacial appears to be a local phenomenon subject to heavy reworking due to the lack of landscape stability. It has previously been suggested that other last glacial Mediterranean loess accumulations are locally derived (Bonifay 1965, Cremaschi *et al.* 1990, Coude-Gaussen 1991, Mücher *et al*. 1991, Günster *et al.* 2001, Garcia *et al.* 2010, 2011), which indicates a regional increase in silt availability through the last glacial. Such an increase in dust availability within the Mediterranean and North Africa could potentially complicate the interpretation of aeolian supply to marine records which have been used to construct atmospheric circulation models.

Additionally, the presence of a North-African derived Holocene loess deposit in southern Spain indicates that a period of sustained dust transport occurred during full Interglacial conditions. This study has also identified a warm isotope-stage interstadial (stage 5) loess, which may have a North African component. This study has therefore demonstrated that the extreme climate conditions of a glacial stadial are not required to produce a sustained supply of North African dust to Iberia.

A full assessment of the timing and provenance of loess in the Mediterranean region would enable further understanding of the local vs. far travelled sources and their relationships to climate and atmospheric conditions, but would also enable regional variability of the conditions optimum for loess accumulation to be understood.

Chapter 13 – Conclusions

This research has, for the first time, provided a comprehensive analysis of loess-palaeosol sequences in southern Spain. Independent dating of these sequences has identified episodes of loess accumulation within MIS 5, 2 and 1. Utilising a multi-proxy approach to analyse loess-palaeosol sequences, it has been possible to highlight their value as palaeoenvironmental archives within the Mediterranean as records of land system response to Late Quaternary climate changes. The principal findings of this study are listed below:

- Previous work has suggested that loess accumulation in southern Spain occurs within Glacial periods, resulting from the deflation of local silt sources. This study provides the first independently dated record of loess accumulations in southern Spain, and identifies that loess deposition occurs during Interglacial, Glacial and warm isotope stage stadials.
- Through the comparison of the sedimentology, grain morphology and geochemistry of loess sediments with local system sediments at each study site, it is clear that loess in southern Spain is not always a locally derived sediment.
- Glacial accumulation of loess (Chimeneas) derives from local silt sources, whereas Holocene loess deposition (La Malaha) records a strong North African dust component.
- Loess deposition in southern Spain is linked to dust supply and vegetation cover, which are both ultimately controlled by climate. It is suggested that, in southern Spain, the potential for loess accumulation and preservation is greatest during ‘warm’ climate intervals such as Interglacial stadial periods.
- Micromorphological and sedimentological analysis of loess-palaeosol sequences has identified that each loess sequence records both accretionary and post-depositional pedogenic alteration. It has been demonstrated that soil forming intervals occur in response to both Milankovitch and sub-Milankovitch climate changes, highlighting the ability of the landscape in southern Spain to respond to rapid climate fluctuations.
- This thesis has demonstrated and highlighted the importance of contextualising analysis of the stable isotopic composition of soil carbonates within a pedo-sedimentary framework, constructed through sedimentological and micromorphological analysis of the sediments, in order to fully understand the origin of the isotopic values recorded.
- Furthermore, contrary to current understanding of the controls on the isotopic composition of soil carbonates within the Mediterranean, this thesis has demonstrated that both temperature and aridity are possible climatic controls.

References

Abreu, L., Shackleton, N.J., Schönfeld, J., Hall, M. and Chapman, M., 2003, Millennial-scale oceanic climate variability off the Western Iberian margin during the last two glacial periods, *Marine Geology,* Vol.196, pp.1-20

Adamiec, G. and Aitken, M., 1998, Dose-rate conversion factors: update, *Ancient TL*, Vol. 16, pp. 37-50

Aitken, M. J., 1985, *Thermoluminescence Dating*, Academic Press, London, pp. 359

Albaréde, F., 2003, Geochemistry: An introduction, Cambridge University Press, Cambridge, UK, pp. 262

Allen, J.R.M., 2009, Vegetation and Ecosystem Dynamics, IN: Woodward, J.C. (Ed), *The Physical Geography of the Mediterranean*, Oxford University Press, Oxford, pp. 203-229

Allen, J.R.M., Brandt, U., Brauer, A., Hans-Wolfgang, H., Huntley, B., Keller, J., Krami, M., Mackensen, A., Mingram, J., Negendank, J.F.W., Nowaczyk, N.R., Oberhansli, H., Watts,W.A.,Wulg, S., Zolitschka, B.,1999. Rapid environmental changes in southern Europe during the last glacial period, *Nature* 400, pp. 740–743

Allen, R.G., Pereira, L.S., Raes, D. and Smith, M., 1998, *Crops evapotranspiration. Guidelines for computing crop requirements.Irrigations and Drainage*, Paper 56, FAO, Rome

Alley, R.B., Clark, P.U., Keigwin, L.D. and Webb, R.S., 1999, Making sense of millenial-scale climate change, *Geophysical monograph,* Vol.112, pp. 385-394

Alonso-Zarza, A.M. and Wright, V.P., 2010, Palustrine Carbonates, IN: Alonzon-Zarza, A.M. and Tanner, LH. (Eds), *Carbonates in continental settings: Geochemistry, diagenesis and applications, Developments in Sedimentology*, Elsevier, pp. 103-132

Amit, R. and Yaalon, D.H., 1996, The micrmomorphology of gypsum and halite in reg soils – the Negev Desert, Israel, *Earth Surface Porcesses and Landforms*, Vol. 21, pp. 1127-1143

An, Z., Kukla, G.J., Porter, S.C. and Xiao, J., 1991, Magnetic Susceptibility Evidence of Monsoon Variation on the Loess Plateau of Central China during the Last 130,000 Years, *Quaternary Research*, Vol. 36, pp. 29-36

Andersen, K.K., Svensson, A., Johnsen, S.J., Rasmussen, S.O., Bigler, M., Bothlisberger, R., Ruth, U., Siggard-Andersen, M.L., Steffensen, J.P., Dahl-Jensen, D., Vinther, B.M. and Clause, H.B., 2006, The Greenland Ice Core Chronology 2005, 15-42ka. Part 1: Constructing the time scale, *Quaternary Science Reviews,* Vol. 25, pp. 3246–3257

Andreucci, S., Bateman, M.D., Zucca, C., Kapur, S., Aks, H, Dunajko, A. and Pascucci, V., in press, Evidence of Saharan dust in upper Pleistocene reworked palaeosols of North-west Sardinia, Italy: palaeoenvironmental implications, *Sedimentology*

Andrews, J.E., 2006, Palaeoclimatic records from stable isotopes in riverine tufas: Synthesis and review, *Earth-Science Reviews*, Vol. 75, pp. 85-104

Andrews, J.E. and Brasier, A.T., 2005, Seasonal records of climatic change in annually laminated tufas: short review and future prospects, *Journal of Quaternary Science*, Vol. 20, pp. 411-421

Andrews, J.E., Riding, R. and Dennis, P.F., 1997, The stable isotope record of environmental and climatic signals in modern terrestrial microbial carbonates from Europe, *Palaeogeography, Palaeoclimatology, Palaeoecology*, Vol. 129, pp. 171 - 189

Antoine, P., Rousseau, D.D., Lautridou, J.P. and Hatté, C., 1999, Last interglacial-glacial climatic cycle in loess-palaeosol successions of north-westem France, *Boreas*, Vol. 28, pp. 551-563

Aqrawi, A.A.M., 1993, Palygorskite in the recent fluvio-lacustrine and deltaic sediments of southern Mesopotamia, *Clay Minerals*, Vol. 28, pp. 153-159

Armitage, S.J. and Bailey, R.M., 2005, The measured dependence of laboratory beta dose rates on sample grain size, *Radiation Measurements*, Vol. 39, pp. 123 – 127

Armitage, S.J., Duller, G.A.T. and Wintle, A.G., 2000, Quartz from southern Africa: sensitivity changes as a result of thermal pretreatment, *Radiation Measurements*, Vol. 32, pp. 571-577

Arpe, K., Leroy, S.A.G. and Mikolajewicz, U., 2011, A comparison of climate simulations for the last glacial maximum with three different versions of the ECHAM model and implications for summer-green tree refugia, *Climates of the Past*, Vol. 7, pp. 91-114

Avery, B.W. and Bascomb, C.L, 1974, Soil survey laboratory methods, *Soil survey of England and Wales*, Harpenden, 83 pp

Avila *et al.* 1996, African dust over Northeastern Spain: Mineralogy and source regions, IN: Guerzoni, S. and Chester, R. (Eds.), *The impact of desert dust across the Mediterranean*, Kluwer academic publishers, Dordrecht, pp. 201-205

Avila, A., Queralt-Mitjans, I., Alarcón, M., 1997, Mineralogical composition of African dust delivered by red rains over northeastern Spain, *Journal of Geophysical Research*, Vol. 102, pp. 21977-23996

Azañón, J.M., García-Dueñas, G. and Goffé, B., 1998, Exhumation of high-pressure metapelites and coeval crustal extension in the Alpujarride complex (Betic Cordillera), *Tectonophysics*, Vol. 285, pp. 231-252

Bai, Y., Fang, X., Nie, J., Wang, Y. and Wu, F., 2009, A preliminary reconstruction of the paleoecological and paleoclimatic history of the Chinese Loess Plateau from the application of biomarkers, *Palaeogeography, Palaeoclimatology, Palaeoecology*, Vol. 271, pp. 161–169

Bailey, H.P., 1979, Semi-arid climates: Their definition and distribution, IN: Hall, A.E., Cannell, G.H., Lawton, H.W. (Eds), *Agriculture in semi-arid environments*, Springer-Verlag, New York, pp. 73-96, CITED IN: Dietz, T.,Verhagen, J. and Ruben, R., 2004, *Impact of Climate Change on Drylands with a focus on West Africa*, Kluwer Academic Publishers, Dordecht, pp. 451

Bailey, R.M., 2000, Circumventing possible inaccuracies of the single aliquot regeneration method for the optical dating of quartz, *Radiation Measurements*, Vol. 32, pp.833–840

Bailey, G.N., Lewin, J., Macklin, M.G. and Woodward, J.C.,1990, The 'Older fill' of the Voidomatis Valley, North-west Greece and its relationship to the Palaeolithic archaeology and glacial history of the region, *Journal of Archaeological Science*, Vol. 17, pp. 145-150

Bajnóczi, B. and Kovács-Kis, V., 2006, Origin of pedogenic needle-fiber calcite revealed by micromorphology and stable isotope composition—a case study of a Quaternary paleosol from Hungary, *Chemie der Erde - Geochemistry*, Vol. 66, pp. 203-212

Balsam, W., Ellwood, B. and Ji, J., 2005, Direct correlation of the marine oxygen isotope record with the Chinese Loess Plateau iron oxide and magnetic susceptibility records, *Palaeogeography, Palaeoclimatology, Palaeoecology*, Vol. 221, pp. 141– 152

Bardaji, T., Goyl, J.L., Zazo, C., Hillaire-Marcel, C., Dabrio, C.J., Cabero, A., Ghlaeb, B., Silva, P.G. and Lario, J., 2009, Sea level and climate changes during OIS 5e in the Western Mediterranean, *Geomorphology*, Vol. 104, pp. 22-37

Bar-Matthews, M. and Ayalon, A., 2011, Mid-Holocene climate variations revealed by high-resolution speleothem records from Soreq Cave, Israel and their correlation with cultural changes, *The Holocene,* Vol. 21, pp. 163-171

Bar-Matthews, M., Ayalon, A. and Kaufman, A., 1997, Late Quaternary Paleoclimate in the Eastern Mediterranean Region from Stable Isotope Analysis of Speleothems at Soreq Cave, *Quaternary Research,* Vol. 47, pp. 155-168

Bar-Matthews, M., Ayalon, A. and Kaufman, A., 2000, Timing and hydrological conditions of Sapropel events in the Eastern Mediterranean, as evident from speleothems, Soreq cave, Israel, *Chemical Geology*, Vol. 169, pp.145-156

Barry, R.G. and Chorley, R.J., 2003, Atmosphere, Weather and Climate (8th Edition), Routledge, London, 412 pp

Barta, G., 2011, Secondary carbonates in loess-paleosoil sequences: a general review, *Central European Journal of Geoscience*, Vol. 3, pp. 129-145

Becze-Deák, J., Langohr, R., and Verrechia, E.P., 1997, Small scale secondary $CaCO_3$ accumulations in selected sections of the European loess belt. Morphological forms and potential for palaeoecological reconstruction, *Geoderma*, Vol.76, pp.221-252

Bell, W.T., 1980, Beta source calibration: some problems associated with the utilisation of the gamma irradiation of quartz and other phosphors, *Ancient TL*, Vol. 11, pp. 2–6

Belnap, J, 2008, Biological Crusts, IN: Lal, R. (Ed), *Encyclopedia of Soil Science*, Taylor & Francis Group, New York, pp.177-191

Benito, G., Thorndycraft, V.R., Rico, M., Sánchez-Moya, Y. and Sopeña, A., 2008, Palaeoflood and floodplain records from Spain: Evidence for long-term climate variability and environmental changes, *Geomorphology*, Vol. 101, pp. 68–77

Berger, A. and Loutre, M.F., 1991, Insolation values for the climate of the last 10 million years, *Quaternary Science Reviews*, Vol. 10, pp.297-317

Berger, A., Loutre, M.F., Kaspar, F. and Lorenz, S.J., 2007, Insolation during Interglacial, IN: Sirocco, F. (Ed), *Climate of past interglacials*, Developments in Quaternary Sciences, Vol. 7, Elsevier, Amsterdam, pp.13-28,

Bethoux, J.P. and Pierre, C., 1999 Mediterranean functioning and sapropel formation: respective influences of climate and hydrological changes in the Atlantic and the Mediterranean, *Marine Geology*, Vol. 153, pp. 29-39

Biscaye, P.E., Grousset, F.E., Revel, M., Van der Gaast, S., Zielinsky, G.A., Vaars, A., Kukla, G., 1997. Asian provenance of last glacial maximum dust in the GISP-2 ice core, Summit, Greenland, *Journal of Geophysical Research*, Vol 102, pp. 26765– 26781

Blaauw, M., Wohlfarth, B. Christen, J.A., 2008, Were last glacial climate events simultaneous between Greenland and western Europe?, *Climate of the Past Discussions*, Vol. 4, pp. 1203-1217

Blunier, T. and Brook, E.J., 2001, Timing of Millennial-Scale Climate Change in Antarctica and Greenland During the Last Glacial Period, *Science,* Vol. 291, pp.109-112

Bond, G., Heinrich, H., Broecker, W., Labeyrie, L., McManus, J., Andrews, J., Huon, S., Jantschik, R., Clasen, S., Simet, C., Tedesco, K., Klas, M., Bonani, G. and Ivy, S., 1992, Evidence for massive discharges of icebergs into the North Atlantic ocean during the last glacial period, *Nature,* Vol.360, pp.245-249.

Bond, G., Broecker, W., Johnsen, S., McManus, J., Labeyrie, L., Jouzel, J. and Bonani, G., 1993, Correlations between climate records from North Atlantic sediments and Greenland ice, *Nature,* Vol.365, pp.143-147

Bond, G., Showers, W., Cheseby, M., Lotti, R., Almasi, P., deMenocal, P., Priore, P., Cullen, H., Hajdas, I. and Bonani, G., 1997, A Pervasive Millennial-Scale Cycle in North Atlantic Holocene and Glacial Climates, *Science,* Vol. 278, pp. 1257-1266

Bonifay, E., 1965, Stratigraphie des loess anciens et récents dans le Sud-Est de la France, *Bulletin de l'Association française pour l'étude du quaternaire*, Vol. 2, pp. 21-34

Bøtter-Jensen, L., Andersen, C.E., Duller, G.A.T. and Murray, A.S., 2003, Developments in radiation,stimulation and observation facilities in luminescence measurements*, Radiation Measurements*, Vol. 37, pp. 535 – 541

Bout-Roumazeilles, V., Combourieu Nebout, N., Peyron, O., Cortijo, E., Landais, A. and Masson-Delmotte, V., 2007, Connection between South Mediterranean climate and North African atmospheric circulation during the last 50,000 yr BP North Atlantic cold events, *Quaternary Science Reviews*, Vol. 26, pp. 3197–3215

Bout-Roumazeilles, V., Combourieu-Nebout, N., Desprat, S., Siani, G. and Turons, J.L., 2012, Tracking atmospheric and riverine terrigenous supplies variability during the last glacial and the Holocene in central Mediterranean, *Climate of the Past Discussions*, Vol. 8, pp. 2921–2968
Brauer, A., Allen, J.R.M., Mingram, J., Dulski, P., Wulf, S. and Huntley, B., 2007, Evidence for last interglacial chronology and environmental change from Southern Europe, *PNAS*, Vol. 104, pp.450-455

Brauer, A., Allen, J.R.M., Mingram, J., Dulski, P., Wulf, S. and Huntley, B., 2007, Evidence for last interglacial chronology and environmental change from Southern Europe, *PNAS*, Vol. 104, pp.450-455

Breecker, D.O., Sharp, Z.D. and McFadden, L.D., 2009, Seasonal bias in the formation and stable isotopic composition of pedogenic carbonate in modern soils from central New Mexico, USA, *Geological Society of America Bulletin,* Vol. 121, pp. 630-640

Bridgland, D. R., 1986, *Clast Lithological Analysis,* Quaternary Research Association, Cambridge, Technical Guide 3, 207 pp

Buchardt, S. and Dahl-Jensen, D, 2008, At what depth is the Eemian layer expected to be found at NEEM?, *Annals of Glaciology*, Vol. 48, pp.100-103 (Abstract only)

Budd, D.A., Pack, S.M. and Fogel, M.L., 2002, The destruction of palaeoclimatic isotopic signals in Pleistocene carbonate soil nodules of Western Australia, *Palaeogeography, Palaeoclimatology, Palaeoecology*, Vol.188, pp. 249-273

Bull, P.A., 1981, Environmental reconstruction by electron microscopy, *Progress in Physical Geography,* Vol. 5, pp. 368-397

Bullock, P., Fedoroff, N., Jongerius, A., Stoops,G. and Tursina, T., 1985, *Handbook for soil thin section description,* Waine Research, Wolverhampton, 152 pp

Cacho, I., Grimalt, J.O., Pelejero, C., Canals, M., Sierro, F.J., Flores, J.A. and Shackleton, N.J., 1999, Dansgaard-Oeschger and Heinrich event imprints in Alboran Sea palaeotemperatures, *Palaeoceanography,* Vol.14, pp.698-705

Cacho, I., Grimalt, J.O., Sierro, F.J., Shackleton, N. and Canals, M., 2000, Evidence for enhanced Mediterranean thermohaline circulation during rapid climatic coolings, *Earth and Planetary Science Letters,* Vol. 183, pp. 417-429

Cacho, I., Grimalt, J.O., Canals, M., Sbaffi, L., Shackleton, N.J., Schönfeld, J. and Zahn, R., 2001, Variability of the western Mediterranean Sea surface temperature during the last 25,000 years and its connection with the Northern Hemisphere climatic changes, *Palaeoceanography*, Vol. 16, pp.40-52

Cacho, I., Shackleton, N., Elderfield, H., Sierro, F.J. and Grimalt, J.O., 2006, Glacial rapid variability in deep-water temperature and $\delta^{18}O$ from the Western Mediterranean Sea, *Quaternary Science Reviews,* Vol. 25, pp. 3294-3311

Candy, I. and Black, S., 2009, The timing of Quaternary calcrete development in semi-arid southeast Spain: Investigating the role of climate on calcrete genesis, *Sedimentary Geology*, Vol. 218, pp. 6–15

Candy, I., Black, S. and Sellwood, B.W., 2004a, Interpreting the response of a dryland river system to Late Quaternary climate change, *Quaternary Science Reviews*, Vol. 23, pp. 2513-2523

Candy, I., Black, S. and Sellwood, B.W., 2004b, Quantifying time scales of pedogenic calcrete formation using U-series disequilibria, *Sedimentary Geology*, Vol. 170, pp. 177–187

Candy, I., Black, S. and Sellwood, B.W., 2005, U-series isochron dating of immature and mature calcretes as a basis for constructing Quaternary landform chronologies for the Sorbas basin, southeast Spain, *Quaternary Research*, Vol. 64, pp. 100 – 111

Candy, I., Stephens, M., Hancock, J. and Waghorne, R., 2011, Palaeoenvironments of Ancient Humans in Britain: The Application of Oxygen and Carbon Isotopes to the Reconstruction of Pleistocene Environments, IN: Ashton, N., Lewis, S.G. and Stringer, C. (Eds), *The Ancient Human Occupation of Britain,* Amsterdam, pp. 23-37

Candy, I., Adamson, K., Gallant, C.E., Whitfield, E. and Pope, R., 2012, Oxygen and carbon isotopic composition of Quaternary meteoric carbonates from western and southern Europe: Their role in palaoenvironmental reconstruction, *Palaeogeography, Palaeoclimatology, Palaeoecology*, Vol. 326–328, pp. 1–11

Canti, M., 1998, Origin of calcium carbonate granules found in buried soils and Quaternary deposits, *Boreas,* Vol. 27, pp. 275-288

Canti, M.C., 2009, Experiments on the origin of 13C in the calcium carbonate granules produced by the earthworm Lumbricus terrestris, *Soil Biology and Biochemistry*, Vol. 41, pp.2588–2592
Caquineau, S., Gaudichet, A., Gomes, L., Magonthier, M.C. and Chatenet, B., 1998, Saharan dust: Clay ratio as a relevant tracer to assess the origin of soil-derived aerosols, *Geophysical Research Letters*, Vol. 25, pp. 983-986

Carrión, J.S., 2002, Patterns and processes of Late Quaternary environmental change in a montane region of southwestern Europe*, Quaternary Science Reviews*, Vol. 21, pp. 2047–2066

Carrión, J.S., 2004, The use of two pollen records from deep sea cores to frame adaptive evolutionary change for humans: a comment on " Neanderthal extinction and the millennial scale climate variability of OIS 3" by d'Errico, F. and Sanchez Goni, M.F., *Quaternary Science Reviews*, Vol. 23, pp. 1217-1224

Carrión, J.S., Munuera, M., Navarro, C., Burjachs, F., Dupré, M. and Walker, M.J., 1999, The palaeoecological potential of pollen records in caves: the case of Mediterranean Spain, *Quaternary Science Reviews,* Vol. 18, pp. 1061-1073

Carrión, J.S., Riquelme, J.A., Navarro, C. and Munuera, M., 2001, Pollen in hyaena coprolites reflects late glacial landscape in southern Spain, *Palaeogeography, Palaeoclimatology, Palaeoecology,* Vol. 176 (1-4), pp. 193-205

Carrión, J.S., Fernández, S., Jiménez-Moreno, G., Fauquette, S., Gil-Romera, G., González-Sampériz, P., Finlayson, C., 2010, The historical origins of aridity and vegetation degradation in southeastern Spain, *Journal of Arid Environments*, Vol. 74, pp. 731–736

Carslaw, H.S. and Jaeger, J.C., 1959, *Conduction of Heat in Solids*, 2nd ed, Oxford, New York

Cegla, J., Buckley, T. and Smalley, I.J., 1971, Microtextures of particles from some European loess deposits, *Sedimentology,* Vol. 17, pp. 129-134

Cerling, T.E., 1984, The stable isotopic composition of modern soil carbonate and its relationship to climate, *Earth and Planetary Science Letters,* Vol. 71, pp. 229-240

Cerling, T.E. and Quade, J., 1993, Stable carbon and oxygen isotopes in soil carbonates, IN: Swart, P.K. Lohmann, K.C. McKenzie, J. and Savin, S. (Eds.), *Climate change in continental isotopic records,* Gemophysical Monograph 78, American Geophysical Union, Washington, pp.217-232

Cerling, T., Quade, J., Wang, Y. and Bowman, J.R., 1989, Carbon isotopes in soils and paleosoils as ecology and paleoecology indicators, *Nature*, Vol. 341, pp.138–139

Cerling, T.E., Solomon, D.K., Quade, J. and Bowman, J.R., 1991, On the isotopic composition of carbon in soil carbon dioxide, *Geochemica cr Cosmochimrca Acta,* Vol. 55, pp. 3403-3405

Cerling, T.E., Harris, J.M., MacFadden, B.J., Leakey, M.G., Quade, J., Eisenmann, V., and Ehleringer, J.R., 1997, Global vegetation change through the Miocene/Pliocene boundary, *Nature*, Vol. 389, pp.153–8

Chappell, J. and Shackleton, N.J., 1986 Oxygen isotopes and sea level, *Nature*, Vol. 324, pp. 137-140

Chappellaz, J., Brook, E., Blunier and Brook, T. and Malaize, B., 1997, CH_4 and $\delta^{18}O$ of O_2 records from Antarctic and Greenland ice: A clue for stratigraphic disturbance in the bottom part of the Greenland Ice Core Project and the Greenland Ice Sheet Project 2 ice cores, *Journal of Geophysical Research*, Vol. 102, pp. 26547-26557

Chen, F.H., Bloemendal, J., Wang, J.M., Li, J.J. and Oldfield, F., 1997, High-resolution multi-proxy climate records from Chinese loess:evidence for rapid climatic changes over the last 75 kyr, *Palaeogeography, Palaeoclimatology, Palaeoecology*, Vol. 130, pp. 323-335

Chen, J., Li, G., Yang, J., Rao, W., Lu, H., Balsam, W., Sun, Y. and Ji, J., 2007, Nd and Sr isotopic characteristics of Chinese deserts: Implications for the provenances of Asian dust, *Geochimica et Cosmochimica Acta*, Vol. 71, pp. 3904–3914

Chester, R., Sharples, E.J., Sanders, G.S. and Saydam, A.C., 1984, Saharan dust incursion over the Tyrrhenian Sea, *Atmospheric environment*, Vol. 18, pp. 929-935

Clark, I. and Fritz, P., 1997, *Environmental Isotopes in Hydeogeology*, Lewis publishers, New York, p. 328

Clark, P.U. and Mix, A.C., 2002, Ice sheets and sea level of the Last Glacial Maximum, *Quaternary Science Reviews*, Vol. 21, pp. 1–7

Cole, J.M., Goldstein, S.L., deMenocal, P.B., Hemming, S.R. and Grousset, F.E., 2009, Contrasting compositions of Saharan dust in the eastern Atlantic Ocean during the last deglaciation and African Humid Period, *Earth and Planetary Science Letters*, Vol. 278, pp. 257–266

Combourieu Nebout, N., Turon, J.L., Zahn, R., Capontondi, L., Londeix, L. and Pahnke, K., 2002, Enhanced aridity and atmospheric high-pressure stability over the western Mediterranean during the North Atlantic cold events of the past 50 k.y, *Geology;* Vol. 30, pp. 863–866

Costa, J.E., 1988, Rheologic, geomorphic and sedimentologic differentiation of water floods, hyperconcentrated flows and debris flows, IN: Baker, V.R., Kockel, R.C. and Patton, P.C. (Eds), *Flood Geomorphology*, Wiley, Chichester, pp. 113-122

Coudé-Gaussen, G., 1987, The peri-Saharan loess: sedimentological characterization and paleoclimatical significance, *Geojournal*, Vol. 15, pp. 177-183

Coudé-Gaussen, G., 1991, The loess and loess-like deposits along the sides of the western Mediterranean Sea: Genetic and palaeoclimatic significance, *Quaternary International*, Vol. 5, pp. 1-8

Craig, H., 1965. The measurement of oxygen isotope palaeotemperatures. In Tongiorgi, E. (Ed), *Stable Isotopes in Oceanographic Studies and Palaeotemperatures*. Pisa, Consiglio Nazionale delle Ricerche Laboratorio di Geologia Nucleare, 161–182.

Cremaschi, M., Fedoroff, N., Guerreschi, A., Huxtable, J., Colombi, N., Castellettill, L. and Masperoll, A., 1990, Loess of Northern Italy, The Bagaggera sequence, *Quaternary International*, Vol. 5, pp. 23-38

Cruz-San Julian, J., Araguas, L., Rozanski, K., Benaventa, J., Cardenal, J., Hidalgo, M.C., Garcia-Lopez, S., Martinez-Garrido, J.C., Moral, F. and Olias, M., 1992, Sources of precipitation over South-Eastern Spain and groundwater recharge. An isotopic study, *Tellus*, Vol. 44B, pp. 226-236

d'Errico, F. and Sánchez Goñi, M.F., 2003, Neanderthal extinction and the millennial scale climatic variability of OIS 3, *Quaternary Science Reviews,* Vol.22, pp.769-788

Dansgaard, W., 1964, Stable isotopes in precipitation, *Tellus*, Vol. 16, pp.436–468

Dansgaard, W., Johnsen, S.J., Clausen, H.B., Dahl-Jensen, D., Gundestrup, N.S., Hammer, C.U., Hvidberg, C.S., Steffensen, J.P., Svelnbjörnsdottir, A.E., Jouzel, J. and Bond, G., 1993, Evidence for general instability of past climate from a 250-kyr ice-core record, *Nature,* Vol.364, pp.218-220

Dasch, E.J., 1969, Strontium isotopes in weathering profiles, deep sea sediments, and sedimentary rocks, *Geochtmica et Cosmochimica Acta*, Vol. 33, pp. 1621-1552

Davis, B.A.S., Brewer, S., Stevenson, A.C. and Guiot, J., 2003, The temperature of Europe during the Holocene reconstructed from pollen data, *Quaternary Science Reviews*, Vol. 22, pp. 1701–1716

Dearing, J.A., 1999, *Environmental magnetic susceptibility*, 2nd Edition, Barington Instruments, Witney, Oxon, pp.104

Dearing, J.A., Livingston, I.P., Bateman, M.D. and White, K.D., 2001, Palaeoclimate records from OIS 8.0-5.4 recorded in loess-palaeosol sequences on the Matmata Plateau, southern Tunisia, based on mineral magnetism and new luminescence dating, *Quaternary International*, Vol. 76/77, pp. 43-56

Decampo, D.M., 2010, The geochemistry of continental carbonates, IN: Alonso-Zarza, A.M. and Tanner, L.H. (eds), *Carbonates in continental settings: Geochemistry, diagenesis and applications*, Developments in Sedimentology, Vol 62, Elsevier, pp.1-60

deMenocal, P., Ortiz, J., Guilderson, T., Adkins, J., Sarnthein, M., Baker, L. and Yarusinsky, M., 2000, Abrupt onset and termination of the African Humid Period: rapid climate responses to gradual insolation forcing, *Quaternary Science Reviews*, Vol. 19, pp. 347-361

Deutz, P., Montanez, I.P., Monger, H.C., 2002, Morphology and stable and radiogenic isotope composition of pedogenic carbonates in late Quaternary relict soils, New Mexico, U.S.A: an integrated record of pedogenic overprinting, Journal of Sedimentary Research, Vol. 72, pp.809–822

Dever, L., Fontes, J.C. and Riche, G., 1987, Isotopic approach to calcite dissolution and precipitation in soils under semi-arid conditions, *Chemical Geology*, Vol. 66, pp. 307-314

Dias, I., Gonzalez, I., Prates, S. and Galan, E., 1997, Palygorskite occurrences in the Portuguese sector of the Tagus basin a preliminary report, *Clay Mineral*, Vol. 32, pp. 323-328

Ding, Z.L., Ranov, V., Yang, S.L., Finaev, A., Han, J.M. and Wang, G.A., 2002, The loess record in southern Tajikistan and correlation with Chinese loess, *Earth and Planetary Science Letters*, Vol. 200, pp. 387-400

Domínguez-Villar, D., Vázquez-Navarro, J.A., Cheng, H. and Edwards, R.L., 2011, Freshwater tufa record from Spain supports evidence for the past interglacial being wetter than the Holocene in the Mediterranean region, *Global and Planetary Change*, Vol. 77, pp. 129–141

Duller, G.A.T., 2003, Distinguishing quartz and feldspar in single grain luminescence measurements, *Radiation Measurements*, Vol. 37, pp.161–165

Durand, N., Monger, H.C., Canti, M.G., 2010, Calcium carbonate features, IN:Stoops, G., Marcelino, V. and Mees, F. (Eds), *Interpretation of micromorphological features of soils and regoliths,* Elsevier, Amsterdam, pp.149-182

Dworkin, S.I., Nordt, L. And Atchely, S., 2005, Determining terrestrial palaeotemperatures using the oxygen isotopic composition of pedogenic carbonate, *Earth and Planetary Science Letters,* Vol.237, pp.56-68

Emiliani*, C,.* 1955*,* Pleistocene temperatures, *Journal of Geology*, Vol. 63, pp. 538-557

Erel, Y. and Torrent, J., 2010, Contribution of Saharan dust to Mediterranean soils assessed by sequential extraction and Pb and Sr isotopes, *Chemical Geology*, Vol. 275, pp. 19–25

Faure, G., 1986, *Principles of Isotope Geology*, John Wiley and Sons, USA, p.589

Federoff, N., 1997, Clay illuviation in Red Mediterranean soils, *Catena*, Vol. 28, pp. 171-189

Feng, J.L., Zhu, L.P., Zhen, X.L. and Hu, Z.G., 2009, Grain size effect on Sr and Nd isotopic compositions in eolian dust: Implications for tracing dust provenance and Nd model age, *Geochemical Journal*, Vol. 43, pp. 123-131

Finlayson, G., Finlayson, C., Giles Pacheco, F., Rodriguez Vidal, J., Carrión, J.S. and Recio Espejo, J.M., 2008, Caves as archives of ecological and climatic changes in the Pleistocene—The case of Gorham's cave, Gibraltar, *Quaternary International,* Vol.181, pp.55-63

Fiol, L.I.A., J.J. Forno´s , B. Gelabert, J.A. Guijarro, 2005, Dust rains in Mallorca (Western Mediterranean): Their occurrence and role in some recent geological processes, *Catena*, Vol. 63, pp. 64–84

Fletcher, W.J. and Sánchez Goñi, M.F., 2008, Orbital- and sub-orbital-scale climate impacts on vegetation of the western Mediterranean basin over the last 48,000 yr, *Quaternary Research,* Vol.70, pp.451-464

Fletcher, W.J. and Zielhofer, C., 2011, Fragility of Western Mediterranean landscapes during Holocene Rapid Climate Changes, *Catena*, *in press*

Fletcher, W.J., Faust, D. and Zeilhoef, C., 2012, Fragile landscapes, Catena, *in press,* pp. 1-2

Florschütz, F., Amor, J.M. and Wijmstra, T.A., 1971, Palynology of a thick Quaternary succession in Southern Spain, *Palaeogeography, Palaeoclimatology, Palaeoecology*, Vol.10, pp. 233-264

Frakes, L.A. and Jianzhong, S., 1994, A carbon isotope record of the upper Chinese loess sequence: Estimates of plant types during stadials and interstadials, *Palaeogeography, Palaeoclimatology, Palaeoecology*, Vol. 108, pp.183-189

Frenchen, M., Oches, E.A. and Kohfeld, K.E., 2003, Loess in Europe-mass accumulation rates during the Last Glacial Period, *Quaternary Science Reviews,* Vol. 22, pp. 1835-1857

Friedli, H. Lötscher, H., Oeschger, Siegenthaler, U., Stauffer, B., 1986, Ice core record of the $^{13}C/^{12}C$ ratio of atmospheric CO_2 in the past two centuries. *Nature,* Vol. 324, pp. 237–239

Frigola, J., Moreno, A., Cacho, I., Canals, M., Sierro, F.J., Flores, J.A. and Grimalt, J.O., 2008, Evidence of abrupt changes in Western Mediterranean Deep Water circulation during the last 50 kyr: A high-resolution marine record from the Balearic Sea, *Quaternary International,* Vol.181, pp.88-104

Frost, C.D., O'Nions, R.K. and Goldstein, S.L., 1986, Mass balance for Nd in the Mediterranean Sea, *Chemical Geology*, Vol. 55, pp. 45-50

Frumkin, A. and Stein, M., 2004, The Sahara-East Mediterranean dust and climate connection revealed by strontium and uranium isotopes in a Jerusalem speleothem, *Earth and Planetary Science Letters*, Vol. 217, pp. 451-464

Fuller, I.C., Macklin, M.G., Lewin, J., Passmore, D.G. and Wintle, A.G., 1998, River response to high-frequency climate oscillations in southern Europe over the past 200 k.y, *Geology,* Vol. 26; pp. 275–278

Gale, S. and Hoare, P., 1992, *Quaternary Sediments: Petrographic methods for the study of unlithified rocks,* John Wiley and Sons, London, 332 pp

Gallant, C.E., Candy, I., van Bogaard, P., Silva, B. and Turner, E., in prep, Stable isotopic evidence for Middle Pleistocene environmental change from a loess palaeosol sequence: Kärlich, Germany

García, R., González, J.A., Petit, M.D. and Rucandio, M.I., 2010. Caracterización de las acumulaciones loéssicas en el Valle medio del Río Tajo, España, *Estudios Geológicos*, Vol. 66, pp. 115–21

García, R., Petit-Domínguez, M.D, Rucandio, M.I. and González, J.A.,2011, Provenance of loess from the Spanish central region: chemometric interpretation, *Geological Magazine*, Vol. 148, pp. 481–491

Gardner, R.A.M., 1977, Evidence Concerning the Existence of Loess Deposits at Tell Fara, Northern Negev, Israel, *Journal of Archaeological Science*, Vol. 4, pp. 377-386

Gasse, F. and van Campo, E., 1994, Abrupt post-glacial climate events in West Asia and North Africa monsoon domains, *Earth and Planetary Science Letters*, Vol. 126, pp. 435-456
Genty, D., Combourieu Nebout, N., Hatté, C., Blamart, D., Ghaleb, B. and Isabello, L., 2005, Rapid climatic changes of the last 90 kyr recorded on the European continent, *Comptes Rendus Geosciences,* Vol. 337, pp.970-982

Gill , R.C.O., Aparicio, A., Azzouzi, M.E., Hernandez, J., Thirlwall, M.F., Bourgois, J. and Marriner, G.F., 2004, Depleted arc volcanism in the Alboran Sea and shoshonitic volcanism in Morocco: geochemical and isotopic constraints on Neogene tectonic processes, *Lithos*, Vol. 78, pp. 363– 388

Gimeno, Luis, Raquel Nieto, Ricardo M. Trigo, Sergio M. Vicente-Serrano, Juan Ignacio López-Moreno, 2010, Where Does the Iberian Peninsula Moisture Come From? An Answer Based on a Lagrangian Approach. *Journal of Hydrometeorology*, Vol. 11, 421–436

Giorgi, F. and Lionello, P., 2008, Climate change projections for the Mediterranean region, *Global and Planetary Change*, Vol. 63, pp. 90–104

Giorgi, F., Hewitson, B., Christensen, J., Hulme, M., Von Storch, H., Whetton, P., Jones, R., Mearns, L., Fu, C., Arritt, R., Bates, B., Benestad, R., Boer, G., Buishand, A., Castro,M., Chen, D., Cramer, W., Crane, R., Crossley, J.F., Dehn, M., Dethloff, K., Dippner, J., Emori, S., Francisco, R., Fyfe, J., Gerstengarbe, F.W., Gutowski, W., Gyalistras, D., Hanssen-Bauer, I., Hantel, M., Hassell, D.C., Heimann, D., Jack,C., Jacobeit, J., Kato, H., Katz, R., Kauker, K., Knutson, T., Lal, M., Landsea, C., Laprise, R., Leung, L.R., Lynch, A.H., May, W., McGregor, J.L., Miller, N.L., Murphy, J. , Ribalaygua, J., Rinke, A., Rummukainen, M., Semazzi, F., Walsh, K., Werner, P., Widmann, M., Wilby, R., Wild, M., Xue, Y., 2001, Regional climate information-evaluation and projections, in Houghton, J.T., Ding, Y., Griggs, D.J., Nouger, M., van der Linden, P.J. and Xiaosu, D. (Eds), *Climate change 2001: The Scientific basis. Contribution of Working Group 1 to the Third Assessment Report of the Intergovernmental Panel on Climate Change,* Cambridge University Press, Cambridge

Gocke, M., Pustovoytov, K., Kühn, P., Wiesenberg, G.L.B., Löscher, M. and Kuzyakov, Y., 2011, Carbonate rhizoliths in loess and their implications for palaeoenvironmental reconstruction revealed by isotopic composition: $\delta^{13}C$, ^{14}C, *Chemical Geology*, Vol. 283, pp. 251–260

Gocke, M., Pustovoytov, K. and Kuzyakov, Y., 2012, Pedogenic carbonate formation: Recrystallization versus migration—Process rates and periods assessed by ^{14}C labelling, *Global biochemical cycles*, Vol. 26, GB1018,

Goldstein, S. L., Onions, R. K., and Hamilton, P. J., 1984, A Sm–Nd isotopic study of atmospheric dusts and particulates from major river systems, *Earth and Planetary Science Letters*, Vol. 70, pp. 221–236

Gómez-Pugnarie, M. T., Ulmer, P., and López-Sánchez-Vizcaíno, V.,. 2000, Petrogenesis of mafic igneous rocks of the Betic Cordilleras: A field, petrological and geochemical study, *Contribution to Mineral Petrology*, Vol. 139, pp. 436-457

González-Sampériz, P., Leroy, S.A.G., Carrión, J.S., Fernández, S., Garcia-Antón, M., Gil-Garcia, M.F., Uzquiano, P., Valero-Garcés, B. and Figueiral, I., 2010, Steppes, savannahs, forests and phytodiversity reservoirs during the Pleistocene in the Iberian Peninsula, *Review of Palaeobotany and Palynology*, Vol. 162, pp.427-457

Goudie, A.S., 1983, Calcrete, IN: Goudie, A.S., Pye, K. (Eds.), *Chemical Sediments and Geomorphology*, Academic Press, London, pp. 93–131

Goudie, A., 2009, Aeolian processes and landforms, IN: Woodward, J.C. (Ed), *The Physical Geography of the Mediterranean*, Oxford University Press, Oxford, pp. 415-432

Goudie, A.S. and Viles, H.A., 1995, The nature and pattern of debris liberation by salt weathering: A laboratory study, *Earth Surface Processes and Landforms*, Volume 20, pp. 437–449 (Abstract only)

Goudie, A.S. and Middleton, N.J., 2001, Saharan dust storms: nature and consequences, *Earth-Science Reviews*, Vol. 56, pp. 179–204

Goudie, A.S., Viles, H.A. and Pentecost, 1993, The late-Holocene tufa decline in Europe, *The Holocene*, Vol. 3, pp.181-186

Grootes, P.M., Stulver, M., White, J.W.C., Johnsen, S. and Jouzel, J., 1993, Comparison of oxygen isotope records from the GISP2 and GRIP Greenland ice cores, *Nature*, Vol. 366, pp.552-554

Grousset, F.E. and Biscaye, P.E., 2005, Tracing dust sources and transport patterns using Sr, Nd and Pb isotopes, *Chemical Geology*, Vol. 222, pp. 149– 167

Grousset, F.E., Biscaye, P.E., Zindler, A., Prospero, J. and Chester, R., 1988, Neodymium isotopes as tracers in marine sediments and aerosols: North Atlantic, *Earth and Planetary Science Letters,* Vol. 87, pp. 367-378

Grousset, F.E., Rognon, P., Coudé-Gaussen, G. and Pédemay, P., 1992, Origins of peri-Saharan dust deposits traced by their Nd and Sr isotopic composition, *Palaeogeography, Palaeoclimatology, Palaeoecology*, Vol.93, pp. 203-212

Grousset , F.E., Parra, M., Bory, A., Martinez, P., Bertrand, P., Shimmield, G. and Ellam, R.M., 1998, Saharan wind regimes traced by the Sr-Nd isotopic composition of Subtropical Atlantic sediments: Last Glacial Maximum vs. today, *Quaternary Science Reviews*, Vol. 17, pp. 395-409

Guieu, C. and Thomas, A.J., 1996, Saharan aerosols: from the soil to the ocean, IN: Guerzoni, S. and Chester, R. (Eds), *The impact of desert dust across the Mediterranean*, Kluwer academic publishers, Dordrecht, pp. 207-216

Günster, H., Eck, P., Skowronek, A. and Zöller, L., 2001, Late Pleistocene loess and their paleosols in the Granada Basin, Southern Spain, *Quaternary International*, Vol. 76/77, pp. 241-245

Gutierrez Elorza, M., 1995, Desert surfaces: pavements, patterned ground, varnishes and crusts, *Developments in Earth Surface Processes*, Vol. 8, pp.259-284

Haase, D., Fink, J., Haase, G., Ruske, R., Pécsi, M., Richter, H., Altermann, M. and Jäger, K.D., 2007, Loess in Europe—its spatial distribution based on a European Loess Map, scale 1:2,500,000, *Quaternary Science Reviews*, Vol. 26, pp. 1301-1312

Harding, A.E., Palutikof, J. and Holt, T., 2009, The climate system, IN: Woodward, J.C. (Ed), *The Physical Geography of the Mediterranean*, Oxford University Press, Oxford, pp. 69-88

Hays, P.D. Grossman, E.L., 1991, Oxygen isotopes in meteoric calcite cements as indicators of continental palaeoclimate, *Geology*, Vol 19, pp. 441-444

Heller, F. and Tung-Sheng, L., 1982, Magnetostratigraphic dating of loess deposits in China, *Nature*, Vol. 300, pp. 431-433

Hemming, S.R., 2007, Terrigenous Sediments, IN: Elias, S.A. (Ed), *Encyclopedia of Quaternary Science,* Elsevier, pp. 1776-1785

Hesse, P.R., 1971, *A Textbook of Soil Chemical Analysis*, John Murray, London, UK

Heusser, L.E., 2000, Rapid oscillations in western North America vegetation and climate during oxygen isotope stage 5 inferred from pollen data from Santa Barbara Basin (Hole 893A), *Palaeogeography, Palaeoclimatology, Palaeoecology*, Vol. 161, pp.407–421

Higgins, P. and MacFadden, B.J., 2004, ‘‘Amount Effect’’ recorded in oxygen isotopes of Late Glacial horse (*Equus*) and bison (*Bison*) teeth from the Sonoran and Chihuahuan deserts, southwestern United States, *Palaeogeography, Palaeoclimatology, Palaeoecology*, Vol. 206, pp. 337– 353

Higgs, E.S. and Vita-Finzi, C., 1966, The climate, Environment and Industries of Stone Age Greece: Part II, *Proceedings of the Prehistoric Society,* Vol. 32, pp. 1-29, Referenced by: Macklin, M.G. and Woodward, J.C., 2009, River systems and environmental change, IN: Woodward, J.C. (Ed), *The Physical Geography of the Mediterranean*, Oxford University Press, Oxford, pp. 319-352

Hoefs, J., 2004, Stable isotope geochemistry (5th Edition), Springer-Verlag, Berlin, p. 241

Hudson, J.D., 1977, Stable isotopes and limestone lithification, *Journal of the Geological Society, Vol.* 133, pp. 637-660

Hughen, K. A., Overpeck, J.T., Peterson, L.C. and Trumbore, S., 1996, Rapid climate changes in the tropical Atlantic region during the last deglaciation, *Nature*, Vol. 380, pp. 51– 54

Hughes, P. D., Woodward, J.C. and Gibbard, P.L., 2006, Quaternary glacial history of the Mediterranean mountains, *Progress in Physical Geography,* Vol. 30, pp. 334-364

Huntley, D.J., Godfrey-Smith, D.I. and Tewalt, M.L.W., 1985, Optical dating of sediments, *Nature*, Vol. 313, pp. 105-107

Imbrie, J., J. D. Hays, D. G. Martinson, A. McIntyre,A. C. Mix, J. J. Morley, N. G. Paces, W. L. Prell, and N. J. Shackleton, 1984,The orbital theory of Pleistocene climate: Support from a revised chronology of the marine $\delta^{18}O$ record, IN: Berger, A.,Imbrie, J., Hays, J., Kukla, G. and Saltzman, B. (Eds), *Milankovitch and Climate, Part I*, Reidel, Dordrecht, pp. 269-305

Iriondo, M.H. and Kröhling, D.M., 2007, Non-classical types of loess, Sedimentary *Geology*, Vol. 202, pp. 352–368

Jacobs, P.M. and Mazon, J.A., 2007, Late Quaternary climate change, loess sedimentation, and soil profile development in the central Great Plains: A pedosedimentary model, *GSA Bulletin*, Vol. 119, pp. 462–475

Jafarzadeh, A.A. and Burnham, C.P., 1992, Gypsum crystals in soils, *Journal of Soil Science*, Vol. 43, pp. 409-420

Jahn, B., Gallet, S. and Han, J., 2001, Geochemistry of the Xining, Xifeng and Jixian sections, Loess Plateau of China: eolian dust provenance and paleosol evolution during the last 140 ka, *Chemical Geology*, Vol. 178, pp. 71–94

Jalut, G., Amat, A.E., Bonnet, L., Gauquelin, T. and Fontugne, M., 2000, Holocene climatic changes in the Western Mediterranean, from south-east France to south-east Spain, *Palaeogeography, Palaeoclimatology, Palaeoecology*, Vol. 160, pp. 255–290

Jenny, H., 1941, *Factors of soil formation: A system of quantitative pedology*, Reprinted 1994, Dover publications, New York

Jiamao, H., Keppens, E., Tungsheng, L., Paepe, R. and Wenying, J., 1997, Stable isotope composition of the carbonate concretion in loess and climate change, *Quaternary International*, Vol.37, pp. 37-43

Johnsen, S., Clausen, H., Dansgaard, W., Fuhrer, K., Gundestrup, N., Hammer, C., Iversen, P., Jouzel, J., Stauffer, B., Steffensen, J., 1992, Irregular glacial interstadials recorded in a new Greenland ice core, *Nature*, Vol. 359, pp. 311 –313

Johnsen, S.J., Dahl-Jensen, D., Gundestrup, N., Steffensen, J.P., Clausen, H.B., Miller, H., Masson-Delmotte, V., Sveinbjo, A.E. and White, J., 2001, Oxygen isotope and palaeotemperature

records from six Greenland ice-core stations: Camp Century, Dye-3, GRIP, GISP2, Renland and NorthGRIP, *Journal of Quaternary Science*, Vol. 16, pp. 299–307

Jones, A.P., Tucker, M.E. and Hart, J.K., 1999, *The description and analysis of Quaternary stratigraphic field sections, Technical guide No. 7*, Quaternary Research Association, London, p. 286

Jouzel, J., Masson-Delmotte, V., Cattani, O., Dreyfus, G., Falourd, S., Hoffmann, G., Minster, B., Nouet, J., Barnola, J.M., Chappellaz, J., Fischer, H., Gallet, J.C., Johnsen, S., Leuenberger, M., Loulergue, L., Luethi, D., Oerter, H., Parrenin, F., Raisbeck, G., Raynaud, D., Schilt, A., Schwander, J., Selmo, E., Souchez, R., Spahni, R., Stauffer, B., Steffensen, J.P., Stenni, B., Stocker, T.F., Tison, J.L., Werner, M. and Wolff, E.W., 2007, Orbital and Millennial Antarctic Climate Variability over the Past 800,000 Years, *Science,* Vol.317, pp.793-796

Kemp, R.A., 1985a, *Soil Micromorphology and the Quaternary,* QRA technical Guide No. 2, Cambridge, 80 pp

Kemp, R.A., 1985b, The decalcified Lower Loam at Swanscombe, Kent: a buried Quaternary soil, *Proceedings of the Geologists' Association*, Vol. 96, pp.343-356

Kemp, R.A., 1995, Distribution and genesis of calcitic pedofeatures within a rapidly aggrading loess-paleosol sequence in China, *Geoderma*, Vol. 65, pp. 303-316

Kemp, R.A., 1999, Micromorphology of loess-palaeosol sequences: a record of palaeoenvironmental change, *Catena,* Vol.35, pp.179-196

Kemp, R.A., 2001, Pedogenic modification of loess: significance for palaeoclimatic reconstructions, *Earth-Science Reviews*, Vol. 54, pp. 145-156

Kemp, R.A., and Derbyshire, E., 1998, The loess soils of China as records of climatic changes, *European Journal of Soil Science*, Vol. 49, pp. 525–539

Kemp, R.A., Derbyshire, E., Xingmin, M., Fahu, C. and Baotian, P., 1995, Pedosedimentary reconstruction of a thick loess-palaeosol sequence near Lanzhou in North-Central China, *Quaternary Research*, Vol. 43, pp. 30-45

Kemp, R.A., Derbyshire, E., Fahu, C. and Haizhou, M., 1996, Pedosedimentary development and palaeoenvironmental significance of the S1 palaeosol on the northeastern margin of the Qinghai-Xizang (Tibetan) Plateau, *Journal of Quaternary Science*, Vol. 11, pp. 95-106

Kemp, R.A., Derbyshire, E., and Meng, X.M., 2001, A high resolution micromorphological record of changing landscapes and climates on the Western Loess Plateau of China during oxygen isotope stage 5, *Palaeogeography, Palaeoclimatology, Palaeoecology*, Vol. 170, pp. 157–169

Kemp, R.A., King, M., Toms, P., Derbyshire, E., Manuel Sayago, J. and Collantes, M. M., 2004, Pedosedimentary development of part of a late Quaternary loess-palaeosol sequence in northwest Argentina, *Journal of Quaternary Science,* Vol. 19, pp. 567-576

Khademi, K. and Mermut, A.R., 1998, Source of palygorskite in gypsiferous Aridisols and associated sedimetns from central Iran, *Clay Minerals,* Vol. 33, pp. 561 578

Kim, S.T. and O'Neil, J.R., 1997, Equilibrium and nonequilibrium oxygen isotope effects in synthetic carbonates, *Geochimica et Cosmochimica Acta*, Vol. 61, pp.3461-3475

King, M., 2000, *Late Quaternary loess-palaeosol sequences in the Palouse, Northwest USA: pedosedimentary and palaeoclimatic significance*, Unpublished PhD Thesis, University of London

Klappa, C.F., 1980, Rhizoliths in terrestrial carbonates: classification, recognition, genesis and significance, *Sedimentology*, Vol. 27, pp. 613-629

Köhler, P., Joos, F., Gerber, S. and Knutti, R., 2005, Simulated changes in vegetation distribution, land carbon storage, and atmospheric CO2 in response to a collapse of the North Atlantic thermohaline circulation, *Climate Dynamics*, Vol. 25, pp 689–708

Krinsley, D.H. and Smalley, I.J., 1972, Sand: The study of quartz sand in sediments provides much information about ancient geological environments, *American Scientist*, Vol. 60, pp. 286-291

Krinsley, D.H. and Doornkamp, J.C., 1973, *Atlas of Quartz sand surface textures*, Cambridge University Press, UK, p.91

Kubilay, N. and Saydam, A.C., 1995, Trace elements in atmospheric particulates over the Eastern Mediterranean; concentrations, sources and temporal variability, *Atmospheric Environment*, Vol. 29, pp. 2289-2300

Kuhlemann, J., Rohling, E.J., Krumrei, I., Kubik, P., Ivy-Ochs, S. and Kucera, M., 2008, Regional Synthesis of Mediterranean Atmospheric Circulation During the Last Glacial Maximum, *Science*, Vol. 321, pp. 1338- 1340

Kukla, G., 1978, The Classical European Glacial Stages: Correlation with Deep-Sea Sediments, *Transactions of the Nebraska Academy of Sciences and Affiliated Societies,* Paper 334, pp.57-93

Kukla, G., 1987, Loess stratigraphy in central China, *Quaternary Science Reviews*, Vol.6, pp.191-219

Kukla, G. and An, Z., 1989, Loess stratigraphy in central China, *Palaeogeography, Palaeoclimatology, Palaeoecology*, Vol. 72, pp. 203-225

Kukla, G., Heller, F., Ming, L.X., Chun, X.T., Sheng, L.T. and Sheng, A., 1988, Pleistocene climates in China dated by magnetic susceptibility, *Geology*, Vol. 16, pp. 811-814

Labeyrie, L., Skinner, L. and Cortijo, E., 2007, Sub-Milankovitch (D-O/Heinrich) Events, In: Scott A. Elias, (Ed), *Encyclopedia of Quaternary Science,* Oxford, Elsevier, pp. 1964-1974

Łącka, B., Łanczont, M. and Madeyska, T., 2009, Oxygen and carbon stable isotope composition in authigenic carbonates in loess sequences from the Carpathian margin and Podolia, as a palaeoclimatic record, *Quaternary International,* Vol. 198, pp.136-151

Lai, Z.P., Wintle, A.G. and Thomas, D.S.G., 2007, Rates of dust deposition between 50 ka and 20 ka revealed by OSL dating at Yuanbao on the Chinese Loess Plateau, *Palaeogeography, Palaeoclimatology, Palaeoecology*, Vol. 248, pp. 431–439

Lambeck, K., Yokoyama, Y., Johnston, P. and Purcel, A., 2000, Global ice volumes at the Last Glacial Maximum and early Lateglacial, *Earth and Planetary Science Letters*, Vol. 181, pp. 513-527

Langmiur, C.H., Vocke, R.D., Hanson, G.N. and Hart, S.R., 1978, A general mixing equation with applications to Icelandic Basalts, *Earth and Planetary Science Letters,* Vol. 37, pp. 380-392

Laskar, J., Robutel, P., Joutel, F., Gastineau, M., Correia, A.C.M. and Levrard, B., 2004, A long-term numerical solution for the insolation quantities of the Earth, *Astronomy and Astrophysics*, Vol. 428, pp. 261-285

Leng, M.J. and Marshall, J.D., 2004, Palaeoclimate interpretation of stable isotope data from lake sediment archives. *Quaternary Science Reviews*, Vol. 23, pp. 811–831

Li, G., Sheng, X., Chen, J., Yang, J. and Chen, Y., 2007, Oxygen-isotope record of paleorainwater in authigenic carbonates of Chinese loess-palaeosol sequences and its paleoclimatic significance, *Palaeogeography, Palaeoclimatology, Palaeoecology*, Vol. 245, pp.551–559

Lindbo, D.L., Stolt, M.H. and Vepraskas, M.J., 2010, Redoximorphic features, IN: Stoops, G., Marcelino, V. and Mees, F. (Eds), *Interpretation of micromorphological features of soils and regoliths*, Elsevier, Amsterdam, pp. 129-147

Lisiecki, L.E. and Raymo, M.E., 2005, A Pliocene-Pleistocene stack of 57 globally distributed benthic $\delta^{18}O$ records, *Palaeoceanography*, Vol. 20, PA1003

Loisy, C. Verrecchia, E.P. and Dufour, P., 1999, Microbial origin for pedogenic micrite associated with a carbonate palaeosol (Champagne, France), *Sedimentary Geology,* Vol.126, pp.193-204

Lopez-Aguayo, F. and Gonzalez-Lopez, J.M., 1995, Fibrous clays in the Almazan Basin (Iberian range, Spain): Genetic pattern in a calcareous lacustrine environment, *Clay Minerals, Vol.* 30, pp. 395-406

Loutre, M.F. and Berger, A., 2003, Marine Isotope Stage 11 as an analogue for the present interglacial, *Global and Planetary Change*, Vol. 36, pp. 209-217

Loÿe-Pilot, M.D. and Martin, J.M., 1996, Saharan dust input to the Western Mediterranean: an eleven years records in Corsica, IN: Guerzoni, S. and Chester, R. (eds), *The impact of desert dust across the Mediterranean*, Kluwer academic publishers, Dorcrecht, pp. 191-199

Loÿe-Pilot, M.D., Martin, J.M. and Morelli, J., 1986, Influence of Saharan dust on the rain acidity and atmospheric input to the Mediterranean, *Nature*, Vol. 321, pp. 427-428

Ložek, V., 1990, Molluscs in loess, their palaeoecological significance and role in geochronology: principles and methods, *Quaternary International*, Vols. 7/8, pp. 71-79

Lu, H.Y., Sun, D.H., 2000, Pathways of dust input to the Chinese Loess Plateau during the last glacial and interglacial periods, *Catena*, Vol. 40, pp. 251–261

Lu, H.Y., van Huissteden, K., An, Z.S., Nugteren, G. and Vandenberghe, J., 1999, East Asia winter monsoon variations on a millennial time-scale before the last glacial-interglacial cycle, *Journal of Quaternary Science*, Vol. 14, pp.101-110

Lui, T.S. and Ding, Z.L., 1993, Stepwise coupling of monsoon circulations to global ice volume variations during the late Cenozoic, *Global and Planetary Change*, Vol. 7, pp. 119-130

Lyamani, H., Olmo, F.J. and Alados-Arboledas, L., 2005, Saharan dust outbreak over southeastern Spain as detected by sun photometer, *Atmospheric Environment*, Vol. 39, pp.7276–7284

Machette, M.N., 1985, Calcic soils of the southwestern United States, *Geological Society of America*, Special paper 303, pp.1-21

Macklin, M.G. and Woodward, J.C., 2009, River systems and environmental change, IN: Woodward, J.C. (Ed), *The Physical Geography of the Mediterranean*, Oxford University Press, Oxford, pp. 319-352

Macklin, M.G., Fuller, I.C., Lewin, J., Maas, G.S., Passmore, D.G., Rose, J., Woodward, J.C., Black, S., Hamlin, R.H.B. and Rowan, J.S., 2002, Correlation of fluvial sequences in the Mediterranean basin over the last 200 ka and their relationship to climate change, *Quaternary Science Reviews,* Vol.21, pp.1633-1641

Magny, M., Miramont, C. and Sivan, O., 2002, Assessment of the impact of climate and anthropogenic factors on Holocene Mediterranean vegetation in Europe on the basis of palaeohydrological records, *Palaeogeography, Palaeoclimatology, Palaeoecology*, Vol. 186, pp. 47-59

Magri, D. and Parra, I., 2002, Late Quaternary western Mediterranean pollen records and African winds, *Earth and Planetary Science Letters*, Vol. 200, pp. 401-408

Maher, B.A., 1998, Magnetic properties of modern soils and Quaternary loessic palaeosols; palaeoclimatic implications, *Palaeogeography, Palaeoclimatology, Palaeoecology,* Vol. 137, pp. 25-54

Markovic, S.B., Hambach, U., Stevens, T., Kukla, G.J., Heller, F., McCoy, W.D., Oches, E.A., Buggle, B. and Zöller, L., 2011, The last million years recorded at the Stari Slankamen (Northern Serbia) loess-palaeosol sequence: revised chronostratigraphy and long-term environmental trends, *Quaternary Science Reviews*, Vol. 30, pp. 1142-1154

Martín-Algarra, A., Martín-Martín, M., Andreo, B., Juliá, R. and González-Gómez, C., 2003, Sedimentary patterns in perched spring travertines near Granada (Spain) as indicators of the paleohydrological and paleoclimatological evolution of a karst massif, *Sedimentary Geology*, Vol. 161, pp. 217–228

Martin-Vide, J. and Lopez-Bustins, J.A., 2006, The western Mediterranean Oscillation and rainfall in the Iberian peninsula, *International Journal of Climatology*, Vol. 26, pp. 1455-1475

Martrat, B., Grimault, J.O., Lopez-Martinez, C., Cacho, I., Sierro, F.J., Flores, J.A., Zahn, R., Canals, M., Curtis, J.H. and Hodell, D.A., 2004, Abrupt temperature changes in the western Mediterranean over the past 250,000 years, *Science*, Vol. 306, pp. 1762-1765

Maslin, M. Seidov, D. and Lowe, J., 2001, Synthesis of the nature and causes of rapid climate transitions during the Quaternary, IN: D. Seidov, B. J. Haupt, and M. Maslin (Eds.), *The oceans and rapid climate change: Past, present and future*, Geophysical Monograph 126, American Geophysical Union

Mattey, D., Lowry, D., Duffet, J., Fisher, R., Hodge, E. and Frisia, S., 2008, A 53 year seasonally resolved oxygen and carbon isotope record from a modern Gibraltar speleothem: Reconstructed drip water and relationship to local precipitation, *Earth and Planetary Science Letters*, Vol. 269, pp. 80–95

Mayewski, P.A., Rohling, E.E., Stager, J.C., Karlen, W., Maasch, K.A., Meeker, L.D., Meyerson, E.A., Gasse, F., van Kreveld, S., Holmgren, K., Lee-Thorp, J., Rosqvist, G., Rack, F., Staubwasser, M., Schneider, R.R., Steig, E.J., 2004, Holocene climate variability, *Quaternary Research*, Vol. 62, pp. 243– 255

Mazzullo, J., Alexander, A., Tieh, T. and Menglin, D., 1992, The effects of wind transport on the shapes of quartz silt grains, *Journal of Sedimentary Petrology*, Vol. 62, pp. 961-971

McCrea, J.M., 1950, On the isotopic chemistry of carbonates and a paleotemperature scale, *The Journal of Chemical Physics*, Vol. 18, pp. 849–857

McGee, D., Broecker, W.S. and Winchler, G., 2010, Gustiness: The driver of glacial dustiness?, *Quaternary Science Reviews*, Vol. *29, pp. 2340-2350*

McManus, J.F., Bond, G.C., Broecker, W.S., Johnsen, S., Labeyrie, L. and Higgins, S., 1994, High-resolution climate records from the North Atlantic during the last interglacial, *Nature*, Vol. 371, pp.326-329

McManus, J.F., Oppo, D.W. and Keigwin, L.D., 2002, Thermohaline circulation and Prolonged Interglacial Warmth in the North Atlantic, *Quaternary Research*, Vol. 58, pp. 17–21

Médial, F., 2008, Mediterranean, IN: Jørgensen, S.E. and Fath, B.D. (Eds), *Ecosystems, Encyclopedia of Ecology*, Elsevier, Oxford, pp.2296-2308

Mejdahl, V., 1979, Thermoluminescence dating: Beta dose attenuation in quartz grains, *Archaeometry*, Vol. 21, pp. 61-72

Meng, X., Derbyshire, E. and Kemp, R.A., 1997, Origin of the magnetic susceptibility signal in Chinese loess, *Quaternary Science Reviews*, Vol. 16, pp. 833-839

Meyers, S.R. and Pagani, M., 2006, Quasi-periodic climate teleconnections between northern and southern Europe during the 17th–20th centuries, *Global and Planetary Change*, Vol. 54, pp. 291–301

Miall, A.D.,1992, Alluvial deposits, IN: Walker, R.G. and James, N.P. (Eds), 1992, *Facies Models*, Geological Association of Canada, Canada, pp. 119-143

Millot, C., 1990, The Gulf of Lions' hydrodynamics, *Continental shelf research*, Vol. 10, pp. 885-894

Moine, O., Rousseau, D. and Antoine, P., 2008, The impact of Dansgaard–Oeschger cycles on the loessic environment and malacofauna of Nussloch (Germany) during the Upper Weichselian, *Quaternary Research,* Vol. 70, pp. 91-104

Molinaroli, E., 1996, Mineralogical characterisation of Saharan dust with a view to its final destination in Mediterranean sediments, IN: Guerzoni, S. and Chester, R. (Eds), *The impact of desert dust across the Mediterranean*, Kluwer academic publishers, Dordrecht, pp. 153-162

Mook, W.G., 2006, *Introduction to Isotope hydrology: Stable and radioactive isotopes of Hydrogen, Oxygen and Carbon*, Taylor and Francis Group, London, p. 256

Moratiel, R., Duran, J.M. and Snyder, R.L., 2010, *Responses of reference evapotranspiration to changes in atmospheric humidity and air temperature in Spain, Climate Research*, Vol. 44, pp.27 – 40

Moreno, A., Cacho, I., Canals, M., Prins, M.A., Sánchez-Goñi, M., Grimalt, J.O. and Weltje, G.J., 2002, Saharan Dust Transport and High-Latitude Glacial Climatic Variability: The Alboran Sea Record, *Quaternary Research,* Vol. 58, pp. 318-328

Moreno, A., Cacho, I., Canals, M., Grimalt, J.O. and Sanchez-Vidal, A., 2004, Millennial-scale variability in the productivity signal from the Alboran Sea record, Western Mediterranean Sea, *Palaeogeography, Palaeoclimatology, Palaeoecology,* Vol. 211, pp. 205-219

Moreno, A., Cacho, I., Canals, M., Grimalt, J.O., Sánchez-Goñi, M.F., Shackleton, N. and Sierro, F.J., 2005, Links between marine and atmospheric processes oscillating on a millennial time-scale. A multi-proxy study of the last 50,000 yr from the Alboran Sea (Western Mediterranean Sea), *Quaternary Science Reviews,* Vol. 24, pp. 1623-1636

Moreno, A., González-Sampériz, P., Morellón, M., Valero-Garcés, B.L. and Fletcher, W., 2012, Northern Iberian abrupt climate change dynamics during the last glacial cycle: A view from lacustrine sediments, *Quaternary Science Reviews*, Vol. 36, pp. 139–153

Moulin, C., Lambert, C.E., Dulac, F. and Dayan, U., 1997, Control of atmospheric export of dust from North Africa by the North Atlantic Oscillation, *Nature*, Vol. 387, pp. 691-694

Mücher, H., Sevink, J., Bergkamp, G. and Jongejans, J.,1991, A pedological and micromorphological study on Mediterranean loessial deposits near Gerona, N.E. Spain, *Quaternary International*, Vol. 5, pp. 9-22

Muhs, D.R., 2007, Loess deposits, origins and properties, IN: Elias, S. E. (Ed), *Encyclopaedia of Quaternary Science*, Elsevier, Oxford, pp. 1405-1418

Muhs, D.R. and Bettis, E.A., 2000, Paleowinds of Midcontinental North America during Last Glaciation, *Quaternary Research*, Vol. 53, pp. 49–61

Muhs, D.R., and Bettis, E.A., 2003, Quaternary loess-paleosol sequences as examples of climate-driven sedimentary extremes, IN: Chan, M.A., and Archer, A.W. (eds), *Extreme depositional environments: Mega end members in geologic time: Boulder, Colorado*, Geological Society of America Special Paper, Vol. 370, p. 53–74

Muhs, D.R., Budahn, J., Avila, A., Skipp, G., Freeman, J. and Patterson, D., 2010, The role of African dust in the formation of Quaternary soils on Mallorca, Spain and implications for the genesis of Red Mediterranean soils, *Quaternary Science Reviews*, Vol. 29, pp. 2518-2543

Mulder, T. and Alexander, J., 2001, The physical character of subaqueous sedimentary density flows and their deposits, *Sedimentology*, Vol. 48, pp. 269-299

Müller, P.J., Cepek, M., Ruhland, G. and Schneider, R.R., 1997, Alkenone and coccolithophorid species changes in late Quaternary sediments from the Walvis Ridge: Implications for the alkenone paleotemperature method, *Palaeogeography, Palaeoclimatology, Palaeoecology*, Vol. 135, pp. 71-96

Murray, A. S. & Wintle, A. G., 2000, Luminescence dating of quartz using an improved single-aliquot regenerative-dose protocol, *Radiation Measurements*, Vol 32, pp.57–73

Murray, A. S., and Wintle, A. G., 2003, The single aliquot regenerative dose protocol: potential for improvements in reliability, Radiation *Measurements*, Vol 37, pp. 377 – 381

Nash, D.J., and Ullyot, J.S., 2007, Silcrete, IN: Nash, D.J. and McLaren, S.J. (Eds), *Geochemical sediments and landscapes*, Blackwell publishing, Oxford, pp.95-144

Nathan, R.P. and Mauz, B., 2008, On the dose-rate estimate of carbonate-rich sediments for trapped charge dating, *Radiation Measurements*, Vol. 43, pp. 14-25

Nicholson, S.E., 2011, *Dryland climatology*, Cambridge University Press, New York

Nobre Silva, I.G., Weis, D. and Scoates, J.S., 2010, Effects of acid leaching on the Sr-Nd-Hf isotopic compositions of ocean island basalts, *Geochemistry, Geophysics, Geosystems*, Vol. 11, Q09011

Nugteren, G., Vandenberghe, J., 2004, Spatial climatic variability on the Central Loess Plateau (China) as recorded by grain size for the last 250 ka, *Global and Planetary Change*, Vol. 41, pp. 185–206

O'Brien, S.R., Mayewski, P.A., Meeker, L.D., Meese, D.A., Twickler, M.S. and Whitlow, S.I., 1995, Complexity of Holocene Climate as Reconstructed from a Greenland Ice Core, *Science*, Vol. 22, pp. 1962-1964

Olley, J.M., Murray, A. and Roberts, R.G., 1996, The effects of disequilibria in the uranium and thorium decay chains on burial dose rates in fluvial sediments, *Quaternary Science Reviews (Quaternary Geochronology),* Vol. 15, pp. 751-760

Oppo, D. W. and Lehman, S.J., 1995, Suborbital timescale variability of North Atlantic Deep Water during the past 200,000 years, *Palaeoceanography*, Vol. 10, pp. 901-910

Oppo, D.W., McManus, J.F. and Cullen, J.L., 2006, Evolution and demise of the Last Interglacial warmth in the subpolar North Atlantic, *Quaternary Science Reviews*, Vol. 25, pp. 3268-3277

Ortiz, J.E., Torres, T., Delgado, A., Julià, R., Lucini, M., Llamas, F.J., Reyes, E., Soler, V. and Valle, M., 2004, The palaeoenvironmental and palaeohydrological evolution of Padul Peat Bog (Granada, Spain) over one million years, from elemental, isotopic and molecular organic geochemical proxies, *Organic Geochemistry,* Vol. 35, pp. 1243-1260

Palmer, A.P. Lee, J.A. Kemp, R.A. and Carr, S.J., unpublished, *Revised laboratory procedures for the preparation of thin sections from unconsolidated sediments,* Centre for Micromorphology, Royal Holloway University of London and Queen Mary University of London

Pantaléon-Cano, J., Yill, E.I., Pérez-Obiol, R. and Roure, J.M., 2003, Palynological evidence for vegetation history in semi-arid areas of the western Mediterranean (Almeria, Spain), *The Holocene*, Vol. 13, pp. 109-119

Paul, H.A., Bernasconi, S.M., Schmid, D.W. and McKenzie, J.A., 2001, Oxygen isotopic composition of the Mediterranean Sea since the Last Glacial Maximum: constraints from pore water analyses, *Earth and Planetary Science Letters*, Vol. 192, pp. 1-14

Pécsi, M., 1990, Loess is not just the accumulation of dust, *Quaternary International*, Vols. 7/8, pp. 1-21

Pécsi, M., 1995, The Role of Principles and Methods in Loess-Paleosol Investigations, GeoJournal, Vol. 36, pp. 117-131

Pedley, H.M., 1990, Classification and environmental models of cool freshwater tufas, *Sedimentary Geology,* Vol. 68, pp. 143-154

Pedley, H.M., 2009, Tufas and travertines of the Mediterranean region: a testing ground for freshwater carbonate concepts and developments*, Sedimentology*, Vol. 56, pp. 221–246

Pelejero, C. and Grimalt, J.O., 1997, The correlation between the uk~ index and sea surface temperatures in the warm boundary: The South China Sea, *Geoehimica et Cosmoehimica Acta*, Vol. 61, pp. 4789-4797

Pérez-Folgado, M., Sierro, F.J., Flores, J.A., Grimault, J.O. and Zahn, R., 2004, Paleoclimatic variations in foraminifer assemblages from the Alboran Sea (Western Mediterranean) during the last 150 ka in ODP Site 977, *Marine Geology*, Vol. 212, pp. 113–131

Petit, J.R., Jouzel, J., Raynaud, D., Barkov, N.I., Barnola, J.M., Basile, I., Bender, M., Chappellaz, J., Davis, M., Delaygue, G., Delmotte, M., Kotlyakov, V.M., Legrand, M., Lipenkov, V.Y., Lorius, C., Pepin, L., Ritz, C., Saltzman, E. and Stievenard, M., Climate and atmospheric history of the past 420,000 years from the Vostok ice core, Antarctica, Nature, Vol. 399, pp. 429.436

Poage, M.A. and Chamberlain, C.P., 2001, Empirical relationships between elevation and the stable isotope composition of precipitation and surface waters: considerations for studies of palaeoelevation change, *American Journal of Science*, Vol. 301, pp. 1–15

Poch, R.M., Artieda, O., Herrero, J. and Lebedeva-Verba, M., 2010, Gypsic features, IN: Stoops, G., Marcelino, V. and Mees, F. (Eds), *Interpretation of micromorphological features of soils and regoliths*, Elsevier, Amsterdam, pp. 195-216

Pons, A. and Reille, M., 1988, The Holocene and upper Pleistocene pollen record from Padul (Granada, Spain): A new study, *Palaeogeography, Palaeoclimatology, Palaeoecology,* Vol. 66, pp.243-249

Porta, J., 1998, Methodologies for the analysis and characterization of gypsum in soils: A review, *Geoderma*, Vol. 87, pp. 31–46

Porta, J. and Herrero, J., 1988, Micromorphology and genesis of soils enriched with gypsum, IN: Douglas, L.A. (Ed), *Soil Micromorphology: A basic and applied science*, Elsevier, Amsterdam, pp. 321-420

Porter, S.C. and Zhisheng, A., 1995, Correlation between climate events in the North Atlantic and China during the last glaciation, *Nature*, Vol. 375, pp. 305-308

Prentice, C. I., Guiot, J and Harrison, S.P., 1992, Mediterranean vegetation, lake levels and palaeoclimate at the Last Glacial Maximum, *Nature*, Vol. 360, pp. 658-660

Prescott, J.R. and Hutton, J.T., 1988, Cosmic ray and gamma ray dosimetry for TL and ESR, *Nuclear Tracks and Radiation Measurements*, Vol. 14, pp. 223-227

Prescott, J.R. and Hutton, J.T., 1994, Cosmic ray contributions to dose rates for luminescence and ESR dating: large depths and long-term time variations, *Radiation Measurements*, Vol. 23, pp. 497-500

Preusser, F., Chitambo, M.L., Gotte, T., Matinia, M., Ramseyer, K., Sendezera, E.J., Susino, G.J. and Wintle, A.G., 2009, Quartz as a natural luminescence dosimeter, *Earth-Science Reviews*, Vol. 97, pp. 184–214

Prins, M.A., Vriend, M., Nugteren, G., Vandenberghe, J., Lu, H., Zheng, H. and Weltje, G.J., 2007,Late Quaternary aeolian dust input variability on the Chinese Loess Plateau: inferences from unmixing of loess grain-size records, *Quaternary Science Reviews*, Vol. 26, pp. 230–242

Prospero, J.M., 1996, Saharan dust transport over the North Atlantic ocean and Mediterranean: an overview, IN: Guerzoni, S. and Chester, R. (eds), *The impact of desert dust across the Mediterranean*, Kluwer academic publishers, Dordrecht, pp. 133-151

Pustovoytov, K. and Terhorst, B., 2004, An isotopic study of a late Quaternary loess-palaeosol sequence in SW Germany, *Revista Mexicana de Ciencias Geológicas,* Vol.21, pp.88-93

Pye, K., 1984, Loess, *Progress in Physical Geography*, Vol. 8, pp. 176-217

Pye, K., 1995, The nature, origin and accumulation of loess, *Quaternary Science Reviews*, Vol.14, pp. 653-667

Pye, K. and Sperling, C.H.B., 1983, Experimental investigation of silt formation by static breakage processes: the effect of temperature, moisture and salt on quartz dune sand and granitic regolith, *Sedimentology*, Volume 30, pp. 49–62 (Abstract only)

Pye, K. and Tsoar, H., 1987, The mechanics and geological implications of dust transport and deposition in deserts with particular reference to loess formation and dune sand diagenesis in the northern Negev, Israel, IN: Frostrick, L. and Reid, I. (eds), *Desert Sediments. Ancient and Modern*, Geological Society Special Publication No. 35, pp. 139-156

Quade, J. and Cerling, T., 2007, Non-Lacustrine terrestrial studies, IN: Elias, S.A., (Ed), *Encyclopaedia of Quaternary Science*, Elsiever, London, pp.329-351

Quade, J., Cerling, T.E. and Bowman, J.B., 1989a, Development of Asian monsoon revealed by marked ecological shift during the latest Miocene in northern Pakistan, *Nature*, Vol. 342, pp.163-166

Quade, J., Cerling, T.E. and Bowman, J.R., 1989b, Systematic variations in the carbon and oxygen isotopic composition of pedogenic carbonate along elevation transects in the southern Great Basin, United States, *Geological Society of America Bulletin*, Vol. 101, pp. 464-475

Quade, J., Solounias, N., and Cerling, T.E., 1994, Stable isotopic evidence from paleosol carbonates and fossil teeth in Greece for forest or woodlands over the past 11 Ma, *Palaeogeography, Palaeoclimatology, Palaeoecology*, Vol. 108, pp.41–53

Quade, J., Garzione, C. and Eiler, J., 2007, Palaeoelevation Reconstruction using Pedogenic Carbonates, *Reviews in Mineralogy & Geochemistry*, Vol. 66, pp. 53-87

Rasmussen, S O, Seierstad, I.K., Andersen, K.K.,Bigler, M., Dahl-Jensen, D. and Johnsen, S.J., 2008 Synchronisation of the NGRIP, GRIP and GISP2 ice cores across MIS 2 and palaeoclimatic implications, *Quaternary Science Reviews, Vol. 27,* pp. 18-28

Rees-Jones, J.,1995, Optical dating of young sediments using fine-grain quartz, *Ancient TL*, Vol. 13, pp. 9-14.

Retallack, G.J., 1991, Untangling the effects of burial alteration and ancient soil formation, Annual Reviews: Earth and Planetary Sciences, Vol. 19, pp. 183-206

Retallack, G.J., 2005,. Soils — palaeosols, IN: Selley, R.C., Cocks, L.R.M. and Plimer, I.R. (Eds), *Encyclopedia of Geology*, Academic Press, London, p. 203-208

Rhodes, E.J., 2011, Optically Stimulated Luminescence Dating of Sediments over the Past 200,000 Years, *Annual Review of Earth and Planetary Sciences*, Vol. 39, pp.461–88

Roberts, H. M., 2007, Assessing the effectiveness of the double-SAR protocol in isolating a luminescence signal dominated by quartz, *Radiation Measurements*, Vol. 42, pp.1627–1636

Roberts, H. M., 2008, The development and application of luminescence dating to loess deposits: a perspective on the past, present and future, *Boreas*, Vol. 37, pp.483–507

Roberts, R.G., Galbraith, R.F., Olley, J.M., Yoshida, H. and Laslett, G.M., 1999, Optical dating of single and multiple grains of quartz from Jinmium rock shelter, northern Australia: Part II, results and implications., *Archaeometry*, Vol. 41, pp. 365–395

Rodriguez, S., Querol, X., Alastuey, A., Kallos, G. and Kakaliagou, O., 2001, Saharan dust contributions to PM10 and TSP levels in Southern and Eastern Spain, *Atmospheric Environment*, Vol. 35, pp. 2433-2447

Rohling, E.J., Mayewski, P.A., Hayes, A., Abu-Zied, R.H., Casford, J.S.L., 2002, Holocene atmosphere–ocean interactions: records from Greenland and the Aegean Sea, *Climate Dynamics*, Vol. 18, pp.573– 592

Rohling, E.J., Abu-Zied, R., Casford, J.S.L., Hayes, A., and Hoogakker, B.A.A. 2009, The Marine Environment: Present and Past, in: Woodward, J.C. (Ed.), *The Physical Geography of the Mediterranean*, Oxford University Press, Oxford, pp. 33-67

Rosanski, K., Araguás-Araguás, L. and Gonfiantini, R., 1993, Isotopic patterns in modern global precipitation, IN: Swart, P.K. (Ed), *Climate change in Continental isotopic records,* Geophysical Monograph 78, pp.1-36, American Geophysical Union, Washington

Rose, J., Meng, X., Watson, C., 1999, Palaeoclimate and palaeoenvironmental responses in the western Mediterranean over the Last 140 ka: evidence from Mallorca, Spain, *Journal of the Geological Society, London*, Vol. 156, pp. 435-448

Rossignol-Strick, M., Nesteroff, W., Olice, P. and Vergnaud-Grazzini, C., 1982, After the deluge: Mediterranean stagnation and sapropel formation, *Nature*, Vol. 295, pp. 105-110

Roucoux, K.H., Shackleton, N.J., de Abreu, L., Schönfeld, J. and Tzedakis, P.C., 2001, Combined Marine Proxy and Pollen Analyses Reveal Rapid Iberian Vegetation Response to North Atlantic Millennial-Scale Climate Oscillations, *Quaternary Research,* Vol. 56(1), pp. 128-132

Rousseau, D.D., 2001, Loess biostratigraphy: new advances and approaches in mollusk studies, *Earth-Science Reviews*, Vol. 54, pp. 157–171

Rousseau, D.D. and Kukla, G., 1994, Late Pleistocene climate record in the Eustis loess section, Nebraska, based on land snail assemblages and magnetic susceptibility, *Quaternary Research*, Vol.42, pp. 176-187

Rousseau, D.D., Zöller, L., Valet, J.P., 1998, Late Pleistocene climatic variations at Achenheim, France based on a magnetic susceptibility and TL chronology of loess, *Quaternary Research*, Vol. 49, pp. 255-263

Rousseau, D.D., Antoine,P., Hatté, C., Lang, A., Zöller, L., Fontugne, M., Othman, D.B., Luck,J.M., Moine, O., Labonne, M., Bentaleb, I. and Jolly, D., 2002, Abrupt millennial climatic changes from Nussloch (Germany) Upper Weichselian eolian records during the Last Glaciation, *Quaternary Science Reviews,* Vol. 21, pp. 1577–1582

Rousseau, D.D., Antoine, P., Hatté, C., Lang, A., Zöller, L., Fontugne, M., Othman, D.B., Luck, J.M., Moine, O., Labonne, M., Bentaleb, I. and Jolly, D., 2002, Abrupt millennial climatic changes from Nussloch (Germnay) Upper Wiechselian eolian records during the Last Glaciation, *Quaternary Science Reviews,* Vol. 21, pp. 1577-1582

Rowe, P.J. and Maher, B.A., 2000, 'Cold' stage formation of calcrete nodules in the Chinese Loess Plateau: evidence from U-series dating and stable isotope analysis, *Palaeogeography, Palaeoclimatology, Palaeoecology*, Vol. 157, pp.109–125

Sánchez, C. and Galán, E., 1995, An approach to the genesis of Palygorskite in a Neogene-Quaternary continental basin using principle factor analysis, *Clay minerals*, Vol. 30, pp. 225-238

Sánchez Goñi, M.F., Turon, J., Eynaud, F. and Gendreau, S., 2000, European climatic response to millennial scale changes in the atmosphere-ocean system during the last glacial period, *Quaternary research,* Vol. 54, pp. 394-403

Sánchez Goñi, M.F., Cacho, I., Turon, J.L., Guiot, J., Sierro, F.J., Peypouquet, J.P., Grimault, J.O. and Shackleton, N.J., 2002, Synchroneity between marine and terrestrial responses to millennial scale climatic variability during the last glacial period in the Mediterranean region, *Climate Dynamics*, Vol. 19, pp. 95-105

Sánchez Goñi, M.F., Loutre, M.F., Crucifix, M., Peyrona, O., Santos, L., Duprat, J., Malaize, B., Turon, J.L. and Peypoquet, J.P., 2005, Increasing vegetation and climate gradient in Western Europe over the Last Glacial Inception (122–110 ka): data-model comparison, *Earth and Planetary Science Letters*, Vol. 231, pp. 111-130

Sánchez Goñi, M.F., Landais, A., Fletcher, W.J., Naughton, F., Desprat, S. and Duprat, J., 2008, Contrasting impacts of Dansgaard–Oeschger events over a western European latitudinal transect modulated by orbital parameters, *Quaternary Science Reviews,* Vol.27 (11-12), pp.1136-1151

Sanz de Galdeano, C., and Andreo, B., 1995, Structure of Sierra Blanca (Alpujarride Complex, West of the Betic Cordillera), *Estudios, Geologica*, Vol. 51, pp.43-55

Schellenberger, A., Heller, F. and Veit, H., 2003, Magnetostratigraphy and magnetic susceptibility of the Las Carreras loess–paleosol sequence in Valle de Tafí, Tucumán, NW-Argentina, *Quaternary International*, Vol. 106–107, pp. 159-167

Schrag, D.P., Adkins, J.F., McIntyre, K., Alexander, J.L., Hoddel, D.A., Charles, C.D. and McManus, J.F., 2002, The oxygen isotopic composition of seawater during the Last Glacial Maximum, *Quaternary Science Reviews*, Vol. 21, pp. 331–342

Seidov, D. and Maslin, M., 2001, Atlantic ocean heat piracy and the bipolar climate see-saw during Heinrich and Dansgaard-Oeschger events, *Journal of Quaternary Science,* Vol. 16, pp. 321-328

Shackleton, N. J., 1967, Oxygen isotope analyses and Pleistocene temperatures re-assessed, *Nature*, Vol. 215, pp. 15-17

Shackleton, N.J., 1987, Oxygen isotopes, ice volume and sea level, *Quaternary Science Reviews,* Vol. 6, pp. 183–190

Shackleton, N.J., Hall, M.A. and Vincent, E., 2000, Phase Relationships Between Millennial-Scale Events 64,000-24,000 Years Ago, *Palaeoceanography,* Vol. 15, pp. 565-569

Shackleton, N.J., Sánchez Goñi, M.F., Pailler, D. and Lancalot, Y., 2003, Marine Isotope Substage 5e and the Eemian Interglacial, *Global and Planetary Change*, Vol. 36, pp. 151–155

Sharpe, W.D., Ludwig, K.R., Chadwick, O.A., Amundson, R., Glaser, L.L., 2003, Dating fluvial terraces by 230Th/U on pedogenic carbonate, Wind River Basin, Wyoming, *Quaternary Research*, Vol. 59, pp. 139-150

Smalley, I.J. and Vita-Finzi, C., 1968, The formation of fine particle in sandy deserts and the nature of 'desert' loess, *Journal of Sedimentary Petrology*, Vol. 38, pp. 766-774

Smalley, I.J. and Krinsley, D.H., 1978, Loess deposits associated with deserts, *Catena,* Vol. 5, pp. 53-66

Smalley, I.J., Kumar, R., Dhand, K.O., Jefferson, I.F. and Evans, R.D., 2005, The formation of silt material for terrestrial sediments: Particularly loess and dust, *Sedimentary Geology*, Vol. 179, pp. 321–328

Smalley, I., Markovic, S.B. and Svirčev, Z., 2011, Loess is [almost totally formed by] the accumulation of dust, *Quaternary International*, Vol. 240, pp. 4-11

Smith, J., Vance, D., Kemp, R.A., Archer, C., Toms, P., King, M and Zárate, M., 2003, Isotopic constraints on the source of Argentinian loess with implications for atmospheric circulation and the provenance of Antarctic dust during recent glacial maxima, *Earth and Planetary Science Letters*, Vol. 212, pp. 181-196

Spötl, C. and Mangini, A., 2002, Stalagmite from the Austrian Alps reveals Dansgaard–Oeschger events during isotope stage 3: Implications for the absolute chronology of Greenland ice cores, *Earth and Planetary Science Letters,* Vol. 203, pp. 507-518

Steig, E.J., Morse, D.L., Waddington, E.D., Stuiver, M., Grootes, P.M., Mayewski, P.A., Twickler, M.S., Whitlow, S., 2000, Wisconsinan and Holocene climate history from an ice core at Taylor Dome, western Ross Sea embayment, Antarctica, *Geografisker Annaler*, Vol. 82A, pp. 213–235

Stevens, T., Armitage, S.J., Lu, H. and Thomas, D.S.G., 2006, Sedimentation and diagenesis of Chinese loess: Implications for the preservation of continuous, high-resolution climate records, *Geology*, Vol. 34, pp. 849–852

Stevens, T., Thomas, D.S.G., Armitage, S.J., Lunn, H.R. and Lu, H., 2007, Reinterpreting climate proxy records from late Quaternary Chinese loess: A detailed OSL investigation, *Earth-Science Reviews*, Vol. 80, pp. 111–136

Stevens, T., Palk, C., Carter, A., Lu, H and Clift, P.D., 2010, Assessing the provenance of loess and desert sediments in northern China using U-Pb dating and morphology of detrital zircons, *GSA Bulletin*, Vol. 122, pp. 1331–1344

Stevens, T., Bird, A.F., Vermeesch, P., Parrish, R.R., Carter, A., Lu, H., Palk, C., Watson, T. and Sevasjanova, I., 2011, Single heavy mineral grains in loess-dust and desert sand provenance analysis in China, *Windy day conference abstract*, http://www.shef.ac.uk/polopoly_fs/1.102990!/file/WindyDay_2011_Abstracts.pdf#page=6

Stolt, M.H. and Lindbo, D.L., 2010, Soil organic matter, Stoops, G., 2010, Micromorphology as a tool in soil and regolith studies, IN: Stoops, G., Marcelino, V. and Mees, F. (Eds), *Interpretation of micromorphological features of soils and regoliths*, Elsevier, Amsterdam, pp.

Stoops, G., 2010, Micromorphology as a tool in soil and regolith studies, IN: Stoops, G., Marcelino, V. and Mees, F. (Eds), *Interpretation of micromorphological features of soils and regoliths*, Elsevier, Amsterdam, pp. 1-8

Strong, G.E., Giles, J.R.A., Wright, V.P., 1992, A Holocene calcrete from North Yorkshire, England: implications for interpreting palaeoclimates using calcretes, Sedimentology, Vol 39, pp. 333–347

Stuiver, M., Grootes, P.M. and Braziunas, T.F., 1995, The GISP2 $\delta^{18}O$ Climate Record of the Past 16,500 Years and the Role of the Sun, Ocean, and Volcanoes, *Quaternary Research,* Vol. 44, pp. 341–354

Stuiver, M., Reimer, P.J., Braziunas, T.F., 1998, High precision radiocarbon age calibration for terrestrial and marine samples, *Radiocarbon*, Vol. 40, pp.1127–1151

Stumpf, R., Frank, M., Schönfeld, J. and Haley, B.A., 2012, Climatically driven changes in sediment supply on the SW Iberian shelf since the Last Glacial Maximum, *Earth and Planetary Science Letters*, Vol. 312, pp. 80–90

Suchodoletz, H., Kuhn, P., Hambach, U., Dietze, M., Zoller, L. and Faust, D., 2009, Loess-like and palaeosol sediments from Lanzarote (Canary Islands/Spain) Indicators of palaeoenvironmental change during the Late Quaternary, *Palaeogeography, Palaeoclimatology, Palaeoecology*, Vol. 278, pp. 71–87

Suchodoletz, H., Glaser, B., Thrippleton, T., Broder, T., Zang, U., Eigenmann, R., Kopp, B., Reichert, M. and Zoller, L*., in press*, The influence of Saharan dust deposits on La Palma soil properties (Canary Islands, Spain), *Catena*, 2011, doi:/10.1016/j.catena.2011.07.005

Sun, J., 2002, Provenance of loess material and formation of loess deposits on the Chinese Loess Plateau, *Earth and Planetary Science Letters*, Vol. 203, pp. 845-859

Sun, J. and Lui, T., 2000, Multiple origins and interpretations of the magnetic susceptibility signal in Chinese wind-blown sediments, *Earth and Planetary Science Letters*, Vol. 180, pp. 287-296

Sun, J., Lü, T., Zhang, Z., Wang, X. and Liu, W., 2012, Stepwise expansions of C4 biomass and enhanced seasonal precipitation and regional aridity during the Quaternary on the southern Chinese Loess Plateau, *Quaternary Science Reviews*, Vol. 34, pp. 57-65

Suwa, M., von Fischer, J.C., Bender, M.L., Landais, A. and Brook, E.J., 2006, Chronology reconstruction for the disturbed bottom section of the GISP2 and the GRIP ice cores: Implications for Termination II in Greenland, *Journal of Geophysical Research*, Vol. 111, pp. 1-12

Svensson, A., Bigler, M., Kettner, E., Dahl-Jensen, D., Johnsen, S., Kipfstuhl, S., Nielsen, M. and Steffensen, J.P., 2011, Annual layering in the NGRIP ice core during the Eemian, *Climates of the Past: Discussions*, Vol. 7, pp. 749–773

Swezey, C., 2001, Eolian sediment responses to late Quaternary climate changes: temporal and spatial patterns in the Sahara, *Palaeogeography, Palaeoclimatology, Palaeoecology*, Vol. 167, pp. 119-155

Taylor, S. R. and McLennan, 1985, *The Continental Crust: Its Composition and Evolution*, Blackwell, Oxford, p. 312

Taylor, S.R., Lennan, S.M. and McCulluch, M.T., 1983, Geochemistry of loess, continental crustal composition and crustal model ages, *Geochemica et Cosmochimica Acta*, Vol. 47, pp. 1897-1905

Taylor, P.N., Moorbath, S., Leube, A. and Hirdes, W., 1992, Early Proterozoic crustal evolution in the birimian of Ghana: constraints from geochronology and isotope geochemistry, Precambrian Research, Vol. 56, pp. 97-111

Thirlwall, M.F., 1991a, Long-term reproducibility of multicollector Sr and Nd isotope ratio analysis, *Chemical Geology*, Vol. 94, pp. 85-104

Thirlwall, M.F., 1991b, High-precision multicollector isotopic analysis of low levels of Nd as oxide, *Chemical Geology*, Vol. 94, pp. 13-22

Thorndycraft, V.R. and Benito, G., 2006, The Holocene fluvial chronology of Spain: evidence from a newly compiled radiocarbon database, *Quaternary Science Reviews*, Vol. 25, pp. 223–234

Thornes, J.B., López-Bermúdez, F. and Woodward, J.C., 2009, Hydrology, river regimes, and sediment yield, IN: Woodward, J.C. (Ed), *The Physical Geography of the Mediterranean*, Oxford University Press, Oxford, pp. 229-253

Thunnel, R.C. and Williams, D.F., 1989, Glacial-Holocene salinity changes in the Mediterranean Sea: hydrographic and depositional effects, Nature, Vol. 338, pp. 493-496

Tsoar, H., Pye, K., 1987. Dust transport and the question of desert loess formation. *Sedimentology*, *Vol.* 34, pp. 139–153 (abstract only)

Tucker, M.E. and Wright, V.P., 1991, *Carbonate Sedimentology*, Wiley, Chichester, p. 496

Tzedakis, C., 2003, Timing and duration of Last Interglacial conditions in Europe: a chronicle of a changing chronology, *Quaternary Science Reviews*, Vol. 22, pp. 763–768

Tzedakis, C., 2005, Towards an understanding of the response of southern European vegetation to orbital and suborbital climate variability, *Quaternary Science Reviews*, Vol. 25, pp. 1585-1599

Tzedakis, C., 2009, Cenozoic climate and vegetation change, IN: Woodward, J.C. (Ed.), *The Physical Geography of the Mediterranean*, Oxford University Press, Oxford, pp. 89-137

Tzedakis, C., Andrieu, V., de Beaulieu, J.-L., Birks, H.J.B., Crowhurst, S., Follieri, M., Hooghiemstra, H., Magri, D., Reille, M., Sadori, L., Shackleton, N.J. & Wijmstra, T.A., 2001, Establishing a terrestrial chronological framework as a basis for biostratigraphical comparisons, *Quaternary Science Reviews*, Vol. 20, pp. 1583-1592

Tzedakis, C.P., McManus, J.F., Hooghiemstra, H., Oppo, D.W. and Wijmstra, T.A., 2003, Comparison of changes in vegetation in northeast Greece with records of climate variability on orbital and suborbital frequencies over the last 450 000 years, *Earth and Planetary Science Letters*, Vol. 212, pp. 197-212

Tzedakis, P.C., Frogley, M.R., Lawson, I.T., Preece, R.C., Cacho, I. and de Abreu, L., 2004, Ecological thresholds and patterns of millennial-scale climate variability: The response of vegetation in Greece during the last glacial period, *Geology,* Vol.32, pp.109-112.

Ufnar, D.E., Grocke, D.R. and Beddows, P.A., 2008 Assessing pedogenic calcite stable-isotope values: Can positive linear covariant trends be used to quantify palaeo-evaporation rates?, *Chemical Geology*, Vol 256, pp. 46-58

Ugidos, J.M., Valladares, M.I., Barba, P. and Ellam, R.M., 2003, The Upper Neoproterozoic–Lower Cambrian of the Central Iberian Zone, Spain: Chemical and isotopic (Sm-Nd) evidence that the sedimentary succession records an inverted stratigraphy of its source, *Geochimica et Cosmochimica Acta*, Vol. 67, No. 14, pp. 2615–2629

Ujvari, G., Varga, A., Ramos, F.C., Kovacs, J., Memeth, T. and Stevens, T., 2012, Evaluating the use of clay mineralogy, Sr–Nd isotopes and zircon U–Pb ages in tracking dust provenance: An example from loess of the Carpathian Basin, *Chemical Geology*, Vol. 304–305, pp. 83–96

van der Hammen, T., Wijmstra, T.A. and Zagwin, H., 1971, The floral record of the Late Cenozoic of Europe, IN: Turekian, K.K. (Ed), *The late Cenozoic Glacial ages,* Yale University Press, New Haven, pp. 391-424 Cited from: Tzedakis, C., 2009, Cenozoic climate and vegetation change, IN: Woodward, J.C. (Ed.), *The Physical Geography of the Mediterranean*, Oxford University Press, Oxford, pp. 89-137

van der Veer, G., Voerkelius, S., Lorentz, G., Heiss, G. and Hoogewerff, J.A., 2009, Spatial interpolation of the deuterium and oxygen-18 composition of global precipitation using temperature as ancillary variable, *Journal of Geochemical Exploration*, Vol. 101, pp. 175–184

Vandenberghe, J., An, Z., Nugteren, G., Lu, H., Van Huissteden, J., 1997, New absolute time scale for the Quaternary climate in the Chinese loess region by grain-size analysis, *Geology*, Vol. 25, pp. 35–38

Vandenberghe, J., Huijzer, B.S., Mücher, H. and Laan, W., 1998, Short climatic oscillations in a western European loess sequence (Kesselt, Belgium), *Journal of Quaternary Science*, Vol. 13, pp.471–485

Verosub, K.L., Fine, P., Singer, M.J. and TenPas, J., 1993, Pedogenesis and palaeoclimate: Interpretation of the magnetic susceptibility record of Chinese loess-palaeosol sequences, *Geology*, Vol. 21, pp. 1011-1014

Verrecchia, E.P. and Verrecchia, K.E., 1994, Needle-fiber calcite; a critical review and a proposed classification *Journal of Sedimentary Research,* Vol. 64, pp. 650-664

Versteegh, E.A.A., Black, S. and Hodson, M., 2011, Earthworm secreted calcium carbonate: A new palaeothermometer?, Geological Society of America, Conference Abstract

Vinther, B.M., Clausen, H.B., Johnsen, S.J., Rasmussen, S.O., Andersen, K.K., Buchardt, S.L., Dahl-Jensen, D., Seierstad, I.K., Siggard-Andersen, M.L., Steffensen, J.P. and Svensson, A., 2006, A synchronized dating of three Greenland ice cores throughout the Holocene, *Journal of Geophysical Research*, Vol. 111, D13102

Vinther, B.M., Buchardt, S.L., Clausen, H.B., Dahl-Jensen, D., Johnsen, S.J., Fisher, D.A., Koerner, R.M., Raynaud, D., Lipenkov, V., Andersen, K.K., Blunier, T., Rasmussen, S.O., Steffensen, J.P. and Svensson, A.M., 2009, Holocene thinning of the Greenland ice sheet, *Nature*, Vol. 461, pp. 385-288

Vita-Finzi, C., 1969, *The Mediterranean Valleys: Geological changes in Historical times,* Cambridge University Press, Cambridge, 150 pp

Wagner, C., Mokhtari, A., Deloule, E. and Chabaux, F., 2003, Carbonatite and alkaline magmatism in Taourirt (Morocco): Petrological, geochemical and Sr-Nd isotope characteristics, *Journal of Petrology*, Vol. 44, pp. 937-963

Wallinga, J., Murray, A. and Wintle, A., 2000, The single-aliquot regenerative-dose (SAR) protocol applied to coarse grain feldspar, *Radiation Measurements*, Vol. 32, pp. 529–533

Wang, Y. and Zheng, S.H., 1989, Palaeosol nodules as Pleistocene paleoclimatic indicators, Luochuan, P.R. China, *Palaeogeography, Palaeoclimatology, Palaeoecology*, Vol. 76, pp. 39–44

Wang, H. and Greenberg, S., 2006, Reconstructing the response of C3 and C4 plants to decadal-scale climate change during the late Pleistocene in southern Illinois using isotopic analyses of calcified rootlets, *Quaternary Research*, Vol. 67, pp. 136-142

Watson, A., 1985, Structure, chemistry and origins of gypsum crusts in southern Tunisia and the central Namib Desert, *Sedimentology*, Vol. 32, pp. 855-875

Weldeab, S., Emeis, K.C., Hemleben, C., Vennemann, T.W. and Schulz, H., 2002, Sr and Nd isotope composition of Late Pleistocene sapropels and nonsapropelic sediments from the Eastern Mediterranean Sea: Implications for detrital influx and climatic conditions in the source areas, *Geochimica et Cosmochimica Acta*, Vol. 66, pp. 3585–3598

Whalley, W.B., Marshall, J.R., Smith, B.J., 1982, Origin for desert loess from some experimental observations, *Nature,* Vol. 300, pp. 433–435

White, R.M.P, Dennis, P.F. Atkinson, T.C., 1999. Experimental Calibration and Field Investigation of the Oxygen Isotopic Fractionation Between Biogenic Aragonite and Water. *Rapid Communications in Mass Spectrometry*, Vol. 13, pp. 1242–1247

Wieder, M. and Yaalon, D.H., 1982, Micromorphological fabrics and developmental stages of carbonate nodular forms related to soil characteristics, *Geoderma*, Vol. 28, pp. 203-220

Wintle, A.G., 1981, Thermoluminescene dating of late Devensian loesses in southern England, *Nature*, Vol. 289, pp. 479-480

Wintle, A.G. and Murray, A.S., 1999, Luminescence sensitivity changes in quartz, *Radiation Measurements*, Vol. 30, pp. 107-118

Wintle, A.G. and Murray, A.S., 2006, A review of quartz optically stimulated luminescence characteristics and their relevance in single-aliquot regeneration dating protocols, *Radiation Measurements*, Vol. 41, pp. 369 – 391

Woillard, G.M. and Mook, G. W., 1987, Carbon-14 Dates at Grande Pile: Correlation of Land and Sea Chronologies, *Science*, Vol. 215, pp. 159-161

Wolff, E.W., Chappellaz, J., Blunier, T., Rasmussen, S.O. and Svenssion, A., 2010, Millennial-scale variability during the last glacial: The ice core record, *Quaternary Science Reviews*, Vol. 29, pp. 2828–2838

Woodward, F.I., Lomas, M.R., and Kelly, C.K., 2004, Global climate and the distribution of plant biomes, *Philosophical Transactions of the Royal Society London B,* Vol. 359, pp.1465–76

Woodward, J.C., Lewin, J. and Macklin, M.G., 1992, Alluvial sediment sources in a glaciated catchment: The Voidomatis basin, Northwest Greece, *Earth Surface Processes and Landforms*, Vol. 17, pp. 205-216

Wright, J.S., 2001, 'Desert' loess versus 'glacial' loess: quartz silt formation, source areas and sediment pathways in the formation of loess deposits, *Geomorphology*, Vol. 36, pp. 231–256

Wright, J.S., Smith, B.J., Whalley, W.B., 1998, Mechanisms of loess sized quartz silt production and their relative effectiveness: laboratory simulations, *Geomorphology*, Vol. 23, pp. 15–34

Wright, V.P., 2007, Calcrete, IN: Nash, D.J. and McLaren, S.J. (Eds), *Geochemical sediments and landscapes*, Blackwell Publishing, Oxford, pp.10-46

Wu, N., Chen, X., Rousseau, D.D., Li, F., Pei, Y. and Wu, B., 2007, Climatic conditions recorded by terrestrial mollusc assemblages in the Chinese Loess Plateau during marine Oxygen Isotope Stages 12–10, *Quaternary Science Reviews*, Vol. 26, pp.1884–1896

Xiao, J., Porter, S.C., An, Z., Kumai, H. and Yoshikawa, S., 1995, Grain size of quartz as an indicator of winter monsoon strength on the Loess Plateau of Central China during the last 130,000yr, *Quaternary Research*, Vol. 43, pp. 22-29

Yaalon, D.H., 1997, Soils in the Mediterranean region: what makes them different? *Catena*, Vol. 28, pp. 157-169

Yang, S., Ding, Z., Wang, X., Tang, Z. and Gu, Z., 2012, Negative $\delta^{18}O$–$\delta^{13}C$ relationship of pedogenic carbonate from northern China indicates a strong response of C3/C4 biomass to the seasonality of Asian monsoon precipitation, *Palaeogeography, Palaeoclimatology, Palaeoecology*, Vol. 317–318, pp.32–40

Zazo, C., Silva, PG., Goy, J.L., Hillaire-Marcel,, H., Ghaleb, B., Lario, J., Bardají, T. and González, A.,1999, Coastal uplift in continental collision plate boundaries: data from the Last Interglacial marine terraces of the Gibraltar Strait area (south Spain), *Tectonophysics*, Vol. 301, pp. 95-109

Zhang, Z., Zhao, M., Eglington, G., Lu, H and Huang, C.Y., 2006, Leaf wax lipids as paleovegetational and paleoenvironmental proxies for the Chinese Loess Plateau over the last 170 kyr, *Quaternary Science Reviews*, Vol. 25, pp. 575–594

Zhou, L.P., Oldfield, F., Wintle, A.G., Robinson, S.G. and Wang, J.T., 1990, Partly pedogenic origin of the magnetic variations in Chinese loess, *Nature*, Vol. 346, pp. 737-739

Online Resources:

Agencia Estatal de Meteorologia, Datos climatológicos, http://www.aemet.es/en/serviciosclimaticos/datosclimatologicos, Date accessed: Aug 2012

Gonzalez, A., Moreno, E.L. and Soria Mingorance, J.M., 1985, Zafarrayah (1040) MAGNA 50 (2ª Serie), 1:50,000, http://www.igme.es/internet/cartografia/cartografia/magna50.asp?hoja=1040&bis=

Martin, A.B., Serrano, A.M. and Mateo, E.P., 1977, Malaga (1053) MAGNA 50 (2ª Serie), 1:50,000, http://www.igme.es/internet/cartografia/cartografia/magna50.asp?hoja=1053&bis=

Stoops, G., Micromorphology slides: Stoops collection, *www.soil.ncsu.edu/lockers/lindbo/soil%20photos/micromorphology%20slides/Stoops%20collection/docs/ch8_cmp.html,* Date Accessed: January 2012

sample	depth	gravel %	sand %	silt %	total clay %	fine clay %	MEDIAN	CaCo3 (%)	LF mean	HF mean	% cfd	% organic carbon
3623	149.00	0.03	1.19	55.81	42.97	25.39	2.87	15.46	64.92	59.30	8.66	0.32
3624	144.00	0.19	1.06	56.58	42.17	26.07	2.96	20.50	63.62	58.06	8.74	0.29
3625	139.00	0.04	1.39	56.68	41.89	26.61	2.98	21.59	62.92	57.66	8.36	0.27
3626	134.00	0.05	1.31	56.03	42.61	28.21	2.96	22.57	63.14	57.78	8.49	0.39
3627	129.00	0.09	1.25	58.02	40.65	27.43	3.14	24.15	60.88	55.24	9.26	0.23
3628	124.00	0.15	1.38	55.24	43.23	27.57	2.77	24.06	66.38	57.34	13.62	0.27
3629	119.00	0.00	1.04	55.52	43.44	26.32	2.75	23.92	68.65	60.84	11.38	0.42
3630	114.00	0.09	1.04	55.27	43.60	26.99	2.68	24.04	71.90	63.18	12.13	0.45
3631	109.00	0.14	1.18	52.40	46.28	27.93	2.36	23.42	71.90	65.98	8.23	0.05
3632	104.00	0.04	1.21	54.21	44.54	27.95	2.57	23.79	72.34	66.10	8.63	0.59
3633	99.00	0.07	0.73	54.56	44.64	28.57	2.61	23.97	72.98	66.04	9.51	0.46
3634	94.00	0.09	0.78	53.33	45.79	29.44	2.43	23.48	70.96	64.46	9.16	0.48
3635	89.00	0.19	1.10	54.19	44.52	27.84	2.57	24.01	72.92	66.52	8.78	0.43
3636	85.00	0.25	1.18	55.30	43.27	27.60	2.74	23.88	77.48	70.40	9.14	0.49
3637	80.00	0.21	1.01	55.02	43.76	28.35	2.73	23.44	77.85	71.56	8.08	0.51
3638	75.00	0.41	1.20	54.02	44.37	27.84	2.63	24.11	76.87	69.66	9.38	0.40
3639	70.00	0.22	1.40	54.50	43.88	27.15	2.64	20.54	68.00	62.36	8.29	0.39
3640	65.00	0.78	1.57	56.24	41.40	25.58	3.04	22.88	70.42	64.84	7.92	0.36
3641	60.00	0.30	2.13	56.20	41.37	25.56	3.04	23.02	67.50	61.98	8.19	0.32
3642	55.00	1.04	2.92	53.88	42.16	25.55	2.96	24.14	64.40	59.24	8.01	0.36
3643	50.00	1.60	3.37	50.84	44.19	27.94	2.70	20.58	67.88	62.40	8.07	0.33
3644	45.00	0.41	5.90	47.79	45.91	27.73	2.50	22.35	69.26	64.00	7.59	0.28
3645	40.00	10.42	6.09	42.75	40.74	26.21	3.30	23.04	66.64	61.66	7.47	0.34
3646	35.00	32.14	6.56	31.82	29.49	18.51	10.44	21.63	65.94	60.62	8.07	0.28
3647	15.00	4.19	4.15	51.60	40.06	25.57	3.56	15.79	60.36	55.50	8.05	0.36

Table a1.1 La Malaha sedimentology data

Disc#	ED	de	ED_Err	de error	N.Signal	BG.signal	Test_Signal	Test_Dose	Residual_Signal	Test_Signal_Change	Recycling1	Recycling1_Err	Recycling2	Recycling2_Err
1	49.40	4.16	2.80	0.24	2871.00	117.00	3253.00	0.00	272.00	1.39	1.02	0.06	0.98	0.06
3	54.10	4.56	2.80	0.24	2918.00	117.00	3025.00	0.00	310.00	1.61	1.05	0.06	0.99	0.06
7	53.10	4.48	3.00	0.25	3219.00	163.00	3273.00	0.00	307.00	1.36	1.02	0.06	0.98	0.06
11	55.90	4.71	3.00	0.25	3197.00	92.00	3149.00	0.00	295.00	1.59	1.04	0.06	0.97	0.05
13	54.10	4.56	3.20	0.27	3247.00	214.00	3205.00	0.00	321.00	1.41	0.99	0.06	0.97	0.06
17	53.10	4.48	3.00	0.25	2692.00	110.00	2703.00	0.00	230.00	1.33	0.98	0.06	1.03	0.06
21	50.40	4.25	2.80	0.24	3040.00	97.00	3259.00	0.00	291.00	1.47	1.02	0.06	0.95	0.05
23	57.30	4.83	3.00	0.25	3588.00	110.00	3449.00	0.00	216.00	1.42	0.99	0.06	1.00	0.06
25	55.40	4.67	3.00	0.25	2706.00	125.00	2722.00	0.00	257.00	1.47	1.03	0.06	0.97	0.06
27	59.10	4.98	3.20	0.27	2848.00	168.00	2753.00	0.00	284.00	1.45	1.05	0.07	0.95	0.06
31	58.20	4.91	3.00	0.25	3415.00	146.00	3402.00	0.00	270.00	1.46	1.03	0.06	0.95	0.05
35	52.70	4.44	2.80	0.24	3030.00	117.00	3181.00	0.00	279.00	1.38	0.99	0.06	0.99	0.06
37	57.30	4.83	3.00	0.25	3423.00	112.00	3413.00	0.00	334.00	1.42	1.04	0.06	1.01	0.06
39	56.80	4.79	3.20	0.27	2887.00	116.00	2802.00	0.00	241.00	1.38	0.98	0.06	1.03	0.06
41	55.00	4.64	3.20	0.27	2955.00	85.00	2979.00	0.00	233.00	1.43	1.02	0.06	1.01	0.06
45	86.90	7.33	4.40	0.37	4978.00	103.00	3239.00	0.00	243.00	1.40	1.02	0.06	0.97	0.06
47	54.50	4.59	2.80	0.24	3717.00	101.00	3596.00	0.00	310.00	1.53	1.01	0.06	1.00	0.05
mean	56.66	4.78	3.07	0.26										

Table a1.2 aliquot data used to construct OSL age estimate MAL 1. Source strength: 0.084309 (Gy/s)

Disc#	ED	de	ED_Err	de error	N.Signal	BG.signal	Test_Signal	Test_Dose	Residual_Signal	Test_Signal_Change	Recycling1	Recycling1_Err	Recycling2	Recycling2_Err
1	85.00	7.15	4.40	0.37	4887.00	126.00	3779.00	0.00	256.00	1.03	0.97	0.06	1.04	0.06
3	86.40	7.27	5.10	0.43	3296.00	114.00	2463.00	0.00	360.00	1.61	0.99	0.06	0.99	0.06
5	83.60	7.03	3.90	0.33	7286.00	101.00	5029.00	0.00	349.00	1.24	1.03	0.06	1.00	0.05
7	81.30	6.84	3.70	0.31	5130.00	101.00	4080.00	0.00	226.00	1.09	0.95	0.06	1.00	0.06
9	93.30	7.85	4.60	0.39	5198.00	108.00	3715.00	0.00	254.00	1.16	1.05	0.06	0.95	0.06
11	94.70	7.97	4.60	0.39	6573.00	117.00	4262.00	0.00	358.00	1.33	1.05	0.06	1.00	0.05
13	92.40	7.77	4.90	0.41	5069.00	102.00	3384.00	0.00	248.00	1.23	1.00	0.06	1.00	0.06
15	80.80	6.80	4.90	0.41	4715.00	116.00	3499.00	0.00	338.00	1.26	0.97	0.06	1.01	0.06
17	79.90	6.72	3.90	0.33	5756.00	112.00	4226.00	0.00	397.00	1.37	0.98	0.06	0.98	0.05
19	78.50	6.60	3.90	0.33	6935.00	125.00	4791.00	0.00	506.00	1.56	0.99	0.05	0.97	0.05
21	84.50	7.11	4.20	0.35	5107.00	105.00	3988.00	0.00	277.00	1.04	1.04	0.06	1.01	0.06
23	91.00	7.66	4.90	0.41	4776.00	89.00	3325.00	0.00	317.00	1.28	1.03	0.06	0.99	0.06
1	92.90	7.82	4.90	0.41	4669.00	122.00	3329.00	0.00	294.00	1.47	0.95	0.06	1.04	0.06
3	82.20	6.92	4.20	0.35	5588.00	110.00	3957.00	0.00	289.00	1.23	0.97	0.06	1.00	0.06
5	86.90	7.31	4.20	0.35	4774.00	104.00	3544.00	0.00	258.00	1.14	1.02	0.06	1.00	0.06
7	87.80	7.39	4.40	0.37	5616.00	122.00	4064.00	0.00	326.00	1.20	1.00	0.06	0.99	0.06
9	92.40	7.77	4.40	0.37	5894.00	114.00	4211.00	0.00	281.00	1.20	1.03	0.06	1.00	0.06
11	78.50	6.60	4.40	0.37	6377.00	112.00	4654.00	0.00	521.00	1.49	1.00	0.05	1.03	0.05
13	90.60	7.62	4.40	0.37	5518.00	116.00	3968.00	0.00	311.00	1.31	1.03	0.06	1.02	0.06
15	85.90	7.23	4.40	0.37	6417.00	118.00	4678.00	0.00	304.00	1.20	1.00	0.06	1.03	0.06
19	86.40	7.27	4.20	0.35	6089.00	103.00	4124.00	0.00	380.00	1.45	0.97	0.05	1.03	0.06
21	85.50	7.19	4.40	0.37	5607.00	107.00	4070.00	0.00	347.00	1.25	0.97	0.06	1.02	0.06
mean	86.39	7.27	4.40	0.37										

Table a1.3 aliquot data used to construct OSL age estimate MAL 2. Source strength: 0.084309 (Gy/s)

	sample number	depth (cm)	gravel %	sand %	silt %	total clay %	fine clay %	MEDIAN	% $CaCO^3$	LF	HF	% CFD	% organic carbon
Log 6	3937	120	0.00	29.28	48.16	22.56	15.13	21.39	26.36	5.90	5.54	6.10	0.11
	3938	125	0.00	27.12	51.16	21.72	14.58	21.29	25.60	5.40	5.38	0.37	0.00
	3939	130	0.00	29.04	50.95	20.01	13.77	22.43	25.74	6.06	5.38	11.22	0.18
	3940	135	0.00	25.90	52.54	21.56	13.93	20.10	21.33	5.88	5.36	8.84	0.15
	3941	140	0.00	27.17	51.20	21.63	13.77	18.95	28.54	5.50	5.28	4.00	0.20
	3942	143	0.00	29.75	50.72	19.53	10.89	20.41	22.40	7.72	7.02	9.07	0.00
	3943	148	0.00	34.83	43.60	21.57	15.38	23.68	22.16	9.84	9.30	5.49	0.15
	3944	153	0.00	27.69	50.11	22.20	18.44	20.50	18.74	16.34	14.58	10.77	0.22
	3945	158	0.00	32.55	45.13	22.33	16.46	23.01	25.34	24.46	21.96	10.22	0.09
	3946	163	0.00	36.67	41.42	21.91	14.44	25.77	36.53	19.98	17.64	11.71	0.00
Log 7	3947	5	0.00	21.27	52.83	25.90	16.14	29.24	33.31	5.98	5.60	6.35	0.14
	3948	10	0.00	21.27	52.83	25.90	16.14	17.81	31.96	6.92	6.58	4.91	0.09
	3949	15	0.00	25.48	49.63	24.89	16.40	17.12	33.64	6.84	6.30	7.89	0.14
	3950	20	0.00	25.94	48.44	25.63	17.18	17.02	32.35	6.68	6.08	8.98	0.17
	3951	25	0.00	26.56	47.07	26.36	21.44	17.08	23.26	6.06	5.50	9.24	0.04
	3952	30	0.00	24.52	48.84	26.65	17.29	15.23	28.47	5.84	5.82	0.34	0.30
	3953	35	0.00	38.44	38.97	22.59	13.79	25.85	24.19	5.34	5.14	3.75	0.13
	3954	40	0.00	37.17	37.38	25.45	16.40	22.73	22.09	6.70	6.22	7.16	0.00
	3955	45	0.00	37.43	37.29	25.28	18.15	23.18	22.61	10.02	9.00	10.18	0.09
	3956	51	0.00	27.61	48.72	23.67	16.58	18.50	24.95	16.10	14.56	9.57	0.32
	3957	56	0.00	36.03	42.47	21.49	14.65	23.97	23.38	17.30	15.20	12.14	0.12
	3958	61	0.00	33.66	43.19	23.15	14.79	21.25	30.23	13.10	11.72	10.53	0.09
	3959	66	0.00	34.63	42.43	22.95	15.23	22.85	29.99	13.34	12.30	7.80	0.04
	3960	71	0.00	28.75	46.31	24.94	15.82	17.58	30.94	12.50	11.52	7.84	0.08
	3961	76	0.00	29.26	44.00	26.74	18.04	16.65	29.39	12.58	11.46	8.90	0.00
	3962	81	0.00	29.12	43.02	27.85	15.45	15.95	27.66	14.92	13.46	9.79	0.10
	3963	86	0.00	32.98	40.41	26.61	17.16	18.02	26.14	19.02	16.60	12.72	0.15
	3964	91	0.00	29.66	46.78	23.56	14.07	18.77	26.57	16.66	15.18	8.88	0.09
	3965	96	0.00	28.27	46.91	24.82	14.49	16.79	28.17	18.46	16.36	11.38	0.13
	3966	101	0.00	25.06	49.76	25.18	15.14	14.93	26.97	14.98	13.22	11.75	0.00
	3967	106	0.00	30.52	45.23	24.25	14.94	19.02	28.87	15.44	14.14	8.42	0.00
	3968	111	0.00	28.93	44.91	26.15	15.56	15.25	35.09	13.42	12.00	10.58	0.04
	3969	116	0.00	30.13	43.95	25.92	16.42	16.52	35.63	19.32	17.42	9.83	0.00
	3970	121	0.00	28.36	43.20	28.44	18.98	13.20	31.97	17.32	15.46	10.74	0.00
	3971	126	0.00	36.04	38.38	25.58	17.14	20.51	29.72	15.30	14.24	6.93	0.28
	3972	131	0.00	25.06	46.24	28.70	18.51	12.49	30.23	17.74	16.36	7.78	0.09
	3973	136	0.00	23.40	49.18	27.42	18.46	13.86	27.95	21.66	19.68	9.14	0.10
	3974	141	0.00	18.71	51.38	29.91	21.30	11.06	26.11	20.88	18.62	10.82	0.13
	3975	146	0.00	23.91	47.56	28.53	18.19	12.33	25.28	22.36	19.74	11.72	0.24
	3976	151	0.00	29.10	41.83	29.07	20.06	12.65	25.25	19.28	16.98	11.93	0.00
	3977	156	0.00	36.77	35.72	27.50	17.51	14.91	26.00	13.56	12.46	8.11	0.14
	3978	161	0.00	38.33	34.78	26.89	18.69	16.47	22.04	17.04	15.62	8.33	0.00
	3979	166	0.00	35.92	35.95	28.13	19.09	15.34	27.23	16.78	15.02	10.49	0.00
Log 8	3980	5	0.00	21.12	48.59	30.29	19.17	9.58	31.46	29.50	26.84	9.02	0.00
	3981	10	0.00	32.98	40.01	27.01	18.77	14.91	31.34	24.52	21.76	11.26	0.00
	3982	15	0.00	32.91	40.32	26.77	17.51	14.57	32.44	26.02	23.26	10.61	0.04
	3983	20	0.00	32.52	40.01	27.46	18.69	13.96	32.53	28.74	25.74	10.44	0.18
	3984	25	0.00	29.45	39.93	30.62	19.47	10.44	31.59	32.26	28.50	11.66	0.18
	3985	30	0.00	33.22	37.73	29.05	18.43	11.57	30.05	27.64	24.22	12.37	0.20
	3986	35	0.00	33.01	38.05	28.94	18.02	10.72	29.07	21.38	18.98	11.23	0.04
	3987	40	0.00	32.11	35.71	32.18	20.84	8.86	31.50	23.60	20.96	11.19	0.14
	3988	45	0.00	31.60	37.07	31.33	19.90	9.62	33.26	23.74	21.46	9.60	0.00
	3989	50	0.00	31.31	35.72	32.97	21.71	8.01	28.19	25.82	23.08	10.61	0.05
	3990	55	0.00	32.74	36.18	31.07	20.78	10.40	32.96	26.38	23.56	10.69	0.04
	3991	60	0.00	40.65	33.36	26.00	19.29	22.63	36.81	23.00	22.92	0.35	0.00
	3992	65	0.00	39.95	32.97	27.08	17.59	20.67	41.44	22.42	22.40	0.09	0.08
	3993	70	0.00	36.65	35.67	27.68	18.88	16.34	37.72	24.36	24.36	0.00	0.00
	3994	75	0.00	33.83	36.99	29.18	19.72	13.45	37.60	26.68	25.98	2.62	0.08
	3995	80	0.00	33.22	37.06	29.72	20.17	12.74	34.33	28.86	25.60	11.30	0.18
	3996	85	0.00	30.65	37.03	32.32	20.80	9.26	33.77	28.00	25.30	9.64	0.32
	3997	88	0.00	27.93	42.23	29.84	16.36	8.86	30.61	27.16	24.68	9.13	0.21
	3998	93	0.00	23.77	43.60	32.63	18.14	6.67	31.79	41.32	37.28	9.78	0.51
	3999	98	0.00	23.91	46.19	29.90	15.98	8.24	32.59	43.50	38.96	10.44	0.05
	4000	103	0.00	22.08	46.44	31.48	17.14	7.31	34.16	47.34	42.02	11.24	0.34

	sample number	depth (cm)	gravel %	sand %	silt %	total clay %	fine clay %	MEDIAN	% $CaCO^3$	LF	HF	% CFD	% organic carbon
Log 8	4001	108	0.00	22.56	44.06	33.38	20.37	6.77	34.77	40.40	36.18	10.45	0.05
	4002	113	0.00	23.94	45.63	30.42	15.97	7.94	31.94	37.86	33.74	10.88	0.14
	4003	118	0.00	23.52	46.04	30.44	17.05	7.65	31.57	45.20	40.10	11.28	0.19
	4004	123	0.00	21.32	48.15	30.53	16.68	6.90	31.10	48.04	43.06	10.37	0.00
	4005	128	0.00	21.27	46.69	32.04	17.72	6.48	28.67	44.94	40.36	10.19	0.05
	4006	133	0.00	17.48	46.87	35.65	19.64	4.69	30.02	49.68	44.18	11.07	0.23
	4007	138	0.00	20.43	45.83	33.74	18.30	5.54	28.69	45.98	40.54	11.83	0.15
	4008	143	0.00	19.71	46.08	34.20	19.59	5.59	30.49	49.08	44.20	9.94	0.14
	4009	148	0.00	21.47	42.96	35.58	20.26	4.80	29.89	43.46	38.56	11.27	0.39
	4010	153	0.00	19.61	45.91	34.49	20.26	5.46	30.09	40.34	35.88	11.06	0.30
	4011	158	0.00	18.84	47.40	33.76	20.45	5.49	31.21	39.70	35.50	10.58	0.14
	4012	163	0.00	18.89	47.05	34.07	19.87	5.66	33.73	24.30	21.32	12.26	0.04
	4013	168	0.00	21.10	44.74	34.16	20.44	5.78	33.91	19.64	17.76	9.57	0.18
	4014	173	0.00	21.38	46.47	32.16	19.42	6.48	33.25	23.56	20.96	11.04	0.17
	4015	178	0.00	18.34	47.28	34.38	20.09	5.61	34.85	26.70	23.40	12.36	0.23
	4016	183	0.00	16.73	47.63	35.64	22.15	5.40	36.18	25.72	23.18	9.88	0.19
	4017	187	0.00	17.64	46.87	35.50	20.84	5.45	35.88	21.88	19.44	11.15	0.15
	4018	192	0.00	15.90	49.20	34.90	20.35	5.16	35.96	28.96	25.68	11.33	0.21
	4019	197	0.00	16.02	47.19	36.78	21.92	4.57	34.68	40.36	35.98	10.85	0.29
	4020	202	0.00	15.30	48.79	35.91	20.67	4.58	33.37	44.10	39.14	11.25	0.20
	4021	207	0.00	17.99	48.39	33.63	19.52	5.76	33.77	39.90	39.92	-0.05	0.24
	4022	212	0.00	17.81	45.62	36.57	22.11	5.15	37.49	38.64	34.14	11.65	0.25
	4023	217	0.00	19.68	45.70	34.62	20.64	6.02	41.11	33.62	29.84	11.24	0.22
	4024	222	0.00	19.65	48.69	31.66	19.53	7.79	44.86	34.02	30.30	10.93	0.18
	4025	227	0.00	16.80	48.25	34.94	20.88	5.52	40.74	40.34	36.02	10.71	0.14
	4026	232	0.00	13.72	54.79	31.49	17.52	6.59	42.10	45.58	40.56	11.01	0.14
	4027	237	0.00	16.91	47.53	35.56	19.94	4.72	36.59	43.84	39.06	10.90	0.13
	4028	242	0.00	16.30	45.95	37.75	21.76	4.14	38.60	44.98	40.04	10.98	0.25
	4029	247	0.00	19.57	49.62	30.80	17.29	7.43	42.12	45.84	41.00	10.56	0.22
	4030	250	0.00	22.75	49.60	27.66	20.78	10.99	46.99	42.60	37.96	10.89	0.12
5	4031	85	30.39	57.43	8.79	3.38	1.83	1175.36	16.22	8.04	7.74	3.73	0.04
5	4032	102	0.00	27.93	53.33	18.74	7.28	14.04	0.61	5.82	5.50	5.50	0.05
6	4033	30	1.83	31.09	43.74	23.35	11.27	10.77	0.22	3.42	3.42	0.00	0.09
6	4034	95	0.00	31.85	51.25	16.90	8.18	19.81	0.64	8.44	7.54	10.66	0.08
9	4035	100	3.08	13.89	47.99	35.04	20.09	5.24	0.15	58.72	52.28	10.97	0.30

Table a2.1 Chimeneas sedimentology data from logs 5-9 (continued from previous page)

sub-unit	sample number	depth in log (cm)	depth in composite	gravel %	sand %	silt %	total clay %	fine clay %	MEDIAN	%CaCO3	lf	hf	% cfd	%organic carbon
1a	4033	30	30	1.83	31.09	43.74	23.35	11.27	10.77	25.17	3.42	3.42	0.00	0.09
1a	4034	95	95	0.00	31.85	51.25	16.90	8.18	19.81	28.52	8.44	7.54	10.66	0.08
1b	3937	120	115	0.00	29.28	48.16	22.56	15.13	21.39	26.36	5.90	5.54	6.10	0.11
1b	3938	125	120	0.00	27.12	51.16	21.72	14.58	21.29	25.60	5.40	5.38	0.37	0.00
b	3939	130	125	0.00	29.04	50.95	20.01	13.77	22.43	25.74	6.06	5.38	11.22	0.18
1b	3940	135	130	0.00	25.90	52.54	21.56	13.93	20.10	21.33	5.88	5.36	8.84	0.15
1b	3941	140	135	0.00	27.17	51.20	21.63	13.77	18.95	28.54	5.50	5.28	4.00	0.20
1c	3942	143	138	0.00	29.75	50.72	19.53	10.89	20.41	22.40	7.72	7.02	9.07	0.00
1c	3943	148	143	0.00	34.83	43.60	21.57	15.38	23.68	22.16	9.84	9.30	5.49	0.15
1c	3944	153	148	0.00	27.69	50.11	22.20	18.44	20.50	18.74	16.34	14.58	10.77	0.22
1c	3945	158	153	0.00	32.55	45.13	22.33	16.46	23.01	25.34	24.46	21.96	10.22	0.09
1c	3946	163	158	0.00	36.67	41.42	21.91	14.44	25.77	36.53	19.98	17.64	11.71	0.00
2a	3957	56	163	0.00	36.03	42.47	21.49	14.65	23.97	23.38	17.30	15.20	12.14	0.12
2a	3958	61	168	0.00	33.66	43.19	23.15	14.79	21.25	30.23	13.10	11.72	10.53	0.09
2a	3959	66	173	0.00	34.63	42.43	22.95	15.23	22.85	29.99	13.34	12.30	7.80	0.04
2a	3960	71	178	0.00	28.75	46.31	24.94	15.82	17.58	30.94	12.50	11.52	7.84	0.08
2a	3961	76	183	0.00	29.26	44.00	26.74	18.04	16.65	29.39	12.58	11.46	8.90	0.00
2a	3962	81	188	0.00	29.12	43.02	27.85	15.45	15.95	27.66	14.92	13.46	9.79	0.10
2a	3963	86	193	0.00	32.98	40.41	26.61	17.16	18.02	26.14	19.02	16.60	12.72	0.15
2a	3964	91	198	0.00	29.66	46.78	23.56	14.07	18.77	26.57	16.66	15.18	8.88	0.09
2a	3965	96	203	0.00	28.27	46.91	24.82	14.49	16.79	28.17	18.46	16.36	11.38	0.13
2a	3966	101	208	0.00	25.06	49.76	25.18	15.14	14.93	26.97	14.98	13.22	11.75	0.00
2a	3967	106	213	0.00	30.52	45.23	24.25	14.94	19.02	28.87	15.44	14.14	8.42	0.00
2a	3968	111	218	0.00	28.93	44.91	26.15	15.56	15.25	35.09	13.42	12.00	10.58	0.04
2a	3969	116	223	0.00	30.13	43.95	25.92	16.42	16.52	35.63	19.32	17.42	9.83	0.00
2a	3970	121	228	0.00	28.36	43.20	28.44	18.98	13.20	31.97	17.32	15.46	10.74	0.00
2a	3971	126	233	0.00	36.04	38.38	25.58	17.14	20.51	29.72	15.30	14.24	6.93	0.28
2a	3972	131	238	0.00	25.06	46.24	28.70	18.51	12.49	30.23	17.74	16.36	7.78	0.09
2a	3973	136	243	0.00	23.40	49.18	27.42	18.46	13.86	27.95	21.66	19.68	9.14	0.10
2a	3974	141	248	0.00	18.71	51.38	29.91	21.30	11.06	26.11	20.88	18.62	10.82	0.13
2a	3975	146	253	0.00	23.91	47.56	28.53	18.19	12.33	25.28	22.36	19.74	11.72	0.24
2a	3976	151	258	0.00	29.10	41.83	29.07	20.06	12.65	25.25	19.28	16.98	11.93	0.00
2a	3977	156	263	0.00	36.77	35.72	27.50	17.51	14.91	26.00	13.56	12.46	8.11	0.14
2a	3978	161	268	0.00	38.33	34.78	26.89	18.69	16.47	22.04	17.04	15.62	8.33	0.00
2a	3979	166	273	0.00	35.92	35.95	28.13	19.09	15.34	27.23	16.78	15.02	10.49	0.00
2b	3998	93	278	0.00	23.77	43.60	32.63	18.14	6.67	31.79	41.32	37.28	9.78	0.51
2b	3999	98	283	0.00	23.91	46.19	29.90	15.98	8.24	32.59	43.50	38.96	10.44	0.05
2b	4000	103	288	0.00	22.08	46.44	31.48	17.14	7.31	34.16	47.34	42.02	11.24	0.34
2b	4001	108	293	0.00	22.56	44.06	33.38	20.37	6.77	34.77	40.40	36.18	10.45	0.05
2b	4002	113	298	0.00	23.94	45.63	30.42	15.97	7.94	31.94	37.86	33.74	10.88	0.14
2b	4003	118	303	0.00	23.52	46.04	30.44	17.05	7.65	31.57	45.20	40.10	11.28	0.19
2b	4004	123	308	0.00	21.32	48.15	30.53	16.68	6.90	31.10	48.04	43.06	10.37	0.00
2b	4005	128	313	0.00	21.27	46.69	32.04	17.72	6.48	28.67	44.94	40.36	10.19	0.05
2b	4006	133	318	0.00	17.48	46.87	35.65	19.64	4.69	30.02	49.68	44.18	11.07	0.23
2b	4007	138	323	0.00	20.43	45.83	33.74	18.30	5.54	28.69	45.98	40.54	11.83	0.15
2b	4008	143	328	0.00	19.71	46.08	34.20	19.59	5.59	30.49	49.08	44.20	9.94	0.14
2b	4009	148	333	0.00	21.47	42.96	35.58	20.26	4.80	29.89	43.46	38.56	11.27	0.39
2b	4010	153	338	0.00	19.61	45.91	34.49	20.26	5.46	30.09	40.34	35.88	11.06	0.30
2c	4011	158	343	0.00	18.84	47.40	33.76	20.45	5.49	31.21	39.70	35.50	10.58	0.14
2c	4012	163	348	0.00	18.89	47.05	34.07	19.87	5.66	33.73	24.30	21.32	12.26	0.04
2c	4013	168	353	0.00	21.10	44.74	34.16	20.44	5.78	33.91	19.64	17.76	9.57	0.18
2c	4014	173	358	0.00	21.38	46.47	32.16	19.42	6.48	33.25	23.56	20.96	11.04	0.17
2c	4015	178	363	0.00	18.34	47.28	34.38	20.09	5.61	34.85	26.70	23.40	12.36	0.23
2c	4016	183	368	0.00	16.73	47.63	35.64	22.15	5.40	36.18	25.72	23.18	9.88	0.19
2c	4017	187	372	0.00	17.64	46.87	35.50	20.84	5.45	35.88	21.88	19.44	11.15	0.15
2d	4018	192	377	0.00	15.90	49.20	34.90	20.35	5.16	35.96	28.96	25.68	11.33	0.21
2d	4019	197	382	0.00	16.02	47.19	36.78	21.92	4.57	34.68	40.36	35.98	10.85	0.29
2d	4020	202	387	0.00	15.30	48.79	35.91	20.67	4.58	33.37	44.10	39.14	11.25	0.20
2d	4021	207	392	0.00	17.99	48.39	33.63	19.52	5.76	33.77	39.90	39.92	-0.05	0.24
2e	4022	212	397	0.00	17.81	45.62	36.57	22.11	5.15	37.49	38.64	34.14	11.65	0.25
2e	4023	217	402	0.00	19.68	45.70	34.62	20.64	6.02	41.11	33.62	29.84	11.24	0.22
2e	4024	222	407	0.00	19.65	48.69	31.66	19.53	7.79	44.86	34.02	30.30	10.93	0.18
2e	4025	227	412	0.00	16.80	48.25	34.94	20.88	5.52	40.74	40.34	36.02	10.71	0.14
2e	4026	232	417	0.00	13.72	54.79	31.49	17.52	6.59	42.10	45.58	40.56	11.01	0.14
2f	4027	237	422	0.00	16.91	47.53	35.56	19.94	4.72	36.59	43.84	39.06	10.90	0.13
2f	4028	242	427	0.00	16.30	45.95	37.75	21.76	4.14	38.60	44.98	40.04	10.98	0.25
2f	4029	247	432	0.00	19.57	49.62	30.80	17.29	7.43	42.12	45.84	41.00	10.56	0.22
2f	4030	250	435	0.00	22.75	49.60	27.66	20.78	10.99	46.99	42.60	37.96	10.89	0.12
3	4035	100	475	3.08	13.89	47.99	35.04	20.09	5.24	39.27	58.72	52.28	10.97	0.30

Table a2.2 Chimeneas composite log sedimentology data

sample ID	original depth	composite depth	Weight (µg)	Peak 2 height (nA)	d13C corr (‰)	error (1s)	d18O corr (‰)	error (1s)	Est % carb
4030	250	440	1045	7.13	-6.58	0.04	-6.23	0.03	59.41
4029	247	437	1102	2.05	-5.45	0.07	-5.42	0.03	18.57
4027	237	427	1017	5.75	-5.75	0.01	-4.82	0.02	56.42
4025	227	417	1014	5.60	-5.94	0.00	-4.87	0.07	48.11
4024	222	412	1036	6.19	-6.35	0.04	-5.22	0.04	59.65
4022	212	402	990	5.58	-6.38	0.03	-5.27	0.04	49.06
4021	207	397	1106	6.75	-6.18	0.00	-5.24	0.03	60.87
4020	202	392	1023	6.37	-6.48	0.00	-5.37	0.01	54.23
4019	197	387	988	7.27	-6.57	0.02	-5.20	0.01	64.12
4016	183	373	963	6.10	-6.03	0.01	-5.03	0.02	55.16
4015	178	368	1084	3.88	-5.97	0.02	-5.05	0.00	35.68
4013	168	358	958	5.84	-6.11	0.02	-5.04	0.01	53.09
4012	163	353	995	1.68	-6.28	0.05	-5.16	0.07	16.81
4011	158	348	1129	6.81	-6.09	0.01	-4.97	0.09	52.56
4008	143	333	997	4.94	-6.42	0.00	-4.95	0.02	43.18
4006	133	323	948	5.00	-5.19	0.01	-4.77	0.06	52.66
4005	128	318	958	5.70	-5.14	0.03	-4.90	0.02	51.78
4003	118	308	969	3.43	-6.48	0.01	-5.35	0.01	35.31
4002	113	303	943	8.14	-4.61	0.03	-4.94	0.07	75.14
3979	166	278	1101	1.65	-6.15	0.04	-4.96	0.11	14.91
3976	151	263	954	4.71	-5.95	0.04	-5.07	0.09	49.29
3973	136	248	1059	4.16	-6.03	0.02	-5.48	0.06	34.18
3970	121	233	945	4.22	-6.25	0.01	-5.30	0.04	38.92
3967	106	218	1101	4.08	-6.03	0.03	-5.88	0.00	32.28
3964	91	203	999	3.03	-5.82	0.02	-5.87	0.03	26.38
3961	76	188	989	3.92	-7.99	0.03	-6.84	0.07	34.50
3958	61	173	979	3.35	-6.25	0.01	-6.20	0.02	29.77
3946	163	163	999	5.54	-5.66	0.01	-5.52	0.00	48.25
3944	153	153	1052	2.84	-6.43	0.02	-6.10	0.02	23.46

Table a2.3 Carbon and oxygen isotope data for Chimeneas

	Disc#	ED	De	ED_Err	De error	N.Signal	BG.signal	Test_Signal	Test_Dose	Residual_Signal	Test_Signal_Change	Recycling1	Recycling1_Err	Recycling2
08-Nov-11	1	238.60	19.60	14.80	1.22	4586.00	88.00	1359.00	0.00	149.00	1.24	1.01	0.08	0.97
08-Nov-11	5	226.00	18.56	13.60	1.12	5988.00	89.00	1785.00	0.00	197.00	1.27	1.01	0.07	0.95
08-Nov-11	15	217.80	17.89	11.40	0.94	6578.00	107.00	1993.00	0.00	167.00	1.14	1.02	0.07	0.99
08-Nov-11	17	226.50	18.60	13.60	1.12	5718.00	120.00	1692.00	0.00	191.00	1.34	0.98	0.07	1.00
08-Nov-11	19	238.60	19.60	15.20	1.25	5085.00	103.00	1470.00	0.00	181.00	1.21	0.97	0.08	0.97
08-Nov-11	21	215.40	17.69	11.10	0.91	8336.00	140.00	2610.00	0.00	314.00	1.22	0.98	0.06	1.04
28-Apr-11	1	241.60	20.13	14.80	1.23	6179.00	103.00	1584.00	0.00	203.00	1.32	0.95	0.07	1.05
28-Apr-11	11	254.10	21.17	15.90	1.32	6763.00	83.00	1649.00	0.00	166.00	1.24	1.04	0.08	0.96
28-Apr-11	15	241.60	20.13	13.90	1.16	7147.00	87.00	1744.00	0.00	214.00	1.19	1.03	0.07	1.04
28-Apr-11	21	240.70	20.05	13.90	1.16	6778.00	70.00	1684.00	0.00	162.00	1.19	1.03	0.08	1.02
28-Apr-11	33	258.30	21.52	15.20	1.27	7269.00	99.00	1654.00	0.00	210.00	1.31	0.99	0.07	0.96
28-Apr-11	41	227.30	18.93	13.40	1.12	6520.00	104.00	1744.00	0.00	215.00	1.22	0.99	0.07	1.00
28-Apr-11	43	205.10	17.09	13.60	1.13	5212.00	126.00	1452.00	0.00	200.00	1.23	0.97	0.08	1.02
28-Apr-11	45	226.80	18.89	14.60	1.22	5496.00	113.00	1460.00	0.00	190.00	1.34	1.02	0.08	0.97
		232.74	19.27	13.93	1.15									
	Source strength:	Apr-11	0.08											
		Nov-11	0.08											

Table a2.4 Aliquot data used to construct OSL age estimate chim2

	Disc#	ED	De	ED_Err	De error	N.Signal	BG.signal	Test_Signal	Test_Dose	Residual_Signal	Test_Signal_Change	Recycling 1	Recycling 1_Err	Recycling 2	Recycling 2_Err
02-Apr-11	1	341.90	28.48	16.40	1.37	14611.00	132.00	2730.00	0.00	287.00	1.29	1.00	0.06	1.00	0.06
02-Apr-11	7	319.20	26.59	17.30	1.44	11330.00	209.00	2257.00	0.00	273.00	1.19	1.00	0.07	1.02	0.07
02-Apr-11	11	318.80	26.56	15.20	1.27	14167.00	128.00	2789.00	0.00	307.00	1.23	0.96	0.06	0.97	0.06
02-Apr-11	13	318.80	26.56	17.10	1.42	13893.00	100.00	2703.00	0.00	221.00	1.22	1.03	0.07	1.00	0.06
02-Apr-11	15	338.20	28.17	18.20	1.52	14377.00	114.00	2680.00	0.00	321.00	1.26	1.00	0.06	1.03	0.06
02-Apr-11	19	339.60	28.29	15.90	1.32	14892.00	126.00	2797.00	0.00	255.00	1.24	1.03	0.06	1.00	0.06
02-Apr-11	21	331.30	27.60	15.20	1.27	16547.00	153.00	3211.00	0.00	316.00	1.28	0.99	0.06	1.01	0.06
08-Nov11	25	327.70	26.92	18.60	1.53	13506.00	169.00	2935.00	0.00	311.00	1.30	0.97	0.06	1.01	0.06
08-Nov11	27	360.60	29.62	15.20	1.25	22059.00	195.00	4335.00	0.00	429.00	1.38	0.99	0.06	1.01	0.05
08-Nov11	29	360.10	29.58	16.50	1.36	17120.00	121.00	3391.00	0.00	292.00	1.45	1.01	0.06	1.00	0.06
08-Nov11	31	338.80	27.83	17.70	1.45	13623.00	144.00	2886.00	0.00	297.00	1.34	0.97	0.06	1.05	0.06
08-Nov11	33	357.70	29.38	19.80	1.63	12057.00	136.00	2540.00	0.00	278.00	1.57	0.92	0.06	1.04	0.06
08-Nov11	37	319.90	26.28	15.20	1.25	15801.00	116.00	3338.00	0.00	310.00	1.28	1.00	0.06	1.04	0.06
08-Nov11	39	332.50	27.31	17.20	1.41	14548.00	158.00	3080.00	0.00	296.00	1.30	1.05	0.06	1.01	0.06
08-Nov11	41	374.60	30.77	18.60	1.53	13659.00	166.00	2660.00	0.00	337.00	1.49	1.02	0.06	0.96	0.06
08-Nov11	43	342.70	28.15	17.20	1.41	13874.00	127.00	2870.00	0.00	289.00	1.31	1.01	0.06	0.98	0.06
		336.08	27.80	16.47	1.39										
	Source strength:	Apr-11	0.08												
		Nov-11	0.08												

Table a2.5 Aliquot data used to construct OSL age estimate chim3

	Disc#	ED	De	ED_Err	De error	N.Signal	BG.signal	Test_Signal	Test_Dose	Residual_Signal	Test_Signal_Change	Recycling 1	Recycling 1_Err	Recycling 2	Recycling 2_Err
02-Apr-11	25	369.60	31.54	20.30	1.73	14128.00	129.00	2518.00	0.00	222.00	1.17	1.00	0.07	1.00	0.06
02-Apr-11	27	377.00	32.17	19.90	1.70	13746.00	108.00	2353.00	0.00	246.00	1.18	1.00	0.07	0.98	0.06
02-Apr-11	29	369.10	31.50	18.50	1.58	14956.00	122.00	2510.00	0.00	296.00	1.20	1.02	0.07	1.01	0.06
02-Apr-11	33	377.90	32.25	19.60	1.67	15075.00	100.00	2520.00	0.00	235.00	1.19	1.00	0.06	1.00	0.06
02-Apr-11	35	383.00	32.68	18.70	1.60	16793.00	112.00	2807.00	0.00	222.00	1.19	1.03	0.06	0.98	0.06
09-Apr-11	23	371.90	31.73	19.40	1.66	15637.00	161.00	2757.00	0.00	329.00	1.36	0.96	0.06	1.03	0.06
09-Apr-11	25	377.90	32.25	18.00	1.54	16179.00	129.00	2714.00	0.00	309.00	1.27	0.95	0.06	1.05	0.06
09-Apr-11	27	357.10	30.47	17.80	1.52	16980.00	102.00	2914.00	0.00	273.00	1.40	1.05	0.06	0.95	0.06
09-Apr-11	33	374.70	31.97	22.40	1.91	12690.00	197.00	2271.00	0.00	320.00	1.35	0.98	0.07	1.00	0.07
09-Apr-11	35	383.50	32.72	21.30	1.82	22931.00	245.00	4031.00	0.00	486.00	1.33	0.99	0.06	1.03	0.06
10-Nov11	1	392.00	32.20	19.60	1.61	15751.00	114.00	2864.00	0.00	230.00	1.30	0.97	0.06	1.03	0.06
10-Nov11	3	376.10	30.89	22.00	1.81	11785.00	143.00	2370.00	0.00	263.00	1.35	0.98	0.07	0.99	0.06
10-Nov11	7	366.90	30.14	19.60	1.61	13851.00	147.00	2667.00	0.00	269.00	1.22	1.01	0.07	1.01	0.06
10-Nov11	9	379.90	31.20	21.10	1.73	14123.00	119.00	2651.00	0.00	242.00	1.28	1.02	0.06	1.03	0.06
10-Nov11	11	392.50	32.24	21.30	1.75	14650.00	139.00	2743.00	0.00	291.00	1.37	0.98	0.06	1.01	0.06
10-Nov11	13	418.20	34.35	23.50	1.93	13097.00	125.00	2373.00	0.00	266.00	1.30	1.05	0.07	1.02	0.06
10-Nov11	17	381.90	31.37	23.00	1.89	13016.00	119.00	2459.00	0.00	211.00	1.19	0.99	0.07	1.02	0.07
10-Nov11	19	393.00	32.28	20.60	1.69	14229.00	114.00	2606.00	0.00	243.00	1.25	0.99	0.06	0.99	0.06
10-Nov11	21	372.20	30.57	18.60	1.53	15754.00	113.00	3027.00	0.00	254.00	1.21	1.02	0.06	1.03	0.06
10-Nov11	23	368.30	30.25	17.90	1.47	12718.00	139.00	2514.00	0.00	234.00	1.31	1.03	0.07	0.97	0.06
		379.14	31.74	20.16	1.69										
	Source strength:	Mar-11	0.09												
		Apr-11	0.09												
		Nov-11	0.08												

Table a2.6 Aliquot data used to construct OSL age estimate chim4

	Disc#	ED	De	ED_Err	De error	N.Signal	BG.signal	Test_Signal	Test_Dose	Residual_Signal	Test_Signal_Change	Recycling 1	Recycling 1_Err	Recycling 2	Recycling 2_Err
07-Mar11	21	356.20	30.46	20.80	1.78	12635.00	123.00	2332.00	0.00	228.00	1.07	1.04	0.07	0.99	0.07
07-Mar11	23	356.70	30.50	17.60	1.50	12400.00	102.00	2153.00	0.00	193.00	1.14	1.00	0.07	1.00	0.07
05-Apr-11	1	299.40	25.55	17.80	1.52	11532.00	262.00	2468.00	0.00	328.00	1.21	0.98	0.07	1.03	0.07
05-Apr-11	3	356.70	30.44	17.80	1.52	15758.00	157.00	2909.00	0.00	359.00	1.22	1.03	0.06	1.01	0.06
05-Apr-11	5	348.30	29.72	16.90	1.44	17963.00	150.00	3303.00	0.00	359.00	1.21	1.02	0.06	0.94	0.06
05-Apr-11	9	374.20	31.93	20.60	1.76	17468.00	161.00	3118.00	0.00	352.00	1.19	1.04	0.06	0.97	0.06
05-Apr-11	11	367.80	31.39	18.50	1.58	19419.00	185.00	3455.00	0.00	331.00	1.16	1.02	0.06	1.00	0.06
05-Apr-11	13	335.40	28.62	15.20	1.30	19357.00	173.00	3655.00	0.00	398.00	1.21	1.03	0.06	0.97	0.06
05-Apr-11	15	300.80	25.67	14.60	1.25	16023.00	140.00	3128.00	0.00	304.00	1.19	0.99	0.06	1.04	0.06
05-Apr-11	17	274.00	23.38	13.20	1.13	17180.00	192.00	3894.00	0.00	383.00	1.33	1.03	0.06	0.98	0.05
05-Apr-11	19	343.30	29.29	17.80	1.52	17460.00	163.00	3258.00	0.00	359.00	1.28	0.99	0.06	0.99	0.06
05-Apr-11	21	327.60	27.95	14.10	1.20	19745.00	165.00	3713.00	0.00	393.00	1.21	1.05	0.06	1.00	0.06
12-Nov11	11	385.30	31.65	18.60	1.53	20694.00	194.00	3871.00	0.00	399.00	1.28	1.05	0.06	0.95	0.05
		340.44	28.97	17.19	1.46										
	Signal strength:	mar	0.09												
		apr	0.09												
		nov	0.08												

Table a2.7 Aliquot data used to construct OSL age estimate for chim5

	Disc#	ED	De	ED_Err	De error	N.Signal	BG.signal	Test_Signal	Test_Dose	Residual_Signal	Test_Signal_Change	Recycling 1	Recycling 1_Err	Recycling 2	Recycling 2_Err
07-Mar11	27	294.80	25.21	14.60	1.25	13799.00	109.00	2829.00	0.00	213.00	1.08	1.03	0.07	0.96	0.06
07-Mar11	29	294.30	25.16	14.60	1.25	16574.00	117.00	3471.00	0.00	253.00	0.97	1.00	0.06	1.01	0.06
05-Apr-11	25	282.30	24.09	13.20	1.13	19003.00	165.00	4243.00	0.00	387.00	1.12	0.98	0.06	1.01	0.06
05-Apr-11	27	268.00	22.87	12.70	1.08	18884.00	154.00	4329.00	0.00	359.00	1.03	1.02	0.06	1.04	0.06
05-Apr-11	29	268.90	22.95	12.50	1.07	17957.00	176.00	4138.00	0.00	382.00	1.15	1.02	0.06	1.00	0.06
05-Apr-11	31	269.80	23.02	12.20	1.04	20988.00	193.00	4861.00	0.00	447.00	1.15	1.02	0.06	0.98	0.05
05-Apr-11	35	284.60	24.29	11.80	1.01	26613.00	194.00	5740.00	0.00	452.00	1.17	1.04	0.06	1.01	0.05
05-Apr-11	37	283.70	24.21	12.90	1.10	23905.00	167.00	5144.00	0.00	420.00	1.14	1.01	0.06	1.01	0.05
05-Apr-11	39	314.60	26.85	14.30	1.22	22034.00	160.00	4422.00	0.00	409.00	1.07	1.03	0.06	1.03	0.06
05-Apr-11	43	276.30	23.58	12.00	1.02	22879.00	182.00	5094.00	0.00	406.00	1.15	1.05	0.06	0.99	0.05
12-Nov11	31	306.40	25.17	14.80	1.22	13251.00	65.00	2887.00	0.00	171.00	1.08	1.04	0.06	1.05	0.06
12-Nov11	23	317.00	26.04	15.00	1.23	14597.00	79.00	3156.00	0.00	217.00	1.25	1.04	0.06	0.99	0.06
		288.39	24.45	13.38	1.13										
	Signal strength:	mar	0.09												
		apr	0.09												
		nov	0.08												

Table a2.8 Aliquot data used to construct OSL age estimate chim6

	Disc#	ED	De	ED_Err	De error	N.Signal	BG.signal	Test_Signal	Test_Dose	Residual_Signal	Test_Signal_Change	Recycling 1	Recycling 1_Err	Recycling 2	Recycling 2_Err
09-Apr-11	3	259.20	22.12	12.20	1.04	18552.00	115.00	4267.00	0.00	287.00	0.96	0.96	0.06	1.01	0.06
09-Apr-11	5	265.60	22.66	11.80	1.01	20192.00	174.00	4595.00	0.00	353.00	1.11	1.01	0.06	0.99	0.06
09-Apr-11	7	253.20	21.61	10.20	0.87	23476.00	153.00	5593.00	0.00	425.00	1.10	1.04	0.06	1.00	0.05
09-Apr-11	11	250.40	21.37	10.40	0.89	24590.00	155.00	5717.00	0.00	384.00	1.11	1.04	0.06	0.97	0.05
09-Apr-11	13	271.70	23.18	11.60	0.99	18552.00	135.00	4244.00	0.00	329.00	1.11	1.03	0.06	1.03	0.06
09-Apr-11	15	254.60	21.73	10.40	0.89	23479.00	155.00	5604.00	0.00	394.00	1.20	1.04	0.06	1.02	0.05
09-Apr-11	17	268.00	22.87	11.80	1.01	19385.00	181.00	4524.00	0.00	327.00	1.08	1.03	0.06	1.00	0.06
09-Apr-11	21	255.50	21.80	11.30	0.96	24768.00	165.00	5898.00	0.00	396.00	1.09	0.98	0.05	1.02	0.05
09-Apr-11	21	255.00	21.76	10.60	0.90	32389.00	247.00	7796.00	0.00	572.00	1.08	1.00	0.05	1.03	0.05
10-Nov11	27	263.30	21.63	11.40	0.94	20275.00	135.00	5217.00	0.00	311.00	1.04	1.02	0.06	1.03	0.06
10-Nov11	29	265.20	21.78	10.60	0.87	27734.00	163.00	7021.00	0.00	386.00	1.04	1.03	0.05	0.98	0.05
10-Nov11	31	272.00	22.34	11.40	0.94	20002.00	140.00	4895.00	0.00	326.00	1.07	1.00	0.06	0.98	0.05
10-Nov11	33	260.90	21.43	10.90	0.90	22502.00	146.00	5711.00	0.00	335.00	1.05	1.01	0.05	1.00	0.05
10-Nov11	37	269.10	22.10	11.40	0.94	17141.00	144.00	4304.00	0.00	330.00	1.06	1.03	0.06	0.96	0.06
10-Nov11	39	275.40	22.62	12.30	1.01	15777.00	119.00	3930.00	0.00	256.00	1.01	1.03	0.06	1.01	0.06
10-Nov11	41	253.60	20.83	10.60	0.87	24665.00	155.00	6525.00	0.00	391.00	1.12	1.01	0.05	0.97	0.05
10-Nov11	43	283.10	23.25	13.30	1.09	18673.00	145.00	4552.00	0.00	252.00	1.02	0.97	0.06	1.01	0.06
10-Nov11	47	271.00	22.26	11.90	0.98	19845.00	190.00	5118.00	0.00	346.00	1.07	1.01	0.06	0.98	0.05
		263.71	22.07	11.34	0.95										
	Signal strength:	mar	0.09												
		apr	0.09												
		nov	0.08												

Table a2.9 Aliquot data used to construct OSL age estimate chim7

TRANSECT 1											
sample number	3408	3409	3410	3411	3412	3413	3414	3415	3416	3417	3418	3419
depth in composite	0	5	10	15	20	25	30	35	39	44	49	54
gravel %	0.00	0.00	0.00	0.00	0.00	0.00	27.30	10.34	0.00	4.04	6.07	0.00
sand %	20.19	20.17	20.53	12.13	12.09	18.86	17.62	24.66	31.79	29.64	32.65	46.49
silt %	57.55	55.40	54.20	58.70	57.67	53.55	34.48	43.42	45.02	44.17	38.36	34.03
total clay %	22.27	24.43	25.27	29.17	30.24	27.59	20.60	21.58	23.19	22.15	22.92	19.48
fine clay %	15.16	18.36	18.04	21.53	22.95	19.55	15.31	17.36	17.39	15.85	16.24	13.70
MEDIAN	15.67	28.98	14.18	9.45	9.29	12.25	35.89	23.85	20.17	21.18	23.97	45.05
%CaCO3	18.28	18.00	16.61	11.56	10.53	11.93	10.84	10.57	13.12	14.82	17.02	17.22
organic carbon	0.37	0.30	0.31	0.35	0.24	0.32	0.19	0.26	0.12	0.14	0.15	0.17
lf	6.28	6.05	6.08	8.03	8.10	7.98	7.95	7.28	6.25	6.15	7.45	8.18
hf	6.10	5.85	6.03	7.53	7.40	7.45	7.40	6.88	6.13	6.10	7.03	7.93
cfd	2.79	3.31	0.82	6.23	8.64	6.58	6.92	5.50	2.00	0.81	5.70	3.06

Table a3.1 Sedimentology data for section 1, transect 1 (composite log depth given)

TRANSECT 2									
sample number	3420	3421	3422	3423	3424	3425	3426	3427	3428
depth in composite	60	65	70	75	80	85	90	95	100
gravel %	0	0	0	0	0	0	0	0	0
sand %	21.20	15.24	20.97	19.48	19.53	29.24	43.25	38.05	28.05
silt %	58.16	61.71	57.69	55.40	56.01	50.38	42.50	46.09	48.64
total clay %	20.65	23.06	21.34	25.12	24.46	20.38	14.24	15.86	23.31
fine clay %	15.29	17.72	14.94	17.71	18.11	14.08	10.33	11.58	17.27
MEDIAN	19.19	15.11	17.89	14.14	13.63	20.65	39.71	28.69	18.88
%CaCO3	17.02	16.30	16.68	14.39	9.02	11.75	20.34	20.91	11.81
organic carbon	0.32	0.23	0.30	0.35	0.43	0.22	0.14	0.15	0.27
lf	35.18	10.73	9.73	8.80	8.18	6.85	4.35	4.25	4.80
hf	32.40	10.05	9.40	8.53	7.93	6.10	4.08	3.98	4.23
cfd	7.89	6.29	3.34	3.13	3.06	10.95	6.32	6.47	11.98

Table a3.2 Sedimentology data for section 1, transect 2 (composite log depth given)

TRANSECT 3																
sample number	3429	3430	3431	3432	3433	3434	3435	3436	3437	3438	3439	3440	3441	3442	3443	3444	3445	3446
depth in composite	273	278	283	288	293	298	303	308	313	318	322	327	332	337	342	347	352	357
gravel %	0.66	0.71	0.82	0.25	0.44	0.53	0.61	0.44	0.47	0.68	1.64	15.50	13.28	0.58	0.15	0.51	0.00	0.27
sand %	6.03	7.34	8.70	6.98	9.35	14.20	16.50	15.99	18.20	20.68	25.48	30.38	26.71	19.15	17.38	23.04	39.29	27.09
silt %	57.10	54.34	53.39	56.40	54.85	46.39	43.19	40.70	45.22	44.59	39.94	30.69	38.46	53.86	52.62	47.17	34.36	39.52
total clay %	36.20	37.61	37.10	36.36	35.36	38.88	39.71	42.87	36.11	34.05	32.94	23.43	21.54	26.41	29.85	29.28	26.35	33.13
fine clay %	25.38	27.49	26.15	27.74	26.97	28.22	29.68	33.68	28.46	26.50	24.49	16.51	14.28	17.90	20.37	21.48	19.06	22.45
MEDIAN	6.21	5.97	6.11	6.07	7.43	6.26	5.96	4.76	8.61	9.53	10.21	36.73	26.87	13.64	10.36	11.65	22.02	10.01
%CaCO3	10.92	8.87	9.03	9.89	8.98	6.31	5.34	4.50	6.08	9.09	17.39	35.86	41.48	20.63	19.37	16.13	15.08	20.70
organic carbon	0.32	0.30	0.24	0.20	0.19	0.40	0.24	0.20	0.25	0.16	0.15	0.33	0.36	0.25	0.34	0.35	0.26	0.29
lf	12.48	13.80	14.33	15.40	14.73	11.48	8.55	6.63	6.13	6.08	5.50	3.98	4.10	5.43	7.10	8.03	8.48	8.10
hf	12.40	13.20	13.90	14.85	14.33	11.18	7.95	6.30	6.00	6.08	5.40	3.70	3.63	5.13	6.73	7.90	8.13	7.75
cfd	0.60	4.35	2.97	3.57	2.72	2.61	7.02	4.91	2.04	0.00	1.82	6.92	11.59	5.53	5.28	1.56	4.13	4.32

Table a3.3 Sedimentology data for transect 3(composite log depth given)

TRANSECT 4																				
sample number	3447	3448	3449	3450	3451	3452	3453	3454	3455	3456	3457	3458	3459	3460	3461	3462	3463	3464	3465	3466	3467	3468
depth in composite	362	367	372	377	380	385	390	395	400	405	407	412	417	422	425	430	435	440	445	450	455	459
gravel %	0	0	0	0	0	0	0	0	0	0	0	0	0	0	0	0	0	0	0	0	0	0
sand %	28.36	27.19	37.88	48.18	41.53	31.83	58.98	33.29	38.07	27.99	29.50	42.21	49.34	39.47	43.88	58.83	66.37	41.37	31.67	29.63	37.37	16.41
silt %	47.00	46.89	42.12	36.85	41.28	48.47	30.11	46.09	42.72	47.60	45.26	34.73	32.02	41.40	39.17	29.36	24.31	40.92	47.83	50.17	44.34	55.25
total clay %	24.64	25.92	20.00	14.98	17.19	19.70	10.91	20.61	19.21	24.41	25.24	23.06	18.64	19.13	16.95	11.82	9.31	17.71	20.50	20.19	18.29	28.34
fine clay %	15.04	15.07	12.67	10.68	11.64	12.20	7.22	12.47	13.20	16.42	16.29	16.30	13.98	14.65	11.28	9.02	6.79	12.19	14.28	13.58	13.28	18.64
MEDIAN	13.60	12.01	23.91	54.15	30.33	19.96	80.12	18.76	26.22	14.81	15.54	28.93	59.77	27.46	37.73	80.04	95.10	32.25	19.34	21.95	25.85	10.15
%CaCO3	21.84	23.09	19.80	19.37	20.99	18.95	23.73	17.80	13.32	16.84	10.81	7.09	9.20	16.21	19.00	18.83	21.17	18.50	19.15	15.96	21.02	21.59
organic carbon	0.20	0.22	0.04	0.07	0.15	0.12	0.14	0.19	0.19	0.23	0.35	0.28	0.11	0.14	0.18	0.14	0.14	0.13	0.17	0.19	0.11	0.22
lf	7.30	6.75	5.38	4.38	4.45	5.23	5.23	5.55	5.25	5.88	6.70	4.58	3.88	4.58	4.63	4.18	4.20	4.83	6.00	7.88	9.43	11.05
hf	7.28	6.25	4.85	4.30	4.13	5.23	4.93	5.35	4.98	5.60	5.83	4.43	3.48	4.23	4.50	3.83	4.03	4.83	6.00	7.88	9.18	10.35
cfd	0.34	7.41	9.77	1.71	7.30	0.00	5.74	3.60	5.24	4.68	13.06	3.28	10.32	7.65	2.70	8.38	4.17	0.00	0.00	0.00	2.65	6.33

Table a3.4 Sedimentology data for transect 4 (composite log depth given)

sample number	depth (cm)	gravel %	sand %	silt %	total clay %	fine clay %	MEDIAN	caco3	organic carbon	lf	hf	cfd
3347	160-165	0.00	33.33	45.93	20.73	12.53	23.79	19.30	0.07	14.00	13.43	4.11
3348	155-160	0.00	32.03	43.71	24.27	15.29	21.32	19.00	0.15	13.73	12.60	8.20
3349	152-155	0.00	31.68	45.77	22.55	13.32	19.19	20.15	0.11	12.75	12.63	0.98
3350	147-152	0.00	38.91	42.21	18.88	11.91	30.28	17.97	0.20	13.08	12.08	7.65
3351	142-147	0.00	41.96	39.87	18.17	12.71	31.37	16.13	0.11	13.30	12.80	3.76
3352	137-142	0.00	48.74	32.81	18.45	13.17	57.65	15.89	0.06	14.35	13.55	5.57
3353	132-137	0.00	45.02	37.66	17.32	11.60	44.31	18.86	0.07	13.55	12.98	4.24
3354	127-132	0.00	44.14	40.05	15.81	10.56	42.55	20.17	0.09	8.83	8.60	2.55
3355	122-127	0.00	32.42	48.12	19.46	13.52	21.00	22.32	0.06	11.60	10.43	10.13
3356	118-122	0.00	28.18	44.53	27.29	19.39	17.43	21.12	0.14	10.93	10.90	0.23
3357	113-118	0.00	24.85	52.23	22.92	16.08	18.41	19.00	0.14	10.38	9.90	4.58
3358	108-113	0.00	32.82	46.42	20.76	14.17	23.01	15.70	0.10	12.33	12.00	2.64
3359	103-108	0.00	38.09	41.61	20.31	14.98	28.82	16.30	0.11	14.80	14.70	0.68
3360	98-103	0.00	46.63	36.40	16.97	10.83	50.99	15.03	0.10	13.65	13.00	4.76
3361	96-98	0.00	59.52	28.38	12.10	8.10	81.74	11.53	0.07	7.98	7.85	1.57
3362	91-96	0.00	59.75	24.99	15.25	10.67	78.97	9.21	0.04	7.93	7.70	2.84
3363	86-91	0.00	54.78	29.89	15.33	11.49	69.96	9.46	0.04	7.78	7.20	7.40
3364	81-86	0.00	52.79	31.35	15.86	11.00	67.23	12.93	0.04	8.95	8.85	1.12
3365	76-81	0.00	39.13	42.97	17.90	12.05	30.43	21.13	0.13	9.00	8.53	5.28
3366	71-76	0.00	41.69	43.38	14.93	11.08	37.43	17.93	0.08	10.15	9.58	5.67
3367	68-71	0.00	59.05	27.40	13.56	10.57	82.66	13.00	0.07	11.63	10.95	5.81
3368	65-68	0.00	50.88	33.60	15.52	13.31	64.85	13.43	0.08	9.68	9.30	3.88
3369	60-65	0.00	15.88	61.16	22.97	15.56	13.90	18.09	0.10	11.55	11.33	1.95
3370	55-60	0.00	21.14	54.81	24.05	16.09	13.03	22.35	0.04	16.43	16.15	1.67
3371	50-55	0.04	29.69	46.66	23.61	16.58	16.97	17.81	0.11	22.08	21.83	1.13
3372	45-50	0.11	27.64	46.02	26.22	18.42	14.05	16.22	0.18	22.73	22.30	1.87
3373	40-45	1.18	22.71	46.58	29.53	19.86	10.45	16.94	0.34	21.63	21.28	1.62
3374	35-40	3.12	18.61	48.21	30.05	19.96	8.94	20.80	0.18	17.40	17.05	2.01
3375	30-35	3.63	18.53	46.47	31.37	21.72	8.35	21.99	0.22	14.38	13.93	3.13
3376	25-30	2.44	21.70	46.12	29.74	20.33	9.34	25.55	0.24	11.00	10.48	4.77
3377	20-25	2.44	26.27	43.48	27.80	17.46	10.74	25.59	0.42	9.30	9.10	3.67
3378	15-20	4.57	40.08	33.93	21.42	14.72	28.54	25.85	0.36	6.13	5.90	3.67
3379	10-15	11.75	42.59	30.18	15.48	10.14	81.14	33.06	0.27	4.30	4.10	4.65
3380	5-10	20.30	41.74	25.40	12.57	8.73	120.38	34.89	0.27	4.13	3.95	4.24
3381	0-5	10.90	43.06	31.72	14.32	9.53	81.67	47.22	0.21	3.65	3.45	5.48

Table a3.5 Sedimentology data Section 1, transect 1 (composite log)

sample number	3382	3383	3384	3385	3386	3387	3388	3389	3390	3391	3392	3393	3394	3395	3396
	5	10	15	20	25	30	35	40	45	50	55	60	64	69	70
depth (cm)	0-5	5-10	10-15	15-20	20-25	25-30	30-35	35-40	40-45	45-50	50-55	55-60	60-64	64-69	69-70
gravel %	0.00	0.00	0.00	0.00	0.00	0.00	0.00	0.00	0.00	0.00	0.00	0.00	0.00	0.00	0.00
sand %	51.39	52.96	45.31	45.69	61.13	66.53	60.85	43.07	37.29	31.51	22.61	15.29	19.36	26.71	26.23
silt %	31.35	30.20	36.64	37.58	26.32	21.99	26.74	37.29	41.52	45.96	52.93	57.43	54.67	45.51	42.56
total clay %	17.26	16.84	18.05	16.73	12.56	11.48	12.41	19.64	21.20	22.53	24.45	27.28	25.97	27.78	31.20
fine clay %	11.28	10.63	11.65	10.81	8.90	7.86	9.08	12.81	14.74	14.79	16.33	18.04	17.34	20.01	21.83
MEDIAN	66.23	70.16	43.28	47.91	81.73	92.75	81.50	32.57	24.29	19.06	13.99	10.91	11.84	13.07	10.45
CaCO3	11.92	12.37	16.59	20.49	23.85	22.73	21.28	25.97	27.87	26.82	31.16	33.72	26.63	19.16	14.27
Organics	0.19	0.10	0.12	0.11	0.08	0.04	0.15	0.19	0.15	0.16	0.24	0.07	0.03	0.15	0.07
if	4.58	4.10	6.25	10.55	12.73	12.83	11.30	13.85	16.28	20.83	24.80	30.80	43.00	60.48	90.08
hf	4.38	3.98	5.90	10.23	12.38	12.75	11.18	12.90	16.00	20.23	23.70	28.95	40.60	56.80	83.98
cfd	4.37	3.05	5.60	3.08	2.75	0.58	1.11	6.86	1.69	2.88	4.44	6.01	5.58	6.08	6.77

Table a3.6 Sedimentology data Maro section 2, transect 2

sample number	3397	3398	3399	3400	3401	3402	3403	3404	3405	3406	3407
	5	10	15	20	25	30	35	40	45	50	55
depth (cm)	0-5	5-10	10-15	15-20	20-25	25-30	30-35	35-40	40-45	45-50	50-55
gravel %	0.00	0.00	0.00	0.00	0.00	0.00	0.00	0.00	0.00	0.00	0.00
sand %	20.77	17.97	15.50	13.06	14.28	16.30	18.40	20.14	26.31	30.75	39.76
silt %	48.49	48.64	51.46	52.95	52.97	52.48	50.10	46.80	43.92	43.56	38.97
total clay %	30.74	33.39	33.04	33.99	32.75	31.22	31.50	33.06	29.77	25.69	21.26
fine clay %	20.04	21.82	21.21	23.47	22.63	21.01	20.81	21.80	21.44	17.10	12.29
MEDIAN	9.77	7.52	7.54	7.46	7.53	7.70	7.25	6.98	9.57	12.59	19.32
CaCO3	15.14	15.34	15.62	13.69	13.62	19.00	25.25	18.89	18.36	29.30	56.47
Organics	0.14	0.21	0.21	0.38	0.17	0.48	0.23	0.11	0.15	0.29	0.25
if	56.40	42.75	34.90	28.48	26.30	26.38	21.68	13.68	8.40	6.20	3.73
hf	54.00	40.10	33.43	27.08	25.10	25.20	20.55	12.83	7.73	6.08	3.70
cfd	4.26	6.20	4.23	4.92	4.56	4.45	5.19	6.22	8.04	2.02	0.67

Table a3.7 Sedimentology data Maro section 2, transect 3

isotope sample #	sample #	13C	18O	%carb	section	unit	material
RDM09 101	3447	-8.64	-6.01	94.39	1	4	ped carb
RDM09 102	3448	-6.34	-3.25	61.13	1	4	ped carb
RDM09 103	3449	-7.07	-4.53	72.53	1	4	ped carb
RDM09 104	3450	-6.45	-5.40	78.20	1	4	ped carb
RDM09 105	3451	-5.87	-4.69	71.72	1	4	ped carb
RDM09 106	3452	-5.49	-3.81	66.41	1	4	ped carb
RDM09 107	3453	-5.67	-4.85	69.12	1	4	ped carb
RDM09 108	3454	-8.05	-5.16	88.58	1	4	ped carb
RDM09 109	3455	-6.21	-3.97	64.85	1	4	ped carb
RDM09 110	3456	-5.63	-3.73	65.43	1	4	ped carb
RDM09 111	3457	-5.29	-3.05	65.92	1	4	ped carb
RDM09 112	3458	-3.28	-3.31	69.77	1	4	ped carb
RDM09 113	3459	-5.24	-2.97	72.27	1	4	ped carb
RDM09 114	3460	-6.03	-3.97	73.61	1	4	ped carb
RDM09 115	3461	-5.56	-2.98	74.91	1	4	ped carb
RDM09 116	3462	-10.16	-6.41	93.82	1	4	ped carb
RDM09 117	3463	-9.78	-6.54	95.72	1	4	ped carb
RDM09 118	3464	-5.31	-3.01	73.73	1	4	ped carb
RDM09 119	3465	-5.52	-2.93	75.56	1	4	ped carb
RDM09 120	3466	-5.46	-2.78	76.36	1	4	ped carb
RDM09 121	3467	-5.86	-3.20	73.95	1	4	ped carb
RDM09 122	3468	-5.14	-4.28	60.60	1	4	ped carb
RDM09 01R	3347	-5.89	-4.11	68.09	2	2	ped carb
RDM09 01A	3347	-5.71	-4.44	74.67	2	2	ped carb
RDM09 02	3348	-5.26	-4.60	66.21	2	2	ped carb
RDM09 03	3349	-4.52	-4.81	50.12	2	2	ped carb
RDM09 04	3350	-5.54	-4.07	69.77	2	2	ped carb
RDM09 05	3351	-5.29	-4.87	65.71	2	2	ped carb
RDM09 06	3352	-5.25	-4.60	62.85	2	2	ped carb
RDM09 07	3353	-5.30	-4.82	70.45	2	2	ped carb
RDM09 08	3354	-5.46	-5.05	69.63	2	2	ped carb
RDM09 09	3355	-6.81	-5.20	73.03	2	2	ped carb
RDM09 10	3356	-6.37	-5.05	64.77	2	2	ped carb
RDM09 11	3357	-6.11	-5.07	63.04	2	2	ped carb
RDM09 12	3358	-5.54	-4.56	69.64	2	2	ped carb
RDM09 13	3359	-4.51	-5.16	59.04	2	2	ped carb
RDM09 14	3360	-4.95	-5.17	67.15	2	2	ped carb
RDM09 15	3361	-4.56	-4.99	74.35	2	2	ped carb
RDM09 16	3362	-5.09	-4.46	70.98	2	2	ped carb
RDM09 17	3363	-5.60	-3.77	74.94	2	2	ped carb
RDM09 18	3364	-3.98	-4.16	66.02	2	2	ped carb
RDM09 19	3365	-4.31	-4.14	62.74	2	2	ped carb
RDM09 20	3366	-5.22	-4.15	71.75	2	2	ped carb
RDM09 21	3367	-3.23	-3.85	69.95	2	2	ped carb
RDM09 22	3368	-4.99	-4.34	62.98	2	2	ped carb
RDM09 23	3369	-5.04	-4.38	61.42	2	2	ped carb
RDMI08-5		-9.25	-7.00	96.40	1	3	oncoid
RDMI08-6		-9.60	-7.30	97.45	1	3	oncoid
RDMI08-7		-9.13	-6.97	94.73	1	3	oncoid
RDMI08-8		-9.32	-7.17	99.93	1	3	oncoid
RDMI08-1		-10.48	-6.76	101.08	1	2	tufa
RDMI08-2		-10.95	-6.56	103.78	1	2	tufa
RDMI08-3		-9.81	-7.25	100.03	2	3	oncoid
RDMI08-4		-9.99	-7.27	102.14	2	3	flowstone
RDMI08-9		-8.33225	-7.38101	99.66	Modern tufa		speleothem
RDMI08-10		-7.58562	-7.3268	95.67	Modern tufa		early onco
RDMI08-11		-8.38396	-7.27492	67.54	Modern tufa		speleothem

Table a3.8 Maro isotope data (all samples)

Name	$d^{13}C$ corr (‰)	error (1s)	$d^{18}O$ corr (‰)	error (1s)	Est % carb
INTERNAL					
RHBNC	3.30	0.05	-10.53	0.05	98.95
RHBNC	3.26	0.00	-10.57	0.00	96.12
RHBNC	3.23	0.03	-10.55	0.03	96.30
RHBNC	3.32	0.01	-10.55	0.06	98.13
RHBNC	3.25	0.02	-10.59	0.03	96.18
RHBNC	3.21	0.02	-10.60	0.01	100.41
RHBNC	3.30	0.07	-10.55	0.03	99.77
RHBNC	3.28	0.04	-10.60	0.04	101.06
RHBNC	3.29	0.05	-10.53	0.05	95.58
RHBNC	3.29	0.05	-10.41	0.03	3.28
RHBNC	3.22	0.00	-10.45	0.04	3.22
RHBNC	3.21	0.03	-10.39	0.06	3.20
RHBNC	3.19	0.02	-10.49	0.05	3.30
RHBNC	3.14	0.00	-10.46	0.00	3.26
RHBNC	3.12	0.01	-10.49	0.07	3.23
RHBNC	3.28	0.02	-10.69	0.03	107.13
RHBNC	3.19	0.03	-10.72	0.03	93.95
RHBNC	3.23	0.09	-10.76	0.05	90.92
RHBNC	3.28	0.03	-10.66	0.01	89.48
RHBNC	3.28	0.02	-10.79	0.06	92.88
RHBNC	3.26	0.01	-10.66	0.03	89.71
average	3.24	0.03	-10.57	0.04	69.81
	0.051953104		0.106892795		
EXTERNAL					
NBS-19	1.94	0.02	-2.16	0.05	100.00
NBS-19	1.94	0.05	-2.15	0.08	100.00
NBS-19	1.91	0.03	-2.16	0.06	100.00
NBS-19	2.00	0.02	-2.56	0.03	1.97
NBS-19	1.85	0.03	-2.60	0.03	1.94
NBS-19	1.96	0.04	-2.20	0.02	100.00
NBS-19	1.94	0.02	-2.20	0.03	100.00
NBS-19	1.94	0.04	-2.20	0.03	100.00
KNOWN	**1.95**		**-2.20**		
EXTERNAL					
LSVEC	-46.50	0.03	-26.68	0.08	103.34
LSVEC	-46.50	0.05	-26.67	0.06	100.75
LSVEC	-46.50	0.03	-26.68	0.04	94.05
LSVEC	-45.44	0.01	-25.98	0.05	-46.50
LSVEC	-45.54	0.07	-25.94	0.06	-46.51
LSVEC	-46.50	0.05	-26.70	0.09	111.68
LSVEC	-46.50	0.03	-26.70	0.09	99.76
LSVEC	-46.50	0.02	-26.70	0.03	96.54
Known	**-46.50**		**-26.70**		

Table a3.9 Isotope standards (for Chimeneas and Maro data)

Disc#	ED	De	ED_Err	De error	N.Signal	BG.signal	Test_Sign	Test_Dose	Residual_	Test_Sign	Recycling	error	Recycling	error
1	3270.30	282.43	208.70	18.02	347475.00	1087.00	23477.00	53.00	251.00	1.04	0.98	0.04	1.02	0.04
3	2946.20	254.44	179.20	15.48	308772.00	950.00	21471.00	53.00	186.00	0.88	0.99	0.04	0.99	0.04
5	3231.00	279.03	198.90	17.18	310735.00	999.00	21979.00	53.00	201.00	0.86	1.02	0.04	1.00	0.04
7	3285.10	283.71	203.80	17.60	304433.00	968.00	20020.00	53.00	242.00	1.06	1.00	0.04	1.02	0.04
11	3452.00	298.12	208.70	18.02	277155.00	851.00	18430.00	53.00	235.00	1.17	1.00	0.04	1.01	0.04
13	2985.50	257.83	179.20	15.48	427337.00	1282.00	32044.00	53.00	366.00	1.14	0.99	0.04	0.99	0.04
15	3064.10	264.62	198.90	17.18	294255.00	898.00	21718.00	53.00	266.00	1.15	1.01	0.04	0.98	0.04
17	3127.90	270.13	191.50	16.54	330493.00	1069.00	24328.00	53.00	247.00	0.99	1.01	0.04	0.98	0.04
19	3147.60	271.83	230.80	19.93	144488.00	614.00	10250.00	53.00	297.00	1.20	1.01	0.05	1.00	0.05
21	3098.50	267.59	194.00	16.75	407058.00	1218.00	28371.00	53.00	226.00	0.89	0.99	0.04	1.01	0.04
23	3231.00	279.03	198.90	17.18	229659.00	829.00	15262.00	53.00	200.00	0.87	0.96	0.04	0.99	0.05
mean	3167.20	273.52	199.33	17.21										
source strength		0.09												

Table a3.10 Aliquot data for OSL age estimate RDM083

Disc#	ED	De	ED_Err	De error	N.Signal	BG.signal	Test_Sign	Test_Dose	Residual_	Test_Sign	Recycling	error	Recycling	error
25	3015.00	260.50	186.60	16.12	276884.00	863.00	17947.00	53.00	125.00	0.79	0.98	0.04	1.01	0.05
27	2980.60	257.52	184.10	15.91	282884.00	861.00	18394.00	53.00	140.00	0.83	0.99	0.04	0.99	0.05
29	3299.80	285.10	213.60	18.46	272108.00	786.00	16851.00	53.00	136.00	0.98	1.01	0.04	0.97	0.04
31	3118.10	269.40	198.90	17.18	266595.00	770.00	17253.00	53.00	156.00	0.98	0.99	0.04	0.98	0.04
33	3132.80	270.67	213.60	18.46	305538.00	899.00	19150.00	53.00	162.00	0.91	0.99	0.04	1.00	0.04
35	3216.30	277.89	198.90	17.18	301879.00	919.00	19045.00	53.00	160.00	0.92	1.00	0.04	0.99	0.04
37	3049.40	263.47	194.00	16.76	260854.00	822.00	17500.00	53.00	136.00	0.87	0.99	0.04	1.01	0.05
39	3137.80	271.11	198.90	17.18	274920.00	871.00	17369.00	53.00	139.00	0.88	1.01	0.05	0.99	0.05
41	2936.40	253.70	201.30	17.39	154500.00	557.00	10944.00	53.00	152.00	0.85	1.02	0.05	1.02	0.05
43	3186.90	275.35	208.70	18.03	279170.00	864.00	18082.00	53.00	139.00	0.90	1.00	0.04	1.00	0.05
45	3078.80	266.01	198.90	17.18	298397.00	868.00	18363.00	53.00	150.00	0.85	1.02	0.05	1.00	0.05
47	3137.80	271.11	196.40	16.97	271774.00	802.00	17307.00	53.00	116.00	0.91	0.98	0.04	0.99	0.05
mean	3107.48	268.49	199.49	17.24										
source strength		0.09												

Table a3.11 Aliquot data for OSL age estimate RDM084

Disc#	ED	De	ED_Err	De error	N.Signal	BG.signal	Test_Sign	Test_Dos	Residual_	Test_Sign	Recycling	error	Recycling	error
1	3491.30	301.65	245.50	21.21	454334.00	1316.00	31277.00	0.00	292.00	0.58	1.03	0.04	1.00	0.04
3	3147.60	271.95	218.50	18.88	480626.00	1344.00	32820.00	0.00	279.00	0.56	1.00	0.04	0.99	0.04
5	3609.20	311.83	243.10	21.00	514828.00	1395.00	33924.00	0.00	457.00	0.79	0.99	0.04	0.99	0.04
7	3010.10	260.07	211.20	18.25	565899.00	1495.00	37805.00	0.00	272.00	0.50	0.99	0.04	1.02	0.04
9	3535.50	305.47	265.20	22.91	468551.00	1298.00	31328.00	0.00	376.00	0.70	1.00	0.04	1.00	0.04
11	3609.20	311.83	240.60	20.79	516004.00	1403.00	36167.00	0.00	418.00	0.68	0.96	0.04	1.01	0.04
13	2956.10	255.41	216.10	18.67	419520.00	1190.00	29311.00	0.00	241.00	0.49	1.02	0.04	0.97	0.04
15	3658.30	316.08	262.70	22.70	530062.00	1414.00	34832.00	0.00	376.00	0.69	0.99	0.04	0.99	0.04
17	3186.90	275.35	235.70	20.36	377571.00	1056.00	26071.00	0.00	270.00	0.59	1.00	0.04	1.00	0.04
19	3452.00	298.25	248.00	21.43	562945.00	1494.00	39494.00	0.00	511.00	0.76	1.02	0.04	0.99	0.04
21	3525.70	304.62	233.20	20.15	539066.00	1427.00	34174.00	0.00	406.00	0.68	0.97	0.04	1.00	0.04
23	3510.90	303.34	230.80	19.94	541430.00	1455.00	34984.00	0.00	340.00	0.63	0.98	0.04	1.01	0.04
mean	3391.07	292.99	237.55	20.52										
source strength		0.09												

Table a3.12 Aliquot data for OSL age estimate RDM085

Disc#	ED	De	ED_Err	De error	N.Signal	BG.signal	Test_Sign	Test_Dos	Residual_	Test_Sign	Recycling	error	Recycling	error
25	3177	274.4928	211.2	18.24768	529795	1588	38515	0	304	0.58	1.01	0.04	1.01	0.04
27	3344	288.9216	228.3	19.72512	517249	1518	34792	0	446	0.66	0.98	0.04	0.99	0.04
29	3299.8	285.1027	228.3	19.72512	492605	1431	35259	0	420	0.73	1	0.04	1	0.04
31	3535.5	305.4672	240.6	20.78784	570901	1602	37723	0	569	0.79	1	0.04	0.99	0.04
33	3520.8	304.1971	245.5	21.2112	457166	1270	31528	0	476	0.84	1	0.04	1.01	0.04
35	3073.9	265.585	225.9	19.51776	304150	839	20819	0	419	1.01	0.99	0.04	1.01	0.04
37	3236	279.5904	228.3	19.72512	504858	1412	35741	0	637	0.91	0.99	0.04	0.98	0.04
39	3673	317.3472	245.5	21.2112	341035	1002	22864	0	333	0.77	1.02	0.04	0.98	0.04
41	3167.2	273.6461	225.9	19.51776	390725	1212	27024	0	376	0.66	1	0.04	0.99	0.04
43	3231	279.1584	216.1	18.67104	559162	1598	38654	0	480	0.72	0.98	0.04	1	0.04
45	3240.9	280.0138	225.9	19.51776	580931	1649	42542	0	601	0.8	0.98	0.04	0.99	0.04
47	3530.6	305.0438	223.4	19.30176	553341	1526	36950	0	462	0.73	1	0.04	1	0.04
mean	3335.808	288.2138	228.7417	19.76328										
source strength		0.0864												

Table a3.13 Aliquot data for OSL age estimate RDM086

date	Disc#	ED	De	ED_Err	De error	N.Signal	BG.signal	Test_Sign	Test_Dos	Residual_	Test_Sign	Recycling	Recycling	Recycling	Recycling
26-May-10	5	3345.00	284.87	277.60	23.64	133381.00	582.00	10054.00	0.00	312.00	0.60	0.98	0.05	0.97	0.05
26-May-10	7	3159.90	269.11	273.00	23.25	105620.00	382.00	7732.00	0.00	119.00	0.73	1.01	0.05	0.99	0.05
02-Jun-10	1	3576.30	303.95	261.40	22.22	273872.00	1132.00	18713.00	0.00	212.00	0.53	0.98	0.05	1.00	0.05
02-Jun-10	3	3317.20	281.93	229.00	19.46	177937.00	861.00	11485.00	0.00	164.00	0.46	0.97	0.05	0.95	0.05
02-Jun-10	5	3155.30	268.17	224.40	19.07	224386.00	957.00	13584.00	0.00	231.00	0.52	0.98	0.05	0.98	0.05
02-Jun-10	7	3275.60	278.39	256.80	21.83	159505.00	699.00	11361.00	0.00	192.00	0.56	0.97	0.05	0.95	0.05
02-Jun-10	9	3395.90	288.62	252.10	21.43	202282.00	841.00	13178.00	0.00	185.00	0.52	1.00	0.05	0.97	0.05
02-Jun-10	15	3067.40	260.70	215.10	18.28	190273.00	870.00	11225.00	0.00	196.00	0.56	0.99	0.05	0.95	0.05
02-Jun-10	19	3072.00	261.09	238.30	20.25	184079.00	865.00	12017.00	0.00	150.00	0.46	1.00	0.05	0.97	0.05
02-Jun-10	21	2924.00	248.51	219.80	18.68	133207.00	738.00	9087.00	0.00	172.00	0.44	0.98	0.06	0.95	0.06
15-Nov-11	1	2671.00	219.39	171.00	14.05	247151.00	1056.00	20167.00	0.00	245.00	0.51	0.98	0.05	0.97	0.05
15-Nov-11	3	3209.90	263.65	187.40	15.39	299881.00	1182.00	22631.00	0.00	224.00	0.57	0.96	0.04	0.99	0.05
15-Nov-11	5	3017.80	247.87	187.40	15.39	329228.00	1224.00	26121.00	0.00	243.00	0.61	0.99	0.04	0.98	0.04
15-Nov-11	7	3130.30	257.11	208.50	17.13	248524.00	848.00	19810.00	0.00	272.00	0.64	0.99	0.04	0.99	0.05
15-Nov-11	11	3153.70	259.03	182.80	15.01	251939.00	1035.00	19506.00	0.00	228.00	0.55	0.95	0.04	1.01	0.05
15-Nov-11	13	2961.60	243.26	171.00	14.05	323795.00	1349.00	23818.00	0.00	292.00	0.58	0.97	0.04	0.96	0.04
15-Nov-11	15	3031.90	249.03	187.40	15.39	259239.00	1003.00	20269.00	0.00	273.00	0.61	0.98	0.04	0.99	0.05
mean		3144.99	263.80	220.18	18.50										
source strengths															
May-10	0.09														
Jun-10	0.08														
Nov-11	0.08														

Table a3.14 Aliquot data for OSL age estimate RDM091

date	Disc#	ED	De	ED_Err	De error	N.Signal	BG.signal	Test_Sign	Test_Dos	Residual_	Test_Sign	Recycling	Recycling	Recycling	Recycling
26-May-10	9	3039.70	258.87	263.70	22.46	77303.00	375.00	5829.00	0.00	118.00	0.70	0.97	0.06	1.04	0.06
26-May-10	11	2905.50	247.44	261.40	22.26	88477.00	538.00	6466.00	0.00	167.00	0.62	0.95	0.05	0.97	0.06
02-Jun-10	25	3062.80	260.31	240.60	20.45	121741.00	604.00	8632.00	0.00	161.00	0.61	1.00	0.05	0.99	0.05
02-Jun-10	39	3220.10	273.67	312.30	26.54	78478.00	427.00	5041.00	0.00	222.00	0.67	0.99	0.06	0.98	0.06
02-Jun-10	45	3072.00	261.09	224.40	19.07	111193.00	637.00	6973.00	0.00	128.00	0.59	0.96	0.05	0.96	0.06
02-Jul-10	3	3173.80	269.21	242.90	20.60	119614.00	736.00	7723.00	0.00	85.00	0.40	0.96	0.06	0.96	0.06
02-Jul-10	5	3081.30	261.36	256.80	21.78	105321.00	727.00	7402.00	0.00	97.00	0.43	0.99	0.06	0.97	0.06
02-Jul-10	9	3095.20	262.54	305.30	25.90	100793.00	627.00	7428.00	0.00	118.00	0.42	0.95	0.06	0.96	0.06
02-Jul-10	11	3113.70	264.11	254.50	21.59	122608.00	587.00	8369.00	0.00	118.00	0.50	0.95	0.05	1.00	0.06
02-Jul-10	13	2988.80	253.51	247.50	20.99	143641.00	795.00	9735.00	0.00	108.00	0.39	0.97	0.05	0.98	0.06
02-Jul-10	25	3229.30	273.91	266.00	22.56	114158.00	643.00	7900.00	0.00	83.00	0.39	1.00	0.06	0.95	0.06
02-Jul-10	29	3072.00	260.57	217.40	18.44	120231.00	703.00	7960.00	0.00	105.00	0.38	0.97	0.06	0.99	0.06
02-Jul-10	35	2873.10	243.70	217.40	18.44	123834.00	706.00	7866.00	0.00	100.00	0.38	0.98	0.06	0.97	0.06
02-Jul-10	37	3136.80	266.07	233.60	19.81	132168.00	752.00	8524.00	0.00	117.00	0.44	0.95	0.05	0.95	0.06
02-Jul-10	39	2831.50	240.17	208.20	17.66	97209.00	627.00	6416.00	0.00	100.00	0.38	0.96	0.06	0.97	0.07
mean		3059.71	259.77	250.13	21.24										
source strength															
may	0.09														
jun	0.08														
jul	0.08														

Table a3.15 Aliquot data for OSL age estimate RDM092

Disc#	ED	de	ED_Err	de error	N.Signal	BG.signal	Test_Sign	Test_Dos	Residual_Signal	Test_Signal_Cha	Recycling	Recycling	Recycling	Recycling
1	3664.20	312.67	254.50	21.72	220324.00	456.00	13302.00	0.00	320.00	1.10	0.99	0.04	0.98	0.04
3	3335.80	284.65	247.50	21.12	143023.00	345.00	7721.00	0.00	188.00	1.05	0.97	0.05	1.00	0.05
5	3169.20	270.43	249.80	21.32	130976.00	317.00	7652.00	0.00	169.00	0.89	0.98	0.05	1.02	0.05
7	3308.00	282.28	229.00	19.54	161021.00	399.00	9106.00	0.00	124.00	0.70	0.97	0.05	0.99	0.05
9	2942.50	251.09	219.80	18.76	145830.00	343.00	7609.00	0.00	122.00	0.67	1.05	0.06	0.96	0.05
11	3025.80	258.20	240.60	20.53	120282.00	306.00	6570.00	0.00	126.00	0.64	0.99	0.05	1.03	0.06
13	3229.30	275.56	256.80	21.91	141028.00	351.00	7979.00	0.00	134.00	0.69	1.00	0.05	1.02	0.05
15	3294.10	281.09	268.30	22.89	112546.00	276.00	6207.00	0.00	122.00	0.75	1.00	0.05	0.97	0.05
17	3567.10	304.39	298.40	25.46	152303.00	359.00	8075.00	0.00	146.00	0.80	1.01	0.05	0.99	0.05
19	3266.40	278.73	268.30	22.89	157453.00	357.00	9072.00	0.00	199.00	1.00	1.01	0.05	0.97	0.05
21	2951.80	251.88	224.40	19.15	126955.00	300.00	6660.00	0.00	113.00	0.67	0.96	0.05	1.02	0.06
23	3474.60	296.49	279.90	23.88	135133.00	337.00	7451.00	0.00	172.00	0.87	1.00	0.05	0.98	0.05
25	3284.90	280.31	289.20	24.68	109042.00	271.00	5654.00	0.00	116.00	0.75	0.99	0.06	1.03	0.06
27	3414.40	291.36	240.60	20.53	150921.00	360.00	8142.00	0.00	193.00	0.85	0.98	0.05	0.97	0.05
29	3793.80	323.73	349.30	29.81	108681.00	284.00	5678.00	0.00	124.00	0.82	0.95	0.05	1.01	0.06
31	2905.50	247.93	236.00	20.14	116270.00	330.00	6617.00	0.00	135.00	0.68	1.00	0.06	0.98	0.06
33	3368.10	287.41	263.70	22.50	154801.00	366.00	8534.00	0.00	284.00	1.21	0.95	0.05	1.03	0.05
35	3423.70	292.15	296.10	25.27	140186.00	340.00	7688.00	0.00	128.00	0.82	1.02	0.05	0.96	0.05
37	3109.10	265.30	229.00	19.54	109184.00	300.00	5647.00	0.00	87.00	0.61	0.97	0.06	1.00	0.06
39	3636.50	310.31	286.80	24.47	129637.00	308.00	6669.00	0.00	148.00	0.93	1.02	0.05	0.99	0.05
41	3525.40	300.83	240.60	20.53	125336.00	333.00	6497.00	0.00	113.00	0.82	0.96	0.05	0.99	0.05
43	3122.90	266.48	231.30	19.74	125173.00	331.00	6503.00	0.00	108.00	0.62	0.95	0.05	1.01	0.06
45	3127.60	266.88	233.60	19.93	123281.00	298.00	6621.00	0.00	131.00	0.76	0.98	0.05	1.02	0.06
47	3146.10	268.46	247.50	21.12	104790.00	262.00	5636.00	0.00	132.00	0.74	0.97	0.05	1.02	0.06
mean	3295.28	281.19	257.54	21.98										
source strength		0.09												

Table a3.16 Aliquot data for OSL age estimate RDM093

date	Disc#	ED	De	ED_Err	De error	N.Signal	BG.signal	Test_Sign	Test_Dos	Residual_	Test_Sign	Recycling	error	Recycling	error
19-Apr-10	1	3011.90	257.01	222.10	18.95	295524.00	967.00	20021.00	0.00	630.00	1.27	0.97	0.04	1.01	0.04
19-Apr-10	3	2280.90	194.63	166.60	14.22	269821.00	891.00	20006.00	0.00	753.00	1.28	0.98	0.04	0.98	0.04
19-Apr-10	5	3095.20	264.12	210.50	17.96	234204.00	778.00	15268.00	0.00	327.00	0.90	0.98	0.04	1.00	0.05
19-Apr-10	9	2956.40	252.27	215.10	18.35	208949.00	755.00	14989.00	0.00	367.00	1.07	0.97	0.04	1.00	0.04
19-Apr-10	11	3331.10	284.25	222.10	18.95	254200.00	811.00	14836.00	0.00	625.00	1.47	0.97	0.04	0.98	0.04
19-Apr-10	13	3002.60	256.22	203.60	17.37	221170.00	753.00	14796.00	0.00	335.00	0.88	1.00	0.04	0.99	0.05
19-Apr-10	15	2979.50	254.25	229.00	19.54	225429.00	787.00	15118.00	0.00	411.00	1.10	0.96	0.04	1.01	0.04
19-Apr-10	17	3294.10	281.09	238.30	20.33	255780.00	821.00	15858.00	0.00	395.00	0.97	0.98	0.04	1.00	0.04
19-Apr-10	19	2789.80	238.06	247.50	21.12	189342.00	683.00	13096.00	0.00	412.00	1.24	0.99	0.04	0.99	0.04
19-Apr-10	21	2424.30	206.87	175.80	15.00	296067.00	939.00	21311.00	0.00	722.00	1.25	0.97	0.04	1.02	0.04
19-Apr-10	23	3035.00	258.98	224.40	19.15	210183.00	714.00	13571.00	0.00	349.00	1.03	1.02	0.04	0.98	0.04
19-Apr-10	25	3261.70	278.33	240.60	20.53	273916.00	856.00	18388.00	0.00	601.00	1.33	0.98	0.04	0.98	0.04
19-Apr-10	27	2766.70	236.09	205.90	17.57	226167.00	777.00	15802.00	0.00	371.00	0.94	0.99	0.04	0.99	0.04
19-Apr-10	29	3437.50	293.33	229.00	19.54	235239.00	770.00	13748.00	0.00	554.00	1.45	0.98	0.04	0.99	0.04
19-Apr-10	31	2961.00	252.67	208.20	17.77	230459.00	771.00	15020.00	0.00	324.00	0.88	1.01	0.04	0.98	0.04
19-Apr-10	33	2951.80	251.88	217.40	18.55	264288.00	866.00	17499.00	0.00	412.00	1.00	0.99	0.04	0.99	0.04
19-Apr-10	35	3021.20	257.80	229.00	19.54	221039.00	732.00	14553.00	0.00	432.00	1.14	0.99	0.04	1.01	0.04
19-Apr-10	37	3164.60	270.04	238.30	20.33	233877.00	805.00	15854.00	0.00	391.00	1.01	0.96	0.04	1.02	0.05
19-Apr-10	39	3122.90	266.48	256.80	21.91	216639.00	780.00	15651.00	0.00	327.00	0.87	1.00	0.04	1.00	0.05
19-Apr-10	41	2382.70	203.32	175.80	15.00	306755.00	993.00	23021.00	0.00	552.00	0.99	0.96	0.04	1.00	0.04
19-Apr-10	43	3210.80	273.98	224.40	19.15	242150.00	799.00	15461.00	0.00	429.00	1.16	0.99	0.04	0.98	0.04
19-Apr-10	45	2516.90	214.77	185.10	15.79	297420.00	958.00	21229.00	0.00	538.00	1.07	0.99	0.04	1.01	0.04
19-Apr-10	47	3229.30	275.56	224.40	19.15	255763.00	817.00	16404.00	0.00	329.00	0.86	0.98	0.04	0.99	0.04
mean		2966.43	253.13	216.95	18.51										
source strength		0.09													

Table a3.17 Aliquot data for OSL age estimate RDM094

Disc#	ED	De	ED_Err	De error	N.Signal	BG.signal	Test_Sign	Test_Dos	Residual_	Test_Sign	Recycling	Recycling	Recycling	Recycling
1	1266.90	109.19	108.00	9.31	61667.00	449.00	7089.00	0.00	356.00	1.14	0.97	0.05	1.00	0.05
3	1163.80	100.30	76.10	6.56	197686.00	907.00	23318.00	0.00	670.00	1.12	0.99	0.04	1.00	0.04
5	1419.10	122.31	103.10	8.89	148706.00	758.00	16172.00	0.00	280.00	0.72	0.99	0.04	0.98	0.04
7	1468.20	126.54	117.80	10.15	170034.00	820.00	18973.00	0.00	502.00	1.15	0.97	0.04	1.02	0.04
9	1694.10	146.01	135.00	11.64	157082.00	759.00	17043.00	0.00	385.00	1.09	1.00	0.04	0.97	0.04
11	1370.00	118.07	103.10	8.89	160071.00	881.00	18383.00	0.00	610.00	1.03	0.97	0.04	1.01	0.04
13	1512.40	130.35	125.20	10.79	125931.00	644.00	14141.00	0.00	224.00	0.82	0.97	0.04	1.00	0.05
15	1203.00	103.68	90.80	7.83	75985.00	433.00	8808.00	0.00	277.00	1.05	1.02	0.05	0.99	0.05
17	1247.20	107.49	95.80	8.26	125601.00	650.00	14263.00	0.00	462.00	1.08	0.97	0.04	1.01	0.04
19	1433.80	123.57	112.90	9.73	156477.00	798.00	16624.00	0.00	425.00	1.00	0.97	0.04	0.98	0.04
21	1379.80	118.92	108.00	9.31	136972.00	766.00	15410.00	0.00	461.00	1.07	0.97	0.04	0.99	0.04
23	1316.00	113.42	98.20	8.46	151781.00	776.00	17325.00	0.00	333.00	0.80	0.96	0.04	1.03	0.05
mean	1372.86	118.32	106.17	9.15										
source strength		0.09												

Table a3.18 Aliquot data for OSL age estimate RDM0822